



UNIVERSITAT DE
BARCELONA

The supramolecular organization of cancer metabolism: From macromolecular crowding to metabolic reprogramming underlying cancer metastasis and drug resistance

Cristina Balcells Nadal

ADVERTIMENT. La consulta d'aquesta tesi queda condicionada a l'acceptació de les següents condicions d'ús: La difusió d'aquesta tesi per mitjà del servei TDX (www.tdx.cat) i a través del Dipòsit Digital de la UB (diposit.ub.edu) ha estat autoritzada pels titulars dels drets de propietat intel·lectual únicament per a usos privats emmarcats en activitats d'investigació i docència. No s'autoritza la seva reproducció amb finalitats de lucre ni la seva difusió i posada a disposició des d'un lloc aliè al servei TDX ni al Dipòsit Digital de la UB. No s'autoritza la presentació del seu contingut en una finestra o marc aliè a TDX o al Dipòsit Digital de la UB (framing). Aquesta reserva de drets afecta tant al resum de presentació de la tesi com als seus continguts. En la utilització o cita de parts de la tesi és obligat indicar el nom de la persona autora.

ADVERTENCIA. La consulta de esta tesis queda condicionada a la aceptación de las siguientes condiciones de uso: La difusión de esta tesis por medio del servicio TDR (www.tdx.cat) y a través del Repositorio Digital de la UB (diposit.ub.edu) ha sido autorizada por los titulares de los derechos de propiedad intelectual únicamente para usos privados enmarcados en actividades de investigación y docencia. No se autoriza su reproducción con finalidades de lucro ni su difusión y puesta a disposición desde un sitio ajeno al servicio TDR o al Repositorio Digital de la UB. No se autoriza la presentación de su contenido en una ventana o marco ajeno a TDR o al Repositorio Digital de la UB (framing). Esta reserva de derechos afecta tanto al resumen de presentación de la tesis como a sus contenidos. En la utilización o cita de partes de la tesis es obligado indicar el nombre de la persona autora.

WARNING. On having consulted this thesis you're accepting the following use conditions: Spreading this thesis by the TDX (www.tdx.cat) service and by the UB Digital Repository (diposit.ub.edu) has been authorized by the titular of the intellectual property rights only for private uses placed in investigation and teaching activities. Reproduction with lucrative aims is not authorized nor its spreading and availability from a site foreign to the TDX service or to the UB Digital Repository. Introducing its content in a window or frame foreign to the TDX service or to the UB Digital Repository is not authorized (framing). Those rights affect to the presentation summary of the thesis as well as to its contents. In the using or citation of parts of the thesis it's obliged to indicate the name of the author.



UNIVERSITAT^{DE}
BARCELONA

UNIVERSITAT DE BARCELONA

FACULTAT DE FARMÀCIA I CIÈNCIES DE L'ALIMENTACIÓ

PROGRAMA DE DOCTORAT EN BIOTECNOLOGIA

**The supramolecular organization of cancer metabolism:
From macromolecular crowding to metabolic reprogramming
underlying cancer metastasis and drug resistance**

Cristina Balcells Nadal

2019



UNIVERSITAT DE BARCELONA

Facultat de Farmàcia i Ciències de l'Alimentació

PROGRAMA DE DOCTORAT EN BIOTECNOLOGIA

Departament de Ciència de Materials i Química Física

Departament de Bioquímica i Biomedicina Molecular

**The supramolecular organization of cancer metabolism:
From macromolecular crowding to metabolic reprogramming underlying
cancer metastasis and drug resistance**

Memòria presentada per **Cristina Balcells Nadal** per
optar al títol de Doctora per la Universitat de Barcelona

Marta Cascante Serratosa

Codirectora

Francesc Mas i Pujadas

Codirector

Josefa Badia Palacín

Tutora

Cristina Balcells Nadal

Doctoranda

Index

Index

1. Introduction	3
1.1. Cancer: An overview	3
1.2. Cancer features.....	5
1.2.1. Cancer and cell cycle	5
1.2.2. Cancer and apoptosis	7
1.3. Cancer metabolism.....	10
1.3.1. Overview of cancer metabolism.....	10
1.3.2. Regulation of cancer metabolism.....	15
1.3.2.1. Pro-anabolic signaling networks	15
1.3.2.2. Pro-catabolic signaling networks	16
1.3.2.3. Regulation of redox balance	17
1.3.2.4. Fine-tuning other aspects of cell metabolism.....	18
1.3.3. Glycolysis and the Warburg effect	19
1.3.4. Tricarboxylic acid cycle and oxidative phosphorylation.....	21
1.3.5. Amino acid metabolism.....	23
1.3.6. Glutamine metabolism	24
1.3.7. Redox balance and ROS metabolism.....	26
1.3.8. Pentose phosphate pathway	27
1.3.9. One-carbon metabolism.....	28
1.3.10. Urea cycle.....	29
1.3.11. Polyamine metabolism	30
1.3.12. Lipid metabolism.....	33
1.4. Metastasis, invasion and stemness	35
1.4.1. Metastasis and epithelial to mesenchymal transitions.....	35
1.4.2. Tumor initiation, stemness, and plasticity	38

1.4.3.	Interplay between the EMT and CSC programs	39
1.4.4.	Metabolic reprogramming associated to metastasis and invasion	40
1.4.5.	Metabolic reprogramming associated with stemness	45
1.5.	Drug resistance	46
1.5.1.	Mechanisms of drug resistance.....	46
1.5.2.	Metabolic reprogramming associated with resistance.....	51
1.5.3.	Platinum-based chemotherapy	52
1.5.4.	Platinum (IV) compounds	53
1.5.5.	Mechanisms of platinum resistance.....	54
1.6.	Macromolecular crowding	54
1.6.1.	Excluded volume effects.....	55
1.6.2.	Macromolecular crowding, metabolism, and cancer.....	57
1.7.	Prostate cancer.....	58
1.7.1.	Histological classification and subsets of prostate cancer	59
1.7.2.	Oncogenic signaling and treatment of prostate cancer	61
1.7.3.	Prostate cancer metabolism.....	62
1.7.4.	Prostate cancer cell models.....	64
1.8.	Colorectal cancer	65
1.8.1.	Oncogenic signaling and treatment of colorectal cancer	66
1.9.	Current approaches for the characterization of cancer cell metabolism	67
1.9.1.	Metabolomics.....	67
1.9.2.	Metabolic target predictions	68
2.	Objectives	73
3.	Materials and methods.....	77
3.1.	Cell culture	77
3.1.1.	Prostate cancer cell lines	77

3.1.2.	Colorectal cancer cell lines	78
3.1.3.	Other cell lines	78
3.2.	Cell proliferation and viability assays	79
3.2.1.	Direct cell counting.....	79
3.2.2.	MTT and Hoechst assays	79
3.3.	Generation of CRPC and CRC acquired platinum resistant cell models and age-matched controls	80
3.4.	Calculation of metabolite consumption or production rates	81
3.5.	Measurement of extracellular metabolites by UV-Vis spectrophotometry .	82
3.6.	Measurement of intracellular glutathione.....	82
3.7.	Metabolite consumptions, productions and intracellular pools by LC-MS/MS and FIA-MS/MS.....	83
3.7.1.	Determination of metabolites in cell pellets.....	84
3.7.2.	Determination of metabolites in culture media	85
3.8.	Enzyme activities under crowded media	86
3.8.1.	Lactate dehydrogenase	86
3.8.2.	Glutamate dehydrogenase	86
3.9.	Spheroid formation assay	88
3.10.	Colony formation assay.....	88
3.11.	Wound healing assay	89
3.12.	Cell cycle analysis by flow cytometry.....	89
3.13.	Apoptosis analysis by flow cytometry	89
3.14.	ROS analysis by flow cytometry	90
3.15.	Western blot.....	91
3.16.	Statistical analysis.....	92
4.	Results and discussion	95

4.1. Chapter 1: Identification of the metabolic signature of metastatic CRPC....	95
4.1.1. Introduction.....	95
4.1.2. Results and discussion	97
4.1.2.1. Proliferation, EMT, and stem cell traits are uncoupled in CRPC.....	97
4.1.2.2. Metastatic prostate CSCs display enhanced glutamine avidity and their proliferation and tumorigenic capacity can be suppressed through glutamine deprivation	102
4.1.2.3. CRPC e-CSC phenotypes present enhanced methionine, lysine and total amino acid consumption rates.....	108
4.1.2.4. CRPC subsets with distinct tumorigenic potential display different polyamine secretory profiles.....	111
4.1.2.5. Intracellular metabolite profiles in CRPC unveil distinct metabolic phenotypes.....	115
4.1.2.6. Distinct urea cycle/polyamine metabolism profiles in different CRPC phenotypes.....	119
4.1.2.7. PC-3M/S display different expression profiles in the urea cycle, ornithine synthesis and polyamine metabolism	124
4.1.2.8. PC-3M/S are arginine auxotrophs and sensitive to different arginine deprivation-based therapies according to OTC, NOS and ASS1 transcript expression levels.....	127
4.1.2.9. Metabolic reprogramming tied to arginine deprivation and glutamine deprivation in PC-3M and PC-3S.....	135
4.1.2.10. PC-3M/S sustain a rewired urea cycle through arginine protein methylation	142
4.1.2.11. PC-3M and PC-3S present differential fuel preference for polyamine synthesis and a Myc-driven response is triggered only upon preferred fuel shortage	146
4.1.2.12. NF- κ B rules over c-Myc in the regulation of glutaminase under AD	149
4.1.2.13. Arginine or glutamine deprivation sensitize PC-3M cells to PRMT5 inhibition	151
4.2. Chapter 2: Characterization of the metabolic reprogramming associated to resistance to platinum-based chemotherapy in CRPC and CRC.....	153
4.2.1. Introduction.....	153
4.2.2. Results and discussion	154

4.2.2.1.	CRPC PC-3 and CRC SW620 models display opposed metabolic signatures in terms of glucose energy metabolism	154
4.2.2.2.	Generation and phenotypic characterization of CRPC and CRC cisplatin-resistant cell lines.....	156
4.2.2.3.	PC-3-MPR and SW620-MPR cells present opposed alterations in glucose and glutamine metabolism	161
4.2.2.4.	PC-3-MPR and SW620-MPR present opposed alterations in amino acid metabolism.....	162
4.2.2.5.	Intracellular metabolite profiling of metastatic multiplatinum-resistant models unveils a common metabolic signature.....	168
4.2.2.6.	PC-3-MPR and SW620-MPR completely suppress cisplatin-induced ROS by enhancing glutathione synthetic capacity	173
4.2.2.7.	PC-3-MPR cells downregulate glycolysis and differentially utilize exogenous glucose and pyruvate	175
4.2.2.8.	SW620-MPR cells upregulate glycolysis and differentially utilize exogenous glucose and pyruvate	178
4.2.2.9.	PC-3-MPR minimize the damage of cisplatin on mitochondrial function and retain respiration levels and mitochondrial ATP production of control cells.....	181
4.2.2.10.	Anaplerosis of glutamine into the TCA cycle is altered in both PC-3-MPR and SW620-MPR	183
4.2.2.11.	SW620-MPR upregulate their polyamine secretory profile	165
4.3.	Chapter 3: Biological evaluation of novel platinum (II) and platinum (IV) compounds in prostate, colorectal and lung cancer	187
4.3.1.	Introduction.....	187
4.3.2.	Results and discussion	188
4.3.2.1.	Effect of cyclometallated platinum (IV) iodido complexes	188
4.3.2.2.	Effect of cyclometallated platinum (IV) chloro and bromo fluorinated complexes	192
4.3.2.3.	Cross-resistance of novel cyclometallated Pt(IV) chloro and bromo fluorinated compounds with multiplatinum-resistant cell lines.....	196
4.3.2.4.	Effect of cyclometallated platinum (IV) complexes containing a para-tolyl ligand	203
4.4.	Chapter 4: Effect of macromolecular crowding on the kinetics of lactate dehydrogenase (LDH).....	209
4.4.1.	Introduction.....	209

4.4.2.	Theoretical framework	211
4.4.3.	Results and discussion	212
4.5.	Chapter 5: Effect of macromolecular crowding on the kinetics of glutamate dehydrogenase (GLDH)	221
4.5.1.	Introduction	221
4.5.1.1.	Glutaminolysis	221
4.5.1.2.	Glutamate dehydrogenase	223
4.5.1.3.	Negative cooperativity of GLDH	225
4.5.2.	Theoretical framework	225
4.5.2.1.	Non-cooperative behavior	227
4.5.2.2.	Negative cooperativity model for hexameric enzymes	229
4.5.3.	Results and discussion	231
4.5.3.1.	Kinetic characterization of negative cooperativity of GLDH in dilute solution	231
4.5.3.2.	Kinetic characterization of GLDH under crowded media	235
4.5.3.3.	Negative cooperativity in crowded media	238
5.	General discussion	245
6.	Conclusions	255
7.	References	259

Abbreviations

Abbreviations

1C: One-carbon	BPTES: Bis-2-(5-phenylacetamido-1,3,4-thiadiazol-2-yl)ethyl sulfide
2-DG: 2-Deoxy-D-glucose	BSA: Bovine serum albumin
2-HG: 2-Hydroxyglutarate	CACT: Carnitine-acylcarnitine translocase
ABC: ATP-binding cassette	CAM: Cell adhesion molecule
ACLY: ATP-citrate lyase	CBS: Cystathionine β -synthase
ADP: Adenosine diphosphate	CDK: Cyclin-dependent kinase
AKT: Protein kinase B	CHK: Checkpoint kinase
ALDH1A1: Aldehyde dehydrogenase 1 A1	COX: Cytochrome C oxidase
ALKP: Alkaline phosphatase	CPS1: Carbamoyl phosphate synthase 1
ALT: Alanine transaminase	CPS2: Carbamoyl phosphate synthase 2
AMD: Adenosylmethionine decarboxylase	CPT1: Carnitine palmitoyltransferase 1
AMPK: AMP-activated protein kinase	CPT2: Carnitine palmitoyltransferase 2
AOAA: Aminoxyacetic acid	CRC: Colorectal cancer
AR: Androgen receptor	CRPC: Castration-resistant prostate cancer
ARG: Arginase	CSC: Cancer stem cell
ASL: Argininosuccinate lyase	CTC: Circulating tumor cells
ASS1: Argininosuccinate synthase 1	DCA: Dichloroacetate
AST: Aspartate transaminase	DCF: 2',7'-Dichlorofluorescein
ATM: Ataxia telangiectasia mutated	dcSAM: decarboxylated S-adenosyl methionine
ATP: Adenosine triphosphate	DDR: DNA damage response
ATR: Ataxia telangiectasia and Rad3-related	DFMO: Difluoromethylornithine
BACAT: Bile acid-CoA: amino acid N-acyltransferase	DHF: Dihydrofolate
BCA: Bicinchoninic acid	DHFR: Dihydrofolate reductase
BCAA: Branched-chain amino acids	DISC: Death-inducing signaling complex
BCRP: Breast cancer resistance protein	DME: Drug-metabolizing enzyme
BPH: Benign prostate hyperplasia	DRI: Drug resistance index

DTNB: 5,5-Dithiobis(2-nitrobenzoic acid)
ECAR: Extracellular acidification rate
EGFR: Epidermal growth factor receptor
eIF5A1: Eukaryotic translation initiation factor 5A1
eIF5A2: Eukaryotic translation initiation factor 5A2
EMT: Epithelial-mesenchymal transition
ER: Endoplasmic reticulum
ER: Estrogen receptor
ERK: Extracellular signal-regulated kinases
ETC: Electron transport chain
FA: Fatty acid(s)
FACS: Fluorescence-activated cell sorting
FADD: Fas-associated death domain
FAK: Focal adhesion kinase
FAO: Fatty acid oxidation
FAS: Fatty acyl-CoA synthase
FBP1: Fructose-1,6-bisphosphatase 1
FH: Fumarate hydratase
FPGS: Folylpolyglutamate synthetase
G6P: Glucose 6-phosphate
G6PDH: Glucose 6-phosphate dehydrogenase
GABA: Gamma-aminobutyric acid
GAD: Glutamic acid decarboxylase
GARBG3: GABA A receptor gamma 3
GFR: Growth factor receptor

GLDH: Glutamate dehydrogenase
GLS: Glutaminase
GLS1: Glutaminase 1
GLS2: Glutaminase 2
GLUT: Glucose transporter
GOT: Glutamate oxaloacetate transaminase
GPT: Glutamate pyruvate transaminase
GSH: Glutathione, reduced form
GSK3 α/β : Glycogen synthase kinase-3 α/β
GSMM: Genome-scale metabolic model
GSSG: Glutathione, oxidized form
GST: Glutathione-S-transferase
GTP: Guanosine-5'-triphosphate
HDAC: Histone deacetylase
H₂DCFDA: 2',7'-Dichlorofluorescein diacetate
HIF: Hypoxia-inducible transcription factor
HK: Hexokinase
HRP: Horseradish peroxidase
IAP: Inhibitor of apoptosis protein
IDH: Isocitrate dehydrogenase
IGF-1: Insulin-like growth factor 1
Keap1: Kelch-like ECH-associated protein 1
KNF: Koshland, Nemethy and Filmer
LDH: Lactate dehydrogenase
LOD: Limit of detection
LOQ: Limit of quantification
MDH: Malate dehydrogenase

MDR: Multidrug resistance protein

ME: Malic enzyme

MEK: Mitogen-activated protein kinase kinase

MET: Mesenchymal-epithelial transition

MetSC: Metastatic stem cells

MOMP: Mitochondrial outer membrane permeabilization

MPC: Mitochondrial pyruvate carrier

MRP: Multidrug resistance-associated protein

MTA: Methylthioadenosine

MTAP: S-methyl-5'-thioadenosine phosphorylase

mTOR: Mammalian target of rapamycin

MTT: 3-(4,5-dimethylthiazol-2-yl)-2,5-diphenyltetrazolium bromide

MS: Methionine synthase

MWC: Monod, Wyman and Changeux

NAD⁺: Nicotinamide adenine dinucleotide, oxidized form

NADH: Nicotinamide adenine dinucleotide, reduced form

NADP⁺: Nicotinamide adenine dinucleotide phosphate, oxidized form

NADPH: Nicotinamide adenine dinucleotide phosphate, reduced form

NE: Neuroendocrine

NEAA: Non-essential amino acid

NEPC: Neuroendocrine prostate cancer

NF- κ B: Nuclear factor κ B

NOX: NAD(P)H oxidase

NQO1: NAD(P)H:quinone oxidoreductase 1

NRF2: nuclear factor (erythroid-derived 2)-like 2

NSCLC: Non-small-cell lung cancer

NSE: Neuron-specific enolase

OAA: Oxaloacetate

OAT: Organic anion transporter

OCR: Oxygen consumption rate

OCT: Organic cation transporter

ODC: Ornithine decarboxylase

OMP: Orotidine 5'-monophosphate

OTC: Ornithine transcarbamylase

OXPHOS: Oxidative phosphorylation

PCa: Prostate cancer

PDH: Pyruvate dehydrogenase

PDK: Pyruvate dehydrogenase kinase

PEG: Polyethylene glycol

PFK: Phosphofructokinase

PFKP: Phosphofructokinase, platelet

PHGDH: Phosphoglycerate dehydrogenase

PI: Propidium iodide

PI3K: Phosphoinositide 3-kinase

PK: Pyruvate kinase

PKB: Protein kinase B

PKM2: Pyruvate kinase isoform M2

PPP: Pentose phosphate pathway

PSA: Prostate-specific antigen

PTEN: Phosphatase and tensin homologue

PTM: Post-translational modification

RB: Retinoblastoma
RFC: Reduced folate carrier
ROS: Reactive oxygen species
RTK: Receptor tyrosine kinases
SAC: Spindle assembly checkpoint
SAM: S-adenosyl methionine
SGOC: Serine, glycine and one-carbon metabolism
SOD: Superoxide dismutase
TALDO: Transaldolase
TCA: Tricarboxylic acid cycle
TF: Transcription factor
TGF β : Transforming growth factor β
THF: Tetrahydrofolate
TIC: Tumor initiating cells
TKT: Transketolase
TKTL1: Transketolase-like-1
TMA: Tissue microarray
TME: Tumor microenvironment
TMZ: Temozolomide
VEGF: Vascular endothelial growth factor
WHO: World health organization
ZEB1: Zinc finger E-box binding homeobox 1
ZEB2: Zinc finger E-box binding homeobox 2

1. Introduction

1. Introduction

1.1. Cancer: An overview

Cancer is a vast group of diseases characterized by the emergence of abnormal cells that circumvent physiological control mechanisms and proliferate in an uncontrolled manner, disseminating through the organism and potentially resulting in death. According to the World Health Organization (WHO) latest statistical report, cancer is the leading cause of disease-related death worldwide, with 18.1 million new cases diagnosed and over 9.6 million deaths registered in 2018. The most frequently diagnosed cancer types worldwide were, listed by incidence, lung (14.5%), prostate (13.5%) and colorectal (10.9%) in men, and breast (24.2%), colorectal (9.5%) and lung (8.4%) in women [1].

Carcinogenic transformation of cells occurs as a consequence of mutagenesis, either occasioned by exogenous factors, such as radiation, chemicals or viral infections; or endogenous factors, such as inherited mutations or defective hormonal or immunological responses [2]. Due to these, specific somatic mutations can enable genes that promote uncontrolled proliferation and malignant transformation (oncogenes) and disable genes that prevent the survival of dysfunctional cells and contribute to healthy cell physiology (tumor suppressor genes).

Once this state is achieved, sustained high rates of uncontrolled mutagenesis and aberrant signaling can drive further development of proliferating cancer cells and tumor progression, in a process that formally resembles Darwinian evolution [3]. In this context, cancer cells are constantly challenged by different selective pressures: achieving higher proliferation rates and anabolic efficiencies [4]; being capable of surviving in hypoxic or nutrient-limited environments [5]; resisting chemotherapeutic treatments [6] or gaining the ability to spread through the organism and encounter more favorable niches, a process commonly referred to as metastasis [7].

Cancer cells become adapted to these harsh environments and succeed in fulfilling their situational energetic and biosynthetic needs mainly by reprogramming their metabolism,

the set of chemical transformations that a cell can perform [8]. Characterizing the metabolic reprogramming that cancer cells display to survive and thrive in each situation (e.g., nutrient scarcity, drug resistance or invasion and metastasis) leads to rationally-designed therapies that target essential metabolic adaptations for cancer cell survival and proliferation, in an approach that can be termed as “metabolic therapy” [8].

However, with such a significant amount of selective pressures, more than one dominant cell subpopulation may emerge, leading to heterogeneity within the tumor. Through the acquisition of different mutations or the activation of various epigenetic and cell signaling programs, cancer cells can differ in proliferation, metabolic profile, pluripotency, motility, adherence, and, ultimately, acquire different specialized functions that collectively contribute to the persistence of the tumor [9]. Indeed, tumor heterogeneity emerges from at least two different sources: (I) the parallel clonal evolution leading to subpopulations harboring different mutations [3], and (II) the hierarchical organization that emerges as pluripotent cancer cells, termed as cancer stem cells (CSCs), give rise to even more tumor subpopulations by multiple events of differentiation and transdifferentiation [10].

In turn, all these different tumor subpopulations, originated either from parallel clonal evolution or differentiation of CSCs, can eventually interact between them and with the tumor microenvironment (TME) in synergistic manners [11], collectively contributing to the persistence and development of the tumor, its metastatic dissemination or to the acquisition of resistance to chemotherapy [9]. In consequence, only the characterization of the different subpopulations in the tumor and the design of specific or combination therapies to target each of them can result in an effective solution for cancer treatment.

The present work focuses on the metabolic characterization of the two main battlefronts in which cancer therapy fails and leads to tumor relapse: metastatic progression and drug resistance. Together, metastasis and resistance to chemotherapy are the leading causes of cancer death [7,12]. Our approach will include the study of isogenic models subjected to different selective pressures to acquire metastatic, invasive, or drug-resistant metabolic phenotypes. Metabolic reprogramming associated to each of them will be investigated, and the crossroads between the metabolic

adaptations tied to metastasis and drug-resistance will be interrogated in a quest to find common vulnerabilities and common potential targets.

1.2. Cancer features

The most successful attempt to systematize all the available knowledge gathered by cancer research is undeniably the classification of cancer features proposed by Hanahan and Weinberg in 2000 [13], which was revisited and expanded by themselves in 2011 [14] and further nuanced by many others thereafter [15–17].

According to this, the most salient features, or hallmarks, of cancer are: sustaining proliferative signaling, evading growth suppressors, enabling replicative immortality, resisting cell death, avoiding immune destruction, deregulating cellular energetics, activating invasion and metastasis and inducing angiogenesis. Moreover, there are two additional hallmarks that, due to their importance in driving tumor progression and enhancing all the previous hallmarks, also receive the distinction of enabling characteristics of cancer: genome instability and mutation and tumor-promoting inflammation [14].

Many of these altered features are linked to the two major processes that fuel the uncontrolled proliferation that defines cancer: cell cycle progression to achieve mitotic division and evasion of programmed cell death (or apoptosis) to achieve cancer cell survival. Mechanistic aspects of these two processes and their cancer-specific alterations will be reviewed hereafter.

1.2.1. Cancer and cell cycle

The cell cycle is a series of sequential and tightly-regulated events that a cell must undergo before being segregated into two daughter cells. These events are classified into three distinct phases: First, G₀/G₁, in which a cell may be quiescent (G₀) or preparing for its DNA replication (gap1 or G₁); synthesis (S), in which the cell is duplicating its genome; and G₂/M (gap2 and mitosis), in which a cell generates an exact copy of itself. Given the importance of this whole process, it is strictly regulated by

several checkpoints and signaling cascades that avoid uncontrolled cell proliferation or the proliferation of damaged cells [18].

The two main families of proteins involved in cell cycle regulation are cyclins and cyclin-dependent kinases (CDKs), which act in coordination to phosphorylate and modulate the activity of all the molecular effectors responsible for each event that is required to achieve cell division [19]. Cyclins and CDKs are only one of the multiple layers of regulation to which the cell cycle is subjected. Other key effectors are p53 and the retinoblastoma (RB) protein, CDK inhibitors (e.g., p16^{INK4A}, p21^{CIP1}, or p27^{KIP1}), Aurora kinases or checkpoint kinases (CHK1 and CHK2), among others [19]. Precisely, the dysfunction of a part of this cell cycle regulatory machinery and the associated cell cycle checkpoints represents a critical driving force of oncogenic transformation, and thus inhibiting cell proliferation through cell cycle arrest constitutes an attractive approach in cancer therapy research. Besides direct chemical inhibitors of CDKs and other cell cycle regulatory proteins [19,20], many other anticancer drugs can also trigger cell cycle arrest at different cell cycle phases and checkpoints (2.2.1).

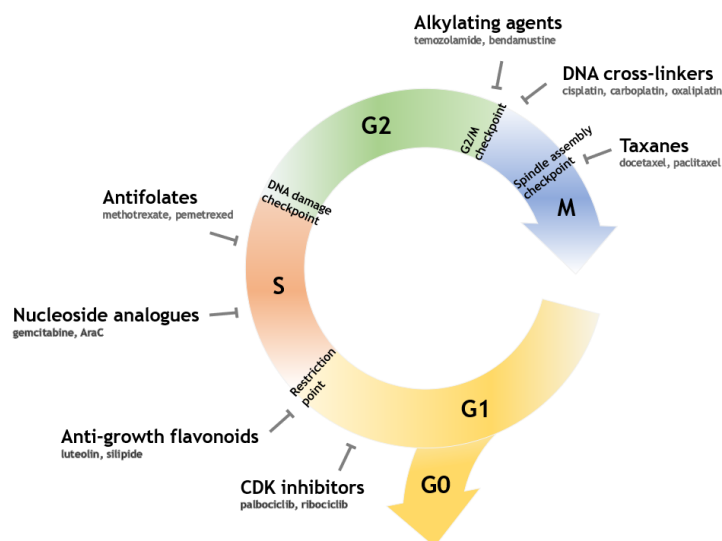


Figure 2.2.1. Cell cycle phases and the effect of different chemotherapeutic agents on cell cycle progression. Schematic representation of chemotherapeutic agents counteracting the successful completion of each cell cycle phase or checkpoint in cancer cells. CDK: cyclin-dependent kinase.

The first checkpoint, referred to as the G0/G1 checkpoint or restriction point, mediates the entrance to the cell division process. An arrest of the cell cycle at this checkpoint has been described for several flavonoid compounds, through interacting with anti-growth and proapoptotic signaling [21,22]. Next, antineoplastic drugs that block nucleotide

synthesis or DNA replication cause an S phase arrest in the cell cycle of proliferating cells. Examples of these are nucleoside analogs, such as AraC or gemcitabine [23], that directly block DNA replication, or antifolates, such as methotrexate and related drugs that impair folate metabolism and subsequently nucleotide synthesis [24].

Upon completion of the S phase, DNA is scanned for defects and repaired if needed through a plethora of enzymes and signaling pathways that are collectively referred to as the DNA damage response (DDR) [25,26]. If this step fails to meet the standards of the G2/M DNA damage checkpoint, the proliferation of defective cells is arrested, and apoptotic signaling is triggered [26]. Massive DNA damage produced by alkylating agents, such as temozolomide (TMZ) and related compounds, or DNA cross-linkers, such as platinum compounds, prevents tumor cell proliferation by arresting the cell cycle at the G2/M checkpoint [27]. Besides, oxidative stress produced by a wide variety of antineoplastic agents also contributes to the aggravation of DNA damage beyond the DNA repair machinery capacity of cancer cells [25].

Finally, the cell cycle can also be blocked by chemotherapy during mitosis by the activation of the mitosis checkpoint or spindle assembly checkpoint (SAC) [20]. Cell cycle arrest at this point is best exemplified by taxanes, such as docetaxel or paclitaxel, compounds that act by stabilizing microtubules and hampering the successful completion of mitosis in proliferating cells [28,29].

In summary, different families of antineoplastic compounds target different phases of the cell cycle of proliferating cancer cells. When cell cycle checkpoints are not completed due to the action of the drug, defective cells cannot progress through cell cycle phases. Instead, their growth can be arrested, or they can be redirected into undergoing programmed cell death or apoptosis.

1.2.2. Cancer and apoptosis

Apoptosis is a homeostatic mechanism that balances cell populations and preserves tissue and organ physiology by the controlled dismantlement of defective or unnecessary cells, minimizing inflammation and perturbation to surrounding cells and tissues [30–32]. As with cell cycle checkpoints, cancer cells also become able to silence the apoptotic stimuli by activating oncogenes that promote cell survival and

proliferation [31]. Thus, countering this anti-apoptotic oncogenic activation and selectively inducing apoptosis in cancer cells also constitutes an appealing therapeutic window.

Cell death by apoptosis can occur via two alternative pathways, termed as extrinsic and intrinsic pathways. In each of them, different effectors are recruited in alternative manners, depending on the stimuli that initially triggers the apoptotic machinery. In the extrinsic pathway, extracellular death ligands bind to cell surface death receptors, inducing an apoptotic intracellular signaling cascade [33]; while, in the intrinsic pathway, intracellular insults or triggers (e.g., cell cycle checkpoint failure, irreparable DNA damage, or oxidative stress) result in the permeabilization of the mitochondria and the release of cytochrome C, irreversibly inducing apoptosis [34,35]. Both types of stimuli and the subsequent signaling cascades lead to the cell being completely dismantled from within through a set of controlled events: chromatin disintegration, nuclear fragmentation, breakdown of DNA and proteins, volume reduction, and externalization of surface markers that label the apoptotic cell for the action of phagocytic cells [31].

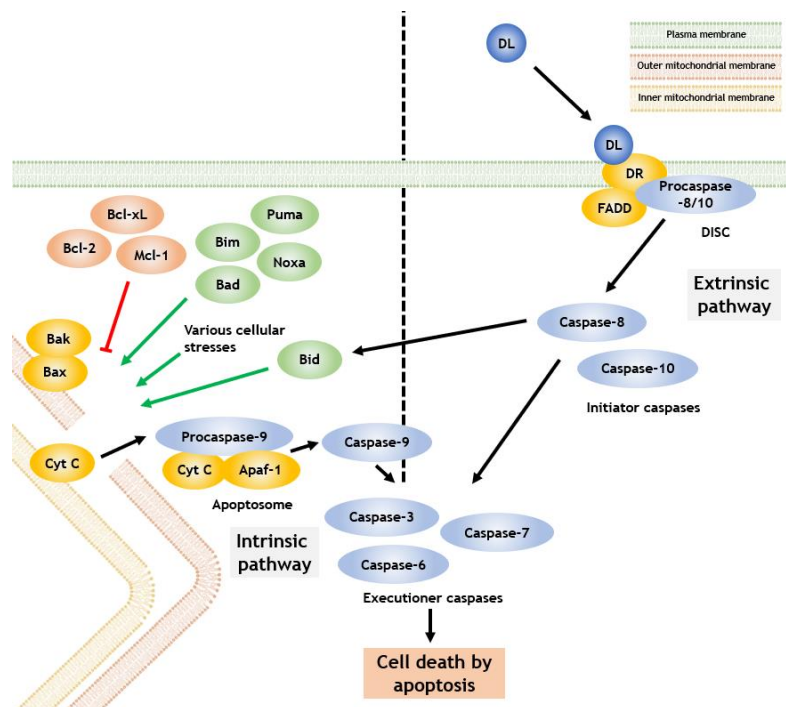


Figure 2.2.2. Schematic representation of the intrinsic and extrinsic apoptotic signaling pathways. The extrinsic pathway is mediated by extracellular stimuli, by the binding of death ligands (DL) to death receptors (DR) on the cell membrane and formation of the death-inducing signaling complex (DISC). The intrinsic pathway is activated by intracellular stresses and initiated by the cytochrome C (Cyt C) release from the mitochondria, triggered by proteins

of the Bcl-2 family. Both pathways converge in the activation of executioner caspases, that will recruit different effectors to trigger a cascade of events that elicits apoptosis.

Many of the events occurring during the apoptotic program are directly or indirectly prompted by a family of cysteine aspartyl proteases termed as caspases. Signal transduction in the apoptotic cascade is propagated through cleavage by hydrolysis of the inactive form of caspases (procaspases) to yield their active cleaved form that can further hydrolyze downstream caspases or other target proteins [33]. Another important family of proteins mediating apoptosis is the Bcl-2 family, containing both pro- and anti-apoptotic members that coordinately balance the integrity of the outer mitochondrial membrane and the release of cytochrome C [34].

In the extrinsic pathway, death ligands from outside the cell bind to death receptors in the cell membrane to recruit the Fas-associated death domain (FADD) protein and caspases-8 and -10, thus promoting the formation of the death-inducing signaling complex (DISC), and the autocatalytic cleavage and activation of caspase-8 and -10, termed as initiator caspases. Cleaved initiator caspases can then cleave and activate caspases-3, -6 or -7, termed as executioner caspases, responsible for the cleavage of many downstream targets that mediate all the apoptotic events [31,36]. Additionally, caspase-8 can also cleave and activate the proapoptotic protein Bid, a member of the Bcl-2 family, which will contribute to the activation of the intrinsic pathway [33].

The intrinsic pathway is triggered by intracellular stimuli, leading to the activation of two proteins from the Bcl-2 family: Bax and Bak. Bax and Bak undergo dimerization and enable the formation of pores on the mitochondrial outer membrane surface, which leads to cytochrome C release to the cytosol. Cytochrome C then recruits Apaf-1 protein and procaspase-9 to assembly the apoptosome complex, which enables the cleavage and activation of caspase-9, which will, in turn, activate the executioner caspases (-3,-6 or -7) [36], converging with the extrinsic pathway. Due to the importance and irreversibility of cytochrome C release, mitochondrial outer membrane permeabilization (MOMP) and Bax/Bak activity are also regulated by many members of the Bcl-2 and other related families of proteins, both promoting (e.g., Bid, Bim, Bad, Puma or Noxa) and preventing (e.g., Bcl-2, Mcl-1 or Bcl-xL) cytochrome C release [37]. Finally, several

proteins collectively termed as inhibitor of apoptosis proteins (IAP) also regulate apoptosis by directly or indirectly inhibiting the function of executioner caspases [33,37].

As mentioned previously in this section, the capacity to evade apoptosis is one of the hallmarks of cancer cells [13], which is often achieved by mutation, functional inactivation, or aberrant expression of apoptosis-governing proteins. Precisely, these dysfunctions encourage the development of novel and existing therapeutic strategies based on modulating death receptor signaling [38] or targeting the anti-apoptotic capacity of Bcl-2 family members [39–41].

1.3. Cancer metabolism

Cancer cells achieve survival through evasion of apoptosis and proliferation through uncontrolled cell cycle progression. For this, they also need to obtain sufficient energy and nutrients to renew and survive and, more importantly, to obtain building blocks to produce a new cell upon each cell cycle completion. Transformation of the uptaken biomass and energy by chemical reactions is required to produce new cells and represents one of the core processes of life.

1.3.1. Overview of cancer metabolism

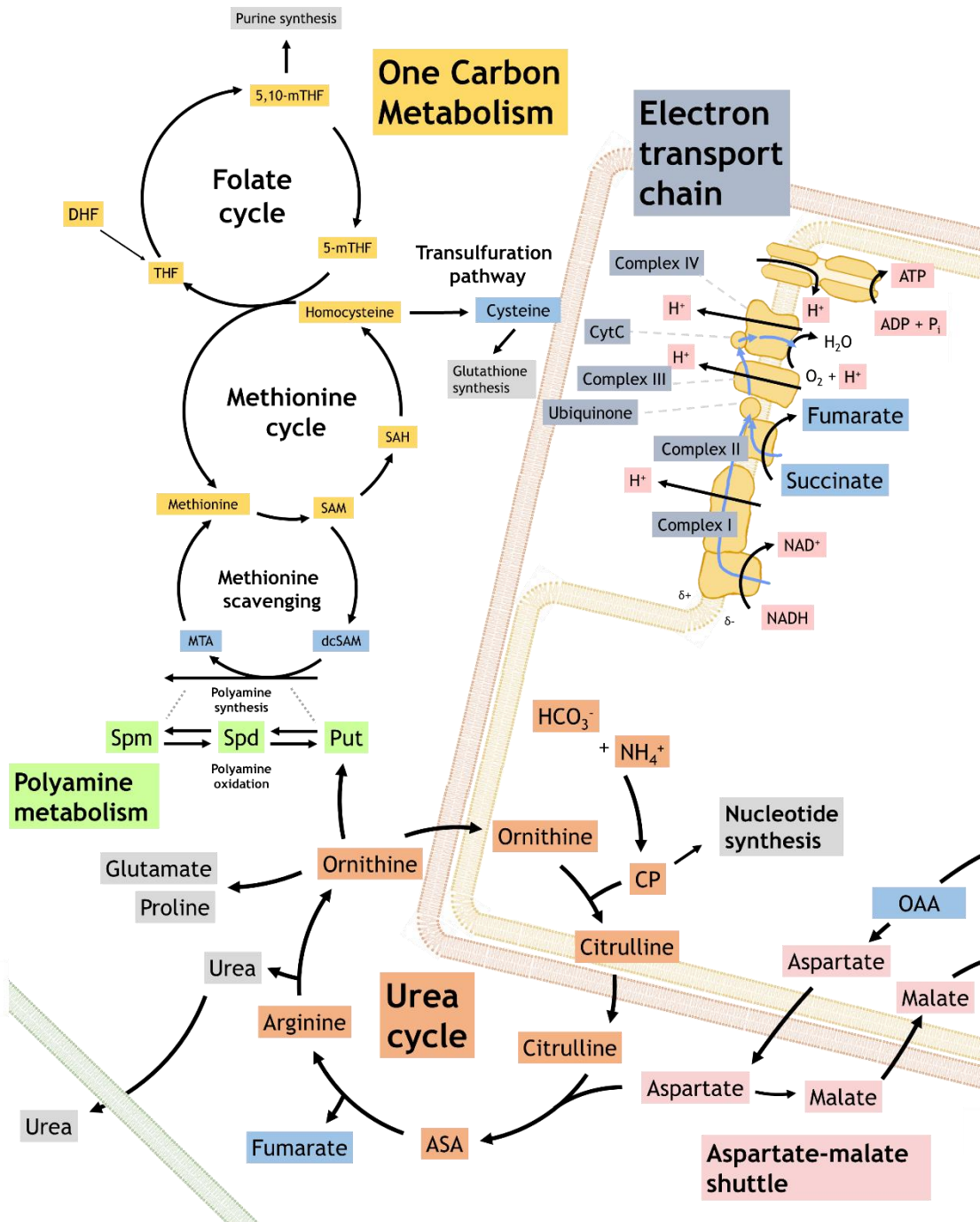
Every cancer cell will require to uptake the sufficient biomass and micronutrients and use them to produce all the essential components of life: nucleic acids, sugars, proteins, lipids, and a myriad of small organic and inorganic molecules of all sort. Sustenance of life and most of its molecular events also requires free energy, carried and transferred by nucleotides containing energy-rich phosphate bonds (e.g., adenosine triphosphate (ATP)); and reducing power, carried by several reduced dinucleotides (e.g., nicotinamide adenine dinucleotide (NADH), nicotinamide adenine dinucleotide phosphate (NADPH), or flavin adenine dinucleotide (FADH₂)). Many of the chemical transformations occurring inside a cell would also be kinetically unfeasible without the presence of proteins functioning as catalyzers (enzymes).

Every cell can host an enormous set of chemical reactions, termed as metabolism, which transforms molecules into other molecules, using enzymes, for a plethora of different

purposes. These reactions are grouped into metabolic pathways, smaller sets of sequential reactions that lead to specific chemical transformations. Metabolic pathways, in turn, are broadly classified into two main sets: ATP-consuming synthesis of small molecules, macromolecules or cellular components (anabolic pathways), and ATP-producing break-down of free energy-containing molecules (catabolic pathways).

In particular, cancer cells need to rewire their metabolism to fulfill the energetic and biosynthetic demands that arise from rapid uncontrolled proliferation and, thus, cancer metabolism is essentially anabolic [8,16]. The diversity of strategies adopted by cancer cells to achieve this highly-proliferative state is so overwhelming that almost every tumor can be considered as unique [11]. Nevertheless, certain strategies are also encountered so frequently that they can be considered as the metabolic hallmarks of cancer. As proposed by Pavlova and Thompson in 2016 [16], the hallmarks of cancer metabolism are: deregulated uptake of glucose and amino acids, use of opportunistic modes of nutrient acquisition, use of glycolysis/tricarboxylic acid (TCA) cycle intermediates for biosynthesis and NADPH production, increased demand for nitrogen, alterations in metabolite-driven gene regulation, and metabolic interactions with the microenvironment.

All these alterations, frequently found in the majority of cancers, are primarily directed towards the achievement of a highly-proliferative state that is sustainable in terms of cell bioenergetics, enhanced biosynthesis and redox balance [8], all supported by a particular set of metabolic pathways that are generally essential for cancer cells, as summarized in **Figure 2.3.1** (pages 12-13).



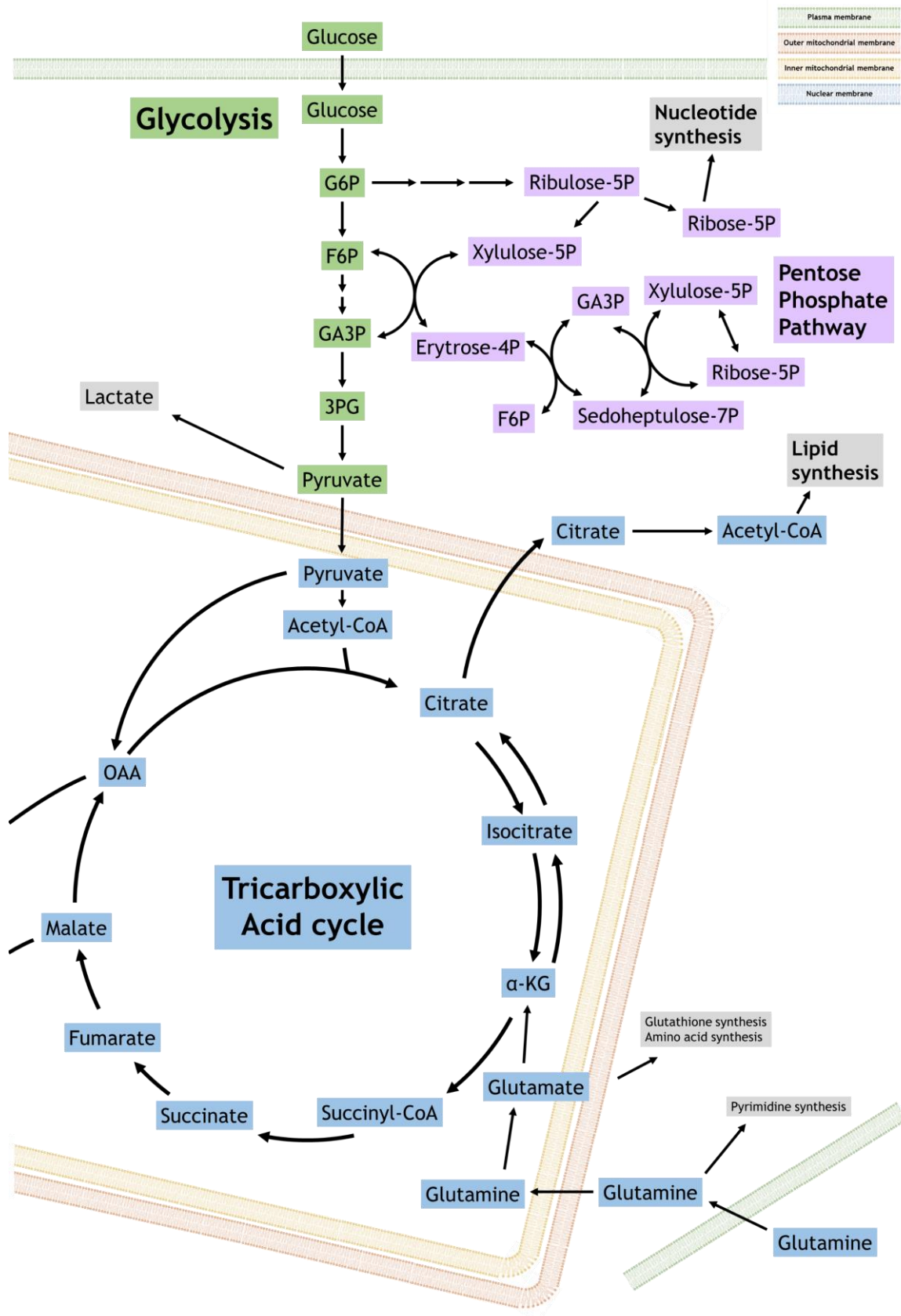


Figure 2.3.1. Schematic representation of the main pathways of cancer cell metabolism. The illustration depicts an overview of the major metabolic pathways involved in cancer metabolism: glycolysis, tricarboxylic acid cycle, electron transport chain, fatty acid synthesis, pentose phosphate pathway, glutaminolysis, methionine cycle, folate cycle,

transulfuration pathway, the aspartate-malate shuttle, polyamine synthesis and the urea cycle. α -KG: alpha-ketoglutarate; ASA: argininosuccinic acid; CP: carbamoyl phosphate; CytC: cytochrome C; dcSAM: decarboxylated S-adenosyl-methionine; DHF: dihydrofolate; ETC: electron transport chain; F6P: fructose-6-phosphate; GA3P: glyceraldehyde 3-phosphate; G6P: glucose-6-phosphate; MTA: methylthioadenosine; 5-mTHF: 5-methyl-tetrahydrofolate; 5,10-mTHF: 5,10-methylene-tetrahydrofolate; OAA: oxaloacetate; 3PG: 3-phosphoglycerate; Put: putrescine; SAH: S-adenosyl-homocysteine; SAM: S-adenosyl-methionine; Spd: spermidine; Spm: spermine; THF: tetrahydrofolate.

Glucose is the main energetic fuel of the cell. Its break-down and partial oxidation in glycolysis yields 2 ATP and two pyruvate moieties per glucose molecule. Pyruvate can then enter the mitochondria and be further oxidized to carbon dioxide in the TCA cycle, a cyclic pathway in which pyruvate is sequentially transformed into acetyl-CoA, citrate, isocitrate, α -ketoglutarate, succinyl-CoA, succinate, fumarate, malate, and oxaloacetate. Also, each turn of the cycle yields several moieties of NADH and FADH₂, two highly-reducing dinucleotides, which can be transformed into ATP in the electron transport chain (ETC). This pathway, alternatively referred to as oxidative phosphorylation (OXPHOS), also occurs in the mitochondria and transfers electrons from molecular oxygen to ATP, reaching a final yield of 36 ATP per glucose molecule [42]. The full oxidation of glucose, through TCA and OXPHOS, is commonly termed as mitochondrial respiration. Altogether, glycolysis, TCA, and OXPHOS constitute the core of cell metabolism and are also commonly referred to as central carbon metabolism, yet this definition can sometimes be relaxed to include additional pathways.

Hundreds of other different metabolic pathways are also part of this intricate network of interconnected reactions occurring inside the cell. Examples of these are the biosynthesis of non-essential amino acids and polyamines; the cycle of urea to detoxify nitrogen from the cell; the synthesis of different families of lipids with structural or signaling functions; the oxidation of some of these lipids to yield ATP; the synthesis of nucleotides and their building blocks through purine and pyrimidine base synthesis and synthesis of pentose moieties in an alternative transformation of glucose through pentose phosphate pathway (PPP), among many others. The metabolic pathways found to be relevant for the present work, along with their regulatory networks, will be reviewed in more detail in the following sections.

1.3.2. Regulation of cancer metabolism

Cancer causes a profound rewiring of cell metabolism in which the altered activity of metabolic enzymes is tightly regulated by transcription factors and post-translational modifications (PTMs) effected by different signaling cascades that orchestrate survival, growth, and proliferation of cancer cells [43]. Most signaling cascades act as sensors of nutrient, oxygen, or energy availability in the cell, and their situational activation results in the reorganization of metabolic fluxes to ensure optimal performance of the cell in each environment.

The endless possibilities that arise from the combined activation of the multiple oncogenic signaling networks that govern metabolism endow cancer cells with the metabolic flexibility to obtain nutrients and prosper in almost any niche of the organism [11]. Indeed, when nutrients are abundant, pro-anabolic signaling networks will promote the transfer of uptaken carbons to lipids, proteins, and nucleic acids to achieve proliferation. On the contrary, when the available nutrients cannot provide the necessary biomass to generate new cells, pro-catabolic signaling will balance energy production to ensure cell maintenance and survival. At the same time, other signaling networks will readjust cancer cell metabolism in other terms, such as redox status, acidity, or oxygen availability. The main signaling networks that can be aberrantly activated or silenced in cancer cells, and cooperate to regulate cancer cell metabolism, being responsible for the emerging metabolic phenotype will be reviewed hereafter.

1.3.2.1. Pro-anabolic signaling networks

Normal cells require exogenous growth stimuli to enter a proliferative and anabolic state. Upon receiving such stimuli by growth factor receptors (GFR), phosphoinositide 3-kinase (PI3K) activates its downstream kinase cascade, centrally represented by protein kinase B (PKB or Akt) and mammalian target of rapamycin (mTOR) [44]. The PI3K/Akt/mTOR signaling network plays a pivotal role in promoting proliferation through modulating cell cycle and apoptosis; and biosynthesis by regulating protein, lipid, and nucleotide synthesis, as well as the central pathways that provide carbon sources: glycolysis and glutaminolysis [8]. Many tumors display aberrantly-activated members of the

PI3K/AKT/mTOR axis, which stimulates all the downstream signaling to elicit growth signal-independent proliferation and anabolic metabolism [44].

Acting in a similar direction than AKT signaling, the transcription factor Myc is another main driving force of oncogenesis, identified as the third most amplified gene in human cancers [45]. Indeed, upregulated Myc is found in many tumors, often amplified and translocated to decrease the dependency of cancer cells on exogenous growth signaling. Its oncogenic activation provides cancer cells with the capacity to fulfill the anabolic demand required for proliferation and growth [46]. It is considered a master regulator of metabolism since it plays a vital role in regulating glycolysis, glutaminolysis [47], mitochondrial metabolism [8,48], or polyamine synthesis [49]. Myc also plays crucial regulatory roles in many other cellular processes besides metabolism, such as cell cycle, cell growth, apoptosis [50] or mitochondrial biogenesis [48].

It is important to distinguish that Myc regulation acts at a transcriptional level, while PI3K/AKT/mTOR axis constitutes the main effector of post-translational metabolic regulation. Thus, Myc modulates the maximal capacity of metabolic pathways by promoting the transcription of its targets, while AKT signaling contributes to a closer adjustment of metabolic fluxes according to the status of the cell by modulating enzyme activity through phosphorylation.

Many other growth-promoting pathways also contain essential oncogenes that drive tumor progression in certain cancers, such as KRAS in colorectal, pancreatic, and lung cancer [51–53], or HER2 in breast cancer [54]. Crosstalk between different oncogenic signaling networks is also common, and it contributes to the overwhelming complexity of cancer regulation and progression. For instance, many oncogenic signaling pathways converge on Myc activation, such as KRAS, ERK, Notch pathway, and the epidermal growth factor receptor (EGFR) downstream signaling [45].

1.3.2.2. Pro-catabolic signaling networks

Another important mediator of cell metabolism that balances the energetic production of the cell is AMP-activated protein kinase (AMPK) signaling [55]. AMPK is activated by upstream kinases upon energy shortage detected by high levels of AMP, low levels of glucose, or changes in NADPH balance. In all these situations, AMPK stimulates ATP

production and energy metabolism and acutely inhibits ATP-consuming pathways. In essence, AMPK activation promotes a catabolic state of the cell, rather than promoting anabolism and proliferation; thus, it can be considered as a metabolic tumor suppressor [55]. In this regard, treatment with AMPK activators such as metformin or several natural anti-inflammatory compounds has recently been postulated as an attractive therapeutic approach for cancer treatment [55]. In this regard, therapeutic promotion of AMPK signaling can, in turn, counteract oncogenic Myc signaling. Myc enhances anabolic metabolism, often to the extent of compromising cellular ATP levels and activating AMPK, which in turn can phosphorylate p53, leading to mitochondria-mediated apoptosis [46].

Tumor suppressor p53, one of the most frequently mutated and silenced genes in human cancers, is also one of the central mediators governing energy balance and cell catabolism, among many other processes such as blocking cell cycle progression and promoting activation of apoptosis. In terms of metabolism, p53 has a crucial role in fine-tuning the balance between glycolysis and mitochondrial respiration, preventing excessive oxidative stress and promoting cell survival [56].

1.3.2.3. Regulation of redox balance

The primary sensor of the redox status of the cell is the Keap1-Nrf2 [Kelch-like ECH-associated protein 1–nuclear factor (erythroid-derived 2)-like 2] system. Nrf2 is a transcription factor that promotes transcription of antioxidant, anti-inflammatory, and detoxification enzymes, leading to a decrease in ROS levels, stress mitigation, and survival, whereas Keap1 acts as its dedicated repressive regulatory protein. In basal conditions, the Keap1-Nrf2 complex is bound, constantly promoting Nrf2 ubiquitination and degradation. Under high ROS levels and oxidative stress, cysteine residues in Keap1 are oxidized, and Keap1 releases Nrf2, which can enter the nucleus and allow the transcription of its target genes [57].

The Keap1-Nrf2 system regulates the expression of phase II enzymes of drug detoxification metabolism [57] (see **Section 1.5.1**). Activation of phase II genes counteracts the action of xenobiotics and oxidative stress, reducing ROS levels and DNA damage, enabling the normalization of the redox balance and promoting survival. Nrf2

implication in cancer has been described as a “double-edged sword”: Nrf2 prevents oxidative stress and DNA damage that drive malignant transformation, but at the same time elevated Nrf2 levels allow cancer cells to maintain redox homeostasis despite the oxidative stress caused by rapid proliferation. In this manner, they can further evade apoptotic stimuli, survive in the presence of chemotherapeutics, and develop drug resistance [57].

In this regard, recurrent somatic mutations of Nrf2 gain-of-function and Keap1 loss-of-function [58–60] have been reported in several types of tumors, including prostate [58], lung [59], and breast [60], describing a role for Keap1-Nrf2 system in oncogenesis [57] and emergence of chemotherapeutic resistance [58]. Besides, Nrf2 can also be differentially-activated through a poorly understood alternative splicing phenomenon. Loss of exon 2 has been reported as related to Nrf2 stabilization and activation of target genes in lung, head, and neck cancers [61]. More recently, Nrf2 has also been linked to mitochondrial metabolism regulation [62], which has yet to be explored in depth.

1.3.2.4. Fine-tuning other aspects of cell metabolism

Besides coping with the metabolic and oxidative stresses arising from rapid proliferation, cancer cell metabolism has often to deal with additional pressures from the TME. During tumor formation and growth, cell proliferation often outpaces blood vessel formation rates, resulting in poorly vascularized areas within the tumor, and deficient oxygen supply. Tumor cells in these hypoxic niches are able to survive by reprogramming their metabolism and using anaerobic glycolysis to cover their energetic needs. The hypoxia response in tumors is mainly activated by the hypoxia-inducible transcription factor (HIF), which globally activates glycolysis, rewires mitochondrial metabolism, and promotes the stimulation of transcription programs associated to angiogenesis and metastatic dissemination [63].

The abnormal activation of glycolysis in cancer cells, either occasioned by hypoxia or by oncogenic signaling pathways, encompasses the secretion of large amounts of lactate to the extracellular milieu. This increasingly acidic TME induces several signaling cascades within the cell, including HIF, nuclear factor- κ B (NF- κ B), or vascular endothelial

growth factor (VEGF), also resulting in a rewiring of cell metabolism, promotion of vascularization and increased invasion [64].

In conclusion, cancer cells reprogram their metabolism in accordance to their particular needs and the cues they receive from their microenvironment, through a wide range of transcription factors and signaling cascades that alter the activity of metabolic enzymes and metabolite transporters, leading to global reprogramming of cell metabolism. Following this, we will raise our focus on how the central metabolic pathways can be rewired in tumors to serve the particular purposes of cancer cell survival and proliferation.

1.3.3. Glycolysis and the Warburg effect

Mammal cells primarily rely on glucose oxidation to obtain ATP. Glucose enters the cell through glucose transporters (GLUT), and it is partially oxidized through glycolysis to yield two pyruvate molecules and two ATP molecules per glucose. Pyruvate, in turn, can then be transformed into lactate by lactate dehydrogenase (LDH), or it can be further oxidized in the mitochondria by the TCA cycle and OXPHOS, achieving complete glucose oxidation to CO₂ and yielding 36 ATP molecules per glucose molecule [42]. Oxygen-requiring complete glucose oxidation is the major source of ATP production in most healthy cells, and it is crucial for the optimal sustenance of life.

Conversely, most cancer cells mainly cover their energy needs through partial glucose oxidation and lactate production, even in the presence of oxygen and fully functional mitochondria [42]. This phenomenon, commonly termed as aerobic glycolysis or Warburg effect, may seem profoundly disadvantageous in terms of energetic yield and, thus, it has encouraged countless research efforts to provide rational explanations behind it. Despite that, the Warburg effect and its causes are still nowadays a matter of debate [65,66].

Due to this utterly common preference for glycolysis, cancer cells generally have a higher demand for glucose and higher glycolytic activity compared to cells with lower rates of proliferation. Moreover, enhanced glycolytic fluxes are generally correlated with higher proliferative states and poor prognosis in many cancer types [11]. In line with this, aberrant activation of glycolytic enzymes, such as hexokinase (HK) [67–69] or

phosphofructokinase (PFK) [70], is also of paramount importance for the maintenance of this glycolytic phenotype.

Predominant aerobic glycolysis is supported in some tumors by preventing the entry of pyruvate, the end-product of glycolysis, into the mitochondria. For instance, this may occur through downregulation or loss of the mitochondrial pyruvate carriers (MPC) [71] or by the inactivating phosphorylation of pyruvate dehydrogenase (PDH), the main entry of pyruvate into the TCA cycle, mediated by a family of dedicated pyruvate dehydrogenase kinases (PDKs) [72,73]. Alternatively, other tumors display high expression of the pyruvate kinase isoform M2 (PKM2), a low activity variant of pyruvate kinase (PK) that allows the accumulation of glycolytic intermediates to be diverted into biosynthetic purposes [74].

Indeed, one of the possible purposes of this glycolytic phenotype is to serve the overall anabolic state of cancer cells. A significant fraction of the glycolytic flux can be funneled into subsidiary pathways that support biosynthesis and proliferation. For instance, it can be diverted to PPP to obtain NADPH and ribose; transamination reactions able to support amino acid and protein synthesis; *de novo* serine and glycine synthesis through phosphoglycerate dehydrogenase (PHGDH) and one-carbon metabolism to obtain reducing equivalents and purine bases [65,66,75,76]; or synthesis of the hydrophilic headgroups of lipids via serine and glycerol-3-phosphate [77].

However, supporting anabolism is not the only postulated rationale behind the Warburg effect. Another feasible explanation is that the use of glycolysis for energy production instead of respiration reduces ROS levels, which contributes to the evasion of proapoptotic signaling [78]. The decrease in ROS levels occurs not only by obtaining ATP while avoiding mitochondrial respiration but also by increasing the capacity to redirect the glycolytic flux into PPP, thereby reducing oxidative stress through increased NADPH production. This redirection can be situationally modulated in response to ROS levels. For instance, the inhibition of PKM2 through cysteine residue oxidation caused by high ROS levels results in the accumulation of glycolytic intermediates and the redirection of glycolytic flux to PPP [79].

Moreover, recent studies emphasize that aerobic glycolysis may not be so disadvantageous under a kinetic point of view: glycolysis is 10 to 100 times faster than mitochondrial metabolism and, in any given time frame, ATP obtained by both aerobic glycolysis and complete glucose oxidation could be comparable [80]. In this regard, also macromolecular crowding, an entropic phenomenon that arises from high fractions of occupied volume and tight-packing of macromolecules inside cells, has been postulated as a kinetic origin for Warburg effect [81]. In this regard, theoretical models point out that aerobic glycolysis would outperform mitochondrial metabolism in terms of energetic yield, not only per unit time but also per unit space, as the glycolytic molecular machinery would be twice more compact and require much less biosynthetic expenditure than OXPHOS [82]. The relation between macromolecular crowding and metabolism, especially glycolysis, will be further addressed in **Section 1.6** of this introductory chapter.

1.3.4. Tricarboxylic acid cycle and oxidative phosphorylation

Differential utilization of mitochondrial metabolism is another distinctive feature of cancer cells. Besides the primary function attributed to mitochondria of being the “powerhouses of the cell”, they also play essential roles in mediating the intrinsic apoptotic cascade, redox homeostasis, and the production of metabolic intermediates for anabolism [48]. Since oncogenic transformation drives cells from a quiescent and catabolic state to a hyperproliferative and anabolic one, mitochondrial metabolism and the TCA cycle are also rewired from their catabolic purpose of energy production through complete glucose oxidation to become a biosynthetic hub to obtain many different precursors for macromolecule synthesis [48,77,83].

Diversion or interconversion of intermediates from the TCA cycle to support biosynthesis can occur at different steps of the cycle. For instance, citrate can be exported to the cytosol to be reconverted to acetyl-CoA by ATP-citrate lyase (ACLY), which can be used for protein acetylation and fatty acid synthesis [77,84]. Apart from that, oxaloacetate (OAA) and α -ketoglutarate (α -KG) can also be interconverted through transamination reactions to balance, directly or indirectly, the intracellular pools of different amino acids: aspartate, asparagine, arginine, glutamate, glutamine or proline

[85,86]. Moreover, two recurrent TCA cycle alterations in cancer, fumarate hydratase (FH) and succinate dehydrogenase (SDH) deficiencies, cause the accumulation of the oncometabolites fumarate and succinate, which can be diverted from the cycle to play different crucial signaling functions for tumor progression and metastasis, through regulating DNA and histone methylation [87–89]. Additionally, accumulated fumarate can be fueled into the urea cycle, reversing its canonic direction, with still unclear implications [90]. Another common mutation of a TCA cycle enzyme is isocitrate dehydrogenase (IDH). Gain-of-function mutations in IDH1/2 isoforms are found in many cancers and are responsible for the generation of the oncometabolite 2-hydroxyglutarate (2-HG), involved in DNA methylation and various oncogenic signaling cascades [87]. The role of certain TCA cycle intermediates in the regulation of epigenetic modifications that alter the metastatic and invasive capacities of cancer cells will be reviewed in the following sections.

From a metabolic perspective, such alterations in TCA cycle enzymes can originate a significant variability on the TCA cycle function in cancer: from truncated TCA cycle caused by severe FH and SDH deficiencies in some tumors, to a net reverse flux from α -ketoglutarate to citrate, termed as reductive carboxylation, mainly fueled by the entrance of glutamine-derived carbons to the TCA cycle [91].

The utilization of TCA cycle intermediates in biosynthesis requires a constant refill of them into the cycle, or anaplerosis, from various carbon sources at different steps. These anaplerotic pathways include glutaminolysis, which fuels α -KG into the TCA cycle from glutamine; pyruvate carboxylation, which fuels OAA from glucose/pyruvate; the urea cycle and the aspartate-malate shuttle that can fuel malate or fumarate from various uptaken amino acids [92]; and the oxidation of branched-chain amino acids (BCAA) such as isoleucine or valine which fuel succinate into the TCA cycle [8], among other anaplerotic sources.

Even if the reliance on aerobic glycolysis and the utilization of the TCA cycle as a biosynthetic hub in cancer cells are frequently found adaptations, many tumors also rely on mitochondrial metabolism and the ETC for energy obtention [93–95]. Briefly, the electron transport process that elicits ATP synthesis occurs in an array of transmembrane protein complexes (Complex I to IV) embedded in the inner

mitochondrial membrane, and two mobile electron carriers, ubiquinone and cytochrome C (2.3.1). Electrons derived from oxidizable substrates obtained from catabolic metabolism, namely NADH and FADH₂, are transported through complexes I to IV in an exergonic manner, allowing the counter-gradient pumping of protons from the mitochondrial matrix to the mitochondrial intermembrane space. In this process, molecular oxygen acts as the final electron acceptor and is reduced to water while NADH or FADH₂ are oxidized. In turn, the energy accumulated through the proton gradient is utilized by ATP synthase (also termed as complex V) to generate ATP [96].

1.3.5. Amino acid metabolism

Amino acids have a dual function as the monomeric subunits of proteins and as central metabolic intermediates that provide carbon and nitrogen for biosynthesis. Indeed, it has been recently shown that the major contribution to the biomass in proliferating and cancer cells is derived from all the non-glutamine amino acids together, rather than from glucose or glutamine [97]. Thus, amino acid metabolism emerges as an important subject of study in cancer metabolism.

The continuous availability of the twenty amino acids within the cell is essential for both proliferating and non-proliferating cells, as in both cases proteins are constantly degraded and synthesized to ensure cell maintenance. Nine of the twenty amino acids are necessarily obtained through diet, as human metabolism does not contain pathways to obtain them *de novo*, and thus considered essential amino acids (EAA). These are phenylalanine, valine, threonine, tryptophan, methionine, leucine, isoleucine, lysine, and histidine [98]. On the contrary, all other amino acids are considered non-essential amino acids (NEAA) as they can be obtained in sufficient amounts through *de novo* biosynthetic pathways in healthy cells. However, the rate of *de novo* synthesis is limited, and it may not be enough to cover the demand of proliferating cancer cells or the reprogramming of metabolic pathways associated with oncogenic transformation [98,99]. In this context, some NEAAs may become essential for cancer cells, and NEAA starvation can become an attractive approach to tackle cancer cell proliferation, as healthy cells can remain invulnerable to it, through satisfying their much lower NEAA demand through endogenous biosynthetic pathways [100].

This emergent essentiality of NEAAs as a result of cancer metabolic reprogramming is often termed as amino acid auxotrophy [101]. This has been reported as important in cancer for several amino acids such as glutamine [102], serine [103] or arginine [104]. The therapeutic approaches to achieve deprivation of a certain NEAA in the clinics are diverse and not limited to dietary restriction or enzyme activity inhibition [101]. For instance, arginine starvation can be achieved through administrating pegylatedⁱ arginase (Arg-PEG) or pegylated arginine deiminase (ADI-PEG), both enzymes causing the degradation of circulating and dietary arginine, approaches currently under multiple clinical trials for various types of cancer, with encouraging results [104,105]. The particular case of arginine auxotrophy displayed by certain tumors is often tied to a deep rewiring of either the TCA cycle or the urea cycle and its related metabolic pathways [92,106,107]. Cancer-tied particularities of arginine metabolism will be further addressed in **Section 1.3.10**.

1.3.6. Glutamine metabolism

Among all amino acids, glutamine has a prominent role in cancer, as it emerges as a crucial carbon and energy source for cancer cells through TCA cycle anaplerosis. Glutamine addiction is probably the second most common and salient feature of cancer metabolism after the Warburg effect [108]. In normal physiological conditions, glutamine is produced by some tissues to scavenge ammonia from amino acid metabolism and is recycled by others as carbon or energy source and, overall, it is the most abundant amino acid both in intracellular pools and in circulation (~500 μM) [109]. However, glutamine is often considered as conditionally essential, since it becomes essential under stress conditions, such as after an injury or surgical intervention; or in highly-proliferative states, such as pregnancy, lactation and neonatal growth [99]. Indeed, its essentiality in these situations provides evidence on the reason why its

ⁱ Pegylation is the covalent attachment of polyethylene glycol (PEG) to small molecules or macromolecules for therapeutic purposes. Pegylation increases solubility, decreases renal clearance by increasing hydrodynamic size, and also masks the therapeutic agent from the host's immune system [105].

importance is so vast in cancer, understood as a similar situation to the abovementioned, yet pathological, in terms of a highly-anabolic and nutrient-demanding situation.

The main role of glutamine in cancer is its anaplerosis of the TCA cycle, functioning as an energetic fuel and as a donor of carbon atoms. Upon cellular uptake, most glutamine is converted to glutamate by glutaminase (GLS), which hydrolyzes the amide group in glutamine to yield glutamate and ammonia. Glutamate can then be converted into α -KG by two divergent pathways: oxidative deamination by glutamate dehydrogenase (GLDH) or transamination, performed by various enzymes that can transfer the amino group to generate other amino acids. These include, for instance, glutamate oxaloacetate transaminase/aspartate transaminase (GOT/AST), which generates aspartate, or glutamate-pyruvate transaminase/alanine transaminase (GPT/ALT), which generates alanine. The metabolic pathway that fuels glutamine into the TCA cycle is generally termed as glutaminolysis [110].

Glutamine, and subsequently its metabolic product glutamate, have diverse and central roles in cell metabolism, which can be divided into different axes: (A) Carbon and energy source through TCA cycle anaplerosis, as abovementioned, (B) Nitrogen donors for amino acid, protein and nucleotide synthesis, (C) Control over acidic homeostasis by balancing ammonia production, and (D) Control over redox homeostasis as precursor of glutathione, a nucleophilic tripeptide (glutamate-cysteine-glycine) that constitutes one of the main systems of ROS detoxification. In addition, glutamine oxidation can also contribute to redox balance by supplying carbons to malic enzyme (ME), which produces NADPH reducing equivalents [111].

Human GLS is encoded by two genes, differentially-expressed across tissues: kidney-type glutaminase (GLS1) and liver-type glutaminase (GLS2). Moreover, alternative splicing of the GLS1 gene can lead to two different isoforms: kidney-type glutaminase (KGA) and glutaminase C (GAC). So far, three allosteric inhibitors of GLS1 have been reported and are commercially available Bis-2-(5-phenylacetamido-1,3,4-thiadiazol-2-yl)ethyl sulfide (BPTES), compound 968 and CB-839 [112], while no commercial inhibitors of GLS2 are available, even if some have been reported in the literature [113].

Glutaminase expression and glutamine metabolism are directly promoted by Myc [47], and glutamine availability and its metabolism are crucial for Myc-driven oncogenesis [47,102,114]. Supporting this notion, Myc can promote apoptosis upon glutamine starvation conditions, but not upon glucose starvation [50].

Glutaminase has been postulated as an appealing therapeutic target in many types of cancer, as its inhibition dramatically compromises the survival of many types of cancer cells [112,115–117]. In triple-negative breast cancer, inhibition of GLS activity leads to suppression of tumor growth *in vitro* and *in vivo*, synergizing with mTOR inhibition [112]. Blocking glutamine-derived TCA anaplerosis has been shown to activate lipid catabolism-derived anaplerosis and autophagy [115], or glucose-derived anaplerosis specifically through pyruvate carboxylase (PC) [116]. Also, relying on glutamine as a carbon and energy source confers cancer cells additional flexibility to adapt and survive in nutrient scarcity, such as glucose shortage [118].

1.3.7. Redox balance and ROS metabolism

Reactive oxygen species (ROS) are oxidant by-products of cell metabolism, including superoxide (O_2^-), hydrogen peroxide (H_2O_2), hydroxyl radical ($\cdot OH$) and singlet oxygen (1O_2). The main source of ROS is mitochondrial metabolism, as ROS are produced by the activity of complex I and complex III of the ETC [57]. Several other metabolic enzymes also contribute to intracellular ROS production: NAD(P)H oxidases (NOX), cytochrome P450-dependent oxygenases, or xanthine oxidase. In normal physiological conditions, ROS levels are low, and they contribute to cell survival, proliferation, homeostasis, and cell signaling [119–121]. On the contrary, high ROS levels are linked to stress and pathological conditions and produce damage to DNA, proteins, and lipids, thus activating cell damage-responsive barriers that can lead to cell senescence or apoptosis triggered by cytochrome c release from the mitochondria [122].

However, prior to the activation of the apoptotic cascade, cells can make use of a vast arsenal of mechanisms to counter and detoxify ROS and preserve redox homeostasis: the nucleophilic tripeptide glutathione (glutamate-cysteine-glycine), the superoxide-inactivating enzyme superoxide dismutase (SOD), thioredoxins, or peroxiredoxins, among others [48], most of them located downstream to the Keap1/Nrf2 axis [57].

In particular, cancer cells can maintain higher ROS levels while evading apoptotic programs. This feature permits sustained DNA damage and genomic instability and allows the constant evolution of tumor cell populations [123], or the modulation of various signaling pathways through the oxidation of cysteine residues. For instance, cysteine oxidation of the PI3K negative regulator phosphatase and tensin homolog (PTEN) impairs its inactivation of the oncogenic PI3K/AKT/mTOR pathway [124]. Elevated ROS levels can also play essential roles in promoting metastasis, exemplified by the oxidation of cysteine residues of tyrosine-protein kinase Src [125].

1.3.8. Pentose phosphate pathway

Cancer cell proliferation also involves a high demand of precursors for nucleic acid synthesis, both DNA and RNA. Nucleotides are the monomeric subunits of nucleic acids, consisting of three essential building blocks: one or more phosphate groups, a purine (adenine and guanine) or pyrimidine base (cytosine, thymine, and uracil), and a pentose sugar (ribose or deoxyribose). Pentose precursors are necessarily provided by the pentose phosphate pathway (PPP), which also generates nicotinamide adenine dinucleotide phosphate (NADPH). NADPH is essential for maintaining redox homeostasis and enabling fatty acid synthesis [126].

PPP is a bi-branched pathway comprised of an oxidative and a non-oxidative branch. The oxidative branch yields NADPH and ribonucleotides through three irreversible reactions that transform glucose-6-phosphate into ribulose-5-phosphate, which will then be further converted into ribose-5-phosphate. On the other hand, the non-oxidative branch is a reversible pathway mainly mediated by the enzymes transketolase (TKT) and transaldolase (TALDO). TKT interconverts glyceraldehyde-3-phosphate and fructose-6-phosphate into xylulose-5-phosphate and erythrose-4-phosphate. In turn, erythrose-4-phosphate and fructose-6-phosphate, via TALDO, can reversibly yield glyceraldehyde-3-phosphate and sedoheptulose-7-phosphate. In the next step, also catalyzed by TKT, glyceraldehyde-3-phosphate and sedoheptulose-7-phosphate are reversibly transformed into xylulose-5-phosphate and ribose-5-phosphate.

Both pathways of PPP can be overexpressed in tumor cells, as pentose requirements for proliferation are significantly increased. However, approximately 80% of required

pentoses are obtained through the non-oxidative pathway in cancer [126]. In this regard, TKT is frequently overexpressed in many tumors, constituting an important biomarker of tumor metabolism, and a druggable target through analogs of its cofactor, thiamine, such as oxythiamine [127]. A non-canonical isoform of TKT, TKT-like-1 (TKTL1), is also frequently overexpressed in tumors, often correlated with poor prognosis [128], and it is postulated to have essential roles in tumorigenesis besides its transketolase activity [129].

1.3.9. One-carbon metabolism

Serine, glycine and one-carbon (SGOC) metabolism is a set of metabolic pathways that mediates the transfer of one-carbon (1C) units required for essential cellular processes such as DNA synthesis and repair (via synthesis of purines and thymidine), amino acid balance (particularly serine, glycine, cysteine and methionine), methylation or redox homeostasis [130,131]. 1C transfers are centrally mediated by two coupled cycles: the folate cycle and the methionine cycle, which require respectively the uptake of folate and methionine, two essential molecules that cannot be synthesized *de novo*.

Inhibiting SGOC is a common therapeutic approach to block proliferation of cancer cells, due to their urge for nucleic acid building blocks to proliferate. Among therapeutic strategies involving SGOC metabolism, the use of folate analogs (or antifolates), such as methotrexate or pemetrexed, to block folate cycle is especially remarkable and used as frontline therapy for different types of cancer, such as breast [100], pleural [132] or lung [133].

Folate is uptaken through reduced folate carrier (RFC). Uptaken folate is first reduced into dihydrofolate (DHF) and then into tetrahydrofolate (THF), as the active form in the folate cycle, consuming reducing power from NADPH in both steps. THF (1C carrier) can then enter the folate cycle and can be loaded with 1C units, mainly coming from serine, glycine, dimethylglycine, or sarcosine (1C donors). 1C-loaded THF, 5,10-methylene-THF, can be used for thymidylate synthesis, or it can transfer its 1C units to the methionine cycle, responsible for the transfer of necessary 1C units for the methylation of DNA, RNA, proteins, and lipids. The methionine cycle is also connected to the transsulfuration

pathway (TSP), a linear pathway that synthesizes cysteine, involved in redox homeostasis as part of the ROS scavenger glutathione [98].

1.3.10. Urea cycle

The urea cycle, occurring canonically in liver cells, is the primary metabolic pathway that permits the non-toxic disposal of excess nitrogen resulting primarily from amino acid and protein catabolism throughout the organism. First, inside the mitochondrial matrix, accumulated ammonia from nitrogen metabolism is converted to carbamoyl phosphate (CP) by carbamoyl phosphate synthase 1 (CPS1). Then, CP is condensed with ornithine to yield citrulline by ornithine transcarbamylase (OTC). Citrulline is exported to the cytosol, condensed with aspartate to yield argininosuccinate by argininosuccinate synthase 1 (ASS1), and argininosuccinate is cleaved into arginine and fumarate by argininosuccinate lyase (ASL). Arginine is then metabolized by arginase (ARG), yielding ornithine, which is imported into the mitochondria to close the cycle, and urea, which is excreted as a waste product.

In tissues other than the liver, not the complete cycle but particular urea cycle enzymes are expressed to endow the cell with the capacity to synthesize the required amounts of arginine, ornithine, and citrulline [92]. The relevance of ornithine relies on its role as a precursor for the synthesis of polyamines, polycations that have a wide arrange of life-sustaining functions within the cell [134]. On the other hand, control over citrulline pools is crucial for nitric oxide synthases (NOS) function [135], which contributes to signaling cascades modulating hypoxia, angiogenesis, and redox homeostasis. Importantly, citrulline levels may also be necessary for a recently-unveiled post-translational modification of proteins through citrullination, potentially relevant for cancer metastasis, as it targets many proteins related to the motile capacity of cells [136].

In cancer cells, metabolism is switched from a catabolic to an anabolic state, and as much nitrogen as possible is scavenged to support biomass production and proliferation [16]. In line with this, nitrogen metabolism is completely rewired, and the urea cycle acquires greater importance in cancerous tissues other than the liver [92]. For instance, ASS1 is frequently encountered to be silenced in many cancers, resulting in arginine auxotrophy and providing a rationale for the efficacy of arginine starvation therapies

[137–139], depicted in **Section 1.3.5**. In some other cancer models, FH deficiency described in **Section 1.3.4** triggers fumarate accumulation to the point that the ASL reaction is reversed, also resulting in arginine auxotrophy and sensitization to arginine starvation therapies [90,140]. Due to the existing links between the urea cycle and the TCA cycle, glutamate transaminases, proline metabolism, and polyamine metabolism, urea cycle alterations reported in cancer have a significant impact on the overall metabolic phenotype displayed by the cell [90,139,141].

GLS and GLDH represent the main contribution to ammonia production in cancer cells, resulting in high concentrations of ammonia in the tumor microenvironment [108]. This situation can remotely resemble the accumulation of ammonia found in liver tissue, responsible for nitrogenous waste disposal through the urea cycle. Such uniquely high concentrations of ammonia in the liver favor the GLDH reaction to function prevalently in the reductive amination direction, incorporating ammonia into α -ketoglutarate [142].

In cancer, a large body of research provides evidence that the GLDH reaction functions in the oxidative deamination direction, contributing to TCA cycle anaplerosis [108,110,143]. However, Spinelli et al. [142] have triggered a novel and interesting hypothesis: ammonia accumulation in the tumor microenvironment can reverse the GLDH reaction, conferring the tumor with a mechanism for coping with ammonia toxicity as well as scavenging the ammonia-derived nitrogen to be incorporated to the biomass. Accordingly, they have recently provided evidence for the reductive amination of glutamate by GLDH in breast cancer cells, by tracking the incorporation of [^{15}N]-amide-glutamine-derived isotopic label into glutamate, proline or aspartate, among other amino acids [142]. Interestingly, the studied models also displayed an absence of label incorporation in urea cycle intermediates, denoting a lack of ammonia incorporation through the CPS1 reaction. Nevertheless, the generality of this behavior for different cancer models and how can this observation be extrapolated to cancer patients needs to be further investigated.

1.3.11. Polyamine metabolism

Polyamines, polycations containing more than one amino group, are involved in various cellular functions: cell fate and differentiation, proliferation, motility, protein and DNA

synthesis and stability, regulation of transcription, oxidative stress response, apoptosis, ion channel regulation, and protein phosphorylation [134,144,145]. Three polyamine compounds are ubiquitous in mammals, and they are responsible for such functions: putrescine, spermidine, and spermine. The role of polyamine metabolism in cancer is poorly understood, yet they are downstream from many key oncogenes, such as Myc, and their metabolism is enhanced in a broad spectra of tumors [49], enhanced in body fluids and downregulated intracellularly in many cancer patients [146], conferring polyamines a potential diagnostic value [144,146–149]. Consequently, many novel therapeutic strategies are based on inhibiting polyamine synthesis and uptake, some of them currently in preclinical and clinical trials [49].

Polyamines are synthesized in a linear pathway that is highly-conserved and tightly controlled. First, ornithine from the urea cycle is converted to putrescine by ornithine decarboxylase (ODC). ODC is the rate-limiting enzyme in polyamine synthesis, and it has found to be overexpressed in many tumors, and inherent or induced overexpression of ODC has been proved to be sufficient to induce tumorigenesis in a wide variety of cell models [150–153]. ODC has one of the shortest lifespans in all the proteome (less than 1 h), it is degraded by the proteasome in a unique ubiquitin-independent manner and tightly regulated by c-Myc [154], polyamine levels, growth factors, hormones and a dedicated system consisting of two regulatory proteins: ODC antizyme (AZ) and ODC antizyme inhibitor (AZI) [145]. Altogether, this suggests that ODC has a pivotal role in polyamine metabolism of cancer cells and that it may also represent an Achilles heel to this pathway. Moreover, ODC overexpression has also been reported to promote angiogenesis by directly regulating the expression of the antiangiogenic factor tumstatin [153].

Following ODC, putrescine is converted to spermidine, and then spermidine to spermine in a linear biosynthetic pathway executed by spermidine synthase (SPDSY) and spermine synthase (SPMSY), respectively. Both SPDSY and SPMSY use a decarboxylated S-adenosyl methionine (dcSAM) moiety, derived from the methionine cycle, which is transformed into methylthioadenosine (MTA). In these reactions, dcSAM acts only as an aminopropyl donor and thus the carbon backbone required for methionine cycle can be recovered through S-methyl-5'-thioadenosine phosphorylase (MTAP), which elicits a way to

by argininosuccinate synthase 1 (ASS1). ASA is metabolized by argininosuccinate lyase (ASL), yielding arginine and fumarate. Arginine can be transformed back to ornithine, via arginase (ARG), also yielding urea, excreted as a waste product. Alternatively, arginine can be converted into citrulline and nitric oxide (NO) by nitric oxide synthase (NOS). Ornithine is also the starting point of polyamine synthesis pathway: ornithine, via ornithine decarboxylase (ODC) yields putrescine (Put). In turn, putrescine will be sequentially converted into spermidine (Spd) and spermine (Spm). Each step of polyamine synthesis also requires decarboxylated S-adenosylmethionine (dcSAM) and produces methylthioadenosine (MTA), in a circular pathway that scavenges methionine and that is coupled to the methionine cycle. In addition, ornithine can be synthesized by other amino acids, such as glutamine, glutamate or proline, via the intermediary metabolite glutamate 5-semialdehyde. Abbreviations: adenosylhomocysteinase (AHCY), adenosylmethionine decarboxylase 1 (AMD1), glutaminase (GLS), S-methyl-5'-thioadenosine phosphorylase (MTAP), 5-methyltetrahydrofolate-homocysteine methyltransferase (MTR), ornithine aminotransferase (OAT), proline dehydrogenase (PRODH), pyrroline-5-carboxylate (P5C), pyrroline-5-carboxylate reductase (PYCR), S-adenosylmethionine (SAM), S-adenosyl homocysteine (SAH).

1.3.12. Lipid metabolism

Cancer cells will also display enhanced demand of lipids for biosynthesis and proliferation, as they constitute essential signaling molecules and the main structural components of cell membranes. However, many tumors also use lipids as fuel for mitochondrial metabolism, serving as both carbon donors for other biosynthetic purposes and as an additional energy source that contributes to the metabolic flexibility of tumor cells [115].

Proliferating cancer cells display a marked avidity for different lipids, displaying enhanced lipid uptake and endogenous biosynthesis [155]. Indeed, the accumulation of excess lipids and cholesterol in lipid droplets within cancer cells is considered indicative of cancer aggressiveness [156].

Reprogramming of fatty acid metabolism is another common hallmark shared by many tumors [157–161]. In this regard, one of the most recurrent metabolic adaptations encountered in cancer cells regarding fatty acid metabolism is the simultaneous activation of both fatty acid synthesis and fatty acid oxidation (FAO), which essentially results in a futile cycle [84]. Still, maintaining both pathways constitutively active can confer metabolic flexibility to tumor cells: fatty acid synthesis is essential for cancer cell proliferation, whereas situational modulation towards FAO to produce NADH and ATP and concomitant activation of metabolic stress pathways such as AMPK can result in a remarkable ability to cope with metabolic stress [162].

Fatty acid synthesis relies on acetyl-CoA availability as a substrate and, subsequently, on the capacity of the TCA cycle to produce citrate through citrate synthase, its export through the citrate shuttle, and its transformation to acetyl-CoA by ACLY [77]. Its catabolic counterpart, fatty acid oxidation, permits the use of fatty acids as fuel for ATP production. It requires the internalization of long-chain fatty acids into the mitochondria, which is mediated by the carnitine system. In brief, cytosolic CoA-bound long-chain acyl groups are bound to carnitine by carnitine palmitoyltransferase 1 (CPT1), yielding acylcarnitine molecules. Then, carnitine-acylcarnitine translocase (CACT) imports acylcarnitines into the mitochondrial matrix, where they are transformed back into long-chain acyl-CoA molecules by carnitine palmitoyltransferase 2 (CPT2) [84,163] (**Figure 2.3.1**).

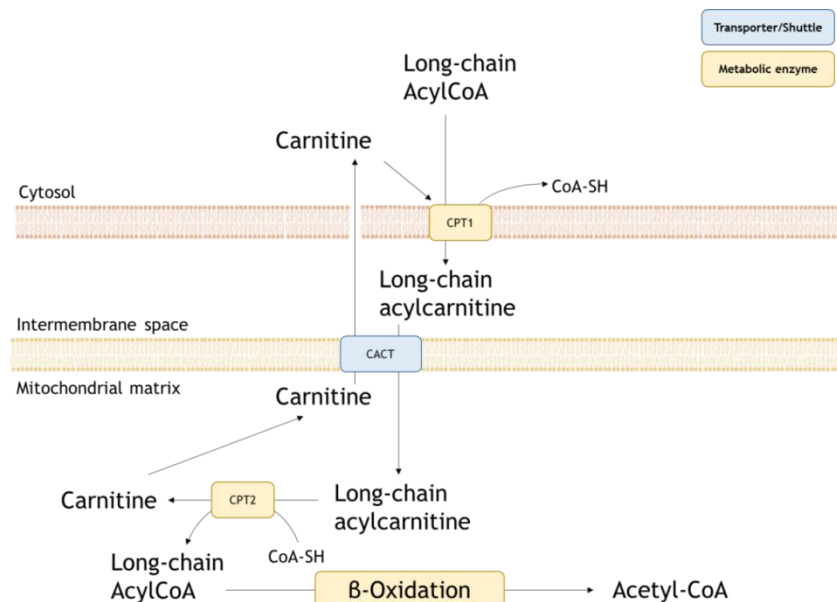


Figure 2.3.4. Transport of fatty acids into the mitochondria through the carnitine system.

CPT1, the rate-limiting enzyme of lipid transport for FAO, has been extensively investigated in terms of its role in carcinogenesis. More recently, three isoforms of CPT1 have been reported: CPT1A, CPT1B, and CPT1C. CPT1A and CPT1B are located on the mitochondrial membrane, whereas CPT1C is located on the endoplasmic reticulum (ER), and it has been reported to have much lower carnitine acyltransferase activity than CPT1A and B [164]. Conversely, it has been recently reported to have signaling functions, such as modulation of autophagy [165].

Sphingolipids constitute another family of lipids that perform structural functions in cell membranes, contributing to the maintenance of membrane fluidity and the capacity of the lipid bilayer to act as a physical barrier [166]. Moreover, they also develop signaling functions in both health and disease by interacting with cell signaling networks. In cancer, they have been implicated in the regulation of cell growth, proliferation, invasion, and metastasis [167]. For instance, oxidative stress and chemotherapy induce the synthesis of sphingosine and ceramide, which act as signaling molecules, triggering apoptosis, senescence, and cell cycle arrest [167].

1.4. Metastasis, invasion and stemness

Tumor progression and the acquisition of new functions by cancer cells are often enabled by the activation of genetic and epigenetic programs that are characteristic of embryonic development [168]. The resemblance between cancer cells and embryonic cells is especially remarkable in the use of transitions between epithelial and mesenchymal states, termed as epithelial-mesenchymal transition (EMT) [169], and in their ability to dedifferentiate and acquire the tumor-initiation and pluripotency capacities that characterize cancer stem cells (CSCs) [170].

These two programs, EMT and stemness, are often intimately linked and coupled since they share common upstream regulators at multiple points of their signaling networks [171,172]. However, rising evidence also opens the possibility for the partially or completely uncoupled activation of both programs [173–177]. Both phenotype-driving programs, stemness and EMT, will be reviewed in this section, together with the crosstalk between both and their implications in cancer cell metabolism.

1.4.1. Metastasis and epithelial to mesenchymal transitions

As tumor cells evolve, they may acquire the capacity to undergo a sequential chain of events that lead to metastasis: invasion of nearby tissues, intravasation into blood or lymph vessels, dissemination through the organism, extravasation to other tissues and establishment of colonies at distant sites. This multi-step process is known as the invasion-metastasis cascade, and it is responsible for about 90% of cancer-associated

deaths [7]. Even if our understanding of the molecular aspects of metastatic lesions is still incomplete, it is well-established that tumor cells require transitions between epithelial and mesenchymal phenotypes to originate metastases.

Epithelial phenotypes are characterized by relatively ordered layers of adjacent cells, tightly attached between them through junctional complexes, displaying an apicobasal polarization [178] and limited migratory capacity [168]. On the opposite, mesenchymal cells loosen their organization, and they present modified adhesion factors that disable cell-cell adhesion, promote the acquisition of front-rear polarity [178] and favor migratory and invasive behaviors [168], including the ability to breach the basement membrane and degrade components of the extracellular matrix (ECM) [169].

EMT can be defined as a series of reversible transitions between epithelial and mesenchymal phenotypes that cells undergo to commit to a certain fate during embryogenesis or to be able to invade and disseminate through the organism during tumorigenesis. In this last scenario, a highly-motile mesenchymal phenotype is required for invasion and intravasation. Conversely, returning to an epithelial one through reverse EMT or mesenchymal-epithelial transition (MET) can be beneficial for the attachment and proliferation that enables colonization and formation of macrometastases.

In molecular terms, epithelial and mesenchymal features of cells are defined by their expression programs of cell adhesion molecules (CAMs). CAMs that drive the epithelial phenotype are E-cadherin, α -catenin, claudins, occludins, or cytokeratins, whereas mesenchymal markers include N-cadherin, vimentin, or fibronectin [169]. Among these, the replacement of E-cadherin for N-cadherin expression is an event of outstanding importance during EMT, commonly termed as the “cadherin switch” [179]. Other alterations in the expression patterns of EMT markers are still a subject of intensive research and debate nowadays, due to the wide range of phenotypes and expression patterns displayed by different tumors and the complexity of the regulatory networks governing this process.

EMT activation in the cell is coordinated by specific EMT-inducing transcription factors (EMT-TFs), such as Snail (Snai1), Slug (Snai2), Twist, or Zeb1, which have been thoroughly

investigated during the last decades [7,172,179–183]. Apart from these, other TFs capable of fine-tuning some aspects of EMT have also been reported, notably Zeb2, Foxc2 or Prrx1, among other TFs [7], and different families of regulatory microRNA and post-translational modifications [169]. The different EMT-TFs can directly promote or repress the transcription of different CAMs and other EMT effector molecules, as well as interacting between them at the transcriptional level. Snail can directly promote transcription of Zeb1 and Twist, which will maintain the loop reinforcing Snail to sustain the mesenchymal phenotype [179]. Zeb2 also represses the epithelial gene program and induces EMT in many cancer types, including CRC [182] and sarcoma [183].

From the distillation of the body of research on this topic, it can be interpreted that metastasizing carcinomas display a wide variety of phenotypes regarding EMT-TFs, CAMs and other molecular effectors of the EMT that can be found active in tumor cells [175,184]. The acquisition of intermediate phenotypes or “partial EMT” has been extensively reported as a highly favorable state driving tumor progression and metastasis [174,185]. Thus, it is now a generally accepted idea that the EMT is a dynamic and multi-stage phenomenon that gives rise to a myriad of different intermediate phenotypes, rather than being a single binary switch between epithelial and mesenchymal opposed states [7,169,179].

Similarly, the invasion-metastasis cascade in general terms is not a fixed and well-defined chain of events that can only occur in one single manner. For instance, circulating tumor cells (CTCs) can migrate through blood or lymph vessels either as individual cells or small clusters of attached cells. These CTC clusters in collective migration display a high grade of heterogeneity in EMT signature that can be beneficial for tumor dissemination: they can include leader mesenchymal cells that will drive the migratory and invasive capacities of the cluster, attached to a bulk of more epithelial ones, better prepared to colonize and proliferate at secondary sites [186]. In consequence, a cell may not necessarily require undergoing EMT to reach its metastatic niche.

Another critical aspect of the invasion-metastasis cascade is the crosstalk between tumor cells and their surrounding stroma. One of the clearest examples is the release by tumor cells of angiogenic factors to their surroundings, promoting the formation of

closer blood vessels by stimulating endothelial cells from the stroma, which will facilitate local invasion [187]. At the same time, stromal cells can also deliver signaling stimuli that will influence the molecular events occurring in tumor cells. Indeed, EMT of cancer cells is triggered by heterotypic signaling received from the surrounding stroma, including transforming growth factor β (TGF- β), Wnt, or different interleukins [7].

1.4.2. Tumor initiation, stemness, and plasticity

CSCs are a relatively rare subset of tumor cells that are endowed with plasticity and self-renewal capacity [171]. These cells are also thought to be the only ones capable of originating a new tumor, and thus, they are sometimes termed as tumor-initiating cells (TICs) [172]. A considerable fraction of tumor heterogeneity and its hierarchical structure is given by these CSC pools, as they can give rise to different lineages of committed daughter subpopulations, potentially in response to the selective pressures to which the tumor is subjected [10,172]. In this manner, CSCs significantly contribute to the adaptation of the tumor to its microenvironment (e.g., nutrients or oxygen availability) and the emergence of resistant phenotypes and tumor relapse after chemotherapy [188] or radiotherapy [189].

The currently accepted CSC model, or hierarchical model, states that every tumor contains a small fraction of CSCs, that are both able to self-renew and to originate differentiated daughter tumor cells with decreased tumorigenic capacity that constitute the bulk of the tumor [171,190]. However, emerging evidence also supports an alternative model, referred to as the stochastic model, in which every tumor subpopulation contributes to tumor plasticity and that committed tumor cells can also dedifferentiate and undergo phenotypic transitions, increasing their tumorigenic capacity [10]. In this regard, Gupta and coworkers proved that each isolated subpopulation of a breast cancer cell line (luminal, basal, and stem) was able to generate the other two and that all three were equally able to originate tumors given the appropriate stimuli [191]. Indeed, deeper insight is still required to fully understand the contribution of cancer cell plasticity and stemness to tumor progression and structure, and the right answer probably lies in between both the hierarchical and the stochastic models, as some studies have already proposed [192,193].

Traditionally, CSCs have been identified and isolated using cell surface markers and receptors, such as CD44 [194,195], CD117 [195] or CD133 [196]. However, a better understanding of the cellular role of these markers, and the detection of false-positives (e.g., CD44+ and CD117+ ovarian cells without TIC capacity [196]) and false-negatives (e.g., both CD133+ and CD133- can initiate tumors in gliomas [197,198]), have led to the use of other means, along with cell surface markers, to accurately identify and characterize CSC populations. Other self-renewal markers that allow identifying CSCs can also be enzymes, such as the aldehyde dehydrogenase 1 A1 (ALDH1A1), involved in retinoic acid synthesis [199,200]; or pluripotency-related transcription factors, such as OCT4 [201], SOX2 [202], Nanog [201,203], Myc [204], KLF4 [205] or Bmi1 [195,206].

1.4.3. Interplay between the EMT and CSC programs

Plasticity, tumorigenic capacity, and EMT activation have been described as phenotypically encompassed in many tumors [207–210]. Notably, the induction of the EMT by ectopic expression of EMT-driving oncogenes and transcription factors concurrently induces the acquisition of a CSC phenotype [211–215]. This phenotypic correlation between both programs is expectable, as the central EMT-TFs (Snail, Twist, and Zeb1/2) can concomitantly elicit the transcription of both EMT-related and CSC-related targets [216].

For instance, Zeb1 represses stemness-inhibiting micro-RNAs [217]. Twist1 upregulates the CSC marker Bmi1, and both Twist1 and Bmi1 act coordinately to repress E-cadherin expression [181]. Combined activation of Slug and Sox9 is sufficient to induce the transformation of differentiated luminal mammary cells into CSCs [210]. Similarly, the ectopic induction of different EMT-TFs has been reported to promote stemness and TIC in mammary cells by activating Hedgehog signaling [218]. Finally, the paramount EMT-TF Snail has been reported to drive both invasiveness and pluripotency in many functional studies of ectopic expression in cancer models [213–215].

Despite this high degree of overlap and redundancy between EMT and CSC signaling, growing evidence suggests that both programs can also be partially or completely uncoupled. Stem-like features have been identified in cells displaying a hybrid EMT phenotype [173,174] or even an entirely epithelial phenotype [175–177]. These

observed differences in the degree of coupling between the EMT and CSC phenotypes rely on the countless possible combinations of EMT-TFs activation. Indeed, even if they are all associated with driving the transcription of the mesenchymal gene program, there is also a significant degree of non-redundancy in their transcriptional targets [219], and it has been shown that their differential activation can determine the CSC state [210,220].

Interestingly, the mechanistic connection between EMT and CSC programs has also been reported as sequential, rather than simultaneous: induction of EMT as a prelude to the acquisition of tumor-initiation capability has been observed in many different types of carcinoma [7]. Consistent with this observation, during the invasion-metastasis cascade, EMT activation is required for achieving dissemination throughout the body, whereas tumor-initiation capability is required at a later phase: the establishment of macrometastases. The cells responsible for tumor initiation at secondary niches are often termed as metastatic stem cells (MetSC) [221]. In order to thrive in their secondary niche, these MetSC need to have a completely or at least partially epithelial phenotype, in order to exit dormancy and proliferate. This can be achieved either by undergoing MET to some degree or by being transported by leader mesenchymal cells throughout the body. The mutually exclusive balance between motility and proliferative capacity has been thoroughly described [222], and thus MetSCs capable of establishing macrometastases will display a phenotype that simultaneously displays stem and epithelial features, often termed as epithelial cancer stem cells (e-CSCS).

Indeed, both TIC capacity and undergoing MET for proliferation at the metastatic site are essential features for success in this later colonization stage, assigning a prominent role to the abovementioned e-CSC phenotype. Consequently, epithelial metastatic stem cells play a decisive role in metastatic colonization, and they could be the most critical tumor subpopulation to target in therapy to eradicate metastases.

1.4.4. Metabolic reprogramming associated to metastasis and invasion

Across the different steps of the invasion-metastasis cascade, tumor cells will be surrounded by a wide variety of different microenvironments that challenge their ability

to survive and preserve their malignancy. Thus, they will need to become adapted to each new scenario by rewiring their metabolic networks to fulfill their energetic and biosynthetic needs with the resources at hand in each particular microenvironment.

This situational rewiring of metabolic pathways to match the evolving requirements of the metastatic cascade is partly triggered by the regulation of metabolic genes by EMT-TFs. The crosstalk between metabolism and EMT-TFs is bidirectional: not only EMT-TFs regulate cell metabolism, but oncogenic signaling functions of metabolites and metabolic enzymes can have a decisive impact on the EMT phenotype through modulating the expression of EMT effectors at transcriptomic and epigenetic levels [87,89,223,224] (2.4.1).

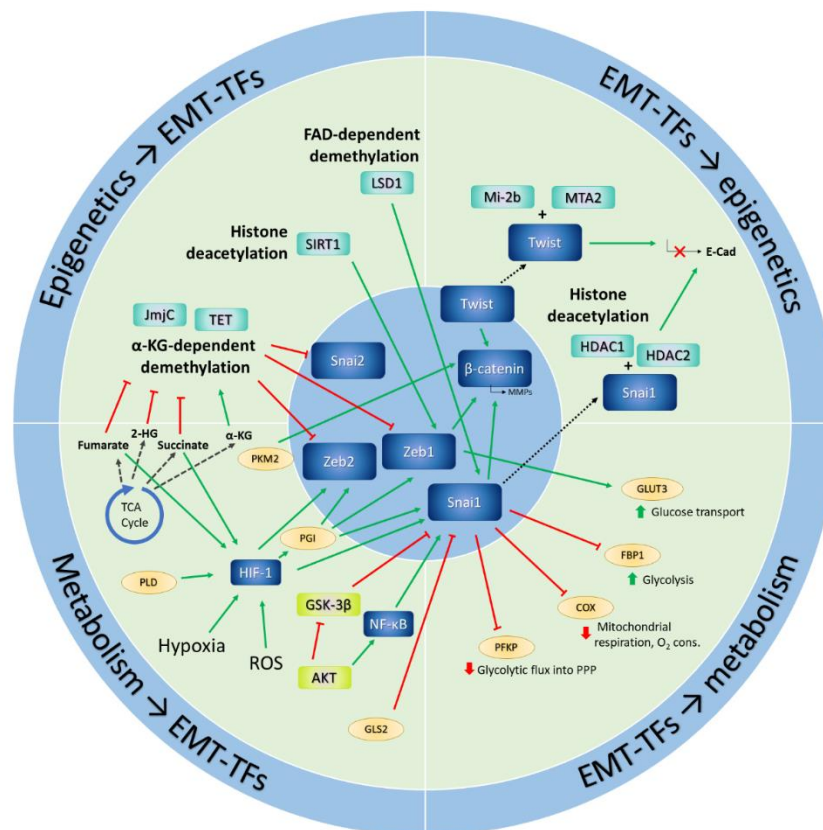


Figure 2.4.1. Relevant examples of crosstalk between metabolism, epithelial-mesenchymal plasticity, and epigenetics. EMT-transcription factors (EMT-TFs) are regulated by histone and DNA methylation and by histone acetylation. These processes are, in turn, modulated by the intracellular levels of metabolic products of the tricarboxylic acid (TCA) cycle. EMT-TFs also cooperate with histone deacetylases to repress the expression of cell adhesion molecules that modulate the EMT phenotype. Metabolic cues such as hypoxia, oxidative stress, or nutrient availability can activate EMT-TFs through various signaling axes such as HIF-1 α , AKT, GSK-3 β , or NF- κ B. Alternatively,

the expression of EMT-TFs can be directly modulated by metabolic enzymes, such as phosphoglucoisomerase (PGI) or pyruvate kinase isoform M2 (PKM2). In turn, EMT-TFs regulate central metabolic pathways, by activating or repressing the transcription of metabolic enzymes and metabolite transporters, such as phosphofructokinase platelet (PFKP), cytochrome c oxidase (COX), fructose-1,6-bisphosphatase 1 (FBP1), or glucose transporter 3 (GLUT3). Adapted from Thomson et al. [222] with the permission of coauthors.

The first challenge that cancer cells must face when undergoing the invasion-metastasis cascade resides in the capacity to be motile enough to degrade the ECM and reach the bloodstream. The motile phenotype is driven in part by lipid rafts, cholesterol, and sphingolipid-rich membranous structures that modulate cell adhesion by partnering with CD44 and are required for ECM degradation and invadopodia formation [225]. Sphingolipids themselves are also part of other oncogenic signaling cascades that lead to motile phenotypes [167]. Finally, different enzymes in fatty acid metabolism are also recruited for the metastatic process [226]. ACLY is required for low molecular weight cyclin E (LMW-E)-mediated transformation, migration, and invasion [227]. Similarly, FASN is also involved in invasion by being able to induce EMT [228,229], and by interacting with Wnt signaling [230].

Upon detachment from an adherent layer, healthy non-hematopoietic cells are unable to uptake sufficient glucose. This cellular state results in anoikis, a particular kind of apoptosis triggered by the lack of ATP that results from loss of anchorage [231,232]. Circulating tumor cells will display metabolic adaptations specifically devoted to permit the evasion of anoikis and to favor anchorage-independent growth, a prerequisite state for metastatic dissemination [233]. Elevated ROS levels can further contribute to the activation of anoikis since ROS accumulation inhibits ATP production [234]. Therefore, many of the alterations exhibited by cancer cells to evade anoikis may also be dedicated to scavenging ROS or diminishing their generation. One of these alterations may be the reinforcement of a highly-glycolytic phenotype, relying on glucose for obtaining ATP, which can decrease cellular ROS levels both by diminished mitochondrial metabolism and increased NADPH production capacity through PPP.

On the contrary, invasive ovarian cancer cells under detachment conditions increase pyruvate uptake for TCA cycle anaplerosis. This engagement on pyruvate favors migration and the adoption of a more oxidative metabolic phenotype [235]. Similarly, the CRC cell line SW620, obtained from lymph node metastasis, exhibits an increase in

EMT markers and invasiveness, and enhanced mitochondrial metabolism in detriment of aerobic glycolysis, when compared to its primary tumor counterpart, SW480 [236].

Indeed, multiple links are emerging between the TCA cycle and metastatic potential of cancer cells, particularly tied to epigenetic signaling (2.4.2). An essential part of these relies on the action of a particular family of α -KG-dependent DNA demethylases termed as ten-eleven translocation (TET) demethylases. Importantly, their demethylating-activity, elicited by α -KG, enables the expression of miRNA-200, an important repressor of EMT-TFs [222]. On the contrary, over the last years, it has been found that succinate [87], the product of TET activity, and fumarate [89], a structural analog of α -KG, inhibit the action of TET enzymes, suppressing miRNA-200 and promoting EMT.

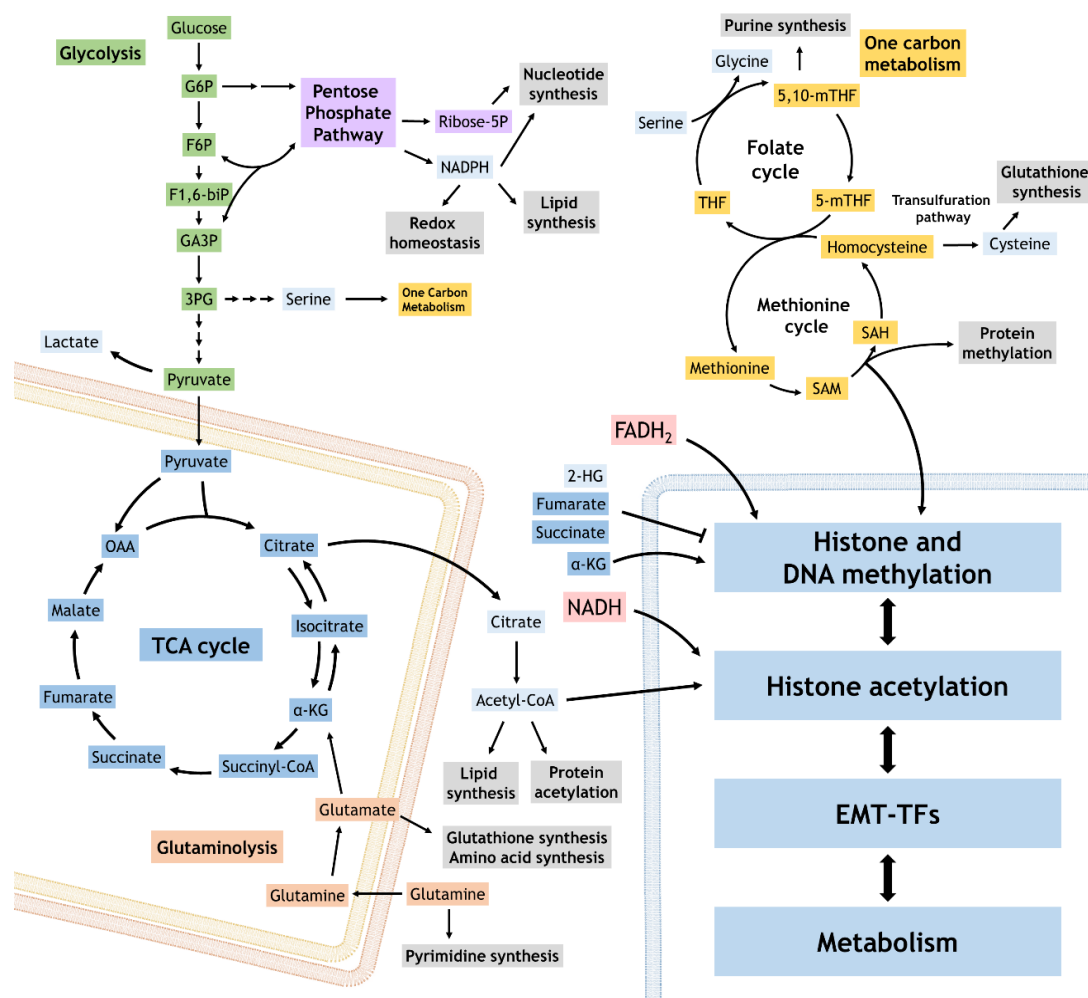


Figure 2.4.2. Metabolic requirements of methylation and acetylation. S-adenosyl-methionine (SAM) acts as a methyl donor for histone and DNA methylation. SAM is produced through one-carbon metabolism. Demethylation can be dependent on the tricarboxylic acid (TCA) cycle intermediate α -ketoglutarate (α -KG) and can be inhibited by other TCA cycle products: succinate, fumarate, or 2-hydroxyglutarate (2-HG). Histone demethylation by lysine-specific

histone deacetylase 1 (LSD1) can also be dependent on FADH₂. FADH₂ pools are dependent on fatty acid oxidation and the TCA cycle. Histone acetylation requires acetyl-CoA, obtained from citrate or fatty acid oxidation in the TCA cycle. Histone deacetylation by sirtuin (SIRT) histone deacetylases is NAD⁺-dependent. NADH pools are dependent on multiple metabolic pathways, including glycolysis, pyruvate dehydrogenase, the TCA cycle, fatty acid oxidation, amino acid oxidation, and oxidative phosphorylation (OXPHOS). Adapted from Thomson et al. [222] with the permission of coauthors.

Not only methylation but also histone acetylation has been reported to have crucial roles in the induction of the EMT program through epigenetic activation of EMT-TFs expression. For instance, an increase in acetyl-CoA pools activates EMT in hepatocellular carcinoma through Twist2 expression by histone acetylation [237]. Similarly, in pancreatic cancer, inhibition of class I histone deacetylase (HDAC) induced the expression of an epithelial gene set [238]. Consequently, mitochondrial metabolism and, more specifically, the preservation of TCA intermediate pools, as well as the balance of NADH and FADH₂, also crucial for methylation and acetylation events, have a prominent impact on the modulation of the EMT program.

Metabolic and EMT signaling cascades display a remarkable level of overlapping that derives in a certain coupling between both in cancer cell phenotype. One of the most evident is through glycogen synthase kinase-3 (GSK3). GSK3 subunits GSK3 α and GSK3 β are one of the busiest signaling kinases in the cell, with over 100 targets [239]. GSK3 β is directly phosphorylated and inactivated by AKT, and one of its target genes is the EMT-TF Snail, hence establishing a link between the metabolic and the EMT phenotypes. GSK3 β inhibits Snail through phosphorylation, targeting it for proteasomal degradation. Importantly, inhibition of GSK3 activates glycogen synthesis and glucose transport [240]. Thus, in mesenchymal phenotypes that encompass inactive GSK3 and subsequently active Snail, enhanced glucose transport and glycogen accumulation may represent a strategy to accumulate carbon and energy reservoirs to sustain potential shortages during the dissemination of motile cells throughout the body. Supporting this idea, Snail also has downstream targets that promote glycolytic flux while inhibiting OXPHOS: Snail represses fructose-1,6-bisphosphatase 1 (FBP1), promoting glucose uptake and the diversion of glycolytic carbons towards biosynthetic pathways, including the pentose phosphate shunt, and impairing respiration and activity of respiratory chain complex I

[241]. Similarly, Snail also represses phosphofructokinase platelet (PFKP) [242] and several subunits of cytochrome C oxidase (COX) [243].

In addition, polyamine metabolism could also play a role in the invasion-metastasis cascade. First, the ROS-balancing capacity of polyamine metabolism can contribute to anoikis evasion, and, second, polyamines may be directly involved in mediating invasion since inhibition of polyamine metabolism directly decreases the expression of different MMPs [244–246]. Finally, other studies have also emphasized the role of glutamate and GABAergic metabolism and metastasis. In particular, glutamic acid decarboxylase (GAD) decarboxylates glutamate to yield γ -aminobutyric acid (GABA), a neurotransmitter molecule that promotes metastasis in oral cancer by causing β -catenin translocation and MMP production in established cell lines and correlates with the occurrence of metastasis in an oral cancer patient cohort [247].

1.4.5. Metabolic reprogramming associated with stemness

The unparalleled ability of CSCs to survive under chemotherapeutic regimes and then instigate tumor relapse has stimulated intensive research on different functional aspects of CSCs, including the metabolic adaptations they display. In this regard, both prominently glycolytic and OXPHOS metabolic phenotypes have been reported in CSC subpopulations, with no identified distinctive feature or particularly tied to specific cancer types [95,248–250].

In glycolytic CSCs, oncogenic activation of Myc has been described as a recurrent link between stemness and the glycolytic phenotype [251,252], mainly contributing to enhanced redox protection due to decreased oxidative mitochondrial metabolism and enhanced flux through PPP [248]. For some models, the isolated CSC fraction displays a greater glycolytic activity than the bulk of the tumor and decreased reliance on mitochondrial respiration [249,250]. However, the role of Myc in the intersection between stemness and glycolytic phenotypes is still unclear. In pancreatic cancer, an OXPHOS-relying CSC pool has been identified, while Myc drives the Warburg phenotype of the more differentiated bulk of the tumor [95]. Besides, Myc, another Yamanaka pluripotency factor, KLF4 [205], has also been reported to have a direct impact on the

glycolysis/OXPHOS balance via targeting TCL1 which drives a Warburg phenotype via AKT activation in induced pluripotent stem cells (iPSCs) [253].

OXPHOS-relying CSCs display greater metabolic flexibility and decrease their dependence on nutrient availability in the TME, as mitochondrial metabolism can be fueled by many substrates other than glucose. In this regard, FAO has shown to be an essential fuel for oxidative mitochondrial metabolism of CSCs [161,254], driven by the pluripotency transcription factor Nanog [161]. Besides, unsaturated fatty acids have been recently described as important markers and mediators of the CSC phenotype through the NF- κ B signaling axis [158,255].

The CSC phenotype is intrinsically encompassed with a high degree of adaptability to the tumor microenvironment and, consequently, the metabolic adaptations they display are also expected to be remarkably plastic and influenced by their particular niche [95]. Some hints on the metabolic particularities tied to CSCs and their regulatory networks have been unveiled, but a much deeper understanding is needed to achieve generalization and systematization on this matter.

1.5. Drug resistance

1.5.1. Mechanisms of drug resistance

Drug resistance in cancer is the process by which cancer cells develop strategies to survive under chemotherapeutic intervention. Resistance can be intrinsic, if a tumor is *per se* irresponsive to a particular chemotherapeutic agent; or acquired, if irresponsiveness emerges after treatment, due to mutagenesis and clonal evolution exerted by the selective pressure of the drug. Moreover, resistance can also be acquired, alone or in combination with clonal evolution, by the plastic phenotypic adaptation of tumor cells through signaling and epigenetics, elicited mainly by their CSC traits [256].

Cancer drug resistance can be limited to a single family of chemical compounds or a wide variety of compounds with distinct cytotoxic mechanisms, termed as multidrug resistance. The mechanisms that contribute to cancer drug resistance are diverse and complex, involving multiple cell signaling pathways, transporters, and molecular

effectors that overlap and can be simultaneously activated in countless manners. In consequence, resistance to single-agent treatments is devastatingly common in cancer. The cancer research community is currently aiming to reverse this situation by developing combination therapies. Multidrug approaches have been proved as highly effective, reducing the risk of clonal selection that leads to resistance [257] and are increasingly used in the clinics [258].

Hereafter, different mechanisms of drug resistance will be reviewed. Aiming to achieve conciseness and clarity in this section, such mechanisms will be discretized and broadly classified into different categories, based on the cellular feature that is altered to contribute to drug resistance: drug transport, drug metabolism, drug target, DNA damage repair, apoptosis evasion, EMT, and stemness.

Drug transport alteration

Drug transport includes all the systems by which a drug can enter or be excreted from a cell. Alteration of either the influx or the efflux of drugs in cancer is an essential mediator in the emergence of resistance. Both reducing the influx or enhancing the efflux result in the reduction of the intracellular accumulation of the drug.

Both processes are mainly mediated by members of the ATP-binding cassette (ABC) transporter family. ABC transporters are transmembrane proteins that consist of a highly conserved nucleotide-binding domain and a transmembrane domain that varies among the 49 members of the family. They mediate the efflux of various substrates out of the cell by consuming an ATP at their nucleotide-binding domain [259]. Three of the members of the ABC transporter family acquire a particular importance in chemotherapy resistance: multidrug resistance protein 1/P-glycoprotein (MDR1/P-gp), multidrug resistance-associated protein 1 (MRP1) and breast cancer resistance protein (BCRP). Due to their low substrate specificity, alteration of these transporters in cancer cells leads to the acquisition of resistance to a broad array of chemotherapeutic agents [6,259].

Alternatively, anticancer drugs can also be excreted from the cell by members of the SLCO and SLC22A transporter superfamilies, including organic cation transporters (OCTs), organic anion transporters (OATs) and organic anion transporting polypeptides

(OATPs). Members of these families are frequently overexpressed in many types of cancer and contribute to the resistance of a wide variety of anticancer drugs, including taxanes, nucleoside analogs, or antifolates [260].

Drug metabolism alteration

Many chemotherapeutic drugs require partial modification to be activated and act on their molecular targets. Upon administration, they are treated as xenobiotics by both tumor and healthy cells, and they undergo biotransformation by drug-metabolizing enzymes (DMEs). These enzymes will transform the prodrug to yield, at a certain step, the bioactive form of the drug, but further progress on these pathways will also lead to drug deactivation and excretion. Drug metabolism can be divided into three distinct phases [261,262]:

Phase I: Modification – Oxidation, reduction, or hydrolysis reactions that decrease toxicity, mainly performed by cytochrome P450 enzymes [263].

Phase II: Conjugation – Conjugation reactions of the drug to glutathione, sulfate, glucuronic acid, mercapturic acid, methyl, and acetyl, performed by specific enzymes with transferase catalytic activity, such as the glutathione-S-transferase (GST) superfamily [261,264].

Phase III: Transport – Shuttling of the drug across the cellular membrane, performed by ABC transporters, OATs, and OCTs of the SLC22A superfamily [261], as described in the previous section.

Two different situations can originate cancer drug resistance by alterations in drug metabolism pathways: downregulation of early drug metabolism that involves less or slower drug activation; or upregulation of late drug metabolism, which leads to faster inactivation and excretion of the active form. Both result in lower intracellular concentration of the active form, and, therefore, decrease in its antineoplastic effect.

Drug target alteration

During long chemotherapeutic regimes, tumors are exposed to the selective pressure resulting from the pharmacological agent. Thus, genomic instability can favor the appearance of subpopulations that deregulate the target pathway or contain an altered

or mutated version of the drug target that can impair the effect of the drug [265]. A clear example of this is the response of breast cancer cells to estrogen receptor (ER)-directed therapies, to which breast cancer cells respond by downregulating or completely losing ER expression, or by mutating or translocating the ER gene, which results in hormone-refractory growth [266]. Acquisition of resistance by alteration of the drug target can also occur due to PTMs resulting from the rewiring of oncogenic signaling cascades. Focal adhesion kinase (FAK)-targeting chemotherapy is counteracted by FAK phosphorylation by receptor tyrosine kinases (RTK), maintaining FAK activation [267]. Moreover, when the drug target is a metabolic enzyme or a metabolic pathway, the emergent metabolic reprogramming counteracting the presence of the drug is an example of a drug target alteration mechanism. This issue will be addressed in more detail in **Section 1.5.2**.

DNA damage response

The mechanism of action of multiple families of antineoplastic agents, such as alkylating agents and DNA crosslinkers, is directed to produce severe amounts of genotoxic damage so that cancer cells become unable to fulfill the conditions of the DNA damage checkpoint, and, therefore, their growth becomes arrested. However, cancer cells can also acquire resistance to genotoxic therapies by upregulating their DNA damage response (DDR) machinery to the extent that sufficient DNA repair is ensured, or that DNA damage checkpoints are ignored [25].

DNA repair occurs through different specific reactions, such as nucleotide excision repair or mismatch repair, depending on the type of lesions produced by the genotoxic agent. When DNA damage is reparable, the cell cycle is arrested as a cytoprotective mechanism, until DNA integrity is recovered. Otherwise, DDR proteins will trigger proapoptotic stimuli [268]. DDR is initially mediated by ataxia telangiectasia mutated (ATM) and ataxia telangiectasia and Rad3-related (ATR), two kinases that recognize DNA damage, recruit effectors for DNA repair, and rewire metabolic pathways to ensure nucleotide availability [25]. Both ATM and ATR contribute to genotoxicity resistance, and, for instance, knockdown of either of them can sensitize glioblastoma and melanoma cells to the alkylating agent TMZ [269]. Downstream to ATM and ATR, checkpoint kinases (Chk1 and Chk2) can block cell cycle progression upon DNA defects, recruiting p53 to

activate the apoptotic cascade. Inhibition of Chk1/Chk2 is able to overcome cisplatin resistance in head and neck cancer [270]. Notably, utterly frequent p53 mutations in many cancers also obstruct the proapoptotic signal transduction that arises from irreparable DNA defects [56].

Apoptosis evasion

One of the hallmarks of cancer cells is their capacity to evade apoptosis, which can be reinforced in cancer cells as a mechanism of resistance to chemotherapeutic agents that are designed to selectively trigger a proapoptotic response in cancer cells. For instance, imatinib-resistant leukemic cells display inhibited apoptosome formation by modulating the function of the apoptosome inhibitor protein Hsp90 β [271]. Indeed, deregulation of the apoptotic signaling cascade is a tremendously common strategy to acquire resistance to a broad spectrum of anticancer drugs, but it can also be counteracted by directly targeting the apoptotic pathway. One clear example is the use of Bcl-2 antagonists, such as AT-101 or navitoclax, in combination with other chemotherapeutic agents to overcome drug resistance. For instance, HDAC inhibition combined with navitoclax has proven to be effective for small cell lung cancer treatment [272]. Similarly, simultaneously targeting Bcl-2 and the PI3K/mTOR axis was effective in triggering apoptosis and enhanced response to tamoxifen in ER+ breast cancer [273].

EMT and stemness

Cancer cell subpopulations can acquire the capability to invade nearby tissues or to intravasate and disseminate through the organism. Different studies with large patient cohorts have unveiled a strong correlation between the EMT phenotype and resistance to chemotherapy [274,275]. Acquiring an invasive phenotype under pharmacological pressure may encompass a combination of different selective advantages. First, gaining the capacity to be motile can enable the possibility to encounter more favorable niches, which can be considered as an adaptation that contributes to escape from the drug pressure. Besides, certain EMT-TFs also mediate the transcription of DDR proteins. For instance, ZEB1 can be activated by the DNA damage-sensitive ATM kinase to promote the stabilization of Chk1 [276,277], a crucial piece of the DDR machinery.

On the other hand, CSCs have also been extensively associated with resistance. They have the potential to become plastically adapted to the drug pressures to which they are subjected, by adopting phenotypes that confer them a selective advantage and improved survival. CSC markers CD117, CD166, and ALDH1, are correlated with resistance in prostate cancer patients [278]. Indeed, certain chemotherapeutic drugs are reported to induce an enrichment in CSC pools [188], and these can lead to tumor relapse many years after chemotherapy has apparently eradicated the tumor [171]. Most frequently, this relapse occurs through metastatic spread, in which latent chemoresistant MetSCs are responsible for cancer regression through distant metastases [221].

Such types of response inevitably arise a question: is the activation of the EMT phenotype a driving force of cancer drug resistance, or a consequence of the activation of EMT-TFs that are simultaneously responsible for multiple functions besides EMT, including DNA damage response and CSC induction?

1.5.2. Metabolic reprogramming associated with resistance

Resistance to chemotherapy can result from the alteration of different parts of the cellular machinery. For instance, amplification or silencing of genes, alteration of signaling cascades, increase in the rate of DNA repair, or upregulation of drug biotransformation and transport. The alteration of any of these mechanisms will necessarily impact the metabolic status of the resistant cancer cells: increased DNA repair rates will raise the demand for nucleotides; increased traffic through ABC transporters will imply additional ATP demand to support active transport; usage of ROS scavenging machinery for drug detoxification will trigger new biosynthetic demands (e.g., glutathione synthesis); alteration of signaling that can infer on the apoptotic cascade, such as p53, Myc or Akt, will also have a profound impact on metabolism.

Even if the source of chemoresistance appears to be, in principle, untied to metabolism, the high degree of interconnection between the different layers of cell physiology can often trigger a noteworthy butterfly effect and have a global impact on cancer cell metabolism. Of course, this global impact will even be more significant when the chemotherapeutic agent directly targets a metabolic enzyme or pathway.

Some authors have found that chemotherapy-resistant cells display increased glycolysis and an exacerbated Warburg phenotype [279]. For instance, long-term exposure to the alkylating agent TMZ derives in GLUT3-overexpressing resistant glioma cells [279]. The rationale behind the resistance-driven glycolytic shift could be tied to the recently-identified signaling functions of lactate [280]. It has been found that lactate can promote DNA repair and resistance in cervical carcinoma, via inhibiting histone deacetylation and activating the hydrocarboxylic acid receptor 1. In line with this, increased aerobic glycolysis also confers radioresistance to glioma and oral carcinoma cells, also tied to an increase in DNA repair rates [281]. This observation suggests that increased lactate production could be a more generalized mechanism to counteract chemo- or radiotherapy-induced DNA damage.

The need for preserving or intensifying a glycolytic phenotype to achieve metabolic resistance to DNA damage can open significant therapeutic windows. In bladder cancer, forced PDH activation by the PDK inhibitor dichloroacetate (DCA) synergized with the DNA crosslinker cisplatin in decreasing the volume of xenografted tumors [282]. Similarly, MCF-7 breast cancer cells resistant to both the antifolate methotrexate and the AMPK activator AICAR, display reversion of their Warburg phenotype, cell cycle arrest, and decreased proliferation upon the combined administration of both drugs [283].

1.5.3. Platinum-based chemotherapy

Platinum (II) compounds have been extensively used in cancer therapy since their accidental discovery in 1965 [284], to the extent that the flagship compound of the family, cisplatin, $\text{cis-[PtCl}_2(\text{NH}_3)_2]$ or CDDP, is often referred as “the penicillin of cancer drugs”. Nowadays, these compounds represent one of the main front lines in solid tumor treatment, despite the ability of many tumors to ultimately become resistant to them. Indeed, cisplatin, carboplatin, and oxaliplatin are extensively used for multiple cancer types, and they are included in the WHO’s Model List of Essential Medicines. Furthermore, some others, such as picoplatin, and more recently, the platinum (IV) compound satraplatin have entered clinical trials [285,286].

The primary mechanism of action of platinum-based chemotherapy is binding to N7 of guanine residues in DNA, inducing massive intra- and inter-strand cross-linking that will ultimately trigger cell death by apoptosis [287]. Apart from that, a plethora of other related and unrelated effects have been reported, such as cell cycle arrest, senescence induction, mitochondrial damage, or ROS induction [288–290].

However, the clinical applicability of these compounds for cancer therapy is often hampered by the emergence of resistant phenotypes. These are driven by a severe reprogramming of cancer cell metabolism that confers to it the ability to surpass mitochondrial impairment caused by platinum drugs, increase DNA repair rates, maintain redox homeostasis, and ultimately evade apoptosis and achieve proliferation and cell growth [286].

1.5.4. Platinum (IV) compounds

In an attempt to overcome the limitations of platinum (II), remarkable research efforts have been set towards the development of platinum (IV) compounds, which act as prodrugs of their platinum (II) precursors. The axial ligands in platinum (IV) compounds enable the modulation of physicochemical properties such as lipophilicity, stability, or reduction potential [287,291].

Platinum (IV) compounds are kinetically inert in comparison to their Pt (II) analogs, which allows their oral administration [292]. Moreover, a large body of evidence suggests that Pt (IV) compounds act as prodrugs since they need to be reduced to Pt (II) and release their two axial ligands in order to be active [287,293]. Thus, in stoichiometric terms, Pt (IV) compounds can potentially consume twice as ROS scavenging molecules as their Pt (II) counterparts, thus generating additional oxidative stress that can contribute to disabling cancer cell survival capacity. These two additional coordination sites can also be rationally designed to act synergistically with the platinum cytotoxic effect; improve their activity, pharmacodynamics, tissue targeting, molecular targeting, and selectivity to decrease systemic toxicity and improve their safety profile [287,292].

1.5.5. Mechanisms of platinum resistance

The molecular mechanisms of resistance encountered in platinum-resistant tumors are partially coincident with the general mechanisms of drug resistance portrayed in **Section 1.5.1**. Particularly, resistance to platinum compounds occurs through increased DNA repair rates, alteration of drug transport, and increased drug inactivation [256]. Hereafter, the different categories depicted in that section will be nuanced for the particular case of platinum compounds.

First, platinum drugs are electrophilic compounds that can be deactivated by different reducing agents that constitute the antioxidant defense mechanisms of the cell [294]. These are mainly reduced glutathione (GSH), cysteine-rich motifs in proteins, and the metallothionein family of proteins. Much of the platinum drug entering the cell is captured and reduced by these means, to the extent that only 1% of the platinum drug entering the cell can enter the nucleus and form cytotoxic platinum-DNA adducts [295].

The interaction between GSH and platinum-based drugs has been extensively characterized, and it can be classified into three types of interaction. First, GSH acts as cytoprotective by reduction or coordination to active platinum (II) or platinum (IV) species, diminishing the amount of free active drug that can enter the nucleus and produce DNA damage. Second, GSH can contribute to platinum drug efflux by ABC transporter-mediated transport or multidrug resistance proteins (MRPs), in which a GSSG-Pt complex is excreted from the cell. Third, it regulates the intracellular copper pool and thus influences platinum efflux through copper-mediated transport [294].

The study of resistance mechanisms to platinum compounds has been approached by the characterization of both short-term exposure, as indicative of innate resistance, and long-term exposure, as indicative of a clonal selection process or acquired resistance [296–298].

1.6. Macromolecular crowding

The interior of living cells is a tightly-packed environment in which a myriad of solutes, macromolecules, and supramolecular structures take about 40% of the total cellular

volume. This occupied fraction can vary among different *in vivo* environments, being on average 200-400 g/l. The most crowded space, the interior of mitochondria, can reach up to 500 g/l, whereas the least crowded one, the bloodstream, contains about 80 g/l of macromolecules [299]. However, even in this least crowded environment, the concentration of macromolecules is much higher than the concentrations reached on *in vitro* biochemical characterization. For instance, *in vitro* enzyme kinetics and enzyme activity studies are typically performed using purified enzymes or protein extracts in the range of 1-10 g/l.

In highly-concentrated environments, all the molecular actors inside the cell will display significant deviations from ideality that will define their *in vivo* behavior, significantly impacting on the function of all the cellular machinery and all the metabolic reactions and pathways. Thus, biochemical measurements performed in dilute solution may lack resemblance to the phenomena occurring in the interior of the cell.

1.6.1. Excluded volume effects

The main difference between diluted and concentrated solutions containing macromolecules relies on excluded volume. Excluded volume theory, developed by Werner Kuhn in 1934 and applied to polymer science by Paul Flory, states that the volume occupied by a given macromolecule in solution excludes an amount of volume to other macromolecules in the solution that is larger than the volume that it actually occupies.

For example, in **Figure 1.6.1**, the small molecule T in panel A (**1.6.1.A**) will be able to occupy all the space (colored in blue) without superposing to other molecules in solution. On the opposite, macromolecule T in panel B (**1.6.1.B**) will not be able to occupy the space between two other macromolecules if the distance between them is smaller than macromolecule T's diameter (pink shade and empty circles in panel **B**). Therefore, the available volume for macromolecule T (colored in blue) will be much less than the real amount of volume that is empty (or occupied by a non-macromolecular solvent). When applying this theory to the biophysics of living cells, it is commonly referred to as macromolecular crowding.

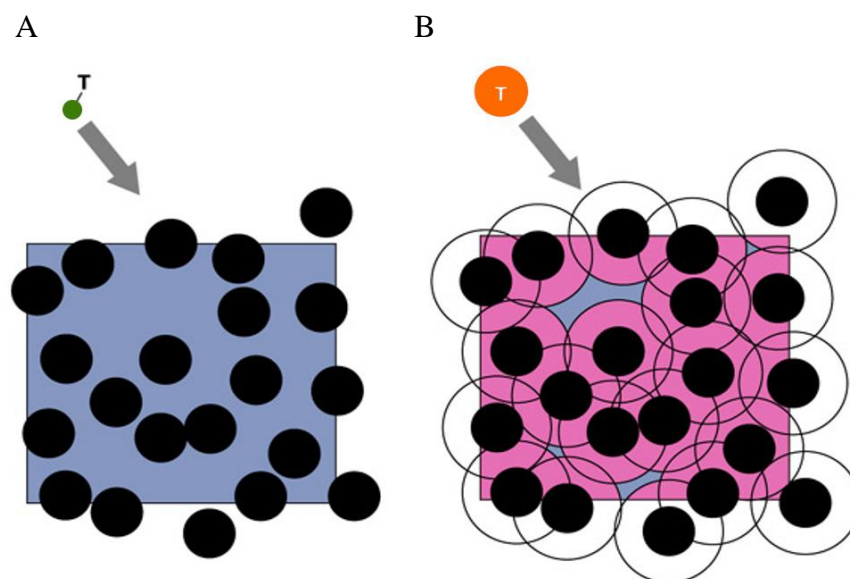


Figure 1.6.1. Graphical representation of the excluded volume effect. Representation of the fraction of available volume (blue) and excluded volume (pink) for a given small molecule (green, panel A) or a macromolecule (orange, panel B) in a macromolecule solution. The amount of excluded volume in a macromolecule solution will be defined by the macromolecule T radius (empty circles in panel B). Extracted and adapted from Rivas G., Minton A. *Trends Biochem. Sci.* 2016, 41, 11, 970-981.

The term macromolecular crowding was coined by Minton and coworkers in 1981 [300], after they had already insinuated its effects in their previous works with concentrated hemoglobin solutions and in previous works by Laurent on enzyme reactions in polymer media in 1971 [301]. Since then, macromolecular crowding has become generally accepted for many different phenomena inside cells: diffusion, where altered or anomalous diffusion phenomena are reported [302,303]; protein folding and stability, where crowding favors protein stabilization and alters folding and conformational equilibria [304]; DNA replication and transcription, where a regulatory role has been found both in experimental and computational studies [305,306]; cell volume sensing, where crowding is proposed as a way for the cell to respond to changes in its volume [307]; and also enzyme activities [308–310]. In addition, computational approaches using Brownian or molecular dynamics tools and metabolic models [81] have also greatly contributed to the understanding of this phenomenon.

In the field of enzyme kinetics, macromolecular crowding addresses the phenomenon of excluded volume in cellular environments, by mimicking the volume exclusion found in the cell with the addition of neutral and relatively inert macromolecules that exclude

volume without introducing significant unspecific interactions with the system of interest. These agents are typically inert neutral polymers, such as Dextran or Ficoll [309].

In particular, the use of Dextran polymers is widely spread due to their lack of reactivity and high solubility in water. Moreover, their flexibility, random coil shape in solution and availability in different sizes comparable to globular proteins typically found inside the cell, make Dextran a suitable option for modelling the effect of excluded volume *in vitro*.

The effects of macromolecular crowding in enzyme kinetics in *in vivo* environments are still unclear but are predicted to have a great impact on cell metabolism regulation, both by directly impacting enzyme conformation and activity and by generating diffusion gradients and non-homogeneous substrate concentrations inside the cell, having an impact not only on metabolic networks, but also on drug metabolism and the action of pharmacological agents inside the cell. The work presented in **Chapter 4** represents a contribution to the understanding of the consequences of macromolecular crowding in enzyme-catalyzed reactions.

1.6.2. Macromolecular crowding, metabolism, and cancer

It has recently been postulated that OXPHOS occupies between 5 to 50 times more volume than aerobic glycolysis to yield the same amount of ATP [311], eliciting the hypothesis that excluded volume could impose a kinetic limitation to rapidly proliferating cells that constraints mitochondrial energy production and promotes aerobic glycolysis. This was cleverly investigated by Vazquez and Oltvai [81]. In their work, they built a central carbon metabolism model that considers volume exclusion effects by introducing solvent capacity constraints for both metabolic enzymes and mitochondria. Their results revealed that aerobic glycolysis is the optimal solution above a threshold metabolic rate, typically displayed by cells under rapid proliferation, or cells with a high ATP demand. Indeed, this suggests a common entropic origin for both the Warburg effect displayed by cancer cells and lactic fermentation exhibited by heavily contracting muscles.

Moreover, macromolecular crowding can also be determinant for the subcellular localization of proteins. Sun et al. described that in cancer cells, SIRT1 is maintained in

the nucleus only due to cytoplasmic crowding, due to cancer-specific nuclear envelope defects [312]. This can be of particular interest for cancer drug development, and the *in vitro* screening of novel compounds or inhibitors targeting cancer metabolism or other molecular aspects of cancer cells. Notably, macromolecular crowding also alters the function of DNA polymerases and nucleases [305,313].

Besides cancer, macromolecular crowding has also been reported to play a role in other diseases. For instance, increasing excluded volume enhances the fibrillation of the Tau protein, the main cause of neurodegenerative diseases [314].

Understanding the actual impact of crowding inside cells or how it is regulated is still a far horizon. However, a recent study has unveiled that the rheology of the cytoplasm is governed by the concentration of ribosomes, being able to occasion 2-fold variations in the diffusion coefficients of cytoplasmic macromolecules [315]. Importantly, the same study also showed that mTORC1, the mediator of ribosome synthesis and degradation, can act as a master regulator of intracellular crowding, along with all the biophysical implications it carries; and the potential role of crowding, regulated by the oncogenic Akt/mTOR pathway, in cancer cells.

1.7. Prostate cancer

Prostate cancer (PCa) is the second most frequently diagnosed cancer in men, with 1.1 million new cases, two-thirds of them in economically developed countries, and 0.37 million deaths worldwide in 2012 [316]. Its increased prevalence in developed countries, where prostate cancer is the most common cancer type and the third cause of cancer death in men, relies on differences in the use of prostate-specific antigen (PSA) screening, the most relevant biomarker for prostate cancer detection [317]. However, an increase in PSA levels can be caused by both prostatic malignancies and benign enlargement of the prostate. The latter, benign prostate hyperplasia (BPH) affects a significant fraction of the population (40% of men in their 40s, 50-60% of men in their 60s, and 80-90% of men in their 70s-80s [318]). Therefore, even if PSA screening persists to be the main PCa biomarker, it is nowadays subject to controversy as it can lead to

deceptive PCa diagnosis and overtreatment [319]. Lately, this situation has encouraged considerable research efforts to the identification of novel PCa biomarkers [147–149].

In this regard, the main problem affecting PCa detection is that malignancies of prostatic origin are usually asymptomatic until an advanced and metastatic stage of the disease. For this reason, regular urologic observation in adult and elderly men and control of PSA levels are crucial for its outcome. Upon early prostate cancer detection, clinical surveillance for the least aggressive tumors or prostatectomy followed by chemotherapy is usually sufficient to permit the disease-free survival of patients [320]. On the opposite, when prostate cancer reaches its metastatic niches, mainly the bones and the brain, the mortality rates are between 70 [278] and 100% [321]. In line with this, available therapeutic options for the metastatic stage of the disease are only palliative, and encountering effective treatments to target prostate cancer metastasis is urgent [321].

Encompassed with the formation of metastasis, another crucial event in prostate cancer progression is the acquisition of insensitivity to androgens, the hormones governing the prostatic function. The androgen receptor (AR) signaling network is a crucial regulatory axis of prostatic cells, which orchestrates in a prominent manner their growth and their metabolism [322]. Thus, first-line chemotherapy for prostate cancer is based on neutralizing AR signaling axis to impair cancer cell proliferation [323]. However, a significant fraction of prostate tumors ultimately relapse and become resistant to androgen ablation therapies, a stage that is commonly referred to as castration-resistant prostate cancer (CRPC) [324,325]. Even if androgen insensitivity worsens prognosis, second-line therapeutic options such as taxanes or radium-223 can also be beneficial for specific subsets of CRPC patients [325].

1.7.1. Histological classification and subsets of prostate cancer

Prostatic glands are composed mainly of basal and secretory epithelial cells, but they also contain a small fraction of neuroendocrine cells (~1%). In contrast to prostatic epithelial cells, prostatic neuroendocrine cells are quiescent, possess neuron-like morphology and secrete biogenic amines, neuropeptides, and endocrine-signaling

molecules, such as chromogranins, serotonin or histamine, which all contribute to the maintenance of homeostasis in epithelial subpopulations of the prostate [326–328].

Most prostate tumors are adenocarcinomas, that is, tumors originated at epithelial tissue with a glandular origin or glandular characteristics. Prostatic adenocarcinomas are histologically classified according to the Gleason score (2.7.1), an index that reflects PCa aggressiveness and deviation from healthy prostate epithelia. Its value ranges from 2, tissue close to healthy prostate epithelia, to 10, aggressive and anaplastic prostatic malignancy. The Gleason score is used to predict the behavior of the malignancy and to determine the best options for its treatment [320].

Besides prostatic carcinogenesis occurring in basal and secretory epithelia, prostate cancer can also originate from the scarce subpopulation of neuroendocrine cells. Neuroendocrine prostate cancer (NEPC) is a relatively rare subset of prostate cancer which is highly-aggressive and associated with poor prognosis [328]. NEPC cells are negative for PSA, tumor progression marker Ki-67, and the AR [329]. Thus, NEPC growth is in origin independent of androgen signaling.

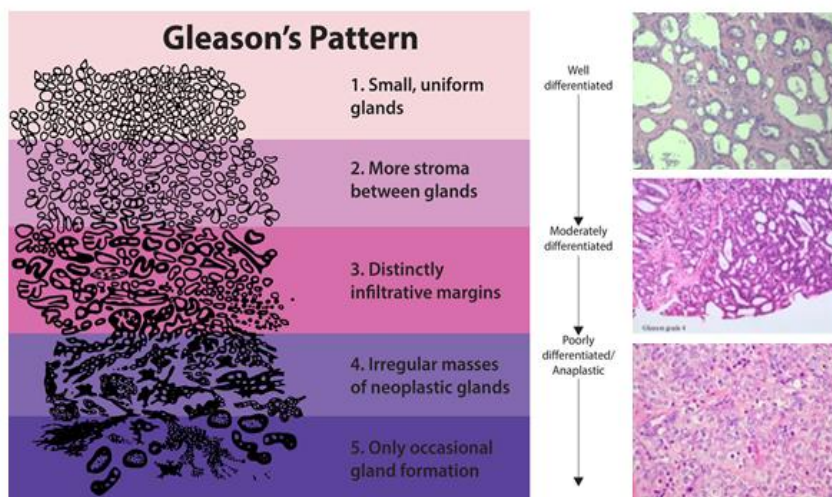


Figure 2.7.1. Histological classification of prostate cancer by the Gleason score. Gleason score is calculated as the sum of scores (N_1+N_2) for the two most prominent areas of the tumor, scored 1 to 5 according to its resemblance to healthy prostate epithelia. The image is an adaptation from Creative Commons content and <http://www.prostates.com.au>, reproduced with the permission of the author.

In this regard, yet another molecular event that also drives prostate cancer progression is the neuroendocrine transdifferentiation of basal and secretory epithelial PCa cells into

NE-like cells. The emergence of NE markers correlates with tumor progression, poor prognosis, and the acquisition of androgen independence [328,330]. Indeed, Wright et al. showed that acquisition of NE-like characteristics is repressed by the activity of AR signaling and that AR knockdown caused NE transdifferentiation in LnCaP androgen-sensitive prostate cancer cells [331], establishing a causal link between NE transdifferentiation and acquisition of castration resistance.

In summary, prostate tumors can be of epithelial or neuroendocrine origin. PCa progression is associated with three different cellular processes: the invasion-metastasis cascade, the acquisition of androgen independence, and the acquisition of neuroendocrine features.

In **Chapter 1** of this work, we have characterized a panel of CRPC cell lines (described in more detail in **Section 1.7.6** from both primary tumor (P4E6) and metastatic origin (PC-3, DU-145, and NCI-H660). Among the metastatic ones, PC-3 and DU-145 are adenocarcinomas displaying opposite EMT signatures, while NCI-H660 displays a NE phenotype. Moreover, to better understand the interplay between the EMT signature and metabolism, we also deepen in the characterization of two different PC-3 subpopulations that display opposite EMT phenotypes: mesenchymal (PC-3S) and epithelial (PC-3M).

Our approach is devoted to identifying therapeutic targets able to impair the proliferation of prostatic neoplasms at their most aggressive state: metastatic and castration-resistant, through a metabolic therapy approach. Moreover, the addition of a metastatic NEPC cell line provides a broader vision of the different cell subpopulations in prostate cancer that need to be targeted to block the metastatic stage of the disease and prevent tumor relapse.

1.7.2. Oncogenic signaling and treatment of prostate cancer

The main signaling axis that drives prostatic function and growth is the androgen receptor. AR signaling is essentially pro-anabolic, as it promotes cell cycle progression and biosynthesis of lipids, nucleotides, and proteins by orchestrating a high number of enzymes in anabolic pathways [322]. For instance, crucial aerobic glycolysis enzymes, GLUT1, HK1/2, and PFK2/PFKFB2, are directly regulated by the AR [322]. Moreover, the

AR can also infer in the redirection of this enhanced glycolytic flux into PPP through G6PD upregulation [332].

The most recently approved AR-targeting drugs include abiraterone acetate, enzalutamide, and apalutamide. Another frequent therapeutic option is taxane-based chemotherapy. Taxanes, such as paclitaxel or docetaxel, act by disrupting microtubule formation and thus hindering mitosis of tumor cells. The combination of both AR-targeting therapy and taxanes has also been proved to be effective in the clinics [323,333].

Another key effector of metabolic reprogramming and oncogenesis in prostate cancer is the frequent loss of PTEN tumor suppressor in prostate tumors [156,334], which elicits the unrestricted activation of PI3K/AKT pathway. Therapeutic strategies aiming at counteracting the upregulated AKT signaling in prostate cancer have been proved to be ineffective, as inhibition of AKT pathway is compensated by cancer cells by the promotion of AR signaling [334]. In this regard, combination therapies that target the AKT and AR axes simultaneously are being explored [335].

Even if metastatic CRPC tumors are currently incurable, a subset of patients can benefit from platinum chemotherapy, especially the ones with NEPC or adenocarcinoma with mutations in DNA repair systems [336].

1.7.3. Prostate cancer metabolism

Healthy prostatic cells display a unique intermediary metabolite profile, as they are programmed to secrete citrate (as a key component of semen) into the prostatic fluid instead of oxidizing it in the TCA cycle [319,337]. Citrate secretion is achieved by an unparalleled ability of prostate epithelia to accumulate zinc, which inhibits aconitase and blocks further progress of the TCA cycle, resulting in net citrate production in benign prostate epithelial cells [319]. Citrate secretion is disadvantageous in bioenergetic terms since it implies high levels of TCA cycle cataplerosis and, therefore, hindered mitochondrial energy production. Because of this, healthy prostate epithelia primarily rely on aerobic glycolysis for ATP production and sustain markedly high glycolytic rates. In comparison, primary prostate cancer does not display a clearer Warburg effect than

healthy tissue as its glycolytic flux is generally similar to the one in benign prostatic tissue [337].

Instead, further enhancement of aerobic glycolysis is associated with prostate tumor progression, as increasingly glycolytic phenotypes are observed in more advanced stages of the disease [11,319,338]. This link between prostate cancer progression and glycolysis can be partly explained in terms of acquisition of androgen independence, since GLUT1, HK1/HK2, and PFK2, crucial glycolytic enzymes, are regulated by the AR [322].

Upon oncogenic transformation, prostate cancer cells also reduce the secretion of citrate to the extracellular medium and redirect it into *de novo* FA synthesis and TCA to sustain uncontrolled proliferation [147,319]. The TCA cycle, partially inactive in healthy prostate epithelia due to aconitase inhibition, emerges as a hub for metabolic precursors and a source of energy production to fuel prostate cancer cell growth. According to the available evidence, citrate accumulation and secretion are reduced as the tumor progresses: intracellular citrate accumulation negatively correlates with the Gleason score, underlining its potential use as a biomarker for PCa aggressiveness [146,147]. Also, it is important to note that citrate accumulation inhibits glycolysis by inhibiting PFK1, prompting the accumulation of energy in the form of fatty acids [339]. Thus, decreasing levels of citrate also contribute to the increasingly glycolytic phenotype tied to PCa progression described earlier in **this Section**.

Moreover, prostate tumors display a marked avidity for lipids and reliance on lipid metabolism [319]. One hallmark of prostate tumors is the apparently futile simultaneous activation of FA synthesis and oxidation [340]. On the one hand, increased *de novo* FA synthesis is a common and early event in prostate carcinogenesis [341]. It is generally effected by FAS overexpression elicited by phosphorylation and nuclear translocation of AKT [342,343]. On the other hand, prostate tumors have a strong reliance on FAO for energy production [344]. Metabolic reprogramming in other families of lipids is also frequent in prostate cancer, as described for phospholipids [337] or cholesterol metabolism [156]. Cholesterol, as a precursor of androgens, acquires additional importance in prostate cancer, since upregulation of cholesterol permits

increased androgen production that leads to self-sufficiency in AR-signaling and insensitivity to androgen deprivation therapies.

Another distinctive feature of the prostate is its polyamine-secreting function to the prostatic fluid. In consequence, dysregulation of polyamine metabolism frequently encountered in other types of cancer displays a unique profile in PCa. Indeed, low intracellular spermine and increased spermine secretion have been postulated as aggressive PCa biomarkers [147–149], and altered polyamine metabolism is also emerging as a hallmark of prostate cancer [345,346].

1.7.4. Prostate cancer cell models

PC-3

PC-3 is one of the best-characterized prostate cancer cell models. It is a castration-resistant model isolated from a metastatic lesion in the bone of a prostate cancer patient. Various studies have reported a lack of AR and PSA in this cell line [347,348]. Even if PC-3 displays mostly basal and luminal cell markers K5, K8 and K18, it has also been reported to express the NE marker neuron-specific enolase (NSE) but to lack other NE markers such as chromogranin A [348]. Recently, histological analysis of PC-3 xenograft tumors revealed resemblance to NEPC as it displays small cell NE markers [347]: lack of AR and PSA expression. This could be a result of either an NEPC origin or NE-transdifferentiation upon acquisition of androgen insensitivity, even if the degree and implications of its partially NE phenotype are not well established.

DU-145

DU-145 is a cell line derived from a prostatic adenocarcinoma that metastasized to the brain. It is negative for both AR and PSA, expresses basal and luminal cell markers K5, K8, and K18, while it lacks any NE marker [348]. DU-145 displays an outstanding capacity to maintain redox homeostasis and detoxify drugs among other prostate cancer cell models, including PC-3, due to a loss-of-function of Keap1 through aberrant splicing that enables high Nrf2 constitutive levels [58].

NCI-H660

NCI-H660 is one of the few available NEPC models, scarcely characterized and displaying a low proliferation rate, with a doubling time of around 100 hours. It was initially reported as a small cell lung cancer cell line [349], which was found to be lymph node metastasis of NEPC after a more in-depth characterization [350]. In this regard, it is important to note that NEPC is histologically indistinguishable from pulmonary and other extra-pulmonary small cell carcinomas [347]. According to its NEPC origin, NCI-H660 does not express AR or PSA, and it is positive for NE markers chromogranin A and NSE [348]. The same study also reports mutations in TP53 in this cell line [348].

P4E6

P4E6 was obtained from an early stage but androgen insensitive adenocarcinoma with a Gleason index of 4 [351]. Its properties have been reported as similar to those of early prostate cancer cells, and it retains expression of many prostate-associated antigens, including PSA [351], and thus it has been used as a model for early-stage PCa primary tumor in different studies [352–354], accounting for its limited metastatic potential. Moreover, its abilities to evade apoptosis and surpass cell cycle checkpoints upon exposure to different chemotherapeutic drugs (e.g., cisplatin or etoposide) are much more limited than the ones displayed by metastatic PCa models such as PC-3 or LnCaP [355], which is also indicative of a low degree of tumor progression in this model.

In **Chapter 1** of this work, we have delineated the metabolic phenotype of these four models, along with two isogenic subpopulations of PC-3 with opposed EMT and CSC signatures, in an attempt to elucidate metabolic alterations tied to metastatic progression in CRPC. In **Chapter 2**, we have obtained a platinum-resistant metastatic PC-3 cell line, and we have unveiled metabolic vulnerabilities tied to platinum resistance. In **Chapter 3**, we have assessed the effect of novel platinum compounds on platinum-sensitive and platinum-resistant CRPC models.

1.8. Colorectal cancer

Colorectal cancer (CRC) includes all malignant growths that occur in the colon and rectal mucosa, being the third most frequently diagnosed malignancy in men and the second

in women worldwide [316]. Its incidence can be attributed to a combination of genetic propensity and environmental factors such as dietary factors, lack of physical activity, obesity, or alcohol consumption [356]. For many years now, CRC screening in risk segments of the population has been proved to be crucial for a positive outcome of the disease, or even its prevention through the removal of colorectal polyps before their malignant transformation [356]. Its metastatic spread, commonly through the lymphatic system, targets predominantly the lymph nodes, liver, and lungs.

1.8.1. Oncogenic signaling and treatment of colorectal cancer

The main oncogenic cascades driving CRC progression are the WNT/ β -catenin pathway, transforming growth factor beta (TGF β), and epidermal growth factor receptor (EGFR) pathway, with its downstream targets RAS, RAF, and PI3K/AKT/mTOR [357]. Metabolic reprogramming accompanying CRC arises mainly from the combined effect of this oncogenic activation.

The two main axes of treatment for CRC are surgical intervention and chemotherapy. Chemotherapeutic options for CRC are mainly based on cytotoxic agents, mainly irinotecan and oxaliplatin, which are often combined with 5-FU, leucovorin, or capecitabine [358]. However, such chemotherapeutic regimes result in an 18-month average survival, as CRC is usually detected at its metastatic stage [358]. In consequence, finding more effective combinations by unveiling the Achilles heel of these two cytotoxic drugs, platins or irinotecan, is a strategy to be prioritized.

In **Chapter 2** of this work, we have obtained and characterized a platinum-resistant metastatic CRC cell line. In **Chapter 3**, we also assessed the effect of novel platinum compounds on platinum-sensitive and platinum-resistant CRC models.

1.9. Current approaches for the characterization of cancer cell metabolism

Different *in vitro* and *in silico* tools allow us to gain a deeper understanding of how cell metabolism is rewired in cancer, and how targeting metabolism can block cancer cell survival and tumor progression. Often, the *in vitro* and the *in silico* approaches are complementary and work symbiotically on characterizing cancer metabolism: empirical data about tumor cells or tissues is obtained through *in vitro* characterization; then it is used to build computational metabolic models to gain an integrated knowledge about the key altered features of the system of interest, and predict its vulnerabilities; then the validity of such predictions is tested *in vitro*; which can lead, in turn, to refine and improve the model, should the predictions not fit the empirical behavior.

In **this Section**, we present a set of tools, directly or indirectly tied to the present work, that are extensively used to characterize cancer cell metabolism, to identify its vulnerabilities, and to discover new biomarkers and targets to be translated to the clinics.

1.9.1. Metabolomics

Metabolomics is the “omic” approach devoted to the quantification of metabolites, and the evaluation of dynamic changes in metabolic pathways and networks, in biological samples such as biological fluids, cells, tissues, organs, or organisms. Two different approaches are currently used in the field: either targeted metabolomics, determination of a pre-established set of metabolites, or untargeted metabolomics, which aims to detect all the metabolites in a biological sample, and thus elicits the discovery of novel metabolites or reactions [359].

Different analytical tools and methods are currently used in metabolomics, along with different sample treatments and metabolite extraction protocols, depending on the type of instrumental platform being used. The most used platforms are either based on nuclear magnetic resonance (NMR) or mass spectrometry (MS). The latter can be standalone, by direct infusion (DI-MS), such as in orbitrap or Fourier transform-ion cyclotron resonance (FT-ICR) technologies or coupled to a previous separative technique.

MS-based coupling to separative techniques gives rise to different technologies, such as capillary electrophoresis-MS (CE-MS), gas chromatography-MS (GC-MS), or liquid chromatography-MS (LC-MS) [360].

The metabolome is the final end-product of gene transcription, and, thus, its study can provide a much closer picture to the actual cellular phenotype than studying the genome, the transcriptome, or the proteome. However, no omic science as standalone can provide a complete picture or be sufficient to understand all the alterations undergone by cancer cells, as they may arise from all different layers, and their implications may spread throughout the different layers in complex manners. Conversely, a comprehensive understanding can only emerge from the integration of different omics in the characterization of the same biological system.

One step further in the understanding of cell metabolism in health and disease is tracing the fate of artificially-labeled metabolites within metabolic pathways. This is usually addressed by feeding the system of interest with a metabolic substrate (e.g., glucose or glutamine) labeled with one or more heavy stable isotopes (e.g., ^2H , ^{13}C , or ^{15}N), and quantifying the metabolites of interest after a given incubation time. This approach is termed as stable isotope-resolved metabolomics (SIRM), and it can be used to estimate metabolic fluxes, defined as reaction and transport rates in living cells. Estimation of a small subset of fluxes can be performed by direct interpretation, or by using simple equations, approaches known as substrate contribution and pathway activity analysis. In contrast, estimations of fluxes at the omic scale can only be addressed by *in silico* approaches [361].

1.9.2. Metabolic target predictions

Integration of different omics can be achieved through genome-scale metabolic models (GSMM). These are based on reconstructing human metabolism, creating a model network containing all the reactions in human metabolism, and integrating into it as many measured extracellular fluxes as possible of the system of interest. This is used to compute all the possible solutions for intracellular fluxes that are in accordance with the extracellular fluxes measured in the system of interest, yielding flux intervals, for any given metabolic reaction or pathway [362].

However, in order for this approach to be useful, the space of solutions obtained needs to be narrow enough to have predictive value about the behavior of the system of interest. To achieve it, the space of solutions needs to be constrained with additional information on what is happening inside the system, besides the information on what enters or leaves the system. This can include genomic, transcriptomic, or proteomic data, intracellular concentrations of metabolites, SIRM data, or, any other empirical data able to further constrain the predictions of the model.

Such predictive capacity can be used to identify metabolic targets that compromise cancer cell viability when the flux through them is blocked. This is achieved by using an objective function, often an artificial function that accounts for biomass production (e.g., amino acids, nucleotides), which aims to be a representation of the ability of a cell to be viable or proliferate. With this setup, a systematic knockout of all reactions can be performed, and the ones resulting on a value for biomass production below a threshold, will be considered as essential for cell viability, known as essential genes or reactions. A similar approach can be used to predict pairs of targets that, when knocked out simultaneously but not individually, also result on a low value for biomass production. These pairs of targets are often termed as synthetic lethal pairs. This approach can be outstandingly useful for the rational design of combination therapies against cancer.

2. Objectives

2. Objectives

The main purpose of this dissertation is to contribute to a better understanding of the two main causes of therapeutic failure in oncology: metastasis and drug resistance. The interplay between them will be interrogated using metabolomics, systems biology and biophysical approaches, in an attempt to find common phenotypic adaptations and metabolic vulnerabilities of metastatic and resistant cancer cells, potentially exploitable in novel combination therapies.

The consecution of this global objective can be addressed through the following specific aims:

1. Characterization of the metabolic phenotype associated to metastatic, invasive and primary tumor prostate cancer. Correlation of the identified phenotypes to the PC-3 isogenic models PC-3M (CSC/metastatic) and PC-3S (non-CSC/invasive) and identification of metastasis-specific metabolic targets (**Chapter 1**).
2. Establishment and metabolic characterization of platinum-resistant prostate and colorectal cancer cell models and identification of platinum resistant-specific metabolic targets (**Chapter 2**).
3. Identification of common potential targets and vulnerabilities associated to both metastasis and platinum-resistance (**Chapters 1 and 2**).
4. Evaluation of novel platinum (II) and platinum (IV) compounds to improve efficacy, selectivity and overcome resistance of platinum-based therapies in prostate and colorectal cancer (**Chapters 2 and 3**).
5. Evaluation of the effect of macromolecular crowding in an aerobic glycolysis-relevant enzyme. Kinetic analysis of lactate dehydrogenase (LDH) under the effect of the excluded volume levels present in the cellular microenvironment. (**Chapter 4**).
6. Evaluation of the effect of macromolecular crowding in a glutaminolysis-relevant enzyme. Kinetic analysis of glutamate dehydrogenase (GLDH) under the effect of the excluded volume levels present in the cellular microenvironment. (**Chapter 5**).

3. Materials and methods

3. Materials and methods

3.1. Cell culture

All cell lines were purchased from the American Type Culture Collection (ATCC, Manassas, VA, USA) or the European Collection of Authenticated Cell Cultures (ECACC, Salisbury, UK), or, when specified, isolated from parental cell lines obtained from either one.

Phosphate buffer saline (PBS), 100x non-essential amino acid solution (NEAA), L-glutamine solution (200 mM), and antibiotic solution (10,000 U mL⁻¹ penicillin, 10 mg mL⁻¹ streptomycin) were obtained from Biological Industries (Kibbutz Beit Haemet, Israel). Trypsin EDTA solution (0.05% trypsin – 0.02% EDTA), sodium pyruvate (100 mM) and fetal bovine serum (FBS) were obtained from Gibco (Thermo Fisher Scientific Inc., Waltham, MA, USA). D-glucose solution (45% in H₂O) and human insulin solution for cell culture were obtained from Sigma Aldrich.

3.1.1. Prostate cancer cell lines

PC-3 (ATCC® CRL-1435™) and DU-145 (ATCC® HTB-81™) cells were cultured in Roswell Park Memorial Institute (RPMI) 1640 (Biowest SAS, Nuaille, France) with final concentrations of 10 mM glucose and 2 mM glutamine, supplemented with 10% FBS and 1% streptomycin/penicillin. NCI-H660 cells (ATCC® CRL-5813™) were cultured in RPMI 1640 (Biowest), supplemented with insulin (0.005 mg/ml), transferrin (0.01 mg/ml), sodium selenite (30 nM), hydrocortisone (10 nM), beta-estradiol (10 nM), glutamine (4 mM), 5% FBS and 1% streptomycin/penicillin, according to manufacturer's instructions. P4E6 cells (ECACC 10112301) were routinely cultured in Keratinocyte-Serum Free Medium (K-SFM, Gibco), supplemented with 10% FBS and 1% streptomycin/penicillin and a final concentration of 10 mM glucose and 4 mM glutamine, according to manufacturer's instructions. Prior to metabolic experiments, all CRPC cell lines were

adapted for at least 10 days to RPMI-1640 10 mM glucose, 2 mM glutamine, 10% FBS and 1% streptomycin/penicillin.

Isogenic subpopulations of PC-3, PC-3M and PC-3S, were obtained as described previously [175]. Briefly, PC-3M cells were selected by limiting dilution of PC-3 cells isolated from liver metastases in nude mice after intrasplenic injection of PC-3 cells, and PC-3S cells were selected by serial enrichment of parental PC-3 cells collected from an invasion chamber. Both cell lines were cultured in RPMI 1640 (Biowest) with a final concentration of 10 mM glucose and 2 mM glutamine, supplemented with 10% FBS and 1% streptomycin/penicillin.

3.1.2. Colorectal cancer cell lines

SW620 (ATCC® CCL-227™) cells were cultured in Dulbecco's Modified Eagle Medium (DMEM) (Gibco) supplemented to final concentrations of 10 mM glucose and 2 mM glutamine, 5% FBS and 1% streptomycin/penicillin. HCT-116 (ATCC® CCL-247™) cells were cultured in DMEM (Gibco) / Ham's Nutrient Mixture F12 (Biological Industries) (DMEM/Ham F12, 1:1 mixture) with final concentrations of 12.5 mM glucose and 2 mM glutamine.

3.1.3. Other cell lines

Human breast adenocarcinoma MCF-7 cells (ATCC® HTB-22™) were cultured in DMEM medium without phenol red (Gibco) containing final concentrations of 10 mM glucose, 2 mM glutamine, 1 mM pyruvate (Biological Industries), 0.01 mg mL⁻¹ insulin and 1% NEAA (Biological Industries). Human lung adenocarcinoma A549 cells (ATCC® CCL-185™) and human breast adenocarcinoma MDA-MB-231 (ATCC® HTB-26™) cells were in DMEM (Gibco) with final concentrations of 10 mM glucose and 2 mM, 10% FBS and 1% streptomycin/penicillin. Human foreskin fibroblasts BJ (ATCC® CRL-2522™) were cultured in DMEM High glucose (Biowest), with final concentrations of 25 mM D-glucose and 4 mM glutamine, supplemented with 10% FBS and 1% streptomycin/penicillin.

All cell lines were routinely cultured in 100 mm treated culture plates and maintained at 37°C in a humidified atmosphere with 5% CO₂ in a ThermoForma SteriCycle incubator.

3.2. Cell proliferation and viability assays

3.2.1. Direct cell counting

For cell proliferation experiments in 6 well or 100 mm plates, cell counting was assessed by flow cytometry using Flow-Count Fluorospheres (Beckman Coulter, Brea, CA, USA) and propidium iodide (PI) staining. Briefly, after the incubation time specified in each experiment, cells in each well were trypsinized, harvested and resuspended in 450 μL of culture medium, 45 μL of fluorosphere solution and 5 μL of PI. Fluorescence of 10^4 PI⁺ cells and the corresponding number of fluorospheres was recorded in a CyAn ADP or Gallios flow cytometers (Beckman Coulter), and the number of cells/mL in each sample was inferred from the known concentration of the fluorosphere solution.

Alternatively, when specified hereafter, cells were stained with trypan blue (Sigma Aldrich) and counted using the digital hemocytometer Countess™ II Automated Cell Counter (Invitrogen, Carlsbad, CA, USA). Cell volume was assessed using a Scepter™ Handheld Automated Cell Counter (Merck Millipore, Billerica, MA, USA), an impedance-based particle sensor.

3.2.2. MTT and Hoechst assays

Cell viability in 96 well plates was evaluated for all cell models at 72 h or 96 h incubation, as specified for each experiment. 24 h after seeding the corresponding number of cells for each cell line, medium of each well was replaced with fresh medium with the specified drug concentrations and allowed to incubate until experiment endpoint (72 h or 96 h).

After that, viability of cells exposed to DNA-interacting compounds (platinum-based drugs in **Chapter 2** and **Chapter 3**) was assessed using a variant of the 3-(4,5-dimethylthiazol-2-yl)-2,5-diphenyltetrazolium bromide (MTT) assay reported previously [363]. At experiment endpoint, 1 mg mL⁻¹ MTT in PBS was mixed 1:1 with fresh culture medium and 100 μL of mixture were added to each well. After 1 h incubation at 37°C, supernatant was removed and the formazan product inside cells was quantitatively retrieved and solubilized by the addition of 100 μL of dimethyl sulfoxide (DMSO).

Absorbance was measured at 550 nm on an ELISA plate reader (Tecan Sunrise MR20-301, TECAN, Salzburg, Austria).

Cell viability was alternatively evaluated using Hoechst staining/HO33342 (2'-[4-ethoxyphenyl]-5-[4-methyl-1-piperazinyl]-2,5'-bi-1H-benzimidazole trihydrochloride trihydrate), Sigma Aldrich). HO33342 is a cell-permeable fluorescent probe that dyes DNA, suitable for testing metabolic inhibitors or drugs that affect mitochondrial respiration. At experiment endpoint, culture medium was aspirated, wells were washed with PBS. Then, 100 μ L of a 0.01% SDS solution were added to each well and plates were frozen and stored at -20°C. Upon measure, plates were allowed to thaw and 100 μ L of 4 μ g mL⁻¹ HO33342 dye in stain solution buffer (1 M NaCl, 1 mM EDTA, and 10 mM Tris-HCl pH 7.4) were added to each well. Plates were incubated at 37°C for 1 h with gentle shaking and minimal light exposure. Then, fluorescence was measured in a fluorescence plate reader (FLUOstar OPTIMA Microplate Reader, BMG LABTECH GmbH, Ortenberg, Germany) at 355 nm excitation and 460 nm emission.

For both assays, relative cell viabilities (compared to the absorbance/fluorescence of untreated cells) and concentrations that inhibited cell growth by 50% (IC₅₀) after 72 h or 96 h of treatment were subsequently calculated by sigmoidal fitting with GraphPad Prism 6 software (La Jolla, CA, USA).

3.3. Generation of CRPC and CRC acquired platinum resistant cell models and age-matched controls

Acquired platinum resistant cell models were obtained from PC-3 and SW620 cells by maintaining them under continuous and increasing cisplatin pressure for up to eight months. PC-3 and SW620 cells (passage 15) were cultured either with or without incremental doses of cisplatin. Initial cisplatin dose was the IC₁₀ at 96 h for each cell line, incremented by Δ IC₁₀ upon the observation of substantial cell viability for 3-4 passages. After eight months, we obtained PC-3- and SW620-derived cell models that increased by 10-fold their IC₅₀ to cisplatin and were cross-resistant to oxaliplatin, thus termed

multiplatinum-resistant (PC-3-MPR or SW620-MPR), and their age-matched/old controls (PC-3-O or SW620-O). Cell viability and IC₅₀ progression for the four cell lines were regularly monitored until passage 43-45, when a large stock of cells was frozen and preserved in liquid nitrogen. In all experiments presented in **Chapter 2** and **Chapter 3**, cells from these stocks were used through passages 45 to 60, routine culturing MPR cell lines under the presence of 5.5 μM cisplatin (SW620-MPR) and 1 μM cisplatin (PC-3-MPR).

3.4. Calculation of metabolite consumption or production rates

Consumption or production rates of metabolites throughout this work have been estimated assuming exponential growth throughout the entire experiment, and a constant rate of uptake or release of the metabolite. Accordingly, consumption or production rate (J_i) of a given metabolite i during a time lapse t can be estimated according to the following system of equations:

$$\begin{cases} \frac{dN_t}{dt} = N_t \times \mu \\ \frac{dM_t}{dt} = N_t \times J_i \end{cases} \quad (\text{Eq. 3.1})$$

where N is the number of cells, M is the amount of metabolite i , and μ is the cellular growth rate.

In experimental terms, this was attained by seeding a suitable number of cells to ensure exponential growth at time t in 100 mm or 6-well plates. Cells were allowed to attach for 24 h, and then cell media was removed and wells were washed with PBS. Fresh media, briefly in contact with the cells was collected (M_0) and triplicate wells were harvested and counted (N_0). For cells further incubated for f hours, fresh media for all the different conditions was added in triplicate wells and, at endpoint, media of each well were collected (M_f) and cells counted (N_f).

Using this experimental scheme, consumption or production rates of glucose, lactate, amino acids and different biogenic amines are presented throughout this work.

3.5. Measurement of extracellular metabolites by UV-Vis spectrophotometry

Glucose, lactate, glutamine and glutamate from culture media were determined using a COBAS Mira Plus spectrophotometric auto-analyzer (Horiba ABX, Kyoto, Japan), by monitoring the changes in NAD(P)H absorbance at 340 nm due to specific enzymatic reactions.

Glucose concentration in culture media was measured using a hexokinase (HK)/glucose-6-phosphate dehydrogenase (G6PDH) kit (ABX Pentra Glucose HK CP, HORIBA ABX, Montpellier, France). Lactate concentration was monitored by the lactate dehydrogenase (LDH) reaction, by adding to the reaction mixture 87.7 U/mL LDH and 1.55 mg/mL NAD⁺ in hydrazine-EDTA buffer (0.2 M hydrazine, 12 mM EDTA, pH 9).

Glutamate was measured through its deamination by glutamate dehydrogenase (GLDH) in presence of ADP. Media samples were added to reaction mixtures containing 2.41 mM ADP, 3.9 mM NAD⁺, and 39 U/mL GLDH in glycine/hydrazine buffer (0.5 M glycine, 0.5 M hydrazine, pH 9.0). For glutamine determination, glutamine was quantitatively converted into glutamate through glutaminase reaction and total glutamate concentration (glutamate + glutamine) was measured as described above. To obtain glutamine concentration, glutamate determined in a parallel sample was deducted. The glutaminase reaction was carried out by adding the media sample into a cuvette containing 125 mU mL⁻¹ of GLS in acetate buffer (125 mM, pH 5.0) and incubating the reacting mixture for 30 minutes at 37°C with gentle shaking, followed by an ice quenching of the reaction.

3.6. Measurement of intracellular glutathione

Total intracellular glutathione concentration was determined by spectrophotometry using the chromogen 5,5-Dithiobis(2-nitrobenzoic acid) (DTNB), also known as Ellman's reagent. DTNB reacts with various sulfhydryl groups (-SH), including free and bound cysteine, to yield a yellow product, TNB, detectable at 412 nm. Specific glutathione

determination was achieved by coupling the DTNB reaction to a known excess of glutathione reductase and NADPH, which recycles glutathione oxidized by DTNB into reduced glutathione. Once the glutathione reductase steady-state is reached, the rate of TNB formation is only proportional to total glutathione concentration, determined using a standard curve for each experiment.

Several p6 plates were seeded and, after 24 hours, fresh medium with or without drug (1 μ M cisplatin for PC-3-MPR and 5.5 μ M for cisplatin for SW620-MPR) was added and then incubated for 2, 6, 12, 24, 30, 48 and 72 hours. At each time point, the cells were harvested, resuspended in 1 mL of PBS and counted. The remaining cell pellet was frozen in liquid nitrogen and stored at -80°C until analysis. Pellets were thawed and resuspended with a 5% SSA solution, then subjected to two cycles of liquid nitrogen freezing and thawing (in a warm bath at 37°C), which released cytoplasmic contents. After 10 minutes at 4°C , cell extracts were centrifuged at 10000 g for 10 minutes and supernatant containing intracellular glutathione was collected. Results were normalized by protein content determined by the BCA method. Moreover, the supernatant volume was to be measured as well. The necessary dilutions of the supernatant were performed with phosphate buffer and then 10 μ L of sample were loaded by duplicates in a 96-well plate, as well as 150 μ L of working mixture (262 μ L DTNB from 1.5 mg/mL stock, 9.2 mL of phosphate buffer and 262 μ L of enzymatic solution, which consisted of 9.7 μ L of glutathione reductase and 280 μ L of phosphate buffer). Finally, 50 μ L of NADPH solution (at 0.16 mg/mL) were added to each well and the 96-well plate was processed with a spectrophotometer (reading at a wavelength of 492 nm). Raw data was treated using Excel software and normalized for cell number, which had been obtained beforehand.

3.7. Metabolite consumptions, productions and intracellular pools by LC-MS/MS and FIA-MS/MS

Excluding the ones mentioned in Sections 3.5 and 3.6, all other metabolites were determined by liquid chromatography tandem-mass spectrometry (LC-MS/MS) or flow injection analysis-tandem mass spectrometry (FIA-MS/MS), using SCIEX 4000 QTRAP

and SCIEX 6500 QTRAP mass spectrometers (SCIEX, Toronto, Canada) ⁱⁱ. All determinations were performed using AbsoluteIDQ[®] p180 (Biocrates Life Sciences AG, Innsbruck, Austria), a targeted metabolomics tool that includes internal standards and standard curves for up to 180 metabolites including hexoses, amino acids, biogenic amines, acyl-carnitines, glycerophospholipids and sphingolipids.

Concentrations for metabolites were determined using the MetIDQ[™] software package, which is an integral part of the AbsoluteIDQ[®] kit. The obtained metabolite concentrations were corrected considering the loaded volume of sample. Results for intracellular metabolites were normalized by protein content when comparing isogenic cell lines or median of amino acids in each sample when comparing non-isogenic cell lines. Results for consumption and production rates were normalized by time and cell number for metabolites in culture media as described in 3.5.

3.7.1. Determination of metabolites in cell pellets

For sample acquisition and processing, triplicates of 5 million cells were trypsinized and washed twice with ice-cold PBS prior to snap-freezing in liquid nitrogen. Cell pellets were stored at -80°C until measure. Right before measuring, cell pellets were thawed at room temperature and resuspended in 70 µL of 85:15 EtOH:PBS solution. Cells were disrupted by two sonication/freezing/defreezing cycles using a titanium probe (VibraCell, Sonics & Materials Inc., Tune: 50, Output: 25), liquid N₂ and a 95°C heat block. Cell lysates were then centrifuged at 20.000 rcf for 5 minutes at 4°C. Supernatants were collected into new tubes and total protein content was determined by Bicinchoninic acid (BCA) assay (Thermo Fisher Scientific, Waltham, MA USA).

Then, standards, internal standards, quality controls (10 µL of each), and up to 50 µL of the samples were loaded into LC and FIA Biocrates plates, which were then processed

ⁱⁱ Determination of both intracellular pools and extracellular exchange flux rates of the CRPC panel (PC-3M, PC-3S, PC-3, DU-145, NCI-H660, and P4E6, **Chapter 1**) were performed in SCIEX 4000 QTRAP. Determination of intracellular pools and extracellular exchange flux rates of PC-3M and PC-3S ctrl vs. arginine or glutamine deprivations (**Chapter 1**), and prostate (PC-3) and colorectal (SW620) long-term platinum resistance studies (**Chapter 2**), were performed in SCIEX 6500 QTRAP.

according to manufacturer instructions, and measured in LC-MC/MS and FIA-MS/MS, respectively.

3.7.2. Determination of metabolites in culture media

For metabolite consumptions and productions in cell culture media, cells were seeded in 6-well plates, incubated for the specified amount of time for each experiment, and initial and final numbers of cells were determined in triplicates for each condition. Initial medium, briefly in contact with cells, and final medium, were collected and stored at -80°C until measure.

Then, standards, internal standards, quality controls (10 µL of each), and up to 50 µL of the samples were loaded into LC and FIA Biocrates plates, which were then processed according to manufacturer instructions, and measured in LC-MC/MS and FIA-MS/MS, respectively.

3.7.3. Seahorse XF Analyzer

The Seahorse XFe96 Analyzer (Agilent Seahorse Bioscience, Santa Clara, CA, USA) is capable of measuring oxygen consumption rate (OCR) and extracellular acidification rate (ECAR) of living cells in a 96-well plate in a real-time manner. A sensor with oxygen- and pH-sensitive fluorophores is placed above the cell monolayer, creating a microchamber that allows the analyzer to determine OCR and ECAR in response to the addition of drugs, inhibitor or substrates.

For a Seahorse assay, the day before the experiment a 96-well plate was seeded, and it was allowed to rest for 1h in the hood to ensure an even seeding (crucial to reduce noise during measurements) before incubating at 37°C and 5% CO₂ for 24h. The sensor cartridge was hydrated overnight with XF Calibrant. The day of the experiment, culture media was replaced by Seahorse media (buffer-free DMEM, Sigma-Aldrich) supplemented as needed for a final volume of 180 µL, and the plate was equilibrated in a non-CO₂ 37°C incubator for 1h. Sensor cartridge ports were loaded with the required compound 10x solutions in volumes of 20, 22, 25 and 27 µL, for then load the cartridge into the analyzer to calibrate the sensors for 15'. Finally, the cell plate was loaded to run the assay.

3.8. Enzyme activities under crowded media

3.8.1. Lactate dehydrogenase

Chemicals

Rabbit muscle L-Lactate Dehydrogenase (E.C. 1.1.1.27) ($140 \text{ U}\cdot\text{mg}^{-1}$), received as a purified and lyophilized powder, sodium pyruvate and β -NADH were acquired from Sigma-Aldrich Chemical (Milwaukee, WI, USA). Four Dextrans (Fluka) of 410, 275, 150 and 50 molecular weight were used without further purification. All the chemicals were of analytical or spectroscopic reagent grade.

LDH reaction under crowded media

The oxidation of NADH was made at 25°C in Imidazole-Acetic Acid buffer (30 mM, pH = 7.5, containing 60 mM of CH_3COOK and 30 mM of MgCl_2). Each sample contains the same concentration of $8.2\cdot 10^{-13}$ M of LDH and $1.17\cdot 10^{-4}$ M of NADH. Michaelis-Menten plots were obtained by measuring initial velocity of the reaction at different pyruvate concentrations, in a range between $7.1\cdot 10^{-5}$ and $5.4\cdot 10^{-4}$ M. This process was first done without the addition of crowding agent. After the incorporation and homogenization of the enzyme into a sample, which contains NADH and pyruvate, the reaction was started.

Subsequently, we dissolved into the same sample mixture different Dextran concentrations (25, 50 and 100 mg/mL) for each Dextran size mentioned above: 410, 275, 150 and 50 kDa, which will be referred as D410, D275, D150 and D50, respectively.

The reaction progress and the data analysis were described in detail in Pastor et al. Briefly, in this case we follow the reaction by the absorbance change that occurs as NADH is oxidized into NAD^+ , which no longer absorbs at 320 nm. Initial reaction velocity, v_0 , was obtained by linear fitting of the initial data points in the absorbance-time plot. Blank solution containing substrate and Dextran in the same concentrations than the sample was measured in each case.

3.8.2. Glutamate dehydrogenase

Chemicals

Bovine liver Glutamate dehydrogenase, type II (EC 1.4.1.3, $M_w=310-350$ kDa in hexameric form) was received already purified and in an aqueous glycerol solution form. The enzyme, L-Glutamic acid and β -Nicotinamide adenine dinucleotide in its oxidised form (NAD⁺) were purchased from Sigma-Aldrich Chemical (Milwaukee, WI, USA). Dextrans with 60, 250 and 500 kDa were acquired from Pharmacosmos (Hoelbrak, Denmark) and used without any further purification. The buffer solution was prepared by diluting a phosphate buffer solution 1M purchased from Sigma-Aldrich Chemical (Milwaukee, WI, USA). All chemicals were of analytical or spectroscopic reagent grade.

Oxidation of L-Glutamate

Spectrophotometric measurements were carried out at 25°C in a 0.01 M phosphate buffer adjusted to pH=7 to enhance enzyme stability (Engel 2011). Each sample contained a constant concentration of L-Glutamate (5 mM), which is in excess to consider the reaction as monosubstrate, and enzyme (0.18 μ M; 1.3 μ g/ml). At protein concentrations below 0.1 mg/ml, the enzyme only exists in the hexameric form. Different NAD⁺ concentrations in a range between 0.1 and 2 mM were used.

Experiments were performed in dilute solution conditions and in crowded conditions by adding increasing concentrations (25-150 g·L⁻¹) of Dextran with 60, 250 and 500 kDa sizes. An increase in absorbance caused by the formation of NADH was measured at 340 nm with a Shimadzu UV-1800 spectrophotometer. The initial reaction rate, v_o , was obtained by linear fitting of first data points in the absorbance-time plot (5-25 seconds). This data was fitted to the proposed models.

Although the oxidative deamination of L-glutamate is a fast reaction, experiments were performed by manual mixing of the reactants. However, some experiments were performed with a stopped-flow system^[36] coupled to the spectrophotometer, which is a rapid mixing device to study fast reactions in solution. Both methods yield to identical results and therefore manual mixing was used to reduce wasting reagents.

Each measurement was repeated at least three times to minimize error and ensure reproducibility. The enzyme activity was controlled by absorbance at 270 nm every day and by measuring a control mixture twice a week.

Data treatment

In order to obtain the initial velocities, the linear section in the absorbance-time plot was selected (5-25 seconds) using Origin 7.0. The slope of that section, dividing among the molar absorptivity (ϵ) of NADH ($6220 \text{ M}^{-1}\text{cm}^{-1}$) and multiplying by the optical path (1 cm), is the initial velocity of the reaction. This data was fitted to the different proposed models using a least square adjustment with GNU Octave.

3.9. Spheroid formation assay

Spheroid formation was evaluated by seeding 10^3 cells in ultra-low attachment 24-well plates in 1 mL of serum-free medium supplemented with the following: 20 ng mL^{-1} EGF, 20 ng mL^{-1} bFGF, $10 \text{ }\mu\text{g mL}^{-1}$ heparine, 1:50 B27 Neuron culture system, $5 \text{ }\mu\text{g mL}^{-1}$ insulin and $0.5 \text{ }\mu\text{g mL}^{-1}$ hydrocortisone. Special media formulations (i.e. amino acid deprivation or addition of chemical compounds) as specified in each experiment were applied simultaneous to cell seeding. Cells were incubated at 37°C and 5% CO_2 for 7 days. After that, spheroids were incubated with 5 mg mL^{-1} MTT for 2-3 h, plates were scanned and spheroid formation was quantified with ImageJ software (National Institutes of Health, USA, <http://rsbweb.nih.gov/ij/>).

3.10. Colony formation assay

Colony formation assay was evaluated by seeding cells at low densities to promote proliferation of single cells through clonal expansion, denoting tumorigenic and self-renewal potential. Cells were cultured in 6-well (10^3 cells/well) or 24-well (250 cells/well) plates under the conditions specified in each experiment and incubated for a seven days. The same number of cells was seeded regardless of proliferation rate. Then, media was removed, wells were washed once with PBS and were incubated with 0.5 mL of ice-cold methanol for 15 minutes. Then, methanol was removed, and cells were incubated for 20 minutes with 1 mL of crystal violet at 0.05%. Finally, wells were thoroughly washed with water and plates were scanned afterwards. *ImageJ* software was used to analyze and quantify the number of colonies, setting a size threshold for colonies greater than 0.3 mm.

3.11. Wound healing assay

Invasive and migratory capacity was evaluated as the closure rate of a rectangular gap in a confluent and synchronized culture. Cells were seeded at confluency in p24 plates in full growth media. After 24 hours, cells were incubated with serum-free media for 24 h to ensure the arrest of proliferation. The next day, media was removed, wells were washed with PBS and a scratch on the middle of the surface of the well was performed using a pipette tip. Then, FBS-containing media was added. Photographs of the cell-free gap were taken with 40x objective lens at 0 h, 3 h, 6 h and 24 h from the scratch. Distance between cell front lines were measured with *ImageJ* software.

3.12. Cell cycle analysis by flow cytometry

Cell cycle was assessed by flow cytometry using a fluorescence activated cell sorter (FACS). For this assay, cells were seeded in 6 well plates with 2 mL of growth medium. After 24 h of incubation, compounds added at their IC₅₀ values, respectively. Following 72 h of incubation, cells were harvested by mild trypsinization, collected by centrifugation and fixed in 70% ethanol and stored at -20°C until measure. Right before measuring, fixed cells were incubated with phosphate buffer solution (PBS) containing 50 mg mL⁻¹ PI and 10 mg mL⁻¹ DNase-free RNase. The cell suspension was incubated for 1 h at room temperature to allow for the staining of the cells with the PI, and afterwards FACS analysis was carried out at 488 nm by employing a *CyAn* flow cytometer (Beckman Coulter, Brea, CA, US). Data from 1 × 10⁴ cells were collected and analyzed using the *FlowJo* software (BD Biosciences, Franklin Lakes, NJ, US).

3.13. Apoptosis analysis by flow cytometry

Relative quantification of healthy, early apoptotic and apoptotic/necrotic fractions of cells under different perturbations or chemical compounds was performed by FACS, by simultaneous labelling of the cells with fluorescein-annexin V (AV-FITC, annexin V-fluorescein isothiocyanate) and propidium iodide [364].

Annexin V-FITC is a fluorescent probe used to detect early apoptotic cells since it binds to phosphatidylserine (PS) residues on the outer membrane of the cell, process that only occurs as one of the initial steps of the apoptotic program [365]. On the other hand, propidium iodide is a fluorescent probe that binds to DNA and is able to stain all cells. However, the signal of the late apoptotic/necrotic cell population is much more intense than the one of alive or early apoptotic cells, since cell membrane integrity is lost at late stages of both cell death programs and larger amounts of PI can permeate the cell membrane. Flow cytometry analysis of cells stained with both probes allows us to relatively quantify three cell populations: alive cells (low PI/low annexin-V), early apoptotic cells (low PI/high annexin-V) and late apoptotic/necrotic cells (high PI).

3.14. ROS analysis by flow cytometry

ROS levels were estimated by flow cytometry using 2',7'-Dichlorofluorescein diacetate (H₂DCFDA, Invitrogen, Carlsbad, CA, US), a general oxidative stress fluorescent probe. Cells were incubated in triplicates for 24, 48 or 72 hours in the presence or absence of the drug at the IC-50 dose. Then, complete medium was replaced by incubation buffer (5,5 mM glucose in PBS containing 5 μ M H₂DCFDA) for 30 minutes at 37°C and 5% CO₂. Afterwards, cells were allowed to recover in complete growth media for 1 hour at 37°C and 5% CO₂. In this manner, acetate groups in H₂DCFDA are hydrolyzed by intracellular esterases and reactive oxygen species within the cell are able to oxidize the probe, thus releasing its fluorescent form: 2',7'-Dichlorofluorescein (DCF). Finally, cells were trypsinized and collected in a 50 μ M H₂DCFDA and 20 μ g/mL PI solution in PBS. Fluorescence of the samples was readily measured in *Cyan ADP* or *Gallios* (Beckman Coulter, Brea, CA, US) using an excitation wavelength of 492 nm, and recording the mean fluorescence intensity of 10⁴ alive cells (PI⁻) emitted at 520 nm. A negative control, incubated without the probe, was included to discard other sources of fluorescence from either cells or drugs.

3.15. Western blot

To analyze protein levels of the cells, confluent p100 plates were aspirated, wash with PBS and lysis buffer (150 mM NaCl, 1% Triton X-100, 0.5% sodium deoxycholate, 0.1% SDS and 50 mM Tris pH 8.0) was added to each plate. Plates were incubated at 4°C for 20 minutes. After that, they were scrapped thoroughly and then sonicated with a titanium probe for three separate five-second cycles. Cells were centrifuged at 12000 g for 20 min at 4°C. The pellet was discarded afterwards, and the supernatant was stored for analysis. Both stacking and separating polyacrylamide gels were polymerized beforehand and mounted. Protein extracts were measured by the Bicinchoninic acid (BCA) assay (Thermo Fisher Scientific, Waltham, MA USA) to determine the protein content. Equal amounts of protein were added to the corresponding wells of the gel. SDS-PAGE was allowed to run for the necessary amount of time. When ready, proteins were transferred onto a nitro-cellulose membrane. Membranes were cut in small pieces for the assessment of proteins of different molecular weights, blocked with powder milk in PBS-Tween 0.1% and incubated with the appropriate primary antibody overnight. After three 10-minute cycles of PBS-Tween washing. Then, membranes were treated with the appropriate secondary antibody for 1 h at room temperature. All blots were detected using with Immobilon ECL Western Blotting Detection Kit Reagent (EMD Millipore, Billerica, MA, USA) and developed after exposure to an autoradiography film. The primary antibodies used were PDH (ab110330), GLS1 (ab93434), MYC (ab32072), from Abcam; P-PDH (ABS204) from Millipore (EMD Millipore); GAC (19958-1-AP) and KGA (20170-1-AP) from Proteintech (Chicago, IL, USA); GDH (GTX105765) from Tebu-Bio (Le-Perray- en-Yvelines, France) and β -actin (#69100) form MP Biomedicals (Santa Ana, CA, USA). The secondary antibodies used were anti-mouse (PO260) from Dako (Glostrup, Denmark), anti-rabbit (NA934V) from Amersham Biosciences (GE Healthcare, Little Chalfont, UK) and anti-goat (sc-2020) from Santa Cruz Biotechnology.

3.16. Statistical analysis

For comparison between mean values of two conditions, we employed t-Student test with $\alpha=0.05$ either assuming equal or unequal variances (variance equality hypothesis was evaluated using an F-test with $\alpha=0.05$). Significance in t-Student test is denoted by the following criteria: NS (non-significant), * ($p<0.05$), ** ($p<0.01$) and *** ($p<0.001$).

For determinations of metabolite consumptions/productions, significance between initial and final metabolite concentrations were evaluated using a t-Student test with $\alpha=0.05$ (previously testing the variance equality hypothesis by F-test $\alpha=0.05$). If the condition of significant consumption/production is met, comparison between cell lines/conditions was performed by two-sided ANOVA and Tukey's multiple comparison testing. Cell lines/conditions sharing the same letter indicates absence of significant differences between them.

Intracellular metabolite pools were normalized by the median of all the amino acids as described previously [366] and comparison between cell lines was performed by one-way ANOVA and Tukey's multiple comparison testing. Cell lines/conditions sharing the same letter indicates absence of significant differences between them.

When ratios of paired empirical measurements are shown, the associated error is calculated as the standard deviation of the ratio for each pair. On the opposite, when ratios of unpaired empirical measurements are shown ($Y=X_1/X_2$), the associated error is propagated as indicated by Eq. 1.

$$\Delta Y = Y \sqrt{\left(\frac{\Delta X_1}{X_1}\right)^2 + \left(\frac{\Delta X_2}{X_2}\right)^2} \quad (1)$$

All calculations and statistical analyses were performed using *Microsoft Excel*, *Origin 7.5* and *GraphPad 6* software.

4. Results and discussion

4. Results and discussion

4.1. Chapter 1: Identification of the metabolic signature of metastatic CRPC

4.1.1. Introduction

Achieving therapeutic control over metastatic spread is the main challenge that urges to be faced to reach complete survival and curation of prostate cancer (PCa). As previously mentioned, even if survival rates of primary PCa patients are relatively high, the mortality rates associated with metastatic PCa are almost 100% [321].

In **this Chapter**, we aim to identify novel metabolic vulnerabilities with potential therapeutic value for metastatic PCa in a representative CRPC panel and two isogenic subpopulations of the metastatic CRPC cell line PC-3. These two isogenic cell lines, PC-3M and PC-3S, represent a unique model to study the interlace between metabolism and the EMT and CSC transcriptional and epigenetic programs: PC-3M was obtained from a metastatic lesion of PC-3 cells xenografted in mice, and PC-3S was obtained from serial enrichment of PC-3 cells in an invasion chamber [175].

In this regard, a thorough phenotypic characterization in terms of EMT and CSC programs previously conducted in our group and collaborators delimited two opposed phenotypes for the two PC-3 subpopulations: PC-3M is highly proliferative, tumorigenic and exhibits traits of having undergone MET; whereas PC-3S displays lower proliferation capacity than parental PC-3, weak tumorigenic capacity, yet high invasivity and an enrichment in mesenchymal traits [175]. Indeed, PC-3M and PC-3S represent one of the few available isogenic models to study metastatic epithelial CSC (e-CSCs) as opposed to non-CSC expressing a stable EMT program [73], thus uncoupling both phenotypic programs.

In terms of metabolism, PC-3M and PC-3S are also radically opposed according to previous studies conducted in our group. PC-3M displays a marked Warburg effect,

partially fueled by a higher glycolytic flux, higher LDH activity, and the inactivation by phosphorylation of PDH; a marked addiction to glutaminolysis and a higher contribution of glutamine to the replenishment of TCA cycle intermediate pools. Further details of the previous metabolic characterization of PC-3M and PC-3S conducted in our group can be found in Aguilar et al. [73].

Bearing this starting point in mind, we aimed to further characterize these two cell models in order to encounter therapeutic options that can selectively target the highly aggressive e-CSC subpopulation (PC-3M), since it is well-established that e-CSC phenotypes play a crucial role in the establishment of proliferating macrometastases and tumor remission after chemotherapy [10,172,221].

Our study will also include a cell panel of other CRPC cell lines with different degrees of metastatic potential, ranging from highly metastatic to non-aggressive early-stage primary tumor. By doing so, we aim to: I) extrapolate and validate previously-identified vulnerabilities of the e-CSC subpopulation PC-3M to a panel of CRPC cell lines, and II) identify new metabolic vulnerabilities tied to metastasis that are unveiled after the simultaneous metabolic characterization of all cell lines of the CRPC panel with different metastatic potentials.

The CRPC panel will include, besides PC-3M and PC-3S, three CRPC cell lines of different metastatic origin: parental PC-3 (bone metastasis), DU-145 (brain metastasis), and NCI-H660 (lymph node metastasis). Finally, we will also explore the metabolism of the prostate primary tumor cell line P4E6 as opposed to all the metastatic CRPC cell lines.

It is worth noting that among the cell lines of metastatic origin, PC-3 and DU-145 belong to the prostate adenocarcinoma subset, whereas NCI-H660 is a cell model for neuroendocrine prostate cancer (NEPC) [350]. As described in detail in the introductory section, NEPC is a subset of PCa that is characterized by exhibiting small cell (SC) phenotype, being relatively quiescent and displaying a particular marker profile that includes a complete absence of AR or PSA expression and production of chromogranin A, synaptophysin and NSE [328,367]. The addition to our panel of a metastatic PCa cell line that is significantly distinct to PCa adenocarcinoma will serve the purpose of

assessing if the identified adaptations and vulnerabilities of metastatic cell lines can be generally valid for distinct PCa subsets.

On the other hand, the primary tumor cell line P4E6 was obtained from an early-stage adenocarcinoma with a Gleason index of 4 [351]. This cell line can be considered as one of the very few available cell models of primary PCa. Despite being obtained from an early stage adenocarcinoma, P4E6 is androgen insensitive, representing a perfect model to uncouple metastatic progression from castration resistance. Indeed, restricting our cell panel to only CRPC cell lines, both metastatic and primary tumor, avoids the undesired masking of the obtained results by the central role that androgen signaling plays in PCa metabolism [130,150,322].

4.1.2. Results and discussion

4.1.2.1. Proliferation, EMT, and stem cell traits are uncoupled in CRPC

We first characterized all the CRPC cell lines in terms of their basic phenotype, attempting to gather readouts that allow us to stratify the different cell lines in terms of cell proliferation and metastatic potential.

In terms of cell proliferation (**4.1.1.AB**), we encountered that PC-3M proliferated at higher rates than the rest of cell lines with a doubling time of around 20 hours, followed by PC-3 and DU-145, with doubling times of around 24 hours. PC-3S and P4E6 proliferated at significantly lower rates, exhibiting doubling times of around 40 hours. Finally, NCI-H660 was more quiescent than the rest of the cell lines, with a doubling time of around 100 hours. In terms of size, all adenocarcinoma cell lines displayed similar cell volumes of around 2.5 to 3 pL, whereas NCI-H660 was significantly smaller, with a cell volume of around 1 pL (**4.1.1.C**). Indeed, the significantly smaller and much less proliferative phenotype of NCI-H660 compared to all PCa adenocarcinoma cell lines is expectable according to previous evidence of neuroendocrine PCa traits [327,368].

According to the current paradigm of the invasion-metastasis cascade, cells that harbor the potential to establish macrometastases and proliferate at secondary niches simultaneously display epithelial and CSC characteristics, and are commonly termed as

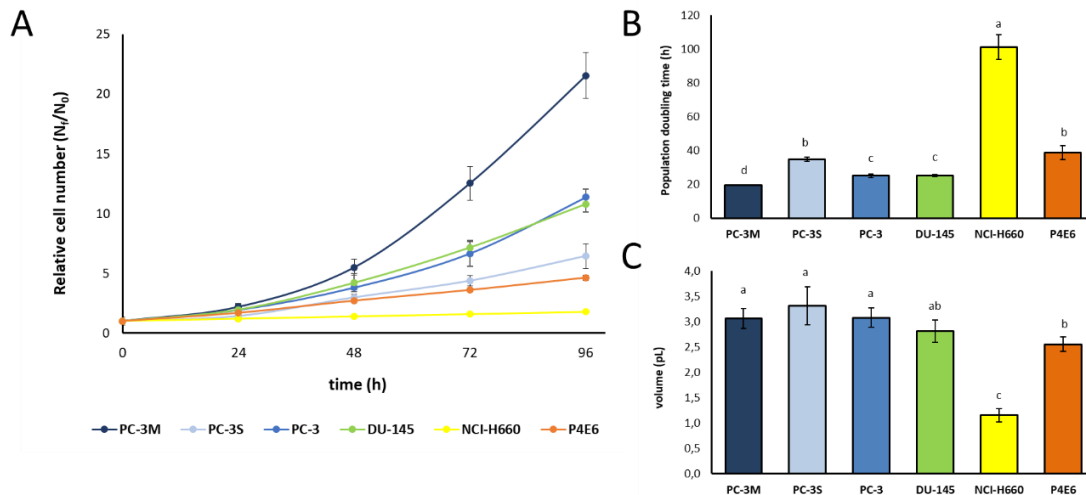


Figure 4.1.1. Comparative cell proliferation, population doubling time and cell volume of CRPC cell panel (A) Growth curves up to 96 h of PC-3M, PC-3S, PC-3, DU-145, NCI-H660, and P4E6 grown in their full media (See Methods 3.1). Proliferation is expressed as the relative cell number N_t/N_0 , where N_t and N_0 are the final and the initial number of cells, respectively. (B) Population doubling time of the CRPC panel under exponential growth phase. (C) Cell volume (pL) measured using a *Scepter* Handheld Automated Cell Counter (Merck Millipore, Billerica, MA, USA). Bars represent mean \pm SD of $n=3$. Cell lines/conditions sharing the same letter indicates absence of significant differences between them (One-way ANOVA and Tukey's multiple comparison test with $\alpha=0.05$).

e-CSCs, which is the phenotype previously ascribed to the PC-3M model [175]. We next attempted to evaluate all CRPC cell lines in these terms, by assessing the spheroid formation capacity (4.1.2.AB) and the expression of several EMT and CSC regulators and effectors (4.1.2.C) in all the cell lines.

We encountered that PC-3M and DU-145 had a markedly increased spheroid-forming capacity than the rest of the cell lines (4.1.2.AB), whereas the early-stage primary tumor P4E6 displayed the lowest. Spheroid growth is a functional assay indicative of the capacity to grow in an anchorage-independent manner, which is tied to cell plasticity, CSC traits, and the tumor initiation potential of cancer cells [369,370]. However, a certain controversy exists on the interpretation of this kind of assay, as it has also been shown that spheroid growth involves the necessary formation of adherens junctions (AJ) mediated by E-cadherin in CRC and that cells that are excluded from spheroids present increased migratory and invasive properties [371]. Either case, spheroid formation represents a highly suitable readout to identify e-CSC phenotypes, since these cells would fulfill both alternative requirements: epithelial and CSC traits, and are thus expected to be the highest spheroid-forming phenotypes.

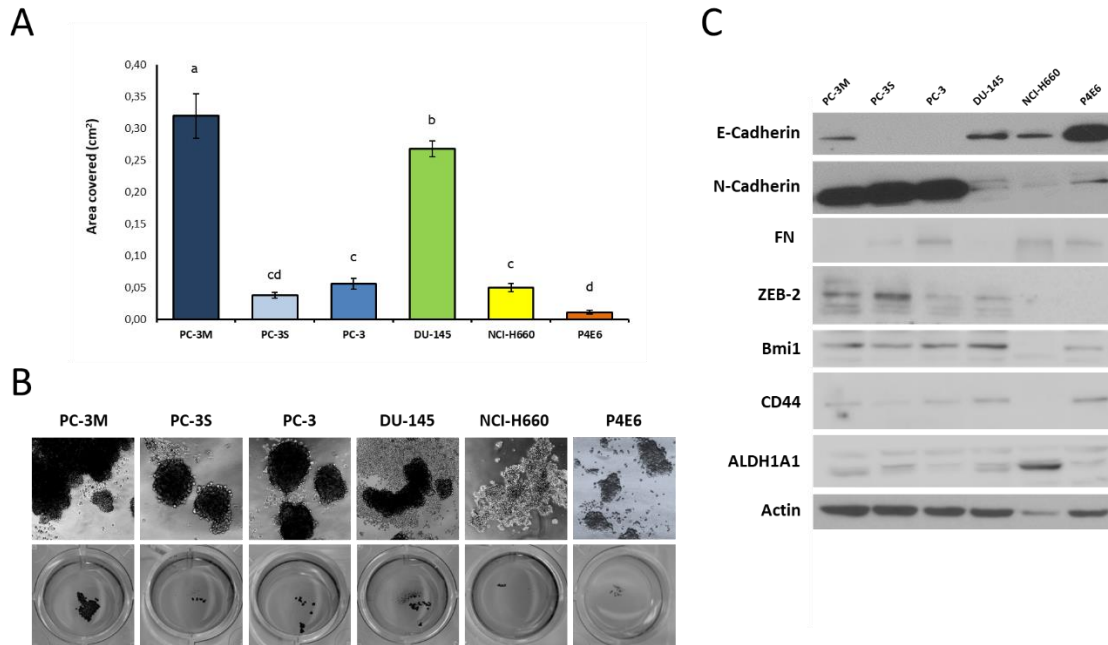


Figure 4.1.2. Characterization of the metastatic phenotype of the CRPC panel. (A) Spheroid formation capacity of CRPC cell lines, assessed by seeding 10^3 cells in ultra-low-attachment plates. Spheroid plates were scanned after 7 days and quantified using *Image J*. (B) Bright-field images (40x) and scans of spheroids in p24 well plates. (C) Protein levels of different EMT and CSC markers and effectors determined by Western Blot. Actin was used as a protein loading control. Results shown are the mean \pm SD from $n=4$. Cell lines sharing the same letter indicates absence of significant differences between them (One-way ANOVA and Tukey's multiple comparison test with $\alpha=0.05$).

Concerning the EMT status, the most widespread and reliable readouts for the identification of epithelial or mesenchymal phenotypes are the expression levels of E-cadherin and N-cadherin, respectively. As explained throughout the introductory section of this dissertation, this “cadherin switch” is a major phenotype-driving event during the EMT [179]. We found that PC-3 and PC-3-derived cell lines expressed significantly higher levels of N-cadherin than the rest of CRPC cell lines, with a slight decrease in the PC-3M subpopulation. On the contrary, among PC-3-derived cell lines, E-cadherin expression was only detected in PC-3M. Both observations are consistent with the previous evidence indicating that PC-3M cells have undergone a partial MET relative to parental PC-3 [175,372]. Similarly, PC-3S displayed the highest ZEB-2 levels, potentially denoting an enrichment in mesenchymal features relative to PC-3.

P4E6 presented the highest E-cadherin expression in the CRPC panel, which supports the notion that this cell line was derived from an early-stage PCa [351], which has evolved to a lesser extent than metastatic cell lines from the normal prostate epithelium.

Finally, the other two metastatic cell lines, DU-145 and NCI-H660, can also be considered as more epithelial than PC-3-derived cell lines, due to the higher E-cadherin expression and the barely detectable N-cadherin expression.

We also analyzed the expression levels of three CSC markers that have been previously reported as relevant for PCa: Bmi1 [208], CD44 [208], and ALDH1A1 [200] (**4.1.2.C**). Our observations denote that, besides a high spheroid formation capacity, both PC-3M and DU-145 also exhibited higher expression of the transcription factor Bmi1, which encodes for a wide variety of targets related to the CSC phenotype [195,206,373].

Among our CRPC panel, the highest Bmi1 expression was found in DU-145, followed by PC-3M, PC-3, and, to a lesser extent, PC-3S. On the contrary, highly epithelial primary tumor P4E6 exhibited lower Bmi1 expression, according to its low capacity to grow in an anchorage-independent manner. Indeed, Bmi1 has also been reported to repress E-cadherin expression along with Twist1 [181]. Possibly, low Bmi1 levels contribute to a marked E-cadherin expression in the P4E6 cell line. However, Bmi1 expression does not totally correlate with E-cadherin expression in the rest of the cell lines, suggesting that the Bmi1-Twist axis may not be dominant in governing E-cadherin expression in CRPC.

Regarding CD44, the highest expression was found in DU-145 and P4E6, only modestly different to PC-3 and its subpopulations PC-3M and PC-3S, whereas it was absent in NCI-H660. Previous works isolating CSC subpopulations of PC-3 had demonstrated that CD44 does not allow to distinguish between CSC and non-CSC PC-3 subpopulations [374]. In partial consonance, a xenograft study including DU-145 and other PCa cell lines suggested that CD44⁺ cells may be either CSCs or the next hierarchical differentiation step, progenitor cells [375]. Apart from that, the CD44 splicing isoform analyzed in our work was CD44v, previously correlated in the literature to strongly epithelial phenotypes in PCa, rather than purely of CSC traits [376]. In support of this, CD44 plays a crucial role in the formation of AJ and the maintenance of the apicobasal epithelial polarity [377]. Consequently, according to E-cadherin and CD44v expression, we could consider DU-145 and P4E6 as the two purely epithelial CRPC cell lines, whereas PC-3M could be described as displaying a partial EMT program, due to retention of N-cadherin expression only mildly lower to PC-3 and PC-3S.

Despite exhibiting lower expression levels of Bmi1 and CD44, NCI-H660 exhibited the highest ALDH1A1 expression. ALDH1A1 is considered a self-renewal and differentiation marker, as it is responsible for retinoic acid synthesis [200]. Retinoic signaling has been linked to the differentiation process in healthy stem cell populations and also found to be relevant in CSCs [199], particularly in prostate cancer [200]. We found that all CRPC cell lines were at least weakly positive for ALDH1A1, consistent with the existence of a scarce pool of CSCs in all of them. However, our observations suggest that the neuroendocrine cell line NCI-H660 is significantly enriched in this CSC marker.

In this regard, a remarkable volume of evidence suggests that ALDH1A1 expression correlates specifically with lymph node metastasis, rather than with neuroendocrine phenotypes or stemness in a plethora of malignancies: ALDH1A1 expression is also correlated with lymph node metastasis in CRC [378–380], breast cancer [381,382] and lung cancer [383]. As mentioned previously, NCI-H660 is also the only cell line in our panel that was isolated from a lymph node metastatic lesion of prostatic origin, which contributes to stimulate the hypothesis that ALDH1A1 could have potential specific predictive value for lymph node metastasis formation regardless of primary tumor site, which, to our knowledge, has not been established previously. Moreover, NCI-H660 displays a lower expression of other CSC markers (Bmi1 and CD44) than other CRPC cell lines, reinforcing the hypothesis that ALDH1A1 overexpression is not purely indicative of CSC enrichment in this cell model. On the contrary, low expression of CD44 in NCI-H660 is in disagreement with previous evidence that reports NEPC tumors were strongly positive for CD44 [326,384], even if, as specified earlier, only the epithelial phenotype-linked CD44v splicing isoform is monitored in our results.

In conclusion, considering both the spheroid formation and western blot results, we can conclude that in the case of our CRPC panel, spheroid formation capacity is indicative of both CSC-enrichment and epithelial features, consistent with previous results regarding PC-3M and termed previously as e-CSC [175,385]. In our case, we found that CRPC cell lines that displayed enhanced spheroid formation capacity are the only ones that can be simultaneously classified according to western blot analysis as CSC-enriched and exhibiting epithelial traits: PC-3M, in accordance with our previous results [175,385], and also DU-145. In this regard, the low capacity to form spheroids of the primary tumor

cell line P4E6, even displaying the most unambiguous epithelial phenotype, contributes to the idea that spheroid formation cannot be interpreted as mere epithelial phenotype [371], but rather to tumor initiation and metastatic capacity [369,370]. In support of this, both PC-3M [175] and DU-145 [386,387] have been previously reported as highly tumorigenic and able to initiate metastases in different organs upon xenotransplantation in mice.

Considering that the cell models included in our CRPC panel exhibited markedly different proliferation rates, we cannot ignore that the result of this assay could be masked by differential proliferation. If this was the case, an underestimation of the spheroid formation capacity of the relatively quiescent cell line NCI-H660 should not be ruled out. Nevertheless, other authors have previously reported the detailed characterization of the inability to form spheroids of this cell line [372], which supports our interpretation of the obtained results. Moreover, our observations underline that neither proliferation nor cell volume of CRPC correlate with metastatic progression. Indeed, both readouts in P4E6 early-stage primary tumor are similar to the average of cell lines obtained from metastatic sites.

Finally, our results also indicate that the abovementioned highly metastatic e-CSC phenotype can only be attributed to PC-3M and DU-145, according to the simultaneous observations of increased spheroid formation capacity, Bmi1 expression, a robust epithelial program, and previous evidence of a high tumorigenic potential in mice [175,386,387].

4.1.2.2. Metastatic prostate CSCs display enhanced glutamine avidity and their proliferation and tumorigenic capacity can be suppressed through glutamine deprivation

After assigning distinct metastatic potentials to all the cell lines in the panel, our ultimate goal in **this Chapter** was the correlation of specific metabolic features to this readout, and the identification of metabolic vulnerabilities that allow us to selectively target the highly aggressive e-CSC tumor subpopulations. We first pursued this goal by characterizing two major sources of carbon and energy in cancer cells, glucose and glutamine, since they represent important metabolic carbon and energy hubs. Hence,

encountering alterations in any of the two necessarily involves a major reprogramming of metabolic pathways that can provide us invaluable clues and guidance towards our aim of finding e-CSC-associated metabolic vulnerabilities.

First, we analyzed the consumption rates of glucose and glutamine, and the subsequent secretion rates of their product metabolites, lactate and glutamate, respectively (4.1.3), in all the cell lines of the CRPC panel.

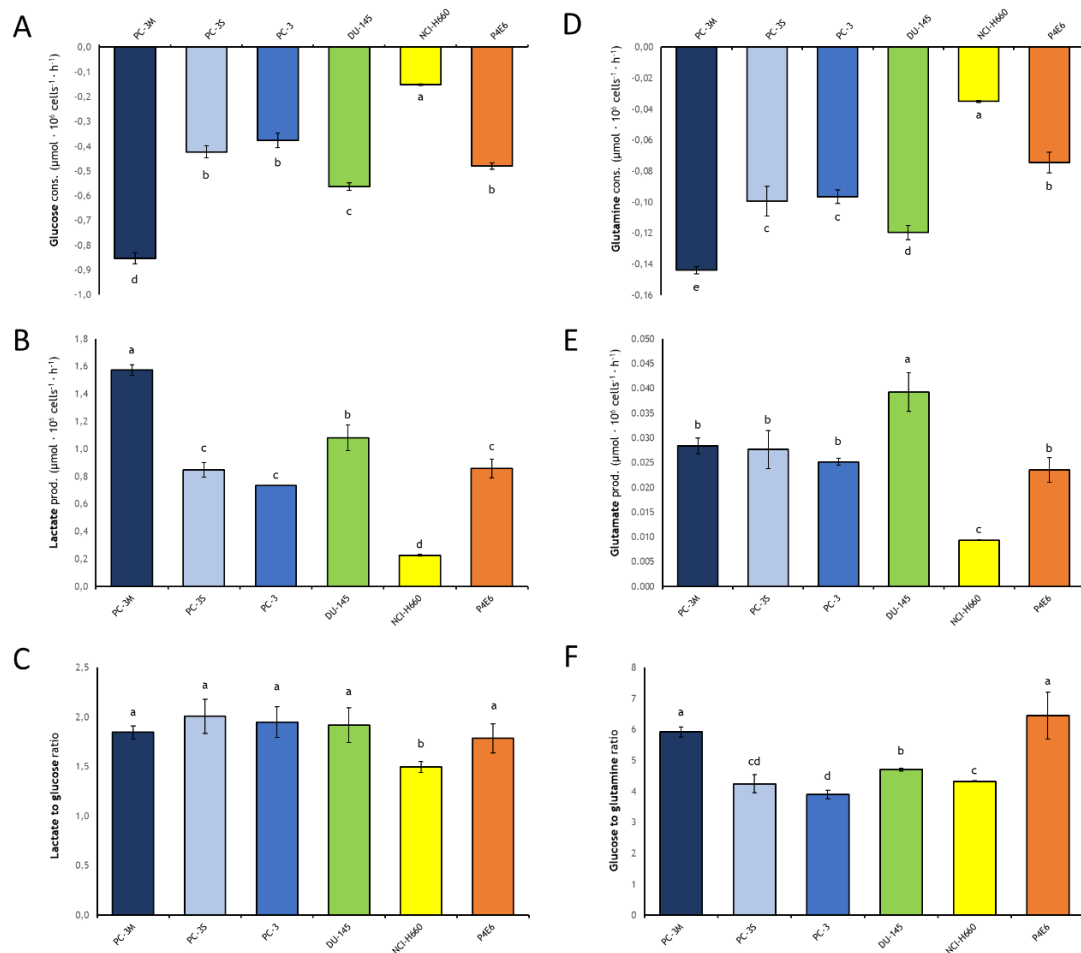


Figure 4.1.3. Extracellular fluxes of glucose, glutamine, lactate and glutamate in the CRPC panel. Glucose consumption (A), lactate production (B), glutamine consumption (D) and glutamate production (E) rates were obtained after 96 h incubation with fresh media and normalized to cell number and proliferation rates. Lactate to glucose ratio (C) and glucose to glutamine ratio (F) were calculated for each replicate. Bars represent mean \pm SD of $n=3$. Cell lines sharing the same letter indicates absence of significant differences between them (One-way ANOVA and Tukey's multiple comparison test with $\alpha=0.05$).

PC-3M exhibited the highest glucose consumption and lactate production rates in our cell panel, followed by DU-145. Next, PC-3, PC-3S and P4E6 exhibited lower glucose consumption and lactate production rates, with no significant differences between the

three cell lines, denoting that glucose consumption does not correlate with proliferation rate, since PC-3 proliferate at a significantly higher rate (pdt ~ 24 h) than PC-3S or P4E6 (pdt ~ 40 h). Finally, both readouts are much lower in the neuroendocrine NCI-H660 than in the rest of cell lines. Despite these significant changes, lactate to glucose ratio (**4.1.3.C**) remained similar and around 2 for all cell lines except for NCI-H660, in which the value of this ratio was around 1.5, which indicates that lactate to glucose ratio depends on PCa subset (neuroendocrine vs. adenocarcinoma).

Similarly, PC-3M and DU-145 also displayed significantly higher glutamine avidity (**4.1.3.D**) compared to the rest of cell lines. Again, our results indicate that glutamine consumption was uncoupled from proliferation in CRPC. Surprisingly, DU-145 also exhibited a higher production of glutamate than the rest of cell lines (**4.1.3.E**), which will be investigated in the following sections, whereas glutamate production was similar across the rest of adenocarcinoma cell lines.

It is worth noting that the lower consumption and production rates of these metabolites in NCI-H660 could also account for its three times smaller volume compared to the rest of cell lines, as described in **Section 4.1.2.1**. Other authors have suggested that the metabolic demands of cancer cells depend on their size, and they propose and validate volume normalization as a way to decouple cell volume variability [388], even if this notion is not yet widespread in the metabolomics field.

According to this, normalization of glucose and glutamine consumption rates by cell volume unveiled that glucose and glutamine metabolism of neuroendocrine CRPC may not be so significantly different than the rest of PCa cell lines (**4.1.4**). In accordance, glucose to glutamine ratio in NCI-H660 is in the average of the rest of PCa cell lines (**4.1.3.F**), which is supported by previous results indicating that NEPC can have glycolytic enzyme levels comparable or even higher than prostate adenocarcinoma [389].

Our results normalized by cell volume still showed that the metastatic cell lines with high tumorigenic capacity exhibited significantly enhanced glucose consumption, yet comparable to the primary tumor P4E6, thus ruling out the hypothesis that the e-CSC phenotype is distinctively more glycolytic. On the contrary, enhanced glutamine consumption appeared to be a characteristic trait of the metastatic phenotype exhibited

by PC-3M and DU-145, with absence of differences among all the other cell lines, regardless of any other variable (i.e. neuroendocrine vs. adenocarcinoma or primary tumor vs. metastatic origin).

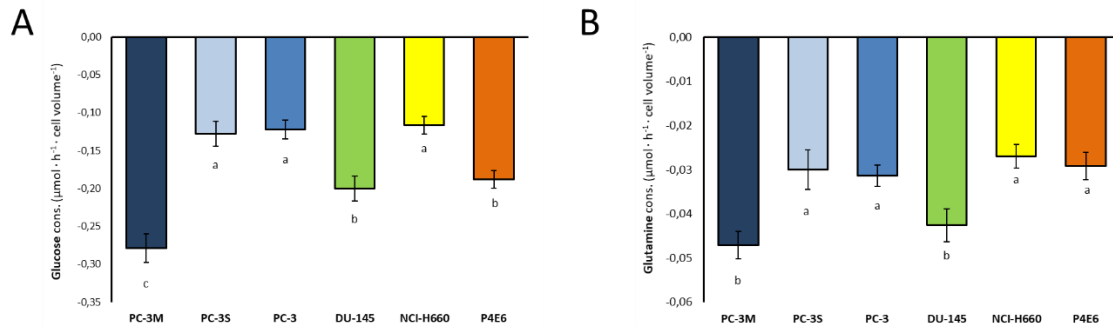


Figure 4.1.4. Extracellular fluxes of glucose and glutamine normalized by cell volume (pL). (A) Glucose and (B) glutamine consumption rates were obtained after 96 h incubation with fresh media and normalized to cell number, proliferation rate and cell volume. Bars represent mean \pm SD of $n=3$. Cell lines sharing the same letter indicates absence of significant differences between them (One-way ANOVA and Tukey's multiple comparison test with $\alpha=0.05$).

In light of these results, we hypothesized that highly metastatic e-CSC adenocarcinoma displays a particular reliance on glutamine uptake that can render this phenotype vulnerable to glutamine starvation or to the inhibition of glutaminolysis. If this was the case, not only cell proliferation, but also the metastatic potential of PC-3M and DU-145 should be compromised under absence of glutamine. To assess this, we evaluated several readouts on the subset of adenocarcinoma cell lines from metastatic origin: PC-3M, PC-3S, PC-3 and DU145.

In particular, we first evaluated the effect of glutamine deprivation (**4.1.5.A**) and the glutaminase 1 inhibitor bis-2-(5-phenylacetamido-1,3,4-thiadiazol-2-yl)ethyl sulfide (BPTES) (**4.1.5.B**) on cell proliferation. We encountered that absence of glutamine in the extracellular medium had a significantly greater impact on the proliferation of PC-3M and DU-145. On the contrary, the decrease in proliferation followed by inhibition of GLS1 by BPTES did show a correlation with metastatic potential within the PC-3-derived cell lines, but not when compared to DU-145. Indeed, we hypothesized that this could also arise from differential GLS1 expression between the cell lines. To validate this hypothesis, we evaluated the protein expression levels of GLS1 (**4.1.5.C**), observing that, in accordance to the higher resistance to GLS1 inhibition by BPTES, DU-145 displayed higher levels of GLS1 than any PC-3-derived cell line. Indeed, this higher GLS1 expression

is also consistent with our previous observation, in **Section 4.1.2.1**, that DU-145 produced significantly more glutamate than any other cell line in the panel.

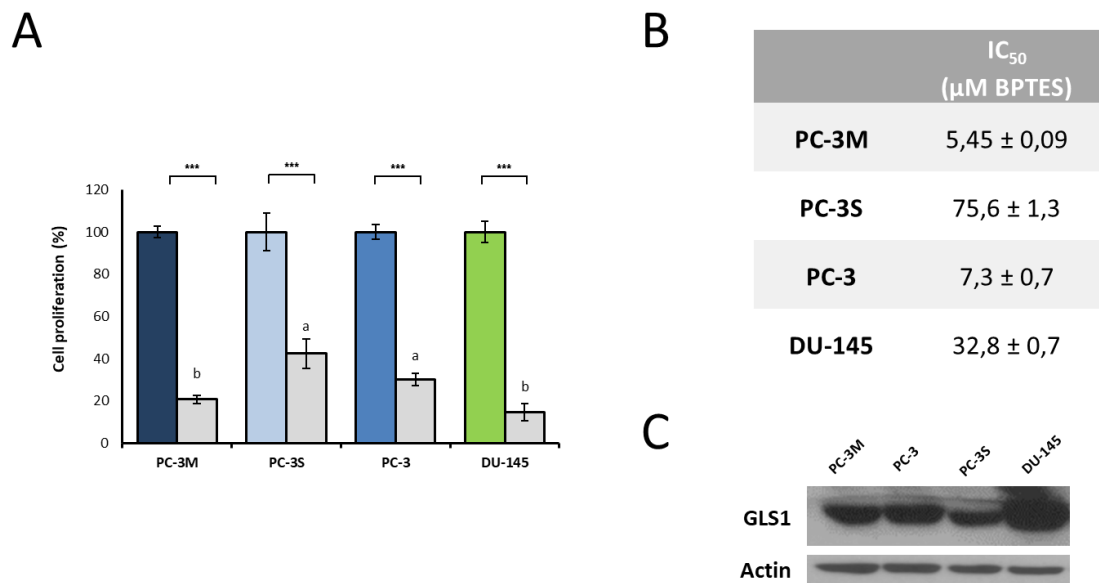


Figure 4.1.5. Effect of glutamine deprivation and glutaminase 1 inhibition on metastatic prostate adenocarcinoma.

(A) Relative cell proliferation of PC-3M, PC-3S, PC-3 and DU-145, after 72 h incubation with full growth medium (colored) or glutamine deprivation (grey). (B) IC₅₀ (μ M) after 72 h incubation with GLS1 inhibitor bis-2-(5-phenylacetamido-1,3,4-thiadiazol-2-yl)ethyl sulfide (BPTES) (C) GLS1 protein expression levels assessed by Western Blot. Actin was used as a loading control. Bars represent mean \pm SD of n=3. In panel A, significant differences of glutamine-deprived conditions (grey) relative to control cells (colored) were evaluated by Student t-test and are indicated at $p < 0.05$ (*), $p < 0.01$ (**), and $p < 0.001$ (***). Relative decreases in proliferation among glutamine-deprived conditions were evaluated by one-way ANOVA and Tukey test for multiple comparisons. Cell lines/conditions sharing the same letter indicates absence of significant differences between them.

In conclusion, we identified that e-CSC phenotypes significantly enhance glutamine consumption and are particularly vulnerable to glutamine removal from the extracellular medium, and we have proven that this vulnerability cannot be explained, at least solely, in terms of GLS1 expression levels. To corroborate the hypothesis that this common vulnerability of PC-3M and DU-145 is tied to their e-CSC phenotype and is functionally related to their metastatic potential, we also assessed the effect of glutamine deprivation on the spheroid formation (**4.1.6.AC**) and colony formation capacities (**4.1.6.BD**) of the adenocarcinoma cell lines.

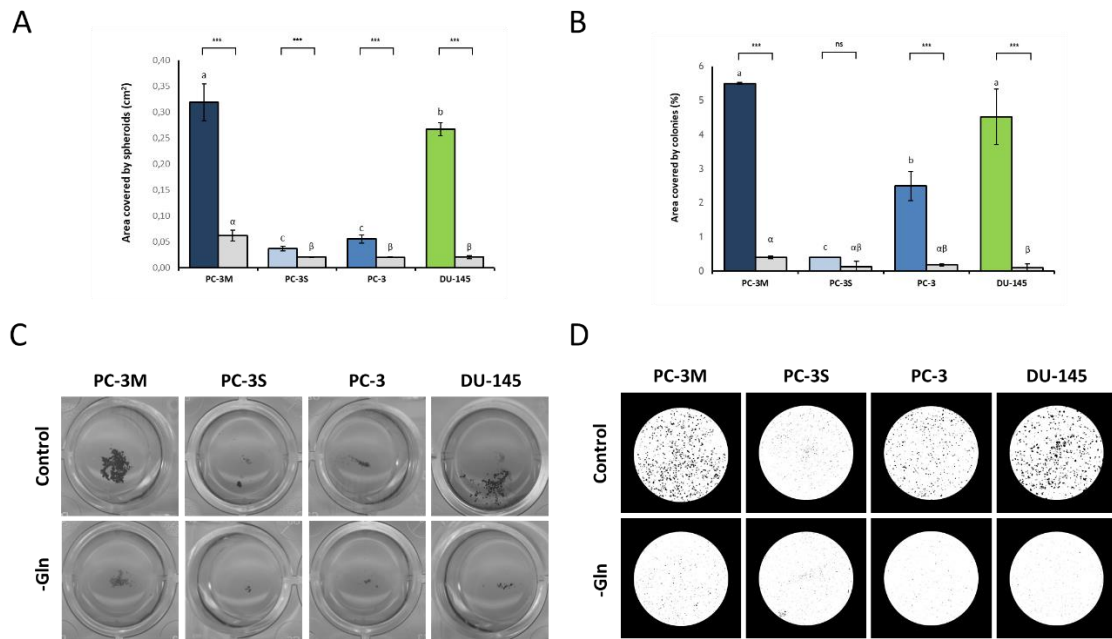


Figure 4.1.6. Effect of glutamine deprivation on the metastatic capacity and tumor-initiating capacity of prostate adenocarcinoma cell lines. (A) Spheroid formation capacity of PCa adenocarcinoma cell lines with full growth medium (colored) or glutamine deprivation (grey), assessed by seeding 10^3 cells in ultra-low-attachment plates. Spheroid plates were scanned after 7 days and quantified using *Image J*. (B) Area covered by cell colonies of PC-3M, PC-3S, PC-3 and DU-145, with full growth medium (colored) or glutamine deprivation (grey), assessed by seeding 10^3 cells in 6-well plates. Plates were scanned after 7 days and quantified using *Image J*. (C) Bright-field images (40x) and scans of spheroids in p24 well plates. (D) Gray-scale conversion of scanned wells of the colony formation assay. Bars represent mean \pm SD of $n=3$. In panels A and B, significant differences of glutamine-deprived conditions (grey) relative to control cells (colored) were evaluated by Student t-test and are indicated at $p < 0.05$ (*), $p < 0.01$ (**), and $p < 0.001$ (***). Relative decreases in proliferation among control or glutamine-deprived conditions were evaluated by one-way ANOVA and Tukey test for multiple comparisons. Significant differences among cell lines are indicated by Latin letters (full-growth medium) or Greek letters (glutamine deprivation).

Similar to spheroid formation introduced in **Section 4.1.2.1**, colony formation assay is also indicative of CSC traits, understood as the ability of a single cell to proliferate through clonal expansion [390,391]. In other words, this assay reflects the capacity to initiate tumors that is essential for the establishment of macrometastases in the last phase of the invasion-metastasis cascade. The spheroid and colony formation capacity assays revealed that glutamine deprivation strikingly diminished the metastatic and tumor-initiating capacities of PC-3M and DU-145, revealing that glutamine availability is essential for these cellular functions and can be an interesting antimetastatic metabolic target to be further explored. Supporting these findings, other recent works have also identified a potential role of glutamine in supporting breast cancer metastasis [392] and

particularly in regulating CSC traits in lung and pancreatic cancers [393], even if the mechanistic connection is far from being established.

4.1.2.3. CRPC e-CSC phenotypes present enhanced methionine, lysine and total amino acid consumption rates

The observed differences in glutamine metabolism associated to highly metastatic phenotypes in CRPC are necessarily connected to other major metabolic pathways, since glutamine represents an important biosynthesis hub for cancer cells. In line with this idea, we next aimed to unveil other metabolic alterations that could be related to the enhanced glutamine avidity in e-CSC phenotypes. To achieve this, we characterized the metabolism of our CRPC panel through targeted metabolomics and lipidomics, simultaneously evaluating intracellular metabolite pools and extracellular consumption and production rates of different families of metabolites.

First, we compared the consumption and production rates of amino acids (**4.1.7**). The obtained results revealed that some amino acid consumption or production rates presented a relatively homogeneous profile across all PCa cell lines cells, such as phenylalanine, tryptophan or tyrosine. On the contrary, other amino acids, notably glycine, aspartate or proline, were consumed in some cell lines while produced in others.

For proline in particular, the previous characterization of PC-3M and PC-3S conducted in our group had identified that PC-3M produced whereas PC-3S consumed proline, and it had been postulated as a potential e-CSC trait [73]. Even if our results agreed with the previous observation that PC-3M shifted from proline consumption to proline production compared to PC-3S (and, as we have identified here, also to parental PC-3), proline secretion was also observed in the poorly tumorigenic cell lines, NCI-H660 and P4E6, whereas this behavior was not observed in the also highly tumorigenic DU-145. These observations ruled out the previous hypothesis that this feature could be tied to e-CSC phenotypes and metastatic progression in CRPC. Indeed, previous studies had pinpointed that proline metabolism could be important in supporting metastasis in breast cancer, in particular due to PRODH and proline catabolism [394]. In spite of that, our results indicate that the role of proline in CRPC metastasis is unclear and that it certainly cannot be ascribed to PRODH, since the previous transcriptomic analysis of PC-

3M and PC-3S revealed an almost complete absence of this enzyme in both cell lines (Appendix 1).

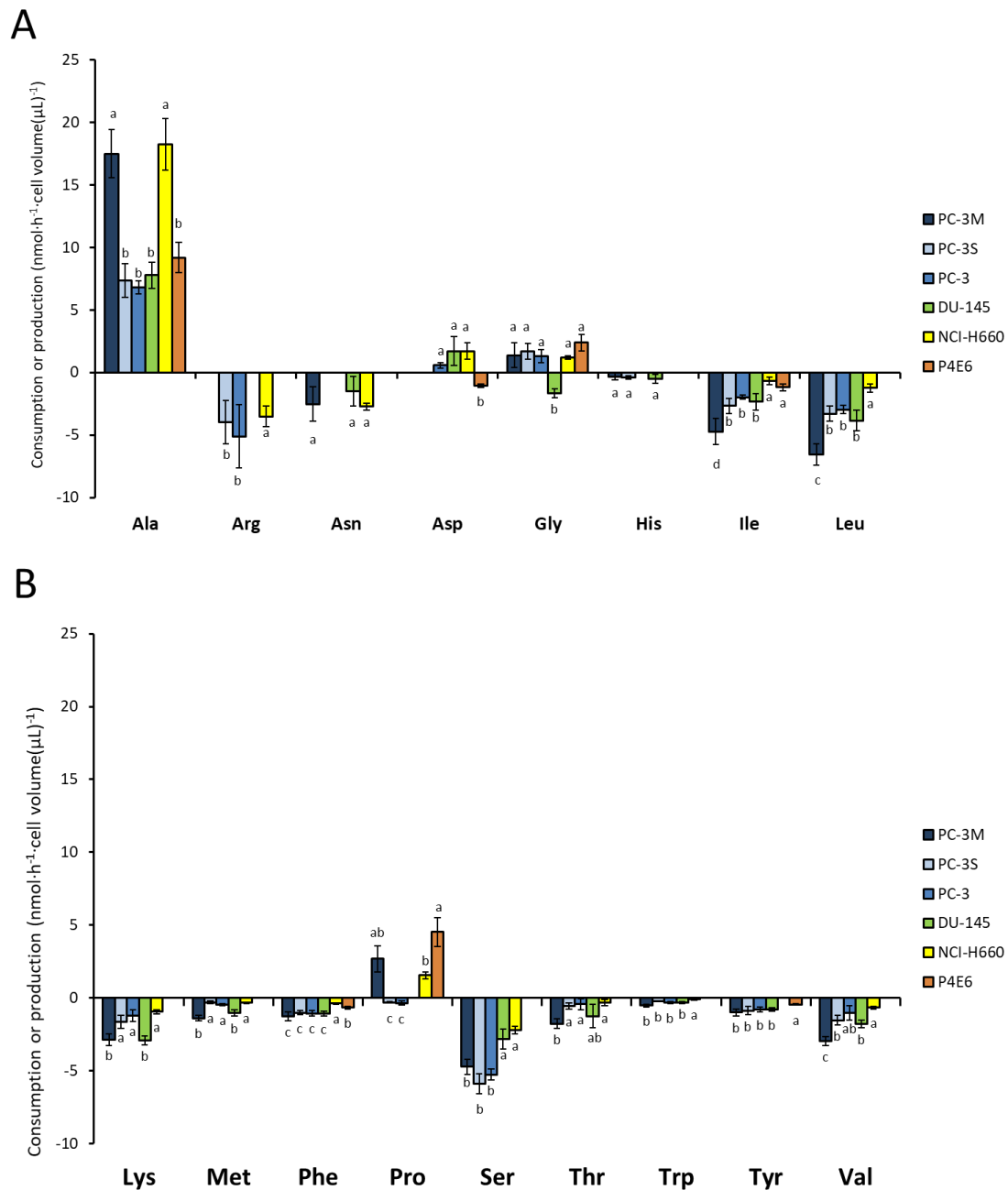


Figure 4.1.7. Amino acid consumption and production rates in the CRPC panel. Amino acid consumption (negative values) or production (positive values) in alphabetic order: (A) Alanine (Ala) to leucine (Leu) and (B) Lysine (Lys) to valine (Val). Abbreviations: arginine (Arg), asparagine (Asn), aspartate (Asp), glycine (Gly), histidine (His), isoleucine (Ile), methionine (Met), phenylalanine (Phe), proline (Pro), serine (Ser), threonine (Thr), tryptophan (Trp) and tyrosine (Tyr). Bars represent mean \pm SD of $n=3$. Significance between initial and final metabolite concentrations were evaluated using a t-Student test with $\alpha=0.05$. If the condition of significant consumption/production was met, comparison between cell lines/conditions normalized by cell volume was performed by one-way ANOVA and Tukey's

multiple comparison testing. Cell lines/conditions sharing the same letter indicates absence of significant differences between them.

Moreover, our results also revealed that PC-3M exhibited a significantly higher consumption rate of the three branched-chain amino acids, isoleucine, leucine, and valine, than the rest of cell lines, which could also be tied to the remarkable overexpression of BCAT in this cell line (**Appendix 1**). Finally, the only significant traits in terms of amino acid consumption and production rates shared by both tumorigenic epithelial cell lines, PC-3M and DU-145, are enhanced lysine and methionine consumption. In this regard, increased methionine consumption could serve the purpose of supporting cysteine production, the rate-limiting amino acid in the synthesis of the ROS scavenger glutathione, which has been functionally linked to *in vivo* metastases previously [395].

Due to the great heterogeneity of amino acid consumption and production profiles among CRPC cell lines, we attempted to compare the contribution of glutamine vs. all amino acids displayed in **Figure 4.1.7**. We encountered that the primary tumor and the neuroendocrine cell lines globally produce the rest of amino acids, whereas the four adenocarcinoma cell lines from metastatic origin have a net consumption of the rest of amino acids (**4.1.8**), even if glutamine constitutes the main amino acid contribution to biomass production in all CRPC cell lines. In this regard, PC-3M and DU-145 also display enhanced global amino acid consumption than the rest of cell lines in the panel.

This adaptation displayed by metastatic adenocarcinoma, as opposed to early stage primary tumor and the relatively quiescent neuroendocrine NCI-H660, could be tied to support the proliferative capacity of these cell models. Others have reported that the uptake of biosynthetic end products such as free amino acids instead of their *de novo* synthesis in proliferating cancer cells allows to decrease the expenditure in ATP, redox equivalents and carbons that is associated to the biosynthetic pathways of NEAAs [97]. Indeed, the uptake of NEAAs instead of their synthesis can foster cancer cell proliferation, by allowing the redirection and investment of such ATP and redox equivalents into the synthesis of other molecules that are scarcer in their microenvironment than NEAAs. Supporting this notion, a recent cohort study unveiled

that increased expression of multiple amino acid transporters including SLC1A5 and SLC7A5 is correlated to poor prognosis in highly proliferative breast cancer [396].

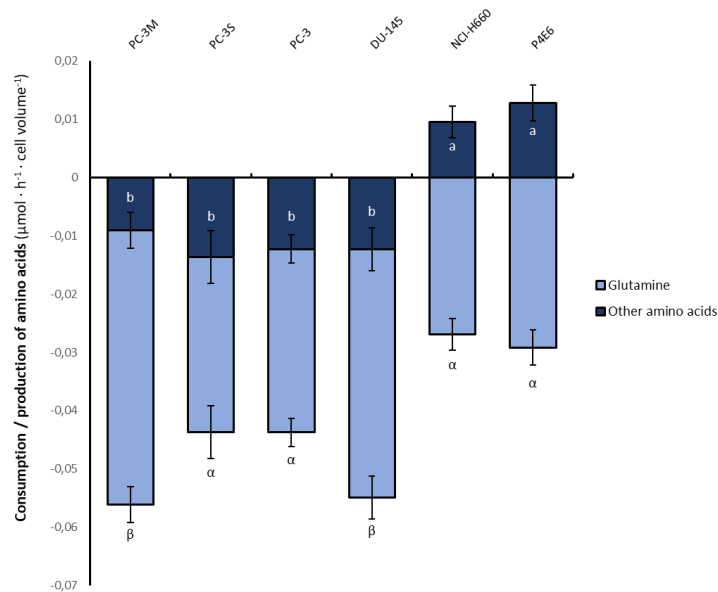


Figure 4.1.8. Contribution of glutamine compared to all other amino acids as carbon and energy sources. Cumulated consumption (negative) or production (positive) of glutamine (light blue) and of all amino acids in Figure 4.1.7 (navy blue) in the cell lines of the CRPC panel. Bars represent mean \pm SD of $n=3$. Significance between initial and final metabolite concentrations were evaluated using a t-Student test with $\alpha=0.05$. If the condition of significant consumption/production is met, comparison between cell lines/conditions normalized by cell volume was performed by one-way ANOVA and Tukey's multiple comparison test. Significant differences among cell lines is indicated by Greek letters (glutamine) or Latin letters (other amino acids).

4.1.2.4. CRPC subsets with distinct tumorigenic potential display different polyamine secretory profiles

Besides amino acids, we also measured the consumption and production rates of several non-proteinogenic amino acids and other biogenic amines, such as the urea cycle intermediates, polyamines, taurine, carnosine or α -aminoadipate (4.1.9). Indeed, secretion of some of these metabolites into the prostatic fluid constitutes an important part of the prostatic metabolism and physiology [397], and thus the evaluation of the alterations of the secretory profile in different PCa subsets can constitute a source of putative biomarker identification.

Our results revealed two different remarkable trends among the CRPC panel that are potentially tied to the highly metastatic e-CSC phenotype. First, we identified that the two e-CSC phenotypes consumed a significantly higher amount of the sulfonic acid taurine than the rest of cell lines (4.1.9.C). Among the many biological roles of this

molecule, it is involved in bile acid conjugation, ROS-scavenging, osmoregulation or modulation of calcium signaling [398]. The role of taurine on the metastatic capacity of cancer cells has been only scarcely addressed, even if it has been previously identified that taurine supplementation induced MET in PCa cells [399]. Thus, this adaptation of increased taurine consumption in PC-3M and DU-145 could be functionally related to their preservation of epithelial traits along with a tumorigenic phenotype, since similar rates of taurine consumption are not detected in the also epithelial but non-tumorigenic cell lines NCI-H660 and P4E6. Of note, alterations found in taurine metabolism could also be linked to the increased methionine consumption found in PC-3M and DU-145 (4.1.7), since taurine is an end-product of the transulfuration pathway, which transforms homocysteine from the methionine cycle into cysteine and other metabolites.

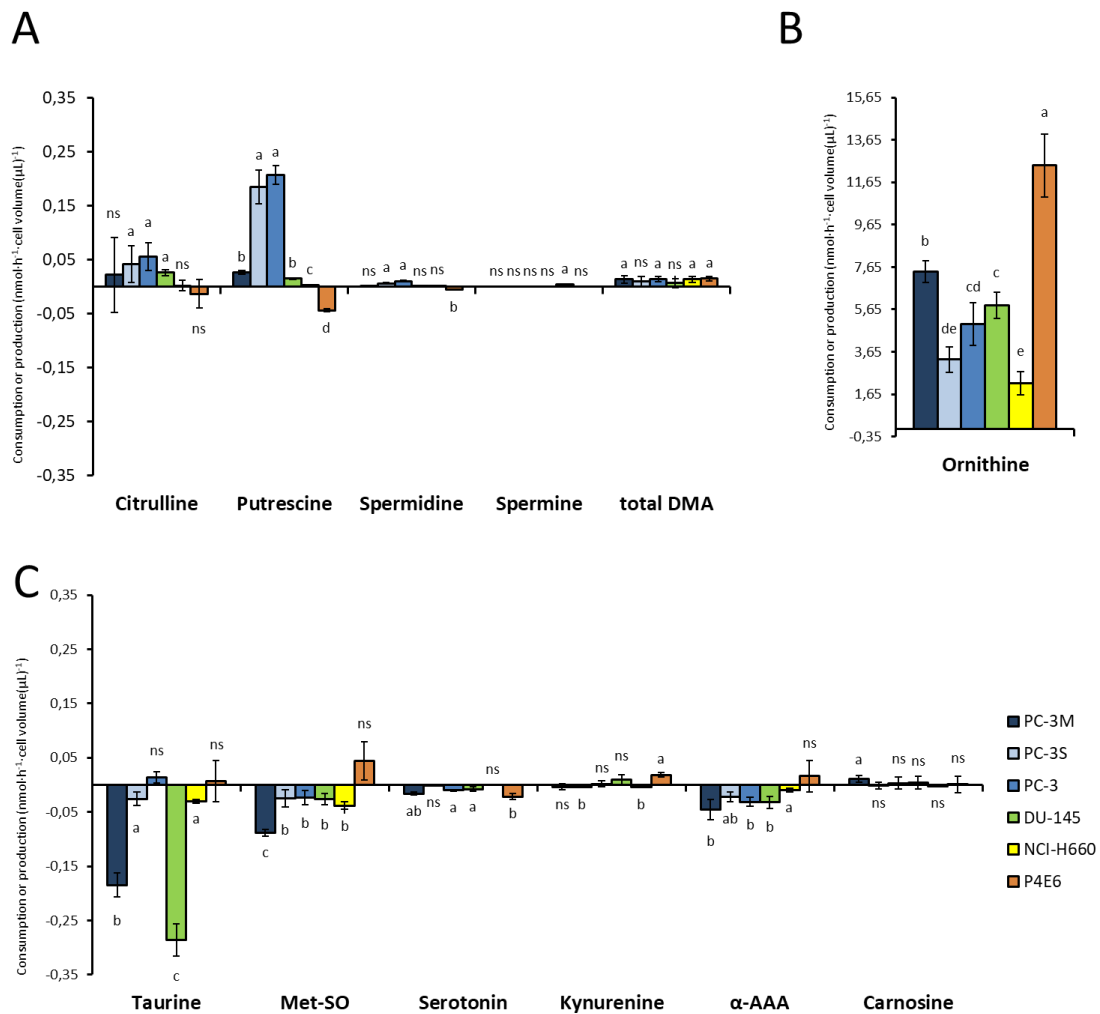


Figure 4.1.9. Consumption and production rates of non-proteinogenic amino acids and other biological amines in the CRPC panel. Consumption (negative values) or production (positive values) of non-proteinogenic amino acids and

biological amines: (A) Related to the urea cycle: citrulline, putrescine, spermidine, spermine, total dimethyl arginine, (B) ornithine, and others: (C) taurine, methionine sulfoxide, serotonin, kynurenine, alpha-aminoadipic acid and carnosine. Bars represent mean \pm SD of n=3. Significance between initial and final metabolite concentrations were evaluated using a t-Student test with $\alpha=0.05$. If the condition of significant consumption/production was met, comparison between cell lines/conditions normalized by cell volume was performed by one-way ANOVA and Tukey's multiple comparison testing. Cell lines/conditions sharing the same letter indicates absence of significant differences between them.

On the other hand, we also encountered several interesting trends among our panel regarding polyamine secretory profiles (**4.1.9.A**). Polyamines constitute an important part of prostatic secretions, and they have been postulated as potential biomarkers for PCa [146–149]. As explained in detail in the introductory section of this work, polyamine synthesis is a linear pathway in which ornithine, a urea cycle intermediate, is sequentially converted into putrescine, spermidine, and spermine, using as an aminopropyl donor decarboxylated SAM (dcSAM), coming from the methionine cycle. Hence, the alterations encountered in polyamine metabolism can also be connected to the altered methionine metabolism reported in the previous section. As mentioned previously, polyamines have important roles in a variety of cellular processes such as proliferation and differentiation, motility, protein translation, DNA synthesis and stability, redox homeostasis or ion channel regulation. However, their implication in such processes is not completely understood [134,144,145].

The first outstanding difference can be found when comparing primary tumor vs. all metastatic origin CRPC cell lines, in which a shift from consuming putrescine and spermidine (primary tumor, P4E6) to synthesizing and secreting them (all CRPC cell lines of metastatic origin) is observed. Moreover, P4E6 also displayed enhanced ornithine production compared to all the metastatic cell lines (**4.1.9.B**). Taken together, both observations denote a decreased or blocked ornithine decarboxylase (ODC) in P4E6 compared to all the metastatic cell lines. ODC is the first and rate-limiting step in polyamine synthesis. ODC expression is clinically correlated with esophageal squamous cell carcinoma tumor progression [152]. ODC activation has been reported to be sufficient to induce tumorigenesis in different cell models [150,151]. Also, direct chemical inhibition of ODC has been proven as outstandingly effective at preventing tumor relapse after standard therapy in high risk neuroblastoma [400]. Importantly, our observation that only primary tumor P4E6 consumes polyamines and excretes high

amounts of ornithine suggests that ODC activation is indeed tied to metastatic progression in CRPC.

Apart from that, PC-3M drastically reduced putrescine secretion (and, to a lesser extent, also spermidine) to the extracellular medium compared to PC-3 and PC-3S (**4.1.9.A**), with DU-145 displaying a similar secretory profile than PC-3M. Alterations in polyamine metabolism have been previously linked to the modulation of the EMT program. Indeed, a recent study including a notable validation in prostate cancer cohorts (n=1519) linked alterations in spermine levels with a non-canonical Wnt signaling pathway that leads to activation of EMT in PCa [146]. Moreover, polyamine depletion through ODC inhibition increased the production of MMPs and exacerbated invasive phenotypes in epithelial cells [401].

Finally, only NEPC cells (NCI-H660) secrete the final product of polyamine synthesis, spermine. Several studies analyzing patient cohorts have underlined the potential of spermine as a PCa biomarker: high spermine secretion in urine and prostatic fluid [148,149] and low intracellular spermine is frequently found in PCa tissue, specifically correlated to tumor aggressiveness [146,147], which is also one of the hallmarks of NEPC tumors compared to prostate adenocarcinoma [330]. Thus, low intracellular spermine and high spermine secretion may be indeed a marker of NEPC or NE-transdifferentiation in PCa, besides denoting tumor aggressiveness. Supporting this notion, a recent metabolomic study of neuroendocrine transdifferentiation in the hormone-naïve LNCaP also found a decrease in intracellular spermine levels in LNCaP cells when they acquired NE features [402].

In summary, primary tumor P4E6 consumed polyamines whereas all cell lines from metastatic origin produced them. Invasive CRPC (PC-3S and PC-3) secreted high amounts of putrescine and, to a lower extent, also spermidine to their surroundings. Highly tumorigenic epithelial cell lines, PC-3M and DU-145, secreted much lower amounts of putrescine and did not significantly secrete spermidine or spermine. Finally, only neuroendocrine NCI-H660 significantly secreted spermine.

4.1.2.5. Intracellular metabolite profiles in CRPC unveil distinct metabolic phenotypes

To achieve a complete picture of the metabolic landscape of each of our CRPC cell lines, we also measured the intracellular pools of all the same metabolites we analyzed in extracellular media, proteinogenic and non-proteinogenic amino acids, urea cycle intermediates, several biogenic amines and different families of lipids.

For the polar metabolite part of our metabolomic analysis, we normalized the obtained concentrations by the median of amino acids in each sample and we scaled and transformed our data as described in Methods 3.16. We attempted to cluster our metabolomic data and achieve a global view of the obtained results by principal component analysis (PCA) (4.1.10.A) and one-way ANOVA (4.1.10.B) to identify relevant trends and the most significant features, and we also presented the obtained concentration matrix for each metabolite as a heatmap (4.1.10.C), clustering the obtained results by condition (cell line) and by feature (metabolite).

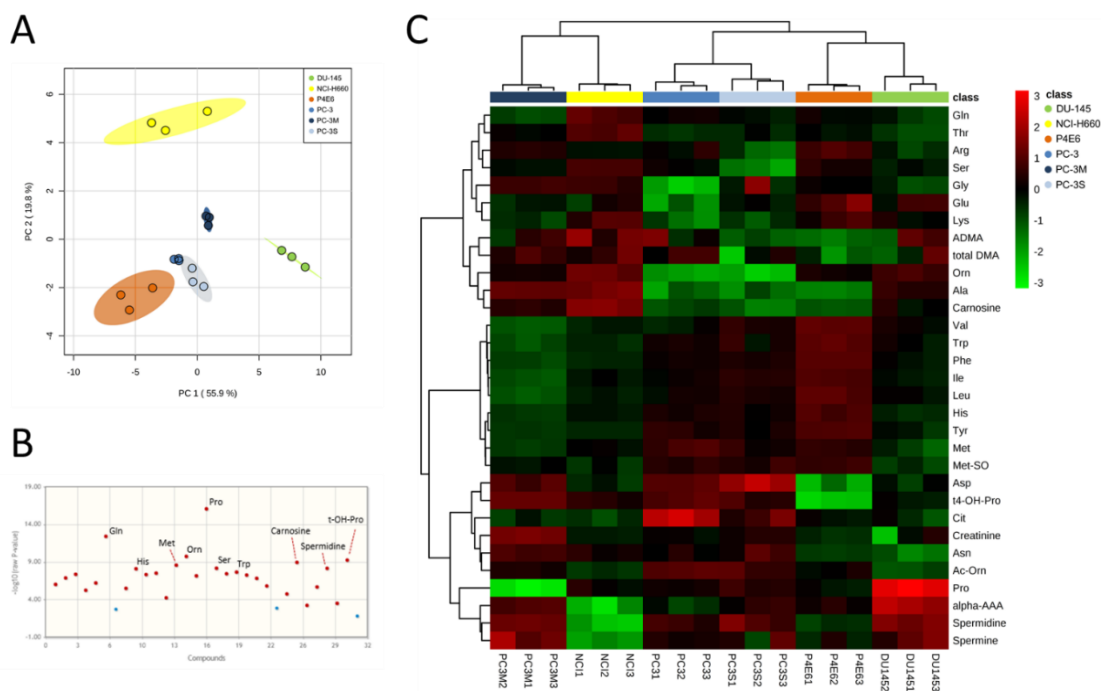


Figure 4.1.10. Intracellular metabolomic profiling of the CRPC panel. (A) Principal component analysis of the metabolomic profiling of the CRPC panel. (B) Top 10 features with highest statistical significance of the presented data, assessed by one-way ANOVA. All significant features are shown in red and features with no significant differences are shown in blue ($\alpha=0.05$). (C) Heatmap and clustering of features and cell lines. Features below or above

the LOQ of the analytical method were removed and all data was normalized by median of amino acids of each sample and log transformed prior to the analysis.

First, PCA analysis delineated clear distances between all the cell lines, except for PC-3 and PC-3S. Indeed, PC-3 and PC-3S intracellular metabolite pools were found to be remarkably similar, whereas PC-3M deviated significantly from both PC-3 and PC-3S (**4.1.7.AC**), consistent with a major phenotypic remodel triggered by the acquisition of CSC traits and the partial MET. Interestingly, PC-3 and PC-3S were also found to be very close to P4E6, while the highly tumorigenic adenocarcinoma cell lines DU-145 and PC-3M, appeared to differ more from the primary tumor cell line, potentially denoting a slight correlation to tumorigenic capacity across PC1 (55.9%).

PC2 (19.8%) showed a clear separation between the neuroendocrine PCa model (NCI-H660) and all adenocarcinoma models. Besides that, PC-3M also appeared to shift slightly closer to both DU-145 in the PC1 axis and NCI-H660 in the PC2 axis, relative to parental PC-3. Indeed, PC-3M, DU-145 and NCI-H660 exhibited remarkable similarities in terms of having lower intracellular pools of a clustered group of different amino acids including all BCAAs, all aromatic amino acids, histidine and methionine; and higher pools of alanine and carnosine (**4.1.10.C**).

At the same time, PC-3M also shared some similarities individually with either NCI-H660 or DU-145. In fact, in the cell line dendrogram clustering, PC-3M and NCI-H660 clustered together (**4.1.10.C**), uncovering the possibility of a slight transdifferentiation to a NE metabolic phenotype in PC-3M. One hypothetical rational basis for this could be the similar levels of 1C metabolites displayed by PC-3M and NCI-H660, since two recent independent studies have linked prostate NE transdifferentiation with altered serine and 1C metabolite intracellular levels [402,403] to support methylation reactions for epigenetic signaling driving the NE program [403].

On the other hand, PC-3M and DU-145, the two highly-metastatic phenotypes of our cell panel, also exhibited remarkable similarities. First, they displayed significantly lower glutamine pools than the rest of cell lines, despite being the two cell lines that consumed glutamine at highest rates (**Section 4.1.2.2**), which implies that consumed glutamine is rapidly transformed into other metabolites in these two cell lines. Interestingly, both cell lines also had a significant greater accumulation of the second and third members of the

polyamine synthetic pathway, spermidine and spermine, while, as described in **Section 4.1.2.4**, they decreased their putrescine and spermidine secretion compared to either PC-3 or PC-3S. These observations, together with higher methionine consumption, suggest a higher polyamine biosynthetic flux in PC-3M and DU-145, which is necessarily coupled to flux through 1C metabolism.

Precisely, the remarkably high spermidine pools in these two cell lines could be devoted to preserve their tumorigenic potential, since polyamines play a crucial role in Myc-driven tumorigenesis. In particular, they elicit a unique PTM termed as hypusination, transference of an aminobutyl group from spermidine to specific lysine residues of eukaryotic translation initiation factor 5A-1 (eIF5A1) and eIF5A2. In turn, eIF5A1 and eIF5A2 are central Myc transcriptional targets and mediate the translation of a high number of Myc downstream genes directly associated with tumor initiation, development, stem cell differentiation and metastasis [404]. Importantly, Myc not only controls the transcription of eIF5A1 and eIF5A2, but also of all the enzymes that are required for spermidine synthesis and consequent eIF5A1 and eIF5A2 hypusination and activation: ODC, AMD1 and SPDSY [404]. In consequence, polyamines, and particularly spermidine, play a key role in Myc-driven tumorigenesis and acquisition of stem cell traits, and thus the observation of enhanced spermidine pools in both PC-3M and DU-145 could be a key driving force of their tumorigenic potential.

Besides glucose and glutamine, fatty acid oxidation (FAO) is another important source of mitochondrial energy production. Due to the glutamine alterations specifically found in PC-3M and DU-145 (enhanced glutamine consumption and yet the lowest intracellular glutamine pools) we hypothesized that FAO could be consequently altered in the CRPC panel. Therefore, we also assessed the intracellular levels of acyl-carnitines in the CRPC panel (**4.1.11**). Enhanced FAO for PC-3M had been suggested previously due to a GSMM model reconstruction of PC-3M and PC-3S and differential antiproliferative effect of the CPT1 inhibitor etomoxir in PC-3M and PC-3S. The fluxes estimated by the model predicted that PC-3M used FAO to fuel the TCA cycle to sustain proliferation, whereas PC-3S used fatty acids as eicosanoid precursors, which could contribute to the maintenance of their invasive phenotype [157]. Metabolomic determination of carnitine and acyl-carnitines was performed in the context of this work in PC-3M and PC-3S cells

to validate the model prediction that long-chain FAO was increased in PC-3M, and the results presented here are included in Marin de Mas et al [157].

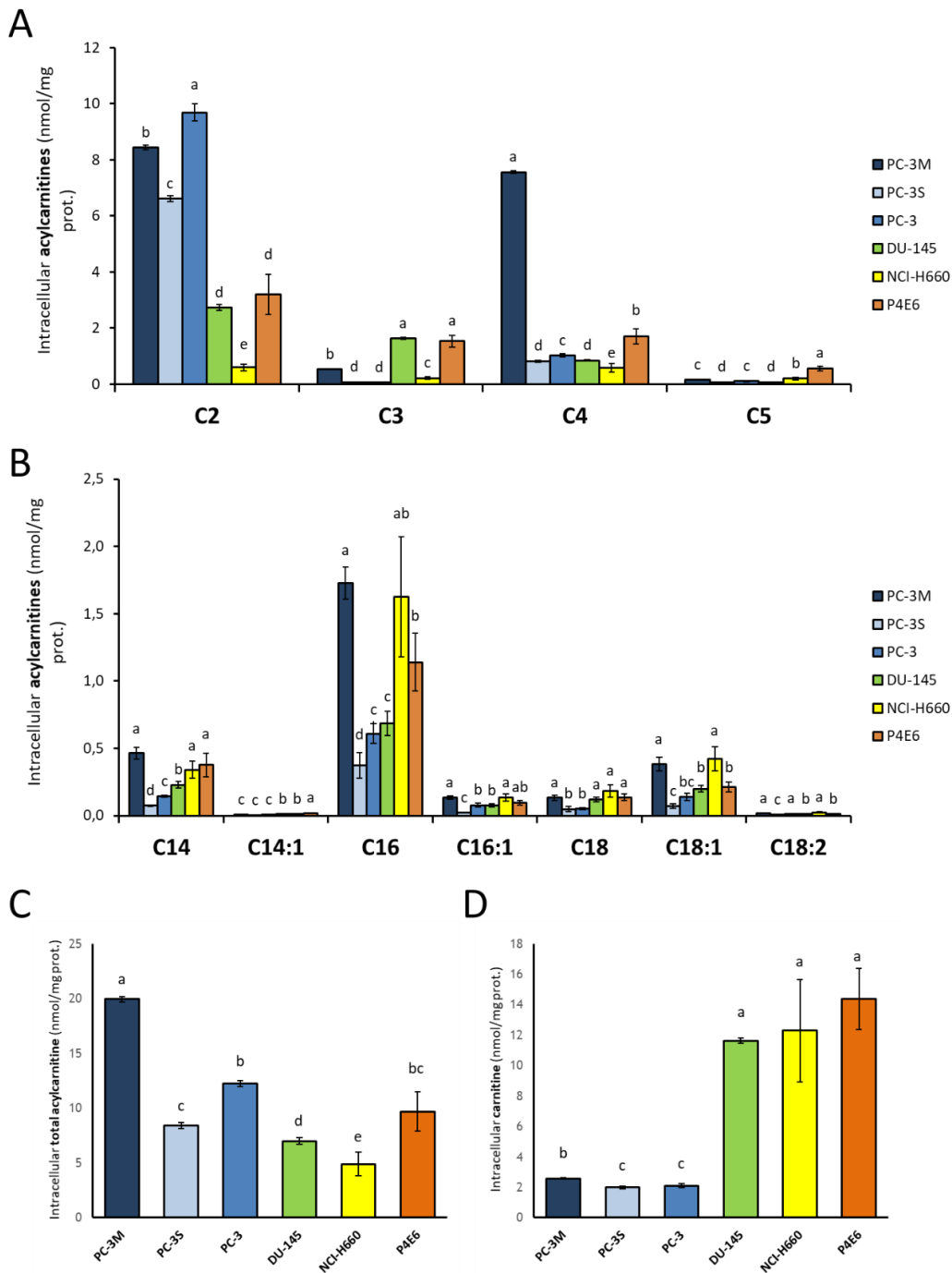


Figure 4.1.11. Acylcarnitine intracellular profiles in the CRPC panel. (A) Short-chain acylcarnitines, (B) long-chain acylcarnitines, (C) total sum of intracellular acylcarnitines and (D) intracellular unbound carnitine. Displayed values are mean \pm SD between three independently-extracted cell pellets for the CRPC cell lines PC-3M, PC-3S, PC-3, DU-145, NCI-H660 and P4E6. Results are normalized by median of protein content in each sample. Cell lines/conditions sharing the same letter indicates absence of significant differences between them.

Interestingly, we also found that levels of free carnitine between PC-3M, PC-3 and PC-3S were similar and significantly much lower than the rest of CRPC cell lines, suggesting that CPT1 activity could be intrinsically higher in PC-3 cell line to lead to decreased pools of unbound carnitine (**4.1.11.D**) and yet higher or similar amounts of acylcarnitines.

Then, we calculated the sum of all acyl-carnitines (**4.1.11.B**) in each cell line, and the sum of total carnitine (free and bound) (**4.1.11.C**). From these results, we can conclude that PC-3M enhanced dependence on FAO to fuel proliferation relies on a combination of two features: enhanced CPT1 activity and higher carnitine synthesis capacity. The first affirmation is sustained on the observation that all the PC-3 subpopulations display a much lower amount of free carnitine than the rest of CRPC cell lines and PC-3M also displays the highest amounts of acyl-carnitines of all the cell lines. The second affirmation is supported by the evidence that PC-3M intracellular pools of total carnitine (the sum of both bound and free carnitine) are higher than PC-3 and PC-3S. This implies that, apart from the reported higher CPT1 activity [157], PC-3M must also have upregulation of carnitine biosynthesis, which leads to a higher amount of total carnitine.

However, the analysis of acylcarnitines of the CRPC panel did not unveil significant trends that can be associated to CRPC metastatic potential in our cell panel, since DU-145 presented acyl-carnitine levels similar to poorly tumorigenic cell lines. Moreover, from the distribution of intracellular levels of short-chain (**4.1.11.A**) and long-chain (**4.1.11.B**) acylcarnitine molecules, as indicative of FAO, we also concluded that, of the three major carbon and energy sources, glucose, glutamine and fatty acids, only alterations in glutamine metabolism can be significantly associated to the tumorigenic potential in our cell panel.

4.1.2.6. Distinct urea cycle/polyamine metabolism profiles in different CRPC phenotypes

Linked to the alterations found in glutamine metabolism, one of the most interesting alterations that arises from integrating our results of consumption and production rates and intracellular metabolite pools is encountered regarding polyamine metabolism, supported by previous studies indicating the potential importance of dysregulated polyamine metabolism in PCa [146–149]. In summary, integrating the intracellular pools

and exchange fluxes of ornithine and polyamines, our analysis revealed up to four distinct metabolic profiles in our CRPC panel (4.1.12).

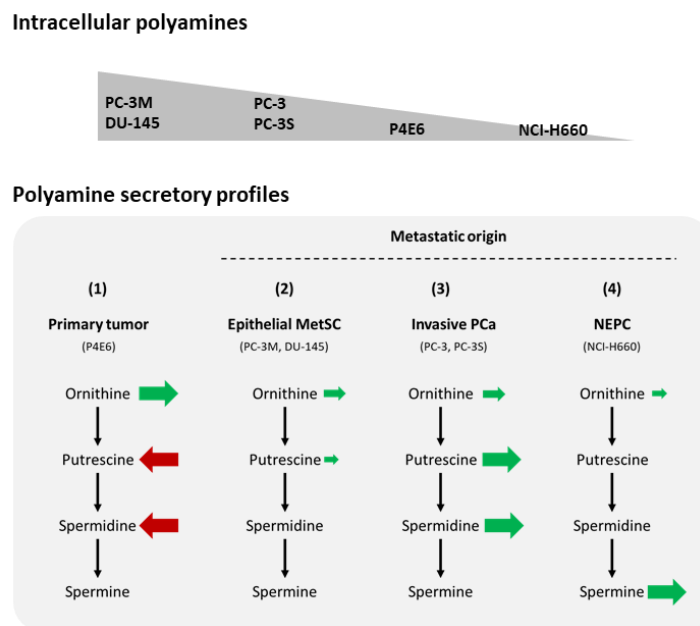


Figure 4.1.12. Four distinct proposed polyamine metabolism profiles for castration resistant prostate cancer (CRPC).

(1) Primary tumor cell line P4E6 displays the greatest rate of ornithine production, and yet is the only cell line that consumes polyamines (putrescine and spermidine) from the extracellular medium. (2) Cell lines previously characterized as highly tumorigenic or metastatic stem cell (MetSC) and prominently epithelial, PC-3M and DU-145, display a moderate ornithine production and slight putrescine production. (3) Parental prostate cancer (PCa) PC-3 and its subpopulation enriched in invasive traits, PC-3S, display moderate ornithine production while high secretion of putrescine and spermidine to the extracellular medium. (4) The neuroendocrine prostate cancer (NEPC) cell line, NCI-H660, displays the lowest production of ornithine and is the only cell line in the panel that produces spermine.

These four profiles can be summarized as: (1) high ornithine excretion and consumption of polyamines from the extracellular medium (primary tumor P4E6), (2) enhanced polyamine synthesis, intracellular accumulation and low secretion (MetSC-like cell lines, PC-3M and DU-145); (3) lower synthesis and significant secretion of putrescine and to a lesser extent spermidine (invasive and poorly tumorigenic PC-3S and PC-3), (4) secretion of spermine and low intracellular polyamine content (neuroendocrine NCI-H660).

Notably, besides these similarities between PC-3M and DU-145 in terms of glutamine and polyamine synthesis, the set of interconnected pathways comprised by the Gln-P5C-Orn axis, the urea cycle and polyamine metabolism also emerged as outstandingly significant in all the cell lines in the CRPC panel, both considering intracellular pools and extracellular secretions. These differences do not only arise between high

metastatic/low metastatic potential, but also among other CRPC traits and they could represent a significant discriminant in PCa metabolic subsets. For this, we decided to obtain a deeper insight on these interconnected pathways to evaluate whether these differences could allow us to determine biomarkers for different CRPC subsets or to design therapeutic strategies targeting the e-CSC phenotype of PC-3M, both in terms of consumption or production rates (4.1.13) and intracellular pools (4.1.14).

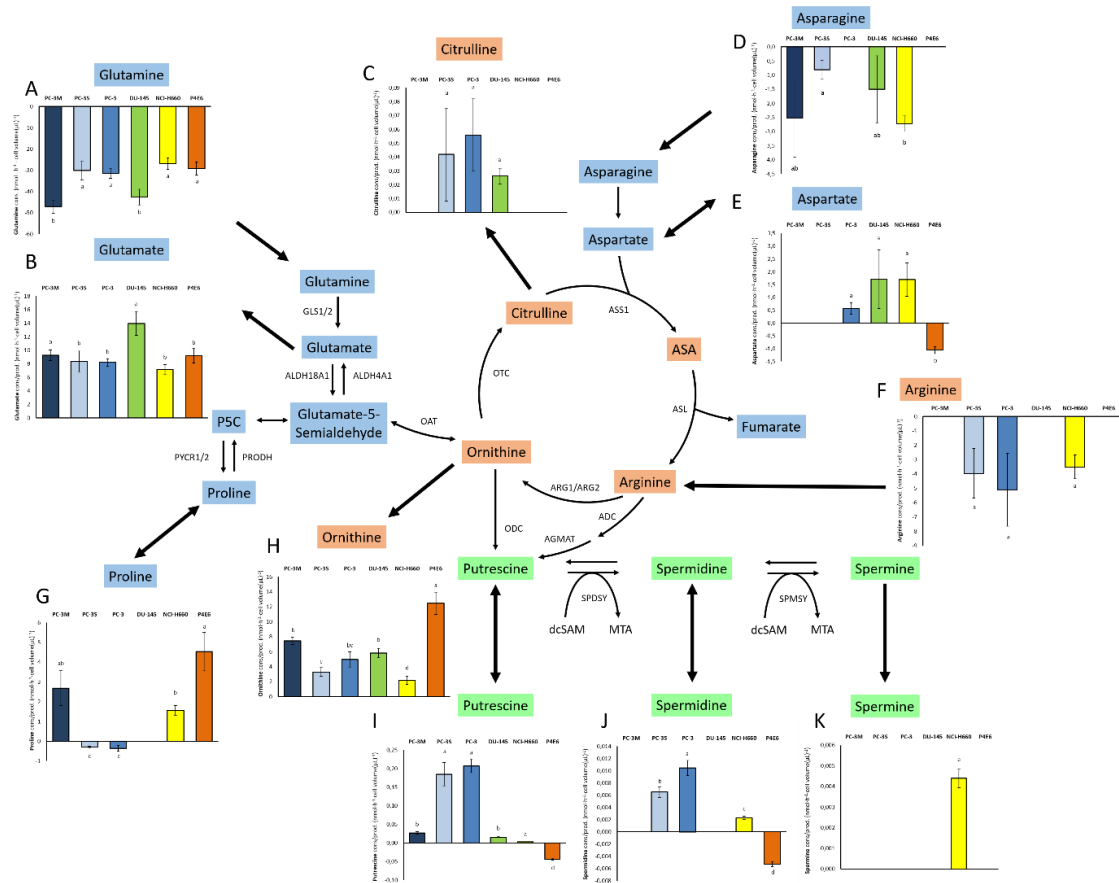


Figure 4.1.13. Metabolite exchange flux rates of urea cycle intermediates, polyamines and related amino acids in the CRPC panel normalized by cell volume. (A) Glutamine, (B) Glutamate, (C) Citrulline, (D) Asparagine, (E) Aspartate, (F) Arginine, (G) Proline, (H) Ornithine, (I) Putrescine, (J) Spermidine, (K) Spermine. Extracellular flux rates are expressed as nmol consumed or produced per hour and normalized by cell number (million cells)/cell volume (pL/cell). Significance between initial and final metabolite concentrations were evaluated using a t-Student test with $\alpha=0.05$. If the condition of significant consumption/production was met, comparison between cell lines/conditions normalized by cell volume was performed by one-way ANOVA and Tukey's multiple comparison testing. Cell lines/conditions sharing the same letter indicates absence of significant differences between them.

First, our results indicated that all the cell lines in the CRPC panel produced and secreted ornithine to the extracellular medium, the necessary precursor for polyamine synthesis

and urea cycle intermediate, and that intracellular ornithine pools did not correlate with other urea cycle intermediates, arginine and citrulline. Moreover, some of the cell lines also significantly excreted a small amount of citrulline to the extracellular medium, without a significant correlation with intracellular citrulline pools.

Indeed, polyamine synthesis from ornithine can be achieved through various amino acids, such as arginine, glutamine, glutamate or proline. Among these, we found that only the three cell lines that displayed strong polyamine secretory programs, PC-3S, PC-3 and NCI-H660, significantly consumed arginine from the culture media, suggesting that arginine may be conditionally essential for invasive CRPC and NEPC survival or phenotype maintenance. On the contrary, PC-3M and DU-145, that accumulate important intracellular polyamine pools, displayed enhanced glutamine consumption, suggesting that, potentially, polyamine pools could be preferentially obtained through glutamine in these two cell lines.

Apart from that, the alterations encountered in glutamine metabolism and polyamine synthesis in PC-3M and DU-145 can be interconnected in two different manners. The most evident is that ornithine, as previously mentioned, can be synthesized from glutamine via glutamate and P5C. The second, far less well-established, is that the recovery of the aminopropyl group of dcSAM after each step of spermidine or spermine synthesis, often termed as methionine scavenging pathway, requires a transamination reaction, in which glutamate, the most common fate of glutamine within the cell, is the most probable amino donor for methionine recovery, according to the scarce available evidence on this pathway in humans [405]. Apart from that, increased methionine consumption in PC-3M and DU-145 and lower intracellular methionine pools could also entail that these cell lines could be consuming uptaken methionine for polyamine production, instead of recycling MTA through the methionine scavenging pathway, or that they could be using both strategies to sustain polyamine synthesis.

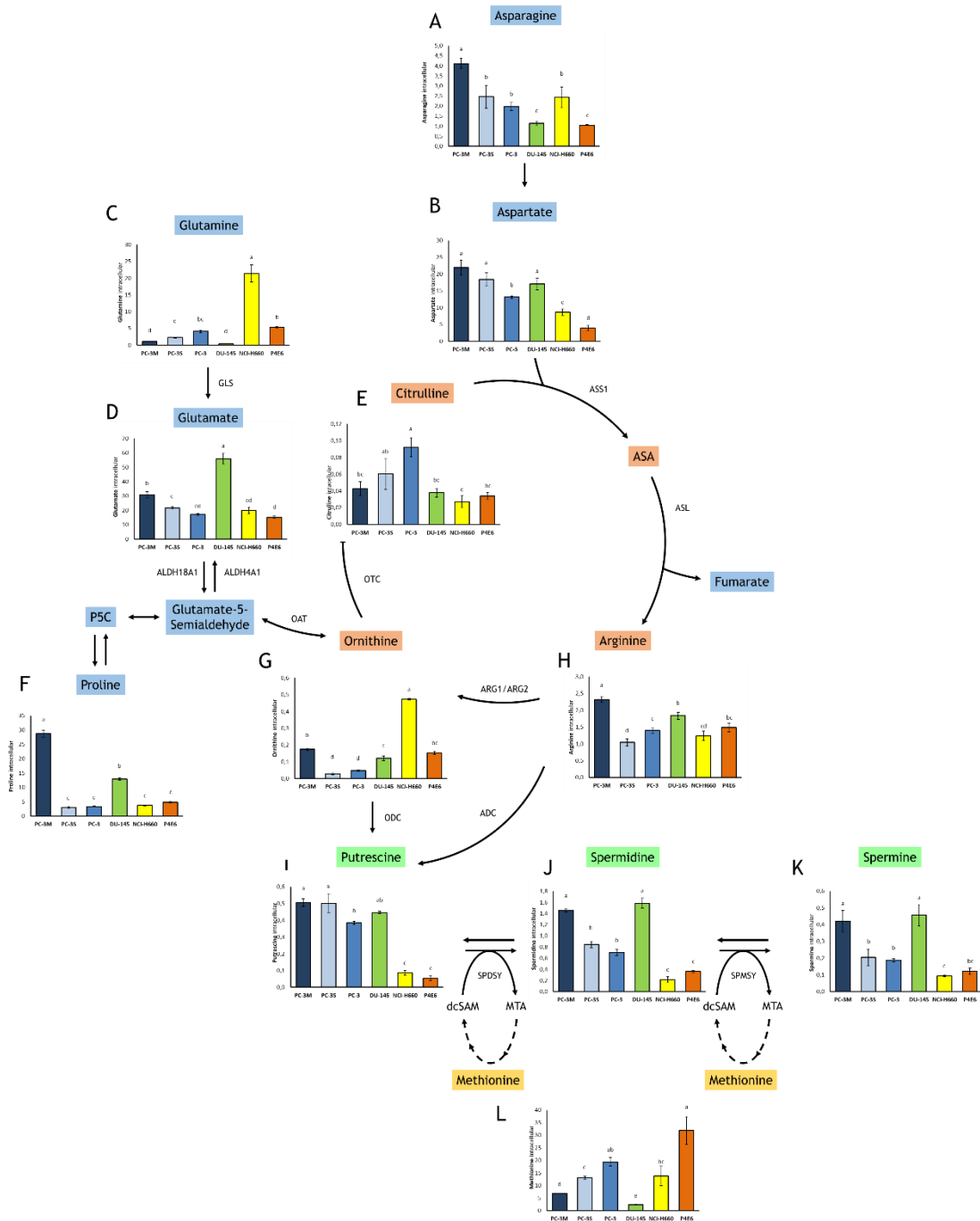


Figure 4.1.14. Metabolite profiling of intracellular polyamines and precursor amino acids and urea cycle intermediates in all lines of the CRPC panel. Displayed values are mean \pm standard deviation between three independently- extracted cell pellets for the CRPC cell lines PC-3M, PC-3S, PC-3, DU-145, NCI-H660 and P4E6. Results are normalized by median of amino acid content in each sample. Panels displayed A) Asparagine, B) Aspartate, C) Glutamine, D) Glutamate, E) Citrulline, F) Proline, G) Ornithine, H) Arginine, I) Putrescine, J) Spermidine, K) Spermine, and L) Methionine. Abbreviations: Argininosuccinate synthase 1 (ASS1), argininosuccinate lyase (ASL), ornithine transcarbamylase (OTC), glutamate oxaloacetate transaminase 1/2 (GOT1/2), glutaminase (GLS), arginine decarboxylase (ADC), ornithine decarboxylase (ODC), spermidine synthase (SPDSY), spermine synthase (SPMSY), decarboxylated S-adenosylmethionine (dcSAM), methylthioadenosine (MTA), argininosuccinic acid (ASA).

4.1.2.7. PC-3M/S display different expression profiles in the urea cycle, ornithine synthesis and polyamine metabolism

Due to the observed differences among the CRPC panel in the urea cycle, polyamine metabolism and arginine, glutamine and methionine metabolism, and the common metabolic phenotype displayed by both highly tumorigenic PC-3M and DU-145 cell lines, we decided to deepen in the functional characterization of these pathways using the PC-3M/S models of tumorigenic potential. Our aim is to assess how the reported alterations in glutamine, methionine and arginine metabolism, the urea cycle and polyamine synthesis pathways are functionally related to the enhanced tumorigenic potential of PC-3M cells.

RNASeq analysis previously conducted in our group revealed significant differences between PC-3M and PC-3S in the transcript levels of almost all the enzymes of the set of interconnected pathways comprised by the urea cycle, polyamine metabolism, P5C metabolism and the methionine cycle (**4.1.15**). First, PC-3M displayed higher levels of polyamine-synthesizing enzymes, SPDSY and SPMSY, whereas PC-3S exhibited higher expression of the polyamine-catabolizing enzyme, PAOX.

Moreover, PC-3S also displayed higher levels of the rate-limiting entrance to the polyamine synthesis pathway, ODC. Taken together, ODC overexpression, decreased polyamine synthesis and increased polyamine oxidation in PC-3S collectively point to a greater accumulation of putrescine in this cell line, which is consistent with the putrescine-secreting phenotype observed in PC-3S in the previous section (**4.1.13**). On the contrary, PC-3M secreted much lower amounts of putrescine to the extracellular medium and exhibited higher levels of intracellular spermidine and spermine (**4.1.14**), denoting increased synthesis, also in accordance with the transcriptomic evidence of increased SPDSY and SPMSY.

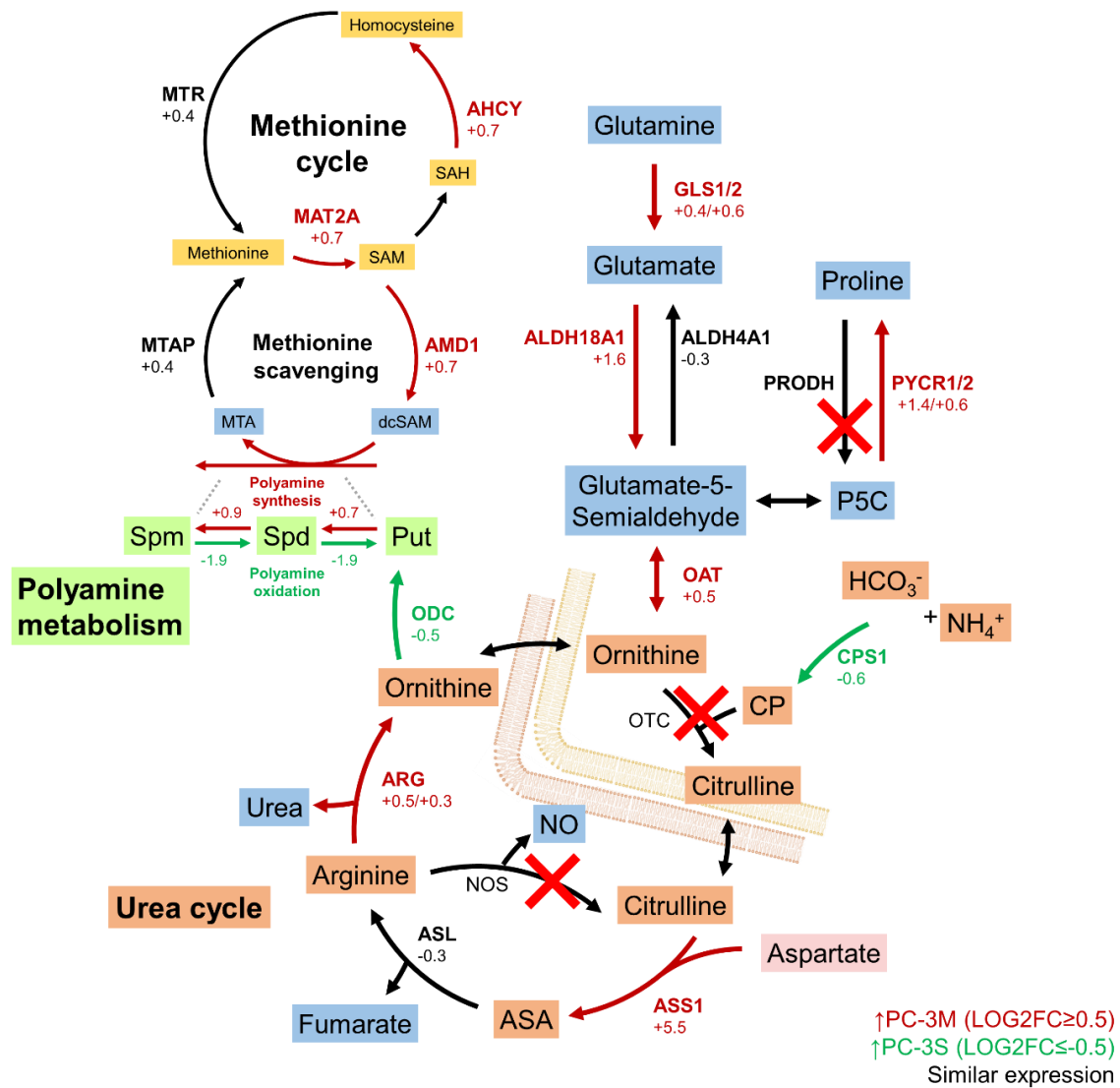


Figure 4.1.15. Schematic representation of the transcriptomic analysis by RNASeq of PC-3M and PC-3S in the urea cycle, polyamine metabolism and related pathways. Arrows and proteins shaded in red correspond to transcripts upregulated in PC-3M (LOG₂FC>0.5), arrows and proteins shaded in green correspond to transcripts upregulated in PC-3S (LOG₂FC<-0.5). Arrows and proteins shaded in black represent similar expression levels between the two cell lines (-0.5<LOG₂FC<0.5). A red cross on top of a reaction indicates that the transcript for that particular enzyme was not detected by RNA sequencing.

Indeed, polyamine synthesis requires ornithine and dcSAM. While ornithine can be obtained through different amino acids, SAM moieties can only be obtained through the methionine cycle, which relies on the uptake of the essential amino acid methionine. SAM is then converted into dcSAM by adenosylmethionine decarboxylase 1 (AMD1). Both decarboxylating enzymes, ODC and AMD have been reported as rate-limiting for polyamine synthesis. Interestingly, at the transcriptomic level, ODC is overexpressed in PC-3S cells, while AMD1 is overexpressed in PC-3M cells. Differential expression of both

enzymes could lead to a shift in polyamine synthesis bottleneck in PC-3M and PC-3S and could be the main cause of putrescine overflow and secretion in PC-3S, and of the increased accumulation of spermidine and spermine in PC-3M, supporting its enhanced tumorigenic potential through hypusination of Myc targets supporting Myc-driven tumorigenesis.

Besides that, the RNASeq analysis also revealed that PC-3M overexpressed the enzymes that allow the conversion of glutamine into proline. In accordance, our metabolomic analysis evidenced that high amounts of proline are secreted and high proline intracellular pools are encountered in this cell line, while PRODH, the enzyme catalyzing the conversion of proline into P5C, is apparently silenced, further reinforcing the proline-producing phenotype observed in PC-3M. However, as previously mentioned, this particularity of PC-3M cannot be ascribed to its highly tumorigenic potential, since similar proline levels and secretion were found in the primary tumor P4E6 and not for the also highly tumorigenic DU-145. In spite of that, this adaptation of the PC-3M/S models will allow us to limit the possible metabolic fuels of the urea cycle to only glutamine and arginine, assuming that proline cannot be converted into ornithine and enter the urea cycle in these cell lines. Moreover, to a lower extent, PC-3M also overexpressed ornithine aminotransferase (OAT), that catalyzes the reversible interconversion between glutamate-5-semialdehyde and ornithine, which could potentially represent a higher flexibility to fuel glutamine-derived carbons into the urea cycle in PC-3M.

More importantly, the transcriptomic results also unveiled a strong overexpression of ASS1 (LOG₂FC~5.5) in PC-3M. In fact, transcript expression levels of ASS1 (**Appendix 1**), would suggest that this enzyme is almost completely silenced in PC-3S. Precisely, ASS1 is the rate-limiting enzyme of the urea cycle, and it has been reported to be frequently altered in cancer, both by silencing [406] and overexpression [407]. Indeed, ASS1 is silenced in many tumors, leading to a proliferative advantage, due to the ability to divert accumulated aspartate into pyrimidine synthesis [408]. This alteration results in arginine auxotrophy, as cells lacking ASS1 cannot synthesize arginine *de novo*, and opens an important therapeutic window against ASS1-deficient tumors, through the enzymatic depletion of arginine in the bloodstream using pegylated arginase or ADI [92]. On the

contrary, ASS1 overexpression has also been reported as correlated to poor prognosis and tumor aggressiveness in gastric cancer [407], with currently unknown mechanistic implications.

In addition to ASS1 overexpression in PC-3M, both PC-3M and PC-3S displayed an apparent inability to synthesize arginine *de novo*, due to a complete lack of ornithine transcarbamylase (OTC) and almost of any nitric oxide synthase (NOS) transcript in both cell lines (**Appendix 1**). Indeed, OTC silencing may be devoted to allowing the redirection of carbamoyl phosphate into pyrimidine synthesis, whereas silencing of all NOS isoforms could be devoted to minimizing the tumor suppressor functions of NO.

Indeed, the simultaneous absence of OTC and NOS results in a necessary dependence on the uptake of exogenous arginine. According to this, both PC-3-derived cell lines would be arginine auxotrophs, or at least display a marked sensitivity to arginine starvation that could be therapeutically relevant. To our knowledge, arginine deprivation strategies to counteract the metabolic reprogramming of ASS1-positive, or even ASS1-overexpressing, metastatic CRPC has not been addressed.

4.1.2.8. PC-3M/S are arginine auxotrophs and sensitive to different arginine deprivation-based therapies according to OTC, NOS and ASS1 transcript expression levels

In light of the transcriptomic and metabolomic evidence gathered, we attempted to validate whether therapies based on arginine deprivation (AD) could be an effective option against highly tumorigenic CRPC.

First, we assessed cell proliferation of PC-3M and PC-3S in full growth medium or an arginine-free medium. Our results point out that the proliferation of both cell lines was impaired under AD, especially in the case of PC-3M (**4.1.16.A**). Moreover, both cell lines appeared to shift to a more epithelial morphology and increase cell-to-cell contacts (**4.1.16.B**), more notably in PC-3S, which displays a more disordered growth and mesenchymal appearance in origin.

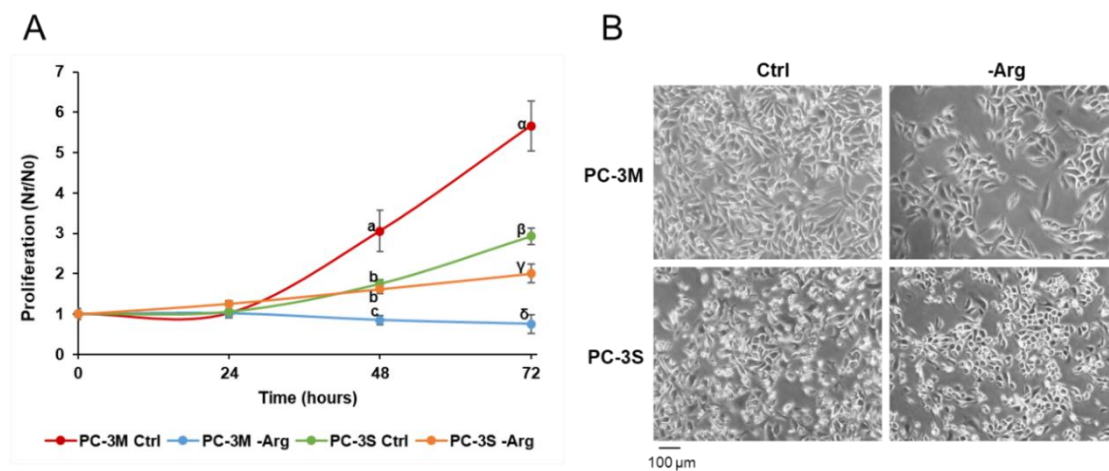


Figure 4.1.16. Cell proliferation and bright field images of PC-3M and PC-3S in full-growth medium vs. arginine deprivation (AD). (A) Growth curves of PC-3M and PC-3S in their control and arginine-depleted media. Proliferation is expressed as the relative cell number N_f/N_0 , where N_f and N_0 are the final and initial number of cells, respectively. Significant differences among cell lines and/or conditions is indicated by Latin letters (48 h) or Greek letters (72 h). In all cases, one-way ANOVA and Tukey's test for multiple comparisons were performed. (B). Bright field images of PC-3M and PC-3S under full growth or arginine-depleted media at 40x.

As explained in the introductory section, current AD-based therapies, designed for ASS-negative tumors, rely on the enzymatic conversion of arginine into citrulline (ADI-PEG) or arginine into ornithine (Arg-PEG). According to the transcriptomic results (4.1.15), due to OTC silencing, the conversion of arginine into ornithine should be effective for both PC-3M and PC-3S, whereas conversion of arginine into citrulline should only be effective for PC-3S, since PC-3M would be able to synthesize arginine from citrulline due to ASS1 reactivation. To validate these hypotheses, we attempted to rescue the decrease in proliferation caused by AD by supplementing stoichiometric amountsⁱⁱⁱ of either ornithine or citrulline in the culture medium. In agreement, the obtained results indicated that ornithine supplementation was unable to rescue the proliferation of either cell line, whereas citrulline supplementation was able to rescue the proliferation of only PC-3M (4.1.17), thus indicating that ASS1 reactivation is functional, and that Arg-

ⁱⁱⁱ Equivalent to the amount that the cells would be able to produce by transforming into ornithine or citrulline all the arginine present in RPMI-1640 full growth medium.

PEG therapy, but not ADI-PEG therapy would be effective against highly tumorigenic CRPC.

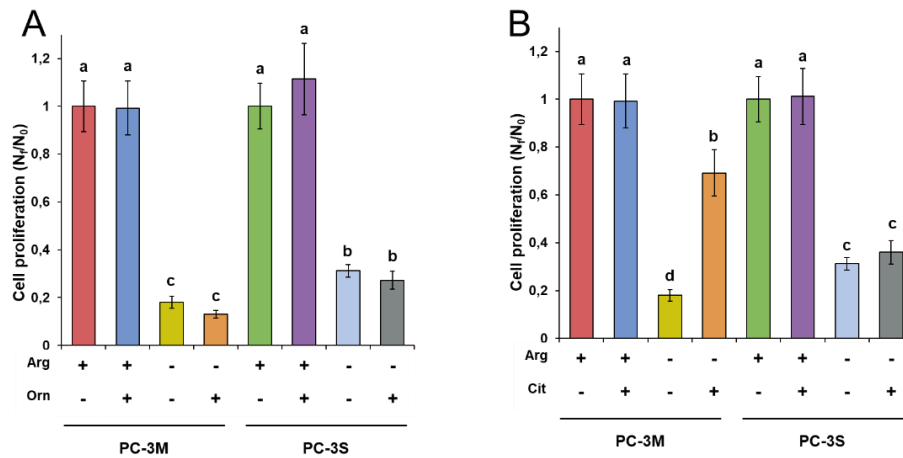


Figure 4.1.17. Rescue of cell proliferation of PC-3M and PC-3S under full growth media and arginine-deprived conditions after 72 h using ornithine (A) or citrulline (B). Rescue of cell proliferation of PC-3M and PC-3S under full growth media and arginine-deprived conditions after 72 h. In all cases, one-way ANOVA and Tukey's test for multiple comparisons were performed. Conditions sharing the same letter do not show significant differences with $\alpha=0.05$.

Next, due to the apparent shift in morphology (4.1.16), and previous evidence that linked the urea cycle to invasion [409], we decided to evaluate the effect of AD on the EMT phenotype of PC-3M and PC-3S. We observed a clear increase in E-cadherin and maintenance of N-cadherin (4.1.18.A) in both cell lines, suggesting that AD inhibits EMT. Supporting this notion, the EMT-TF ZEB1 clearly decreased in both cell lines and the EMT marker FN, only detectable in PC-3S, also decreased (4.1.18.A).

To analyze the functional implications of the observed MET, we also evaluated the migratory capacity of PC-3M and PC-3S cells under AD by wound healing assay (4.1.18.B). Our results indicate that, despite the previous identification of PC-3S as enriched in mesenchymal traits [175], PC-3M and PC-3S presented similar rates of wound closure in the wound healing assay, indicating that their functional invasive capacities are indeed similar. This is in agreement with our recent molecular characterization of EMT and CSC drivers in these cell models, which reveal that PC-3S and PC-3M overexpress different sets of molecular drivers and effectors of the EMT program [410]. Concerning AD, our results indicate that invasive capacity was substantially reduced only in PC-3M at 3, 6 and 24 h. Indeed, this indicates that the reprogramming of the EMT transcriptional cascade occurs faster in PC-3M, potentially tied to a higher urea cycle flux elicited by

ASS1 overexpression, whereas the inhibition of EMT is only evident in PC-3S in terms of EMT-TFs and CAMs after 72 h incubation (4.1.18.A).

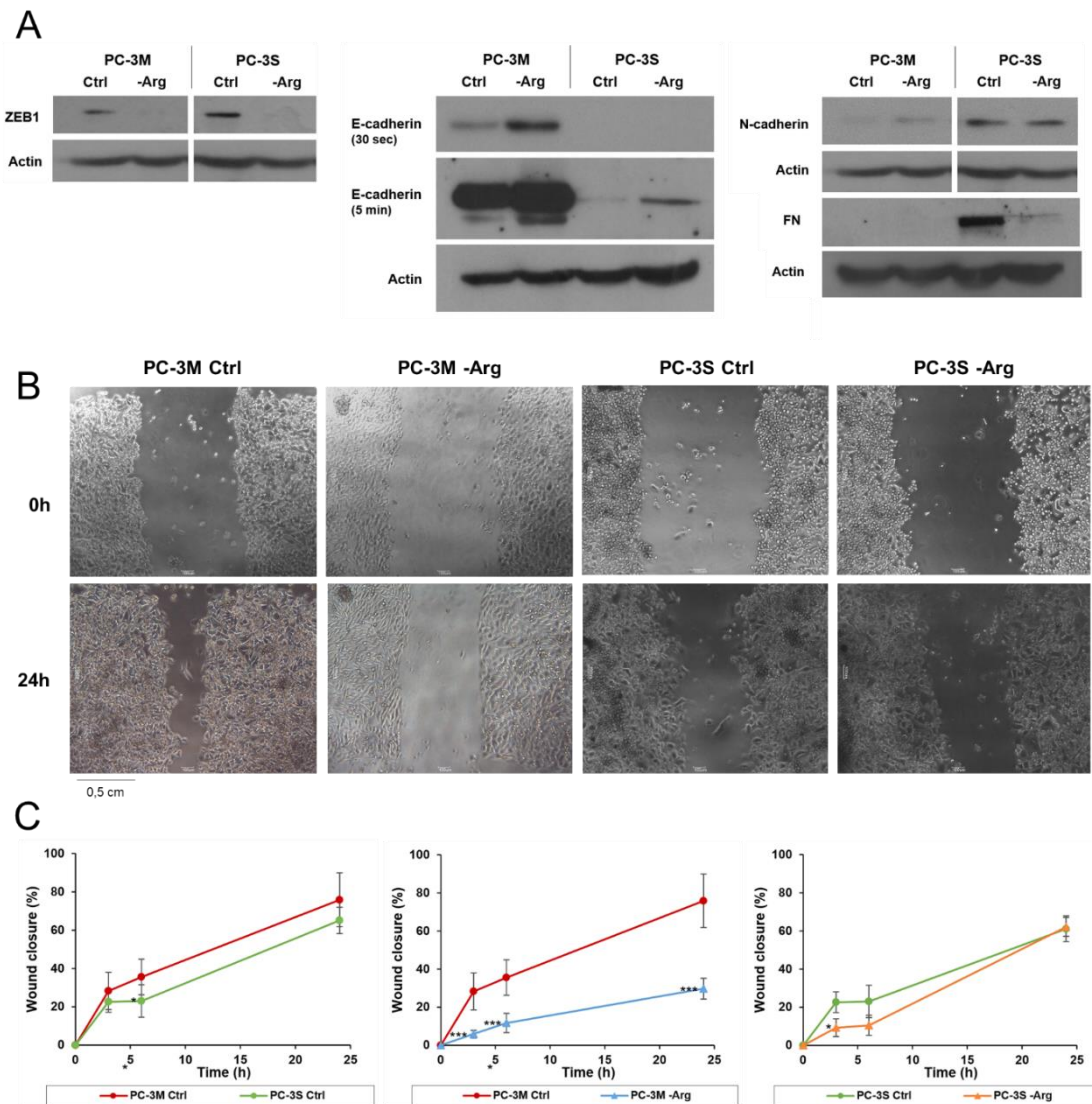


Figure 4.1.18. Effect of arginine deprivation (AD) on the EMT and the invasive phenotype of PC-3M and PC-3S. (A) Protein levels of epithelial marker E-cadherin, mesenchymal markers, N-cadherin and fibronectin (FN), and epithelial-mesenchymal transition-related transcription factor Zeb1 (n=2, α -actin was used as loading control). (B) Representative bright field images from *in vitro* wound healing assays. (C) Summary graphs showing wound closure expressed as the area covered by the cells. (n=2; *p<0.05 versus control; **p<0.01 versus control; ***p<0.001 versus control).

In light of these results, we also assessed the effect of AD on the tumorigenic capacity of PC-3M and PC-3S cells. Consistent with previous observations in **this Chapter**, all the readouts for tumorigenic traits were significantly enhanced in PC-3M compared to PC-3S (**4.1.19**). Interestingly, spheroid (**4.1.19.ABD**) and colony formation (**4.1.19.C**) capacities, and the expression of the CSC markers ALDH1A1 and Bmi1 (**4.1.19.E**) decreased under AD, whereas CD44 increased in both cell lines (**4.1.19.E**). Of note, the splicing isoform assessed is the CD44v variant (124 kDa), which has been previously identified as a marker of epithelial prostate cancer [376], and also implicated in the regulation of EMT [194]. Therefore, in our case, CD44v protein levels correlate with the EMT inhibition we observed under AD, rather than being a suitable marker of CSC traits.

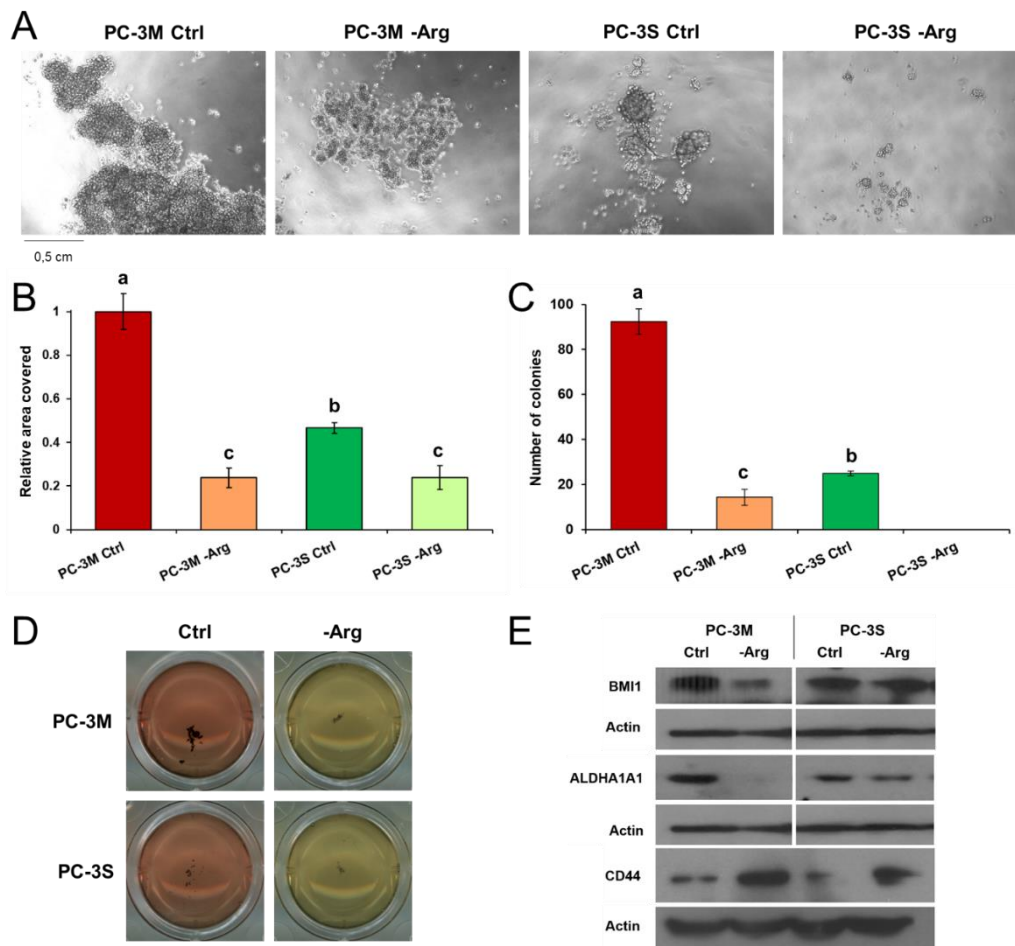


Figure 4.1.19. Effect of arginine deprivation on the tumorigenic capacity of PC-3M and PC-3S. (A) Representative bright field images of spheroids at 40x. (B) Quantification of percentage of area covered by spheroids (n=2). (C) Colony formation assay quantification represented as number of colonies (n=2). (D) Images of the spheroid mass in a representative well. (E) Western blot analysis of CSC markers (n=2). α -actin was used as loading control. In all cases, one-way ANOVA and Tukey's test for multiple comparisons were performed. Conditions sharing the same letter do not show significant differences with $\alpha=0.05$.

In summary, we have found that AD, besides greatly impairing cell proliferation of PC-3M cells, simultaneously suppressed their invasive and tumorigenic traits, being a highly appealing therapeutic perspective against metastatic CRPC in both the e-CSC and invasive steps of the invasion-metastasis cascade. To infer whether these effects in EMT and CSC programs arise from the reported urea cycle rewiring, or if they are functionally related to ASS1 overexpression in PC-3M, we intended to rescue the alteration of EMT/CSC phenotypes caused by AD with ornithine and citrulline supplementation.

First, we assessed the effect of ornithine and citrulline supplementation in the EMT phenotype, though wound healing assay (4.1.20). Interestingly, citrulline was able to completely rescue the invasive capacity of PC-3M at all time points after 3 hours, whereas ornithine had no effect on invasivity. In line with previous results shown, neither ornithine nor citrulline had any visible effect on the invasive capacity of PC-3S cells.

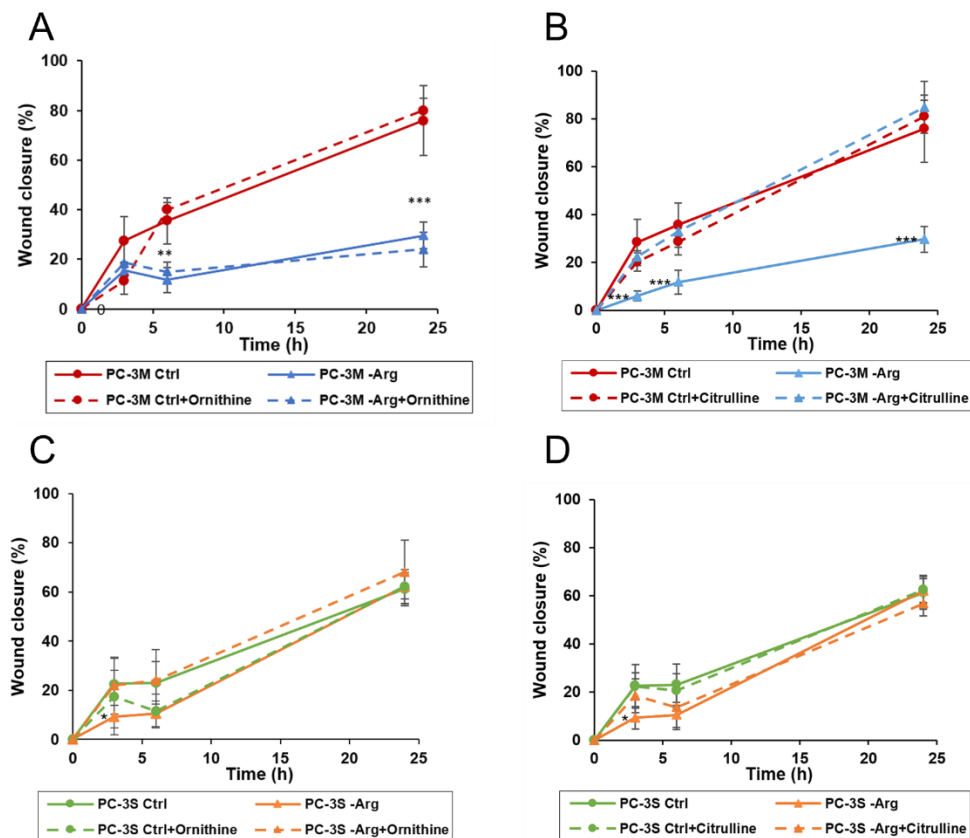


Figure 4.1.20. Rescue of wound healing capacity of PC-3M and PC-3S under full growth media and arginine-depleted conditions using ornithine and citrulline after 3,6, and 24 h using ornithine in PC-3M (A), citrulline in PC-3M (B),

ornithine in PC-3S (C), or citrulline in PC-3S (D). All panels show summary graphs showing wound closed expressed as the area covered by the cells. (n=2; *P<0.05 versus control; **P<0.01 versus control; ***P<0.001 versus control).

Outstandingly, we observed that the same pattern obtained for proliferation was reproduced in colony formation assay (4.1.21): citrulline was able to recover the tumorigenic traits of PC-3M, but not PC-3S, whereas ornithine was unable to rescue the altered phenotype in neither cell line.

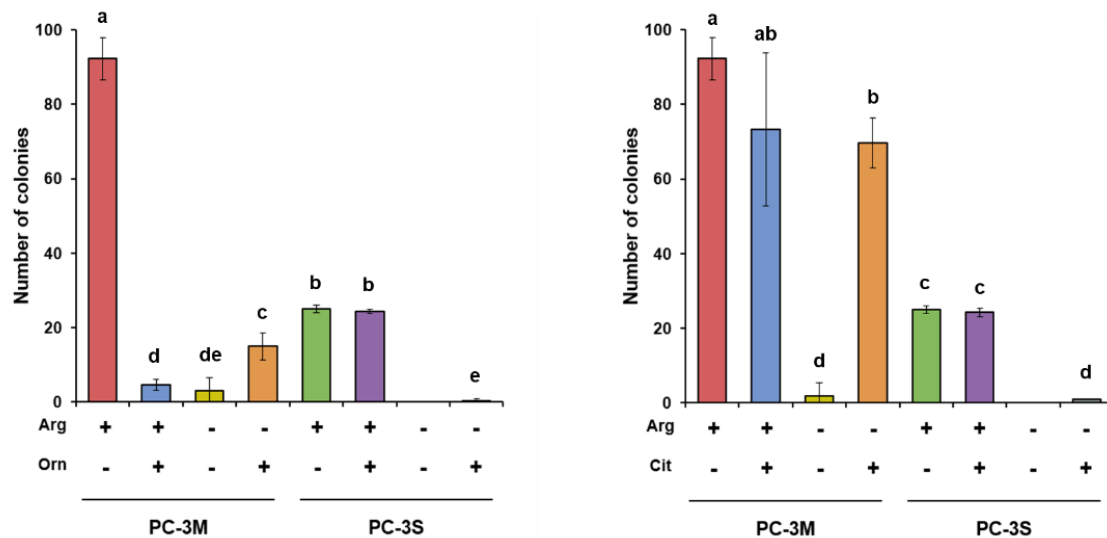


Figure 4.1.21. Rescue of colony formation capacity of PC-3M and PC-3S under full growth media and arginine-deprived conditions using ornithine and citrulline. All panels show summary graphs showing wound closed expressed as the area covered by the cells. (n=2; *P<0.05 versus control; **P<0.01 versus control; ***P<0.001 versus control).

Intriguingly, we also found that ornithine supplementation had a strong inhibitory effect on the colony formation capacity of PC-3M cells in full growth medium conditions. We hypothesized that this observation could be explained in terms of an imbalance in polyamine pools caused by ornithine addition to full-growth conditions, in which PC-3M exhibits highly-active polyamine synthesis. As stated previously, polyamine metabolism is directly linked to tumorigenic potential due to their inference in Myc signaling, which is a known regulator of ODC, AMD1 and SPDSY, and thus modulates polyamine synthesis rates. Thus, to assess if the observed drop in colony formation capacity in PC-3M after ornithine supplementation could be explained in terms of a polyamine imbalance, we evaluated the effect of adding putrescine to the culture medium in control or AD

conditions. Strikingly, we observed that, even if the addition of putrescine to the culture medium had no significant effect in PC-3M proliferation in full growth medium, the same pattern observed with ornithine was found with putrescine regarding colony formation capacity (4.1.22), suggesting that the effect of ornithine supplementation on PC-3M tumorigenesis in full growth medium can be completely explained in terms of a polyamine synthesis pathway imbalance. Notably, the observed effect with both ornithine or putrescine supplementation can be unequivocally ascribed to tumorigenic capacity, since cell proliferation was unaffected. The same pattern was also detectable to a lesser extent in the much lower colony formation capacity of PC-3S.

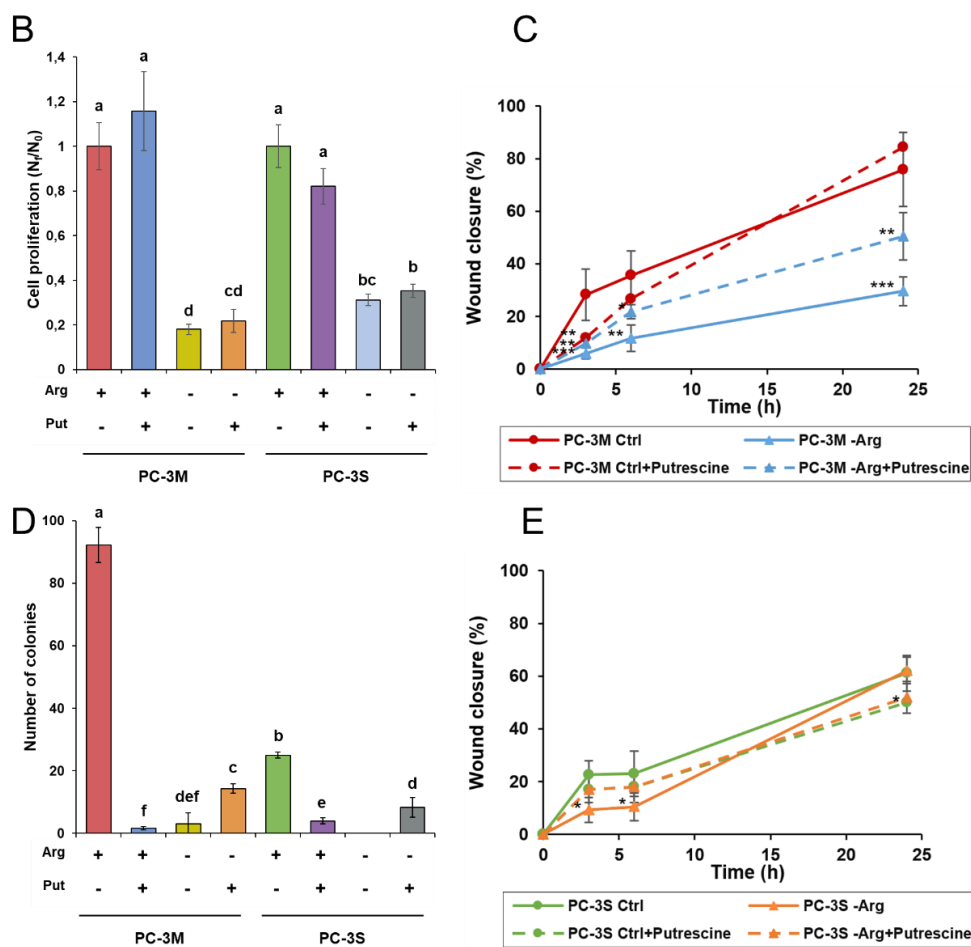


Figure 4.1.22. Rescue of colony formation and wound healing capacity of PC-3M and PC-3S under full growth media and arginine-deprived conditions using putrescine after 3,6, and 24 h using ornithine in PC-3M (A), citrulline in PC-3M (B), ornithine in PC-3S (C), or citrulline in PC-3S (D). All panels show summary graphs showing wound closed expressed as the area covered by the cells. (n=2; *P<0.05 versus control; **P<0.01 versus control; *P<0.001 versus control).**

Whereas the addition of ornithine or putrescine to full growth conditions decreased the tumorigenic capacity of PC-3M and PC-3S cells, the opposite effect than was observed in colony formation of PC-3M and PC-3S under AD. Under AD, putrescine supplementation slightly rescued the tumorigenic capacity of both cell lines, which suggests that AD may cause a major reprogramming of polyamine biosynthesis and polyamine pools that could lead to opposing effects of ornithine and putrescine in full growth medium versus AD. Nevertheless, the decreased proliferation and stemness triggered by AD could not be rescued through putrescine addition, and only a partial rescue of invasion was found in PC-3M-AD. This suggests that polyamines are indeed tied to invasion in CRPC, as reported by previous studies [144,244], but that the observed response to AD occurs, at least partially, through a mechanism that is independent to polyamine metabolism, and that arises from the urea cycle or from other pathways connected to arginine metabolism.

4.1.2.9. Metabolic reprogramming tied to arginine deprivation and glutamine deprivation in PC-3M and PC-3S

The availability of arginine and the flux through the urea cycle appear to be important contributions to the maintenance of the partial EMT and CSC phenotypic programs that lead to the high degree of malignancy exhibited by PC-3M. In particular, the rewiring of the urea cycle and arginine metabolism could be at least partially devoted to the differential replenishment and fine-tuning of polyamine pools, as evidenced by the differential effect of ornithine and putrescine supplementation in full growth medium or AD conditions. However, the simultaneous remarkable decrease in tumorigenic and invasive capacities of PC-3M under arginine restriction cannot be explain, at least solely, in terms of depletion of polyamines, as putrescine addition does not rescue completely any of the two cellular functions: tumorigenesis or invasiveness. On the other hand, glutamine was also identified as an e-CSC vulnerability previously in **this Chapter**, functionally tied to tumorigenic potential, and it can also contribute to the urea cycle and polyamine flux through its subsequent conversion onto P5C and ornithine and, possibly, also through the donation of nitrogen atoms for the re-amination of dcSAM.

Indeed, the results presented up until this point, have revealed that both glutamine and arginine are key vulnerabilities specific for highly tumorigenic phenotypes of CRPC.

Indeed, both amino acids can contribute to the urea cycle and polyamine metabolism, which we have identified as profoundly deregulated in CRPC and with a specific metabolic signature in highly tumorigenic models: higher accumulation of intracellular polyamines and decreased polyamine secretory profiles compared to lesser tumorigenic phenotypes of CRPC. Thus, in order to have a complete functional picture of these metabolic pathways in our cell models and to elucidate common mechanistic links between both, we next assessed the metabolic reprogramming of arginine deprivation (AD) and glutamine deprivation (GD) in PC-3M and PC-3S. Bearing this approach in mind, we explored the alteration of intracellular pools (4.1.24) by targeted metabolomics in PC-3M and PC-3S, under full growth media, arginine deprivation (AD), and glutamine deprivation (GD). The analysis of intracellular pools normalized by protein content revealed that the metabolic shift occasioned by GD is greater than by AD, as revealed by both the heatmap dendrogram and PCA analysis, consistent with the broader role of glutamine in cell metabolism, that impacts on the carbon and energy balance of the cell, through TCA cycle anaplerosis, and also has an important role as a precursor for glutathione synthesis.

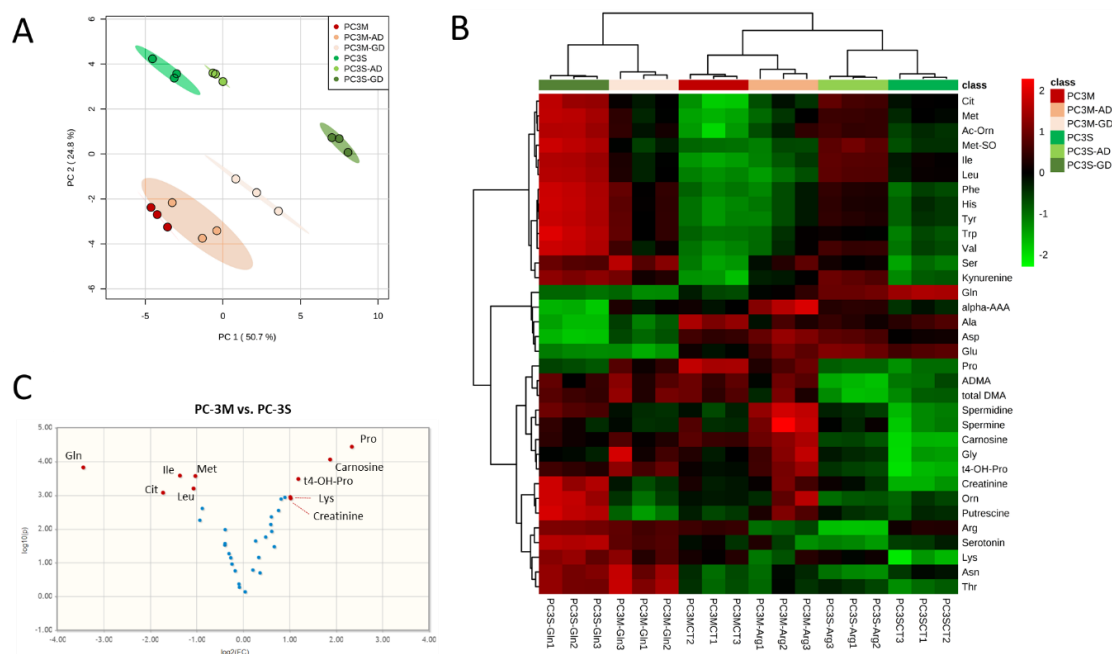


Figure 4.1.24. Metabolomic intracellular profiling of PC-3M, PC-3S under full growth medium vs. arginine deprivation (AD) or glutamine deprivation (GD). (A) Principal component analysis of the metabolomic profiling of the PC-3M, PC-3S under full growth medium, AD or GD. (B) Volcano plot ($\log_{10}(p)$ vs \log_2FC) of PC-3M and PC-3S, where p is the p value assessed by Student's t test with $\alpha=0.05$ and FC stands for fold change. All significant features

are shown in red and features with no significant differences are shown in blue. (C) Heatmap and clustering of features and cell lines/conditions. Features below or above the LOQ of the analytical method were removed and all data was normalized by protein content of each sample and log transformed prior to the analysis.

Nevertheless, performing a volcano plot analysis (4.1.25) also revealed that AD in PC-3M and GD in PC-3S caused a significant common alteration that is not present in the opposite condition (PC-3M-GD and PC-3S-AD): a marked increase in spermidine intracellular content. Notably, as described earlier, spermidine is the key polyamine required for Myc-driven oncogenesis. Besides that, the heatmap also revealed that PC-3S-GD and PC-3M-AD exhibit higher putrescine and ornithine intracellular pools than the rest of conditions. This differential response to AD and GD in both cell lines suggests that polyamine pools are sensitive to GD in PC-3S and to AD in PC-3M, which will be further investigated hereafter.

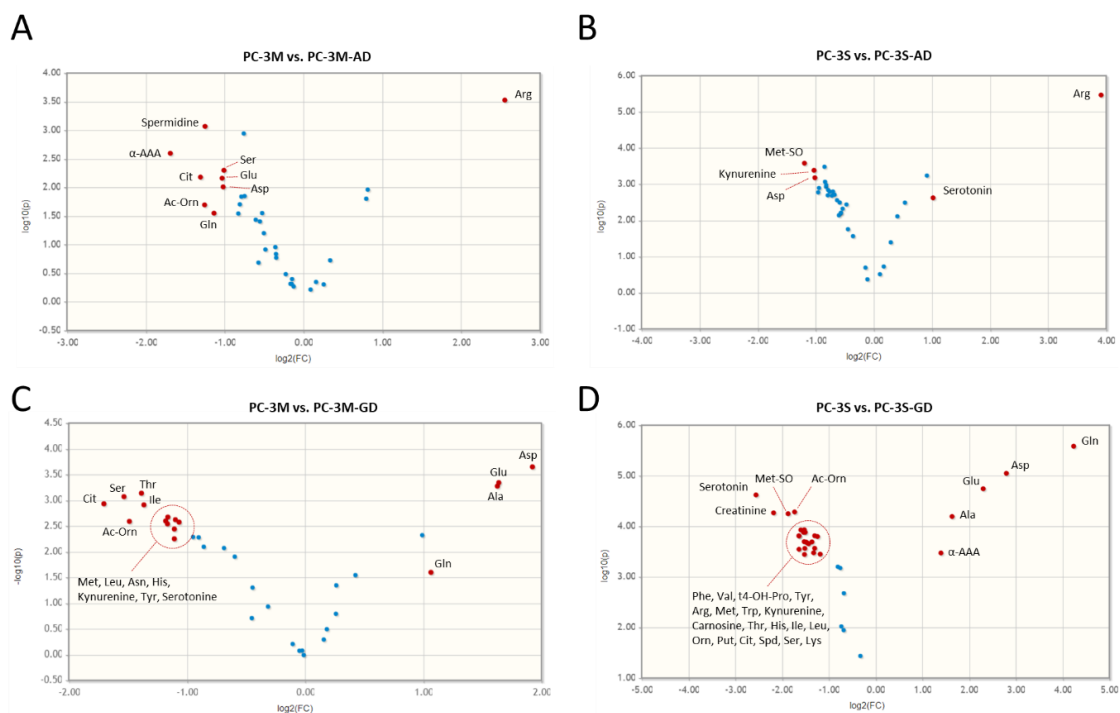


Figure 4.1.25. Volcano plots for PC-3M and PC-3S full growth media vs. arginine or glutamine deprivation. Volcano plot ($\log_{10}(p)$ vs $\log_2(\text{FC})$) of PC-3M and PC-3S, where p is the p value assessed by Student's t test with $\alpha=0.05$ and FC stands for fold change. All significant features are shown in red and features with no significant differences are shown in blue.

Interestingly, the metabolic phenotype of PC-3S-GD shifts closer to all PC-3M phenotypes, both indicated by the PCA analysis and a set of metabolites that can be identified in the heatmap, such as arginine, dimethylated arginine, carnosine or

polyamines. The rationale behind this observation may be related to the constitutively much lower glutamine pools in PC-3M than in PC-3S, in spite of higher glutamine consumption, due to increased glutaminase and glutamine utilization. This observation implicates that the constitutive low intracellular glutamine in PC-3M appears to be largely responsible for the distribution of intracellular pools of metabolites in PC-3M, since removing glutamine in PC-3S significantly increases its resemblance to PC-3M in PC2 (24.8%). Importantly, this suggests that arginine and polyamine metabolism rewiring in PC-3M could be an adaptative response to low levels of intracellular glutamine. Consistently, all these metabolites do not display significant alterations in PC-3M-GD compared to PC-3M control, suggesting that PC-3M in full growth medium could rely on arginine, rather than glutamine to support these pathways.

As reported earlier in **this Chapter** and in an associated publication [157], PC-3M cells rely on long-chain FAO, whereas PC-3S cells preferentially use fatty acids for the production of eicosanoid precursors. Strikingly, under AD and GD we observed that intracellular pools of long-chain carnitines (C14, C16 and C18) decrease in PC-3M and increase in PC-3S. Moreover, according to the total amount of circulating carnitine (free + bound), AD and GD cause a significant increase in carnitine synthesis in PC-3S, whereas total carnitine levels remain similar in PC-3M (4.1.26).

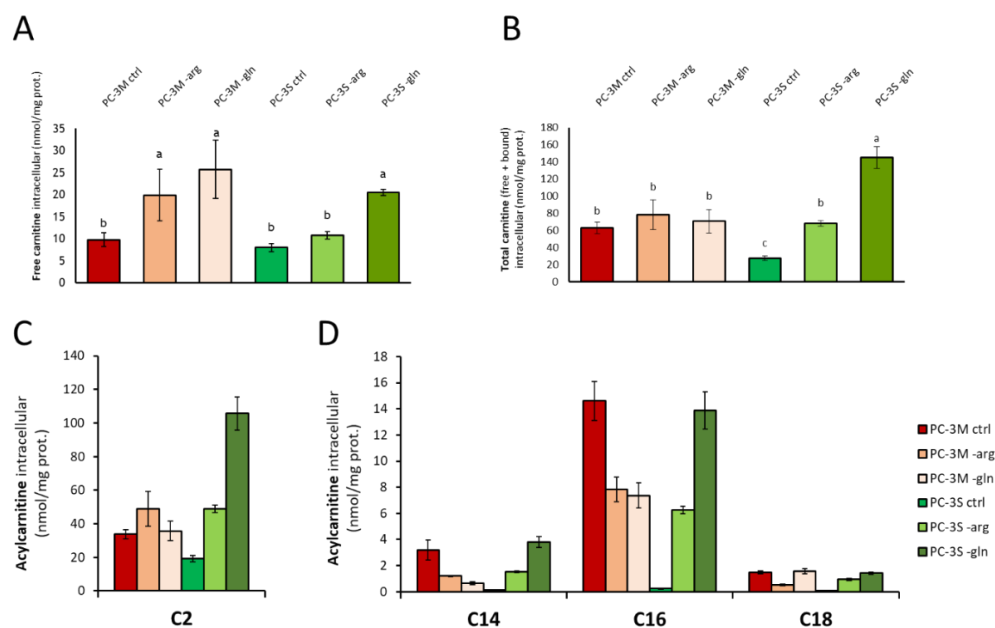


Figure 4.1.26. Intracellular carnitine and acylcarnitine profiles in PC-3M and PC-3S under AD and GD. Intracellular pools of metabolites are expressed relative to protein content: (A) Intracellular ornithine, putrescine, spermidine and

spermine in PC-3M and PC-3S in full growth media and arginine starvation. (B) Intracellular ornithine, putrescine, spermidine and spermine in PC-3M and PC-3S in full growth media and glutamine starvation.

To our knowledge, alterations in FAO as a response to AD have not been previously reported in the literature and they represent an encouraging perspective of potential source of vulnerabilities that can be exploited through combination therapies through simultaneous inhibition of FAO and arginine or glutamine metabolism.

Due to the observation that indeed spermidine could be differentially involved in only PC-3M-AD and PC-3S-GD, we have set our focus on these pathways, by displaying a further nuanced version of intracellular metabolite pools per mg of protein (**4.1.26**) and metabolite consumption or production rates (**4.1.27**).

Our targeted metabolomics analysis revealed that ornithine and citrulline pools are not depleted under either AD or GD. In the case of ornithine, its levels can be replenished by arginine under GD or glutamine under AD. On the contrary, according to the transcriptomic analysis, citrulline pools under AD can only be replenished through citrulline consumption. Moreover, all the conditions displayed significant intracellular citrulline pools, without significant citrulline consumption in either control or GD conditions. However, both PC-3M and PC-3S exhibited a lack of OTC and NOS expression, which implies that the two conventional citrulline-producing pathways are silenced.

Interestingly, this analysis also showed that the pools of the first two polyamines, putrescine and spermidine are increased in PC-3M AD, whereas they are maintained under PC-3M GD. On the contrary, putrescine and spermidine pools increased in PC-3S GD, but not in PC-3S AD. Maintenance of polyamine pools in PC-3S under AD could be at least partially aided by the suppression of the polyamine-secreting phenotype of PC-3S under AD, consisting on a decrease in putrescine production and the complete blockage of spermidine production.

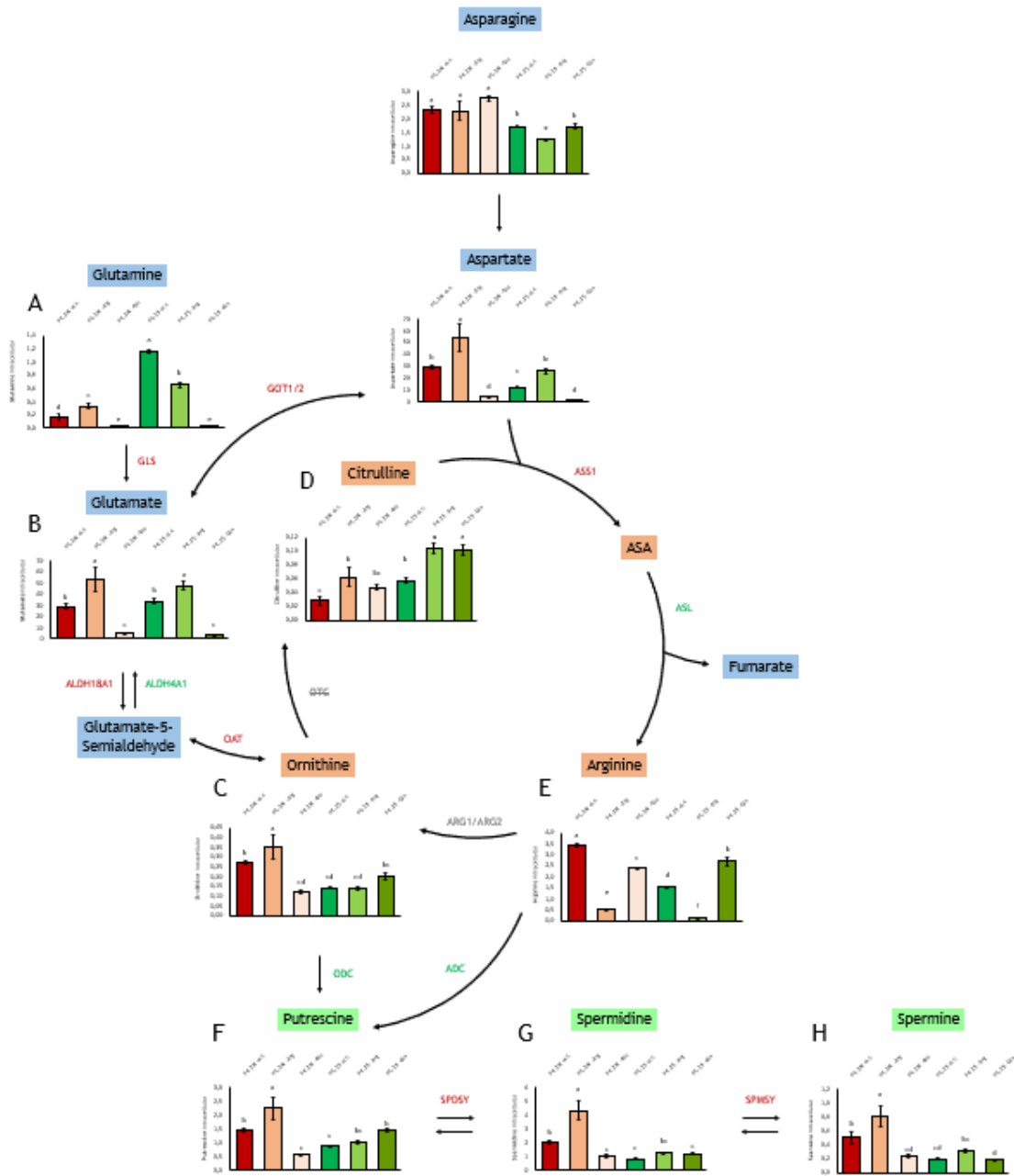


Figure 4.1.27. Intracellular pools of urea cycle intermediates, polyamines and related amino acids in PC-3M and PC-3S under arginine or glutamine starvation. Intracellular pools of metabolites are expressed relative to the median of amino acids: (A) Asparagine, (B) Aspartate, (C) Glutamine, (D) Glutamate, (E) Ornithine, (F) Arginine, (G) Putrescine, (H) Spermidine, (I) Spermine. Extracellular flux rates are expressed as μM consumed or produced per hour and million cells:

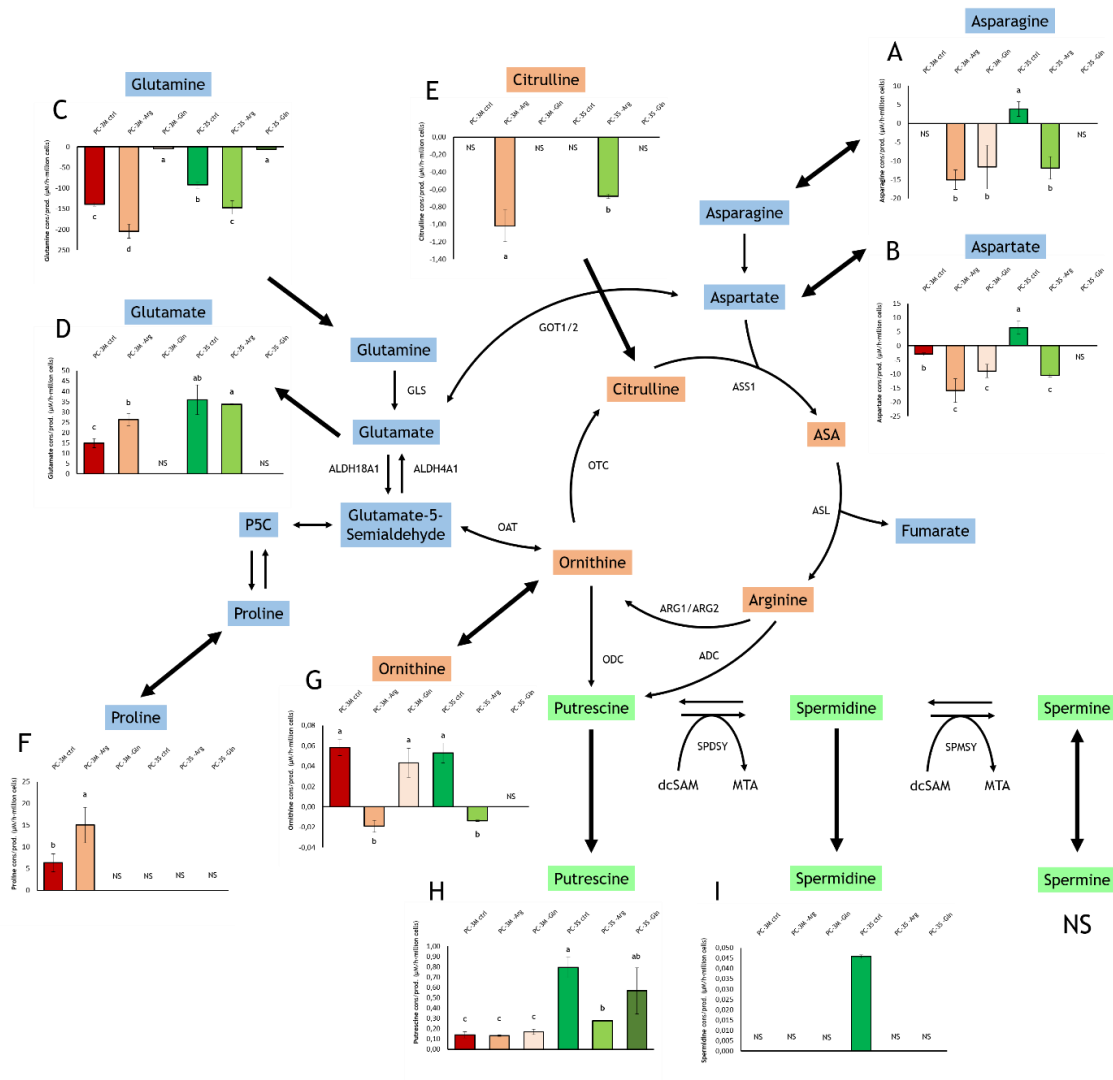


Figure 4.1.28. Exchange flux rates of urea cycle intermediates, polyamines and related amino acids in PC-3M and PC-3S under arginine or glutamine starvation. Intracellular pools of metabolites are expressed relative to the median of amino acids: (A) Asparagine, (B) Aspartate, (C) Glutamine, (D) Glutamate, (E) Ornithine, (F) Arginine, (G) Putrescine, (H) Spermidine, (I) Spermine. Extracellular efflux rates are expressed as μM consumed or produced per hour and million cells.

Moreover, AD triggers an enhanced consumption of glutamine in both cell lines, whereas enhanced secretion of glutamate and proline was only observed in PC-3M. Consumption of citrulline, ornithine, asparagine and aspartate were also stimulated in both cell lines under AD. In the case of ornithine, both cell lines shifted from a clear overflow to a slight consumption, but insufficient to explain the observed sustenance of intracellular pools of polyamines and part of their secretory profiles.

4.1.2.10. PC-3M/S sustain a rewired urea cycle through arginine protein methylation

The apparent inability to achieve the conversion of ornithine into citrulline in the PC-3M and PC-3S cell models that arose from the transcriptomic evidence and the ornithine supplementation functional assays, showed some inconsistency with the metabolomic analysis performed. Besides net citrulline pools and net citrulline production in PC-3S, our analysis also revealed important alterations in the metabolism of dimethylated arginine (DMA) species: asymmetrical dimethylarginine (ADMA) and symmetrical dimethylarginine (SDMA). Arginine methylation is an important PTM of histone and non-histone targets elicited by the protein arginine methyltransferase (PRMT) family, with a prominent role in the pluripotency and developmental program, among many other signaling functions [411].

We encountered that PC-3M and PC-3S shifted from net production of ADMA and SDMA, under full growth medium, to ADMA and SDMA consumption under AD (**4.1.29**). However, these species only constitute the by-product of protein catabolism after PRMT-mediated posttranslational modification of arginine in proteins with signaling purposes. The observed induction of DMA uptake under AD can be explained in terms of the activation of arginine transporters, which are also able to uptake DMA according to previous studies [412]. A lack of net DMA consumption or production under GD may respond to the growth arrest and previously reported global protein synthesis decrease caused by GD [413] and, consequently, an expected decrease in protein turnover.

Our results also revealed that total DMA production was significant in both PC-3M and PC-3S. Also, in accordance to the transcriptomic evidence, PC-3M contained total intracellular DMA pools, which could indicate higher arginine methylation rates, also supported by increased methionine and serine consumption, and lower methionine intracellular pools.

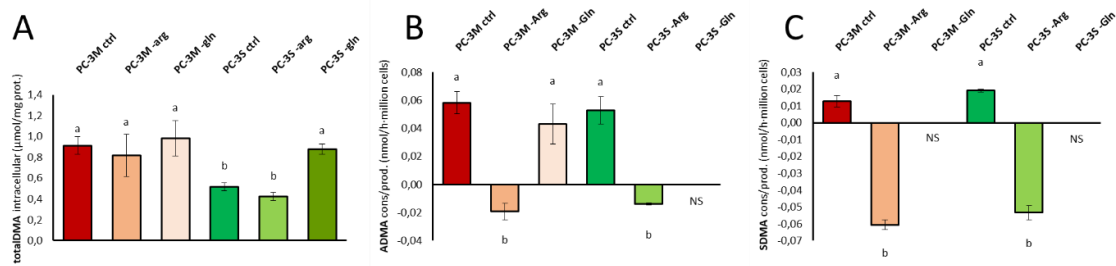


Figure 4.1.29. Total DMA intracellular pools, ADMA and SDMA consumption/production rates in PC-3M and PC-3S in control, AD, and GD conditions. Intracellular pools of metabolites are expressed relative to protein content: (A) total DMA (ADMA+SDMA) in PC-3M and PC-3S in full growth media, AD and GD. Consumption or production rate of ADMA (B) and SDMA (C) in PC-3M and PC-3S in control, AD and GD conditions.

The observations of both net citrulline production in spite of OTC and NOS silencing in PC-3M and PC-3S, and the shift from production to a clear consumption of methylated arginine species under AD made us hypothesize whether PC-3M and PC-3S cells could be using these methylated arginine species to close their apparently truncated urea cycle. Moreover, the ASS1 overexpression displayed by PC-3M, which we have already proven to be functionally relevant in these cells, would lack physiological significance if its substrate, citrulline, could not be produced in the cell and is not significantly consumed in control conditions. In this regard, the transcriptomic analysis revealed that a non-canonical version of the urea cycle, in which citrulline production was possible through arginine methylation, was more than feasible, compared to the expression levels of the canonical urea cycle citrulline-producing reactions, and was compatible with the results obtained from the metabolomic analysis.

Indeed, we hypothesize that the urea cycle in our cell lines could only be completed and citrulline production could be achieved through protein arginine methylation, elicited by PRMTs and dimethylarginine dimethylaminohydrolases (DDAH) (**4.1.30.B**). Importantly, PRMT and DDAH transcript expression levels are outstandingly much higher than OTC or NOS (**4.1.30.D**), and this alternative pathway could potentially be the main contribution to the flux through the urea cycle in our cell models.

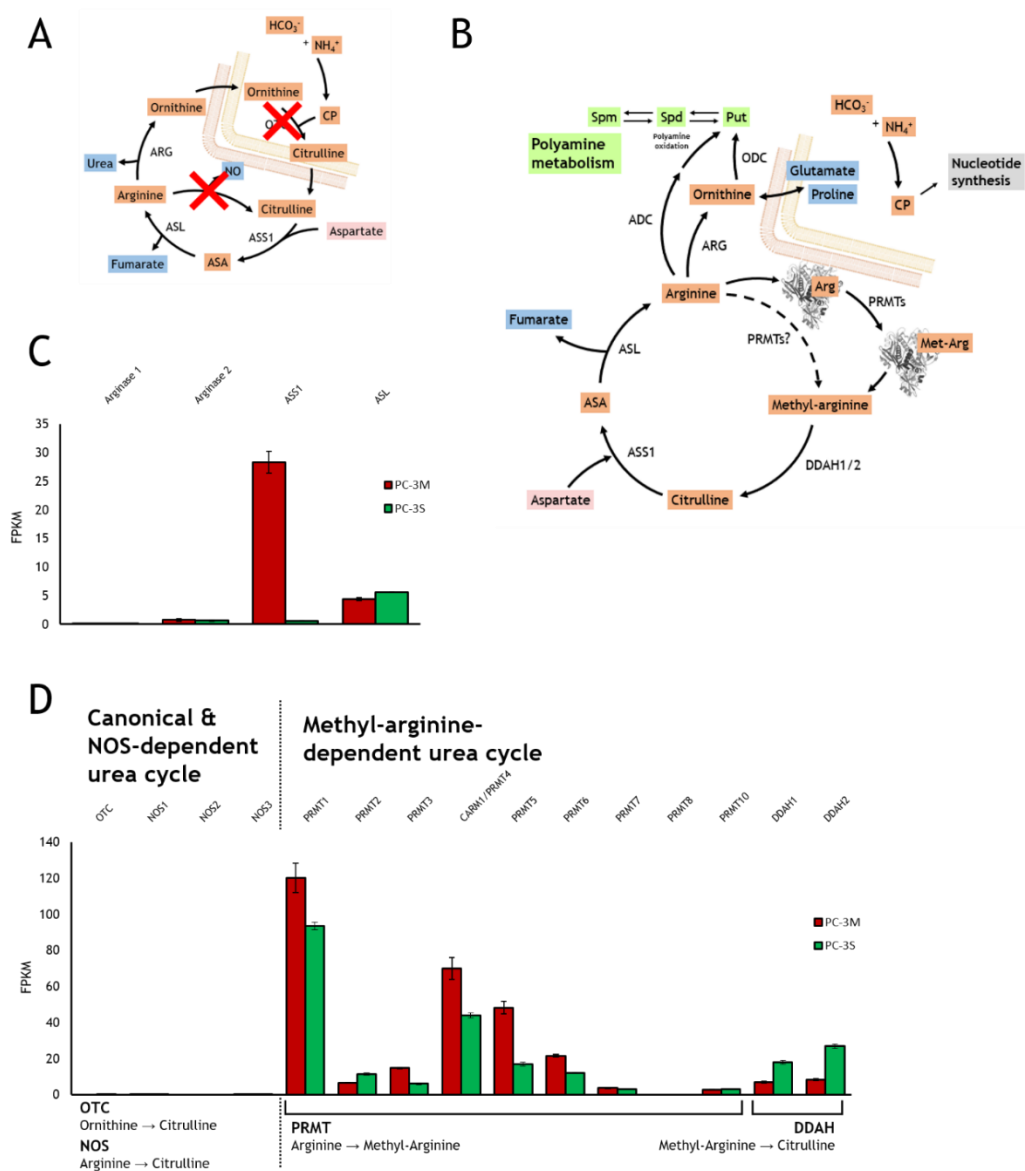


Figure 4.1.30. Transcript levels (FPKM) of the urea cycle reactions. A) Canonical and nitric oxide synthase (NOS)-dependent urea cycle versions. B) Methyl-arginine-dependent version of the urea cycle unveiled by the transcriptomic analysis of our cell models. C) Transcriptomic levels of reactions shared by both pathways: arginase 1 and 2, argininosuccinate synthase (ASS1) and argininosuccinate lyase (ASL). D) Transcriptomic levels of canonical and NOS-dependent reactions (ornithine transcarbamylase (OTC), NOS1, NOS2, and NOS3); and the proposed methyl-arginine-dependent pathway, through protein arginine methyltransferases (PRMTs) and dimethylarginine dimethylaminohydrolase (DDAH).

PRMTs are the effectors of the mono-methylation or di-methylation of arginine in histone and non-histone proteins, involved in signaling and epigenetic regulation through controlling mRNA splicing and translation and cell signaling. Indeed, PRMTs have recently bloomed in attention, due to their implication in cell differentiation, the EMT program, cancer progression and neurodegeneration [411]. Each PRMT family

member has specificity for a set of histone and non-histone protein targets. In particular, PRMT1 is involved in the regulation of EMT, by direct methylation of Twist1, required for its E-cadherin repression [414], PRMT2 is related to glucose sensing and hypoxia response, or PRMT3 is responsible for regulation of lipogenesis. Most PRMTs, notably PRMT1, PRMT4/CARM1, PRMT5, PRMT6 and PRMT7 are involved in the induction of pluripotency programs and activated during development. PRMT8 has been reported as a tumor suppressor with unclear mechanism. Similarly, PRMT10 has been identified but with currently unknown functions. Overexpression of most PRMTs tied to pluripotency programs in PC-3M (notably PRMT1, PRMT3, PRMT4/CARM1, PRMT5, PRMT6 and PRMT7) can contribute to explain the increase in stem-like features and tumorigenic capacity in this cell line. PRMT5 is a major driver of pluripotency to the extent that it is often considered among the *Yamanaka* pluripotency factors [411]. Functional studies reveal that depletion of PRMT5 reduced the number of induced pluripotent stem (iPS) cells, whereas the ectopic co-expression of Myc and PRMT5 increased the number of iPS-like cells compared to Myc alone.

On the other hand, overexpression of DDAHs has been previously linked to invasive and migratory phenotypes, in consistence with the increase in mesenchymal markers observed in PC-3S. The link between invasion and DDAH overexpression has been so far ascribed to the depletion of DMAs, known inhibitors of NO synthesis [415]. In particular, DDAHs have been found overexpressed in PCa tissue compared to BPH or healthy prostatic tissue [415]. In our case, however, the rationale behind overexpression of DDAH would be less clear and would rule out the currently established hypothesis, due to the apparent silencing of all NOS genes, and could serve a different purpose, potentially tied to the ASS1 status. Nevertheless, the proposed model is consistent with the observation of higher accumulation of intracellular citrulline pools in PC-3S than in PC-3M (**4.1.28**), which agrees with both higher DDAH expression and decreased ASS1 relative to PC-3M.

Notably, the proposed rewiring of urea cycle (**4.1.30.B**) can confer metastatic CRPC several potential advantages: silencing of OTC and arginase enable the redirection of excess mitochondrial ammonia to pyrimidine synthesis. Inhibition of NOS can avoid the tumor-suppressing functions of NO, such as activation of apoptosis or suppression of

invasiveness [409], whereas an increased flux and turnover through PRMTs may contribute to an increased stem cell and tumorigenic capacities. In spite of that, the role of ASS1 reactivation in PC-3M in this scenario remains to be elucidated.

Consistent to the proposed rewiring of urea cycle, all CRPC cell lines analyzed displayed significant ADMA intracellular pools, and all except DU-145 significantly excreted DMA to the extracellular medium, denoting overflow DMA production (4.1.19)^{iv}. Moreover, all CRPC cell lines secreted amounts of ornithine to the extracellular medium similar or higher to PC-3M and PC-3S, with silenced OTC, suggesting that OTC silencing could potentially be a widespread alteration in CRPC, as it occurs for other cancer types such as CRC [107].

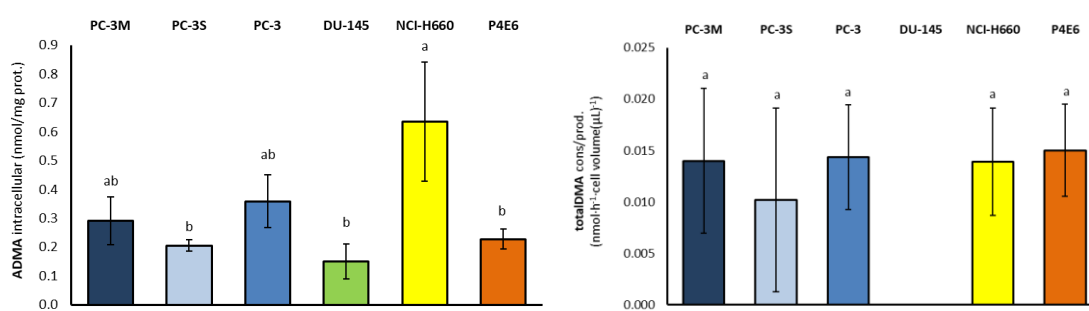


Figure 4.1.31. Intracellular pools of asymmetrical dimethyl arginine (ADMA) and total dimethylarginine (DMA) secretion in the CRPC panel.

4.1.2.11. PC-3M and PC-3S present differential fuel preference for polyamine synthesis and a Myc-driven response is triggered only upon preferred fuel shortage

The described interplay between polyamine levels and PRMT5 on the one hand, and PRMT5 and Myc on the other, lead us to the hypothesis that the polyamine-sensing ability of PRMT5 could be a dedicated regulatory mechanism that would allow Myc to sense and fine-tune spermidine levels, necessary for hypusination that activates the translation of Myc targets. Precisely, PRMT5 is a known Myc transcriptional regulator

^{iv} SDMA intracellular pools were also detected below the LOQ of the analytical method in the LC-MS/MS AB SCIEX QTRAP 4000. ADMA and SDMA quantification in cell pellets and culture media was assessed and found significant for PC-3M and PC-3S in the more sensitive model LC-MS/MS AB SCIEX QTRAP 6500.

that is sensitive to the polyamine synthesis product MTA. In particular, MTA accumulation inhibits PRMT5, which in turn results in Myc downregulation. This loop could elicit a tight feedback regulation of polyamine levels, since Myc is responsible for the transcription of ODC, AMD1 and SPDSY, prominently governing polyamine synthesis until spermidine. Indeed, the surprising increase in intracellular polyamine pools in PC-3M in response to AD, could be mediated by Myc. Potentially, an initial drop in polyamine levels could trigger PRMT5 activation, which in turn would activate Myc and cause the upregulation of ODC, AMD1 and SPDSY [154]. This hypothesis is also sustained on the observation that the maximal difference between PC-3M control and AD is found in spermidine, and that the difference between both conditions is greatly attenuated in spermine, since Myc regulates the transcription of ODC, AMD1, SPDSY, and several genes upstream to ornithine, but not SPMSY, because Myc oncogenic action requires spermidine, but not spermine. Accordingly, we observed that Myc was remarkably overexpressed under AD in PC-3M cells, but not in PC-3S, in complete agreement with the observed polyamine pools.

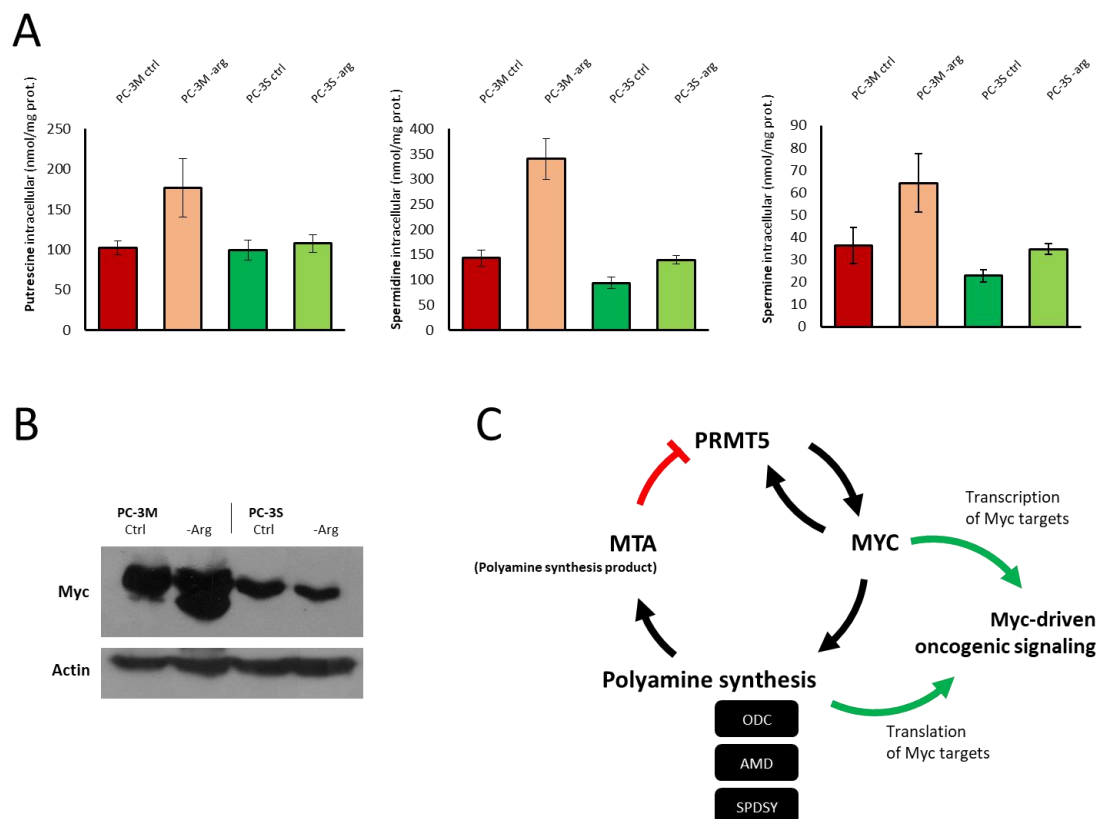


Figure 4.1.32. Intracellular polyamine pools and Myc protein levels in PC-3M and PC-3S in full growth media
Intracellular pools of metabolites are expressed relative to protein content: (A) Intracellular putrescine, spermidine

and spermine in PC-3M and PC-3S in full growth media and arginine starvation. (B) Myc protein levels in PC-3M and PC-3S in full growth media and arginine starvation. Postulated model of PRMT5-dependent regulation of polyamine pools by Myc.

Possibly, the key difference between the two cell lines that would explain all our results could rely on a differential amino acid source for the replenishment of putrescine pools. Indeed, an alternative source of putrescine production through arginine decarboxylase (ADC) has also been described in humans. Arginine decarboxylation yields agmatine, an aminoguanidinic compound with a potent inhibitory effect on polyamine synthesis. Subsequently, agmatinase (AGMAT) can hydrolyze the guanidino group, yielding putrescine. Interestingly, ADC is strongly overexpressed in PC-3S while agmatinase is strongly overexpressed in PC-3M. This would in principle lead to an accumulation of agmatine in PC-3S, causing further inhibition of polyamine synthesis, which is consistent with the metabolic phenotype described so far along **this Chapter**. On the contrary, the pattern of expression of ADC and AGMAT in PC-3M suggests a rapid conversion of agmatine to putrescine in PC-3M, representing an alternative pathway to ODC, and avoiding the accumulation of agmatine, inhibitor of polyamine synthesis, further contributing to a higher polyamine synthesis flux in PC-3M. Moreover, according to our observation that AD causes fluctuations in polyamine pools of PC-3M, this alternative pathway of putrescine synthesis could even be dominant in PC-3M.

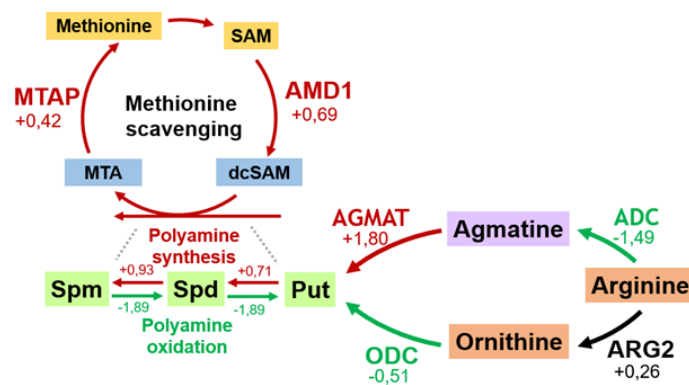


Figure 4.1.33. Schematic representation of the transcriptomic analysis by RNASeq of PC-3M and PC-3S in two known entries of polyamine biosynthetic pathway. Arrows and proteins shaded in red correspond to transcripts upregulated in PC-3M ($\text{LOG}_2\text{FC} > 0.5$), arrows and proteins shaded in green correspond to transcripts upregulated in PC-3S ($\text{LOG}_2\text{FC} < -0.5$). Arrows and proteins shaded in black represent similar expression levels between the two cell lines ($-0.5 < \text{LOG}_2\text{FC} < 0.5$).

Remarkably, the flux through ADC and AGMAT can only be fueled by arginine in our models, due to OTC deficiency. On the contrary, flux through ODC (overexpressed in PC-3S) could in principle rely on both glutamine or arginine to produce ornithine. However, the expression levels of all enzymes that convert glutamine into ornithine (GLS, ALDH18A1 and OAT) are much higher than arginase expression, which is close to zero in both PC-3M and PC-3S, and only its mitochondrial form, ARG2, is detected, which would imply that ornithine can be produced from arginine in the mitochondria, not in the cytosol, where polyamine synthesis occurs. These expression patterns would suggest that an important fraction of ornithine produced, and thus of putrescine produced through ODC, comes from glutamine, whereas the flux through ADC-AGMAT can only derive from arginine. In line with these ideas, we observed that while AD triggered a spermidine increase in PC-3M, triggered by Myc overexpression, a parallel mechanism could be triggered in PC-3S under GD, denoting that the majority of polyamine flux in PC-3S could be fueled by glutamine through ODC. Consistently, glutamine pools in PC-3S are much greater than in PC-3M.

In this regard, a recent study in PCa has shown that Myc regulation as the main director of polyamine synthesis also depends on the peroxisome proliferator-activated receptor gamma coactivator 1-alpha (PGC1 α), indicating that PGC1 α expression inhibits polyamine synthesis and PCa aggressiveness through Myc downregulation in various PCa models, delineating the role of PGC1 α as a tumor suppressor that acts by depleting polyamine pools in PCa [416]. Interestingly, this alternative mechanism may also be PRMT5-dependent, as another study also found that PRMT5 KD caused PGC1 α activation, and that PRMT5 enzymatic activity was required for PGC1 α regulation [417]. Our transcriptomic results indicate that PGC1 α is scarcely detectable in our cell models, whereas Myc and PRMT5 display high levels in both cell lines, and are both overexpressed in PC-3M, suggesting that PRMT5 can also regulate Myc in a PGC1 α -independent manner.

4.1.2.12. NF- κ B rules over c-Myc in the regulation of glutaminase under AD

To gather additional evidence on the implications of Myc overexpression in PC-3M under AD, we decided to evaluate the protein expression levels of GLS1, one of the most

characteristic Myc targets. According to our hypothesis, it would be logical to assume that, to preserve and even enhance polyamine pools under AD, polyamine biosynthetic pathway would shift from arginine to glutamine in PC-3M, reinforcing the enzymatic machinery to produce ornithine from glutamine, which is also regulated by Myc. Consistently, we had observed an increase in glutamine consumption in both PC-3M and PC-3S under AD.

However, to our surprise, we encountered a clear downregulation of GLS1 in both cell lines under AD. Indeed, GLS expression is inhibited by Myc through miRNA23, which can be inhibited by both Myc and NF- κ B [418]. Intriguingly, our results showed that Myc and NF- κ B displayed opposite behaviors under an arginine starvation regime, and that NF- κ B apparently governs GLS1 expression over Myc in our cell models, whereas Myc overexpression in PC-3M permits the activation of polyamine biosynthetic machinery, uncoupled to GLS1 protein levels.

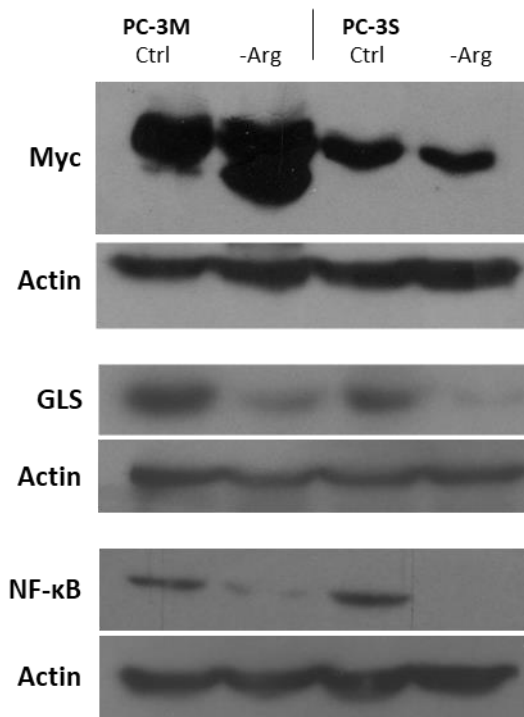


Figure 4.1.34. Protein expression levels of Myc, β -catenin, NF- κ B and GLS in PC-3M and PC-3S cells under arginine starvation.

Importantly, the observed almost complete downregulation of NF- κ B under AD in both cell lines contributes to provide a mechanistical explanation to the observed alterations in the EMT signature of PC-3M and PC-3S under AD, since NF- κ B has been extensively

reported to be tied to metastasis and regulate several EMT-TFs [419,420]. Nevertheless, another possible explanation of the observed inhibition of EMT in PC-3M and PC-3S, according to the rewiring of the urea cycle through PRMT activity we proposed, is a decrease in PRMT1 activity, which has been described as an important mediator of EMT, since direct PRMT1 methylation of Twist1 is required for E-cadherin repression [414].

4.1.2.13. Arginine or glutamine deprivation sensitize PC-3M cells to PRMT5 inhibition

To further elucidate the importance of PRMT5 in driving polyamine biosynthesis in our cell models, we next decided to evaluate the effect of PRMT5 inhibition, using its selective chemical inhibitor EPZ015666. PRMT5 inhibition has previously been reported as effective in blocking the proliferation *in vitro* and *in vivo* of mantle cell lymphoma [421]; and PRMT5 inhibition alone or synergistically with PRMT1 inhibition has also been recently described to have antiproliferative potential against diffuse large B cell lymphoma [422].

Our results point out that PC-3M cells are resistant to EPZ015666 up to 200 μ M, whereas PC-3S proliferation is decreased to roughly 50% at the same concentration (4.1.34).

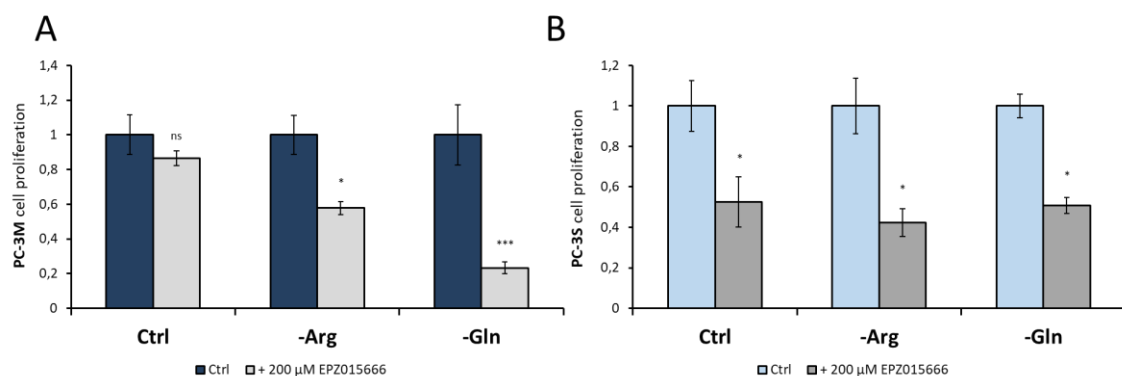


Figure 5.1.35. Effect of addition of PRMT5 inhibitor EPZ015666 on cell proliferation of PC-3M and PC-3S cells under full growth medium, arginine deprivation or glutamine deprivation. Significant differences of EPZ015666-treated cells relative to PC-3M or PC-3S cells under control, arginine-free or glutamine-free medium were evaluated by Student t-test and are indicated at $p < 0.05$ (*) and $p < 0.001$ (***)

This is consistent with the transcriptomic evidence that PC-3M cells overexpress PRMT5. Outstandingly, when assessing the effect of PRMT5 inhibition under AD or GD, we observed that such treatments sensitized PC-3M cells to PRMT5 inhibition, in particular glutamine deprivation. Interestingly, this could entail that, as described throughout **this**

Chapter, PC-3M cells could be relying on PRMTs for urea cycle and polyamine fluxes, in which both arginine and glutamine are implicated. When any of the two is removed, even if polyamine pools are preserved, the metabolic flexibility of PC-3M is compromised. This sensitization can be explained in terms of an outstanding decrease in PRMT flux upon removal of one of the two amino acids, leading to a shift from net production to consumption of DMA species in AD or no significant production or consumption in GD.

The mild efficacy of the inhibitor in full growth medium may be explained in terms of a redirection of arginine methylation from PRMT5 to other PRMTs, since a recent study has shown that simultaneous inhibition of PRMT1 (type I PRMT, ADMA-producing) and PRMT5 (type II PRMT, SDMA-producing) is highly synergistic in decreasing lymphoma tumor volume, by decreasing the production of both ADMA and SDMA, compared to each inhibitor alone [422]. PC-3M, overexpressing most PRMTs, may be particularly capable to redirect such flux and achieve resistance to PRMT5 inhibition.

Altogether, our results suggest that additional metabolic regulation networks become activated after PRMT5 inhibition that allow the replenishment of polyamine pools, whereas these mechanisms can be hampered under the shortage of either one or the other source of polyamines in our cell models, decreasing the metabolic flexibility of PC-3M cells. The mechanistic implications of the differential effect of PRMT5 inhibition in PC-3M and PC-3S remain to be elucidated, but these results reinforce the idea that PRMTs are crucial in mediating urea cycle and polyamine synthesis flux in our cell models, and that these fluxes may rely on different amino acids in a CSC and ASS1-proficient versus a non-CSC and ASS1-deficient subpopulation of metastatic CRPC. Moreover, ASS1 reactivation in PC-3M could possibly act by supporting the CSC phenotype, by avoiding the accumulation of excess DMA species despite higher global PRMT activity in PC-3M, which would cause product inhibition and hamper sustained high rates of arginine methylation in PC-3M. In any case, the observed synergy between amino acid deprivation treatments and PRMT5 inhibition opens up an important therapeutic window to further improve the efficacy of arginine- or glutamine-based therapies in CRPC.

4.2. Chapter 2: Characterization of the metabolic reprogramming associated to resistance to platinum-based chemotherapy in CRPC and CRC

4.2.1. Introduction

Platinum-based compounds are of capital importance for cancer therapy. They are extensively used in many types of tumors, including prostate [336,423] and colorectal [356,424]. Still, many tumors can circumvent the multitarget antineoplastic effect of platinum drugs by increasing drug efflux, altering active transport, enhancing DNA damage repair rates, upregulating drug detoxification mechanisms, and suppressing apoptotic stimuli [256,286].

All these processes are necessarily tied to a major reprogramming of metabolic pathways that enables an increased synthesis of nucleotides for DNA damage repair [25], allows the alteration of active transport and redox balance, or nurtures the synthesis of drug-metabolizing enzyme (DME) machinery and antioxidant response [289]. However, the metabolic adjustments that are required to meet these newly-developed needs may be different depending on the metabolic profile of the cancer tissue of origin.

For this, in **this Chapter**, we intended to investigate the metabolic reprogramming that arises in metastatic CRPC and CRC as a response to long term treatment with platinum compounds. *In vitro* long term acquired resistance approaches have been previously reported in the literature to investigate other molecular aspects of platinum resistance, such as apoptosis evasion [425], cell cycle dynamics [425], inflammatory protein secretion [426], EMT signature [427] and CSC signature [425]. All these studies were performed in many cell models, including esophageal carcinoma [426], neuroblastoma [427], NSCLC [425], or ovarian cancer [298]. The total time of drug exposure varies among studies between six and twelve months [425,427], whereas some authors use alternative approaches, such as multiple treatment cycles [426] or intermittent pulsed exposure [297] to platinum compounds.

In this work, we have generated isogenic cell models of CRPC (PC-3) and CRC (SW620) resistant to cisplatin, after continuous exposure to increasing cisplatin concentrations upon eight months, along with their age-matched controls. We expect that this approach will allow us to uncouple the effects of aging from acquired platinum resistance and will reveal the metabolic alterations that can be genuinely ascribed to acquired platinum resistance. By comparing CRPC and CRC models that are in origin radically opposed in metabolic terms, we will attempt to match the metabolic profiling obtained for each of them, seeking to unveil a common metabolic signature of platinum resistance across radically different types of metastatic solid tumors.

4.2.2. Results and discussion

4.2.2.1. CRPC PC-3 and CRC SW620 models display opposed metabolic signatures in terms of glucose energy metabolism

In **Chapter 1**, we thoroughly characterized PC-3 in metabolic terms, along with a cell panel that included different CRPC cell lines. Our results pointed out that all CRPC cell lines relied prominently on aerobic glycolysis as a carbon and energy source. Indeed, as mentioned earlier in this work, this is a metabolic feature that arises from healthy prostatic tissue, with blocked TCA cycle at the aconitase step to achieve citrate secretion. Hence, both healthy prostatic tissue and CRPC can be considered to display pronounced Warburg phenotypes [319]. In opposition, CRC has previously been reported to have a prominently oxidative metabolism, with higher rates of OXPHOS than surrounding healthy tissue and without significant overexpression of glycolytic enzymes [93,94].

First, we attempted to corroborate whether the selected parental cell models, PC-3 and SW620, could be considered as opposed in terms of glucose energy metabolism. To do so, we assessed glucose consumption (**4.2.1.A**), lactate production (**4.2.1.B**), and glutamine consumption (**4.2.1.C**), and we evaluated the cellular respiration (**4.2.1.D**) and glycolytic function (**4.2.1.E**) of both parental cell lines. Cells were cultured as specified in the Methods section.

As expected, we encountered that PC-3 cells significantly consumed more glucose and produced more lactate than SW620 cells, and their glycolysis and glycolytic capacity were significantly higher. On the contrary, SW620 displayed higher glutamine

consumption, basal respiration, higher mitochondrial ATP production, and increased spare respiratory capacity relative to PC-3 cells.

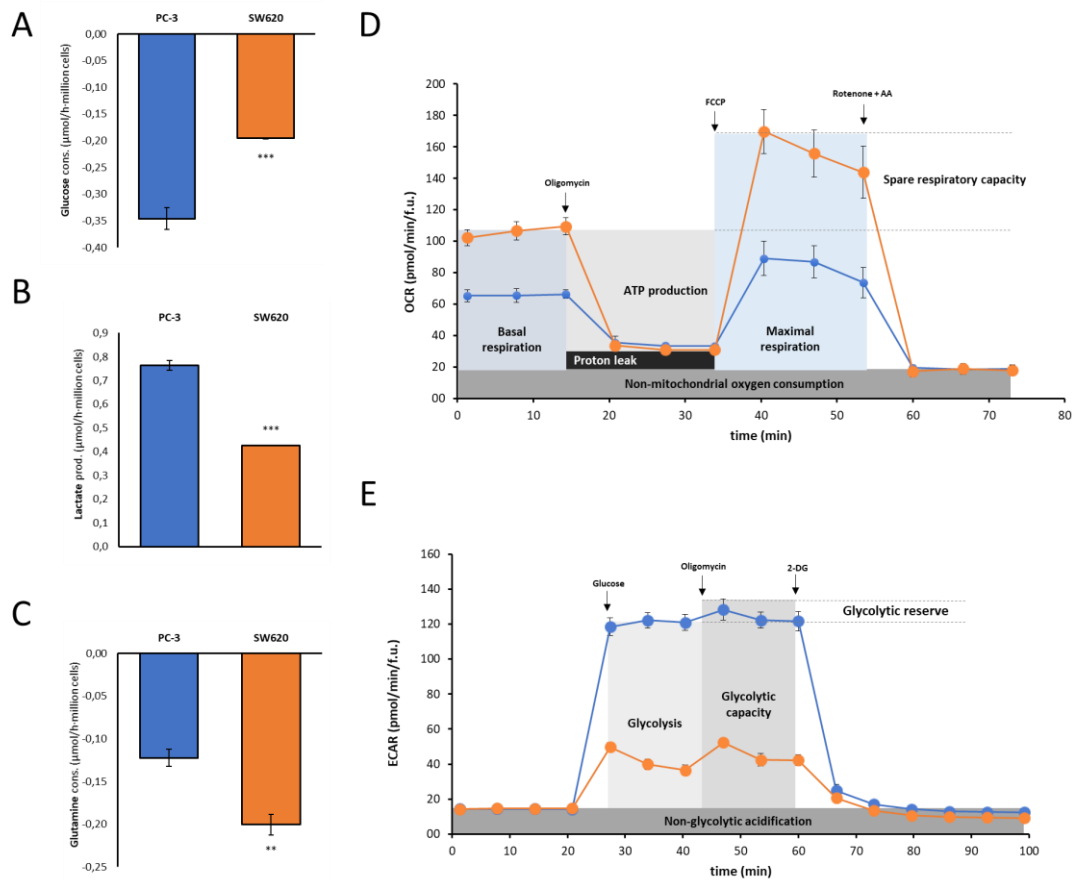


Figure 4.2.1. Compared mitochondrial and glycolytic function of PC-3 and SW620 cells (A) Glucose consumption rate, (B) Lactate production rate, (C) Glutamine consumption rate, (D) Representative example of the assessment of the mitochondrial function of PC-3 and SW620 cells and schematic representation of regions illustrating the calculation of different cell respiration-related parameters in XF *MitoStress Test*, (E) Representative example of the assessment of the glycolytic function in PC-3 and SW620 cells and schematic representation of regions illustrating the calculation of different glycolysis-related parameters in XF *Glycolysis Test*. Bars represent mean \pm SD of n=3 (AB) and n=8 (CD). Significant differences relative to PC-3 are indicated in panels A and B at $p < 0.05$ (*), $p < 0.01$ (**), and $p < 0.001$ (***)

Altogether, these results validate our parental cell models as contrasting in terms of glucose utilization and mode of energy obtention inside the cell and will allow us to evaluate the impact of platinum resistance in cancer cell metabolism when originated in glycolytic versus oxidative metastatic solid tumors.

4.2.2.2. Generation and phenotypic characterization of CRPC and CRC cisplatin-resistant cell lines

In order to generate the platinum-resistant cell lines, PC-3 and SW620 cells were incubated with increasing concentrations of cisplatin, $\Delta(IC_{10})$, along eight months. At endpoint, final IC_{50} value for cisplatin and oxaliplatin were evaluated, and the resulting cells were found to display stable minimum 10-fold increases in IC_{50} to both platinum compounds over splits 45 to 60 (See Figure **4.2.2.C** for PC-3 cells and **4.2.3.C** for SW620 cells). Indeed, the mechanisms developed by both cell models when exposed to cisplatin for a long term have also greatly increased their resistance to oxaliplatin, and thus will be termed hereafter as multiplatinum resistant (MPR), PC-3-MPR and SW620-MPR. In parallel, PC-3 and SW620 cells in full growth media without platinum exposure were subcultured to obtain an age-matched control of the resistant cells (PC-3-O and SW620-O, split 45 to 60, no drug exposure). PC-3 or SW620 (split 15 to 30)^v were also characterized as the parental cells from which their respective isogenic models (O and MPR) were obtained. All experiments were performed between split 45 and 60 for PC-3-O, PC-3-MPR, SW620-O, and SW620-MPR cells and between split 15 and 30 for PC-3 and SW620.

First, cell proliferation of all three CRPC cell lines was evaluated, finding that PC-3 and PC-3-O did not show significant differences between them, whereas PC-3-MPR displayed markedly decreased proliferation (**4.2.2.A**) as they increased about 10-fold their IC_{50} to cisplatin (**4.2.2.C**). Also, PC-3-MPR cells appeared to undergo significant morphological alterations that suggested the reinforcement of a front-rear polarity and lack of cell-cell contacts compared to PC-3 or PC-3-O (**4.2.2.B**). Indeed, PC-3 parental cell line already displayed a markedly mesenchymal phenotype, according to the EMT characterization carried out in **Chapter 1**.

Finally, we also evaluated if the addition of cisplatin to all PC-3 cell lines significantly induced apoptosis (**4.2.2.D**). Even if slight significant changes were observed, our results

^v In **Chapter 1** and **Chapter 3** of this work, PC-3 and SW620 were also used between passages 15-30 and thus are comparable to the parental cell lines used in **this Chapter**.

globally indicated that all PC-3 cells, both parental and resistant, were outstandingly capable of evading cisplatin-induced apoptosis at a concentration that significantly affected their proliferation (their respective IC₅₀ values). Indeed, percentages of healthy cell populations vary only between 98 and 92%. These results indicate that the effect of cisplatin on the proliferation of PC-3 cells is essentially cytostatic.

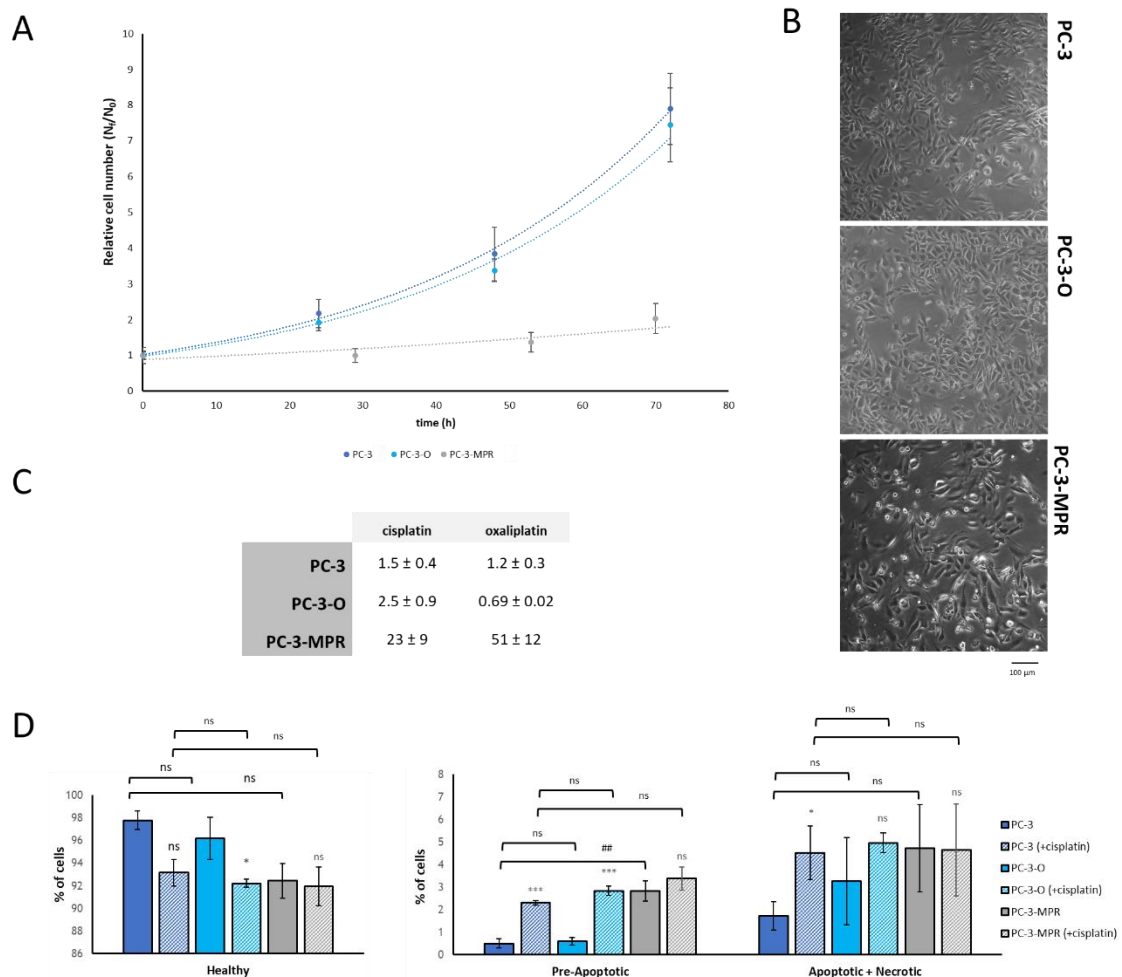


Figure 4.2.2. Cell proliferation, bright field images, and effect of cisplatin addition on apoptosis of PC-3, PC-3-O, and PC-3-MPR (A) Growth curves of PC-3, PC-3-O, and PC-3-MPR. Proliferation is expressed as the relative cell number N_f/N_0 , where N_f and N_0 are the final and the initial number of cells, respectively. (B) Bright-field images of PC-3, PC-3-O, PC-3-MPR at 40x. (C) IC₅₀ (µM) of cisplatin and oxaliplatin in PC-3, PC-3-O, and PC-3-MPR. (D) Percentage variations of alive, early apoptotic and late apoptotic/necrotic cell populations at 72 h incubation with cisplatin at their respective IC₅₀ concentrations in PC-3, PC-3-O, and PC-3-MPR. Cells were stained with propidium iodide (PI) and FITC-annexin and were analyzed by flow cytometry. Bars represent mean ± SD of $n=3$. Significant differences between cisplatin addition and the untreated condition were evaluated by Student t-test ($\alpha=0.05$) and are indicated at $p < 0.05$ (*), $p < 0.01$ (**), and $p < 0.001$ (***). Significant differences among cell lines (untreated) relative to PC-3 are indicated at $p < 0.05$ (#), $p < 0.01$ (##), and $p < 0.001$ (###). Statistical significance is not shown in panel A.

Similarly, SW620 and SW620-O were found to proliferate at similar rates, whereas SW620-MPR proliferation rate was markedly lower (4.2.3.A). Moreover, SW620-MPR also increased by more than 10-fold their IC₅₀ to cisplatin and oxaliplatin (4.2.3.C), and, unlike PC-3, apoptosis was induced to a significant extent in the parental and the SW620-O cell lines (4.2.3.D). Interestingly, SW620-O showed enhanced resistance to cisplatin-induced apoptosis relative to SW620, potentially denoting a certain acquired capacity to evade apoptosis with cell aging. On the other hand, SW620-MPR did not show any significant increase in apoptosis (Annexin V⁺ cells) or other kinds of cell death (PI⁺ cells) upon addition of cisplatin at their IC₅₀ concentration, denoting an increased capacity to evade apoptosis and that the antiproliferative effect of cisplatin in SW620-MPR cells is essentially cytostatic.

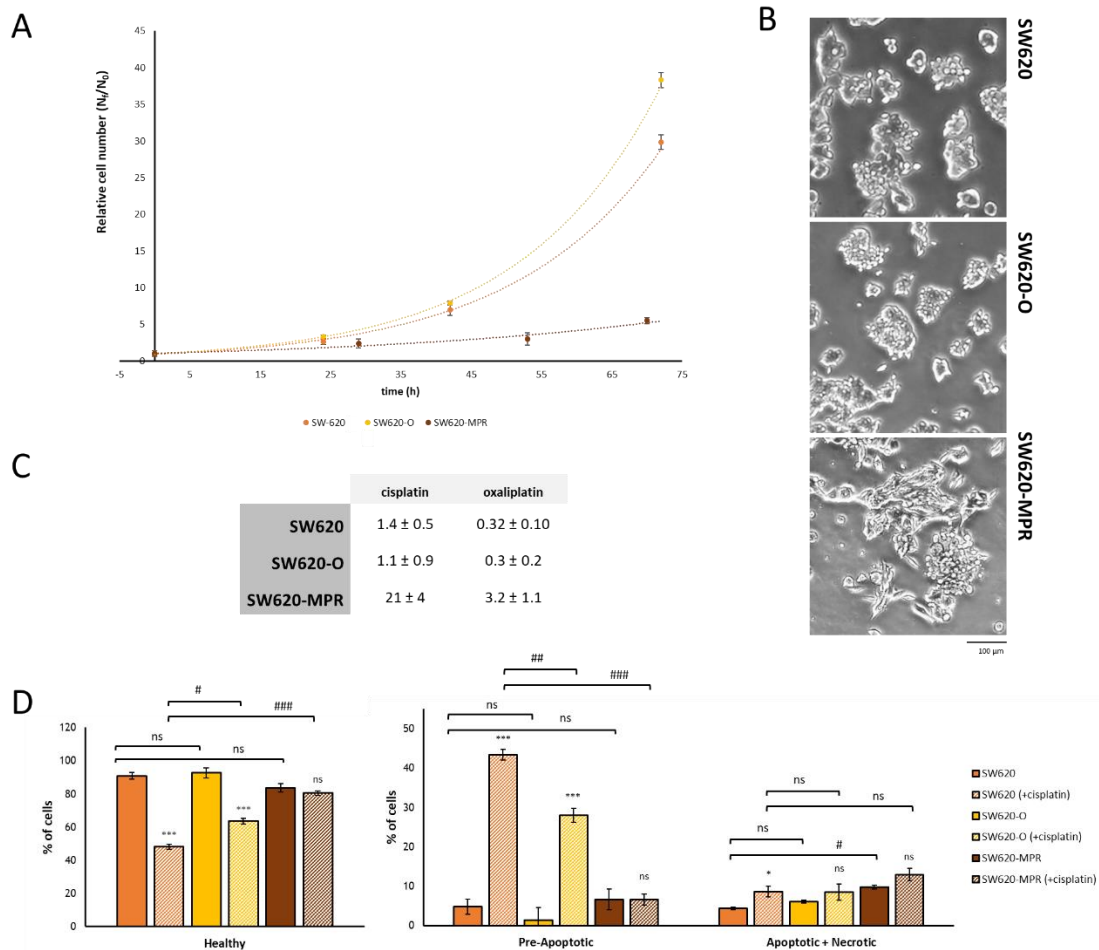


Figure 4.2.3. Cell proliferation, bright-field images and effect of cisplatin addition on apoptosis of SW620, SW620-O, and SW620-MPR (A) Growth curves of SW620, SW620-O, and SW620-MPR. Proliferation is expressed as the relative cell number N_t/N_0 , where N_t and N_0 are the final and initial number of cells, respectively. (B) Bright-field images of SW620, SW20-O, SW620-MPR at 40x. (C) IC₅₀ (μ M) of cisplatin and oxaliplatin in SW620, SW620-O, and

SW620-MPR. (D) Percentage variations of alive, early apoptotic and late apoptotic/necrotic cell populations at 72 h incubation with cisplatin at their respective IC_{50} concentrations in SW620, SW620-O, and SW620-MPR. Cells were stained with propidium iodide (PI) and FITC-annexin and were analyzed by flow cytometry. Bars represent mean \pm SD of $n=3$. Significant differences between cisplatin addition and the untreated condition were evaluated by Student t-test ($\alpha=0.05$) and are indicated at $p < 0.05$ (*), $p < 0.01$ (**), and $p < 0.001$ (***). Significant differences among cell lines (untreated) relative to SW620 are indicated at $p < 0.05$ (#), $p < 0.01$ (##), and $p < 0.001$ (###). Statistical significance is not shown in panel A.

Bright field images of SW620 revealed that they tend to proliferate in cell clusters, with a high degree of cell-cell contacts and marked apicobasal cell polarity, denoting a clear epithelial status (**4.2.3.B**), particularly when compared to PC-3. On the contrary, SW620-MPR appeared to shift to a much more disordered and contact-independent growth, with an evident front-rear polarity, hinting to the activation of EMT [216]. Notably, the morphological differences between SW620-MPR and both untreated cell lines are qualitatively more evident than the ones observed in PC-3, PC-3-O, and PC-3-MPR.

In light of the apparent morphological alterations in MPR cell lines we next characterized the EMT state and tumorigenic potential of parental, aged and platinum resistant cell lines, with the hypothesis that, in both cases, the activation of EMT is triggered upon acquisition of platinum resistance. In accordance to our hypothesis, both cell lines showed signs of having undergone EMT (**4.2.4.AB**). In all PC-3-derived cell lines, only N-cadherin was detected, and its expression was notably increased upon acquisition of MPR. On the contrary, for SW620 and its isogenic cell lines, only E-cadherin was detected, denoting a significantly more epithelial phenotype in origin. SW620-MPR gradually decreased expression of E-cadherin upon acquisition of resistance, but a switch to expressing N-cadherin was not detected.

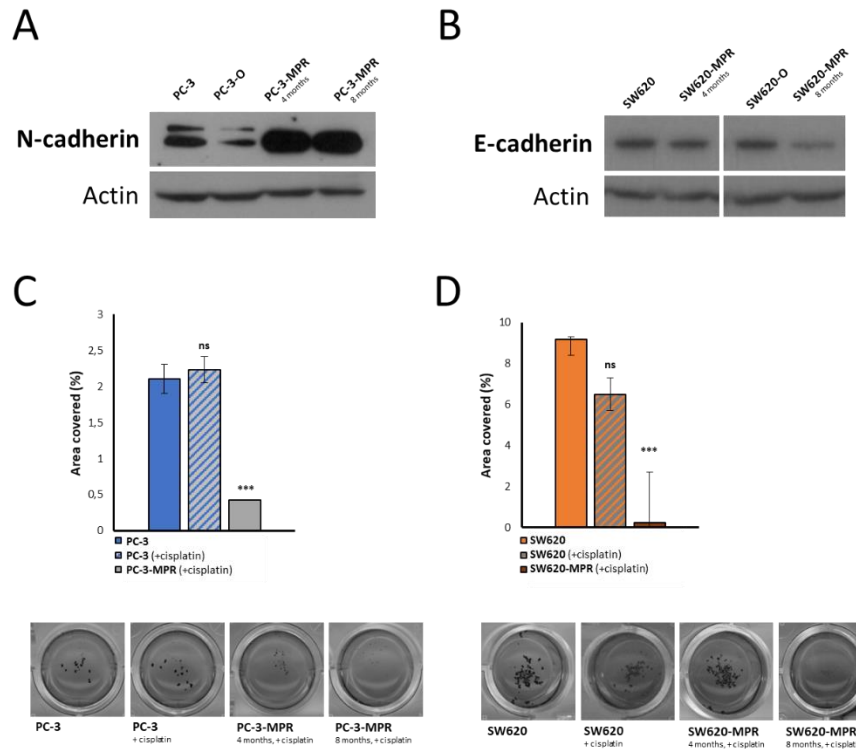


Figure 4.2.4. Characterization of E-cadherin and N-cadherin expression and spheroid formation capacity of PC-3/O/MPR and SW620/O/MPR. (A) N-cadherin protein levels in PC-3, PC-3-O and PC-3-MPR determined by Western Blot. Actin was used as a protein loading control. (B) E-cadherin protein levels in SW620, SW620-O and SW620-MPR determined by Western Blot. Actin was used as a protein loading control. (C) Spheroid formation capacity of PC-3-derived cell lines. When specified, cisplatin was added to the medium to a final concentration of 1 μ M. (D) Spheroid formation capacity of SW620-derived cell lines, assessed seeding 10^3 cells in ultra-low-attachment plates. When specified, cisplatin was added to the medium to a final concentration of 5.5 μ M. For C and D panels, spheroid formation capacity was assessed by seeding 10^3 cells in ultra-low-attachment plates. Spheroid plates were scanned after 7 days and quantified using *Image J*. Data shown is the mean \pm SD from at least $n=3$. Significant differences relative to PC-3 or SW620 control cells were evaluated by Student t-test and are indicated at $p < 0.05$ (*), $p < 0.01$ (**), and $p < 0.001$ (***).

Indeed, both cell lines transitioned to a more mesenchymal phenotype, which has also been reported for other platinum-resistant solid tumors such as neuroblastoma [427]. This same study also identified that, even if EMT was functionally activated in all resistant cell lines, expression of EMT-TFs ZEB1 and Snai1 were suppressed upon acquisition of resistance. Indeed, this represents a potential link between the observed EMT activation and the metabolic phenotype of resistant cells. For instance, Snai1 has been reported to promote a Warburg-like phenotype, by inhibiting respiratory complexes and isoforms of glycolytic enzymes that divert the glycolytic flux into PPP, such as FBP1 or PFKP [241,435]. Hypothetically, this decrease in Snai1 upon platinum

resistance could be devoted to diverting glycolytic flux to PPP to increase NADPH production for ROS mitigation.

On the other hand, both CRC and CRPC markedly decreased their spheroid-forming capacity (**4.2.4.C**). As discussed along **Chapter 1**, a decrease in the capacity to form spheroids, besides indicating a loss in CSC potential, can also denote a loss in epithelial traits, since the adherens junctions responsible for the formation of the epithelial mass through cell-cell contact require E-cadherin expression [371]. In accordance, the results of our spheroid formation assays would be consistent with the results obtained regarding E-cadherin and N-cadherin expression in both cell lines.

4.2.2.3. PC-3-MPR and SW620-MPR cells present opposed alterations in glucose and glutamine metabolism

Our aim in **this Chapter** is to perform a metabolic characterization of acquired platinum resistance in metastatic tumors, either prostate or colorectal, displaying opposite metabolic profiles. This approach can potentially allow us to unveil a common metabolic signature of platinum resistance that can serve as a prognostic biomarker for radically-different metastatic solid tumors or that could be targeted in combination therapies in the future in order to overcome multiplatinum resistance.

In an approach parallel to the followed in **Chapter 1** for the CRPC panel, we first attempted to evaluate whether the generated resistant cell lines differed significantly from their age-matched controls in terms of central metabolism, by examining the glucose and glutamine consumption rates (**4.2.5**). To our surprise, we encountered that PC-3-MPR and SW620-MPR cell lines had deviated from their age-matched controls in opposite directions. PC-3, essentially glycolytic in origin, had decreased glucose and glutamine consumption upon acquisition of resistance since PC-3-MPR exhibited lower consumption rates than both PC-3 and PC-3-O (**4.2.5.AC**). On the contrary, SW620 cells, more oxidative in origin, significantly increased glucose and glutamine consumption rates upon acquisition of resistance since SW620-MPR displayed higher consumption rates than SW620 and SW620-O (**4.2.5.BD**).

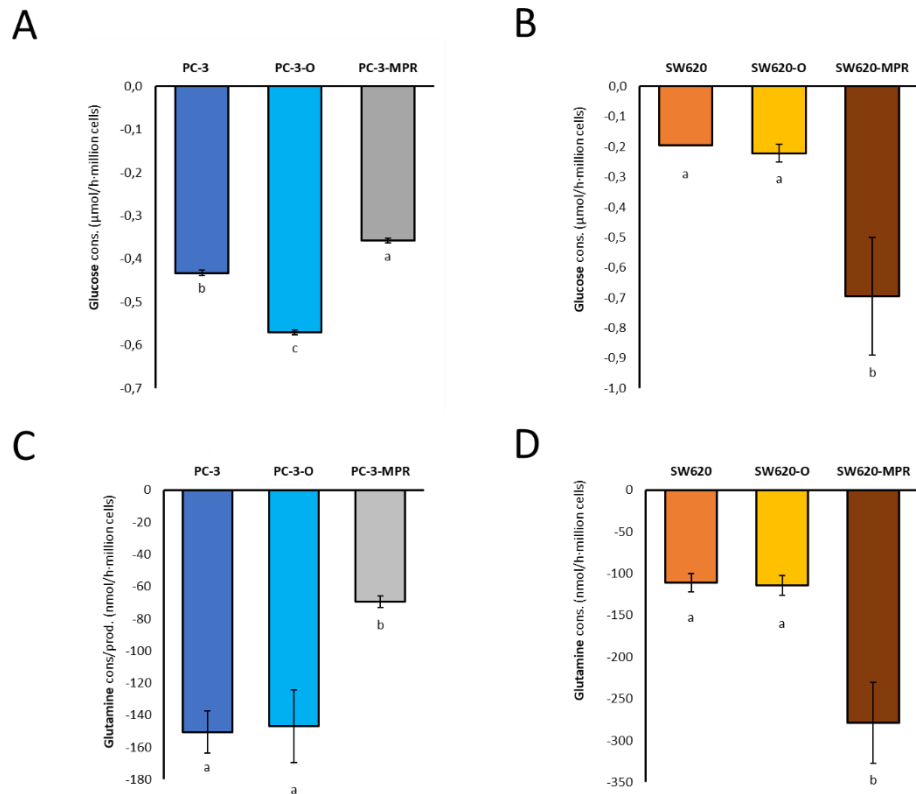


Figure 4.2.5. Compared glucose and glutamine consumption rates of PC-3 and SW620 cells. Glucose consumption rates of PC-3-derived (A) and SW620-derived (B) cells. Glutamine consumption rates of PC-3-derived (C) and SW620-derived (D) cells. Bars represent mean \pm SD of $n=3$. In all cases, one-way ANOVA and Tukey test for multiple comparisons were performed. Cell lines/conditions sharing the same letter indicates the absence of significant differences between them.

Apart from that, our analysis also revealed that both parental and age-matched control cell lines did not differ significantly in terms of glutamine consumption, which implies that the observed changes in glutamine metabolism can unequivocally be ascribed to acquired platinum resistance. On the other hand, PC-3-O appeared to be slightly more glycolytic than the parental cell line.

4.2.2.4. PC-3-MPR and SW620-MPR present opposed alterations in amino acid metabolism

To evaluate how these alterations in glucose and glutamine metabolism are translated into the metabolism of other amino acids, we next assessed the consumption and production rates of the rest of amino acids in PC-3, PC-3-O and PC-3-MPR (4.2.6) and SW620, SW620-O and SW620-MPR (4.2.7).

In the PC-3 model, we observed the general trend that both controls displayed similar and enhanced amino acid consumption rates compared to PC-3-MPR. The slightly higher glucose consumption rate in PC-3-O compared to PC-3 does not have any impact on the majority of amino acids, except for alanine, which can probably be correlated to the enhanced glucose uptake through an enhanced flux through alanine transaminase (ALT), due to enhanced pyruvate production [428].

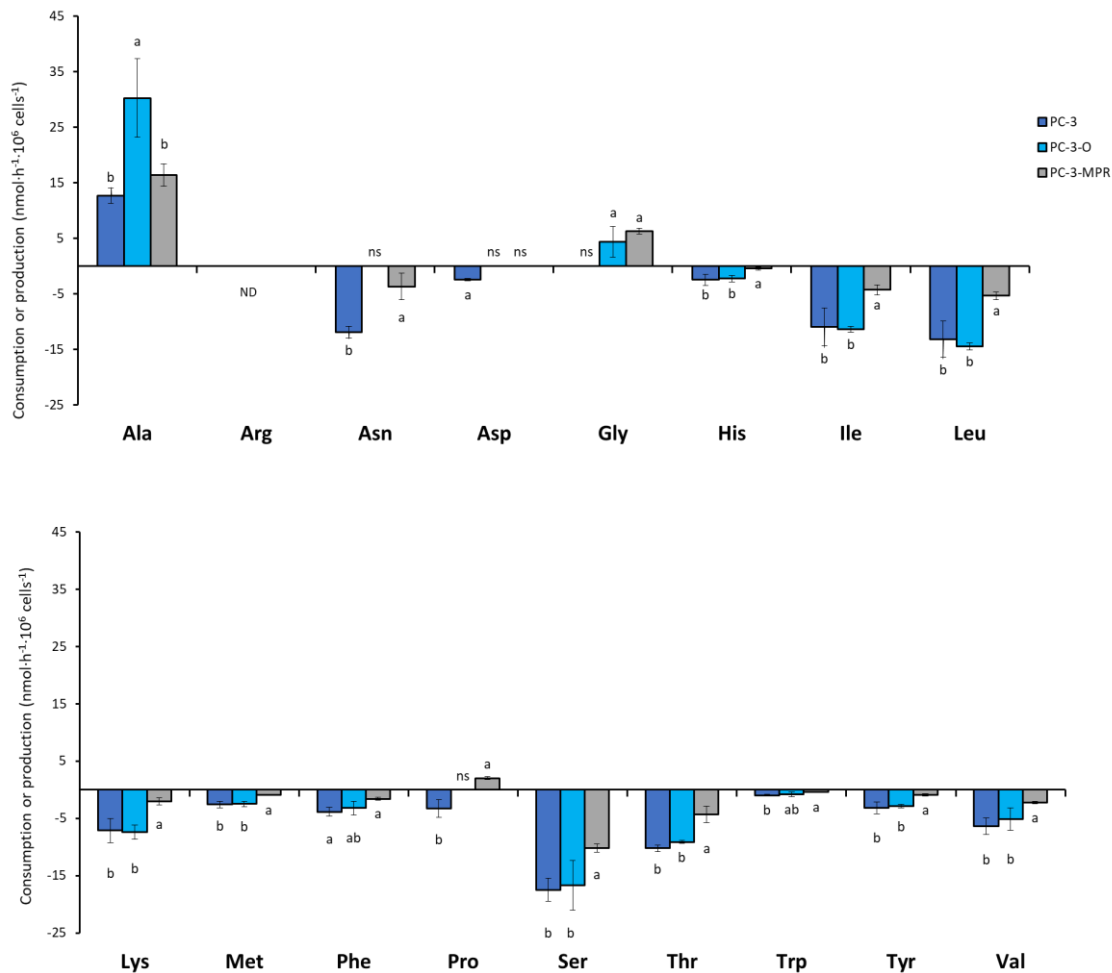


Figure 4.2.6. Amino acid consumption and production rates of PC-3, PC-3-O, and PC-3-MPR cells. Amino acid consumption (negative values) or production (positive values) in alphabetic order: (A) Alanine (Ala) to leucine (Leu) and (B) Lysine (Lys) to valine (Val). Abbreviations: arginine (Arg), asparagine (Asn), aspartate (Asp), glycine (Gly), histidine (His), isoleucine (Ile), methionine (Met), phenylalanine (Phe), proline (Pro), serine (Ser), threonine (Thr), tryptophan (Trp) and tyrosine (Tyr). Bars represent mean \pm SD of $n=3$. Significance between initial and final metabolite concentrations were evaluated using a t-Student test with $\alpha=0.05$. Absence of significant consumption or production is denoted by ns. If the condition of significant consumption/production is met, comparison between cell lines/conditions normalized by cell volume was performed by one-way ANOVA and Tukey's multiple comparison testing. Cell lines/conditions sharing the same letter indicates absence of significant differences between them.

Besides that, a shift from proline consumption in PC-3 to no significant consumption or production in PC-3-O and significant proline production in PC-3-MPR was also observed. Interestingly, a shift from proline consumption to proline production was also observed between PC-3S and PC-3M in **Chapter 1**. However, this shift could not be ascribed to an increase in tumorigenesis, since the other highly-metastatic cell line, DU-145, displayed an opposed behavior than PC-3M. Nevertheless, even if the role of proline production remains elusive in the PC-3 model, a correlation between metastasis and acquired platinum resistance has been found, and it could denote that proline production could be tied to tumor progression or tumor aggressiveness, but both cell aging and acquired platinum resistance contribute to this shift in the isogenic PC-3 models of **Chapter 2**.

As expected for the SW620-MPR cell model, due to its increased glycolytic and glutaminolytic metabolic phenotypes, SW620-MPR significantly enhanced the production of amino acids that can be synthesized from either glutamate or pyruvate, such as alanine, aspartate, glycine, serine, arginine, or proline (**4.2.7**).

Apart from that, a significant increase in the consumption of methionine and serine was also found in the resistant cell line, potentially denoting the activation of 1C metabolism, which would allow SW620-MPR cells to increase nucleotide synthesis to nurture DNA damage repair and palliate the effects of platin-DNA crosslinks.

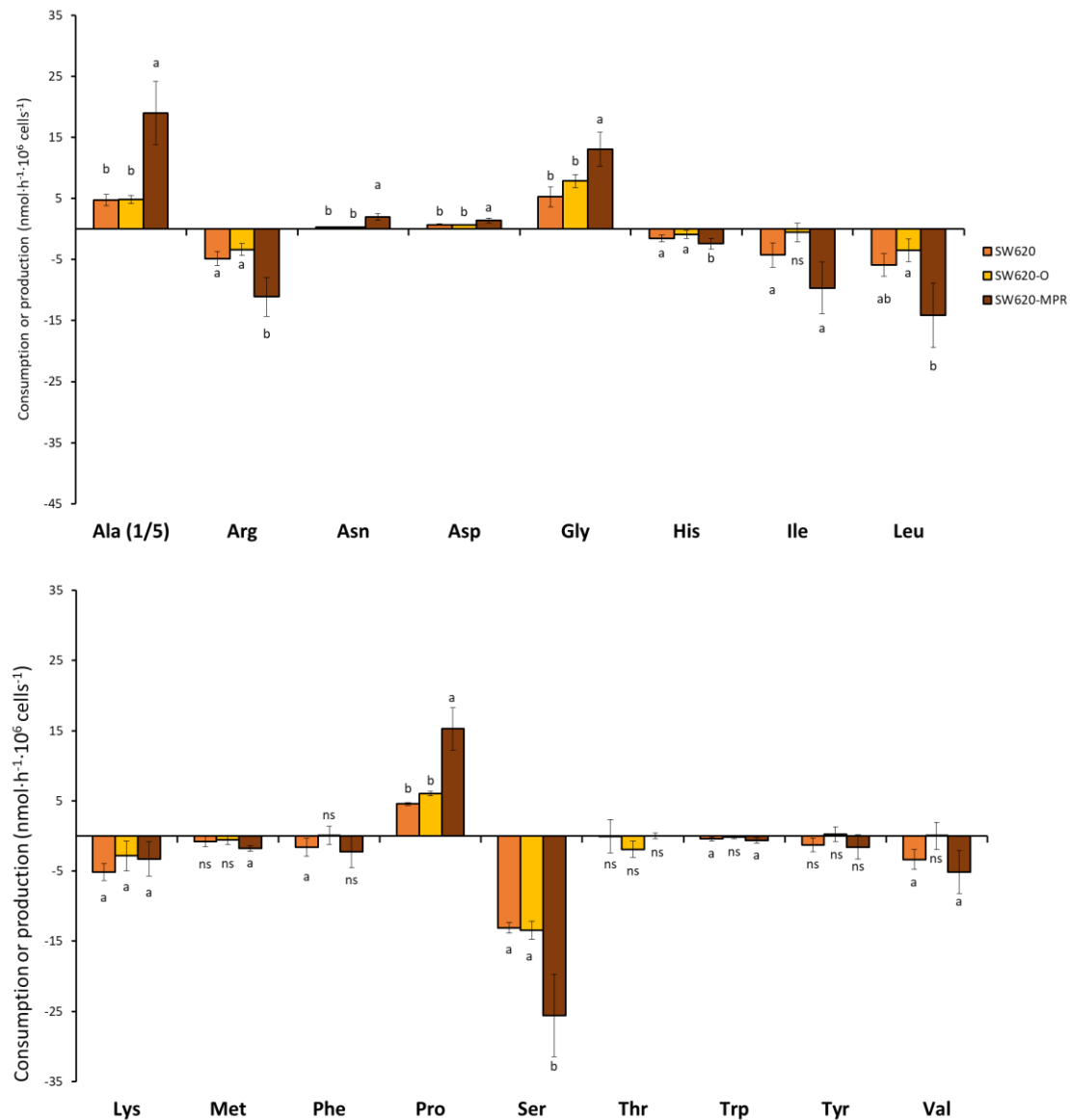


Figure 4.2.7. Amino acid consumption and production rates of SW620, SW620-O, SW620-MPR cells Amino acid consumption (negative values) or production (positive values) in alphabetic order: (A) Alanine (Ala) to leucine (Leu) and (B) Lysine (Lys) to valine (Val). Abbreviations: arginine (Arg), asparagine (Asn), aspartate (Asp), glycine (Gly), histidine (His), isoleucine (Ile), methionine (Met), phenylalanine (Phe), proline (Pro), serine (Ser), threonine (Thr), tryptophan (Trp) and tyrosine (Tyr). Bars represent mean \pm SD of $n=3$. Significance between initial and final metabolite concentrations was evaluated using a t-Student test with $\alpha=0.05$. Absence of significant consumption or production is denoted by ns. If the condition of significant consumption/production is met, comparison between cell lines/conditions normalized by cell volume was performed by one-way ANOVA and Tukey's multiple comparison testing. Cell lines/conditions sharing the same letter indicates the absence of significant differences between them.

4.2.2.5. SW620-MPR upregulate their polyamine secretory profile

However, in line with our results in **Chapter 1**, the simultaneous increase in arginine, glutamine, and methionine consumption in the SW620-MPR cell line also led us to the hypothesis whether polyamine metabolism could be altered in SW620-MPR. Indeed,

polyamines require either arginine or glutamine to produce putrescine and decarboxylated S-adenosylmethionine (dcSAM) as an aminopropyl donor.

In accordance to our hypothesis, SW620-MPR increased putrescine secretion compared with SW620 and SW620-O and, remarkably, also began to significantly secrete spermidine (**4.2.8**), a capacity that was not found in neither control cell line. Spermine was not detected in the culture media of any of the conditions for SW620 cell lines above our lower limit of quantification (LOQ) (5 nM). Remarkably, this increase in polyamine secretion can further contribute to scavenge ROS, since polyamines are polycations that can react with oxidant species, including ROS [432]. Moreover, the observation of increased putrescine and spermidine in SW620-MPR contribute to stimulate the hypothesis that Pt-polyamine complexes could be formed and constitute an alternative manner to achieve platinum excretion in the resistant cell lines. In line with this, other authors have reported the synthesis of such platinum-polyamine complexes, and have determined that they possess antiproliferative activity against cisplatin-resistant ovarian cancer [433].

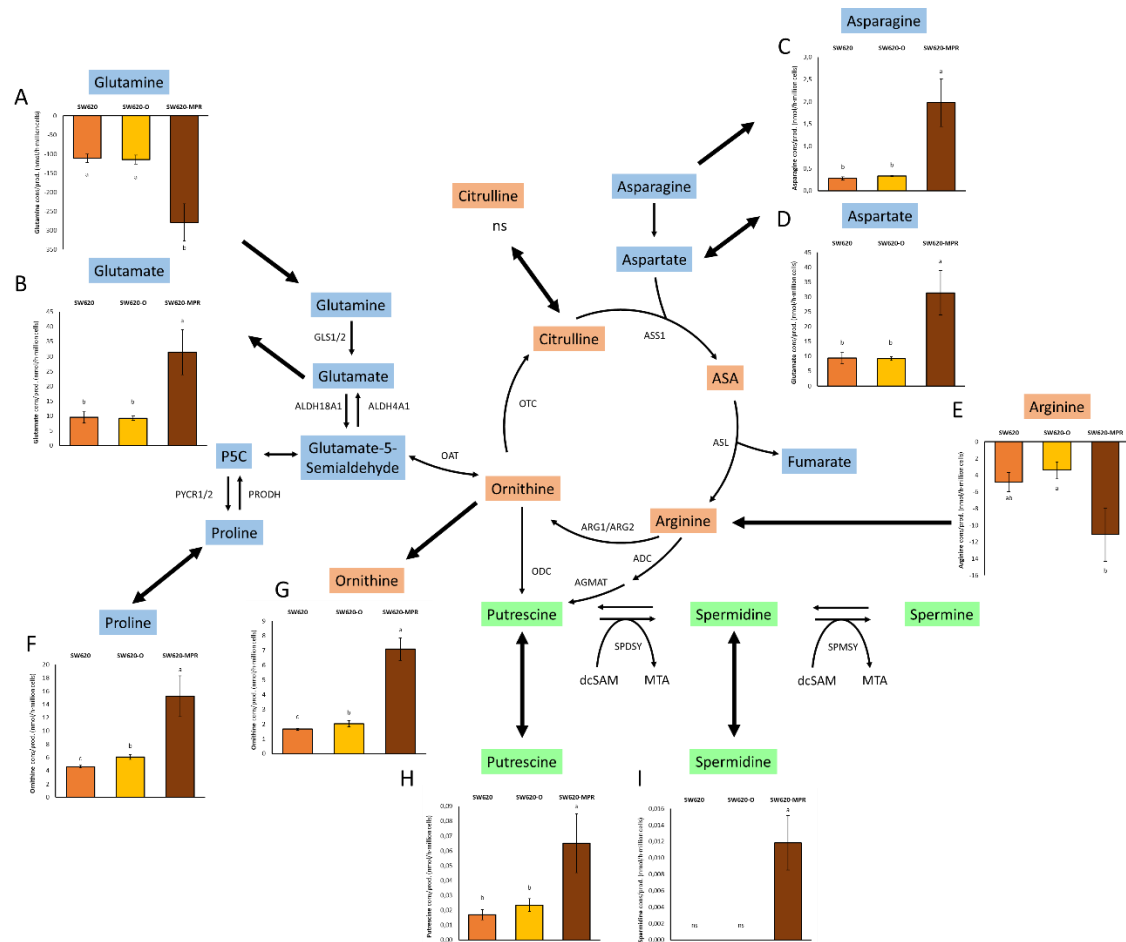
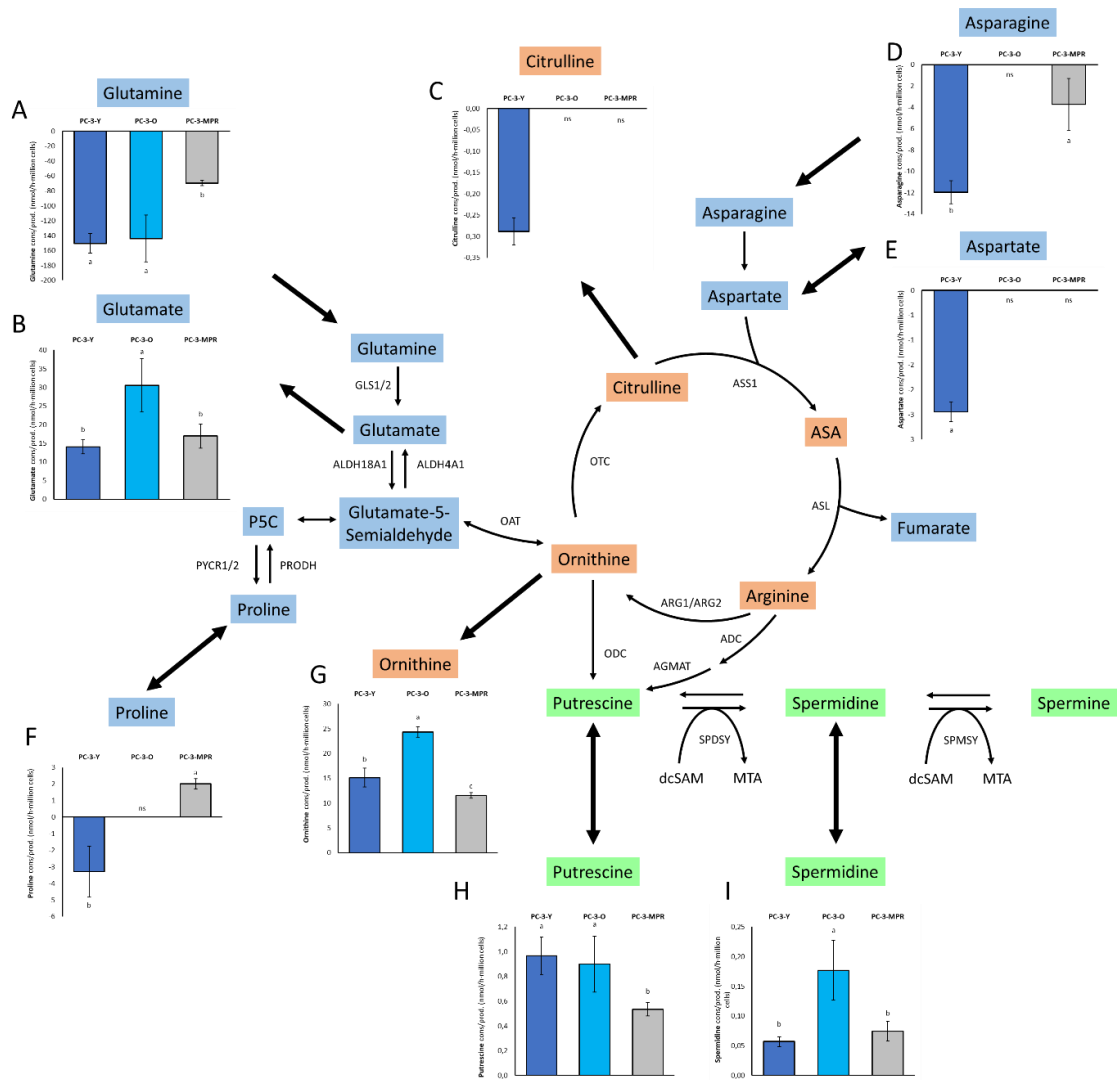


Figure 4.2.8. Metabolite exchange flux rates of urea cycle intermediates, polyamines and related amino acids in SW620, SW620-O and SW620-MPR. (A) Glutamine, (B) Glutamate, (C) Asparagine, (D) Aspartate, (E) Arginine, (F) Proline, (G) Ornithine, (H) Putrescine, (I) Spermidine. Extracellular flux rates are expressed as nmol consumed or produced per hour and million cells. Significance between initial and final metabolite concentrations were evaluated using a t-Student test with $\alpha=0.05$. If the condition of significant consumption/production was met, comparison between cell lines/conditions normalized by cell volume was performed by one-way ANOVA and Tukey's multiple comparison testing. Cell lines/conditions sharing the same letter indicates absence of significant differences between them. Abbreviations: Argininosuccinate synthase 1 (ASS1), argininosuccinate lyase (ASL), ornithine transcarbamylase (OTC), glutamate oxaloacetate transaminase 1/2 (GOT1/2), glutaminase (GLS), arginine decarboxylase (ADC), ornithine decarboxylase (ODC), spermidine synthase (SPDSY), spermine synthase (SPMSY), decarboxylated S-adenosylmethionine (dcSAM), methylthioadenosine (MTA), argininosuccinic acid (ASA).

On the contrary, for PC-3-derived cell lines, polyamine secretion was slightly reduced (4.2.9), correlated with the consumption or production rates of glutamine, glutamate and ornithine.



4.2.2.6. Intracellular metabolite profiling of metastatic multiplatinum-resistant models unveils a common metabolic signature

To complete the metabolic characterization of acquired platinum resistance uncoupled from cell aging in both models, we also evaluated intracellular pools of amino acids, several non-proteinogenic amino acids, polyamines and some other relevant biogenic

amines through targeted metabolomics, evaluating our results separately for the PC-3 model (4.2.10) and SW620 (4.2.11), and then matching the results for both cell models (4.2.12), to obtain a common fingerprint for acquired platinum resistance, despite the opposed effects of platinum resistance in glucose and glutamine metabolism in CRPC and CRC.

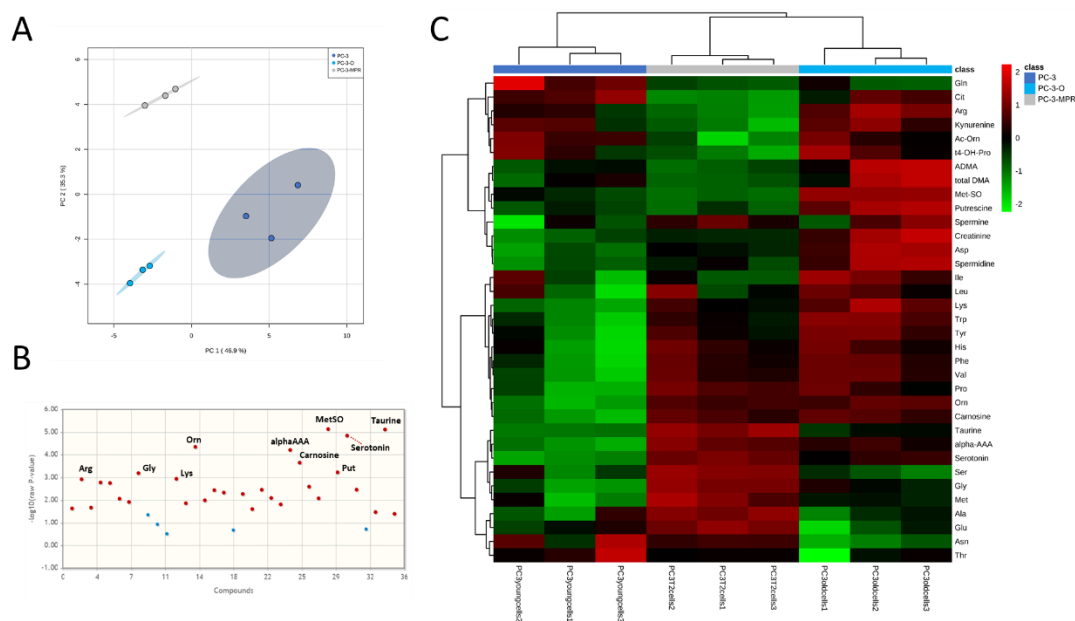


Figure 4.2.10. Intracellular metabolomic profiling of PC-3, PC-3-O and PC-3-MPR. (A) Principal component analysis of the metabolomic profiling of PC-3, PC-3-O and PC-3-MPR. (B) Top 10 features with highest statistical significance of the presented data, assessed by one-way ANOVA. All significant features are shown in red and features with no significant differences are shown in blue ($\alpha=0.05$). (C) Heatmap and clustering of features and conditions of PC-3, PC-3-O and PC-3-MPR. Features below or above the LOQ of the analytical method were removed and all data was normalized by median of amino acids of each sample and log transformed prior to the analysis.

Concerning the CRPC model, our results indicated that PC-3-O and PC-3-MPR were more similar in metabolic terms between them than to the parental PC-3, indicating that they both co-evolved and that a significant part of the metabolic alterations observed can be associated to cell aging. Indeed, in the principal component analysis (PCA) analysis, PC 1 (46,9%) could be ascribed to cell aging, whereas PC 2 (36,3%) to the acquisition of platinum resistance (4.2.10.A). This observation is of particular interest, considering that there are no significant differences in terms of proliferation between PC-3 and PC-3-O, whereas PC-3-MPR is markedly less proliferative. Thus, such observed effects are completely uncoupled from cell proliferation. Apart from that, we also identified certain alterations that can only be associated to acquired platinum resistance, since MPR

displayed the opposite trend than PC-3 and PC-3-O. Interestingly, these resistance-tied features include arginine, citrulline, or glutamate intracellular pools hinting, as found in **Chapter 1**, alterations potentially tied to the urea cycle in this cell line. In support of this notion, arginine, ornithine or putrescine appear among the most significantly different features in our analysis (**4.2.10.B**).

Performing a similar analysis in the SW620 model, revealed that the majority of alterations of metabolite intracellular pools were associated to the acquisition of platinum resistance. Significant differences between SW620-MPR and the two control cell lines were found, as shown by both PCA (**4.2.11.A**), in which the component that can be associated to resistance weights 87%, and the heatmap (**4.2.11.C**), in which SW620-MPR displayed the opposite behavior than the two other cell lines in the vast majority of metabolites, whereas SW620 and SW620-O were remarkably similar.

As with PC-3-derived cell lines, alterations in the Gln-Orn-Pro axis and polyamine metabolism also appeared to be amongst the most relevant features upon acquisition of platinum resistance in CRC (**4.2.11.B**), similar to our findings for the PC-3 model.

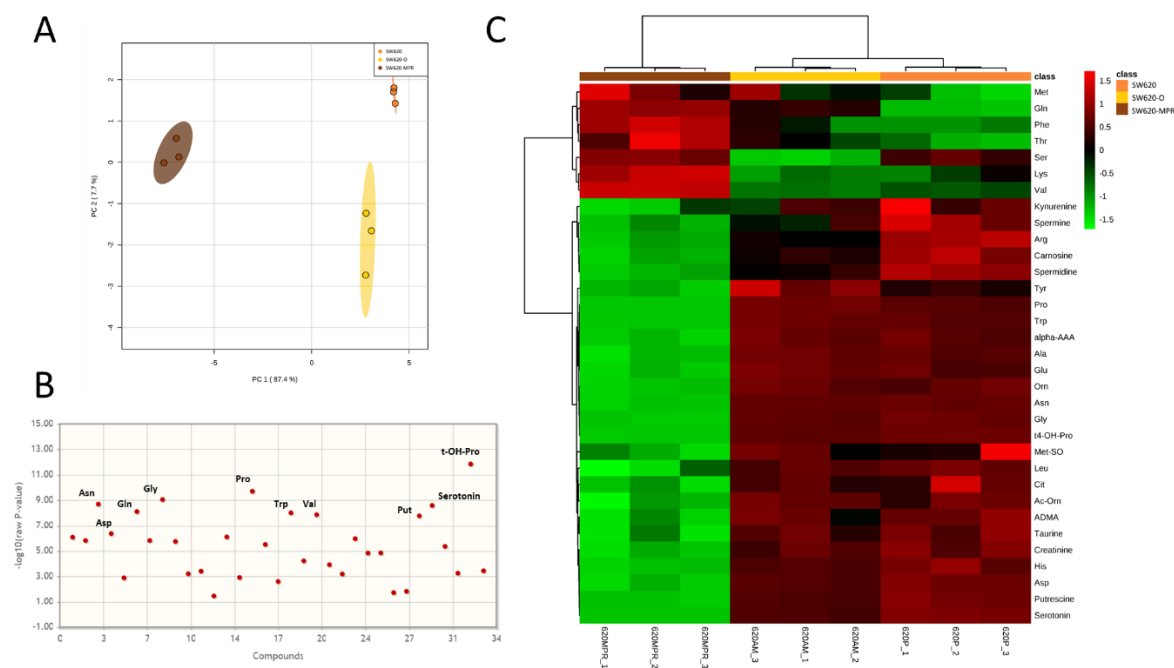
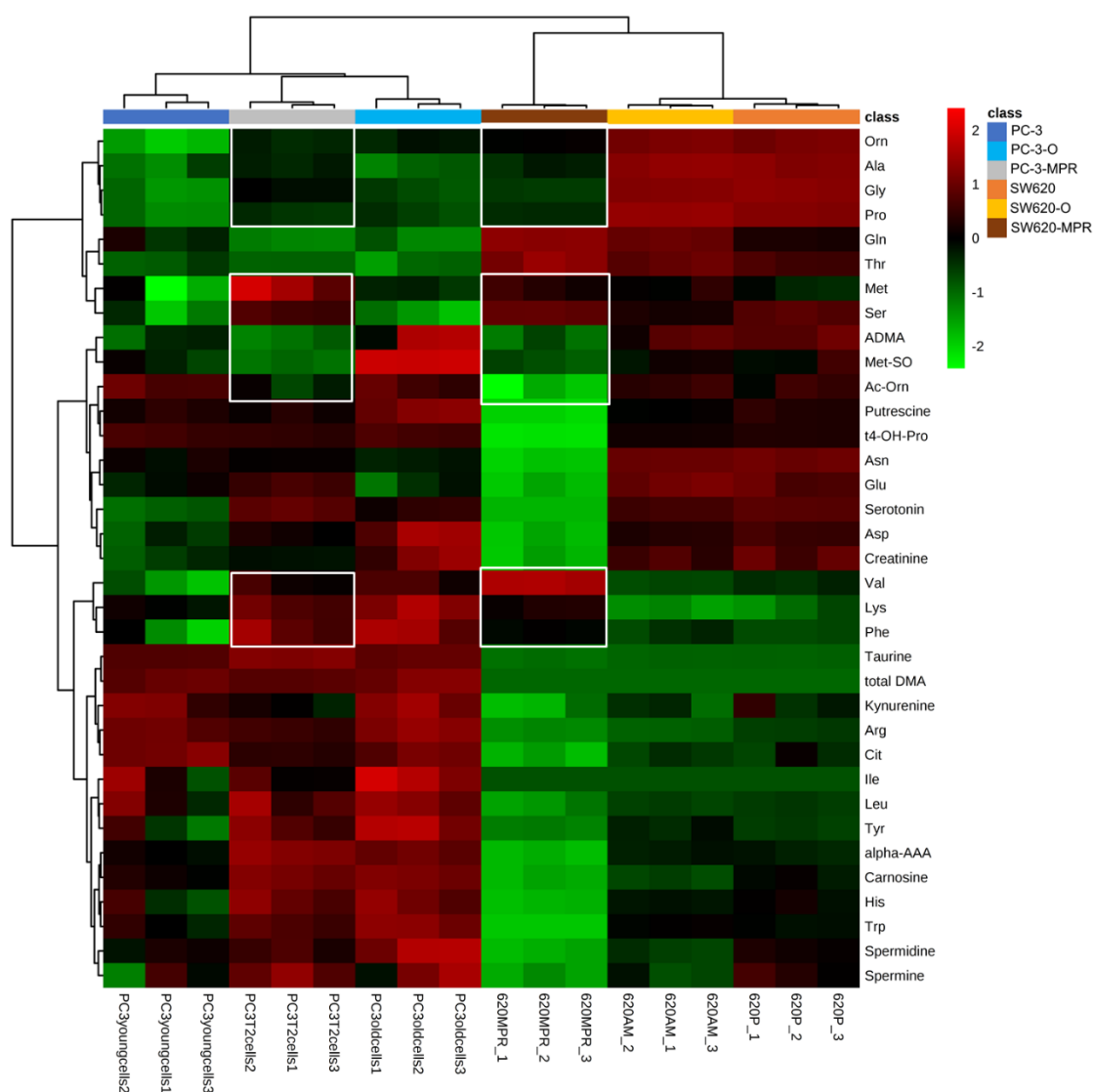


Figure 4.2.11. Intracellular metabolomic profiling of SW620, SW620-O and SW620-MPR. (A) Principal component analysis of the metabolomic profiling of SW620, SW620-O and SW620-MPR. (B) Top 10 features with highest statistical significance of the presented data, assessed by one-way ANOVA. All significant features are shown in red ($\alpha=0.05$). (C) Heatmap and clustering of features and conditions of SW620, SW620-O and SW620-MPR. Features below or above

the LOQ of the analytical method were removed and all data was normalized by median of amino acids of each sample and log transformed prior to the analysis.

Finally, we also attempted to match the results obtained for both cell models to unveil a common metabolic fingerprint of acquired platinum resistance and, indeed, we encountered that the levels of a definite set of metabolites converge in PC-3-MPR and SW620-MPR (**4.2.12**), despite their adaptations in opposite directions regarding glucose and glutamine metabolism. Namely, the metabolites that converge in normalized levels in both cell lines are amino acids (alanine, glycine, proline, methionine, serine, valine, lysine, and phenylalanine), non-proteinogenic amino acids (ornithine, ADMA, acetyl-ornithine) and the polyamine putrescine.

Interestingly, in some of these identified metabolites, namely ornithine, alanine and glycine, PC-3-MPR displayed levels comparable to both PC-3 controls, whereas SW620-MPR shifted towards PC-3. The opposite was found in some others, in which PC-3-MPR shifted towards SW620, such as methionine or serine levels. Regarding the other identified common metabolites, we encountered distinct patterns including partial association to aging. Besides that, this joint analysis also revealed that the metabolic alterations found in SW620-MPR relative to its controls are markedly larger in magnitude than in PC-3-MPR. Indeed, these results could indicate that the metabolic alterations that are necessary for the acquisition of a similar degree of platinum resistance may occur to different extents depending on the metabolic phenotype of the original tumor.



4.2.12. Comparison of the metabolic profile of acquired multiplatinum resistance in CRPC and CRC. Heatmap and clustering of features and conditions of PC-3, PC-3-O, PC3-MPR, SW620, SW620-O and SW620-MPR. Features below or above the LOQ of the analytical method were removed and all data was normalized by median of amino acids of each sample and log transformed prior to the analysis. Metabolites that displayed similar levels in the resistant cell lines and different to controls are denoted by a white square.

In this regard, we hypothesize that cancer cells originally relying prominently in OXPHOS for energy obtention (SW620) need to readjust their central metabolism to a greater extent than cancer cells prominently relying on aerobic glycolysis (PC-3). Potentially, SW620 cells would require more significant adaptations due to their necessity to simultaneously cope with cisplatin-derived ROS and mitochondrial metabolism-derived ROS. In line with this, the encountered increase in glutamine consumption could also be devoted to increase glutathione synthesis to further contribute to ROS scavenging.

Thus, we next aimed to investigate whether PC-3-MPR and SW620-MPR presented distinct capacities to mitigate oxidative stress, and if they achieve redox homeostasis by increasing their capacity to produce glutathione in response to exposure to the drug or if they do so by altering their glycolytic function or their mitochondrial respiration. Furthermore, from our results in **this Section** we have identified that PC-3-O and SW620-O are suitable controls for uncoupling cell aging from acquired platinum resistance, and that their metabolic phenotypes have not deviated significantly from the parental models. Thus, in the following sections, PC-3-MPR and SW620-MPR will only be compared to their age-matched controls.

4.2.2.7. PC-3-MPR and SW620-MPR completely suppress cisplatin-induced ROS by enhancing glutathione synthetic capacity

As a starting point of the metabolic characterization of our cell models, we first hypothesized that the most direct impact of cisplatin on cell metabolism would be on cellular redox balance and ROS homeostasis. As mentioned previously, Pt(II) compounds can oxidize a wide variety of biomolecules inside the cell and, in particular, highly nucleophilic cellular ROS scavengers such as cysteine residues, ascorbic acid or glutathione. The oxidation of such molecules by platinum compounds necessarily decreases the availability of their reduced forms, damaging the capacity of the cell to quench ROS that are normally produced in the ETC during mitochondrial respiration.

Hence, we evaluated ROS levels in our CRPC and CRC cell models. Our results indicated that addition of cisplatin (at the IC₅₀ of each cell line) caused a 50% increase in ROS in PC-3-O and almost no increase in PC-3-MPR (**4.2.13.A**), whereas it caused a 350% increase in SW620-O and almost no increase in SW620-MPR (**4.2.13.B**). These results indicate that both MPR cell lines have acquired a notable capacity to mitigate cisplatin-induced oxidative stress. Besides that, the remarkable difference obtained between both control cell lines could certainly be ascribed to the prominently more oxidative metabolism of SW620, which renders them more vulnerable to a ROS imbalance than PC-3 cells, mainly relying on aerobic glycolysis.

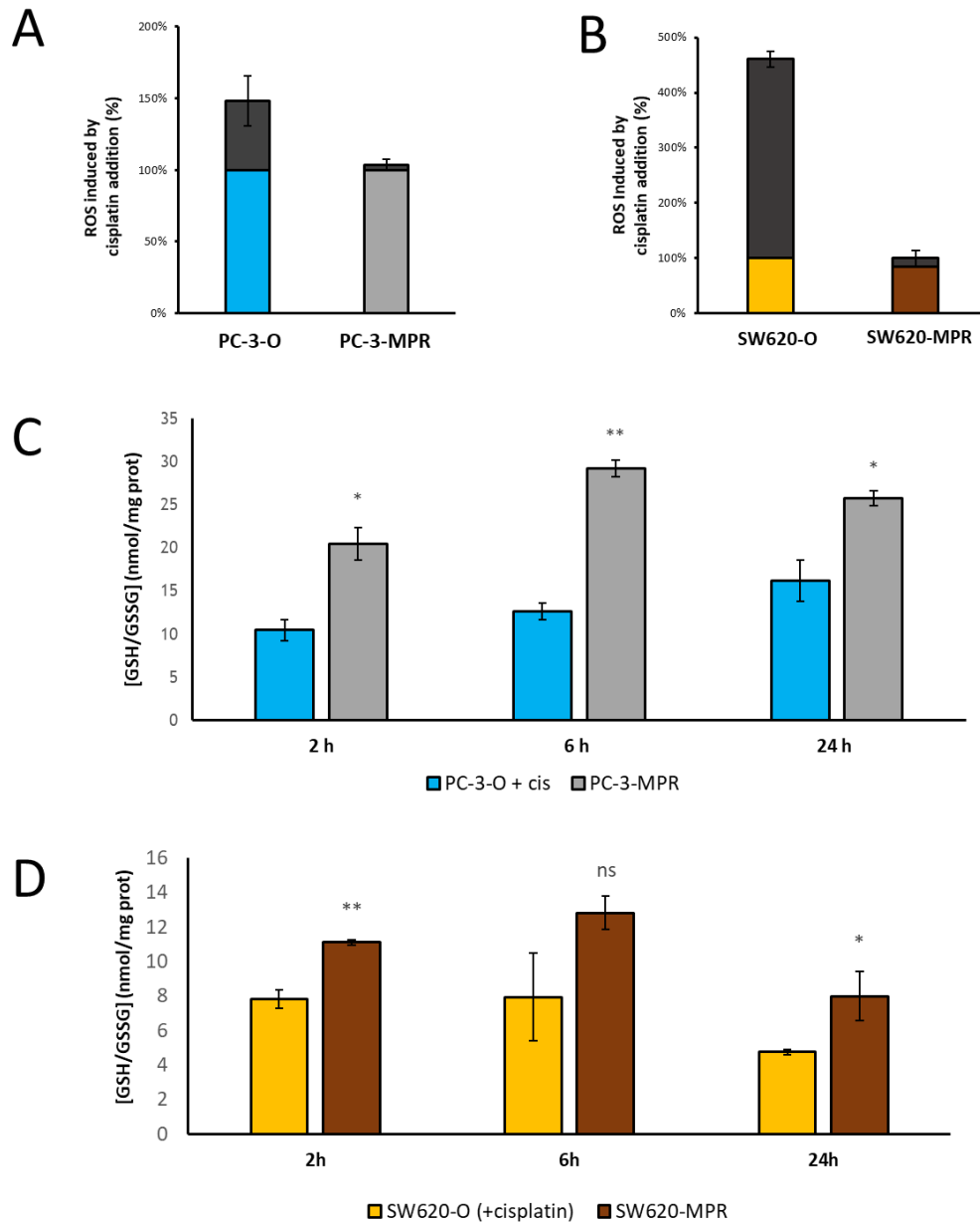


Figure 4.2.13. ROS levels and total intracellular glutathione in PC-3-O/MPR and SW620-O/MPR cells. ROS levels after 72 h incubation with cisplatin at the IC_{50} concentration in the PC-3-O/MPR (A) and SW620-O/MPR cells (B). Cells were stained with 2',7'-dichlorofluorescein diacetate. Total intracellular glutathione content (GSSG+GSSH) at different time points (2-24 h) after the addition of cisplatin to the culture medium of PC3/O/MPR (C) and SW620/O/MPR (D). Bars represent mean \pm SD of $n=3$. Significant differences relative to parental PC-3 or SW620 were evaluated by Student t-test and are indicated at $p < 0.05$ (*), $p < 0.01$ (**), and $p < 0.001$ (***)

Moreover, we had previously determined that PC-3-MPR and SW620-MPR displayed similar degrees of platinum resistance and they both had completely suppressed any apoptotic stimuli upon incubation with cisplatin, which is in accordance with the absence of ROS induction upon cisplatin exposure. Apart from that, we also unveiled that PC-3 cells are intrinsically resistant to apoptosis, whereas we detected significant

levels of apoptosis activation in SW620-O than in PC-3-O. Those results are also in accordance to the induction of higher ROS levels by cisplatin in SW620-O, since accumulation of ROS is an important trigger of proapoptotic stimuli.

On the other hand, achieving the complete suppression of such a significant ROS induction in SW620-MPR (from 350% in SW620-O to almost 0% increase in SW620-MPR) necessarily requires a significant reprogramming of their oxidative metabolism, which could involve several significant hypothetical alterations. First, in order to decrease their vulnerability to cisplatin-induced oxidative stress, SW620-MPR could have shifted their energy production to aerobic glycolysis, adopting a more Warburg phenotype. Also, they could have upregulated their synthesis of ROS scavengers, to be able to quench both cisplatin and the amounts of ROS produced through mitochondrial metabolism.

To validate this second hypothesis, we also analyzed the effect of cisplatin addition on the total glutathione content in PC-3 and SW620, since glutathione is the most abundant antioxidant and the main contributor to ROS scavenging in human cells [395]. Our results showed that PC-3-MPR cells had significantly higher total intracellular glutathione pools than PC-3-O (**4.2.13.C**). SW620-MPR also had significantly higher glutathione levels than SW620-O, but such increase was not significant at 6 h (**4.2.13.D**).

4.2.2.8. PC-3-MPR cells downregulate glycolysis and differentially utilize exogenous glucose and pyruvate

As mentioned previously, enhancement of glycolysis and PPP are frequently encountered metabolic adaptations in chemotherapy-resistant cancer cell models, especially in the case of electrophilic drugs such as platinum compounds [429]. The increased levels of intracellular glutathione detected in PC-3-MPR and SW620-MPR could also entail an increase in the NADPH demand for ROS detoxification, since NADPH, mainly produced in PPP, provides the necessary reducing power to fuel the ROS-scavenging machinery of the cell [430]. Apart from that, a shift from oxidative to glycolytic metabolism could also represent an additional mechanism to mitigate cisplatin-derived oxidative stress.

Thus, to deepen in the changes in glucose consumption encountered in **Section 4.2.2.3**, we first interrogated the glycolytic function of our MPR PC-3 model. In line with the

observed decrease in glucose consumption, our findings also underlined a slight diminishment in glycolytic flux through decreased glucose consumption and lactate production (4.2.14.B), supported by a significant decrease in ECAR upon glucose addition (4.2.14.E) in PC-3-MPR. However, the ratio between both metabolites was maintained, indicating that the rate of glycolysis, but not the fate of glucose inside the cell, was significantly altered. Indeed, these differences between both cell lines could be ascribed to decreased proliferation of the PC-3-MPR model.

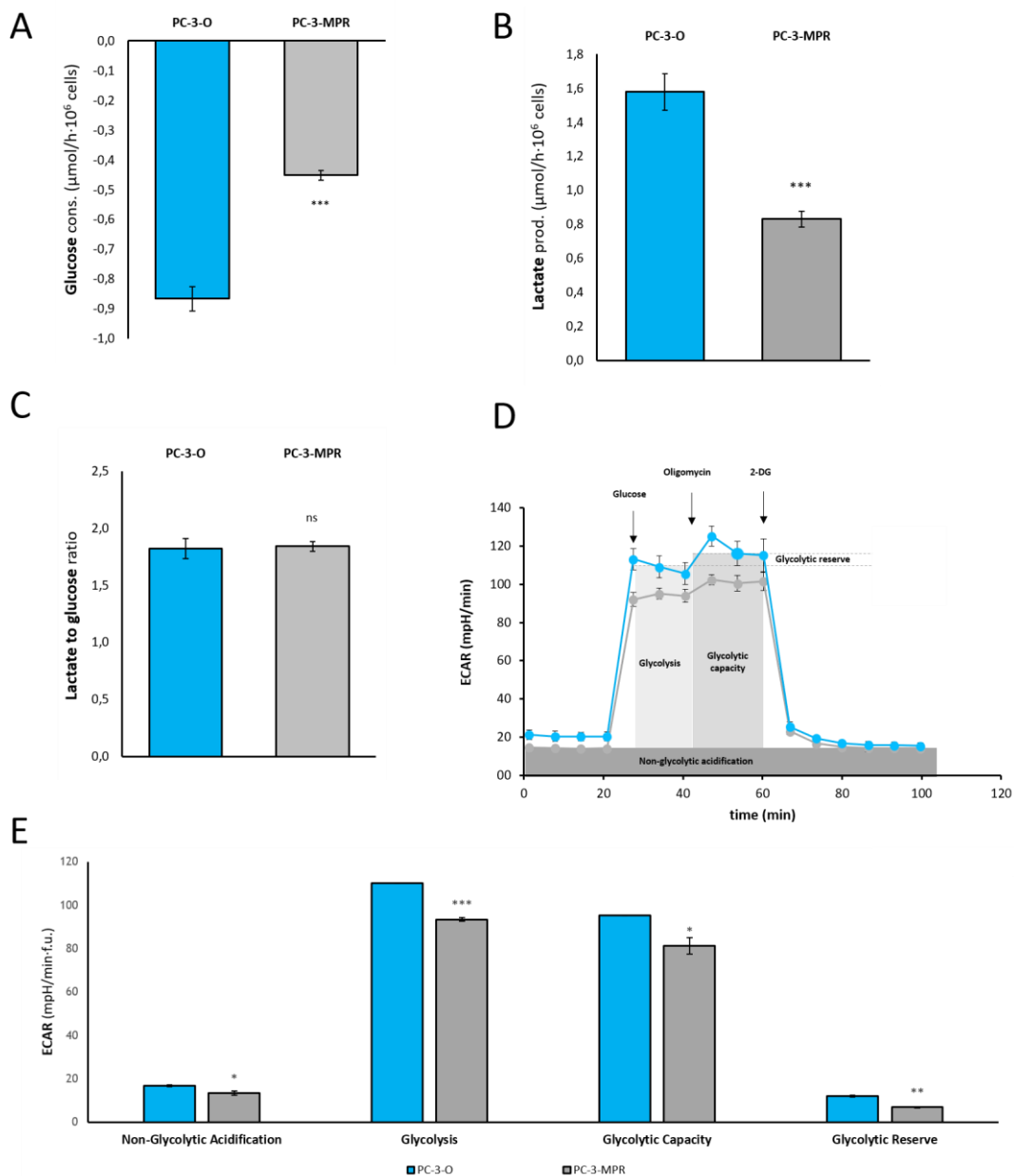


Figure 4.2.14. Glycolytic function of PC-3-O and PC-3-MPR cells (A) Glucose consumption rate, (B) Lactate production rate, (C) Lactate to glucose ratio, (D) Representative example of glycolysis test in PC-3-O/MPR and schematic representation of regions illustrating the calculation of different glycolysis-related parameters in XF Glycolysis Test,

(E) Functional parameters of the glycolytic function of PC-3-O/MPR. Bars represent mean \pm SD of $n=3$. Significant differences relative to PC-3-O are indicated at $p < 0.05$ (*), $p < 0.01$ (**), and $p < 0.001$ (***)

In light of the observed decrease in the glycolytic rate in PC-3-MPR, we decided to also interrogate if the addition of glucose or pyruvate contributed differentially to the respiration and acidification rates of PC-3-O and PC-3-MPR cells. Interestingly, the addition of glucose decreased mitochondrial respiration in both cell models (4.2.15.A), especially in PC-3-MPR up to 10 mM, whereas pyruvate addition increased respiration in both cell lines (4.2.15.C), in particular in PC-3-O up to 1 mM. On the contrary, both glucose (4.2.15.B) and pyruvate (4.2.15.D) caused an increase in ECAR in both cell lines. Notably, the increase in ECAR in PC-3-MPR is significantly lower than in PC-3-O at 1.5 and 2 mM.

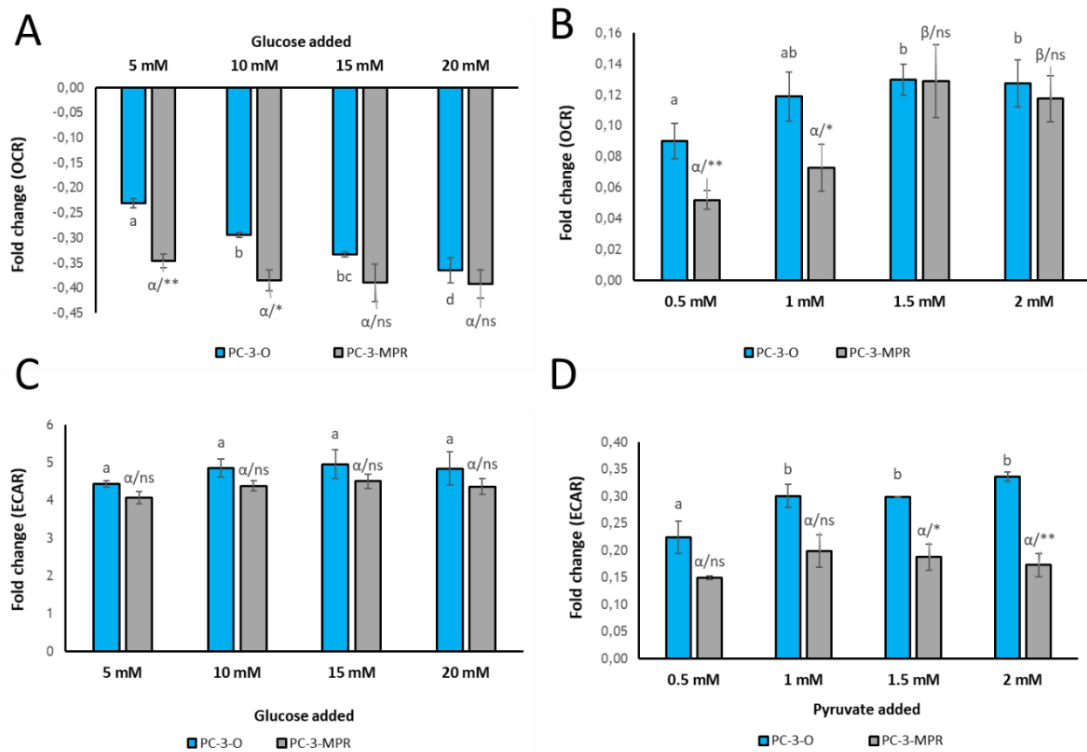


Figure 4.2.15. Contribution of glucose and pyruvate to mitochondrial respiration and extracellular acidification of PC-3-O and PC-3-MPR cells (A) Effect of glucose addition on OCR of PC-3-O and PC-3-MPR cells, (B) Effect of pyruvate addition on OCR of PC-3-O and PC-3-MPR cells, (C) Effect of glucose addition on ECAR of PC-3-O and PC-3-MPR cells, (D) Effect of pyruvate addition on the ECAR of PC-3-O and PC-3-MPR cells. Significant differences among the addition of different concentrations of metabolite is indicated by Latin letters (PC-O) or Greek letters (PC-3-MPR). In all cases, one-way ANOVA and Tukey's test for multiple comparisons were performed ($\alpha=0.05$). Significant differences between PC-3-MPR and PC-3-O at each metabolite addition were evaluated by Student t-test ($\alpha=0.05$) and are indicated at $p < 0.05$ (*), $p < 0.01$ (**), and $p < 0.001$ (***)

This indicates that the response to the addition of glucose in both cell lines is a clear shift from oxidative to glycolytic metabolism, indicating that they both preferentially adopt a Warburg-like phenotype if glucose is available. Moreover, the decrease in respiration at 5 and 10 mM is higher in PC-3-MPR, potentially denoting an enhanced contribution of glucose to ATP production in basal conditions. On the contrary, the addition of pyruvate causes the simultaneous activation of OXPHOS (**4.2.15.C**) and apparently increased lactate excretion (**4.2.15.D**), even if a slight contribution of H⁺ produced to the extracellular medium can also be generated through CO₂ production in OXPHOS. In either case, this entails that exogenous pyruvate, but not exogenous glucose, causes inhibition of PDK forcing the entrance of pyruvate to the TCA cycle. At the same time, lactate is simultaneously produced from excess pyruvate and excreted; since pyruvate, lactate and alanine pools tend to exist in equilibrium in mammal cells [428]. The lower decrease in ECAR in PC-3-MPR could entail decreased LDH activity than PC-3-O, which would also be coherent with results presented earlier regarding the glycolytic function of PC-3-MPR (**4.2.14**).

4.2.2.9. SW620-MPR cells upregulate glycolysis and differentially utilize exogenous glucose and pyruvate

We next performed a similar analysis of the glycolytic function of SW620-derived cell lines. Unlike PC-3-MPR cells, SW620-MPR significantly shifted towards a markedly glycolytic behavior compared the aged control cell lines, increasing significantly glucose consumption (**4.2.16.A**) and lactate production (**4.2.16.B**). In spite of that, even if SW620-MPR presented slightly increased glycolytic capacity, glycolysis was not significantly altered (**4.2.16.CD**).

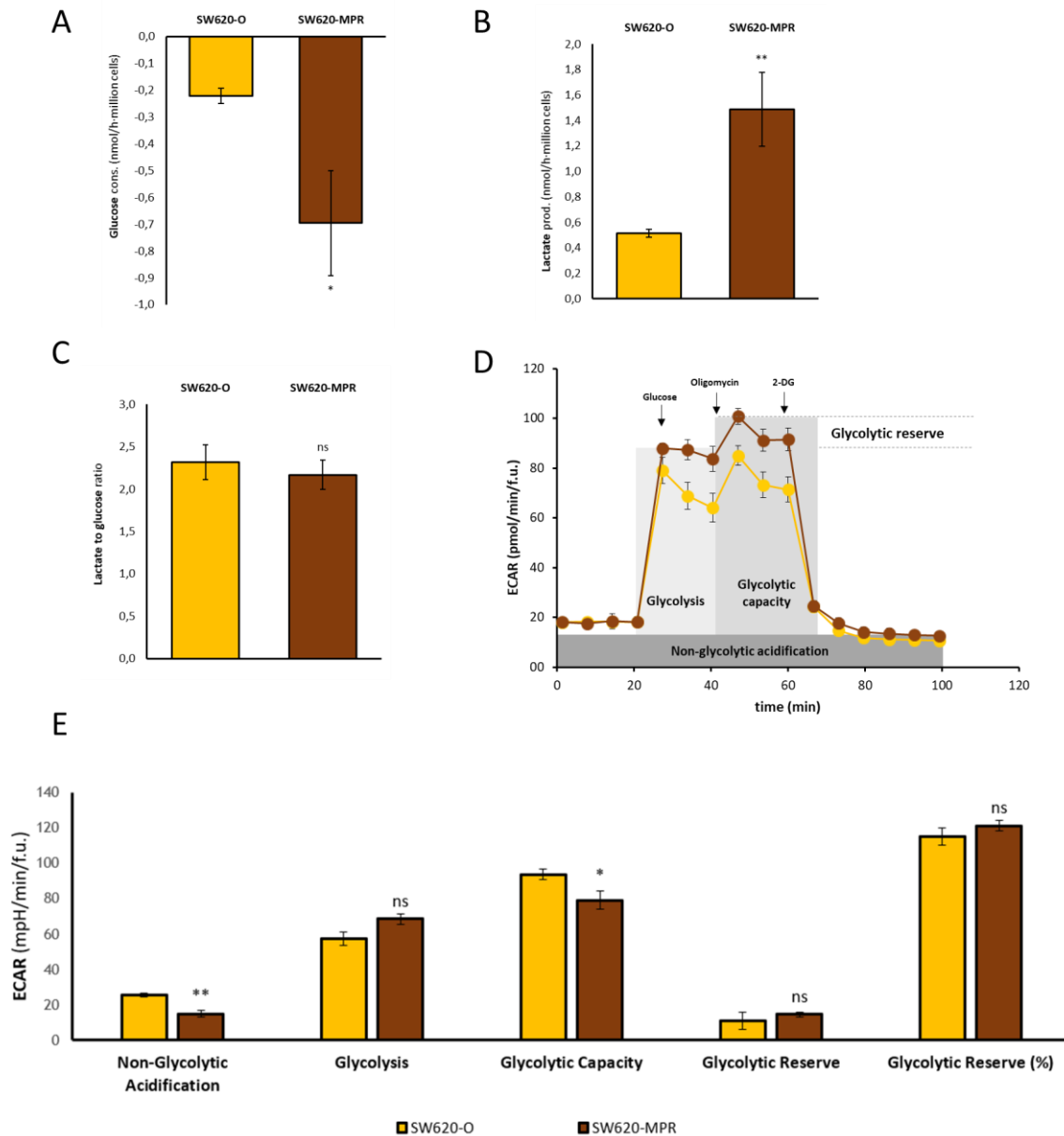


Figure 4.2.16. Glycolytic function of SW620, SW620-O and SW620-MPR cells (A) Glucose consumption rate, (B) Lactate production rate, (C) Lactate to glucose ratio, (D) Representative example of glycolysis test in SW620/O/MPR and schematic representation of regions illustrating the calculation of different glycolysis-related parameters in XF Glycolysis Test, (E) Functional parameters of the glycolytic function of SW620/O/MPR. Bars represent mean \pm SD of $n=3$. Significant differences relative to SW620-O are indicated at $p < 0.05$ (*), $p < 0.01$ (**), and $p < 0.001$ (***)

Indeed, glucose consumption and lactate production were found to be about three times higher in the SW620-MPR than in the parental and aged control cell lines (4.2.17.AB). However, the ratio between uptaken glucose and excreted lactate was similar in both cell lines (4.2.17.C). In the extracellular acidification assay, glycolysis was found to be enhanced in both SW620-O and SW620-MPR relative to the parental cell line. Indeed, the increase changes found in SW620 regarding glucose consumption were,

in magnitude, much greater than the changes encountered in PC-3 (-0.5 nmol/h·million cells in SW620 vs. +0.15 nmol/h·million cells in PC-3).

We also evaluated the dose-dependent addition of glucose and pyruvate on OCR and ECAR of SW620-O and SW620-MPR cells. As with the PC-3 model, we also encountered that the effect on the OCR of the addition of glucose (4.2.17.A) and pyruvate (4.2.17.B) had opposite directions. The decrease in OCR in both cell lines upon adding glucose was similar in both cell lines, denoting a similar capacity to oxidize other fuels when glucose is not present. However, the addition of glucose caused a significantly higher increase in ECAR in the SW620-MPR model, which implies a higher glycolytic rate. On the other hand, pyruvate doses up to 2 mM progressively enhanced OCR in a similar manner in both cell lines (4.2.17.C), whereas a higher increase in ECAR was found in SW620-MPR than in SW620-O (4.2.17.D). Considering the similarity in the OCR result, a greater increase in ECAR in SW620-MPR could imply an increase in pyruvate transport into the cell and the conversion of excess pyruvate into lactate.

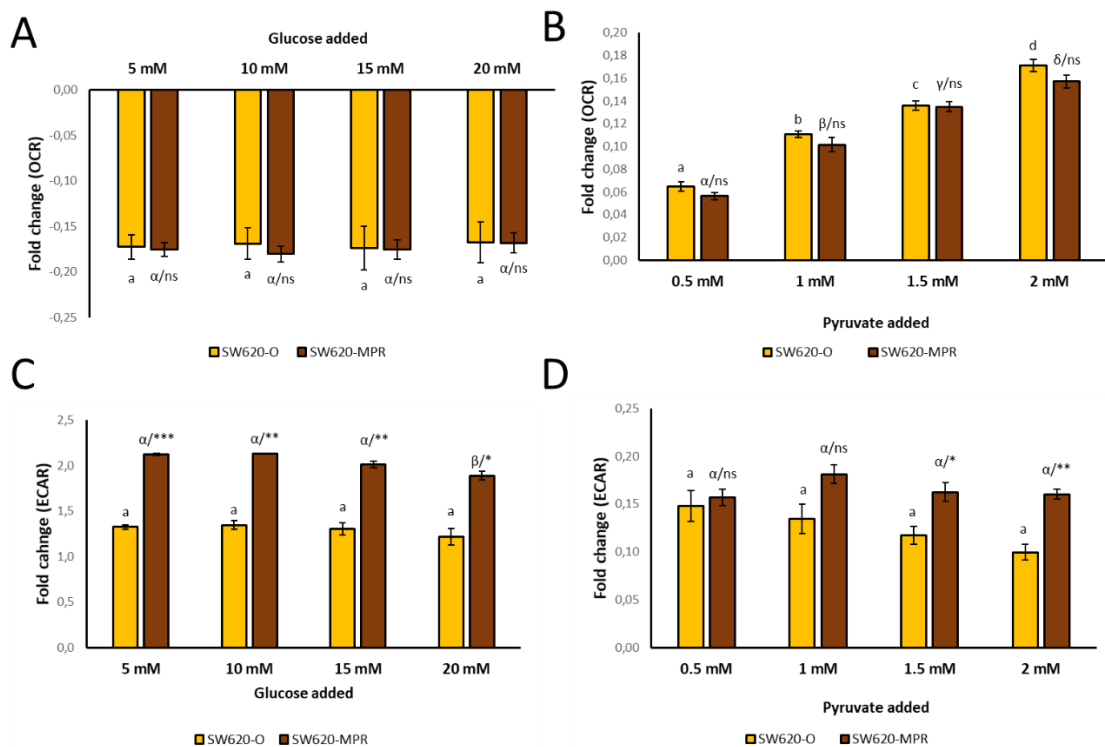


Figure 4.2.15. Contribution of glucose and pyruvate to mitochondrial respiration and extracellular acidification of PC-3-O and PC-3-MPR cells (A) Effect of glucose addition on OCR of PC-3-O and PC-3-MPR cells, (B) Effect of pyruvate addition on OCR of PC-3-O and PC-3-MPR cells, (C) Effect of glucose addition on ECAR of PC-3-O and PC-3-MPR cells, (D) Effect of pyruvate addition on the ECAR of PC-3-O and PC-3-MPR cells. Significant differences among the addition

of different concentrations of metabolite is indicated by Latin letters (PC-O) or Greek letters (PC-3-MPR). In all cases, one-way ANOVA and Tukey's test for multiple comparisons were performed ($\alpha=0.05$). Significant differences between PC-3-MPR and PC-3-O at each metabolite addition were evaluated by Student t-test ($\alpha=0.05$) and are indicated at $p < 0.05$ (*), $p < 0.01$ (**), and $p < 0.001$ (***)

4.2.2.10. PC-3-MPR minimize the damage of cisplatin on mitochondrial function and retain respiration levels and mitochondrial ATP production of control cells

After characterizing the glycolytic function of our cell models, we next moved to analyze whether PC-3-MPR displayed an altered mitochondrial metabolism. It is well-established that cisplatin binds to mitochondrial DNA, impairing normal mitochondrial physiology [290]. Moreover, platinum-based compounds are highly electrophilic and they oxidize a wide variety of biomolecules inside the cell, including ROS-scavenging molecules. This implies decreased availability of antioxidant defenses, compromising the maintenance of high rates of oxidative metabolism to support proliferation.

For this, we evaluated the mitochondrial function of our cell models by monitoring OCR during the addition of oligomycin, CCCP and rotenone + antimycin A. Our results indicate that the mitochondrial function of PC-3-MPR was not significantly impaired despite their continuous exposure to a high dose of cisplatin: basal respiration and mitochondrial ATP production were similar to PC-3-O (**4.2.18.A**). Indeed, this implies that PC-3-MPR cells have completely reverted the impact of the drug on mitochondrial metabolism, which mainly involves ATP depletion via mitochondrial damage and collapse of mitochondrial membrane potential [431]. Supporting this notion, we also found that the addition of increasing doses of cisplatin caused a more significant decrease in the respiration of PC-3-O than in PC-3-MPR cells (**4.2.18.C**), indicating an acquired capacity to minimize cisplatin-induced mitochondrial impairment.

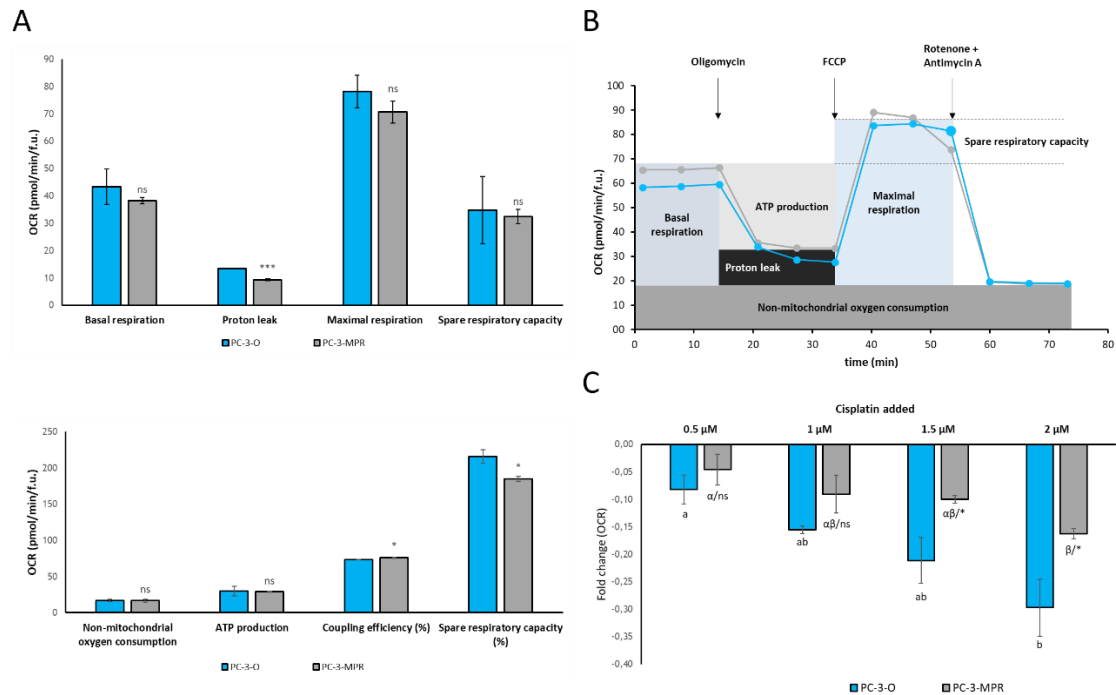


Figure 4.2.18. Mitochondrial function of PC-3, PC-O and PC-3-MPR and effect of cisplatin addition on the respiration of PC-3-O and PC-3-MPR.

On the other side, SW620-MPR decreased basal respiration and mitochondrial energy production relative to SW620-O control (4.2.19.AB), which could be understood as a mechanism to decrease overall levels of ROS and mitigate the effect of the drug in this regard while, as discussed earlier in **this Chapter** it shifts its energy production to aerobic glycolysis. Interestingly, unlike PC-3-MPR, which have an improved capacity to mitigate the effect of cisplatin addition on mitochondrial respiration (4.2.19.C), SW620-MPR cells present a similar impairment of mitochondrial respiration compared to SW620-O, denoting that these cells are less proficient on mitigating the effect of cisplatin in the mitochondria.

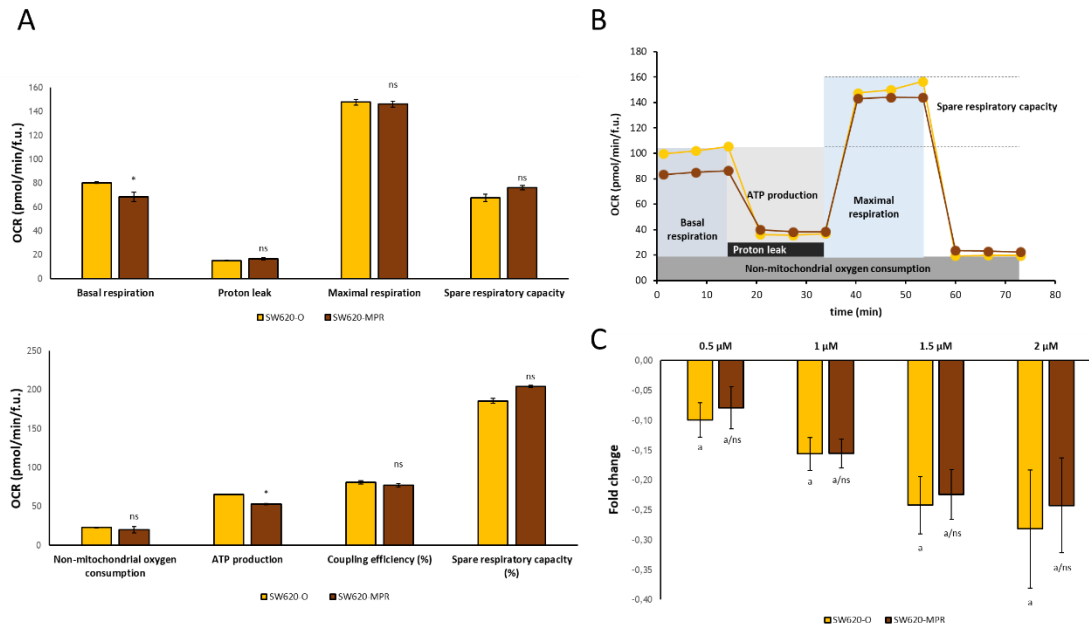


Figure 4.2.19. Mitochondrial function of SW620, SW620-O and SW620-MPR and effect of cisplatin addition on the respiration of PC-3-O and PC-3-MPR.

4.2.2.11. Anaplerosis of glutamine into the TCA cycle is altered in both PC-3-MPR and SW620-MPR

We also expected to find alterations in glutamine metabolism in our MPR models as glutamine plays an important role in mitochondrial metabolism, deeply altered by the action of cisplatin. Moreover, glutamine is also an important precursor of the ROS scavenger glutathione, enhanced in both MPR cell lines as described earlier in **Section 4.2.2.3**.

First, we evaluated glutamine consumption and glutamate production for all six cell lines (**4.2.20.AD**). We encountered that PC-3-MPR reduced their glutamine uptake, whereas SW620-MPR increased it relative to both parental cell lines. PC-3-O produced more glutamate than both the parental and the resistant cell lines. In SW620, correlated with glutamine consumption, SW620-MPR secreted significantly more glutamine than both untreated cell lines. Importantly, the ratio glutamine to glutamate was maintained between the three cell lines.

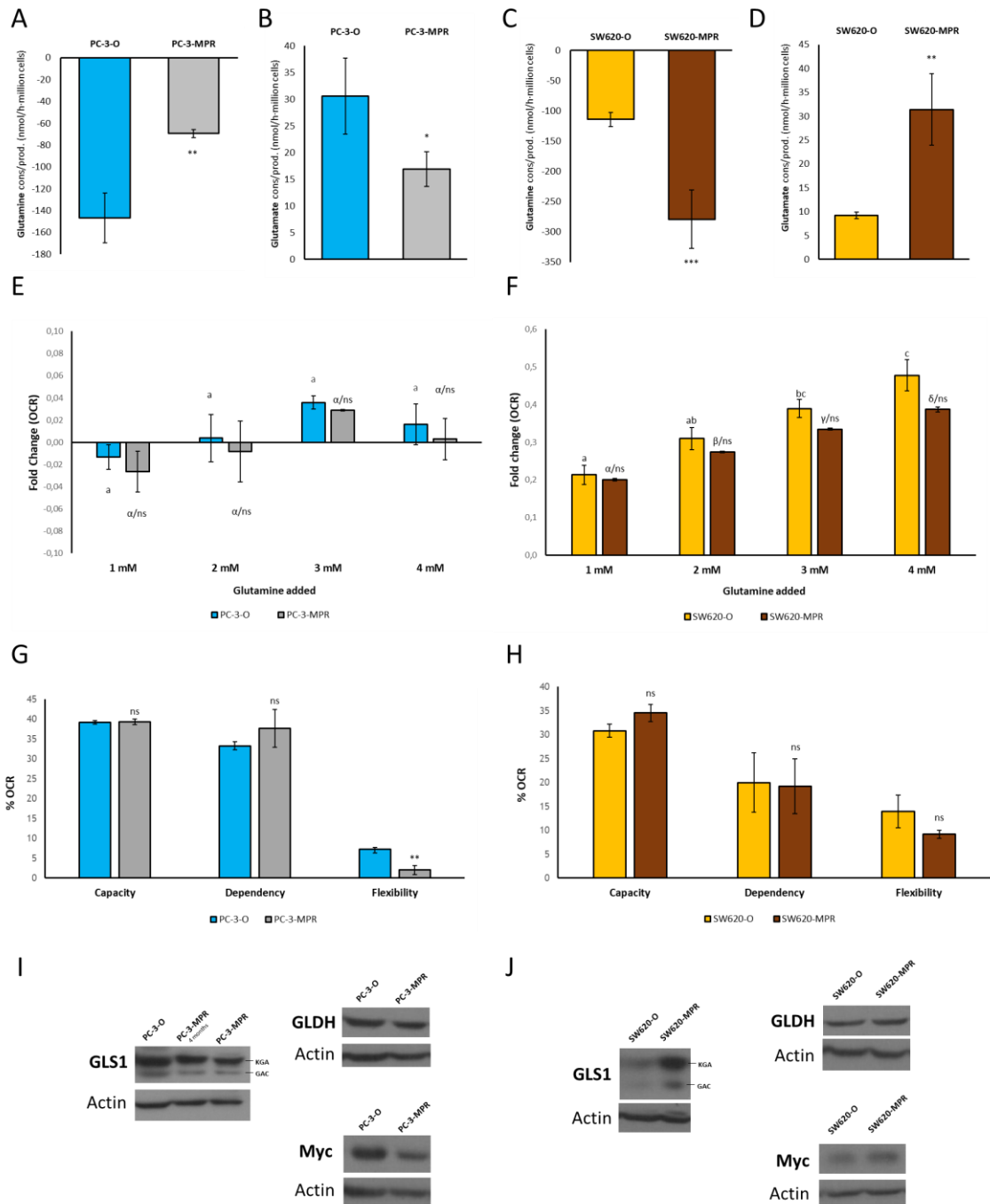


Figure 4.2.20. Glutaminolytic signature of PC-3/O/MPR and SW620/O/MPR cells. (A) Glutamine consumption and (B) glutamate production of PC-3, PC-3-O and PC-3-MPR cells; (C) glutamine consumption and (D) glutamate production of SW620, SW620-O and SW620-MPR cells; effect of the addition of glutamine to the OCR of (E) PC-3-O and PC-3-MPR cells and (F) SW620 and SW620-MPR cells; (G) Glutamine *MitoFuel* test for PC-3, PC-3-O and PC-3-MPR cells; (H) Glutamine *MitoFuel* test for SW620-O and SW620-MPR cells; protein levels of GLS1, GLDH and Myc in (I) PC-3-derived cell lines and (J) SW620-derived cell lines. Actin was used as the loading control. Bars represent mean \pm SD of n=3. For panel A-F statistical significance was evaluated using one-way ANOVA followed by a Tukey test for multiple comparisons. In panels A-D, cell lines/conditions sharing the same letter indicates absence of significant differences between them. In panels E and F, significant differences among the addition of different concentrations of glutamine is indicated by Latin letters (PC-O and SW620-O) or Greek letters (PC-3-MPR and SW620-MPR). Significant differences

between PC-3/SW620 aged control and MPR were evaluated by t-test ($\alpha=0.05$). In panels G and H, statistical significance was also evaluated by t-test ($\alpha=0.05$). Significant differences relative to PC-3-O (E,G) or SW620-O (F,H) are indicated at $p < 0.05$ (*), $p < 0.01$ (**), $p < 0.001$ (***) and $p < 0.0001$ (****).

We also evaluated the relative changes in OCR upon the addition of increasing concentrations of glutamine in PC-3-O/PC-3-MPR (**4.2.20.E**) and SW620-O/SW620-MPR (**4.2.20.F**). Our results showed almost no significant alteration of OCR upon glutamine addition in any of PC-3 cell lines, and no significant correlation to the concentration of glutamine added, denoting that glutamine contribution to mitochondrial respiration is limited in this cell line or in its platinum resistant version. On the contrary, SW620 showed 10 times higher fold change increase in OCR upon glutamine addition and a dose-dependent response up to 4 mM in both SW620-O and SW620-MPR. Importantly, we encountered no significant differences between SW620-O and SW620-MPR in the effect of glutamine addition to respiration. This is indicative that the relative contribution of glutamine to respiration in SW620-O and SW620-MPR is maintained. This result is supported by the complete lack of significant differences between both cell lines in the glutamine *MitoFuel* test (**4.2.20.H**), which evaluates the contribution of glutamine to respiration relative to the sum of glucose, glutamine and fatty acids.

Interestingly, we observed an increase in GLS1 expression in SW620-MPR (**4.2.20.J**), whereas GLDH expression was maintained. Together with the extracellular flux rates and the Seahorse assays, our results for SW620-MPR indicate that this cell line does not increase the contribution of glutamine to TCA cycle anaplerosis, but it does increase glutamine consumption and its conversion into glutamate, probably to support enhanced glutathione synthesis. Other authors have also found an upregulation of glutamine transporter ASCT2 and an increase in glutaminase in cisplatin-resistant ovarian cancer [296].

On the contrary, PC-3-MPR decreased the expression of both Myc and GLS1 relative to PC-3-O (**4.2.20.I**), consistent with decreased glutamine uptake in this cell line. The relative contribution of glutamine to TCA cycle anaplerosis was not altered significantly between PC-3-O and PC-3-MPR cell lines (**4.2.20.G**). Thus, we can conclude that no clear changes in glutaminolysis associated to acquisition of platinum resistance are observed in the PC-3 model.

In summary, we have unveiled that PC-3-MPR and SW620-MPR cells exhibit opposed metabolic alterations in terms of glucose and glutamine metabolism. PC-3 cells, glycolytic in origin, undergo very little alterations in intracellular metabolite pool distributions, whereas they generally decreased the consumption and production rates of the vast majority of metabolites measured, possibly tied to a decrease in proliferation. Indeed, our results indicate that PC-3-MPR enter into a metabolically more quiescent state, which could be compatible with the acquisition of CSC traits [434]. Indeed, the acquisition of a CSC-enriched quiescent state upon acquisition of platinum resistance has been previously reported in the literature [188].

On the contrary, SW620-MPR, originally more OXPHOS-dependent, display a set of metabolic adaptations in response to acquired cisplatin resistance: they increase their glucose and glutamine consumption and upregulate Myc, deriving in increased glutathione synthesis and they acquire the capacity to secrete significantly greater amounts of putrescine and spermidine.

4.3. Chapter 3: Biological evaluation of novel platinum (II) and platinum (IV) compounds in prostate, colorectal and lung cancer

4.3.1. Introduction

The unparalleled importance of platinum compounds in the history of chemotherapy and their continuous usage up to the present days propitiate constant research and development of new platinum compounds with improved antineoplastic potential [292]. Over the last years, platinum (IV) compounds have drawn considerable attention as novel chemotherapeutic agents since their axial ligands can be rationally designed to improve efficacy and selectivity of their platinum (II) precursors, or modulate physicochemical parameters such as lipophilicity, stability or reduction potential [287,291].

The final aim of platinum research, to which platinum (IV) compounds can greatly contribute, is to encounter a compound that has cytotoxic specificity for tumor cells and can be administered at low doses with minimal side effects. For this reason, in **this Chapter**, we present the antiproliferative screening of over 40 novel platinum (II) and platinum (IV) compounds. All compounds presented here were synthesized and structurally characterized by the laboratory of Prof. Margarita Crespo (Faculty of Chemistry, University of Barcelona), and were evaluated in this work in different cancer cell panels that include prostate, colorectal, lung and breast cancer cell lines.

The main molecular mechanism of action of platinum compounds is the formation of platin-DNA intra-strand cross-links via platin-N7 guanine adducts. These will impair DNA replication and repair, inducing cell cycle arrest at S or G2/M phases and triggering apoptosis [286]. Moreover, due to the electrophilic nature of platinum compounds, they react with the ROS-scavenging machinery of the resulting in the reduction of platinum (sequentially, Pt(IV) to Pt(II), and Pt(II) to Pt(0)) impacting on redox homeostasis and generating oxidative stress. In consequence, the lead candidates of each family of related chemical structures have been further evaluated in terms of their effect on the

progression of cell cycle and their ability to induce oxidative stress and apoptosis in the treated cells. Moreover, we also investigated the effect of some of these lead compounds on the multiplatinum resistant CRPC and CRC models generated in **Chapter 2**, in an attempt to find platinum compounds with low cross-resistance with conventional platinum anticancer agents (namely cisplatin, carboplatin and oxaliplatin) that could circumvent the mechanisms of acquired platinum resistance, and potentially be effective as second-line treatments for platinum-resistant tumors.

4.3.2. Results and discussion

4.3.2.1. Effect of cyclometallated platinum (IV) iodo complexes

First, we investigated the antineoplastic effect of a set of platinum (IV) derivatives obtained from three different platinum (II) compounds displaying the general structure $[\text{PtX}\{(\text{CH}_3)_2\text{N}(\text{CH}_2)_3\text{NCH}(4\text{-ClC}_6\text{H}_3)\}]$ (**4.3.1.A**), with three different substitutions **1a** ($\text{X}=\text{Cl}$), **1b** ($\text{X}=\text{CH}_3$) and **1c** ($\text{X}=\text{I}$). Six different derivatives (**4.3.1.B**) were obtained by intermolecular oxidative addition with methyl iodide (compounds **2a-2c**) or iodine (compounds **3a-3c**). Further details on the synthesis of these compounds and additional biological characterization of their effect can be found in the associated publication [436].

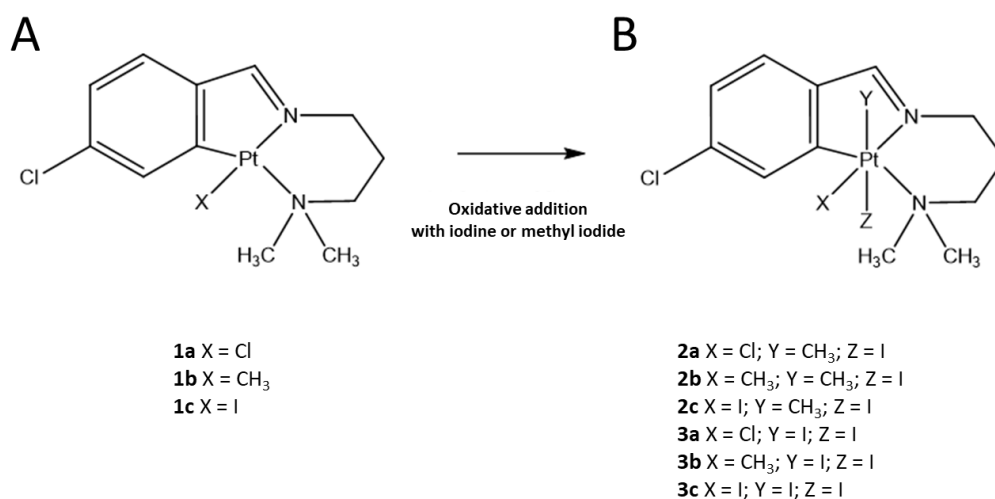


Figure 4.3.1. Chemical structures of the cyclometallated platinum (II) parental compounds and their iodo platinum (IV) derivatives. (A) Chemical structures of the three parental compounds, $[\text{PtX}\{(\text{CH}_3)_2\text{N}(\text{CH}_2)_3\text{NCH}(4\text{-ClC}_6\text{H}_3)\}]$, where $\text{X}=\text{Cl}$ (**1a**), $\text{X}=\text{CH}_3$ (**1b**) or $\text{X}=\text{I}$ (**1c**). (B) Chemical structures of the six platinum (IV) derivatives obtained by oxidative addition of iodine or methyl iodide, containing as axial ligands (Y,Z) either methyl or iodide groups.

The antiproliferative effect of series 1 (square planar Pt(II) compounds) and series 2 and 3 (octahedral Pt(IV) derivatives) was tested on A549 lung cancer cell line, MDA-MB-231 and MCF-7 breast cell lines and HCT-116 CRC cell line (4.3.2). Platinum (II) compounds, **1a-1c**, were generally comparable to cisplatin in terms of antiproliferative capacity. **1a** and **1c** displayed improved efficacy relative to cisplatin only in MCF-7 cell line.

Series 2 (**2a**, **2b** and **2c**), containing methyl or iodine as axial ligands, showed the lowest IC₅₀ values, particularly for A549 lung (1.4–2.6 μM), HCT-116 colorectal (1.3–5.4 μM) and MDA-MB-231 (2.1–4 μM) breast cancer cells.

	Compound	Cell line			
		A549	MDA-MB-231	MCF-7	HCT-116
	1a	6 ± 4	8 ± 4	7.7 ± 0.8	6.3 ± 0.3
	1b	10 ± 2	7.3 ± 0.6	31.3 ± 0.5	10.6 ± 0.2
	1c	6 ± 3	10 ± 3	10.2 ± 0.5	7.1 ± 0.2
	2a	2.5 ± 0.2	2.3 ± 0.3	12.4 ± 0.8	5.4 ± 0.1
	2b	2.6 ± 0.3	2.1 ± 0.5	7.9 ± 0.7	2.3 ± 0.3
	2c	1.4 ± 0.1	4 ± 2	6.8 ± 0.4	1.3 ± 0.2
	3a	5 ± 4	5 ± 2	8.4 ± 0.4	5.1 ± 0.1
	3b	6.7 ± 1.3	7.3 ± 0.2	7.7 ± 0.1	4 ± 2
	3c	23 ± 3	14 ± 4	>100	12.1 ± 0.7
	cisplatin	5.2 ± 0.1	12.3 ± 0.4	24.9 ± 0.4	6.5 ± 0.4

Table 4.3.2. Antiproliferative activity on A549 lung, MDA-MB-231 and MCF-7 breast, and HCT-116 colorectal cancer cell lines for the novel platinum (II) and platinum (IV) compounds and cisplatin as reference compound. IC₅₀ values (μM) of compounds 1a-3c and cisplatin (cis-[PtCl₂(NH₃)₂]), assessed by MTT cell viability assay. Data shown represents mean ± SD of n=3 of at least two independent experiments. Cisplatin is taken as the reference compound.

Compound **2c**, containing one iodido group arranged in trans to the imine nitrogen, was particularly effective, significantly more potent than cisplatin in all cell lines of the cancer cell line panel. Interestingly, series 2 displayed selectivity for the triple negative^{vi} breast

^{vi} Triple negative breast cancer is an aggressive subset of breast cancer defined by the absence of expression of estrogen receptor (ER), progesterone receptors (PR) and hormone epidermal growth factor receptor 2 (HER-2).

cancer cell line, MDA-MB-231 (2.3–4 μM) relative to the ER and PR positive cell line, MCF-7 (6.8–12.4 μM). Regarding series 3, **3a** and **3b** platinum (IV) compounds showed higher efficacy than cisplatin for all the cell lines. Contrarily, compound **3c** displayed much higher IC_{50} values than the rest of the compounds, possibly due to its low solubility in cell culture media.

In summary, compounds **2b** and **2c** were significantly more potent than cisplatin in all cell lines and thus they were selected for further investigation of their molecular mechanisms of action in the lung adenocarcinoma cell line A549, in terms of cell cycle progression, apoptosis and generation of intracellular ROS.

Our results indicated that both **2b** and **2c** were capable of triggering apoptosis in A549 cells (**4.3.3.A**), since a significant fraction of cells treated with either **2b** or **2c** were detected as annexin V⁺/PI⁻. However, an increase in PI⁺ cells relative to control was only detected in **2b**-treated A549 cells after 72 h incubation. On the contrary, only **2c**-treated A549 cells displayed a percentual increase in ROS (**4.3.3.B**), evaluated through the incubation with the H₂O₂-reacting fluorescent probe 2',7'-dichlorofluorescein diacetate.

Finally, both compounds triggered a similar cell cycle arrest in the synthesis phase (**4.3.3.C**), denoting a similar effect in impairing DNA replication in A549 cells. However, differential effects between both compounds on the induction of apoptosis or the generation of ROS in A549 cells could indicate additional mechanisms of action. Remarkably, in the associated publication we also reported a marked inhibitory effect of compound **2b** on topoisomerase II α [436], which was significantly stronger than etoposide, the conventional anticancer therapy based on topoisomerase inhibition. Topoisomerase inhibition by chemical compounds has been extensively reported to be accompanied by significant induction of apoptosis [437,438], which is in accordance to our results. Indeed, topoisomerase II α inhibitory activity was detected for compound **2b**, but not **2c**, which is consistent with our observation of markedly higher apoptosis induction in **2b**-treated cells.

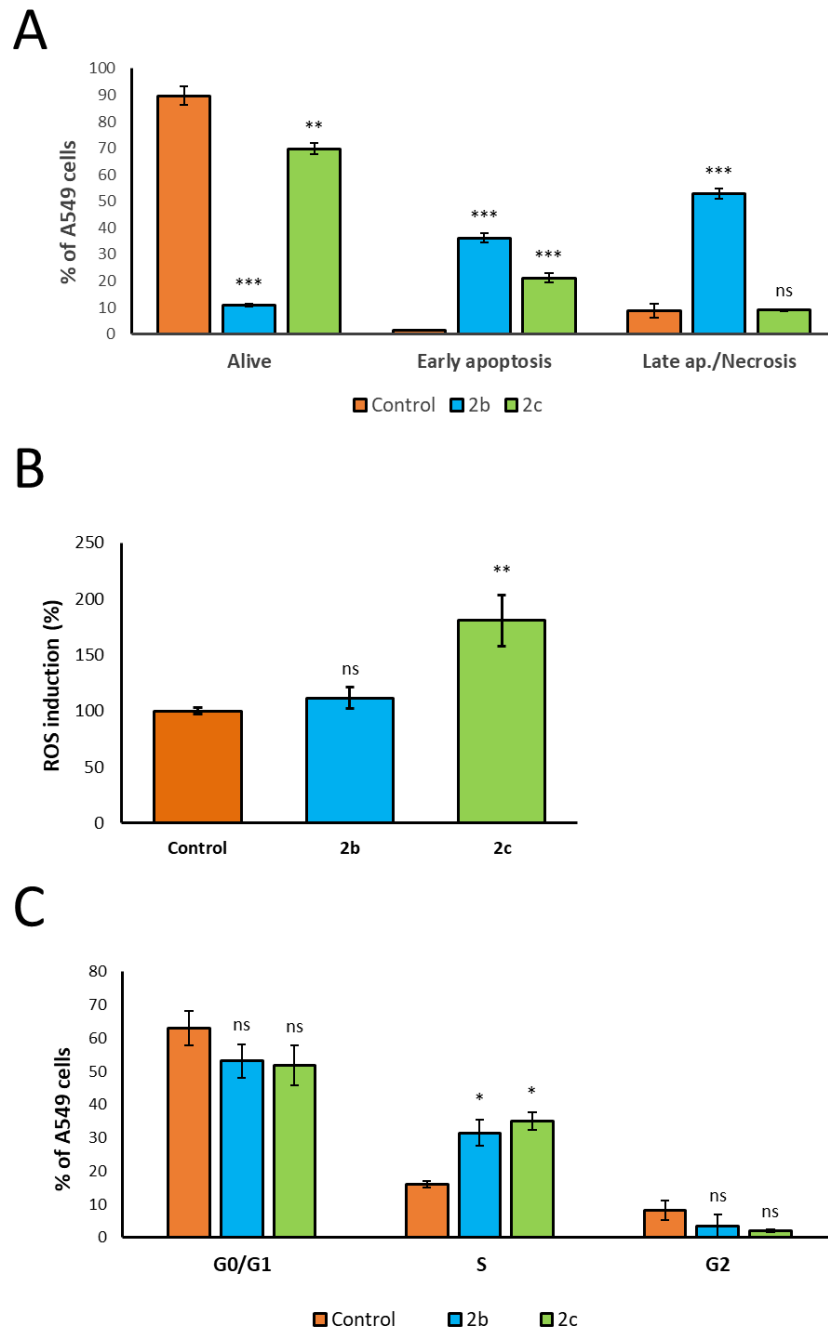


Figure 4.3.3. Effect of compounds 2b and 2c on the cell cycle distribution, apoptosis and generation of reactive oxygen species (ROS) of A549 lung adenocarcinoma cells. (A) Percentage variations of alive, early apoptotic and late apoptotic/necrotic cell populations at 72 h incubation with compounds 2b and 2c at their IC50 concentration in the A549 lung adenocarcinoma cell line. Cells were stained with propidium iodide (PI) and FITC-annexin and were analyzed by flow cytometry. (B) ROS levels after 72 h incubation with compounds 2b and 2c at their IC50 concentration in the A-549 lung adenocarcinoma cell line. Cells were stained with 2',7'-dichlorofluorescein diacetate. (C) Cell cycle phase distribution at 72 h incubation with compounds 2b and 2c at their IC50 concentration in the A549 lung adenocarcinoma cell line. Cells were stained with PI and their DNA content was analyzed by flow cytometry. Bars represent mean \pm SD of $n=3$. Significant differences relative to A549 control were evaluated by Student t-test and are indicated at $p < 0.05$ (*), $p < 0.01$ (**), and $p < 0.001$ (***)

4.3.2.2. Effect of cyclometallated platinum (IV) chloro and bromo fluorinated complexes

Some members of the cyclometallated families of compounds of the previous section were found to be highly effective and able to hinder cancer cell viability via different molecular mechanisms. However, as described in detail in the associated publication, we did not detect *in vitro* oxidation of ascorbic acid after 10 day incubation with the compounds **2b** and **2c** [436]. Indeed, oxidation of cell endogenous ROS scavengers is desirable in the design of platinum compounds with antineoplastic potential, since it leads to increased oxidative stress in cancer cells, which ultimately can contribute to cancer cell death. Thus, we next aimed to refine the structures obtained in the previous section by introducing subtle modifications in the cyclometallated structure and the axial ligands, which could potentially increase the reduction potential of the obtained species. For this, we obtained the Pt (II) structures [PtX{(CH₃)₂N(CH₂)₃NCH(4-FC₆H₃)}] (**4.3.4.A**) and [PtX{(CH₃)₂N(CH₂)₂NCH(4-FC₆H₃)}] (**4.4.4.C**), in which, for both, X can be a chloride or bromide substituent. Then, by oxidative addition with either chlorine or bromine, we also obtained four Pt(IV) derivatives in total, with chloride or bromide axial ligands (**4.3.4.BD**).

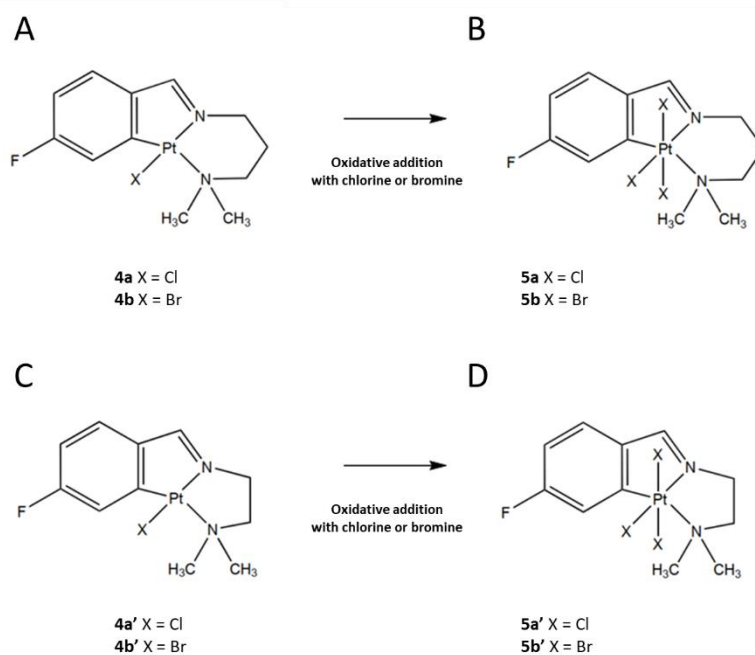


Figure 4.3.4. Chemical structures of the cyclometallated platinum (II) parental compounds and their chloro and bromo platinum (IV) derivatives. (A) Chemical structures of the two parental compounds, [PtX{(CH₃)₂N(CH₂)₃NCH(4-

FC₆H₃}}], where X=Cl (4a) or X=Br (4b) (B) Chemical structures of the two platinum (IV) derivatives obtained by oxidative addition of chlorine or bromine, containing as axial ligands (X) either chloride (5a) or bromide groups (5b). (C) Chemical structures of the two parental compounds, [PtX{(CH₃)₂N(CH₂)₂NCH(4-FC₆H₃)}], where X=Cl (4a') or X=Br (4b') (D) Chemical structures of the two platinum (IV) derivatives obtained by oxidative addition of chlorine or bromine, containing as axial ligands (X) either chloride (5a') or bromide (5b') groups.

The antiproliferative capacity of this series of compounds was tested in NSCLC cell line A549, CRC SW620, breast cancer MCF-7, and CRPC PC-3, using both cisplatin and oxaliplatin as reference compounds (4.3.5). Remarkably, the IC₅₀ of all the compounds except **4a'** and **4b'** were significantly lower than both cisplatin and oxaliplatin for the breast cancer cell line MCF-7. Also, some of the Pt(IV) derivatives of both series of compounds displayed IC₅₀ values in the nanomolar range for SW620 and PC-3, being significantly more potent than cisplatin and, in some cases, also oxaliplatin. In particular, our results indicate that **5a'** was the most effective compound against SW620 (0.41 μM), whereas **5a** displayed the highest efficacy against PC-3 (0.9 μM), A549 (1.4 μM) and MCF-7 (5.4 μM). In particular, the Pt(II) structure **4a** had a similar effect than the Pt(IV) derivatives in PC-3. In A549, all four Pt(IV) derivatives were slightly more potent than cisplatin and the best of them, compound **5a**, had an efficacy similar to oxaliplatin.

Compound	Cell line			
	A549	SW620	MCF-7	PC-3
4a	5 ± 2	5.7 ± 1.1	6 ± 2	1.1 ± 0.6
4b	5 ± 2	5.5 ± 0.4	7 ± 2	2.1 ± 1.3
4a'	57 ± 3	4.6 ± 0.8	>100	19 ± 5
4b'	48 ± 5	3.1 ± 1.1	>100	66 ± 13
5a	1.4 ± 0.5	0.9 ± 0.3	3.3 ± 0.5	0.9 ± 0.2
5b	3.39 ± 0.12	1.8 ± 0.7	6.6 ± 0.8	1.46 ± 0.13
5a'	4.1 ± 0.3	0.41 ± 0.04	5.4 ± 1.0	1.2 ± 0.5
5b'	4 ± 2	0.7 ± 0.4	8.0 ± 0.8	1.46 ± 0.11
cisplatin	5.5 ± 0.2	1.4 ± 0.5	25.6 ± 0.7	1.5 ± 0.4
oxaliplatin	1.3 ± 0.2	0.3 ± 0.2	23.4 ± 0.2	1.2 ± 0.3

Table 4.3.5. Antiproliferative activity on A549 lung, SW620 colorectal, MCF-7 breast, and PC-3 prostate cancer cell lines for the novel platinum (II) and platinum (IV) compounds with cisplatin and oxaliplatin as reference compounds. IC₅₀ values (μM) of compounds 4a-5b', cisplatin (cis-[PtCl₂(NH₃)₂]) and oxaliplatin (C₈H₁₂N₂O₄Pt), assessed by MTT cell viability assay. Data shown represents mean ± SD of n=3 of at least two independent experiments. Cisplatin and oxaliplatin are taken as the reference compounds.

In summary, the antiproliferative effect of this series of compounds against the studied cancer cell line panel was highly heterogeneous, even if compounds **4a'** and **4b'** were generally much less effective than the rest of compounds. Such heterogeneous effects among cell lines potentially indicates the existence of more than one molecular mechanism of action for the studied compounds. Furthermore, unlike the previous series of compounds, in which Pt(IV) compounds were significantly better than their Pt(II) precursors, in the present case structures **4a** and **4b** had similar effect than some of their Pt(IV) derivatives.

In general terms, compound **5a** (best in PC-3, MCF-7 and A549) and compound **5a'** (best in SW620) could be selected as the lead compound of this series. Moreover, the parental Pt(II) structure **4a** was also highly effective *per se* and has the potential of leading to even more promising results than the obtained with its derivative **5a** when being further investigated with different axial ligands. For this reason, we next decided to investigate the selectivity of **4a**, **5a** and **5a'** for cancer cells, by studying the antiproliferative effect of the three compounds in a healthy immortalized fibroblast cell line, BJ, in the range of doses that is sufficient to completely block the proliferation of all four investigated cancer cell lines. Encouragingly, our results showed that compound **5a** is highly selective for all four cell lines in doses equal or higher than 5 μ M, and also at 1 μ M for PC-3 and SW620 (**4.3.6.A**). Importantly, at this dose the proliferation of BJ cells was completely unaffected by the drug, which could open an important therapeutic window against highly proliferative metastatic solid tumors. Compound **5a'** was also highly selective for all cell lines at 5 μ M and, unlike **5a**, it did not have any effect on BJ cells at this dose (**4.3.6.B**). Importantly, compound **5a'** also displayed a significant selectivity for SW620 at 1 μ M. Finally, compound **4a** was also highly selective for PC-3, SW620 and A549 at 5 μ M, and also for MCF-7 at 10 μ M (**4.3.6.C**), denoting also a good selectivity profile for cancer cell lines.

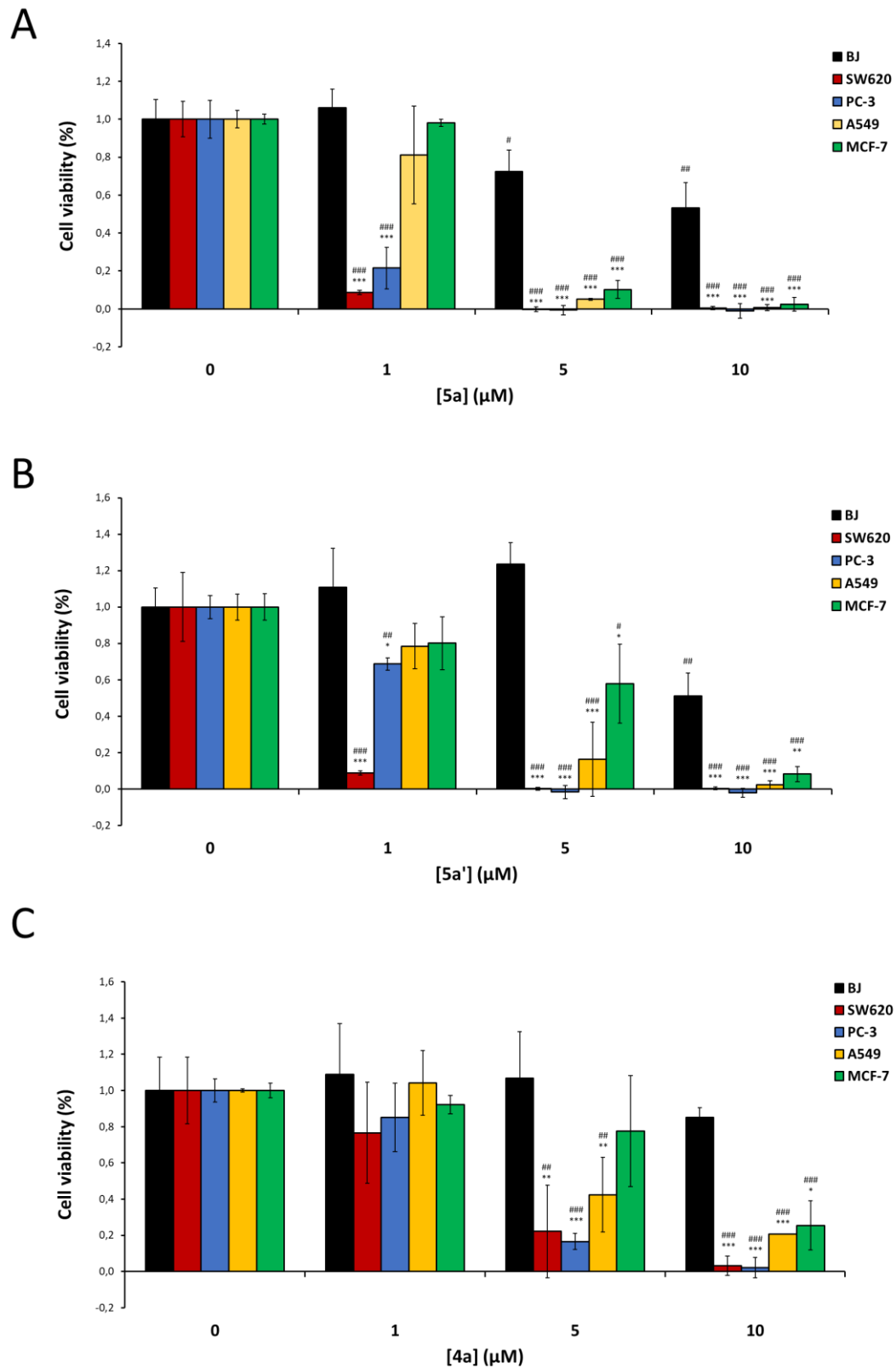


Figure 4.3.6. Selectivity of Pt(II) compound 4a and Pt(IV) compounds 5a and 5a' for cancer cells. Normalized cell viability after 72 h incubation with 0, 1, 5 or 10 μM of 5a (A), 5a' (B), or 4a (C) in BJ healthy foreskin fibroblasts, SW620 colorectal cancer, PC-3 metastatic prostate adenocarcinoma, A549 lung adenocarcinoma and MCF-7 breast cancer cells determined by MTT antiproliferative assay. Bars represent mean ± SD of n=3. Significant differences between a given compound concentration relative to the respective untreated control cells were evaluated by Student t-test

and are indicated at $p < 0.05$ (#), $p < 0.01$ (##), and $p < 0.001$ (###). Significant differences in response to the same dose between cancer cells (SW620, PC-3, A549 or MCF-7) and BJ cells (healthy control) at each dose were evaluated by Student t-test and are indicated at $p < 0.05$ (*), $p < 0.01$ (**), and $p < 0.001$ (***). Absence of the specified symbols denotes absence of statistical significance.

4.3.2.3. Cross-resistance of novel cyclometallated Pt(IV) chloro and bromo fluorinated compounds with multiplatinum-resistant cell lines

Compounds in **Section 4.4.2.1** and **Section 4.4.2.2** displayed an encouraging potential to be further developed as anticancer agents due to their high efficacy, selectivity for cancer cells and their multiple molecular mechanisms of action, which collectively hinder the emergence of acquired resistance: cell cycle arrest, inhibition of topoisomerase activity, induction of apoptosis and disruption of redox homeostasis of cancer cells. Bearing this in mind, we next interrogated the capacity of these compounds to circumvent the resistance to cisplatin, carboplatin and oxaliplatin acquired by the CRPC and CRC platinum resistant cell models generated in **Chapter 2**, PC-3-MPR and SW620-MPR, respectively.

To assess this, we evaluated the cell viability of age-matched parental cell lines PC-3-O and SW620-O and multiplatinum resistant cell lines PC-3-MPR and SW620-MPR. We used the drug resistance index (DRI), defined as the ratio between the IC_{50} values of the same compound in two cell lines [439,440]. We used this index to evaluate the degree of resistance to a certain compound acquired by either cell aging, DRI_{aging} (PC-3 vs. PC-3-O); prolonged exposure to cisplatin, $DRI_{resistance}$ (PC-3-O vs. PC-3-MPR); or the combination of both factors, DRI_{total} (PC-3 vs. PC-3-MPR), or equivalently in the isogenic CRC cell lines, SW620, SW620-O and SW620-MPR. Strikingly, our results unveiled that the acquisition of conventional multiplatinum resistance was completely uncoupled from resistance to the novel cyclometallated compounds for both resistant PC-3 (**Table 4.3.7**) and SW620 (**Table 4.3.8**). In the majority of cases, the antiproliferative effect of PC-3-MPR and SW620-MPR was indistinguishable from their respective age-matched control.

On the other hand, these experiments also allowed us to detect a slight general tendency to acquire resistance to both conventional platinum compounds and the cyclometallated compounds as cancer cells aged in cell culture, denoting the mutational

burden acquired during cell aging contributes to span the arsenal of mechanisms that cancer cells can use to dodge the effect of a broad spectrum of chemotherapeutic agents.

	Compound						
	4a	5a	5b	5a'	5b'	cisplatin	oxaliplatin
PC-3	1.1 ± 0.7	0.9 ± 0.2	1.46 ± 0.13	1.2 ± 0.5	1.46 ± 0.11	1.5 ± 0.4	1.2 ± 0.3
PC-3-O	0.67 ± 0.11	1.4 ± 0.8	5.3 ± 0.3	2 ± 2	4 ± 2	2.5 ± 0.9	0.69 ± 0.02
PC-3-MPR	1.6 ± 0.2	1.5 ± 0.3	3.7 ± 1.3	2.9 ± 0.4	3.7 ± 0.4	23 ± 9	51 ± 12
DRI _{aging}	0.6	1.5	3.7	1.9	2.4	1.7	0.6
DRI _{resistance}	2.5	1	0.7	1.3	1	9.1	74
DRI _{total}	1.5	1.6	2.5	2.4	2.5	15	42

Table 4.3.7. Antiproliferative activity of Pt(IV) compounds 4a, 5a-5b', cisplatin and oxaliplatin on PC-3, PC-3-O and PC-3-MPR and drug resistance index (DRI) between cell lines. IC₅₀ values (μM) of compounds 5a-5b', cisplatin (cis-[PtCl₂(NH₃)₂]) and oxaliplatin (C₈H₁₂N₂O₄Pt), assessed by MTT cell viability assay. DRI is defined as the ratio of IC₅₀ values of: PC-3-O to PC-3 (DRI_{aging}), PC-3-MPR to PC-3-O (DRI_{resistance}) and PC-3-MPR to PC-3 (DRI_{total}). Data shown represents mean ± SD of n=3 of at least two independent experiments. Cisplatin and oxaliplatin are taken as the reference compounds.

	Compound						
	4a	5a	5b	5a'	5b'	cisplatin	oxaliplatin
SW620	5.7 ± 1.1	0.9 ± 0.3	1.8 ± 0.7	0.41 ± 0.04	0.7 ± 0.4	1.4 ± 0.5	0.32 ± 0.10
SW620-O	7 ± 3	2.2 ± 0.3	3.6 ± 1.2	1.1 ± 0.7	0.8 ± 0.4	1.1 ± 0.9	0.3 ± 0.2
SW620-MPR	7.1 ± 0.6	3 ± 2	4.8 ± 1.4	1.64 ± 0.01	1.4 ± 0.7	21 ± 4	3.2 ± 1.1
DRI _{aging}	1	2.4	2	2.8	1.2	0.8	1
DRI _{resistance}	1	1.2	1.3	1.4	1.7	19	10
DRI _{total}	1.3	2.8	2.7	4	2	15	10

Table 4.3.8. Antiproliferative activity of Pt(IV) compounds 4a, 5a-5b', cisplatin and oxaliplatin on SW620, SW620-O and SW620-MPR and drug resistance index (DRI) between cell lines. IC₅₀ values (μM) of compounds 5a-5b', cisplatin (cis-[PtCl₂(NH₃)₂]) and oxaliplatin (C₈H₁₂N₂O₄Pt), assessed by MTT cell viability assay. DRI is defined as the ratio of IC₅₀ values of: SW620-O to SW620 (DRI_{aging}), SW620-MPR to SW620-O (DRI_{resistance}) and SW620-MPR to SW620 (DRI_{total}). Data shown represents mean ± SD of n=3 of at least two independent experiments. Cisplatin and oxaliplatin are taken as the reference compounds.

Other recent studies, such as the one by Li et al. with Pt(IV) prodrugs containing microtubule inhibitors as axial ligands have also found low DRIs against a cisplatin resistant ovarian cancer [440]. Similarly, another work by Qin et al. also found low resistance indexes in cisplatin resistant gastric cancer to Pt(IV) compounds conjugated to chlorambucil, a nitrogen mustard agent typically used in chemotherapy [441]. Indeed,

a common factor between both studies is the combination of Pt(IV) with axial ligands that have molecular mechanisms of action that do not overlap with the action of Pt(II). Thus, in both cases upon release of the axial ligands, these can act either independently or in combination with Pt(II) to impair cancer cell proliferation. However, in our case the axial ligands are bromide and chloride ions, which are unlikely to promote any independent cytotoxic effect. In support of this notion, Pt(II) precursor **4a** also displayed similar cross-resistance levels than the Pt(IV) derivatives. In consequence, the absence of cross-resistance necessarily relies on the square-planar cyclometallated structure that surrounds the platinum atom, and not on the axial ligands. Indeed, the alteration of the platinum mechanism of action in the lead compound of this series will require further investigation in the near future.

Also, the observation that both PC-3/SW620-O and -MPR cells behave in a similar manner to **5a-5b'**, but they are both slightly more resistant than the parental cell line reinforces our idea that **5a-5b'** act, at least in part, through different mechanisms than conventional platinum compounds, and thus hold great promise as an effective alternative for tumors no longer responding to conventional platinum drugs. In addition, the fact that parallel effects are observed in completely different cancer types, CRPC and CRC, supports the idea that this response could be also exportable to other solid tumor types, such as breast or lung, in which we have also observed that the compounds have similar efficacy than in prostate and CRC. This would be of particular interest for lung cancer in which, for certain subsets, platinum compounds are the only available therapeutic option [442].

Given the promising results of the compounds in the PC-3/SW620-MPR cell lines, we also analyzed the selectivity of compounds **5a** and **5a'** against the immortalized healthy fibroblast cell line BJ. We also found that both compounds were highly selective at 5 and 10 μM (**4.3.9**), doses at which cell viability of PC-3/SW620-O and -MPR cell lines is drastically compromised.

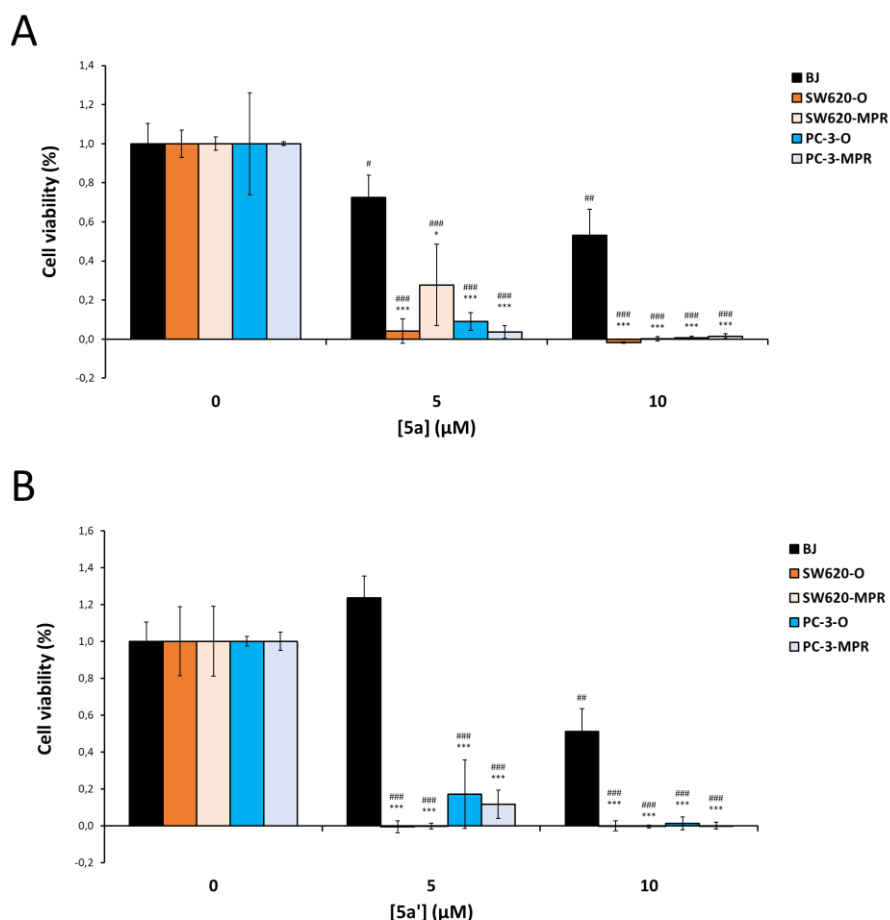


Figure 4.3.9. Selectivity of Pt(IV) compounds 5a and 5a' for multiplatinum resistant (MPR) colorectal and prostate cancer cell models, SW620-MPR and PC-3-MPR, and their age-matched controls, SW620-O and PC-3-O. Normalized cell viability after 72 h incubation with 0, 5 or 10 μM of 5a (A) or 5a' (B), in BJ healthy foreskin fibroblasts, SW620-MPR, PC-3-MPR, SW620-O and PC-3-O determined by MTT antiproliferative assay. Bars represent mean \pm SD of $n=3$. Significant differences between a given compound concentration relative to the respective untreated control cells were evaluated by Student t-test and are indicated at $p < 0.05$ (#), $p < 0.01$ (##), and $p < 0.001$ (###). Significant differences in response to the same dose between cancer cells (SW620-MPR, PC-3-MPR, SW620-O and PC-3-O) and BJ cells (healthy control) at each dose were evaluated by Student t-test and are indicated at $p < 0.05$ (*), $p < 0.01$ (**), and $p < 0.001$ (***). Absence of the specified symbols denotes absence of statistical significance.

In **Chapter 2** we concluded that part of the metabolic reprogramming undergone by both prostate and colorectal cancer cells to become platinum-resistant was devoted to increase intracellular glutathione content. In consequence, our platinum resistant cell models would, in principle, also be resistant to any electrophilic cytotoxic agent that could be inactivated by glutathione, including all the novel compounds described in **this Chapter**.

However, the DRI of the novel lead compounds analyzed here is much lower than the ones of cisplatin and oxaliplatin in our multiplatinum resistant cell models. This could hypothetically be ascribed to the higher oxidation state of the Pt(IV) central atom of the lead compounds. To inactivate the cytotoxicity of platinum compounds, ROS scavenging machinery of the cell must reduce the Pt atom to Pt(0). In consequence, Pt(IV) compounds would need stoichiometrically twice as ROS scavenging agents as Pt(II) to be completely inactivated. Despite that, if Pt(IV) was the only reason why these novel compounds display low cross-resistance with conventional platinum drugs in our cell models, the expected DRI value would be about half the DRI of cisplatin or oxaliplatin, which is far from what our results suggest.

Bearing this idea in mind, and to further characterize the effect of compound **5a'** on platinum-resistant cells, we next evaluated the effect of either cisplatin or **5a'** in SW620-O and SW620-MPR, in terms of cell cycle progression, apoptosis and intracellular ROS levels. Our results indicated that the effect of cisplatin and **5a'** on the cell cycle of SW620-O and SW620-MPR cells was radically different. First, cisplatin caused a remarkable G2/M arrest in SW620-O (**4.3.10.A**), while a much smaller but still significant G2/M arrest in SW620-MPR (**4.3.10.B**). In this case, it is worth noting that the cisplatin dosage in both cell lines for this experiment is the IC₅₀ dose for each cell line, which is about one order of magnitude greater for the resistant cell line. Still, our results showed that the relative contribution of cell cycle arrest to the 50% decrease in proliferation (IC₅₀) is decreased in the resistant cell line relative to SW620-O (roughly 10% vs 40% in decrease in G0/G1, in SW620-MPR and SW620-O respectively). On the other hand, **5a'** caused a significant arrest in S phase, in detriment to G2/M phase in SW620-O and had no significant effect on the cell cycle of the resistant cell line. Interestingly, both the results obtained with cisplatin and **5a'** for SW620-MPR indicate that acquired multiplatinum resistance in CRC involves the minimization of DNA-platinum interactions or their consequences, either by improving DNA repair and replication mechanisms or by reducing the amount of platinum that can enter the nucleus. Either way, the fact that the IC₅₀ for **5a'** is similar in SW620-O and SW620-MPR necessarily implies that other cytotoxic mechanisms emerge, potentially inexistent in conventional platinum compounds, to which SW620-MPR has not developed resistance.

Indeed, these could be tied to the alteration of redox homeostasis and related metabolic networks. In this regard, cisplatin caused a dramatic increase in ROS production in SW620-O cell line, whereas a much lesser increase in the SW620-MPR cell line, given the 10-fold increase in cisplatin dose (**4.3.10.C**). On the contrary, compound **5a'** only caused a significant ROS increase in SW620-MPR but not on the parental cell line. This observation would be consistent with the idea that SW620-MPR are reprogrammed to reduce the amount of platinum compound that enters the nucleus. In this way, increased cytosolic **5a'** in SW620-MPR could potentially be responsible for this increase in intracellular ROS in the resistant cell line. Still, further experiments would be required to deepen in this matter.

Unlike the differences found in cell cycle and ROS production between the control and resistant cell lines, compound **5a'** was able to significantly induce apoptosis in both cell lines after 72 h incubation (**4.3.10.DE**). Our flow cytometry analyses detected about 70% of PI⁺ cells in SW620-O and 50% of PI⁺ cells in SW620-MPR. Cisplatin displayed much more modest effects than compound **5a'** on inducing apoptosis in both cell lines. Remarkably, despite the 10-fold increase in dose, the effect on the resistant cell line was significantly decreased: only 10% reduction on the healthy population, whereas a 25% reduction was found on SW620-O when exposed to cisplatin.

In general terms, our results indicate that conventional platins rely more on cell cycle arrest and less on induction of apoptosis than the cyclometallated structures we have generated. In accordance, the resistant cell line SW620-MPR is adapted to such cell cycle disruption, and minimizes its effects, but is still similarly vulnerable to the induction of apoptosis caused by **5a'**, and potentially the rest of compounds in the series.

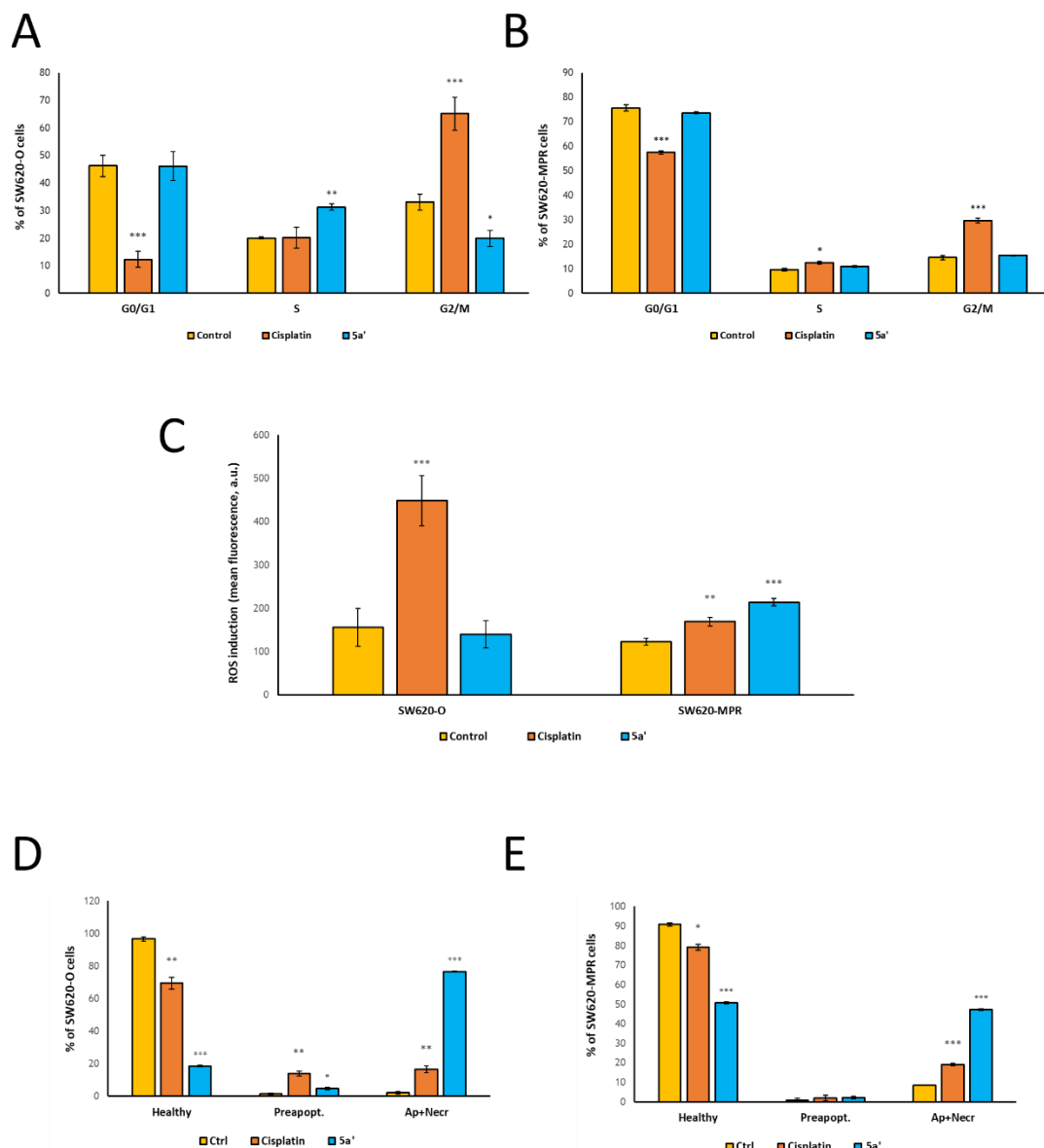


Figure 4.3.10. Effect of cisplatin and compound 5a' on the cell cycle distribution, apoptosis and generation of reactive oxygen species (ROS) of SW620-O and SW620-MPR cells. Percentage variations of alive, early apoptotic and late apoptotic/necrotic cell populations at 72 h incubation with cisplatin and compound 5a' at their respective IC₅₀ concentrations in SW620-O (A) and SW620-MPR (B). Cells were stained with propidium iodide (PI) and FITC-annexin and were analyzed by flow cytometry. (C) ROS levels after 72 h incubation with cisplatin and compound 5a' at their IC₅₀ concentrations in the SW620-O and SW620-MPR cells. Cells were stained with 2',7'-dichlorofluorescein diacetate. Cell cycle phase distribution at 72 h incubation with cisplatin and compound 5a' at their respective IC₅₀ concentrations in SW620-O (D) and SW620-MPR (E) cell lines. Cells were stained with PI and their DNA content was analyzed by flow cytometry. Bars represent mean ± SD of n=3. Significant differences relative to the untreated condition in each cell line were evaluated by Student t-test and are indicated at p < 0.05 (*), p < 0.01 (**), and p < 0.001 (***).

4.3.2.4. Effect of cyclometallated platinum (IV) complexes containing a para-tolyl ligand

Given the promising antineoplastic effect introduced by the oxidative addition of halogen and methyl groups on cyclometallated platinum structures, explored in **Sections 4.3.2.1 to 4.3.2.3**, we next decided to further evaluate similar cyclometallated structures by generating a third subset of platinum (IV) complexes. We introduced para-tolyl ligands and tridentate [C,N,N'] or a bidentate [C,N] ligands, to explore if the tridentate structure (similar to the ones in **Section 4.3.2.1** and **4.3.2.2**) is indeed partly responsible of the cytotoxic effect of the novel Pt(II) and Pt(IV) compounds, as hypothesized in the previous sections.

All three parental compounds (**4.3.11**) were prepared from the reaction of a common platinum precursor $[\text{Pt}(4\text{-CH}_3\text{C}_6\text{H}_4)_2\{\mu\text{-S}(\text{CH}_2\text{CH}_3)_2\}]_2$ and two different imines L_1 and L_2 (**4.3.12**), leading to parental compounds **cm1** and **cm2**. Parental compound **cm3** was prepared by substitution of the diethyl sulfide ligand in **cm2** by triphenylphosphine (PPh_3). Finally, Pt(IV) derivatives of **cm1**, **cm2** and **cm3** were obtained by intermolecular oxidative addition reaction with methyl iodide (**cm1-3MeI** series) or iodine (**cm1-3I₂** series). Further synthetic details for all the compounds can be found in the publication associated to the synthesis and biological evaluation of the compounds analyzed in this section [443].

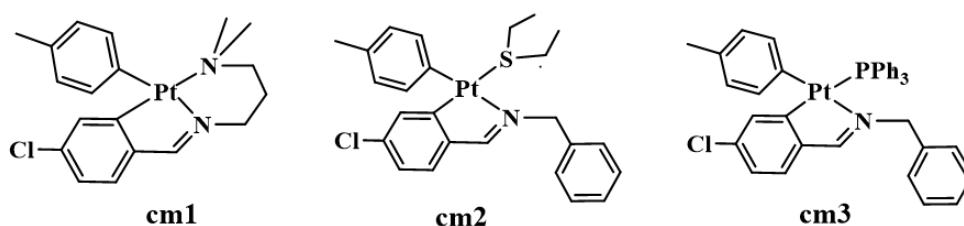


Figure 4.3.11. Chemical structures of the cyclometallated platinum (II) parental compounds. Square planar Pt(II) compounds derived from the general precursor $[\text{Pt}(4\text{-CH}_3\text{C}_6\text{H}_4)_2\{\mu\text{-S}(\text{CH}_2\text{CH}_3)_2\}]_2$ all containing a para-tolyl ligand. Compound **cm1** contains a tridentate [C,N,N'] ligand, whereas compounds **cm2** and **cm3** contain the same bidentate [C,N] ligand and a diethyl sulfide (**cm2**) and triphenylphosphine (**cm3**), respectively.

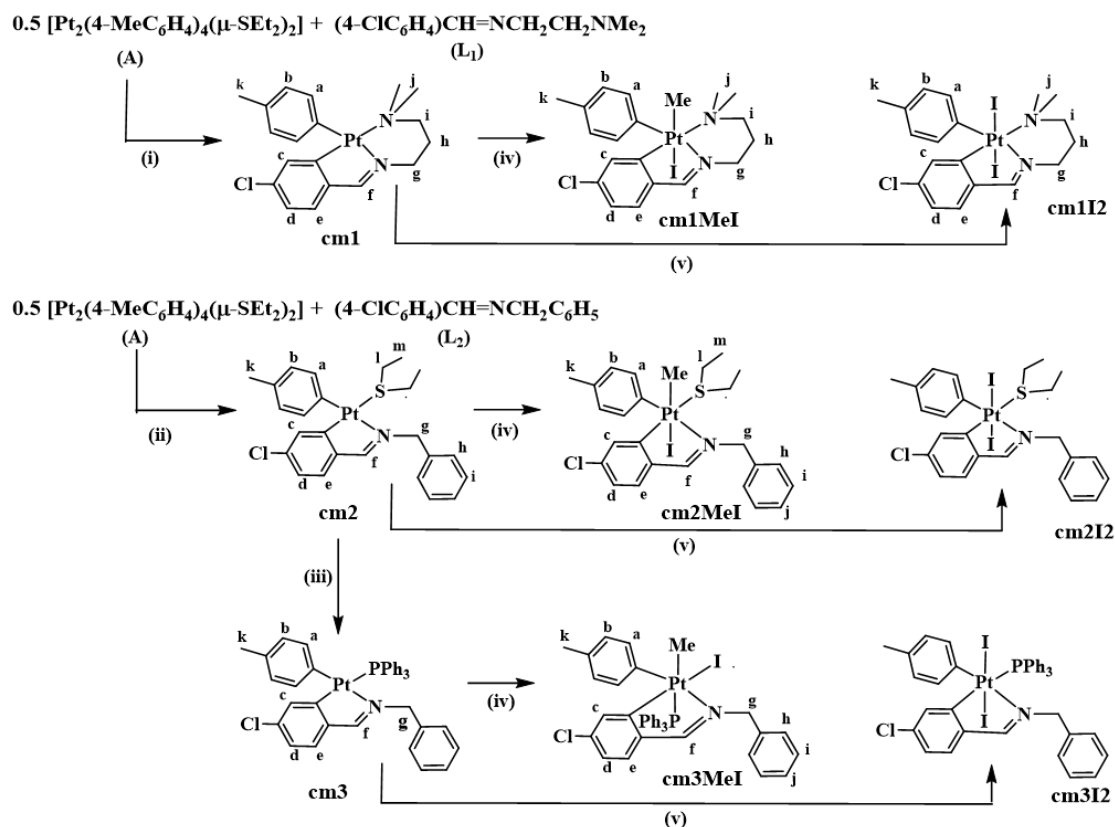


Figure 4.3.12. Chemical structures and synthetic details of the cyclometallated platinum (II) parental compounds and their methyl-iodo and iodo platinum (IV) derivatives. Chemical structures of the three parental compounds, derived from the general structure [Pt(4-CH₃C₆H₄)₂{μ-S(CH₂CH₃)₂}₂], and synthetic procedure of all compounds used in this series: (i) Toluene, 90 °C, 6 h; (ii) toluene, RT, 24 h; (iii) +PPh₃, acetone, 2 h; (iv) +CH₃I, acetone, RT, 24 h; (v) +I₂, acetone, RT, 2 h.

First, we evaluated the antiproliferative capacity of all compounds of the **cm1**, **cm2** and **cm3** series, with the structures detailed in (4.3.12). Our results of the antiproliferative screening (4.3.13) revealed that, in general, **cm1** and **cm2** Pt(II) precursors had an efficacy similar to cisplatin for lung and CRC cell lines A549 and HCT-116. Interestingly, in both breast cancer cell lines the IC₅₀ values of both **cm1** and **cm2** are significantly smaller than cisplatin. This is particularly relevant for the breast cancer cell line MCF-7, inherently more resistant to cisplatin than the rest of cell lines in the panel. For this cell line, the values of both **cm1** and **cm2** are reduced by half compared to cisplatin. On the contrary, **cm3** displayed no cytotoxic activity up to 100 μM in any of the cell lines in our cell panel.

Regarding the Pt(IV) derivatives, some of them notably improved the efficacy of their Pt(II) precursor. In particular, **cm1MeI** had a stronger effect than cisplatin in all four cell

lines, whereas **cm1I₂** was also more potent than cisplatin in all cell lines except A549. On the other hand, **cm2MeI** and **cm3MeI** were far less effective.

Interestingly, for the case of **cm2MeI**, the introduction of the axial ligands decreased the activity of the parental compound, while **cm3MeI** had the opposite effect, probably due to the alteration of the lipophilic profile of the precursors. In this regard, compounds **cm2I₂** and **cm3I₂** could not be analyzed due to strong insolubility in cell culture medium.

Compound	Cell line			
	A549	MDA-mb-231	MCF-7	HCT-116
cm1	9.8 ± 0.3	7.7 ± 1.0	13.8 ± 3.3	6.5 ± 1.3
cm2	6.5 ± 0.3	5.5 ± 0.2	10.2 ± 0.6	4.0 ± 0.4
cm3	>100	>100	>100	>100
cm1I₂	9.7 ± 0.4	7 ± 2	11.1 ± 0.8	5.13 ± 0.03
cm1MeI	3 ± 2	1.6 ± 0.6	10 ± 4	1.8 ± 0.6
cm2MeI	76 ± 13	26 ± 3	>100	8.6 ± 0.9
cm3MeI	>100	38 ± 7	>100	31 ± 7
cisplatin	5.19 ± 0.09	12 ± 2	24.8 ± 0.4	6.5 ± 0.4

Table 4.3.13. Antiproliferative activity on A549 lung, MDA-MB-231 and MCF-7 breast, and HCT-116 colorectal cancer cell lines for the novel platinum (II) and platinum (IV) compounds and cisplatin as reference compound. IC₅₀ values (μM) of compounds **cm1**, **cm2**, **cm3**, **cm1I₂**, **cm1MeI**, **cm2MeI**, **cm3MeI** and cisplatin (cis-[PtCl₂(NH₃)₂]), assessed by MTT cell viability assay. Data shown represents mean ± SD of n=3 of at least two independent experiments. Cisplatin is taken as the reference compound.

For this set of compounds, we selected **cm1MeI** and **cm1I₂** as representative of the family, and the CRC cell line HCT-116 to further evaluate the biological activity of these compounds on cancer cells. Importantly, between both compounds the only difference is one axial ligand (methyl or iodine). Thus, any differences encountered between both compounds can, in principle, be directly ascribed to the lability of the axial ligands. In this regard, we found that, after incubation with the IC₅₀ value for 72 h, the fractions of annexin⁺ and/or PI⁺ cells were significantly larger for **cm1MeI** than **cm1I₂** (**4.3.14.A**). One possible explanation could be that the higher lability of iodine as leaving group upon a nucleophilic attack by ROS scavengers can result in an easier deactivation of the Pt atom in **cm1I₂** than in **cm1MeI**. In accordance, **cm1MeI** has enhanced cytotoxic activity in all cell lines tested, except in MCF-7, in which both compounds display similar results. In

spite of that, when incubated at their IC₅₀, both compounds display a similar increase of intracellular ROS at 72 h (4.3.14.B) and a similar cell cycle arrest both in S phase and in G2/M phase (4.3.14.C).

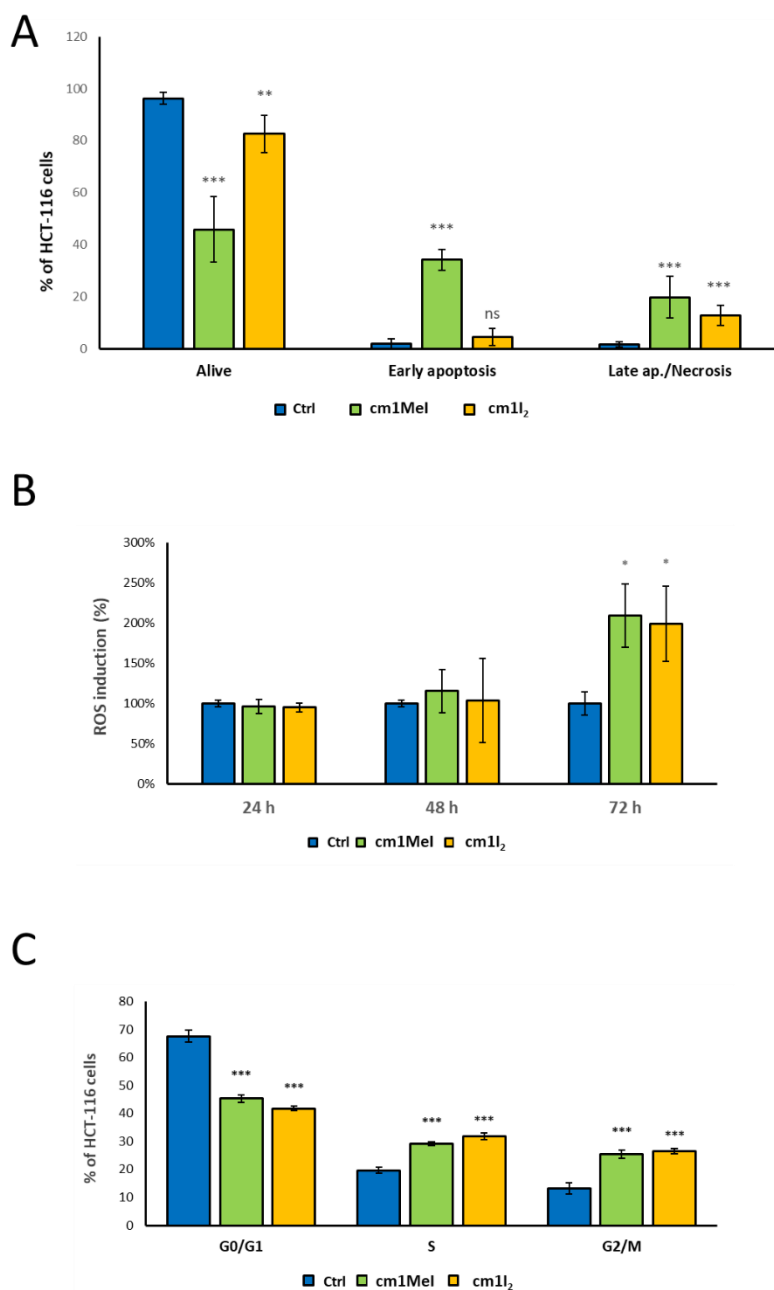


Figure 4.3.14. Effect of compounds cm1Mel and cm1I₂ on the cell cycle distribution, apoptosis and generation of reactive oxygen species (ROS) of HCT-116 colorectal cancer cells. (A) Percentage variations of alive, early apoptotic and late apoptotic/necrotic cell populations at 72 h incubation with compounds cm1Mel and cm1I₂ at their IC₅₀ concentration in HCT-116 cells. Cells were stained with propidium iodide (PI) and FITC-annexin and were analyzed by flow cytometry. (B) ROS levels after 24, 48 or 72 h incubation with compounds cm1Mel and cm1I₂ at their IC₅₀ concentration in the HCT-116 colorectal cancer cell line. Cells were stained with 2',7'-dichlorofluorescein diacetate. (C) Cell cycle phase distribution at 72 h incubation with compounds cm1Mel and cm1I₂ at their IC₅₀ concentration in HCT-

116 cells. Cells were stained with PI and their DNA content was analyzed by flow cytometry. Bars represent mean \pm SD of $n=3$. Significant differences relative to HCT-116 control cells were evaluated by Student t-test and are indicated at $p < 0.05$ (*), $p < 0.01$ (**), and $p < 0.001$ (***)

Given the promising cytotoxic activity of **cm1Mel** and **cm1I₂**, we decided to also explore their ability to selectively impair cancer cell proliferation. For this, we compared their cytotoxic effect at selected concentrations with the effected on healthy fibroblast cell line BJ. Our results indicate that **cm1I₂** (4.3.15.B) is selective for cancer cells against all evaluated the tumor models, whereas **cm1Mel** (4.3.15.A) is only selective against HCT-116 and MDA-mb-231. However, it is remarkable that at 5 μM of **cm1Mel** concentration we have a complete inhibition of MDA-mb-231 and HCT-116 proliferation with no significant effect on the healthy control. Instead, **cm1I₂** shows a slight decrease ($\sim 20\%$) in BJ proliferation for all the concentrations tested.

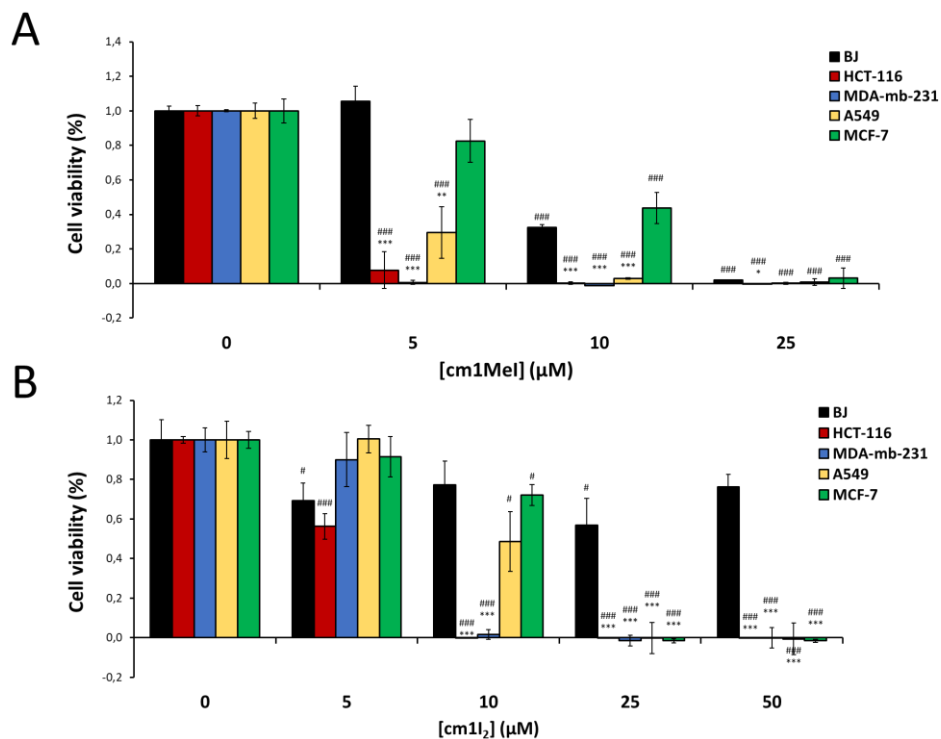


Figure 4.3.15. Selectivity of compounds cm1Mel and cm1I₂ for cancer cells. Normalized cell viability after 72 h incubation with 0, 5, 10, 25 or 50 μM of cm1Mel (A) or cm1I₂ (B) in BJ healthy foreskin fibroblasts, HCT-116 colorectal cancer, MDA-mb-231 and MCF-7 breast cancer, and A549 lung adenocarcinoma cells determined by MTT antiproliferative assay. Bars represent mean \pm SD of $n=3$. Significant differences between a given compound concentration relative to the respective untreated control cells were evaluated by Student t-test and are indicated at $p < 0.05$ (#), $p < 0.01$ (##), and $p < 0.001$ (###). Significant differences in response to the same dose between cancer cells (HCT-116, MDA-mb-231, MCF-7, A549) and BJ cells (healthy control) at each dose were evaluated by Student t-

test and are indicated at $p < 0.05$ (*), $p < 0.01$ (**), and $p < 0.001$ (***). Absence of the specified symbols denotes absence of statistical significance.

Finally, two more sets of Pd(II) cyclometallated compounds containing nitro ligands and ester/methyl-ester ligands, with eight members in each family, were also screened and found to display lower antiproliferative activities than the ones presented in **this Chapter**, which discouraged any further biological evaluation. The results of the screening of these sixteen additional compounds are presented in **Appendix 2**.

As a general conclusion, in **this Section** we have characterized a set of Pt(II) and Pt(IV) compounds with para-tolyl ligands containing either tridentate [C,N,N'] ligands, similar to the ones in **Sections 4.3.2.1** and **4.3.2.2**, as opposed to bidentate [C,N] ligands. We unveiled that Pt(IV) compounds that belong to the **cm1** series, with a tridentate structure, displayed enhanced cytotoxicity than the Pt(IV) compounds of the other two series of this set, **cm2** and **cm3**. On the contrary, the parental Pt(II) structures **cm1** and **cm2** displayed similar results. Indeed, this observation validates our hypothesis of the previous sections that the tridentate [C,N,N'] structure plays a crucial role in the cytotoxicity of the studied compounds, and that it may act through molecular mechanisms that are distinct to the ones of conventional platinum compounds. However, the similarity between Pt(II) precursors **cm1** and **cm2** also indicates that both the cyclometallated structure and the oxidation state of the Pt atom are necessary to explain the enhanced cytotoxicity of the lead compounds of each series. Also, the distinct mechanisms of action that arise from the combination of these two features, allow cyclometallated compounds to completely circumvent acquired multiplatinum resistance in prostate and colorectal metastatic tumors.

Indeed, Pt(IV) is emerging as a trend in platinum-based drug design and as an encouraging alternative to conventional Pt(II) [287], since other authors have also recently reported enhanced anticancer activity of different Pt(IV) structures relative to their Pt(II) precursor structures [444–446]. Our results in **this Chapter** encourage further development of these compounds as a novel class of platinum chemotherapeutic agents, either as second-line chemotherapeutic options after the appearance of platinum resistance, or even as first-line substitutes to conventional platinum compounds.

4.4. Chapter 4: Effect of macromolecular crowding on the kinetics of lactate dehydrogenase (LDH)

4.4.1. Introduction

The interior of living cells is a highly occupied space, where the total concentration of macromolecules ranges from 200 to 400 g L⁻¹ [308]. However, determinations involving enzyme kinetics and activities are commonly performed in protein extracts typically around 1-10 g L⁻¹, including the ones performed in **Chapters 1** and **2** of this work.

Consistent with this idea of a high-volume occupancy inside the cell, *in vitro* metabolic readouts will significantly differ from the ones that would be obtained within the cellular environment. First, diffusion coefficients of any solute moving through the intracellular environment will be altered due to macromolecular crowding, either being reduced or presenting anomalous diffusion at short times [303,447–449]. Indeed, mTORC regulation of ribosome synthesis has been recently postulated as crucial for modulating *in vivo* diffusion coefficients [315], which, due to the prominent oncogenic role of AKT/mTOR signaling, alterations in diffusion could be essential for cancer metabolism.

Besides hindering diffusion, macromolecular crowding has also been extensively reported to affect biochemical reactions, by altering the structure of enzymes in terms of protein folding, self-association or protein-protein interactions [300,304,450–452], which in turn will alter enzymatic activity. Therefore, in order to achieve a better predictive capacity through *in vitro* experiments of enzyme activity, the effect of macromolecular crowding on the *in vivo* function of enzymes should be mimicked. In this regard, an important number of works have studied how enzyme kinetics is affected by crowded environments [305,313,453–455].

An optimal approach for this sort of studies would certainly be using concentrated cell extracts. However, the experimental data collection and interpretation would be challenging due to the high heterogeneity in cell extract geometrical and physical properties. Indeed, as postulated recently by Rivas and coworkers, it is expected that

the discrepancies encountered between *in vitro* and *in vivo* account for additional phenomena besides macromolecular crowding [308]. Thus, the implications and consequences of crowding need to be understood in depth first, before addressing further complexity. Therefore, the majority of experimental studies on macromolecular crowding effect currently use purified globular and inert macromolecules as crowding agents.

In recent years, the effects of crowding on enzyme catalysis have been explored by different works, outstandingly reviewed by Minton and coworkers [308,456]. Most of them indicate that under Michaelis-Menten conditions in crowded media, excluded volume is a major player in modulating enzymatic behavior. Moreover, gathering many different the contributions published so far, some general trends are encountered. For instance, a slight reduction in the apparent substrate-binding affinity constant, K_m is usually reported, despite of the characteristics of the crowding agent [300,313,455,457–460]. In contrast, in crowded media experiments k_{cat} can increase in some cases [305,453,457,460], or it can also decrease [300,313,453,455].

In previous studies conducted in our group we reported the effect of crowding on the hydrolysis of N-succinyl-L-phenyl-Ala-p-nitroanilide catalyzed by alpha-chymotrypsin [310]. We encountered that the total volume fraction occupied by Dextran, but not Dextran size, triggers significant changes on the reaction rate. We obtained a v_{max} decrease and an K_m increase upon increasing Dextran concentrations. We also showed that the slower diffusion of alpha-chymotrypsin in presence of Dextran was responsible for the observed rise in K_m , whereas the decrease in v_{max} could be explained in terms of a mixed inhibition by product, enhanced by crowding. In another study performed previously in our group, we reported the effect of macromolecular crowding the oxidation of 2,2'-azino-bis(3-ethylbenzothiazoline-6-sulfonate) (ABTS) by H_2O_2 catalyzed by Horseradish Peroxidase (HRP) [461]. Our results revealed that the reaction rate was also significantly influenced by the excluded volume effect, but it was independent of the Dextran size. Both v_{max} and K_m decayed when increasing the concentration of the crowder in solution, suggesting an activation control. In other words, the catalytic constant (k_{cat}) brings a significant contribution as a result of the environmental surroundings influence. This contribution may be the consequence of one or the additive

effect of the following aspects: the rise of the ratio of the activity coefficients between the enzyme and the complex formed by enzyme and substrate as a consequence of a crowded microenvironment; the boost of water chemical activity favored by a dense solution; or the conformational change of the enzyme active site induced by crowding.

Here, we studied how the crowding by Dextrans at several concentrations and sizes affects the catalytic reaction of lactate dehydrogenase (LDH), a crucial player of the Warburg effect in cancer cells and, unlike our two previous case studies, an oligomeric enzyme. Besides that, we also chose this enzymatic reaction as a model process for other several reasons. First, it is a well-known reaction in which small substrates and products lead to the occurrence of the reaction without a significant variation in excluded volume. Second, there are no interactions between the enzyme and the Dextrans used as crowding agents. And third, the LDH size ($M_w = 140$ kDa) is intermediate between those of the selected Dextrans (from 50 to 410 kDa).

Therefore, here we illustrate how the reaction catalyzed by LDH is strongly influenced by different amounts of neutral polymers of different dimensions, mimicking the known intracellular crowding levels. Specifically, we studied the dependence of v_{max} and K_m parameters on the total volume of the solution excluded by the crowder and the individual volume occupied by each of the polymeric coils.

4.4.2. Theoretical framework

The oxidation of NADH by pyruvate catalyzed by LDH can be treated as a single substrate reaction and its kinetic study can be performed using the scheme proposed by Henri [462]:



where k_1 , k_{-1} , and k_2 are rate constants. This system can be described using Michaelis-Menten equation [462,463]:

$$v_0 = \frac{v_{max}[S]_0}{K_m + [S]_0} \quad (2)$$

where v_{\max} is the maximum velocity and K_m is the Michaelis-Menten constant. With the combination of (1) and (2) some definitions can be stated: K_m can be defined as $K_m = ((k_{-1}) + k_2) / k_1$, and for v_{\max} , $v_{\max} = k_{\text{cat}} [E]_T$, and $k_{\text{cat}} = k_2$.

Since Michaelis and Menten studies, it has been assumed that enzyme activity can be studied applying equation (2), obtaining data to fit that equation by performing measurements of the initial rate of product formation at different substrate concentrations.

4.4.3. Results and discussion

For a suitable evaluation of the influence exerted by macromolecular crowding on the kinetic parameters, one must consider at least two important features of the study. First, the reactions under investigation should be processes the kinetic behavior of which has an established and generally accepted interpretation. In our case, the reaction between NADH and pyruvate catalyzed by LDH is a well-known process following a Michaelis-Menten mechanism and it can easily be monitored by UV-spectroscopy. Second, the crowding induced effect should be accounted only by the changes incurred by the crowding polymers with regard to its dimensions and concentration. Besides, as stated above, the selected reaction is accompanied by an insignificant variation of excluded volume during the progression of the reaction, owing to the small size of NADH, pyruvate, NAD^+ and L-lactate.

We studied how the selected system presents a different kinetic response than in dilute solution when different concentrations and sizes of Dextran are added to the reaction media. An initial linear decrease followed by a plateau is observed when measuring the absorbance of NADH at 320 nm in all the studied cases (results not shown). As explained in Material and Methods, initial velocity (v_0) values were acquired by the fitting of the linear part of the absorbance-time plot for each sample.

Figure 4.4.1 shows v_0 values as a function of the substrate concentration. Each data point is obtained from the mean between 3 to 5 samples with the same reaction conditions in terms of substrates, enzyme and Dextran concentrations. Each figure, A to D, represents a given Dextran size, from the smallest to the biggest Dextran. Dextran concentration in mg/mL and excluded volume are directly proportional. A significant

dependence of v_0 on both the excluded volume and the obstacle dimension is clearly found.

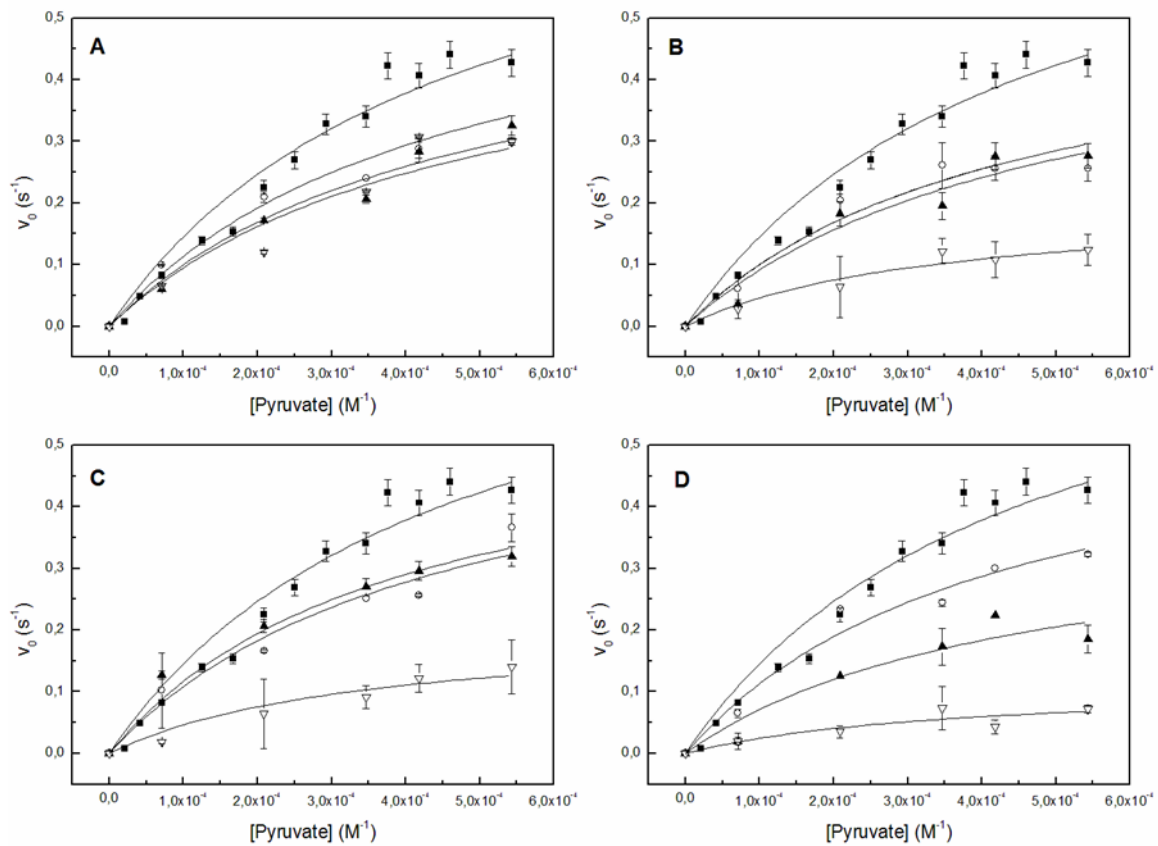


Figure 4.4.1. v_0 versus substrate concentration plot for the oxidation of NADH in presence of pyruvate catalyzed by LDH in Dextran crowded media with different Dextran sizes: (A) $M_w = 50$ kDa; (B) $M_w = 150$ kDa; (C) $M_w = 275$ kDa and (D) $M_w = 410$ kDa. In each figure, the curves corresponding to four Dextran concentrations are plotted: 0 mg/mL (solid square), 25 mg/mL (open circle), 50 mg/mL (solid up-triangle) and 100 mg/mL (open down-triangle).

Figure 4.4.2 reveals that reaction rate decreases as a function of Dextran size when high Dextran concentrations (> 50 mg/mL) are used. In this case, the process behavior depends not only on the excluded volume but also on the dimension of the obstructive particles present in the reaction media. This result is consistent with the results of Homchaudhuri et al. [459]. These authors stated that alkaline phosphatase makes the hydrolysis of p-nitrophenyl phosphate with a velocity which depends on the crowder size for a given excluded volume conditions. They showed that for samples of Dextran of about 20% (w/w) the reaction rates decrease with the increase of Dextran size: a decrease of about 2, 5 and 7-fold was observed for Dextran of 15-70, 200 and 500 kDa,

respectively. However, it is in contrast with the results showed in our previous works [310,461] and with the results of Minton et al. [447,450,456]. In all these works, only excluded volume but not obstacle size was presented as a major factor influencing enzymatic reactions occurring in reaction media crowded by macromolecules.

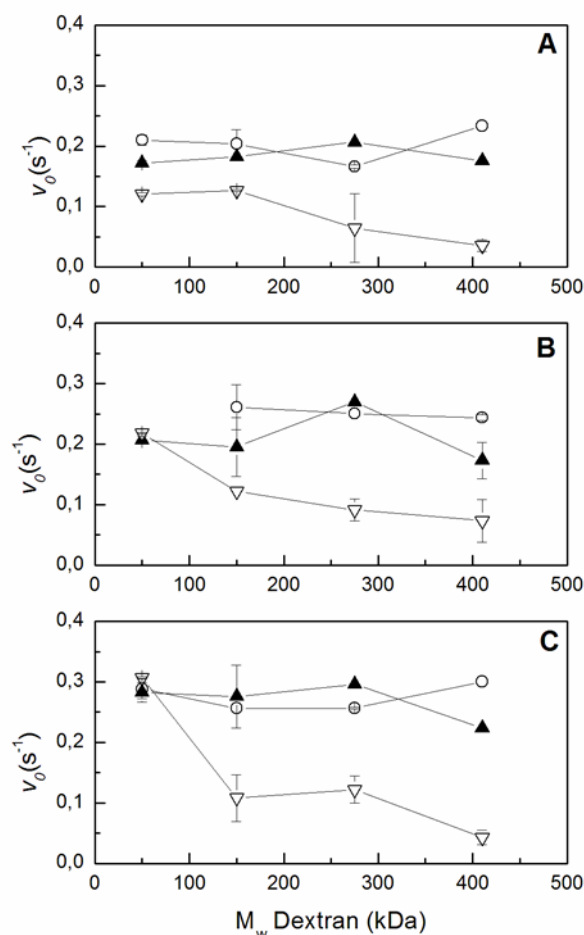


Figure 4.4.2. Example of v_0 variation with Dextran size and concentration for the oxidation of NADH in presence of pyruvate catalyzed by LDH for three fixed substrate concentrations: 0.22 mM (A), 0.34 mM (B) and 0.40 mM (C). In each figure, three Dextran concentrations are plotted: 25 mg/mL (open circle), 50 mg/mL (solid up-triangle) and 100 mg/mL (open down-triangle).

The major difference between the studies is the relative dimension of the protein in respect to the obstacle. It has to be acknowledged that the size of alkaline phosphatase (105 kDa) is comparable with that of LDH (140 kDa). As such, the rate of the reactions they catalyze has similar behavior in crowded media unlike the rate of the other investigated processes catalyzed by much smaller proteins: alpha-chymotrypsin (25 kDa) and HRP (42 kDa). As revealed by Homchaudhuri et al. [459], occasioned by the big size of the protein, large crowding agents make enzyme and substrates to come across less

often. However, this effect is partially offset when using small obstacles and the decrease is less significant, due to a certain caging effect that causes an enhanced enzymatic activity. Our results underline the fact that the degree of crowding effect relies both on the size and concentration of the obstructive particles. In spite of that, the relative size of the enzyme in respect to the crowder seems to exert a significant influence when larger molecules are present in the system.

The values of Michaelis Menten constants, K_m and v_{max} , were estimated by fitting Eq. 2 to each data set in Figure 4.4.1, in order to get information about how the excluded volume could affect the oxidation of NADH by LDH in crowded media. Figures 4.4.3 and 4.4.4 show how K_m and v_{max} are dependent on the amount of volume excluded by macromolecular inert obstacles. In fact, we can perceive that only high concentrations and large sizes of Dextran affect both v_{max} and K_m values, whereas for smaller sizes of Dextran, the enzymatic system behaves in a similar way to our previous studies with α -Chymotrypsin [310].

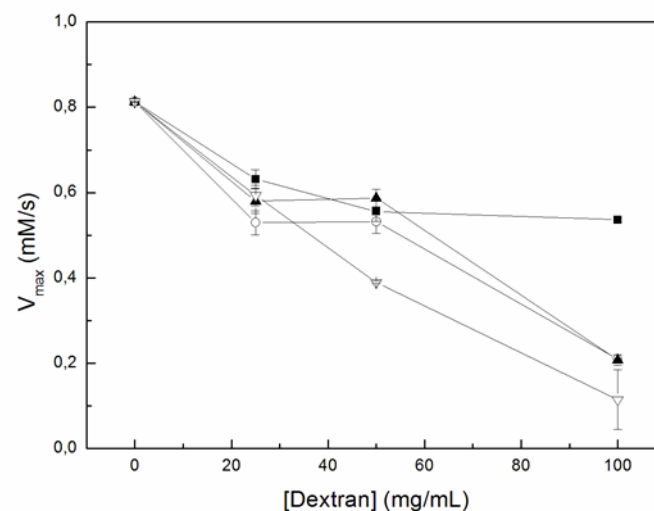


Figure 4.4.3. Variation of v_{max} values with Dextran size and concentration for the oxidation of NADH in presence of pyruvate catalyzed by LDH. The four Dextran sizes used are plotted: D50 (solid square), D150 (open circle), D275 (solid up-triangle) and D410 (open down-triangle).

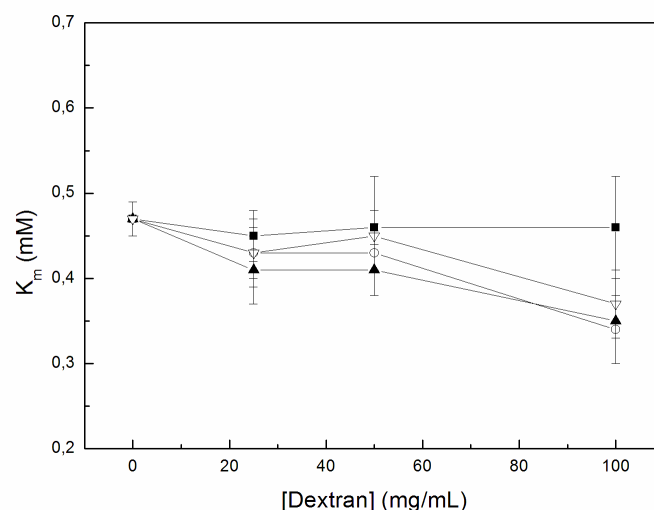


Figure 4.4.4. Variation of K_m values with Dextran size and concentration for the oxidation of NADH in presence of pyruvate catalyzed by LDH. The four Dextran sizes used are plotted: D50 (solid square), D150 (open circle), D275 (solid up-triangle) and D410 (open down-triangle).

Firstly, examining v_{max} values we see (Figure 4.4.3 and Table 4.4.5) that they diminish with the increase of size and concentration of Dextran. In the Figure it is shown that the value of v_{max} in presence of D50, which size is lower than LDH, decreases slightly with respect to the value in diluted solution, but it is independent of the concentration of D50. Moreover, the presence of low concentrations (25 and 50 mg/mL) of D150 and D410, whose sizes are, respectively, equal and two times the LDH size, affects the value of v_{max} in the same sense, i.e. its value decays slightly with respect to the value in diluted solution, but it is independent of the concentration. However, high concentration of both Dextrans, D150 and D275, decreases hugely the value of v_{max} . In the same direction but even enhanced, the presence of a high concentration of D410, which size is three times the LDH size, causes biggest decreases of v_{max} .

	Concentration (mg/mL)	v_{max} (mM/s)	K_m (mM)	v_{max}/K_m (s ⁻¹)	r^2
Diluted Solution	-	0.81 ± 0.01	0.47 ± 0.01	1.7 ± 0.1	0.9825
D50	25	0.63 ± 0.02	0.45 ± 0.01	1.4 ± 0.1	0.9893
	50	0.57 ± 0.02	0.46 ± 0.01	1.2 ± 0.1	0.9758
	100	0.54 ± 0.05	0.46 ± 0.01	1.2 ± 0.1	0.9733

D150	25	0.53 ± 0.03	0.43 ± 0.01	1.2 ± 0.1	0.9879
	50	0.53 ± 0.03	0.43 ± 0.01	1.2 ± 0.1	0.9820
	100	0.21 ± 0.01	0.34 ± 0.01	0.6 ± 0.1	0.9918
D275	25	0.58 ± 0.03	0.41 ± 0.01	1.4 ± 0.1	0.9865
	50	0.59 ± 0.02	0.41 ± 0.01	1.4 ± 0.1	0.9846
	100	0.21 ± 0.01	0.35 ± 0.01	0.6 ± 0.1	0.9965
D410	25	0.59 ± 0.02	0.43 ± 0.01	1.4 ± 0.1	0.9925
	50	0.39 ± 0.03	0.43 ± 0.01	0.9 ± 0.1	0.9855
	100	0.11 ± 0.07	0.37 ± 0.01	0.3 ± 0.1	0.9970

Table 4.4.5. Obtained kinetic parameters for the kinetics of LDH under crowded media

As stated previously, v_{\max} is defined as $v_{\max}=k_{\text{cat}}[E]_T$, with $k_{\text{cat}}=k_2$. Therefore, its decrease with high concentration or large size of Dextrans could be due to two main reasons: the variation of the effective enzyme concentration or the deviation of the catalytic rate constant (k_{cat}). On the one hand, the excluded volume in crowded media is responsible for an increase of the effective enzyme concentration [300,447,456]. In fact, an increase of v_{\max} in crowding situations is usually explained as a result of a raise in the effective enzyme concentration [305,457,460]. On the other hand, when a decrease in v_{\max} is found in crowding situations, it is normally explained by the reduction of k_{cat} as a result of conformational changes of the catalytic center of the protein derived from surrounding variations induced by the crowded media [305,313,455,464]. In our case, it is reasonable to assume that k_{cat} would be unaffected by the presence of Dextran. Since the catalytic site is protected from the bulk solution, Dextran cannot denaturize or somehow alter the inner cavities of the protein in contrast with other molecules [301,305,313,455,457,464]. In fact, in this particular case we should also consider the comparable size between LDH and the obstacles to understand the decrease of v_{\max} in crowded media. In presence of large obstacles, the comparable size between both, LDH and Dextrans, causes a reduction of the encounters between enzyme and substrates. On the contrary, a minor decrease in the v_{\max} value is found in presence of small obstacles because the crowding effect is partially compensated by the improvement of

enzymatic activity that a certain cage effect can induce. In our opinion, only this situation could explain our results.

Secondly, we analyzed the K_m behavior. As it is shown in Figure 4.4.4 and Table 4.4.5, only a high concentration of large Dextran, 100 mg/mL of D150, D275 or D410, decays the K_m value. As was explained in Materials and Methods section, the Michaelis-Menten constant is defined by $K_m=(k_{(-1)}+k_2)/k_1$ following the general chemical equation for enzymatic processes presented in Eq. 1.

In a situation of diffusion control, an increase in K_m value can be expected since the bimolecular constant (k_1) will decrease with crowding [465,466]. In the literature, there are few works that report this situation [310,465–467]. In these reported cases, a high diffusion resistance in the sample is responsible of a K_m increase with Dextran concentration. However, most of the enzymatic reaction studies in crowding situations showed a slight decrease in K_m compared to that of the dilute solution. These studies excluded a diffusion control of the enzymatic process and the modification of k_1 by the presence of crowding agents (e.g. [460]). A variation in k_{cat} with crowding is usually found in the cases where a K_m decrease is reported. The K_m constant is sensitive to the sample composition since it depends on the substrate activity coefficient. Therefore, a decrease in K_m with crowding is usually attributed to several factors. On the one hand, due to non-ideal conditions of the crowded solution, chemical activity of the substrate is modified. On the other hand, there is an increase of the activity coefficients relation between the free enzyme and the complex formed by enzyme and substrate [313,455]. Moreover, substrate binding event is depending on water activity, because both the substrate and the active site must be dehydrated for the binding to occur. Therefore, k_2 value may be affected. In our opinion, as it was explained in detail in our previous work [310], both hindered diffusion and alterations in the active site must be considered to better understand the results. In fact, the behavior showed in this study by K_m at high concentration of large Dextrans is in agreement with these previous studies. In this case, at high concentration of large Dextrans, the decrease of both constants, v_{max} and K_m , are in agreement with a decrease in the k_2 value, which depends on the amount of encounters between enzyme and substrates. The existence of a high quantity of large Dextrans reduces the number of these encounters and consequently the constant value.

In addition, if we compute the v_{\max}/K_m ratio (Table 4.4.5), we observe a decrease in its value at high concentration of large Dextran, which could indicate some possible effect of inhibition. Excess-substrate inhibition of rabbit muscle LDH is well documented for the case of pyruvate [468,469]. However, we observe a slight and constant decrease of the value of the v_{\max}/K_m ratio with respect to the case of diluted solution until the excluded volume achieves some limit value. This behavior suggests that the possible substrate inhibition reported in the earlier literature does not explain the obtained values. Recent simulation and experimental studies reported on diffusion processes of enzymes in crowded media [303,470] show that the effective diffusion coefficient is higher in dilute samples than in crowding situations. A decrease in the diffusion coefficient may imply a decrease in the bimolecular constant (k_1) with crowding [465,466]. In a situation where the enzymatic reaction depends on the diffusion, the K_m value should increase because of the decrease of k_1 . However, we find that K_m remains constant until high concentration of large Dextran. On the other hand, our results show that k_2 decreases with crowding, which is in agreement with an activation control. Thus, a mixed activation-diffusion control could explain the rough decreases of the experimental fitted values of v_{\max} and K_m for high Dextran sizes and concentrations. In particular, the decrease v_{\max} is produced by the decrease of k_2 with size and concentration of Dextran. The quasi-constant value of K_m can be seen as a result of the combined effect of the decreasing of the diffusion-controlled constant k_1 , with size and concentration of Dextran and the decreasing of k_2 . This concordance breaks for high concentration of large Dextran when K_m is not constant anymore.

In conclusion, our results reveal, on the one hand, that the initial velocity of the reaction depends on both the size and amount of Dextran present in the media. In addition, and in contrast with previous reported works, we have found that the enzyme relative size respect to the crowding molecules represents another important factor influencing the velocity of the reactions occurring in crowded media. When enzymes are small the reaction rate mainly relies on the excluded volume of the solution. However, for large enzymes (in our case LDH) the reaction rate is also influenced by the size of obstacles present in the reaction environment. On the other hand, we obtained a decrease in both Michaelis-Menten constants, v_{\max} and K_m , with the amount of crowding agent in the

sample, but this decrease is only significant in the case of samples with high concentrations of large Dextran. The decrease in v_{max} also depends on the size of Dextran present in the media. This result is attributable to the activation control of the enzymatic process, but it must be taken into account the fact that as a result of the relative large size of LDH, large obstacles reduce the encounters among enzymes and substrates. However, an activation control of the LDH reaction is against the decay found in K_m only in cases with high concentration of large Dextran. This decrease can be explained by a mixed activation-diffusion control of this enzymatic process in crowding media produced by Dextran. Only a mixed control can explain the behavior found in both Michaelis-Menten constants, and probably it is due to the relative large size of the LDH and the difference between the enzyme and the crowding agent size. In our opinion, the enzyme relative size with respect to the crowding agent represents a significant factor to be considered in enzymatic reaction studies carried out in macromolecular crowded media.

4.5. Chapter 5: Effect of macromolecular crowding on the kinetics of glutamate dehydrogenase (GLDH)

4.5.1. Introduction

After having studied the impact of macromolecular crowding on the kinetics of LDH, as a determinant kinetic step in the Warburg phenotype of cancer cells, we next assessed the impact of crowding on the glutaminolytic pathway, which is also a major source of carbon and energy for cancer cells through TCA cycle anaplerosis, and identified as a phenotype-defining pathway in the metastatic cell models studied in **Chapter 1** and **Chapter 2**.

4.5.1.1. Glutaminolysis

Glutaminolysis, as described throughout the introductory section of this work, is comprised by two sequential reactions that convert glutamine into α -ketoglutarate. The first, conversion of glutamine into glutamate, can be performed by three different enzymes (KGA, GAC or LGA) termed generally as glutaminase, which are encoded by two different genes (GLS1 and GLS2). Next, glutamate is converted into α -ketoglutarate by glutamate dehydrogenase (GLDH) and it can then enter the TCA cycle (**4.5.1**).

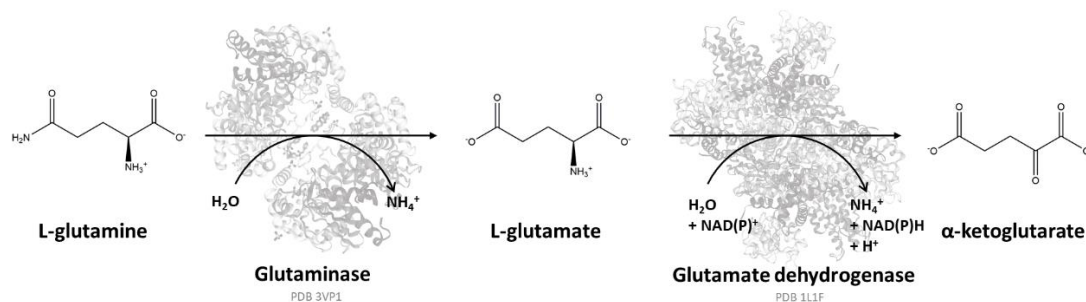


Figure 4.5.1. Schematic representation of glutaminolysis. L-glutamine is converted into L-glutamate by glutaminase (PDB structure: 3VP1) and L-glutamate is converted into α -ketoglutarate in an NAD(P)⁺-dependent manner by glutamate dehydrogenase (PDB structure: 1L1F). Both deamination reactions require H₂O and also yield ammonia.

Throughout **Chapter 1** and **Chapter 2** of this work, we have identified that glutaminase protein expression levels in cancer cells are extremely sensitive to different

perturbations, such as amino acid starvation (e.g. arginine), acquisition of platinum resistance or cell aging, whereas the protein expression levels of GLDH remained largely unaltered. We selected GLDH as a model for study since, to our understanding, unlike glutaminase, it truly represents the flux through TCA cycle anaplerosis, whereas the previous step can be directed to other biosynthetic purposes such as glutathione, proline synthesis or urea cycle anaplerosis.

Moreover, different classical kinetic studies established a marked negative cooperative behavior in GLDH kinetics and that its activity can be fine-tuned by a wide variety of allosteric effectors [471], as summarized in Table 4.5.2. In particular, GLDH is activated by ADP and inhibited by GTP or ATP, denoting a capacity to sense and respond to the mitochondrial energy status. In line with this, it is also inhibited by the presence of palmitoyl-CoA and other fatty acid-CoA esters, implying that the utilization of glutamine as a carbon and energy source for the TCA cycle is inhibited at the GLDH step when cells can oxidize fatty acids instead [471]. Collectively, all these regulation mechanisms support the notion that GLDH could be the limiting step of glutaminolytic TCA cycle anaplerosis in the mitochondria.

ALLOSTERIC ACTIVATORS	Adenosine diphosphate (ADP) Leucine Monocarboxylic acids
ALLOSTERIC INHIBITORS	Guanosine-5'-triphosphate (GTP) NADH Adenosine triphosphate (ATP) Steroid hormones such as diethylbestrol (DES) Hydrophobic compounds such as Palmitoyl CoA Zn ²⁺
NEGATIVE COOPERATIVITY	Coenzyme (NAD(P) ⁺)
SUBSTRATE INHIBITION	Glutamate (high pH) α -Ketoglutarate (low pH)

Table 4.5.2. Summary of glutamate dehydrogenase allosteric regulation. Adapted from Smith, T.J. and Stanley, C.A. *Trends. Biochem. Sci.* 2008 33: 557-564 [471].

Thus, in **this Chapter**, we hypothesized that the overall rate of glutaminolysis, determined by the GLDH reaction, could be heavily influenced by macromolecular crowding, as it occurs entirely inside the mitochondrial matrix, which is the intracellular

microenvironment with highest volume occupancies (up to 500 g/L) [472]. Bearing this in mind, we have performed a thorough study of the kinetic behavior of GLDH in absence and presence of macromolecular crowding mimicked by dextrans of different sizes and at different concentrations.

Importantly, another important reason for choosing GLDH as a model for study in crowded media experiments is that, to our knowledge, the impact of macromolecular crowding on the cooperative behavior of oligomeric enzymes has not yet been addressed.

4.5.1.2. Glutamate dehydrogenase

GLDH is an homohexameric enzyme found in all living organisms that catalyzes the reversible oxidative deamination of glutamate to α -ketoglutarate by converting NAD^+ or NADP^+ (with nearly equal affinity in mammals [473]) to their corresponding reduced forms, NADH and NADPH. Importantly, product inhibition of GLDH by NADH has been reported previously [471]. Under physiological conditions in mammals, the GLDH reaction is expected to occur only in the oxidative deamination direction, due to the high K_M for ammonia. However, a recent work by Spinelli et al. has postulated that the high ammonia concentrations found in cancer cells could force the reverse reaction [142].

The GLDH homohexamer is assembled as a dimer of trimmers stacked directly on top of each other (**4.5.3**). Each subunit is composed of at least three domains: the bottom domain that makes extensive contacts with a subunit from the other trimer, the NAD-binding domain which is on top of the bottom domain and the antenna which rises above the NAD-binding domain and lies immediately behind the adjacent, counter-clockwise neighbor [471].

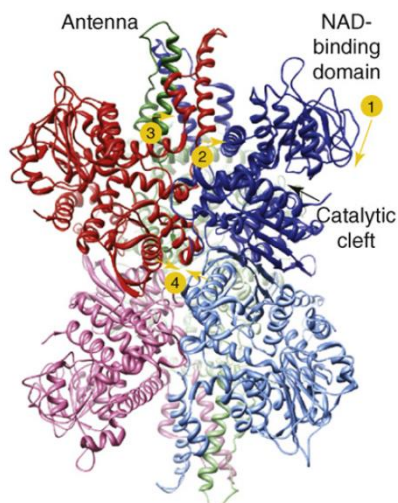


Figure 4.5.3. Glutamate dehydrogenase structure. Schematic representation of the six identical monomers of GLDH (shown in different colors). The NAD-binding domain (1), the catalytic cleft (2), the antenna (3) and the trimmer-trimmer interaction loop (4) are highlighted. Adapted from *Smith, T.J. and Stanley, C.A. Trends. Biochem. Sci. 2008 33: 557-564.*

Substrate binds in the depths of the cleft between the NAD-binding domain and the bottom domain. Coenzyme binds on the NAD-binding domain and it closes down upon the substrate and coenzyme. As the catalytic site closes, the base of each antenna rotates out in a counter-clockwise manner, pushing away the pivot helix of the adjacent subunit. The three pairs of subunits move rigid towards each other, compressing the cavity at the core of the hexamer [474].

Unlike bacterial GLDH, only regulated at a transcriptional level, mammalian GLDH presents a rich variety of allosteric regulation, as described earlier in this section. The structural basis for such mechanisms lies in the antenna-like domain, only found in the allosteric regulated forms of GLDH [471].

On the other hand, the possible roles for negative cooperativity of GLDH are not completely understood, even if the main consequence of negative cooperativity is that enzymes displaying it become significantly less sensitive to fluctuations in substrate concentration [475]. This could be relevant in the case of GLDH, since decreasing its dependence on $\text{NAD}^+/\text{NADP}^+$ pools could magnify GLDH sensitivity to the energy status (ATP/ADP ratio), mitochondrial pH, or to the availability of fatty acyl-CoA esters (see Table 4.5.2).

4.5.1.3. Negative cooperativity of GLDH

Glutamate dehydrogenase exhibits an unusual kinetic behavior with an unclear physiological role, negative cooperativity. This phenomenon was first reported for this enzyme in 1969 [476], in a study in which deviation from Michaelis-Menten behavior was detected when varying NAD^+ and NADP^+ concentrations.

Negative cooperativity in GLDH is caused by coenzyme-induced conformational changes and requires a dicarboxylic acid substrate or an analog with a 2-position substituent [473]. With alternative amino acidic substrates, such as norvaline, cooperative interactions are absent [476].

Over the years some studies have explained negative cooperativity in GLDH with a compulsory order mechanism, two different mechanisms depending on pH. However, some mathematical inconsistencies detected in 1970 [477] provided clear proof that the enzyme does not follow a compulsory mechanism. Independent evidence [478] for a random-order mechanism obtained by studying isotope exchange at equilibrium was also found. Although alternative models have been proposed [479], a model to explain the negative cooperativity in GLDH is still not found.

The unusual kinetic behavior exhibited by glutamate dehydrogenase has been attributed to the interactions between its six sites (or subunits) and also by different conformational transitions. The presence of cooperativity caused by interactions within the sites was demonstrated by the ideal kinetic behavior presented by a bacterial form of the enzyme when performing experiments deactivating five of the six subunits [480]^[34]. By mutating tryptophan and phenylalanine residues at the trimer-trimer interface results suggest that conformational transitions between different active sites mediate the cooperative behavior [481].

4.5.2. Theoretical framework

The behavior of an oligomeric enzyme, with s sites, can be described by the following reaction scheme:



where $-E$ represents the free binding sites, S is the substrate and $-ES$ are the occupied sites. K_c is the mean effective association function of the substrate at each different value of substrate concentration, $[S]$, and can be expressed as [482]:

$$K_c([S]) = \frac{[E-S]}{[E-][S]} = \frac{1}{[S]} \cdot \left(\frac{\theta}{1-\theta} \right) = \frac{1}{[S]} \cdot \left(\frac{\nu}{s-\nu} \right) \quad (2)$$

ν is the average number of occupied sites, and it is related to the fractional occupancy of the sites, θ , as:

$$\nu = s \cdot \theta \quad (3)$$

The fractional occupancy can be experimentally approximated as a ratio between the initial and maximum velocities of the reaction (2) and, therefore, the average number of occupied sites also depends on that ratio:

$$\theta \equiv \frac{v_0}{v_{max}} ; \nu \equiv s \cdot \frac{v_0}{v_{max}} \quad (4)$$

where v_0 is the initial rate and v_{max} is the maximum velocity.

With this kinetics parameters, the mean effective association function (2) can also be written as:

$$K_c(S) = \frac{1}{[S]} \cdot \left(\frac{v_0}{v_{max}-v_0} \right) \quad (5)$$

In terms of the macroscopic or stoichiometric association constants (K_i), the average number of occupied sites can be written in terms of the Adair's equation [483]:

$$\nu(S) = \frac{\sum_{j=1}^s j \cdot b_j \cdot [S]^j}{\sum_{i=0}^s b_i \cdot [S]^i} ; b_j \equiv \prod_{i=1}^j K_i ; b_0 = 1 \quad (6)$$

Where j represents the number of catalytic centres ($j=1, \dots, s$) and b_j parameters are the products of the macroscopic association constants (K_i).

The Adair equation can also be expressed in terms of the binding polynomial, $\Xi(S)$, which is the macrocanonical partition function of the sites, $\Xi(S) = \sum_{j=0}^s b_j [S]^j$ [484,485]. Then

$$\nu(S) = \frac{\partial \ln \Xi(S)}{\partial (S)} \Rightarrow \nu(S) = \langle j \rangle = \sum_{j=0}^s p_j j \quad (7)$$

where, p_j , are the probability of have j sites occupied, $p_j(S) = b_j[S]^j/\Xi(S) \in(0,1)$. With this interpretation, the coefficients of the binding polynomial can be seen as the canonical partition function of the macrostates with j occupied sites.

It is important to define the intrinsic constants and its relation with the macroscopic ones. An intrinsic constant, K_j^{int} , is an effective association constant that represents the average binding properties of a site when $(j-1)$ sites have already been occupied, independently of the statistical factor of choosing a specific free site between the total of $(s-j)$ free sites. The relationship between macroscopic or stoichiometric and the intrinsic constants are given elsewhere [485,486]:

$$K_j = \binom{s-j+1}{j} \cdot K_j^{int} \quad (8)$$

4.5.2.1. Non-cooperative behavior

The non-cooperative or ideal behavior corresponds to the Michaelis-Menten [463] model. It is important to describe this model because it is commonly used to characterize kinetic behaviors, even when they are cooperative.

First, the model involves an enzyme (E) which is combined with the substrate (S) in a first and reversible step to form the enzyme-substrate complex (ES). The dissociation of this complex yields to the product (P) and the recovery of the enzyme. This can be schematized as:



Where k_f and k_b are the rate constants of formation (forward) and decomposition (backward) of the complex, respectively, and k_{cat} is the rate constant for product formation (catalytic). By assuming that product formation is an irreversible step and supposing the stationary state conditions, *i.e.* assuming constant value for the complex concentration, which holds for cases of excess substrate concentration (constant) over enzyme concentration, the Michaelis-Menten equation for the initial rate (v_0) can be written down as [463]:

$$v_0 = \frac{v_{max} \cdot [S]}{K_M + [S]} \quad (10)$$

where v_{max} is the maximum velocity and can be expressed as:

$$v_{max} = \lim_{[S] \rightarrow \infty} v_0 = k_{cat} \cdot [E] \quad (11)$$

and K_m is the pseudo-dissociation constant for the complex, which is named as Michaelis constant, and can be related to the enzyme affinity for the substrate:

$$K_M \equiv \frac{[E][S]}{[ES]} = \frac{k_{cat} + k_b}{k_f} \quad (12)$$

The Michaelis-Menten equation gives a sigmoidal behavior, typical for non-ideal behavior or non-cooperativity behavior (4.5.4).

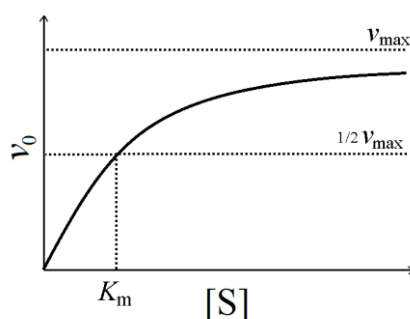


Figure 4.5.4. Plot of the Michaelis-Menten equation as the variation of the initial rate with substrate concentration.

The parameters v_{max} and K_M are used to describe kinetic behaviors even when they are cooperative; in that case they are used as apparent parameters (v_{max}^{app} , K_M^{app})

$$v_0 = \frac{v_{max}^{app} \cdot [S]}{K_M^{app} + [S]} \quad (13)$$

The non-cooperative case can be also described by Adair's equation (6) in which the association intrinsic constants of all the sites will be equal:

$$K_c^{id} \equiv K = K_1^{int} = \dots = K_s^{int} = K_M^{-1} \quad (14)$$

and

$$v^{id}([S]) = \frac{s \cdot K \cdot [S]}{1 + K \cdot [S]} \quad (15)$$

If the expression is rearranged in terms of the Michaelis constant, which is the inverse of an association constant, the Michaelis-Menten equation is obtained

$$v^{id}([S]) = \frac{s \cdot [S]}{K_M + [S]}; K_c^{id} \equiv K = K_M^{-1} \quad (16)$$

In general, $K_c^{id} \equiv K$, can be obtained as:

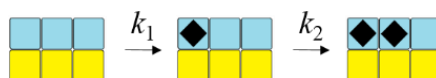
$$K_c^{id} \equiv K = \lim_{[S] \rightarrow 0} K_c = K_1^{int} = \frac{K_1}{s} \quad (17)$$

4.5.2.2. Negative cooperativity model for hexameric enzymes

One of the objectives of this study was to properly define the cooperative behavior of GLDH by proposing a model that fits the experimental data and allow some interpretation of its functioning. To this end and owing to the background of the group [37], some microscopic models compatible with the Adair's equation (see section 3.1) were proposed and are outlined.

The $\{b_j\}$ parameters of Adair's equation in the proposed models depend on other microscopic parameters, in which are included microscopic association constants, $\{k_j\}$, and the interaction between trimmers. Four types of models have been proposed varying the number and type of these parameters, they can be schematized as:

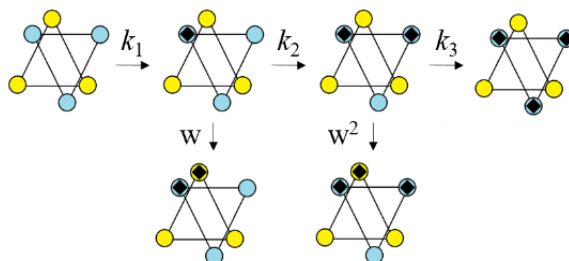
Two parameters (k_1, k_2)



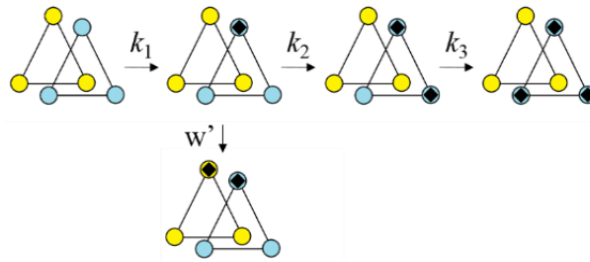
Three parameters (k_1, k_2, k_3)



Four parameters (k_1, k_2, k_3, w), with an alternated conformation of the two trimmers



Four parameters (k_1, k_2, k_3, w') with an eclipsed conformation of the two trimmers



The terms of the interaction between trimmers (w and w') are Boltzmann's factors associated to the free energy of interactions:

$$w = e^{-E_{int}/k_B T} ; w' = e^{-E'_{int}/k_B T} \tag{18}$$

Where E_{int} is the energy associated with the interaction, k_B is Boltzmann constant and T is temperature.

In table 4.5.5, the relationship between $\{b_j\}$ parameters and the microscopic association constants $\{k_j\}$ is presented for the four different models, obtained from mechanical statistics development in the microcanonical collective.

b_i	Config.	Statistical weight	Relationship of microscopic parameters			
			2 parameters (k_1, k_2)	3 parameters (k_1, k_2, k_3)	4 parameters (k_1, k_2, k_3, w)	4 parameters (k_1, k_2, k_3, w')
0		1	1	1	1	1
1		6	$6k_1$	$6k_1$	$6k_1$	$6k_1$
2		9	$9k_1^2 + 6k_1k_2$	$9k_1^2 + 6k_1k_2$	$3k_1^2 + 6k_1^2w + 6k_1k_2$	$6k_1^2 + 3k_1w' + 6k_1k_2$
		6				
3		18	$18k_1^2k_2 + 2k_1k_2^2$	$18k_1^2k_2 + 2k_1^2k_3$	$12k_1^2k_2w + 6k_1^2k_2w^2 + 2k_1^2k_3$	$12k_1^2k_2w' + 6k_1^2k_2 + 2k_1^2k_3$
		2				
4		9	$9k_1^2k_2^2 + 6k_1k_2^3$	$9k_1^2k_2^2 + 6k_1^2k_2k_3$	$3k_1^2k_2^2w^2 + 6k_1^2k_2^2w^3 + 6k_1^2k_2k_3w^2$	$3k_1^2k_2^2w' + 6k_1^2k_2^2w'^2 + 6k_1^2k_2k_3w'$
		6				
5		6	$6k_1k_2^4$	$6k_1^2k_2^2k_3$	$6k_1^2k_2^2k_3w^4$	$6k_1^2k_2^2k_3w'^2$


6		1	k_2^6	$k_1^2 k_2^2 k_3^2$	$k_1^2 k_2^2 k_3^2 w^6$	$k_1^2 k_2^2 k_3^2 w'^3$
---	---	---	---------	---------------------	-------------------------	--------------------------

Table 4.5.5. Relationship of microscopic parameters for each b_i parameter and schematic representation of substrate binding on the possible configurations

It should be noticed that for each configuration there is a product of microscopic association parameters $\{k_j\}$, and the resulting b_i parameter is the sum of the products for all the possible configurations.

These b_i parameters are introduced in Adair's equation to obtain the final fitting equation for each model. The data was fitted by a least square adjustment with *GNU Octave*, varying the microscopic parameters.

4.5.3. Results and discussion

4.5.3.1. Kinetic characterization of negative cooperativity of GLDH in dilute solution

First, we obtained experimental initial velocities as a function of NAD^+ for a range of NAD^+ concentrations evenly distributed between 0.1 and 2 mM (4.5.6.A), maintaining a constant excess concentration of L-glutamate so that the reaction can be considered as monosubstrate. All these experiments were performed in dilute solution conditions. As expected, the Scatchard plot (4.5.6.B) presented the typical curvature expected for negative cooperativity. This dilute solution data was fitted into the different microscopic models proposed in Section 4.5.2.2.

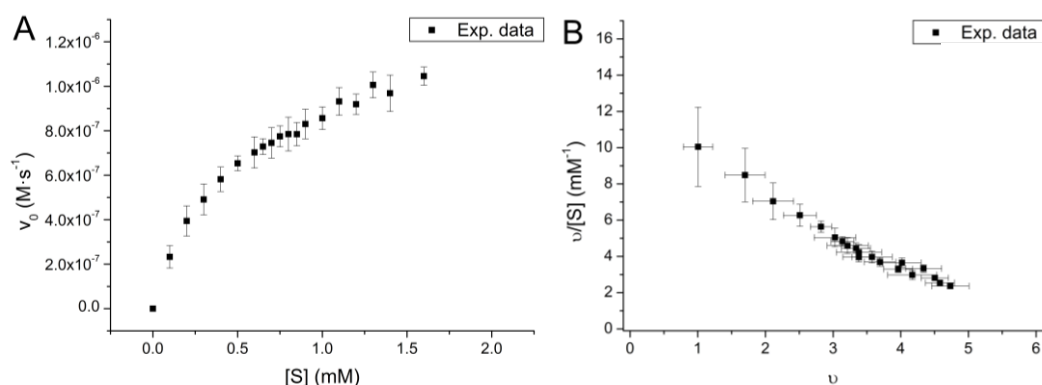


Figure 4.5.6. Initial rate variation with substrate concentration (A) and Scatchard plot (B) of the experimental data obtained in dilute solution conditions. Substrate (S) concentration (NAD^+) was increased from 0.1 to 2 mM. Data shown represents mean \pm SD of $n = 10-15$.

In order to fit the data to the proposed models, it was necessary to obtain the v_{\max} value, which was initially obtained by fitting our data to the Michaelis-Menten equation (13) using *Origin 7*. The v_{\max}^{app} value obtained was $(1.39 \pm 0.03) \cdot 10^{-6} \text{ M} \cdot \text{s}^{-1}$.

Next, we fitted the obtained experimental data to the four proposed models, using GNU Octave. The obtained results with the four different models are presented in the form of v vs. $[S]$ representation and Scatchard plot (4.5.7).

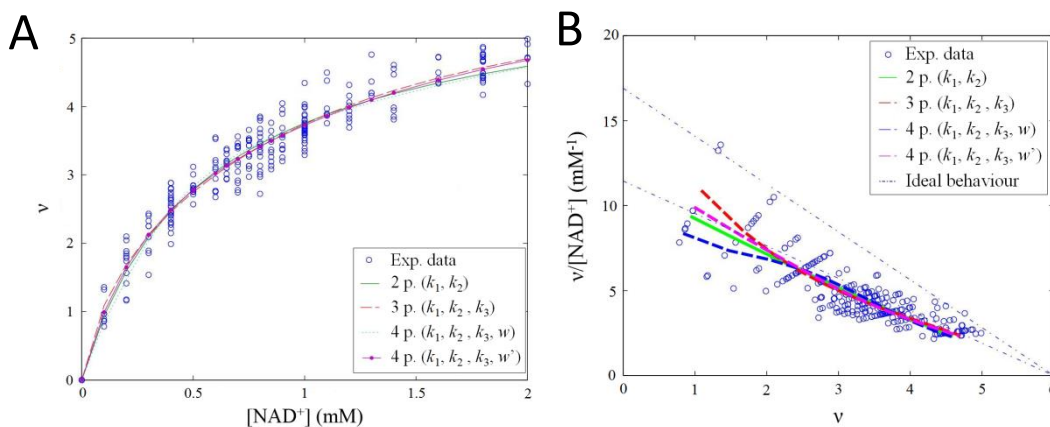


Figure 4.5.7. Variation of the average number of occupancy with substrate concentration (A) and Scatchard plot (B) of the experimental data and the fittings to the different models (different numbers of parameters). In the Scatchard plot, the ideal behavior expected is also plotted (depends on k_1 obtained by fitting).

The plot for v on substrate concentration (4.5.7.A) showed a good fitting for all the models, although the 3 parameters and 4 parameters (w') models seemed to fit better the experimental data. On the other hand, the fitting of each model in a Scatchard plot (4.5.7.B) showed that only the 3 parameters and the 4 parameters (w') models achieved a proper fitting of the data. The 2 parameters model seemed to represent a non-cooperative behavior and the 4 parameters (w) clearly did not fit the data.

In order to numerically compare the models, the values and errors of the microscopic parameters and also the reduced chi-squared, χ_r^2 , for every model are depicted (in Table 4.5.8).

Model	Fitted parameters				χ_r^2
2 parameters	k_1	1.91	\pm 0.10	(mM)	0.0618
	k_2	1.72	\pm 0.02	(mM)	
3 parameters	k_1	2.8	\pm 0.3	(mM)	0.0590

	k_2	1.0	\pm	0.2	(mM)	
	k_3	2.6	\pm	0.4	(mM)	
4 parameters (w)	k_1	3.6	\pm	1.3	(mM)	0.0674
	k_2	1.2	\pm	1.3	(mM)	
	k_3	14	\pm	8	(mM)	
	w	$-(5 \pm 2) \cdot 10^2$				
4 parameters (w')	k_1	2.3	\pm	0.4	(mM)	0.0592
	k_2	1.4	\pm	0.6	(mM)	
	k_3	8	\pm	5	(mM)	
	w'	$(3.9 \pm 1.2) \cdot 10^2$				

Table 4.5.8. Parameters values and reduced chi-squared, χ_r^2 , obtained from fitting the experimental data to four different models.

The first two models have reasonable microscopic parameters and their corresponding errors. The 4 parameters (w) model has greater relative errors and a negative constant, which means that it does not fit well the data, which is in accordance with the graphical representation (4.5.5.B). The 4 parameters (w') model has also higher errors than the 2 and 3 parameters models.

In terms of χ^2 reduced, the 3 parameters model has the smallest χ^2 reduced. Therefore, the 3 parameters model is the one that fitted best the experimental data and, consequently, the one that defines better with the minimum number of parameters GLDH's negative cooperativity.

In Figure 4.5.7, the fitting of the data to the 3 parameters model can be seen in different plots. It is also noteworthy that the K_c plot (4.5.7.C) showed a decrease relative to the ideal behavior depicted in the graphical representation.

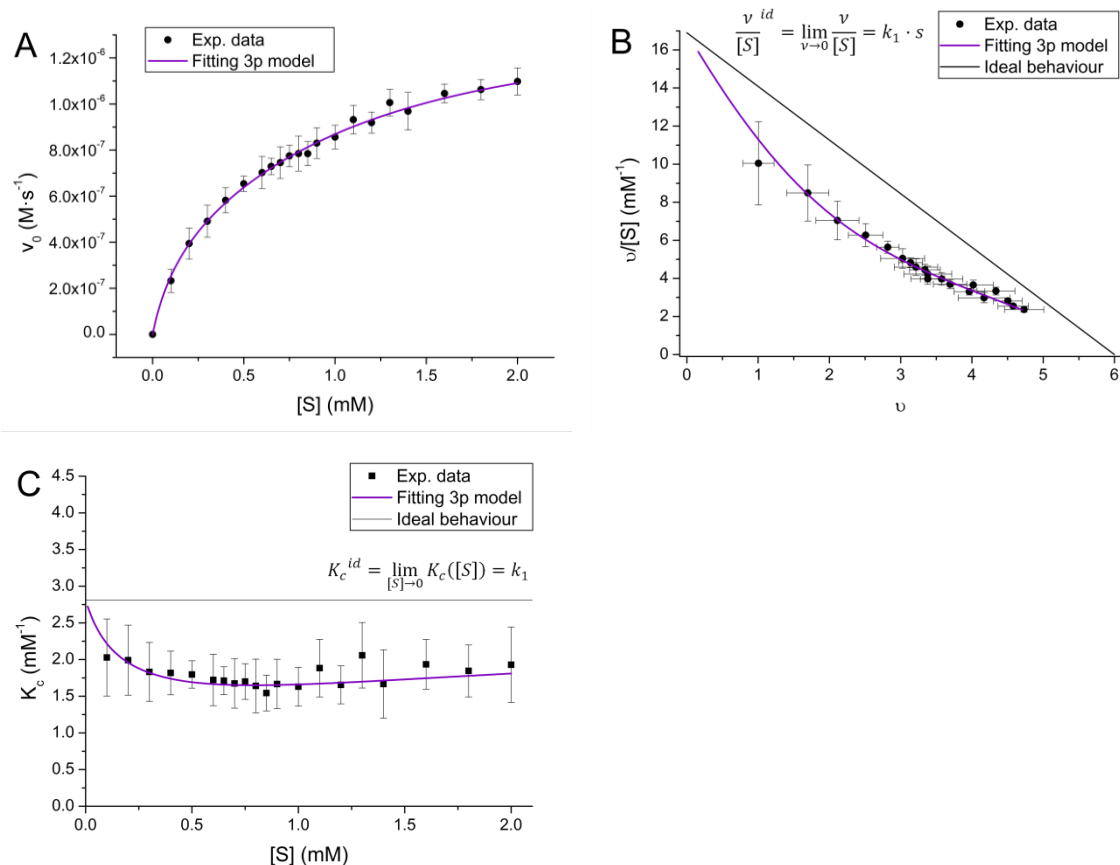


Figure 4.5.7. Alternative graphical representations of the fitting to the 3p model. Variation of the initial rate with substrate concentration plot (A), Scatchard plot (B) and variation of the effective association constant (K_c) with substrate concentration plot (C) of the experimental data and the fitting to the 3 parameters model. The ideal or non-cooperative behavior is shown in B and C, with its deduction.

The $\{b_j\}$ parameters and the intrinsic association constants (8) obtained by fitting the data are depicted in Table 4.5.8.

Fitted $\{b_j\}$ parameters

b_1 (mM^{-1})	b_2 (mM^{-2})	b_3 (mM^{-3})	b_4 (mM^{-4})	b_5 (mM^{-5})	b_6 (mM^{-6})
17 ± 2	$(9 \pm 2) \cdot 10$	$(1.5 \pm 0.4) \cdot 10^3$	$(10 \pm 4) \cdot 10$	$(2.1 \pm 1.3) \cdot 10$	1.4 ± 1.5

Intrinsic association constants (mM^{-1})

K_1^{int}	K_2^{int}	K_3^{int}	K_4^{int}	K_5^{int}	K_6^{int}
2.8 ± 0.3	2.1 ± 0.2	1.6 ± 0.2	1.4 ± 0.2	1.6 ± 0.2	2.6 ± 0.4

Table 4.5.8. Values for the $\{b_j\}$ parameters and the intrinsic association constants obtained by fitting the experimental data to the proposed model.

The values of the intrinsic association constants allow us to predict the mean affinity of the enzyme for the substrate at every situation. As can be deduced by observing the values of the K_i^{int} in Table 4.5.8, the enzyme seems to present negative cooperativity, the constants values decrease, until four substrates are bind. It also seems to recover its initial affinity in the last two binding events. This behavior can be clearly seen when representing the intrinsic association constants and the variation of the effective association constant (K_c) with the average number of occupied sites (4.5.9).

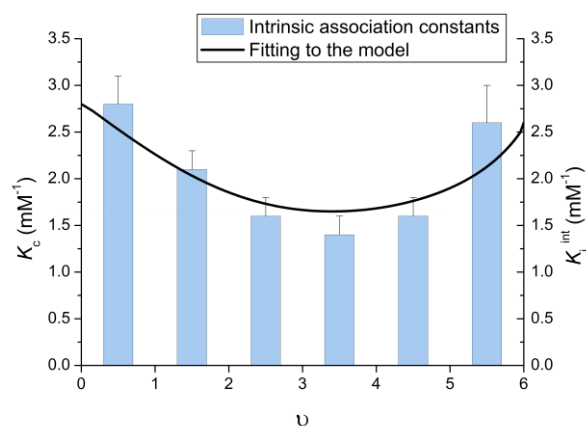


Figure 4.5.9. Plot of the intrinsic association constants (K_i^{int}) values and the variation of the fitted mean effective association constant (K_c) with the average number of occupied sites (v).

Although it seems to recover its initial association affinity, there is not an experimental evidence about this because the last experimental point was obtained before $v=5$ (it can be clearly seen in the Scatchard plot in 4.5.7.B). It was not possible to obtain values at higher site occupancies than $v=5$ in the conditions of this work since the assumption of excess glutamate would be compromised and the reaction could not be considered as monosubstrate. These results are further discussed in Section 4.5.3.3.

4.5.3.2. Kinetic characterization of GLDH under crowded media

Effect of the crowder concentration

To focus only in the effect of crowder concentration, the results shown in this section were all obtained working with the same size of Dextran, which is 250 kDa. This size was chosen due to its similarity to the enzyme size (310-350 kDa). He hypothesized that using crowders with similar size to the enzyme increases the crowding effect, as previous results by our group and others suggested [487].

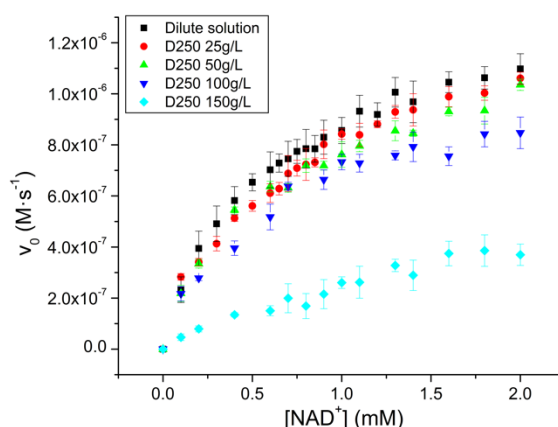


Figure 4.5.10. Experimental data obtained for the variation of the initial rate with substrate concentrations in dilute solution conditions and working with different concentrations of 250 kDa Dextran (crowder).

In Figure 4.5.10, the experimental data obtained in dilute solution conditions and with increasing concentrations of Dextran is displayed. First, it can be noticed that the initial rates generally decrease in crowded media and tend to decrease more with crowder concentration. It follows that v_{max} seems to decrease in crowded media. Secondly, the greater decrease in the initial rate corresponds to $150 \text{ g}\cdot\text{L}^{-1}$ concentration. This curve presents a different shape than the rest of curves.

Finally, fittings to Michaelis-Menten equation were performed to the data in order to quantify variations in the kinetic parameters. Although this enzyme does not behave ideally, this strategy is a simple way to compare the effect of crowding in terms of the kinetic parameters, which in this case, as our enzyme is cooperative, they are apparent.

	Dilute solution	Dextran $25 \text{ g}\cdot\text{L}^{-1}$	Dextran $50 \text{ g}\cdot\text{L}^{-1}$	Dextran $100 \text{ g}\cdot\text{L}^{-1}$	Dextran $150 \text{ g}\cdot\text{L}^{-1}$
$K_m^{app} \text{ (mM)}$	0.58 ± 0.03	0.73 ± 0.06	0.60 ± 0.06	0.58 ± 0.08	~ 3
$v_{max}^{app} \text{ (} 10^{-7} \text{ M}\cdot\text{s}^{-1}\text{)}$	13.9 ± 0.3	14.2 ± 0.5	12.5 ± 0.5	10.9 ± 0.5	~ 10

Table 4.5.11. Michaelis constant and maximum velocity values obtained by fitting the experimental data in several crowded conditions to a Michaelis-Menten equation using Origin. The crowder size used was 250 kDa.

The results of the fitting to Michaelis-Menten equation are shown in Table 5. The $150 \text{ g}\cdot\text{L}^{-1}$ data was not well fitted to Michaelis-Menten equation due to its shape, the results shown for this data can only be taken as orientative. The Michaelis constant remains practically equal for all the crowded conditions except for the highest one, in which K_m

seems to increase. Maximum velocity decreases with crowder concentration as predicted by observing the plot. For $25 \text{ g}\cdot\text{L}^{-1}$ of crowder concentration v_{\max} is almost equal to the one obtained in dilute solution, but the initial rates in general are lower than in dilute solution (as seen in Figure 15). The maximum velocity of $150 \text{ g}\cdot\text{L}^{-1}$ seems to be lower than the value obtained by the fitting.

In conclusion, the concentration of crowder diminishes initial rates and maximum velocity but does not affect K_m it seems to increase at high concentrations of crowder.

Effect of the crowder size

It is also important to analyze the effect of crowder size. For this purpose, experimental data obtained with different concentrations and sizes of Dextran is depicted in this section.

For 25 and $100 \text{ g}\cdot\text{L}^{-1}$ crowder concentrations the initial rate remains essentially equal independently of the crowder size used as can be seen in Figure 4.5.12.

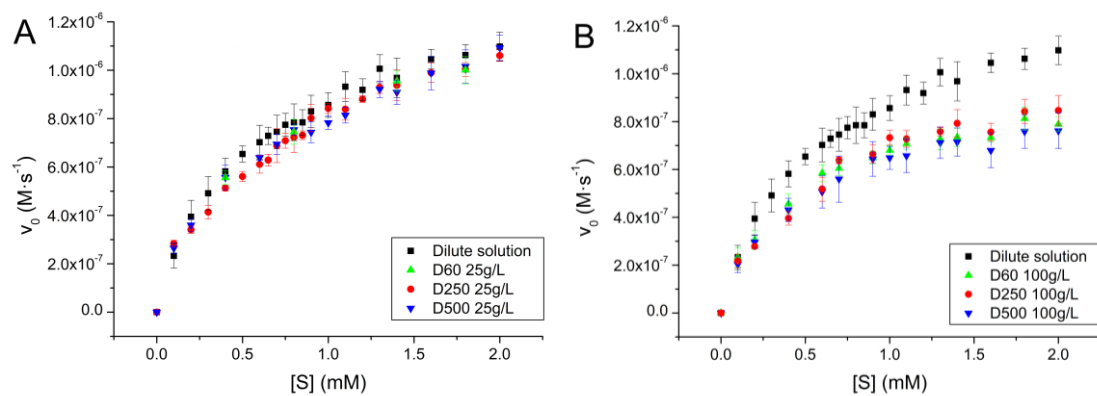


Figure 4.5.12. Experimental data obtained for the variation of the initial rate with substrate concentration working in dilute solution conditions and with two concentrations: $25 \text{ g}\cdot\text{L}^{-1}$ (A) and $100 \text{ g}\cdot\text{L}^{-1}$ (B). Both were obtained with different Dextran sizes: 60, 250 and 500 kDa.

Experimental data for $150 \text{ g}\cdot\text{L}^{-1}$ of crowder with different sizes is shown in Figure 4.5.13.

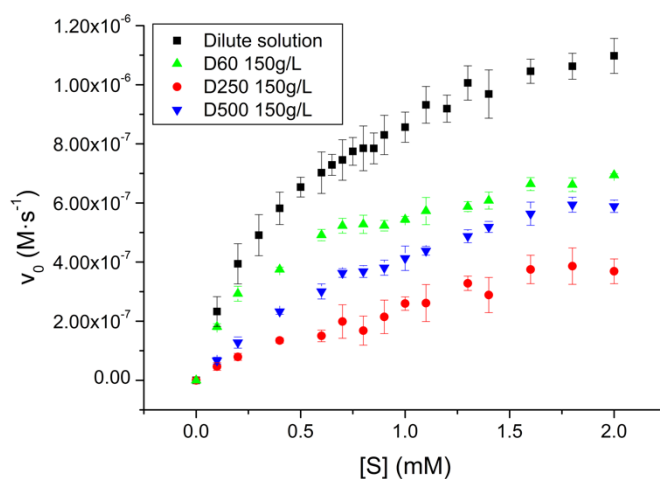


Figure 4.5.13. Experimental data obtained for the variation of the initial rate with substrate concentration working in dilute solution conditions and with a $150 \text{ g}\cdot\text{L}^{-1}$ concentration and different Dextran sizes (60, 250 and 500 kDa).

It can be noticed that the initial rate, for a $150 \text{ g}\cdot\text{L}^{-1}$ crowder concentration, depends on the crowder size and it depends in an unexpected manner. The decrease on the initial rate is higher with the 250 kDa Dextran, which is the intermediate crowder size used. The 500 kDa Dextran has less decreasing effect than the 250 kDa and the 60 kDa Dextran has the lower decreasing effect.

To properly analyze the effect of the different size in $150 \text{ g}\cdot\text{L}^{-1}$ crowder concentration, it would be useful to fit the data to a Michaelis-Menten equation to compare the kinetic constants but, due to the shape of the obtained curves, it was not possible to fit the data correctly to that model.

4.5.3.3. Negative cooperativity in crowded media

The last objective of this work was to analyze the cooperative behavior of the enzyme in crowded media. With this purpose, some data series obtained in crowded conditions (Dextran 250 kDa) were fitted to the proposed model (3 parameters).

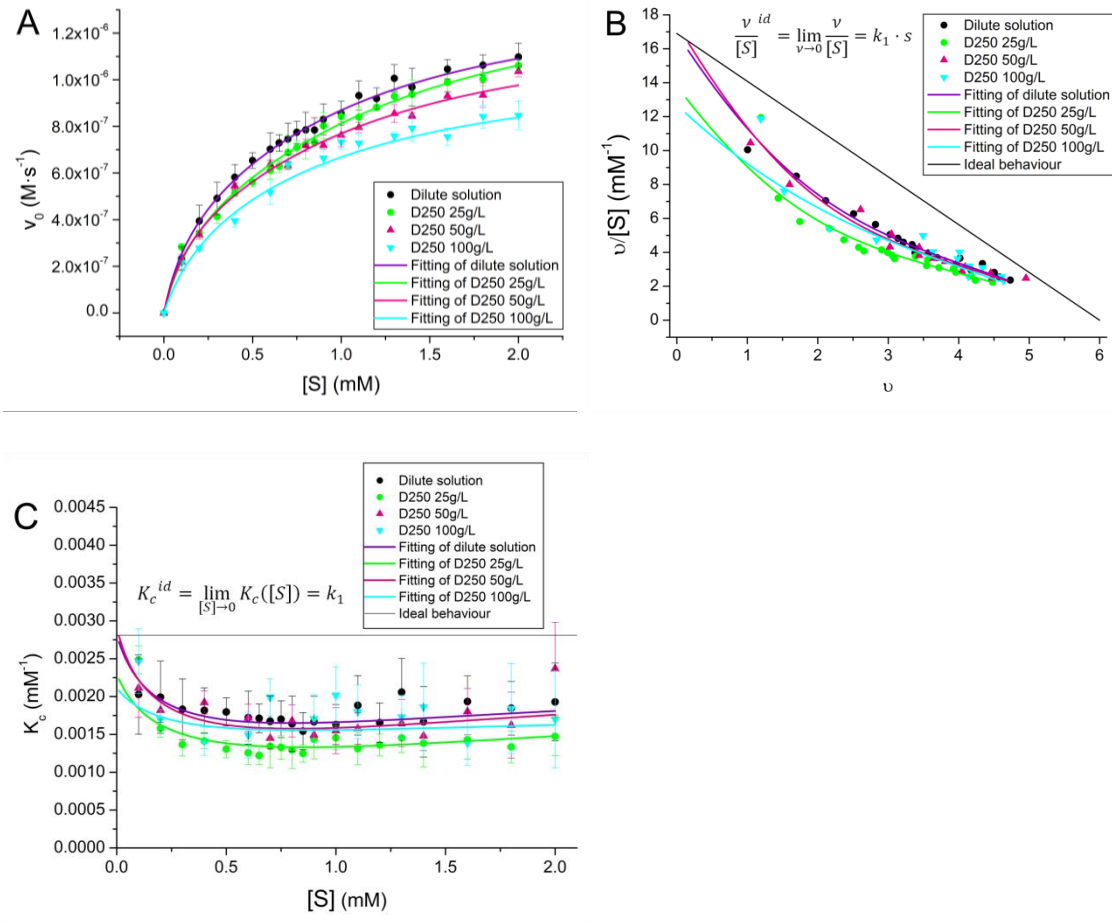


Figure 4.5.14. Variation of the initial rate with substrate concentration (A), Scatchard (B) and variation of K_c with substrate concentration (C) plots of the experimental data in dilute solution and in crowded conditions (250 kDa) and fittings to the model proposed (3p). To clarify the goodness of the fitting, the Scatchard plot (B) does not include errors.

As shown in Figure 4.5.14, the fitting of the data was performed with great results. All the plots corroborate that the 3 parameters model proposed is capable to fit the data in crowded conditions. Now, to properly analyze the effect of crowding in the cooperative behavior of GLDH the values obtained for the fitted parameters are depicted in Table 4.5.15.

Conditions	k_1 (mM $^{-1}$)	k_2 (mM $^{-1}$)	k_3 (mM $^{-1}$)	χ_r^2
Dilute solution	2.8 ± 0.3	1.0 ± 0.2	2.6 ± 0.4	0.059
25 g/L crowding agent	2.3 ± 0.3	0.7 ± 0.2	2.6 ± 0.6	0.031

50 g/L crowding agent	2.9 ± 0.4	0.9 ± 0.2	2.7 ± 0.6	0.032
100 g/L crowding agent	2.1 ± 0.5	1.2 ± 0.3	2.0 ± 0.5	0.093

Table 4.5.15. Parameters obtained by fitting the experimental data to the proposed model (3 parameters) and reduced chi-squared, χ_r^2 , of the fitting.

The first thing that should be noticed is that the reduced χ^2 for the 25 and 50 g·L⁻¹ is lower than the obtained fitting dilute solution data, which means that the fitting is even better for these crowding conditions. For the 100 g·L⁻¹ the reduced χ^2 is worse than for the dilute solution fitting, which is probably caused by some dispersion on the shape of the curve. Now, focusing on the parameter's values, it can be seen that they remain equal with increasing crowder concentrations. Even the 100 g·L⁻¹ the parameters are practically equal to the rest of parameters for different conditions. The explanation for these results would be discussed in the section below.

First, four cooperative models were proposed to characterize the negative cooperativity observed in glutamate dehydrogenase. The fitting of the experimental data to the models revealed that the best model, with the minimum number of parameters, is the one with 3 parameters. Therefore, this was chosen to explain the cooperative behavior and also to fit the data obtained in crowded conditions. The proposed model has only microscopic association constants (it does not include the interaction between trimmers term), which means that the enzyme works as two equal trimmers. In each trimmer, the union of a substrate to a site affects the rest of the sites.

Analyzing the intrinsic constants obtained, it can be seen that the enzyme decreases its affinity for the substrate until the first four sites are occupied and, in the last two, it seems to recover its initial affinity. This combination of two different behaviors could be explained by: the presence of negative cooperativity, until the fourth site is occupied. But, considering that there is experimental evidence only before the fifth intrinsic association constant (or $v=5$), this recovery cannot be confirmed. To obtain data with substrate concentration above the concentrations used in this study is necessary to rethink all the experiments, due to the fact that in higher substrate concentrations glutamate would not be in excess and the reaction could not be considered as

Where the product (P) acts as a mixed inhibitor, instead of a competitive inhibitor, due to the fact that it binds to a different form of the enzyme (E') than the one that substrate binds (E). The effect of this inhibition affects the v_{max}^{app}/K_m^{app} ratio as:

$$\frac{v_{max}^{app}}{K_m^{app}} = \left(\frac{1}{1 + \frac{[P]}{K_{ic}}} \right) \cdot \frac{v_{max}}{K_m} ; K_{ic} = \frac{(k_{-1} + k_2) \cdot k_3}{k_1 \cdot k_{-2}} \quad (20)$$

As can be seen in Eq. 13, the term multiplying the v_{max}/K_m ratio is <1 and, therefore, it is able of diminish the value of v_{max}^{app}/K_m^{app} if it decreases with crowding. Crowding increases the effective concentrations of the species present in solution and, therefore, it increases the product concentration. If product concentration is higher, the term multiplying the v_{max}/K_m ratio decreases and the apparent maximum velocity decreases.

The following topic to discuss is the effect of crowder size. It has been found that, only in the highest crowding conditions, the initial rates depend on the size of the crowding agent. In fact, the size that highly affects the rates has a 250 kDa size. Considering that our enzyme size is about 310-350 kDa, it seems that the crowder with similar size to the enzyme is the one exerting a highest effect. The effect of the crowder size in this case is similar than in other enzymes reported as ALKP [459] and MDH [454]. As previously mentioned, this size-dependence effect can be explained by the rise of depletion forces [487].

Finally, the effect of macromolecular crowding on negative cooperativity has been found to not affect the values of the parameters, which means that the cooperative behavior of GLDH is not affected by crowding.

These results suggest that crowding is not affecting the enzyme conformation, because it would probably alter the cooperativity exerted by GLDH. Instead of that, it seems more likely to think that crowding is only diminishing the diffusion and hindering the encounters between the substrates and the enzymes. Binding experiments in crowded media would be a great alternative to confirm and corroborate the results presented in this study.

5. General discussion

5. General discussion

Cancer is a heterogeneous group of diseases with multiple layers of complexity that accounts for the majority of disease-related deaths [1]. Due to its complex nature and multilevel organization, approaching it through one single scientific discipline provides only a picture of one of such layers and tackles only a small fraction of the problem, deeming to non-definitive improvements and incomplete solutions. Instead, to fully comprehend and confront cancer, knowledge from many distinct areas must be gathered and integrated. Namely, cell, tissue and organism physiology, histology, genetics, nutrition, molecular and cell biology, biochemistry, biophysics, toxicology, among a long etcetera.

In this work, we have intended to contribute to the understanding of the two main cancer features that drive to malignancy and therapeutic failure: metastasis [7,488] and drug resistance [6,12,489], by combining different perspectives and approaches from the fields of metabolomics, molecular biology, biophysics and drug discovery approaches.

First, we have encountered several potential metabolic correlations to tumorigenic potential in a cell panel of CRPC, validating such findings in two extreme cell models of metastatic progression derived from PC-3. Metabolomic characterization of different stages of prostate cancer can lead not only to better therapeutic options, but also to the identification of new potential biomarkers with improved predictive capacity.

In this regard, we have identified that highly tumorigenic CRPC is markedly vulnerable to glutamine restriction and accumulates higher amounts of intracellular polyamines and reduces their secretion to the extracellular medium. Potentially, these polyamine reservoirs can fuel a situational activation of methionine scavenging pathway, under increased nucleotide demand. Also, polyamines could be an alternative mechanism to fine-tune ROS homeostasis, since the situational shift towards their synthesis or oxidation can either produce or scavenge ROS [134]. On the other hand, intracellular accumulation of polyamines could also be understood as a consequence of a highly active methionine recycling through higher AMD1 activity in these cell lines, as discussed

through **Chapter 1**. Our results are supported by recent works that link these pathways with mTORC1 signaling [346] or sustain that polyamine biosynthesis can unveil novel vulnerabilities of CRPC [345]. Either case, our results delineate the suitability of intracellular polyamine content as a putative biomarker of remarkably tumorigenic and metabolically-plastic CRPC phenotypes. This find is biomedically relevant considering the emerging controversy on the PSA screening [319,490]. Indeed, the reliance on PSA as a biomarker has led to overtreatment with aggressive chemotherapy in PCa cases in which surveillance of the non-aggressive tumor could have been sufficient[319], since PSA is not able to discriminate between aggressive and benign subsets of the disease [490].

Additionally, our results also unveiled a significant metabolic rewiring of the urea cycle and subsequently of polyamine metabolism that is ubiquitously present across very different CRPC phenotypes and that could be therapeutically approachable, as we have already proven *in vitro*, through specific arginine deprivation therapies that are already reaching the clinics for other types of cancer [92,491].

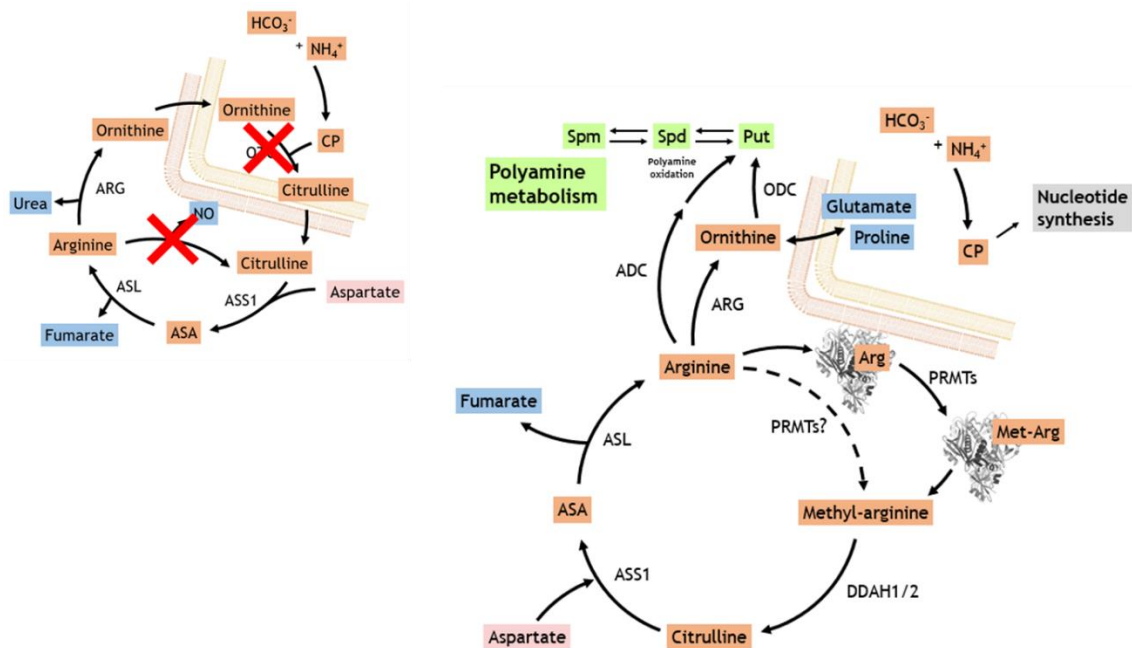


Figure 6.1. Schematic representation of the proposed rewiring of urea cycle in CRPC

Indeed, this set of interconnected metabolic pathways comprising arginine, glutamine and proline metabolism, the urea cycle and polyamine metabolism have also been identified as important for the acquisition of multiplatinum resistance in **Chapter 2**. This

observation rises the possibility that these pathways represent a common metabolic signature that can be ascribed to different cellular processes associated to cancer malignancy. In this regard, we identified that the extent to which cancer cell metabolism needs to be reprogrammed in response to achieve prolonged platinum resistance depends on the metabolic phenotype of the tissue of origin: highly glycolytic phenotypes are *per se* compatible with the acquisition of platinum resistance and only minor metabolic alterations are required, whereas tumors that prominently rely on OXPHOS need to completely rewire their energy and carbon sources to be able to cope with platinum-induced ROS.

Pharmacological management of platinum resistance in the clinics persists to be an urgent issue to be faced, as many cancer patients rely on platinum drugs as the only effective therapeutic option. The metabolic characterization performed in the multiplatinum resistant cell lines in **Chapter 2** has also unveiled a common set of metabolic features that are altered in the same direction in both CRPC and CRC. This paves the way for targeting the metabolic rewiring underlying the acquisition drug of resistance.

In addition to characterizing in depth the metabolic reprogramming associated to resistance to platinum compounds already used in the clinics, we also explored the possibility to design of novel platinum drugs able to counter platinum-resistant tumors. The rational basis of this second parallel strategy is to exploit the fact that Pt(IV) compounds are emerging as relevant therapeutic tools in oncology, due to the possibility to rationally design the additional axial ligands to modulate pharmacokinetic properties, improving drug activity, selectivity and safety profiles [292]. Additionally, due to their higher oxidation state, Pt(IV) drugs can potentially further disrupt the redox homeostasis of cancer cells, which we identified as a crucial feature for CRPC and CRC resistant models generated in **Chapter 2**.

With this aim, in our team we had the possibility to synthesize different families of Pt(IV) cyclometallated compounds that were tested in the context of this work. Thus, in **Chapter 3**, we have also identified a new family of cyclometallated Pt(IV) compounds that do not exhibit cross-resistance with conventional platinum compounds, which could also be used as part of the therapeutic arsenal against platinum resistance.

Potentially, they could also benefit from the combination with the metabolic targets unveiled in **Chapter 2** to further accentuate their anticancer effect.

Indeed, platinum-based research is blooming into a new generation of improved anticancer agents, undeniably shifting to Pt(IV) compounds [291,444,446,492]. The increasing interest in Pt(IV) relies in the prodrug traits of their axial ligands that allow to improve efficacy and selectivity, as supported by our results in **Chapter 3**, along with an encouraging complete absence of cross-resistance with cisplatin or oxaliplatin. We have identified that these novel families of Pt(IV) compounds display different cytotoxic mechanisms than conventional platinum compounds, by being able to arrest cell cycle at earlier stages and promoting enhanced cytotoxicity in both sensitive and resistant cell lines. However, the particular molecular mechanisms that account for these differences remain to be fully elucidated.

At least in part, these mechanisms could potentially be related to the commonly underestimated effect that platinum compounds have on different structural aspects of the cell such as tubulin assembly or cell polarity [493,494]. These can severely affect internal cell architecture, causing fluctuations in the levels of macromolecular crowding inside cells and having an impact on the supramolecular organization of cell metabolism. In turn, this has been proved to have a profound impact on the kinetic behavior of metabolic enzymes that govern the rate of metabolic pathways that we have identified as important throughout this work.

Indeed, signaling networks that govern metabolism act as sensors of metabolite pools, acidity, redox status or oxygen availability, and they rewire metabolic fluxes accordingly to ensure optimal performance of the cell [4,8]. Thus, an interesting future prospect is the possibility that some of these metabolic regulators may also be sensitive to intracellular volume exclusion through conformational changes that alter their activity (e.g. kinase activity) and promote metabolic pathways that are compatible with rapid proliferation in entropic terms, such as aerobic glycolysis [81].

Evidence of alterations of conformational equilibria and oligomerization has been reported for different proteins, including metabolic enzymes [454,495], and direct mechanistic links with signaling cascades governing cell metabolism will probably be

unveiled in the near future. Indeed, how crowding levels are modulated inside the cell by mTOR activation and subsequent ribosome synthesis has been recently unveiled [315]. However, the reciprocal relation, how those crowding levels can influence cell signaling cascades and, by extension, cell metabolism, remains unclear and represents a thrilling future perspective.

The effect of volume exclusion also directly impacts the kinetic behavior of metabolic enzymes. In **Chapter 1** and **Chapter 2** we assessed the impact of glycolysis and glutaminolysis in correlation with the metastatic potential and the acquisition of platinum resistance in metastatic solid tumor models. We theorize that the kinetic particularities of such pathways could be substantially altered *in vivo*, due to the high-volume occupancy encountered inside the cell. Thus, in **Chapter 4** and **Chapter 5** we studied the kinetic behavior of two relevant enzymes of glycolysis and glutaminolysis, LDH and GLDH respectively, by mimicking the conditions present inside the cells in terms of excluded volume, systematically exploring different obstacle sizes and total obstacle concentrations.

The effect of macromolecular crowding has been explored *in silico* for the case of the complete glycolytic pathway, unveiling that one of the reasons underlying the Warburg effect in proliferating cells may be precisely the kinetic limitation that macromolecular crowding imposes inside cells [81,82]. In this regard, one can think that OXPHOS could be more efficient than aerobic glycolysis as a mode of energy obtention in terms of yield per glucose moiety, but glucose availability is hardly ever a limiting factor *in vivo*. On the contrary, *in silico* predictions sustain that aerobic glycolysis could be actually more efficient than OXPHOS when considering yield per unit time and yield per unit space [81], which could actually allow cancer cells to maximize their proliferation rate.

In line with this idea, in this work we have explored the kinetic behavior of LDH under the presence of globular obstacles that do not introduce specific interactions with either LDH or its substrates, dextran polymers. We have systematically assessed the kinetic behavior of LDH in the presence of different concentrations and sizes of such obstacles, obtaining that LDH kinetics is impaired in an obstacle size- and concentration-dependent manner. Additionally, we unveiled that LDH kinetic behavior shifts from activation control to diffusion control as crowding increases, implying that the behavior of LDH

inside cells could be significantly different than previous dilute solution kinetic studies of this enzyme had predicted.

On the other hand, the effect of macromolecular crowding on glutaminolysis had not been explored prior to this work. This is of special interest since, unlike glycolysis, glutaminolysis occurs inside the mitochondrial matrix, which is the intracellular compartment displaying the highest volume occupancy [472]. We selected GLDH as a model for study because its flux can be unequivocally ascribed to TCA cycle anaplerosis, whereas glutaminase can represent flux of glutamate to other pathways, such as glutathione or proline synthesis. Moreover, mammalian GLDH displays a rich variety of allosteric regulation that renders it sensitive to important metabolic stimuli such as the mitochondrial energy status and fatty acid availability, thus allowing GLDH to regulate the anaplerosis of glutamine into the TCA cycle. Apart from that, negative cooperativity is also well described for GLDH [474,475], which is a phenomenon that had never been addressed under the influence of macromolecular crowding.

Interestingly, we encountered that GLDH kinetic behavior is also obstacle size- and concentration-dependent, but that negative cooperativity is not significantly altered by macromolecular crowding. The preservation of negative cooperativity across the fluctuations in crowding levels inside the mitochondrial matrix suggests that negative cooperativity could be a highly robust and well-preserved mechanism which plays an important role in the physiological behavior and the regulation of the GLDH function.

Gathering the knowledge obtained through **Chapter 4** and **Chapter 5**, along with works previously conducted in our group and others [309,310,454] we can reach the conclusion that the kinetic behavior of monomeric enzymes does not depend on obstacle size, whereas oligomeric enzymes ($n=2-6$) under crowded media behave in a crowder size-dependent manner. Moreover, for some enzymes, such as LDH, this dependence is linear with obstacle size: the larger the obstacle, the bigger the hindrance exerted on the kinetic behavior of the enzyme. On the contrary, in the case of GLDH, macromolecular crowding reaches the maximum inhibition when faced with obstacles that are comparable to the GLDH hexamer in size (the 250 kDa dextran). This observation, also encountered in other enzymes such as ALKP or MDH, can be explained

in terms of a maximization of the depletion forces when both the enzyme and the obstacles are similar in size [487].

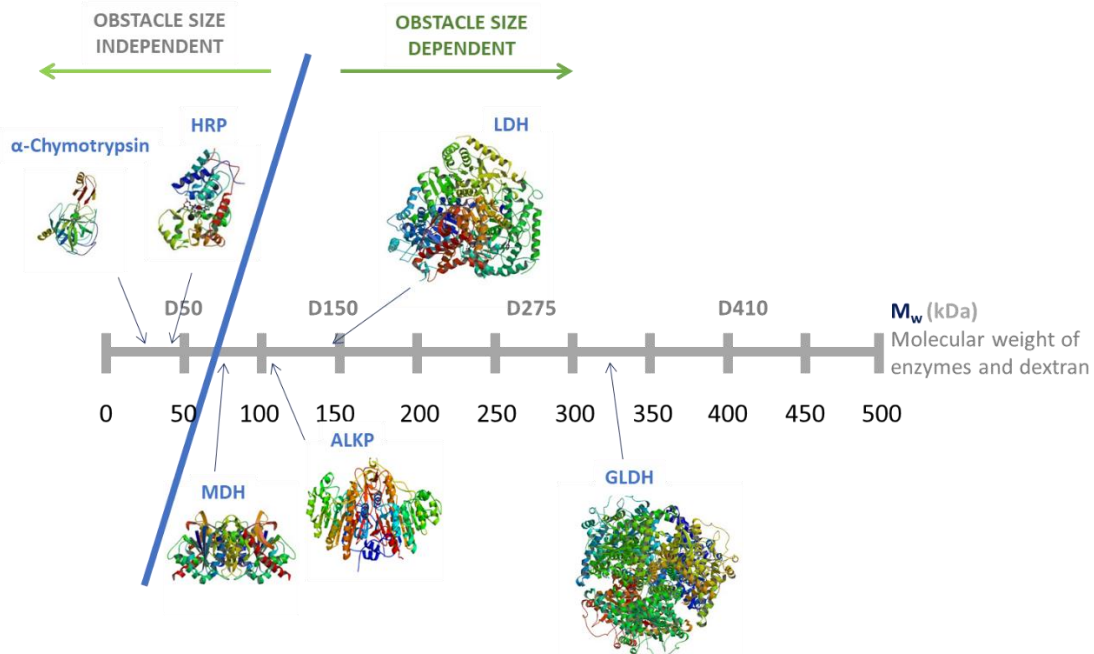


Figure 6.2. Schematic representation of enzyme and dextran obstacle size by M_w (kDa)

The actual impact of macromolecular crowding on cell metabolism has been scarcely explored and we are just scratching the surface of the understanding of the multiple implications that this phenomenon may entail for cell physiology and, in particular, for the metabolic alterations of cancer cells. The main existing limitation is the overwhelmingly interdisciplinary knowledge that is required, involving physics, chemistry and biology but, encouragingly, interdisciplinary science is and will definitely continue being on the rise in the coming years. Our observations throughout this work will hopefully have contributed to set grounds onto this enthralling enterprise, as long as meaningfully contributed to encounter valuable therapeutic tools against metastatic CRPC and CRC that can circumvent platinum resistance, both with new generations of platinum compounds and novel metabolic targets that selectively target metastatic solid tumors.

6. Conclusions

6. Conclusions

1. Highly metastatic e-CSC phenotypes of CRPC present particular metabolic vulnerabilities that can potentially lead to establishing putative biomarkers and metabolic targets that are specific for PCa subsets with high tumorigenic potential. These include enhanced glutamine avidity, a shift to taurine consumption and intracellular accumulation, increased sensitivity to disruption of one carbon metabolism, and a deep rewiring of polyamine synthesis and secretion profiles.
2. Targeting arginine metabolism and the urea cycle can be an effective therapeutic approach against metastatic CRPC. In particular PC-3M, and to a lesser extent also PC-3S, rely on exogenous arginine due to the silencing of OTC and NOS. This rewiring renders them extremely vulnerable to arginine deprivation therapies and is functionally relevant for their EMT and CSC programs, as arginine deprivation simultaneously suppresses tumorigenic and invasive capacities. In particular, PC-3M cells present a *de novo* reactivation of ASS1 that alters their sensitivity profile to arginine-based therapies and can be functionally relevant for the EMT and CSC phenotypic programs through protein arginine methylation.
3. Metastatic solid tumors with originally opposed metabolic profiles can lead to different metabolic adaptations as they acquire platinum resistance. CRPC, mainly glycolytic, does not undergo a substantial metabolic reprogramming as platinum resistance is acquired. On the contrary, largely oxidative CRC undergoes a shift to a more glycolytic metabolic profile to recover ROS homeostasis. A common metabolic signature of acquired platinum resistance arises, which also includes alterations in proline and one carbon metabolism, glutathione synthesis and ROS production.
4. Cyclometallated platinum (II) and platinum (IV) compounds exhibit strong antiproliferative effects in the low micromolar range against a wide variety of

solid tumors. The leading compounds of each series also exhibit remarkable selectivity for cancer cells and the capacity to arrest the cell cycle at S and G2/M phases, induce apoptosis and increase intracellular ROS levels. The multiple combinations of equatorial and axial ligands explored, allowed us to conclude that octahedral Pt(IV) compounds containing tridentate [C,N,N'] ligands are the optimal design to improve efficacy and selectivity against cancer cell lines. Moreover, compounds **5a-5b'** exhibit a complete absence of cross-resistance in CRPC and CRC multiplatinum resistant cell models generated in this work.

5. Simulating *in vitro* macromolecular crowding levels close to the ones encountered inside cells reveals that the glycolytic rate is remarkably affected. LDH kinetics is significantly impaired in an obstacle size- and concentration-dependent manner. Additionally, we unveiled that LDH kinetic control can be described as mixed between activation and diffusion under crowded media.
6. GLDH kinetics is decreased by macromolecular crowding, depending on both obstacle size and concentration. The velocity of the enzymatic reaction reaches a minimum when enzyme and obstacle are similar in size, corresponding to the theoretical maximization of depletion forces in the system.
7. We studied the phenomenon of negative cooperativity of GLDH kinetics under dilute solution and crowded media. To do so, we first developed and experimentally validated different models that achieve a remarkable fitness to describe the obtained experimental results, both in dilute solution and crowded media. We unveiled that negative cooperativity remains stable when varying crowder size or concentration, denoting that it may represent a well-preserved regulatory mechanism that is independent to crowding fluctuations inside the mitochondrial matrix.

7. References

7. References

- [1] F. Bray, J. Ferlay, I. Soerjomataram, R.L. Siegel, L.A. Torre, A. Jemal, Global cancer statistics 2018: GLOBOCAN estimates of incidence and mortality worldwide for 36 cancers in 185 countries., *CA. Cancer J. Clin.* 68 (2018) 394–424. doi:10.3322/caac.21492.
- [2] C.B. Blackadar, Historical review of the causes of cancer, *World J. Clin. Oncol.* 7 (2016) 54–86. doi:10.5306/wjco.v7.i1.54.
- [3] A. Rübber, A. Araujo, Cancer heterogeneity : converting a limitation into a source of biologic information, *J. Transl. Med.* 15 (2017) 1–10. doi:10.1186/s12967-017-1290-9.
- [4] L.K. Borouh, R.J. Deberardinis, Metabolic pathways promoting cancer cell survival and growth, *Nat. Cell Biol.* 17 (2015) 351–359. doi:10.1038/ncb3124.
- [5] K.L. Eales, K.E.R. Hollinshead, D.A. Tennant, Hypoxia and metabolic adaptation of cancer cells, *Oncogenesis.* 5 (2016) e190. doi:10.1038/oncsis.2015.50.
- [6] G. Housman, S. Byler, S. Heerboth, K. Lapinska, M. Longacre, N. Snyder, S. Sarkar, Drug resistance in cancer: An overview, *Cancers (Basel).* 6 (2014) 1769–1792. doi:10.3390/cancers6031769.
- [7] A.W. Lambert, D.R. Pattabiraman, R.A. Weinberg, Emerging Biological Principles of Metastasis, *Cell.* 168 (2017) 670–691. doi:10.1016/j.cell.2016.11.037.
- [8] R.J. DeBerardinis, N.S. Chandel, Fundamentals of cancer metabolism, *Sci. Adv.* 2 (2016). doi:10.1126/sciadv.1600200.
- [9] A.A. Alizadeh, V. Aranda, A. Bardelli, C. Blanpain, C. Bock, C. Borowski, C. Caldas, A. Califano, M. Doherty, M. Elsner, M. Esteller, D. Pe, K. Polyak, C.W.M. Roberts, L. Siu, A. Snyder, H. Stower, Toward understanding and exploiting tumor heterogeneity, *Nat. Med.* 21 (2015) 1–8. doi:10.1038/nm.3915.
- [10] E. Batlle, H. Clevers, Cancer stem cells revisited, *Nat. Med.* 23 (2017) 1124–1134. doi:10.1038/nm.4409.
- [11] C. LeHuede, F. Dupuy, R. Rabinovitch, R.G. Jones, P.M. Siegel, Metabolic plasticity as a determinant of tumor growth and metastasis, *Cancer Res.* 76 (2016) 5201–5208. doi:10.1158/0008-5472.CAN-16-0266.
- [12] M. Leary, S. Heerboth, K. Lapinska, S. Sarkar, Sensitization of Drug Resistant Cancer Cells : A Matter of Combination Therapy, *Cancers (Basel).* 10 (2018) 1–18. doi:10.3390/cancers10120483.
- [13] D. Hanahan, R.A. Weinberg, The Hallmarks of Cancer, *Cell.* 100 (2000) 57–70. doi:10.1016/S0092-8674(00)81683-9.
- [14] D. Hanahan, R.A. Weinberg, Hallmarks of cancer: the next generation., *Cell.* 144 (2011) 646–74. doi:10.1016/j.cell.2011.02.013.

- [15] P.S. Ward, C.B. Thompson, Metabolic Reprogramming: A Cancer Hallmark Even Warburg Did Not Anticipate, *Cancer Cell*. 21 (2012) 297–308. doi:10.1016/j.ccr.2012.02.014.
- [16] N.N. Pavlova, C.B. Thompson, The Emerging Hallmarks of Cancer Metabolism, *Cell Metab.* 23 (2016) 27–47. doi:10.1016/j.cmet.2015.12.006.
- [17] K. Pietras, A. Östman, Hallmarks of cancer: Interactions with the tumor stroma, *Exp. Cell Res.* 316 (2010) 1324–1331. doi:10.1016/j.yexcr.2010.02.045.
- [18] A. Satyanarayana, P. Kaldis, Mammalian cell-cycle regulation: Several cdks, numerous cyclins and diverse compensatory mechanisms, *Oncogene*. 28 (2009) 2925–2939. doi:10.1038/onc.2009.170.
- [19] T. Otto, P. Sicinski, Cell cycle proteins as promising targets in cancer therapy, *Nat. Rev. Cancer*. 17 (2017) 93–115. doi:10.1038/nrc.2016.138.
- [20] S. Diaz-Moralli, M. Tarrado-Castellarnau, A. Miranda, M. Cascante, Targeting cell cycle regulation in cancer therapy, *Pharmacol. Ther.* 138 (2013) 255–271. doi:10.1016/j.pharmthera.2013.01.011.
- [21] D. Wang, Q. Sun, J. Wu, W. Wang, G. Yao, T. Li, X. Li, L. Li, Y. Zhang, W. Cui, S. Song, A new Prenylated Flavonoid induces G0/G1 arrest and apoptosis through p38/JNK MAPK pathways in Human Hepatocellular Carcinoma cells, *Sci. Rep.* 7 (2017) 1–13. doi:10.1038/s41598-017-05955-0.
- [22] X. ling Song, Y. jiao Zhang, X. feng Wang, W. jie Zhang, Z. Wang, F. Zhang, Y. jian Zhang, J. hua Lu, J. wei Mei, Y. ping Hu, L. Chen, H. feng Li, Y. yuan Ye, Y. bin Liu, J. Gu, Casticin induces apoptosis and G0/G1 cell cycle arrest in gallbladder cancer cells, *Cancer Cell Int.* 17 (2017) 1–10. doi:10.1186/s12935-016-0377-3.
- [23] Z. Shi, A. Azuma, D. Sampath, Y.X. Li, P. Huang, W. Plunkett, S-phase arrest by nucleoside analogues and abrogation of survival without cell cycle progression by 7-hydroxystaurosporine, *Cancer Res.* 61 (2001) 1065–1072.
- [24] M. Tsurusawa, M. Niwa, N. Katano, T. Fujimoto, Methotrexate cytotoxicity as related to irreversible S phase arrest in mouse L1210 leukemia cells, *Jpn J. Cancer Res.* 81 (1990) 85–90.
- [25] M.-O. Turgeon, N.J.S. Perry, G. Pouligiannis, DNA Damage, Repair, and Cancer Metabolism, *Front. Oncol.* 8 (2018). doi:10.3389/fonc.2018.00015.
- [26] J.E. Haber, Deciphering the DNA Damage Response, *Cell*. 162 (2015) 1183–1185. doi:10.1016/j.cell.2015.08.034.
- [27] S. Müller, DNA Damage-inducing Compounds: Unraveling their Pleiotropic Effects Using High Throughput Sequencing, *Curr. Med. Chem.* 24 (2017) 1558–1585. doi:10.2174/0929867324666170124143710.
- [28] B.A. Weaver, How Taxol/paclitaxel kills cancer cells, *Mol. Biol. Cell*. 25 (2014) 2677–2681. doi:10.1091/mbc.E14-04-0916.
- [29] D.L. Morse, Docetaxel induces cell death through mitotic catastrophe in human breast cancer cells, *Mol. Cancer Ther.* 4 (2005) 1495–1504. doi:10.1158/1535-

- 7163.MCT-05-0130.
- [30] R.C. Taylor, S.P. Cullen, S.J. Martin, Apoptosis: Controlled demolition at the cellular level, *Nat. Rev. Mol. Cell Biol.* 9 (2008) 231–241. doi:10.1038/nrm2312.
- [31] J.L. Koff, S. Ramachandiran, L. Bernal-Mizrachi, A time to kill: Targeting apoptosis in cancer, *Int. J. Mol. Sci.* 16 (2015) 2942–2955. doi:10.3390/ijms16022942.
- [32] S. Elmore, Apoptosis: A Review of Programmed Cell Death, *Toxicol. Pathol.* 35 (2007) 495–516. doi:10.1080/01926230701320337.
- [33] D.R. Mcilwain, T. Berger, T.W. Mak, Caspase Functions in Cell Death and Disease, (2015) 1–29. doi:10.1101/cshperspect.a008656.
- [34] J. Kale, E.J. Osterlund, D.W. Andrews, BCL-2 family proteins: Changing partners in the dance towards death, *Cell Death Differ.* 25 (2018) 65–80. doi:10.1038/cdd.2017.186.
- [35] P.E. Czabotar, G. Lessene, A. Strasser, J.M. Adams, Control of apoptosis by the BCL-2 protein family: implications for physiology and therapy, *Nat. Rev. Mol. Cell Biol.* 15 (2013) 49–63. doi:10.1038/nrm3722.
- [36] S. Nagata, Apoptosis and Clearance of Apoptotic Cells, *Annu. Rev. Immunol.* 36 (2018) 489–517. doi:10.1146/annurev-immunol-042617-053010.
- [37] J.L. Fox, M. MacFarlane, Targeting cell death signalling in cancer: Minimising “Collateral damage,” *Br. J. Cancer.* 115 (2016) 5–11. doi:10.1038/bjc.2016.111.
- [38] B. Lim, J.E. Allen, V. V Prabhu, M.K. Talekar, N.K. Finnberg, W.S. El-Deiry, Targeting TRAIL in the treatment of cancer: new developments, *Expert Opin. Ther. Targets.* 19 (2015) 1171–1185. doi:10.1517/14728222.2015.1049838.
- [39] J.T. Opferman, Attacking cancer’s Achilles heel: antagonism of anti-apoptotic BCL-2 family members, *FEBS J.* 283 (2016) 2661–2675. doi:10.1111/febs.13472.
- [40] A.W. Roberts, M.S. Davids, J.M. Pagel, B.S. Kahl, S.D. Puvvada, J.F. Gerecitano, T.J. Kipps, M.A. Anderson, J.R. Brown, L. Gressick, S. Wong, M. Dunbar, M. Zhu, M.B. Desai, E. Cerri, S. Heitner Enschede, R.A. Humerickhouse, W.G. Wierda, J.F. Seymour, Targeting BCL2 with Venetoclax in Relapsed Chronic Lymphocytic Leukemia, *N. Engl. J. Med.* 374 (2016) 311–322. doi:10.1056/NEJMoa1513257.
- [41] J. Shi, Y. Zhou, H.C. Huang, T.J. Mitchison, Navitoclax (ABT-263) accelerates apoptosis during drug-induced mitotic arrest by antagonizing Bcl-xL, *Cancer Res.* 71 (2011) 4518–4526. doi:10.1158/0008-5472.CAN-10-4336.
- [42] M.G. Vander Heiden, L.C. Cantley, C.B. Thompson, P. Mammalian, C. Exhibit, A. Metabolism, Understanding the Warburg Effect : The Metabolic Requirements of Cell Proliferation, *Science* (80-.). 324 (2009) 1029–1034.
- [43] A. Martín-Bernabé, C. Balcells, J. Tarragó-Celada, C. Foguet, S. Bourgoin-Voillard, M. Seve, M. Cascante, The importance of post-translational modifications in systems biology approaches to identify therapeutic targets in cancer metabolism, *Curr. Opin. Syst. Biol.* 3 (2017) 161–169. doi:10.1016/j.coisb.2017.05.011.

- [44] C. Porta, C. Paglino, A. Mosca, Targeting PI3K/Akt/mTOR Signaling in Cancer, *Front. Oncol.* 4 (2014) 88–93. doi:10.3389/fonc.2014.00064.
- [45] Z.E. Stine, Z.E. Walton, B.J. Altman, A.L. Hsieh, C. V. Dang, MYC, Metabolism, and Cancer, *Cancer Discov.* 5 (2015) 1024–1039. doi:10.1158/2159-8290.CD-15-0507.
- [46] F.R. Dejure, M. Eilers, MYC and tumor metabolism: chicken and egg, *EMBO J.* (2017) 1–12.
- [47] P. Gao, I. Tchernyshyov, T. Chang, Y. Lee, K. Kita, T. Ochi, K.I. Zeller, A.M. De Marzo, J.E. Van Eyk, J.T. Mendell, C. V Dang, c-Myc suppression of miR-23a / b enhances mitochondrial glutaminase expression and glutamine metabolism, *Nature.* 458 (2009) 762–765. doi:10.1038/nature07823.
- [48] S. Vyas, E. Zaganjor, M.C. Haigis, Mitochondria and Cancer, *Cell.* 166 (2016) 555–566. doi:10.1016/j.cell.2016.07.002.
- [49] R.A. Casero Jr, T. Murray Stewart, A.E. Pegg, Polyamine metabolism and cancer: treatments, challenges and opportunities, *Nat. Rev. Cancer.* (2018). doi:10.1038/s41568-018-0050-3.
- [50] M. Yuneva, N. Zamboni, P. Oefner, R. Sachidanandam, Y. Lazebnik, Deficiency in glutamine but not glucose induces MYC-dependent apoptosis in human cells, 178 (2007) 93–105. doi:10.1083/jcb.200703099.
- [51] H. Ying, A.C. Kimmelman, C.A. Lyssiotis, S. Hua, G.C. Chu, E. Fletcher-Sananikone, J.W. Locasale, J. Son, H. Zhang, J.L. Coloff, H. Yan, W. Wang, S. Chen, A. Viale, H. Zheng, J.H. Paik, C. Lim, A.R. Guimaraes, E.S. Martin, J. Chang, A.F. Hezel, S.R. Perry, J. Hu, B. Gan, Y. Xiao, J.M. Asara, R. Weissleder, Y.A. Wang, L. Chin, L.C. Cantley, R.A. Depinho, Oncogenic kras maintains pancreatic tumors through regulation of anabolic glucose metabolism, *Cell.* 149 (2012) 656–670. doi:10.1016/j.cell.2012.01.058.
- [52] D. Gaglio, C.M. Metallo, P.A. Gameiro, K. Hiller, L.S. Danna, C. Balestrieri, L. Alberghina, G. Stephanopoulos, F. Chiaradonna, Oncogenic K-Ras decouples glucose and glutamine metabolism to support cancer cell growth, *Mol. Syst. Biol.* 7 (2011) 1–15. doi:10.1038/msb.2011.56.
- [53] K. Kawada, K. Toda, Y. Sakai, Targeting metabolic reprogramming in KRAS-driven cancers, *Int. J. Clin. Oncol.* 22 (2017) 651–659. doi:10.1007/s10147-017-1156-4.
- [54] U. Krishnamurti, J.F. Silverman, HER2 in breast cancer: A review and update, *Adv. Anat. Pathol.* 21 (2014) 100–107. doi:10.1097/PAP.000000000000015.
- [55] W. Li, S.M. Saud, M.R. Young, G. Chen, Targeting AMPK for cancer prevention and treatment, *Oncotarget.* 6 (2015) 7365–7378.
- [56] F. Kruiswijk, C.F. Labuschagne, K.H. Vousden, P53 in survival, death and metabolic health: A lifeguard with a licence to kill, *Nat. Rev. Mol. Cell Biol.* 16 (2015) 393–405. doi:10.1038/nrm4007.
- [57] P. Deshmukh, S. Unni, G. Krishnappa, B. Padmanabhan, The Keap1–Nrf2 pathway: promising therapeutic target to counteract ROS-mediated damage in cancers and

- neurodegenerative diseases, *Biophys. Rev.* 9 (2017) 41–56. doi:10.1007/s12551-016-0244-4.
- [58] P. Zhang, A. Singh, S. Yegnasubramanian, D. Esopi, P. Kombairaju, M. Bodas, H. Wu, S.G. Bova, S. Biswal, Loss of Kelch-Like ECH-Associated Protein 1 Function in Prostate Cancer Cells Causes Chemoresistance and Radioresistance and Promotes Tumor Growth, *Mol. Cancer Ther.* 9 (2010) 336–346. doi:10.1158/1535-7163.MCT-09-0589.
- [59] R. Romero, V.I. Sayin, S.M. Davidson, M.R. Bauer, S.X. Singh, S.E. Leboeuf, T.R. Karakousi, D.C. Ellis, A. Bhutkar, F.J. Sánchez-Rivera, L. Subbaraj, B. Martinez, R.T. Bronson, J.R. Prigge, E.E. Schmidt, C.J. Thomas, C. Goparaju, A. Davies, I. Dolgalev, A. Heguy, V. Allaj, J.T. Poirier, A.L. Moreira, C.M. Rudin, H.I. Pass, M.G. Vander Heiden, T. Jacks, T. Papagiannakopoulos, Keap1 loss promotes Kras-driven lung cancer and results in dependence on glutaminolysis, *Nat. Med.* 23 (2017) 1362–1368. doi:10.1038/nm.4407.
- [60] P. Nioi, T. Nguyen, A mutation of Keap1 found in breast cancer impairs its ability to repress Nrf2 activity, *Biochem. Biophys. Res. Commun.* 362 (2007) 816–821. doi:10.1016/j.bbrc.2007.08.051.
- [61] L.D. Goldstein, J. Lee, F. Gnad, C. Klijn, A. Schaub, J. Reeder, A. Daemen, C.E. Bakalarski, T. Holcomb, D.S. Shames, R.J. Hartmaier, J. Chmielecki, S. Seshagiri, R. Gentleman, D. Stokoe, Recurrent Loss of NFE2L2 Exon 2 Is a Mechanism for Nrf2 Pathway Activation in Human Cancers, *Cell Rep.* 16 (2016) 2605–2617. doi:10.1016/j.celrep.2016.08.010.
- [62] A.T. Dinkova-Kostova, A.Y. Abramov, The emerging role of Nrf2 in mitochondrial function, *Free Radic. Biol. Med.* 88 (2015) 179–188. doi:10.1016/j.freeradbiomed.2015.04.036.
- [63] S. Soni, Y.S. Padwad, HIF-1 in cancer therapy: two decade long story of a transcription factor, *Acta Oncol. (Madr.)* 56 (2017) 503–515. doi:10.1080/0284186X.2017.1301680.
- [64] Y. Kato, S. Ozawa, C. Miyamoto, Y. Maehata, A. Suzuki, T. Maeda, Y. Baba, Acidic extracellular microenvironment and cancer, *Cancer Cell Int.* 13 (2013) 1. doi:10.1186/1475-2867-13-89.
- [65] S.Y. Lunt, M.G. Vander Heiden, Aerobic Glycolysis : Meeting the Metabolic Requirements of Cell Proliferation, *Annu. Rev. Cell Dev. Biol.* 27 (2011) 441–464. doi:10.1146/annurev-cellbio-092910-154237.
- [66] M. V Liberti, J.W. Locasale, The Warburg Effect : How Does it Benefit Cancer Cells ?, *Trends Biochem. Sci.* 41 (2016) 211–218. doi:10.1016/j.tibs.2015.12.001.
- [67] K.C. Patra, Q. Wang, P.T. Bhaskar, L. Miller, Z. Wang, W. Wheaton, N. Chandel, M. Laakso, W.J. Muller, E.L. Allen, A.K. Jha, G. a Smolen, M.F. Clasquin, R.B. Robey, N. Hay, Hexokinase 2 is required for tumor initiation and maintenance and its systemic deletion is therapeutic in mouse models of cancer., *Cancer Cell.* 24 (2013) 213–28. doi:10.1016/j.ccr.2013.06.014.

- [68] D. DeWaal, V. Nogueira, A.R. Terry, K.C. Patra, S.M. Jeon, G. Guzman, J. Au, C.P. Long, M.R. Antoniewicz, N. Hay, Hexokinase-2 depletion inhibits glycolysis and induces oxidative phosphorylation in hepatocellular carcinoma and sensitizes to metformin, *Nat. Commun.* 9 (2018). doi:10.1038/s41467-017-02733-4.
- [69] D.J. Roberts, S. Miyamoto, Hexokinase II integrates energy metabolism and cellular protection: Acting on mitochondria and TORCing to autophagy, *Cell Death Differ.* 22 (2015) 248–257. doi:10.1038/cdd.2014.173.
- [70] T. Houles, S.P. Gravel, G. Lavoie, S. Shin, M. Savall, A. Meant, B. Grondin, L. Gaboury, S.O. Yoon, J. St-Pierre, P.P. Roux, RSK regulates PFK-2 activity to promote metabolic rewiring in melanoma, *Cancer Res.* 78 (2018) 2191–2204. doi:10.1158/0008-5472.CAN-17-2215.
- [71] J.C. Schell, K.A. Olson, L. Jiang, A.J. Hawkins, J.G. VanVranken, J. Xie, R.A. Egnatchik, E.G. Earl, R.J. DeBerardinis, J. Rutter, A role for the mitochondrial pyruvate carrier as a repressor of the warburg effect and colon cancer cell growth, *Mol. Cell.* 56 (2014) 400–413. doi:10.1016/j.molcel.2014.09.026.
- [72] J. Kim, I. Tchernyshyov, G.L. Semenza, C. V Dang, HIF-1-mediated expression of pyruvate dehydrogenase kinase: A metabolic switch required for cellular adaptation to hypoxia, *Cell Metab.* 3 (2006) 177–185. doi:10.1016/j.cmet.2006.02.002.
- [73] E. Aguilar, I. Marin de Mas, E. Zodda, S. Marin, F. Morrish, V. Selivanov, O. Meca-Cortés, H. Delowar, M. Pons, I. Izquierdo, T. Celià-Terrassa, P. de Atauri, J. Centelles, D. Hockenbery, T. Thomson, M. Cascante, Metabolic reprogramming and dependencies associated with epithelial cancer stem cells independent of the epithelial-mesenchymal transition program, *Stem Cells.* 34 (2016) 1163–1176. doi:10.1002/stem.2286.
- [74] H.R. Christofk, M.G. Vander Heiden, M.H. Harris, A. Ramanathan, R.E. Gerszten, R. Wei, M.D. Fleming, S.L. Schreiber, L.C. Cantley, The M2 splice isoform of pyruvate kinase is important for cancer metabolism and tumour growth, *Nature.* 452 (2008) 230–233. doi:10.1038/nature06734.
- [75] J.W. Locasale, L.C. Cantley, Metabolic flux and the regulation of mammalian cell growth, *Cell Metab.* 14 (2011) 443–451. doi:10.1016/j.cmet.2011.07.014.
- [76] G.M. DeNicola, L.C. Cantley, Cancer's Fuel Choice: New Flavors for a Picky Eater, *Mol. Cell.* 60 (2015) 514–523. doi:10.1016/j.molcel.2015.10.018.
- [77] C.S. Ahn, C.M. Metallo, Mitochondria as biosynthetic factories for cancer proliferation, *Cancer Metab.* 3 (2015) 1–10. doi:10.1186/s40170-015-0128-2.
- [78] D.C. Ngo, K. Ververis, S.M. Tortorella, T.C. Karagiannis, Introduction to the molecular basis of cancer metabolism and the Warburg effect, *Mol. Biol. Rep.* 42 (2015) 819–823. doi:10.1007/s11033-015-3857-y.
- [79] D. Anastasiou, G. Pouligiannis, J.M. Asara, M.B. Boxer, J. Jiang, M. Shen, G. Bellinger, A.T. Sasaki, J.W. Locasale, D.S. Auld, C.J. Thomas, M.G. Vander Heiden, L.C. Cantley, Inhibition of Pyruvate Kinase M2 by Reactive Oxygen Species

- Contributes to Cellular Antioxidant Responses, *Science* (80-.). 334 (2011) 1278–1283. doi:10.1126/science.1211485.
- [80] A.A. Shestov, X. Liu, Z. Ser, A.A. Cluntun, Y.P. Hung, L. Huang, D. Kim, A. Le, G. Yellen, J.G. Albeck, J.W. Locasale, Quantitative determinants of aerobic glycolysis identify flux through the enzyme GAPDH as a limiting step, *Elife*. 3 (2014) 1–18. doi:10.7554/eLife.03342.
- [81] A. Vazquez, Z.N. Oltvai, Molecular crowding defines a common origin for the warburg effect in proliferating cells and the lactate threshold in muscle physiology, *PLoS One*. 6 (2011) 1–9. doi:10.1371/journal.pone.0019538.
- [82] A. Vazquez, Z.N. Oltvai, Macromolecular crowding explains overflow metabolism in cells, *Sci. Rep.* 6 (2016) 1–7. doi:10.1038/srep31007.
- [83] P.E. Porporato, N. Filigheddu, J.M.B.S. Pedro, G. Kroemer, L. Galluzzi, Mitochondrial metabolism and cancer, *Cell Res.* 28 (2018) 265–280. doi:10.1038/cr.2017.155.
- [84] M.A.B. Melone, A. Valentino, S. Margarucci, U. Galderisi, A. Giordano, G. Peluso, The carnitine system and cancer metabolic plasticity, *Cell Death Dis.* 9 (2018) 1–12. doi:10.1038/s41419-018-0313-7.
- [85] J. Zhang, J. Fan, S. Venneti, J.R. Cross, T. Takagi, B. Bhinder, H. Djaballah, M. Kanai, E.H. Cheng, A.R. Judkins, B. Pawel, J. Baggs, S. Cherry, J.D. Rabinowitz, C.B. Thompson, Asparagine plays a critical role in regulating cellular adaptation to glutamine depletion, *Mol. Cell.* 56 (2014) 205–218. doi:10.1016/j.molcel.2014.08.018.
- [86] J. Son, C.A. Lyssiotis, H. Ying, X. Wang, S. Hua, M. Ligorio, R.M. Perera, C.R. Ferrone, E. Mullarky, N. Shyh-Chang, Y. Kang, J.B. Fleming, N. Bardeesy, J.M. Asara, M.C. Haigis, R.A. Depinho, L.C. Cantley, A.C. Kimmelman, Glutamine supports pancreatic cancer growth through a KRAS-regulated metabolic pathway, *Nature*. 496 (2013) 101–105. doi:10.1038/nature12040.
- [87] M. Sciacovelli, C. Frezza, Oncometabolites: Unconventional triggers of oncogenic signalling cascades, *Free Radic. Biol. Med.* 100 (2016) 175–181. doi:10.1016/j.freeradbiomed.2016.04.025.
- [88] M. Yang, T. Soga, P.J. Pollard, J. Adam, The emerging role of fumarate as an oncometabolite, *Front. Oncol.* 2 (2012) 1–7. doi:10.3389/fonc.2012.00085.
- [89] M. Sciacovelli, E. Gonçalves, T.I. Johnson, V.R. Zecchini, A.S.H. Da Costa, E. Gaude, A.V. Drubbel, S.J. Theobald, S.R. Abbo, M.G.B. Tran, V. Rajeeve, S. Cardaci, S. Foster, H. Yun, P. Cutillas, A. Warren, V. Gnanapragasam, E. Gottlieb, K. Franze, B. Huntly, E.R. Maher, P.H. Maxwell, J. Saez-Rodriguez, C. Frezza, Fumarate is an epigenetic modifier that elicits epithelial-to-mesenchymal transition, *Nature*. 537 (2016) 544–547. doi:10.1038/nature19353.
- [90] L. Zheng, E.D. MacKenzie, S.A. Karim, A. Hedley, K. Blyth, G. Kalna, D.G. Watson, P. Szlosarek, C. Frezza, E. Gottlieb, Reversed argininosuccinate lyase activity in fumarate hydratase-deficient cancer cells, *Cancer Metab.* 1 (2013) 12.

- doi:10.1186/2049-3002-1-12.
- [91] A.R. Mullen, W.W. Wheaton, E.S. Jin, P.H. Chen, L.B. Sullivan, T. Cheng, Y. Yang, W.M. Linehan, N.S. Chandel, R.J. Deberardinis, Reductive carboxylation supports growth in tumour cells with defective mitochondria, *Nature*. 481 (2012) 385–388. doi:10.1038/nature10642.
- [92] R. Keshet, P. Szlosarek, A. Carracedo, A. Erez, Rewiring urea cycle metabolism in cancer to support anabolism, *Nat. Rev. Cancer*. 18 (2018) 634–645. doi:10.1038/s41568-018-0054-z.
- [93] A. Kaldma, A. Klepinin, V. Chekulayev, K. Mado, I. Shevchuk, N. Timohhina, K. Tepp, M. Kandashvili, M. Varikmaa, A. Koit, M. Planken, K. Heck, L. Truu, A. Planken, V. Valvere, E. Rebane, T. Kaambre, An in situ study of bioenergetic properties of human colorectal cancer: The regulation of mitochondrial respiration and distribution of flux control among the components of ATP synthasome, *Int. J. Biochem. Cell Biol.* 55 (2014) 171–186. doi:10.1016/j.biocel.2014.09.004.
- [94] V. Chekulayev, K. Mado, I. Shevchuk, A. Koit, A. Kaldma, A. Klepinin, N. Timohhina, K. Tepp, M. Kandashvili, L. Ounpuu, K. Heck, L. Truu, A. Planken, V. Valvere, T. Kaambre, Metabolic remodeling in human colorectal cancer and surrounding tissues: alterations in regulation of mitochondrial respiration and metabolic fluxes, *Biochem. Biophys. Reports*. 4 (2015) 111–125. doi:10.1016/j.bbrep.2015.08.020.
- [95] P. Sancho, E. Burgos-Ramos, A. Tavera, T. Bou Kheir, P. Jagust, M. Schoenhals, D. Barneda, K. Sellers, R. Campos-Olivas, O. Graña, C.R. Viera, M. Yuneva, B. Sainz, C. Heeschen, MYC/PGC-1 α balance determines the metabolic phenotype and plasticity of pancreatic cancer stem cells, *Cell Metab.* 22 (2015) 590–605. doi:10.1016/j.cmet.2015.08.015.
- [96] R.U.Z. Zhao, S. Jiang, L. Zhang, Z.-B. Yu, Mitochondrial electron transport chain, ROS generation and uncoupling, *Int. J. Mol. Med.* 44 (2019) 3–15. doi:10.3892/ijmm.2019.4188.
- [97] A.M. Hosios, V.C. Hecht, L. V. Danai, M.O. Johnson, J.C. Rathmell, M.L. Steinhauser, S.R. Manalis, M.G. Vander Heiden, Amino Acids Rather than Glucose Account for the Majority of Cell Mass in Proliferating Mammalian Cells, *Dev. Cell*. 36 (2016) 540–549. doi:10.1016/j.devcel.2016.02.012.
- [98] M. Yang, K.H. Vousden, Serine and one-carbon metabolism in cancer, *Nat. Rev. Cancer*. 16 (2016) 650–662. doi:10.1038/nrc.2016.81.
- [99] M. Watford, Glutamine and glutamate: Nonessential or essential amino acids?, *Anim. Nutr.* 1 (2015) 119–122. doi:10.1016/j.aninu.2015.08.008.
- [100] R.C. Geck, A. Toker, Nonessential amino acid metabolism in breast cancer, *Adv. Biol. Regul.* 62 (2016) 11–17. doi:10.1016/j.jbior.2016.01.001.
- [101] M.J. Lukey, W.P. Katt, R.A. Cerione, Targeting amino acid metabolism for cancer therapy, *Drug Discov. Today*. 22 (2017) 796–804. doi:10.1016/j.drudis.2016.12.003.

- [102] D.R. Wise, C.B. Thompson, Glutamine addiction: a new therapeutic target in cancer, *Trends Biochem. Sci.* 35 (2010) 427–433. doi:10.1016/j.tibs.2010.05.003.
- [103] O.D.K. Maddocks, C.R. Berkers, S.M. Mason, L. Zheng, K. Blyth, E. Gottlieb, K.H. Vousden, Serine starvation induces stress and p53-dependent metabolic remodelling in cancer cells, *Nature*. 493 (2013) 542–546. doi:10.1038/nature11743.
- [104] M.D. Patil, J. Bhaumik, S. Babykutty, U.C. Banerjee, D. Fukumura, Arginine dependence of tumor cells: Targeting a chink in cancer’s armor, *Oncogene*. 35 (2016) 4957–4972. doi:10.1038/onc.2016.37.
- [105] V. Gupta, S. Bhavanasi, M. Quadir, K. Singh, G. Ghosh, K. Vasamreddy, A. Ghosh, T.J. Siahaan, S. Banerjee, S.K. Banerjee, Protein PEGylation for cancer therapy: bench to bedside, *J. Cell Commun. Signal.* (2018). doi:10.1007/s12079-018-0492-0.
- [106] J.C. Kremer, B.C. Prudner, S.E.S. Lange, G.R. Bean, M.B. Schultze, C.B. Brashears, M.D.A. Radyk, N. Redlich, S.C. Tzeng, K. Kami, L. Shelton, A. Li, Z. Morgan, J.S. Bomalaski, T. Tsukamoto, J. McConathy, L.S. Michel, J.M. Held, B.A. Van Tine, Arginine Deprivation Inhibits the Warburg Effect and Upregulates Glutamine Anaplerosis and Serine Biosynthesis in ASS1-Deficient Cancers, *Cell Rep.* 18 (2017) 991–1004. doi:10.1016/j.celrep.2016.12.077.
- [107] C. Alexandrou, S.S. Al-aqbi, J.A. Higgins, W. Boyle, A. Karmokar, C. Andreadi, J. Luo, D.A. Moore, M. Viskaduraki, M. Blades, G.I. Murray, L.M. Howells, A. Thomas, K. Brown, P.N. Cheng, A. Rufini, Sensitivity of Colorectal Cancer to Arginine Deprivation Therapy is Shaped by Differential Expression of Urea Cycle Enzymes, *Sci. Rep.* (2018) 1–14. doi:10.1038/s41598-018-30591-7.
- [108] B.J. Altman, Z.E. Stine, C. V. Dang, From Krebs to clinic: Glutamine metabolism to cancer therapy, *Nat. Rev. Cancer*. 16 (2016) 619–634. doi:10.1038/nrc.2016.71.
- [109] J.R. Mayers, M.G. Vander Heiden, Famine versus feast: Understanding the metabolism of tumors in vivo, *Trends Biochem. Sci.* 40 (2015) 130–140. doi:10.1016/j.tibs.2015.01.004.
- [110] L. Yang, S. Venneti, D. Negrath, Glutaminolysis: A Hallmark of Cancer Metabolism, *Annu. Rev. Biomed. Eng.* 19 (2017) 163–194. doi:10.1146/annurev-bioeng-071516-044546.
- [111] J. Zhang, N.N. Pavlova, C.B. Thompson, Cancer cell metabolism: the essential role of the nonessential amino acid, glutamine, *EMBO J.* 36 (2017) 1302–1315. doi:10.15252/embj.201696151.
- [112] M. Lampa, H. Arlt, T. He, B. Ospina, J. Reeves, B. Zhang, J. Murtie, G. Deng, C. Barberis, D. Hoffmann, H. Cheng, J. Pollard, C. Winter, V. Richon, C. Garcia-Escheverria, F. Adrian, D. Wiederschain, L. Srinivasan, Glutaminase is essential for the growth of triple-negative breast cancer cells with a deregulated glutamine metabolism pathway and its suppression synergizes with mTOR inhibition, *PLoS One*. 12 (2017). doi:10.1371/journal.pone.0185092.

- [113] Y.-Z. Lee, C.-W. Yang, H.-Y. Chang, H.-Y. Hsu, I.-S. Chen, H.-S. Chang, C.-H. Lee, J. Lee, C.R. Kumar, Y.-Q. Qiu, Y.-S. Chao, S.-J. Lee, Y.-Z. Lee, C.-W. Yang, H.-Y. Chang, H.-Y. Hsu, I.-S. Chen, H.-S. Chang, C.-H. Lee, J. Lee, C.R. Kumar, Y.-Q. Qiu, Y.-S. Chao, S.-J. Lee, Discovery of selective inhibitors of Glutaminase-2, which inhibit mTORC1, activate autophagy and inhibit proliferation in cancer cells, *Oncotarget*. 5 (2014) 6087–6101. doi:10.18632/oncotarget.2173.
- [114] D.R. Wise, R.J. DeBerardinis, A. Mancuso, N. Sayed, X.-Y. Zhang, H.K. Pfeiffer, I. Nissim, E. Daikhin, M. Yudkoff, S.B. McMahon, C.B. Thompson, Myc regulates a transcriptional program that stimulates mitochondrial glutaminolysis and leads to glutamine addiction, *Proc. Natl. Acad. Sci.* 105 (2008) 18782–18787. doi:10.1097/00152192-198605000-00048.
- [115] A. Halama, M. Kulinski, S.S. Dib, S.B. Zaghlool, K.S. Siveen, A. Iskandarani, J. Zierer, K.S. Prabhu, N.J. Satheesh, A.M. Bhagwat, S. Uddin, G. Kastenmüller, O. Elemento, S.S. Gross, K. Suhre, Accelerated lipid catabolism and autophagy are cancer survival mechanisms under inhibited glutaminolysis, *Cancer Lett.* 430 (2018) 133–147. doi:10.1016/j.canlet.2018.05.017.
- [116] T. Cheng, J. Sudderth, C. Yang, A.R. Mullen, E.S. Jin, J.M. Matés, R.J. DeBerardinis, Pyruvate carboxylase is required for glutamine-independent growth of tumor cells, *PNAS*. 108 (2011) 8674–8679. doi:10.1073/pnas.1016627108/-/DCSupplemental.www.pnas.org/cgi/doi/10.1073/pnas.1016627108.
- [117] M.J. Seltzer, B.D. Bennett, A.D. Joshi, P. Gao, A.G. Thomas, D. V. Ferraris, T. Tsukamoto, C.J. Rojas, B.S. Slusher, J.D. Rabinowitz, C. V. Dang, G.J. Riggins, Inhibition of glutaminase preferentially slows growth of glioma cells with mutant IDH1, *Cancer Res.* 70 (2010) 8981–8987. doi:10.1158/0008-5472.CAN-10-1666.
- [118] Y. Chendong, J. Sudderth, D. Tuyen, R.G. Bachoo, J.G. McDonald, R.J. DeBerardinis, Glioblastoma cells require glutamate dehydrogenase to survive impairments of glucose metabolism or Akt signaling, *Cancer Res.* 69 (2009) 7986–7993. doi:10.1158/0008-5472.CAN-09-2266.
- [119] M.W. Lee, S.C. Park, Y.G. Yang, S.O. Yim, H.S. Chae, J.H. Bach, H.J. Lee, K.Y. Kim, W.B. Lee, S.S. Kim, The involvement of reactive oxygen species (ROS) and p38 mitogen-activated protein (MAP) kinase in TRAIL/Apo2L-induced apoptosis., *FEBS Lett.* 512 (2002) 313–8. doi:10.1016/S0014-5793(02)02225-1.
- [120] E. Giannoni, F. Buricchi, G. Raugei, G. Ramponi, P. Chiarugi, Intracellular Reactive Oxygen Species Activate Src Tyrosine Kinase during Cell Adhesion and Anchorage-Dependent Cell Growth Intracellular, *Mol. Cell. Biol.* 25 (2005) 6391–64033. doi:10.1128/MCB.25.15.6391.
- [121] P. Gao, H. Zhang, R. Dinavahi, F. Li, Y. Xiang, V. Raman, Z.M. Bhujwalla, D.W. Felsher, L. Cheng, J. Pevsner, L.A. Lee, G.L. Semenza, C. V. Dang, HIF-Dependent Antitumorigenic Effect of Antioxidants In Vivo, *Cancer Cell.* 12 (2007) 230–238. doi:10.1016/j.ccr.2007.08.004.
- [122] C. Garrido, L. Galluzzi, M. Brunet, P.E. Puig, C. Didelot, G. Kroemer, Mechanisms of cytochrome c release from mitochondria, *Cell Death Differ.* 13 (2006) 1423–

1433. doi:10.1038/sj.cdd.4401950.
- [123] A. Tubbs, A. Nussenzweig, Endogenous DNA Damage as a Source of Genomic Instability in Cancer, *Cell*. 168 (2017) 644–656. doi:10.1016/j.cell.2017.01.002.
- [124] L.B. Sullivan, N.S. Chandel, Mitochondrial reactive oxygen species and cancer, *Cancer Metab.* 2 (2014) 1–12. doi:10.1186/2049-3002-2-17.
- [125] P.E. Porporato, V.L. Payen, J. Pérez-Escuredo, C.J. De Saedeleer, P. Danhier, T. Copetti, S. Dhup, M. Tardy, T. Vazeille, C. Bouzin, O. Feron, C. Michiels, B. Gallez, P. Sonveaux, A mitochondrial switch promotes tumor metastasis, *Cell Rep.* 8 (2014) 754–766. doi:10.1016/j.celrep.2014.06.043.
- [126] K.C. Patra, N. Hay, The pentose phosphate pathway and cancer, *Trends Biochem. Sci.* 39 (2014) 347–354. doi:10.1016/j.tibs.2014.06.005.
- [127] L.G. Boros, J. Puigjaner, M. Cascante, W.N.P. Lee, J.L. Brandes, S. Bassilian, F.I. Yusuf, R.D. Williams, P. Muscarella, W.S. Melvin, W.J. Schirmer, Oxythiamine and dehydroepiandrosterone inhibit the nonoxidative synthesis of ribose and tumor cell proliferation, *Cancer Res.* 57 (1997) 4242–4248. doi:10.1158/0008-5472.can-09-4615.
- [128] S. Langbein, M. Zerilli, A. Zur Hausen, W. Staiger, K. Rensch-Boschert, N. Lukan, J. Popa, M.P. Ternullo, A. Steidler, C. Weiss, R. Grobholz, F. Willeke, P. Alken, G. Stassi, P. Schubert, J.F. Coy, Expression of transketolase TKTL1 predicts colon and urothelial cancer patient survival: Warburg effect reinterpreted, *Br. J. Cancer.* 94 (2006) 578–585. doi:10.1038/sj.bjc.6602962.
- [129] L.E. Meshalkina, V.L. Drutsa, O.N. Koroleva, O.N. Solovjeva, G.A. Kochetov, Is transketolase-like protein, TKTL1, transketolase?, *Biochim. Biophys. Acta - Mol. Basis Dis.* 1832 (2013) 387–390. doi:10.1016/j.bbadis.2012.12.004.
- [130] J.M. Corbin, M.J. Ruiz-Echevarría, One-carbon metabolism in prostate cancer: The role of androgen signaling, *Int. J. Mol. Sci.* 17 (2016). doi:10.3390/ijms17081208.
- [131] G.S. Ducker, J.D. Rabinowitz, One-Carbon Metabolism in Health and Disease, *Cell Metab.* 25 (2017) 27–42. doi:10.1016/j.cmet.2016.08.009.
- [132] Y. Sato, S. Matsuda, A. Maruyama, J. Nakayama, T. Miyashita, H. Udagawa, S. Umemura, K. Yanagihara, A. Ochiai, M. Tomita, T. Soga, K. Tsuchihara, H. Makinoshima, Metabolic characterization of antifolate responsiveness and nonresponsiveness in malignant pleural mesothelioma cells, *Front. Pharmacol.* 9 (2018) 1–12. doi:10.3389/fphar.2018.01129.
- [133] N. Fleeman, A. Bagust, C. McLeod, J. Greenhalgh, A. Boland, Y. Dundar, R. Dickson, C. Tudur Smith, H. Davis, J. Green, M. Pearson, Pemetrexed for the first-line treatment of locally advanced or metastatic non-small cell lung cancer., *Health Technol. Assess.* 14 Suppl 1 (2010) 47–53. doi:10.3310/hta14Suppl1/07.
- [134] A.E. Pegg, Functions of polyamines in mammals, *J. Biol. Chem.* 291 (2016) 14904–14912. doi:10.1074/jbc.R116.731661.
- [135] N. Burrows, G. Cane, M. Robson, E. Gaude, W.J. Howat, P.W. Szlosarek, R.B.

- Pedley, C. Frezza, M. Ashcroft, P.H. Maxwell, Hypoxia-induced nitric oxide production and tumour perfusion is inhibited by pegylated arginine deiminase (ADI-PEG20), *Sci. Rep.* 6 (2016) 1–14. doi:10.1038/srep22950.
- [136] A.E. Yuzhalin, Citrullination in Cancer, *Cancer Res.* 79 (2019) 1274–1284. doi:10.1158/0008-5472.CAN-18-2797.
- [137] K. Ohshima, S. Nojima, S. Tahara, M. Kurashige, Y. Hori, K. Hagiwara, D. Okuzaki, S. Oki, N. Wada, J.I. Ikeda, Y. Kanai, E. Morii, Argininosuccinate Synthase 1-Deficiency Enhances the Cell Sensitivity to Arginine through Decreased DEPTOR Expression in Endometrial Cancer, *Sci. Rep.* 7 (2017) 1–14. doi:10.1038/srep45504.
- [138] A. Thongkum, C. Wu, Y.Y. Li, M. Wangpaichitr, P. Navasumrit, V. Parnlob, T. Sricharunrat, V. Bhudhisawasdi, M. Ruchirawat, N. Savaraj, The combination of arginine deprivation and 5-fluorouracil improves therapeutic efficacy in argininosuccinate synthetase negative hepatocellular carcinoma, *Int. J. Mol. Sci.* 18 (2017). doi:10.3390/ijms18061175.
- [139] Y. Long, W. Bin Tsai, D. Wang, D.H. Hawke, N. Savaraj, L.G. Feun, M.C. Hung, H.H.W. Chen, M.T. Kuo, Argininosuccinate synthetase 1 (ASS1) is a common metabolic marker of chemosensitivity for targeted arginine- and glutamine-starvation therapy, *Cancer Lett.* 388 (2017) 54–63. doi:10.1016/j.canlet.2016.11.028.
- [140] J. Adam, M. Yang, C. Bauerschmidt, M. Kitagawa, L. O’Flaherty, P. Maheswaran, G. Özkan, N. Sahgal, D. Baban, K. Kato, K. Saito, K. Iino, K. Igarashi, M. Stratford, C. Pugh, D.A. Tennant, C. Ludwig, B. Davies, P.J. Ratcliffe, M. El-Bahrawy, H. Ashrafian, T. Soga, P.J. Pollard, A Role for Cytosolic Fumarate Hydratase in Urea Cycle Metabolism and Renal Neoplasia, *Cell Rep.* 3 (2013) 1440–1448. doi:10.1016/j.celrep.2013.04.006.
- [141] L.A. Bateman, W.M. Ku, M.J. Heslin, C.M. Contreras, C.F. Skibola, D.K. Nomura, Argininosuccinate Synthase 1 is a Metabolic Regulator of Colorectal Cancer Pathogenicity, *ACS Chem. Biol.* 12 (2017) 905–911. doi:10.1021/acscchembio.6b01158.
- [142] J.B. Spinelli, H. Yoon, A.E. Ringel, S. Jeanfavre, C.B. Clish, M.C. Haigis, Metabolic recycling of ammonia via glutamate dehydrogenase supports breast cancer biomass, *Science* (80-.). 358 (2017) 941–946.
- [143] L. Jin, G.N. Alesi, S. Kang, Glutaminolysis as a target for cancer therapy, *Oncogene.* 35 (2016) 3619–3625. doi:10.1038/onc.2015.447.
- [144] K. Soda, The mechanisms by which polyamines accelerate tumor spread, *J. Exp. Clin. Cancer Res.* 30 (2011) 1–9. doi:10.1186/1756-9966-30-95.
- [145] L. Miller-Fleming, V. Olin-Sandoval, K. Campbell, M. Ralser, Remaining Mysteries of Molecular Biology: The Role of Polyamines in the Cell, *J. Mol. Biol.* 427 (2015) 3389–3406. doi:10.1016/j.jmb.2015.06.020.
- [146] E. Sandsmark, A.F. Hansen, K.M. Selnaes, H. Bertilsson, A.M. Bofin, A.J. Wright, T.

- Viset, E. Richardsen, F. Drabløs, T.F. Bathen, M.-B. Tessem, M.B. Rye, A novel non-canonical Wnt signature for prostate cancer aggressiveness., *Oncotarget*. 8 (2017) 9572–9586. doi:10.18632/oncotarget.14161.
- [147] G.F. Giskeødegård, H. Bertilsson, K.M. Selnes, A.J. Wright, T.F. Bathen, T. Viset, J. Halgunset, A. Angelsen, I.S. Gribbestad, M.B. Tessem, Spermine and Citrate as Metabolic Biomarkers for Assessing Prostate Cancer Aggressiveness, *PLoS One*. 8 (2013) 1–9. doi:10.1371/journal.pone.0062375.
- [148] N.J. Serkova, E.J. Gamito, R.H. Jones, C. O'Donnell, J.L. Brown, S. Green, H. Sullivan, T. Hedlund, E.D. Crawford, The metabolites citrate, myo-inositol, and spermine are potential age-independent markers of prostate cancer in human expressed prostatic secretions, *Prostate*. 68 (2008) 620–628. doi:10.1002/pros.20727.
- [149] T.H. Tsoi, C.F. Chan, W.L. Chan, K.F. Chiu, W.T. Wong, C.F. Ng, K.L. Wong, Urinary polyamines: A pilot study on their roles as prostate cancer detection biomarkers, *PLoS One*. 11 (2016) 1–13. doi:10.1371/journal.pone.0162217.
- [150] A. Shukla-Dave, M. Castillo-Martin, M. Chen, J. Lobo, N. Gladoun, A. Collazo-Lorduy, F.M. Khan, V. Ponomarev, Z. Yi, W. Zhang, P.P. Pandolfi, H. Hricak, C. Cordon-Cardo, Ornithine Decarboxylase Is Sufficient for Prostate Tumorigenesis via Androgen Receptor Signaling, *Am. J. Pathol.* 186 (2016) 3131–3145. doi:10.1016/j.ajpath.2016.08.021.
- [151] T.G.O. O'Brien, L.C. Megosh, G. Gilliard, G.O. Brien, C. Megosh, Ornithine Decarboxylase Overexpression Is a Sufficient Condition for Tumor Promotion in Mouse Skin, *Cancer Res*. 57 (1997) 2630–2637.
- [152] W. He, E. Roh, K. Yao, K. Liu, X. Meng, F. Liu, P. Wang, A.M. Bode, Z. Dong, Targeting ornithine decarboxylase (ODC) inhibits esophageal squamous cell carcinoma progression, *Npj Precis. Oncol.* 1 (2017) 13. doi:10.1038/s41698-017-0014-1.
- [153] W.E.I. Wang, C. Xu, G. Hou, Y. Chen, J. Xin, X. Liu, Downregulation of tumstatin expression by overexpression of ornithine decarboxylase, (2013) 2042–2048. doi:10.3892/or.2013.2708.
- [154] C. Bello-fernandez, G. Packham, J.L. Cleveland, The ornithine decarboxylase gene is a transcriptional target of c-Myc, 90 (1993) 7804–7808.
- [155] S. Beloribi-Djefafli, S. Vasseur, F. Guillaumond, Lipid metabolic reprogramming in cancer cells, *Oncogenesis*. 5 (2016) e189. doi:10.1038/oncsis.2015.49.
- [156] S. Yue, J. Li, S.Y. Lee, H.J. Lee, T. Shao, B. Song, L. Cheng, T.A. Masterson, X. Liu, T.L. Ratliff, J.X. Cheng, Cholesteryl ester accumulation induced by PTEN loss and PI3K/AKT activation underlies human prostate cancer aggressiveness, *Cell Metab.* 19 (2014) 393–406. doi:10.1016/j.cmet.2014.01.019.
- [157] I. Marín de Mas, E. Aguilar, E. Zodda, C. Balcells, S. Marin, G. Dallmann, T.M. Thomson, B. Papp, M. Cascante, Model-driven discovery of long-chain fatty acid metabolic reprogramming in heterogeneous prostate cancer cells, *PLoS Comput. Biol.* 14 (2018) 1–20. doi:10.1371/journal.pcbi.1005914.

- [158] A. Mukherjee, H.A. Kenny, E. Lengyel, Unsaturated Fatty Acids Maintain Cancer Cell Stemness, *Cell Stem Cell*. 20 (2017) 291–292. doi:10.1016/j.stem.2017.02.008.
- [159] A. Dueregger, B. Schöpf, T. Eder, J. Höfer, E. Gnaiger, A. Aufinger, L. Kenner, B. Perktold, R. Ramoner, H. Klocker, I.E. Eder, Differential Utilization of Dietary Fatty Acids in Benign and Malignant Cells of the Prostate, *PLoS One*. 10 (2015) e0135704. doi:10.1371/journal.pone.0135704.
- [160] M. Knobloch, G.A. Pilz, B. Ghesquière, W.J. Kovacs, T. Wegleiter, D.L. Moore, M. Hruzova, N. Zamboni, P. Carmeliet, S. Jessberger, A Fatty Acid Oxidation-Dependent Metabolic Shift Regulates Adult Neural Stem Cell Activity, *Cell Rep.* (2017). doi:10.1016/j.celrep.2017.08.029.
- [161] C.L. Chen, D.B. Uthaya Kumar, V. Punj, J. Xu, L. Sher, S.M. Tahara, S. Hess, K. Machida, NANOG Metabolically Reprograms Tumor-Initiating Stem-like Cells through Tumorigenic Changes in Oxidative Phosphorylation and Fatty Acid Metabolism, *Cell Metab.* 23 (2016) 206–219. doi:10.1016/j.cmet.2015.12.004.
- [162] S.M. Jeon, Regulation and function of AMPK in physiology and diseases, *Exp. Mol. Med.* 48 (2016) e245. doi:10.1038/emm.2016.81.
- [163] C.S. McCoin, T.A. Knotts, S.H. Adams, Acylcarnitines—old actors auditioning for new roles in metabolic physiology, *Nat. Rev. Endocrinol.* 11 (2015) 617–625. doi:10.1038/nrendo.2015.129.
- [164] A.Y. Sierra, E. Gratacós, P. Carrasco, J. Clotet, J. Ureña, D. Serra, G. Asins, F.G. Hegardt, N. Casals, CPT1c is localized in endoplasmic reticulum of neurons and has carnitine palmitoyltransferase activity, *J. Biol. Chem.* 283 (2008) 6878–6885. doi:10.1074/jbc.M707965200.
- [165] X. Roa-Mansergas, R. Fadó, M. Atari, J.F. Mir, H. Muley, D. Serra, N. Casals, CPT1C promotes human mesenchymal stem cells survival under glucose deprivation through the modulation of autophagy, *Sci. Rep.* 8 (2018) 1–13. doi:10.1038/s41598-018-25485-7.
- [166] Y.A. Hannun, L.M. Obeid, Principles of bioactive lipid signalling: Lessons from sphingolipids, *Nat. Rev. Mol. Cell Biol.* 9 (2008) 139–150. doi:10.1038/nrm2329.
- [167] B. Ogretmen, Sphingolipid metabolism in cancer signalling and therapy, *Nat. Rev. Cancer.* 18 (2017) 33–50. doi:10.1038/nrc.2017.96.
- [168] J.P. Thiery, H. Acloque, R.Y.J. Huang, M.A. Nieto, Epithelial-Mesenchymal Transitions in Development and Disease, *Cell*. 139 (2009) 871–890. doi:10.1016/j.cell.2009.11.007.
- [169] M.A. Nieto, R.Y.Y.J. Huang, R.A.A. Jackson, J.P.P. Thiery, EMT: 2016, *Cell*. 166 (2016) 21–45. doi:10.1016/j.cell.2016.06.028.
- [170] C. Hadjimichael, K. Chanoumidou, N. Papadopoulou, P. Arampatzi, J. Papamatheakis, A. Kretsovali, Common stemness regulators of embryonic and cancer stem cells, *World J Stem Cells*. 7 (2015) 1150–1184. doi:10.4252/wjsc.v7.i9.1150.

- [171] T. Shibue, R.A. Weinberg, EMT, CSCs, and drug resistance: The mechanistic link and clinical implications, *Nat. Rev. Clin. Oncol.* 14 (2017) 611–629. doi:10.1038/nrclinonc.2017.44.
- [172] R. Sato, T. Semba, H. Saya, Concise Review: Stem Cells and Epithelial-Mesenchymal Transition in Cancer: Biological Implications and Therapeutic Targets, *Stem Cells*. 34 (2016) 1997–2007. doi:10.1002/stem.2406.
- [173] B. Bierie, S.E. Pierce, C. Kroeger, D.G. Stover, D.R. Pattabiraman, P. Thiru, J. Liu Donaher, F. Reinhardt, C.L. Chaffer, Z. Keckesova, R.A. Weinberg, Integrin- β 4 identifies cancer stem cell-enriched populations of partially mesenchymal carcinoma cells, *Proc. Natl. Acad. Sci.* 114 (2017) E2337–E2346. doi:10.1073/pnas.1618298114.
- [174] A. Grosse-Wilde, A.F. D’Hérouël, E. McIntosh, G. Ertaylan, A. Skupin, R.E. Kuestner, A. Del Sol, K.A. Walters, S. Huang, Stemness of the hybrid epithelial/mesenchymal state in breast cancer and its association with poor survival, *PLoS One*. 10 (2015) 1–28. doi:10.1371/journal.pone.0126522.
- [175] T. Celià-terrassa, Ó. Meca-cortés, F. Mateo, A.M. De Paz, N. Rubio, A. Arnal-estapé, B.J. Ell, R. Bermudo, A. Díaz, M. Guerra-rebollo, J.J. Lozano, C. Estarás, C. Ulloa, D. Álvarez-simón, J. Milà, R. Vilella, R. Paciucci, M. Martínez-balbás, A.G. De Herreros, R.R. Gomis, Y. Kang, Epithelial-mesenchymal transition can suppress major attributes of human epithelial tumor-initiating cells, *J. Clin. Invest.* 122 (2012) 1849–1868. doi:10.1172/JCI59218.itly.
- [176] J. Stingl, P. Eirew, I. Ricketson, M. Shackleton, F. Vaillant, D. Choi, H.I. Li, C.J. Eaves, Purification and unique properties of mammary epithelial stem cells, *Nature*. 439 (2006) 993–997. doi:10.1038/nature04496.
- [177] G.G. Jinesh, G.C. Manyam, C.O. Mmeje, K.A. Baggerly, A.M. Kamat, Surface PD-L1, E-cadherin, CD24, and VEGFR2 as markers of epithelial cancer stem cells associated with rapid tumorigenesis, *Sci. Rep.* 7 (2017) 1–12. doi:10.1038/s41598-017-08796-z.
- [178] W.J. Nelson, Remodeling epithelial cell organization: transitions between front-rear and apical-basal polarity., *Cold Spring Harb. Perspect. Biol.* 1 (2009) a000513. doi:10.1101/cshperspect.a000513.
- [179] M. Singh, N. Yelle, C. Venugopal, S.K. Singh, EMT: Mechanisms and therapeutic implications, *Pharmacol. Ther.* 182 (2018) 80–94. doi:10.1016/j.pharmthera.2017.08.009.
- [180] Y. Wang, J. Shi, K. Chai, X. Ying, B. Zhou, The Role of Snail in EMT and Tumorigenesis, *Curr. Cancer Drug Targets*. 13 (2013) 963–972. doi:10.2174/15680096113136660102.
- [181] M.H. Yang, D.S.S. Hsu, H.J.H.W. Wang, H.J.H.W. Wang, H.Y. Lan, W.H. Yang, C.H. Huang, S.Y. Kao, C.H. Tzeng, S.K. Tai, S.Y. Chang, O.K.S. Lee, K.J. Wu, Bmi1 is essential in Twist1-induced epithelial-mesenchymal transition, *Nat. Cell Biol.* 12 (2010) 982–992. doi:10.1038/ncb2099.

- [182] S.X. Li MZ, Wang JJ, Yang SB, Li WF, Xiao LB, He YL, ZEB2 promotes tumor metastasis and correlates with poor prognosis of human colorectal cancer., *Am J Transl Res.* 9(6)2838-2851. 9 (2017) 2838–2851.
- [183] E.T. Wiles, R. Bell, D. Thomas, M. Beckerle, S.L. Lessnick, ZEB2 Represses the Epithelial Phenotype and Facilitates Metastasis in Ewing Sarcoma, *Genes and Cancer.* 4 (2013) 486–500. doi:10.1177/1947601913506115.
- [184] A. Bonnomet, L. Syne, A. Brysse, E. Feyereisen, E.W. Thompson, A. Noël, J.M. Foidart, P. Birembaut, M. Polette, C. Gilles, A dynamic in vivo model of epithelial-to-mesenchymal transitions in circulating tumor cells and metastases of breast cancer, *Oncogene.* 31 (2012) 3741–3753. doi:10.1038/onc.2011.540.
- [185] V.B. Sampson, J.M. David, I. Puig, P.U. Patil, A.G. de Herreros, G. V Thomas, A.K. Rajasekaran, Wilms' tumor protein induces an epithelial-mesenchymal hybrid differentiation state in clear cell renal cell carcinoma., *PLoS One.* 9 (2014) e102041. doi:10.1371/journal.pone.0102041.
- [186] P. Friedl, J. Locker, E. Sahai, J.E. Segall, Classifying collective cancer cell invasion, *Nat. Cell Biol.* 14 (2012) 777–783. doi:10.1038/ncb2548.
- [187] D.R. Bielenberg, B.R. Zetter, The Contribution of Angiogenesis to the Process of Metastasis, *Cancer J.* 21 (2015) 267–273. doi:10.1097/PPO.0000000000000138.
- [188] B. Thakur, P. Ray, Cisplatin triggers cancer stem cell enrichment in platinum-resistant cells through NF- κ B-TNF α -PIK3CA loop, *J. Exp. Clin. Cancer Res.* 36 (2017) 1–14. doi:10.1186/s13046-017-0636-8.
- [189] S. Bao, Q. Wu, R.E. McLendon, Y. Hao, Q. Shi, A.B. Hjelmeland, M.W. Dewhirst, D.D. Bigner, J.N. Rich, Glioma stem cells promote radioresistance by preferential activation of the DNA damage response, *Nature.* 444 (2006) 756–760. doi:10.1038/nature05236.
- [190] M.F. Clarke, J.E. Dick, P.B. Dirks, C.J. Eaves, C.H.M. Jamieson, D.L. Jones, J. Visvader, I.L. Weissman, G.M. Wahl, Cancer stem cells - Perspectives on current status and future directions: AACR workshop on cancer stem cells, *Cancer Res.* 66 (2006) 9339–9344. doi:10.1158/0008-5472.CAN-06-3126.
- [191] P.B. Gupta, C.M. Fillmore, G. Jiang, S.D. Shapira, K. Tao, C. Kuperwasser, E.S. Lander, Stochastic state transitions give rise to phenotypic equilibrium in populations of cancer cells, *Cell.* 146 (2011) 633–644. doi:10.1016/j.cell.2011.07.026.
- [192] Y. Song, Y. Wang, C. Tong, H. Xi, X. Zhao, Y. Wang, L. Chen, A unified model of the hierarchical and stochastic theories of gastric cancer, *Br. J. Cancer.* 116 (2017) 973–989. doi:10.1038/bjc.2017.54.
- [193] W. Wang, Y. Quan, Q. Fu, Y. Liu, Y. Liang, J. Wu, G. Yang, C. Luo, Q. Ouyang, Y. Wang, Dynamics between cancer cell subpopulations reveals a model coordinating with both hierarchical and stochastic concepts, *PLoS One.* 9 (2014) 1–9. doi:10.1371/journal.pone.0084654.
- [194] T. Chanmee, P. Ontong, K. Kimata, N. Itano, Key Roles of Hyaluronan and Its CD44

- Receptor in the Stemness and Survival of Cancer Stem Cells, *Front. Oncol.* 5 (2015) 1–11. doi:10.3389/fonc.2015.00180.
- [195] S. Zhang, C. Balch, M.W. Chan, H.C. Lai, D. Matei, J.M. Schilder, P.S. Yan, T.H.M. Huang, K.P. Nephew, Identification and characterization of ovarian cancer-initiating cells from primary human tumors, *Cancer Res.* 68 (2008) 4311–4320. doi:10.1158/0008-5472.CAN-08-0364.
- [196] J.M. Stewart, P. a Shaw, C. Gedye, M.Q. Bernardini, B.G. Neel, L.E. Ailles, Phenotypic heterogeneity and instability of human ovarian tumor-initiating cells, *PNAS.* 108 (2011) 6468–6473. doi:10.1073/pnas.1005529108/-/DCSupplemental.www.pnas.org/cgi/doi/10.1073/pnas.1005529108.
- [197] P.B. Singh, Sheila K.; Clarke, Ian D.; Terasaki, Mizuhiko; Bonn, Victoria E.; Hawkins, Cynthia; Squire, Jeremy; Dirka, Identification of a cancer stem cell in human brain tumors, *Cancer Res.* 63 (2003) 5821–5828.
- [198] J. Wang, P. Sakariassen, O. Tsinkalovsky, H. Immervoll, S.O. Bøe, A. Svendsen, L. Prestegarden, G. Røslund, F. Thorsen, L. Stuhr, A. Molven, R. Bjerkvig, P. Enger, CD133 negative glioma cells form tumors in nude rats and give rise to CD133 positive cells, *Int. J. Cancer.* 122 (2008) 761–768. doi:10.1002/ijc.23130.
- [199] H. Tomita, K. Tanaka, T. Tanaka, A. Hara, Aldehyde dehydrogenase 1A1 in stem cells and cancer, *Oncotarget.* 7 (2016). doi:10.18632/oncotarget.6920.
- [200] T. Li, Y. Su, Y. Mei, Q. Leng, B. Leng, Z. Liu, S.A. Stass, F. Jiang, ALDH1A1 is a marker for malignant prostate stem cells and predictor of prostate cancer patients outcome, *Lab. Investig.* 90 (2010) 234–244. doi:10.1038/labinvest.2009.127.
- [201] X. Yin, B.H. Zhang, S.S. Zheng, D.M. Gao, S.J. Qiu, W.Z. Wu, Z.G. Ren, Coexpression of gene Oct4 and Nanog initiates stem cell characteristics in hepatocellular carcinoma and promotes epithelial-mesenchymal transition through activation of Stat3/Snail signaling, *J. Hematol. Oncol.* 8 (2015) 1–13. doi:10.1186/s13045-015-0119-3.
- [202] W.S. Song, Y.P. Yang, C.S. Huang, K.H. Lu, W.H. Liu, W.W. Wu, Y.Y. Lee, W.L. Lo, S.D. Lee, Y.W. Chen, P.I. Huang, M.T. Chen, Sox2, a stemness gene, regulates tumor-initiating and drug-resistant properties in CD133-positive glioblastoma stem cells, *J. Chinese Med. Assoc.* 79 (2016) 538–545. doi:10.1016/j.jcma.2016.03.010.
- [203] S. Shaheen, M. Ahmed, F. Lorenzi, A.S. Nateri, Spheroid-Formation (Colonsphere) Assay for in Vitro Assessment and Expansion of Stem Cells in Colon Cancer, *Stem Cell Rev. Reports.* 12 (2016) 492–499. doi:10.1007/s12015-016-9664-6.
- [204] H. Akita, J.U. Marquardt, M.E. Durkin, M. Kitade, D. Seo, E.A. Conner, J.B. Andersen, V.M. Factor, S.S. Thorgeirsson, MYC activates stem-like cell potential in hepatocarcinoma by a p53-dependent mechanism, *Cancer Res.* 74 (2014) 5903–5913. doi:10.1158/0008-5472.CAN-14-0527.
- [205] F. Yu, J. Li, H. Chen, J. Fu, S. Ray, S. Huang, H. Zheng, W. Ai, Kruppel-like factor 4

- (KLF4) is required for maintenance of breast cancer stem cells and for cell migration and invasion, *Oncogene*. 30 (2011) 2161–2172. doi:10.1038/onc.2010.591.
- [206] R. Bhattacharya, S. Banerjee Mustafi, M. Street, A. Dey, S.K.D. Dwivedi, Bmi-1: At the crossroads of physiological and pathological biology, *Genes Dis.* 2 (2015) 225–239. doi:10.1016/j.gendis.2015.04.001.
- [207] S. Geng, Y. Guo, Q. Wang, L. Li, J. Wang, Cancer stem-like cells enriched with CD29 and CD44 markers exhibit molecular characteristics with epithelial-mesenchymal transition in squamous cell carcinoma, *Arch. Dermatol. Res.* 305 (2013) 35–47. doi:10.1007/s00403-012-1260-2.
- [208] G.J. Klarmann, E.M. Hurt, L.A. Mathews, X. Zhang, M.A. Duhagon, T. Mistree, S.B. Thomas, W.L. Farrar, Invasive prostate cancer cells are tumor initiating cells that have a stem cell-like genomic signature, *Clin. Exp. Metastasis*. 26 (2009) 433–446. doi:10.1007/s10585-009-9242-2.
- [209] A.H.K. Cheung, D.N. Iyer, C.S.C. Lam, L. Ng, S.K.M. Wong, H.S. Lee, T. Wan, J. Man, A.K.M. Chow, R.T. Poon, R. Pang, W.L. Law, Emergence of CD26+ cancer stem cells with metastatic properties in colorectal carcinogenesis, *Int. J. Mol. Sci.* 18 (2017). doi:10.3390/ijms18061106.
- [210] W. Guo, Z. Keckesova, J.L. Donaher, T. Shibue, V. Tischler, F. Reinhardt, S. Itzkovitz, A. Noske, U. Zürrer-Härdis, G. Bell, W.L. Tam, S.A. Mani, A. van Oudenaarden, R.A. Weinberg, Slug and Sox9 Cooperatively Determine the Mammary Stem Cell State, *Cell*. 148 (2012) 1015–1028. doi:10.1016/j.cell.2012.02.008.
- [211] A.P. Morel, M. Lièvre, C. Thomas, G. Hinkal, S. Ansieau, A. Puisieux, Generation of breast cancer stem cells through epithelial-mesenchymal transition, *PLoS One*. 3 (2008) 1–7. doi:10.1371/journal.pone.0002888.
- [212] S.A. Mani, W. Guo, M.J. Liao, E.N. Eaton, A. Ayyanan, A.Y. Zhou, M. Brooks, F. Reinhard, C.C. Zhang, M. Shipitsin, L.L. Campbell, K. Polyak, C. Brisken, J. Yang, R.A. Weinberg, The Epithelial-Mesenchymal Transition Generates Cells with Properties of Stem Cells, *Cell*. 133 (2008) 704–715. doi:10.1016/j.cell.2008.03.027.
- [213] I. Ota, T. Masui, M. Kurihara, J.I. Yook, S. Mikami, T. Kimura, K. Shimada, N. Konishi, K. Yane, T. Yamanaka, T. Kitahara, Snail-induced EMT promotes cancer stem cell-like properties in head and neck cancer cells, *Oncol. Rep.* 35 (2016) 261–266. doi:10.3892/or.2015.4348.
- [214] F. Fan, S. Samuel, K.W. Evans, J. Lu, L. Xia, Y. Zhou, E. Sceusi, F. Tozzi, X.-C. Ye, S.A. Mani, L.M. Ellis, Overexpression of Snail induces epithelial-mesenchymal transition and a cancer stem cell-like phenotype in human colorectal cancer cells, *Cancer Med.* 1 (2012) 5–16. doi:10.1002/cam4.4.
- [215] L.F. Zhu, Y. Hu, C.C. Yang, X.H. Xu, T.Y. Ning, Z.L. Wang, J.H. Ye, L.K. Liu, Snail overexpression induces an epithelial to mesenchymal transition and cancer stem cell-like properties in SCC9 cells, *Lab. Investig.* 92 (2012) 744–752. doi:10.1038/labinvest.2012.8.

- [216] M.A. Nieto, Epithelial plasticity: A common theme in embryonic and cancer cells, *Science* (80-.). 342 (2013). doi:10.1126/science.1234850.
- [217] U. Wellner, J. Schubert, U.C. Burk, O. Schmalhofer, F. Zhu, A. Sonntag, B. Waldvogel, C. Vannier, D. Darling, A. Hausen, V.G. Brunton, J. Morton, O. Sansom, J. Schöler, M.P. Stemmler, C. Herzberger, U. Hopt, T. Keck, The EMT-activator ZEB1 promotes tumorigenicity by repressing stemness-inhibiting microRNAs, *Nat. Cell Biol.* 11 (2009) 1487–1495. doi:10.1038/ncb1998.
- [218] V.J. Guen, T.E. Chavarria, C. Kröger, X. Ye, R.A. Weinberg, J.A. Lees, EMT programs promote basal mammary stem cell and tumor-initiating cell stemness by inducing primary ciliogenesis and Hedgehog signaling, *Proc. Natl. Acad. Sci.* 114 (2017) E10532–E10539. doi:10.1073/pnas.1711534114.
- [219] M.P. Stemmler, R.L. Eccles, S. Brabletz, T. Brabletz, Non-redundant functions of EMT transcription factors, *Nat. Cell Biol.* 21 (2019) 102–112. doi:10.1038/s41556-018-0196-y.
- [220] X. Ye, W.L. Tam, T. Shibue, Y. Kaygusuz, F. Reinhardt, E. Ng Eaton, R.A. Weinberg, Distinct EMT programs control normal mammary stem cells and tumour-initiating cells., *Nature.* 525 (2015) 256–60. doi:10.1038/nature14897.
- [221] T. Oskarsson, E. Batlle, J. Massagué, Metastatic Stem Cells: Sources, Niches, and Vital Pathways, *Cell Stem Cell.* 14 (2014) 306–321. doi:10.1016/j.stem.2014.02.002.
- [222] T.M. Thomson, C. Balcells, M. Cascante, Metabolic Plasticity and Epithelial-Mesenchymal Transition, *J. Clin. Med.* 8 (2019) 1–24.
- [223] E. Gonçalves, M. Sciacovelli, A.S.H. Costa, M.G.B. Tran, T.I. Johnson, D. Machado, C. Frezza, J. Saez-Rodriguez, Post-translational regulation of metabolism in fumarate hydratase deficient cancer cells., *Metab. Eng.* 45 (2018) 149–157. doi:10.1016/j.ymben.2017.11.011.
- [224] A. Hamabe, M. Konno, N. Tanuma, H. Shima, K. Tsunekuni, K. Kawamoto, N. Nishida, J. Koseki, K. Mimori, N. Gotoh, H. Yamamoto, Y. Doki, M. Mori, H. Ishii, Role of pyruvate kinase M2 in transcriptional regulation leading to epithelial-mesenchymal transition, *Proc. Natl. Acad. Sci.* 111 (2014) 15526–15531. doi:10.1073/pnas.1407717111.
- [225] T. Murai, The role of lipid rafts in cancer cell adhesion and migration, *Int. J. Cell Biol.* 2012 (2012). doi:10.1155/2012/763283.
- [226] X. Luo, C. Cheng, Z. Tan, N. Li, M. Tang, L. Yang, Y. Cao, Emerging roles of lipid metabolism in cancer metastasis, *Mol. Cancer.* 16 (2017) 1–10. doi:10.1186/s12943-017-0646-3.
- [227] K.S. Lucenay, I. Doostan, C. Karakas, T. Bui, Z. Ding, G.B. Mills, K.K. Hunt, K. Keyomarsi, Cyclin e associates with the lipogenic enzyme ATP-citrate lyase to enable malignant growth of breast cancer cells, *Cancer Res.* 76 (2016) 2406–2418. doi:10.1158/0008-5472.CAN-15-1646.
- [228] L. Jiang, H. Wang, J. Li, X. Fang, H. Pan, X. Yuan, P. Zhang, Up-regulated FASN

- expression promotes transcoelomic metastasis of ovarian cancer cell through epithelial-mesenchymal transition, *Int. J. Mol. Sci.* 15 (2014) 11539–11554. doi:10.3390/ijms150711539.
- [229] J. Li, L. Dong, D. Wei, X. Wang, S. Zhang, H. Li, Fatty acid synthase mediates the epithelial-mesenchymal transition of breast cancer cells, *Int. J. Biol. Sci.* 10 (2014) 171–180. doi:10.7150/ijbs.7357.
- [230] H. Wang, Q. Xi, G. Wu, Fatty acid synthase regulates invasion and metastasis of colorectal cancer via Wnt signaling pathway, *Cancer Med.* 5 (2016) 1599–1606. doi:10.1002/cam4.711.
- [231] Z.T. Schafer, A.R. Grassian, L. Song, Z. Jiang, Z. Gerhart-Hines, H.Y. Irie, S. Gao, P. Puigserver, J.S. Brugge, Antioxidant and oncogene rescue of metabolic defects caused by loss of matrix attachment, *Nature.* 461 (2009) 109–113. doi:10.1038/nature08268.
- [232] G.F. Weber, Metabolism in cancer metastasis, *Int. J. Cancer.* 138 (2016) 2061–2066. doi:10.1002/ijc.29839.
- [233] P. Paoli, E. Giannoni, P. Chiarugi, Anoikis molecular pathways and its role in cancer progression, *Biochim. Biophys. Acta - Mol. Cell Res.* 1833 (2013) 3481–3498. doi:10.1016/j.bbamcr.2013.06.026.
- [234] C.L. Buchheit, R.R. Rayavarapu, Z.T. Schafer, The regulation of cancer cell death and metabolism by extracellular matrix attachment, *Semin. Cell Dev. Biol.* 23 (2012) 402–411. doi:10.1016/j.semcd.2012.04.007.
- [235] C.A. Caneba, N. Bellance, L. Yang, L. Pabst, D. Nagrath, Pyruvate uptake is increased in highly invasive ovarian cancer cells under anoikis conditions for anaplerosis, mitochondrial function, and migration, *AJP Endocrinol. Metab.* 303 (2012) E1036–E1052. doi:10.1152/ajpendo.00151.2012.
- [236] C.S. Lin, L.T. Liu, L.H. Ou, S.C. Pan, C.I. Lin, Y.H. Wei, Role of mitochondrial function in the invasiveness of human colon cancer cells, *Oncol. Rep.* 39 (2018) 316–330. doi:10.3892/or.2017.6087.
- [237] M. Lu, W. Zhu, X. Wang, J. Chen, J. Lu, M. Lu, W. Zhu, X. Wang, J. Tang, K. Zhang, G. Yu, W. Shao, ACOT12-Dependent Alteration of Acetyl-CoA Drives Hepatocellular Carcinoma Metastasis by Epigenetic Induction of Epithelial-Mesenchymal Transition, *Cell Metab.* 29 (2019) 886–900. doi:10.1016/j.cmet.2018.12.019.
- [238] V.K. Mishra, F. Wegwitz, R.L. Kosinsky, M. Sen, R. Baumgartner, T. Wulff, J.T. Siveke, H. Schildhaus, Z. Najafova, V. Kari, H. Kohlhof, E. Hessmann, A. Johnsen, Histone deacetylase class-I inhibition promotes epithelial gene expression in pancreatic cancer cells in a BRD4- and MYC-dependent manner, *Nucleic Acids Res.* 45 (2017) 6334–6349. doi:10.1093/nar/gkx212.
- [239] E. Beurel, S.F. Grieco, R.S. Jope, Glycogen synthase kinase-3 (GSK3): Regulation, actions, and diseases, *Pharmacol. Ther.* 148 (2015) 114–131. doi:10.1016/j.pharmthera.2014.11.016.

- [240] S.J. Oreña, A.J. Torchia, R.S. Garofalo, Inhibition of glycogen-synthase kinase 3 stimulates glycogen synthase and glucose transport by distinct mechanisms in 3T3-L1 adipocytes, *J. Biol. Chem.* 275 (2000) 15765–15772. doi:10.1074/jbc.M910002199.
- [241] C. Dong, T. Yuan, Y. Wu, Y. Wang, T.W.M. Fan, S. Miriyala, Y. Lin, J. Yao, J. Shi, T. Kang, P. Lorkiewicz, D. St Clair, M.C. Hung, B.M. Evers, B.P. Zhou, Loss of FBP1 by snail-mediated repression provides metabolic advantages in basal-like breast cancer, *Cancer Cell.* 23 (2013) 316–331. doi:10.1016/j.ccr.2013.01.022.
- [242] N.H. Kim, Y.H. Cha, J. Lee, S.H. Lee, J.H. Yang, J.S. Yun, E.S. Cho, X. Zhang, M. Nam, N. Kim, Y.S. Yuk, S.Y. Cha, Y. Lee, J.K. Ryu, S. Park, J.H. Cheong, S.W. Kang, S.Y. Kim, G.S. Hwang, J.I. Yook, H.S. Kim, Snail reprograms glucose metabolism by repressing phosphofructokinase PFKP allowing cancer cell survival under metabolic stress, *Nat. Commun.* 8 (2017) 1–12. doi:10.1038/ncomms14374.
- [243] S.Y. Lee, H.M. Jeon, M.K. Ju, C.H. Kim, G. Yoon, S.I. Han, Wnt / Snail Signaling Regulates Cytochrome c Oxidase and Glucose Metabolism, 2 (2012) 3607–3618. doi:10.1158/0008-5472.CAN-12-0006.
- [244] G.L. Matters, A. Manni, J.S. Bond, Inhibitors of polyamine biosynthesis decrease the expression of the metalloproteases mepirin α and MMP-7 in hormone-independent human breast cancer cells, *Clin. Exp. Metastasis.* 22 (2005) 331–339. doi:10.1007/s10585-005-0660-5.
- [245] A. Coker-Gurkan, M. Celik, M. Ugur, E.D. Arisan, P. Obakan-Yerlikaya, Z.B. Durdu, N. Palavan-Unsal, Curcumin inhibits autocrine growth hormone-mediated invasion and metastasis by targeting NF- κ B signaling and polyamine metabolism in breast cancer cells, *Amino Acids.* 50 (2018) 1045–1069. doi:10.1007/s00726-018-2581-z.
- [246] S. Muthukumar, R. Bhuvanandar, V. Umashankar, K.N. Sulochana, Insights on ornithine decarboxylase silencing as a potential strategy for targeting retinoblastoma, *Biomed. Pharmacother.* 98 (2018) 23–28. doi:10.1016/j.biopha.2017.12.030.
- [247] R. Kimura, A. Kasamatsu, T. Koyama, C. Fukumoto, Y. Kouzu, M. Higo, Y. Endo-Sakamoto, K. Ogawara, M. Shiiba, H. Tanzawa, K. Uzawa, Glutamate acid decarboxylase 1 promotes metastasis of human oral cancer by beta-catenin translocation and MMP7 activation, *BMC Cancer.* 13 (2013) 555. doi:10.1186/1471-2407-13-555.
- [248] P. Sancho, D. Barneda, C. Heeschen, Hallmarks of cancer stem cell metabolism, *Br. J. Cancer.* 114 (2016) 1305–1312. doi:10.1038/bjc.2016.152.
- [249] P.P. Liu, J. Liao, Z.J. Tang, W.J. Wu, J. Yang, Z.L. Zeng, Y. Hu, P. Wang, H.Q. Ju, R.H. Xu, P. Huang, Metabolic regulation of cancer cell side population by glucose through activation of the Akt pathway, *Cell Death Differ.* 21 (2014) 124–135. doi:10.1038/cdd.2013.131.
- [250] R. Palorini, G. Votta, C. Balestrieri, A. Monestiroli, S. Olivieri, R. Vento, F. Chiaradonna, Energy metabolism characterization of a novel cancer stem cell-like

- line 3AB-OS, *J. Cell. Biochem.* 115 (2014) 368–379. doi:10.1002/jcb.24671.
- [251] M. Gabay, Y. Li, D. Felsher, MYC Activation Is a Hallmark of Cancer Initiation, *Cold Spring Harb. Perspect. Med.* (2014) 1–13. doi:10.1101/cshperspect.a014241.
- [252] C.D.L. Folmes, A. Martinez-Fernandez, R.S. Faustino, S. Yamada, C. Perez-Terzic, T.J. Nelson, A. Terzic, Nuclear reprogramming with c-Myc potentiates glycolytic capacity of derived induced pluripotent stem cells, *J. Cardiovasc. Transl. Res.* 6 (2013) 10–21. doi:10.1007/s12265-012-9431-2.
- [253] K. Nishimura, S. Aizawa, F.L. Nugroho, E. Shiomitsu, Y.T.H. Tran, P.L. Bui, E. Borisova, Y. Sakuragi, H. Takada, A. Kurisaki, Y. Hayashi, A. Fukuda, M. Nakanishi, K. Hisatake, A Role for KLF4 in Promoting the Metabolic Shift via TCL1 during Induced Pluripotent Stem Cell Generation, *Stem Cell Reports.* 8 (2017) 787–801. doi:10.1016/j.stemcr.2017.01.026.
- [254] I. Samudio, R. Harmancey, M. Fiegl, H. Kantarjian, M. Konopleva, B. Korchin, K. Kaluarachchi, W. Bornmann, S. Duvvuri, H. Taegtmeier, M. Andreeff, Pharmacologic inhibition of fatty acid oxidation sensitizes human leukemia cells to apoptosis induction, *J. Clin. Invest.* 120 (2010) 142–156. doi:10.1172/JCI38942.
- [255] J. Li, S. Condello, J. Thomes-Pepin, X. Ma, Y. Xia, T.D. Hurley, D. Matei, J.X. Cheng, Lipid Desaturation Is a Metabolic Marker and Therapeutic Target of Ovarian Cancer Stem Cells, *Cell Stem Cell.* 20 (2017) 303-314.e5. doi:10.1016/j.stem.2016.11.004.
- [256] L. Amable, Cisplatin resistance and opportunities for precision medicine, *Pharmacol. Res.* 106 (2016) 27–36. doi:10.1016/j.phrs.2016.01.001.
- [257] M. Rahman, M.R. Hasan, Cancer metabolism and drug resistance, *Metabolites.* 5 (2015) 571–600. doi:10.3390/metabo5040571.
- [258] E.C. Saputra, L. Huang, Y. Chen, L. Tucker-Kellogg, Combination therapy and the evolution of resistance: The theoretical merits of synergism and antagonism in cancer, *Cancer Res.* 78 (2018) 2419–2431. doi:10.1158/0008-5472.CAN-17-1201.
- [259] J.I. Fletcher, R.T. Williams, M.J. Henderson, M.D. Norris, M. Haber, ABC transporters as mediators of drug resistance and contributors to cancer cell biology, *Drug Resist. Updat.* 26 (2016) 1–9. doi:10.1016/j.drup.2016.03.001.
- [260] M. Roth, A. Obaidat, B. Hagenbuch, OATPs, OATs and OCTs: The organic anion and cation transporters of the SLCO and SLC22A gene superfamilies, *Br. J. Pharmacol.* 165 (2012) 1260–1287. doi:10.1111/j.1476-5381.2011.01724.x.
- [261] C.J. Omiecinski, J.P. Vanden Heuvel, G.H. Perdew, J.M. Peters, Xenobiotic metabolism, disposition, and regulation by receptors: From biochemical phenomenon to predictors of major toxicities, *Toxicol. Sci.* 120 (2010) S49–S75. doi:10.1093/toxsci/kfq338.
- [262] K. Bachmann, *Drug Metabolism*, 1st ed., Academic press, Burlington, MA, 2009. doi:10.1016/B978-0-12-369521-5.00008-7.
- [263] F.P. Guengerich, Common and uncommon cytochrome P450 reactions related to

- metabolism and chemical toxicity, *Chem. Res. Toxicol.* 14 (2001) 611–650. doi:10.1021/tx0002583.
- [264] H. Zahreddine, K.L.B. Borden, Mechanisms and insights into drug resistance in cancer, *Front. Pharmacol.* 4 MAR (2013) 1–8. doi:10.3389/fphar.2013.00028.
- [265] C.M. Worsley, E.S. Mayne, R.B. Veale, Clone wars: The evolution of therapeutic resistance in cancer, *Evol. Med. Public Heal.* 2016 (2016) 180–181. doi:10.1093/EMPH/EOW015.
- [266] F.H. Groenendijk, R. Bernards, Drug resistance to targeted therapies: déjà vu all over again., *Mol. Oncol.* 8 (2014) 1067–83. doi:10.1016/j.molonc.2014.05.004.
- [267] T.A. Marlowe, F.L. Lenzo, S.A. Figel, A.T. Grapes, W.G. Cance, Oncogenic Receptor Tyrosine Kinases Directly Phosphorylate Focal Adhesion Kinase (FAK) as a Resistance Mechanism to FAK-Kinase Inhibitors, *Mol. Cancer Ther.* 15 (2016) 3028–3039. doi:10.1158/1535-7163.MCT-16-0366.
- [268] L. Galluzzi, L. Senovilla, I. Vitale, J. Michels, I. Martins, O. Kepp, M. Castedo, G. Kroemer, Molecular mechanisms of cisplatin resistance, *Oncogene.* 31 (2012) 1869–1883. doi:10.1038/onc.2011.384.
- [269] M. Eich, W.P. Roos, T. Nikolova, B. Kaina, Contribution of ATM and ATR to the Resistance of Glioblastoma and Malignant Melanoma Cells to the Methylating Anticancer Drug Temozolomide, *Mol. Cancer Ther.* 12 (2013) 2529–2540. doi:10.1158/1535-7163.MCT-13-0136.
- [270] M.A. Gadhikar, M.R. Sciuto, M.V.O. Alves, C.R. Pickering, A.A. Osman, D.M. Neskey, M. Zhao, A.L. Fitzgerald, J.N. Myers, M.J. Frederick, Chk1/2 Inhibition Overcomes the Cisplatin Resistance of Head and Neck Cancer Cells Secondary to the Loss of Functional p53, *Mol. Cancer Ther.* 12 (2013) 1860–1873. doi:10.1158/1535-7163.MCT-13-0157.
- [271] M. Kurokawa, C. Zhao, T. Reya, S. Kornbluth, Inhibition of Apoptosome Formation by Suppression of Hsp90 Phosphorylation in Tyrosine Kinase-Induced Leukemias, *Mol. Cell. Biol.* 28 (2008) 5494–5506. doi:10.1128/MCB.00265-08.
- [272] W. Nakajima, K. Sharma, M.A. Hicks, N. Le, R. Brown, G.W. Krystal, H. Harada, Combination with vorinostat overcomes ABT-263 (navitoclax) resistance of small cell lung cancer, *Cancer Biol. Ther.* 17 (2016) 27–35. doi:10.1080/15384047.2015.1108485.
- [273] F. Vaillant, D. Merino, L. Lee, K. Breslin, B. Pal, M.E. Ritchie, G.K. Smyth, M. Christie, L.J. Phillipson, C.J. Burns, G.B. Mann, J.E. Visvader, G.J. Lindeman, Targeting BCL-2 with the BH3 Mimetic ABT-199 in Estrogen Receptor-Positive Breast Cancer, *Cancer Cell.* 24 (2013) 120–129. doi:10.1016/j.ccr.2013.06.002.
- [274] P. Farmer, H. Bonnefoi, P. Anderle, D. Cameron, P. Wirapati, P. Wirapati, V. Becette, S. André, M. Piccart, M. Campone, E. Brain, G. Macgrogan, T. Petit, J. Jassem, F. Bibeau, E. Blot, J. Bogaerts, M. Aguet, J. Bergh, R. Iggo, M. Delorenzi, A stroma-related gene signature predicts resistance to neoadjuvant chemotherapy in breast cancer., *Nat. Med.* 15 (2009) 68–74. doi:10.1038/nm.1908.

- [275] L.A. Byers, L. Diao, J. Wang, P. Saintigny, L. Girard, M. Peyton, L. Shen, Y. Fan, U. Giri, P.K. Tumula, M.B. Nilsson, J. Gudikote, H. Tran, R.J.G. Cardnell, D.J. Bearss, S.L. Warner, J.M. Foulks, S.B. Kanner, V. Gandhi, N. Krett, S.T. Rosen, E.S. Kim, R.S. Herbst, G.R. Blumenschein, J.J. Lee, S.M. Lippman, K.K. Ang, G.B. Mills, W.K. Hong, J.N. Weinstein, I.I. Wistuba, K.R. Coombes, J.D. Minna, J. V. Heymach, An epithelial-mesenchymal transition gene signature predicts resistance to EGFR and PI3K inhibitors and identifies Axl as a therapeutic target for overcoming EGFR inhibitor resistance, *Clin. Cancer Res.* 19 (2013) 279–290. doi:10.1158/1078-0432.CCR-12-1558.
- [276] P. Zhang, Y. Sun, L. Ma, ZEB1: At the crossroads of epithelial-mesenchymal transition, metastasis and therapy resistance, *Cell Cycle*. 14 (2015) 481–487. doi:10.1080/15384101.2015.1006048.
- [277] P. Zhang, Y. Wei, L. i. Wang, B.G. Debeb, Y. Yuan, J. Zhang, J. Yuan, M. Wang, D. Chen, Y. Sun, W.A. Woodward, Y. Liu, D.C. Dean, H. Liang, Y. Hu, K.K. Ang, M.C. Hung, J. Chen, L. Ma, ATM-mediated stabilization of ZEB1 promotes DNA damage response and radioresistance through CHK1, *Nat. Cell Biol.* 16 (2014) 864–875. doi:10.1038/ncb3013.
- [278] K.S. Harris, B.A. Kerr, Prostate Cancer Stem Cell Markers Drive Progression, Therapeutic Resistance, and Bone Metastasis, *Stem Cells Int.* 2017 (2017) 1–9. doi:10.1155/2017/8629234.
- [279] B. Le Calvé, M. Rynkowski, M. Le Mercier, C. Bruyère, C. Lonez, T. Gras, B. Haibe-Kains, G. Bontempi, C. Decaestecker, J.-M. Ruyschaert, R. Kiss, F. Lefranc, Long-term In Vitro Treatment of Human Glioblastoma Cells with Temozolomide Increases Resistance In Vivo through Up-regulation of GLUT Transporter and Aldo-Keto Reductase Enzyme AKR1C Expression, *Neoplasia*. 12 (2010) 727–739. doi:10.1593/neo.10526.
- [280] W. Wagner, W.M. Ciszewski, K.D. Kania, L- and D-lactate enhance DNA repair and modulate the resistance of cervical carcinoma cells to anticancer drugs via histone deacetylase inhibition and hydroxycarboxylic acid receptor 1 activation, *Cell Commun. Signal.* 13 (2015) 1–16. doi:10.1186/s12964-015-0114-x.
- [281] A.N. Bhatt, A. Chauhan, S. Khanna, Y. Rai, S. Singh, R. Soni, N. Kalra, B.S. Dwarakanath, Transient elevation of glycolysis confers radio-resistance by facilitating DNA repair in cells, *BMC Cancer*. 15 (2015) 1–12. doi:10.1186/s12885-015-1368-9.
- [282] B.L. Woolbright, D. Choudhary, A. Mikhalyuk, C. Trammel, S. Shanmugam, E. Abbott, C.C. Pilbeam, J.A. Taylor, The Role of Pyruvate Dehydrogenase Kinase-4 (PDK4) in Bladder Cancer and Chemoresistance., *Mol. Cancer Ther.* 3 (2018) molcanther.0063.2018. doi:10.1158/1535-7163.MCT-18-0063.
- [283] T. Fodor, M. Szántó, O. Abdul-Rahman, L. Nagy, Á. Dér, B. Kiss, P. Bai, Combined treatment of MCF-7 cells with AICAR and methotrexate, arrests cell cycle and reverses warburg metabolism through AMP-activated protein kinase (AMPK) and FOXO1, *PLoS One*. 11 (2016) 1–16. doi:10.1371/journal.pone.0150232.

- [284] B. Rosenberg, L. Van Camp, T. Krigas, Inhibition of cell division in *Escherichia coli* by electrolysis products from a platinum electrode, *Nature*. 205 (1965) 698–699. doi:10.1038/205698a0.
- [285] N.J. Wheate, S. Walker, G.E. Craig, R. Oun, The status of platinum anticancer drugs in the clinic and in clinical trials, *Dalt. Trans.* 39 (2010) 8113–8127. doi:10.1039/c0dt00292e.
- [286] A.-M. Florea, D. Büsselberg, Cisplatin as an Anti-Tumor Drug: Cellular Mechanisms of Activity, Drug Resistance and Induced Side Effects, *Cancers (Basel)*. (2011) 1351–1371. doi:10.3390/cancers3011351.
- [287] M.D. Hall, H.R. Mellor, R. Callaghan, T.W. Hambley, Basis for design and development of platinum(IV) anticancer complexes, *J. Med. Chem.* 50 (2007) 3403–3411. doi:10.1021/jm070280u.
- [288] S. Dasari, P. Bernard Tchounwou, Cisplatin in cancer therapy: Molecular mechanisms of action, *Eur. J. Pharmacol.* 740 (2014) 364–378. doi:10.1016/j.ejphar.2014.07.025.
- [289] J. Gumulec, J.A.N. Balvan, M. Sztalmachova, M. Raudenska, V. Dvorakova, L. Knopfova, H. Polanska, K. Hudcova, B. Ruttkay-Nedecky, P. Babula, V. Adam, R. Kizek, M. Stiborova, M. Masarik, Cisplatin-resistant prostate cancer model: Differences in antioxidant system, apoptosis and cell cycle, *Int. J. Oncol.* 44 (2014) 923–933. doi:10.3892/ijo.2013.2223.
- [290] Z. Yang, L.M. Schumaker, M.J. Egorin, E.G. Zuhowski, Z. Quo, K.J. Cullen, Cisplatin preferentially binds mitochondrial DNA and voltage-dependent anion channel protein in the mitochondrial membrane of head and neck squamous cell carcinoma: Possible role in apoptosis, *Clin. Cancer Res.* 12 (2006) 5817–5825. doi:10.1158/1078-0432.CCR-06-1037.
- [291] E. Schreiber-Brynzak, V. Pichler, P. Heffeter, B. Hanson, S. Theiner, I. Lichtscheidl-Schultz, C. Kornauth, L. Bamonti, V. Dhery, D. Groza, D. Berry, W. Berger, M. Galanski, M.A. Jakupec, B.K. Keppler, Behavior of platinum(IV) complexes in models of tumor hypoxia: Cytotoxicity, compound distribution and accumulation, *Metallomics*. 8 (2016) 422–433. doi:10.1039/c5mt00312a.
- [292] U. Basu, B. Banik, R. Wen, R.K. Pathak, S. Dhar, The Platin-X series: activation, targeting, and delivery, *Dalt. Trans.* 45 (2016) 12992–13004. doi:10.1039/C6DT01738J.
- [293] M. Crespo, Cyclometallated platinum(IV) compounds as promising antitumour agents, *J. Organomet. Chem.* 879 (2019) 15–26. doi:10.1016/j.jorganchem.2018.10.008.
- [294] H.H.W. Chen, M.T. Kuo, Role of Glutathione in the Regulation of Cisplatin Resistance in Cancer Chemotherapy, *Met. Based. Drugs*. 2010 (2010) 1–7. doi:10.1155/2010/430939.
- [295] F. Arnesano, M. Losacco, G. Natile, An updated view of cisplatin transport, *Eur. J. Inorg. Chem.* (2013) 2701–2711. doi:10.1002/ejic.201300001.

- [296] C.D. Hudson, A. Savadelis, A.B. Nagaraj, P. Joseph, S. Avril, A. DiFeo, N. Avril, C.D. Hudson, A. Savadelis, A.B. Nagaraj, P. Joseph, S. Avril, A. DiFeo, N. Avril, Altered glutamine metabolism in platinum resistant ovarian cancer, *Oncotarget*. 7 (2016) 41637–41649. doi:10.18632/oncotarget.9317.
- [297] M. Sonego, I. Pellizzari, A.D. Acqua, E. Pivetta, I. Lorenzon, S. Benevol, R. Bomben, P. Spessotto, R. Sorio, V. Gattei, M. Schiappacassi, G. Baldassarre, Common biological phenotypes characterize the acquisition of platinum-resistance in epithelial ovarian cancer cells, *Sci. Rep.* 7 (2017) 1–12. doi:10.1038/s41598-017-07005-1.
- [298] X. Yan, M.I.N. Li, Y.E. Yuan, N. Mao, L. Pan, Biological comparison of ovarian cancer resistant cell lines to cisplatin and Taxol by two different administrations, *Oncol. Rep.* 17 (2007) 1163–1169.
- [299] S. Mittal, R.K. Chowhan, L.R. Singh, Macromolecular crowding : Macromolecules friend or foe, *Biochim. Biophys. Acta.* 1850 (2015) 1822–1831. doi:10.1016/j.bbagen.2015.05.002.
- [300] a P. Minton, J. Wilf, Effect of macromolecular crowding upon the structure and function of an enzyme: glyceraldehyde-3-phosphate dehydrogenase., *Biochemistry.* 20 (1981) 4821–6. <http://www.ncbi.nlm.nih.gov/pubmed/7295652>.
- [301] T.C. Laurent, Enzyme Reactions in Polymer Media, *Eur. J. Biochem.* 21 (1971) 498–506. doi:10.1111/j.1432-1033.1971.tb01495.x.
- [302] B.D. Slaughter, J.W. Schwartz, R. Li, Mapping dynamic protein interactions in MAP kinase signaling using live-cell fluorescence fluctuation spectroscopy and imaging., *Proc. Natl. Acad. Sci. U. S. A.* 104 (2007) 20320–5. doi:10.1073/pnas.0710336105.
- [303] I. Pastor, E. Vilaseca, S. Madurga, J.L. Garcés, M. Cascante, F. Mas, Diffusion of alpha-chymotrypsin in solution-crowded media. A fluorescence recovery after photobleaching study., *J. Phys. Chem. B.* 114 (2010) 4028–4034. doi:10.1021/jp910811j.
- [304] Y. Phillip, G. Schreiber, Formation of protein complexes in crowded environments-From in vitro to in vivo, *FEBS Lett.* 587 (2013) 1046–1052. doi:10.1016/j.febslet.2013.01.007.
- [305] Y. Sasaki, D. Miyoshi, N. Sugimoto, Regulation of DNA nucleases by molecular crowding, *Nucleic Acids Res.* 35 (2007) 4086–4093. doi:10.1093/nar/gkm445.
- [306] H. Matsuda, G.G. Putzel, V. Backman, I. Szleifer, Macromolecular crowding as a regulator of gene transcription., *Biophys. J.* 106 (2014) 1801–10. doi:10.1016/j.bpj.2014.02.019.
- [307] M. Al-Habori, Macromolecular crowding and its role as intracellular signalling of cell volume regulation, *Int. J. Biochem. Cell Biol.* 33 (2001) 844–864. doi:10.1016/S1357-2725(01)00058-9.
- [308] G. Rivas, A.P. Minton, Macromolecular Crowding In Vitro, In Vivo, and In Between, *Trends Biochem. Sci.* 41 (2016) 970–981. doi:10.1016/j.tibs.2016.08.013.

- [309] I. Pastor, L. Pitulice, C. Balcells, E. Vilaseca, S. Madurga, A. Isvoran, M. Cascante, F. Mas, Effect of crowding by Dextrans in enzymatic reactions., *Biophys. Chem.* 185 (2014) 8–13. doi:10.1016/j.bpc.2013.10.006.
- [310] I. Pastor, E. Vilaseca, S. Madurga, J.L. Garcés, M. Cascante, F. Mas, Effect of crowding by dextrans on the hydrolysis of N-Succinyl-L-phenyl-Ala-p-nitroanilide catalyzed by α -chymotrypsin., *J. Phys. Chem. B.* 115 (2011) 1115–21. doi:10.1021/jp105296c.
- [311] A. Vazquez, J. Liu, Y. Zhou, Z.N. Oltvai, Catabolic efficiency of aerobic glycolysis: The Warburg effect revisited, *BMC Syst. Biol.* 4 (2010) 1–9. doi:10.1186/1752-0509-4-58.
- [312] L. Sun, J. Fang, Macromolecular crowding effect is critical for maintaining SIRT1's nuclear localization in cancer cells, *Cell Cycle.* 15 (2016) 2647–2655. doi:10.1080/15384101.2016.1211214.
- [313] Y. Sasaki, D. Miyoshi, N. Sugimoto, Effect of molecular crowding on DNA polymerase activity, *Biotechnol. J.* 1 (2006) 440–446. doi:10.1002/biot.200500032.
- [314] Y. Wu, N. Teng, S. Li, Effects of macromolecular crowding and osmolyte on human Tau fibrillation, *Int. J. Biol. Macromol.* 90 (2016) 27–36. doi:10.1016/j.ijbiomac.2015.11.091.
- [315] M. Delarue, G.P. Brittingham, S. Pfeffer, I.V. Surovtsev, S. Pinglay, K.J. Kennedy, M. Schaffer, J.I. Gutierrez, D. Sang, G. Poterewicz, J.K. Chung, J.M. Plitzko, J.T. Groves, C. Jacobs-Wagner, B.D. Engel, L.J. Holt, mTORC1 Controls Phase Separation and the Biophysical Properties of the Cytoplasm by Tuning Crowding, *Cell.* 174 (2018) 338–349.e20. doi:10.1016/j.cell.2018.05.042.
- [316] J. Ferlay, I. Soerjomataram, R. Dikshit, S. Eser, C. Mathers, M. Rebelo, D.M. Parkin, D. Forman, F. Bray, Cancer incidence and mortality worldwide: Sources, methods and major patterns in GLOBOCAN 2012, *Int. J. Cancer.* 136 (2015) E359–E386. doi:10.1002/ijc.29210.
- [317] L. Torre, R. Siegel, A. Jemal, *Global Cancer Facts & Figures 3rd Edition.*, Am. Cancer Soc. (2015) 1–64. doi:10.1002/ijc.27711.
- [318] C.G. Roehrborn, Benign Prostatic Hyperplasia: An Overview, *Rev. Urol.* 7 (2005) S3–S14. doi:10.1016/S0090-4295(98)00532-9.
- [319] E. Eidelman, J. Twum-Ampofo, J. Ansari, M.M. Siddiqui, The Metabolic Phenotype of Prostate Cancer, *Front. Oncol.* 7 (2017) 1–6. doi:10.3389/fonc.2017.00131.
- [320] M.S. Litwin, H.-J. Tan, The Diagnosis and Treatment of Prostate Cancer, *Jama.* 317 (2017) 2532. doi:10.1001/jama.2017.7248.
- [321] E.D. Crawford, C.S. Higano, N.D. Shore, M. Hussain, D.P. Petrylak, Treating patients with metastatic castration resistant prostate cancer: A comprehensive review of available therapies, *J. Urol.* 194 (2015) 1537–1547. doi:10.1016/j.juro.2015.06.106.

- [322] C.E. Massie, A. Lynch, A. Ramos-Montoya, J. Boren, R. Stark, L. Fazli, A. Warren, H. Scott, B. Madhu, N. Sharma, H. Bon, V. Zecchini, D.M. Smith, G.M. Denicola, N. Mathews, M. Osborne, J. Hadfield, S. MacArthur, B. Adryan, S.K. Lyons, K.M. Brindle, J. Griffiths, M.E. Gleave, P.S. Rennie, D.E. Neal, I.G. Mills, The androgen receptor fuels prostate cancer by regulating central metabolism and biosynthesis, *EMBO J.* 30 (2011) 2719–2733. doi:10.1038/emboj.2011.158.
- [323] E. Nevedomskaya, S.J. Baumgart, B. Haendler, Recent Advances in Prostate Cancer Treatment and Drug Discovery, *Int. J. Mol. Sci.* 19 (2018) 1–25. doi:10.3390/ijms19051359.
- [324] S.J. Hotte, F. Saad, Current management of castrate-resistant prostate cancer, *Curr. Oncol.* 17 (2010) 72–79. doi:10.3747/co.v17i0.718.
- [325] T.A. Yap, A.D. Smith, R. Ferraldeschi, B. Al-Lazikani, P. Workman, J.S. De Bono, Drug discovery in advanced prostate cancer: Translating biology into therapy, *Nat. Rev. Drug Discov.* 15 (2016) 699–718. doi:10.1038/nrd.2016.120.
- [326] G.S. Palapattu, C. Wu, C.R. Silvers, H.B. Martin, K. Williams, L. Salamone, T. Bushnell, L.S. Huang, Q. Yang, J. Huang, Selective expression of CD44, a putative prostate cancer stem cell marker, in neuroendocrine tumor cells of human prostate cancer, *Prostate.* 69 (2009) 787–798. doi:10.1002/pros.20928.
- [327] A.D. Grigore, E. Ben-Jacob, M.C. Farach-Carson, Prostate Cancer and Neuroendocrine Differentiation: More Neuronal, Less Endocrine?, *Front. Oncol.* 5 (2015) 1–19. doi:10.3389/fonc.2015.00037.
- [328] S. Terry, H. Beltran, The Many Faces of Neuroendocrine Differentiation in Prostate Cancer Progression, *Front. Oncol.* 4 (2014) 1–9. doi:10.3389/fonc.2014.00060.
- [329] J. Huang, J.L. Yao, P.A. di Sant' Agnese, Q. Yang, P.A. Bourne, Y. Na, Immunohistochemical Characterization of Neuroendocrine Cells in Prostate Cancer, *Prostate.* 66 (2006) 1399–1406. doi:10.1002/pros.
- [330] T.C. Yuan, S. Veeramani, M.F. Lin, Neuroendocrine-like prostate cancer cells: Neuroendocrine transdifferentiation of prostate adenocarcinoma cells, *Endocr. Relat. Cancer.* 14 (2007) 531–547. doi:10.1677/ERC-07-0061.
- [331] M.E. Wright, M.-J. Tsai, R. Aebersold, Androgen Receptor Represses the Neuroendocrine Transdifferentiation Process in Prostate Cancer Cells, *Mol. Endocrinol.* 17 (2003) 1726–1737. doi:10.1210/me.2003-0031.
- [332] E. Tsouko, A.S. Khan, M.A. White, J.J. Han, Y. Shi, F.A. Merchant, M.A. Sharpe, L. Xin, D.E. Frigo, Regulation of the pentose phosphate pathway by an androgen receptor-mTOR-mediated mechanism and its role in prostate cancer cell growth, *Oncogenesis.* 3 (2014) e103-10. doi:10.1038/oncsis.2014.18.
- [333] R.E. Miller, C.J. Sweeney, Chemotherapy for metastatic castrate-sensitive prostate cancer., *Prostate Cancer Prostatic Dis.* 19 (2016) 139–44. doi:10.1038/pcan.2016.10.
- [334] T. Jamaspishvili, D.M. Berman, A.E. Ross, H.I. Scher, A.M. De Marzo, J.A. Squire, T.L. Lotan, Clinical implications of PTEN loss in prostate cancer, *Nat. Rev. Urol.* 15

- (2018) 222–234. doi:10.1038/nrurol.2018.9.
- [335] B.S. Carver, C. Chapinski, J. Wongvipat, H. Hieronymus, Y. Chen, S. Chandralapaty, V.K. Arora, C. Le, J. Koutcher, H. Scher, P.T. Scardino, N. Rosen, C.L. Sawyers, Reciprocal Feedback Regulation of PI3K and Androgen Receptor Signaling in PTEN-Deficient Prostate Cancer, *Cancer Cell*. 19 (2011) 575–586. doi:10.1016/j.ccr.2011.04.008.
- [336] M.S. Humeniuk, R.T. Gupta, P. Healy, M. McNamara, S. Ramalingam, M. Harrison, D. George, T. Zhang, Y. Wu, A.J. Armstrong, Platinum sensitivity in metastatic prostate cancer: does histology matter?, *Prostate Cancer Prostatic Dis.* 21 (2018) 92–99. doi:10.1038/s41391-017-0017-6.
- [337] X. Wu, G. Daniels, P. Lee, M.E. Monaco, Lipid metabolism in prostate cancer., *Am. J. Clin. Exp. Urol.* 2 (2014) 111–20. <http://www.ncbi.nlm.nih.gov/pubmed/25374912><http://www.pubmedcentral.nih.gov/articlerender.fcgi?artid=PMC4219300>.
- [338] F. Giunchi, M. Fiorentino, M. Loda, The Metabolic Landscape of Prostate Cancer, *Eur. Urol. Oncol.* In press (2018) 1–9. doi:10.1016/j.euo.2018.06.010.
- [339] M.E. Mycielska, A. Patel, N. Rizaner, M.P. Mazurek, H. Keun, A. Patel, V. Ganapathy, M.B.A. Djamgoz, Citrate transport and metabolism in mammalian cells: Prostate epithelial cells and prostate cancer, *BioEssays*. 31 (2009) 10–20. doi:10.1002/bies.080137.
- [340] G. Deep, I.R. Schlaepfer, Aberrant lipid metabolism promotes prostate cancer: Role in cell survival under hypoxia and extracellular vesicles biogenesis, *Int. J. Mol. Sci.* 17 (2016). doi:10.3390/ijms17071061.
- [341] J. V. Swinnen, T. Roskams, S. Joniau, H. Van Poppel, R. Oyen, L. Baert, W. Heyns, G. Verhoeven, Overexpression of fatty acid synthase is an early and common event in the development of prostate cancer, *Int. J. Cancer*. 98 (2002) 19–22. doi:10.1002/ijc.10127.
- [342] T. Van De Sande, E. Schrijver, W. Heyns, G. Verhoeven, J. V Swinnen, Role of the Phosphatidylinositol 3'-Kinase/PTEN/Akt Kinase Pathway in the Overexpression of Fatty Acid Synthase in LNCaP Prostate Cancer Cells, *Cancer Res.* 62 (2002) 642–646.
- [343] T. Van de Sande, T. Roskams, E. Lerut, S. Joniau, H. Van Poppel, G. Verhoeven, J. V Swinnen, High-level expression of fatty acid synthase in human prostate cancer tissues is linked to activation and nuclear localization of Akt/PKB, *J. Pathol.* 206 (2005) 214–219. doi:10.1002/path.1760.
- [344] Y. Liu, Fatty acid oxidation is a dominant bioenergetic pathway in prostate cancer, *Prostate Cancer Prostatic Dis.* 9 (2006) 230–234. doi:10.1038/sj.pcan.4500879.
- [345] J. Pey, E. San José-Eneriz, M.C. Ochoa, I. Apaolaza, P. De Atauri, A. Rubio, X. Cendoya, E. Miranda, L. Garate, M. Cascante, A. Carracedo, X. Agirre, F. Prosper, F.J. Planes, In-silico gene essentiality analysis of polyamine biosynthesis reveals APRT as a potential target in cancer, *Sci. Rep.* 7 (2017) 1–10. doi:10.1038/s41598-

017-14067-8.

- [346] A. Zabala-Letona, A. Arruabarrena-Aristorena, N. Martín-Martín, S. Fernandez-Ruiz, J.D. Sutherland, M. Clasquin, J. Tomas-Cortazar, J. Jimenez, I. Torres, P. Quang, P. Ximenez-Embun, R. Bago, A. Ugalde-Olano, A. Loizaga-Iriarte, I. Lacasa-Viscasillas, M. Unda, V. Torrano, D. Cabrera, S.M. Van Liempd, Y. Cendon, E. Castro, S. Murray, A. Revandkar, A. Alimonti, Y. Zhang, A. Barnett, G. Lein, D. Pirman, A.R. Cortazar, L. Arreal, L. Prudkin, I. Astobiza, L. Valcarcel-Jimenez, P. Zuñiga-García, I. Fernandez-Dominguez, M. Piva, A. Caro-Maldonado, P. Sánchez-Mosquera, M. Castillo-Martín, V. Serra, N. Beraza, A. Gentilella, G. Thomas, M. Azkargorta, F. Elortza, R. Farràs, D. Olmos, A. Efeyan, J. Anguita, J. Muñoz, J.M. Falcón-Pérez, R. Barrio, T. Macarulla, J.M. Mato, M.L. Martinez-Chantar, C. Cordon-Cardo, A.M. Aransay, K. Marks, J. Baselga, J. Tabernero, P. Nuciforo, B.D. Manning, K. Marjon, A. Carracedo, MTORC1-dependent AMD1 regulation sustains polyamine metabolism in prostate cancer, *Nature*. 547 (2017) 109–113. doi:10.1038/nature22964.
- [347] S. Tai, Y. Sun, J.M. Squires, H. Zhang, W.K. Oh, C.Z. Liang, J. Huang, PC3 is a cell line characteristic of prostatic small cell carcinoma, *Prostate*. 71 (2011) 1668–1679. doi:10.1002/pros.21383.
- [348] A. van Bokhoven, M. Varella-García, C. Korch, W.U. Johannes, E.E. Smith, H.L. Miller, S.K. Nordeen, G.J. Miller, M.S. Lucia, Molecular characterization of human prostate carcinoma cell lines, *Prostate*. 57 (2003) 205–225. doi:10.1002/pros.10290.
- [349] D.N. Carney, A.F. Gazdar, G. Bepler, J.G. Guccion, P.J. Marangos, T.W. Moody, M.H. Zweig, J.D. Minna, Establishment and identification of small cell lung cancer cell lines having classic and variant features., *Cancer Res*. 45 (1985) 2913–23. <http://www.ncbi.nlm.nih.gov/pubmed/2985257>.
- [350] K.D. Mertz, S.R. Setlur, S.M. Dhanasekaran, F. Demichelis, S. Perner, S. Tomlins, J. Tchinda, B. Laxman, R.L. Vessella, R. Beroukhim, C. Lee, A.M. Chinnaiyan, M.A. Rubin, Molecular characterization of TMPRSS2-ERG gene fusion in the NCI-H660 prostate cancer cell line: a new perspective for an old model., *Neoplasia*. 9 (2007) 200–6. doi:10.1593/neo.07103.
- [351] N.J. Maitland, C.A. Macintosh, J. Hall, M. Sharrard, G. Quinn, S. Lang, In vitro models to study cellular differentiation and function in human prostate cancers., *Radiat. Res*. 155 (2001) 133–142. doi:10.1667/0033-7587(2001)155{[]0133:IVMTSC]2.0.CO;2.
- [352] M. Mourtada-Maarabouni, M.R. Pickard, V.L. Hedge, F. Farzaneh, G.T. Williams, GAS5, a non-protein-coding RNA, controls apoptosis and is downregulated in breast cancer, *Oncogene*. 28 (2009) 195–208. doi:10.1038/onc.2008.373.
- [353] M.R. Pickard, M. Mourtada-Maarabouni, G.T. Williams, Long non-coding RNA GAS5 regulates apoptosis in prostate cancer cell lines, *Biochim. Biophys. Acta - Mol. Basis Dis*. 1832 (2013) 1613–1623. doi:10.1016/j.bbadis.2013.05.005.
- [354] J. Schmitt, A. Noble, M. Otsuka, P. Berry, N.J. Maitland, M.G. Rumsby, Phorbol

- ester stimulates ethanolamine release from the metastatic basal prostate cancer cell line PC3 but not from prostate epithelial cell lines LNCaP and P4E6, *Br. J. Cancer*. 111 (2014) 1646–1656. doi:10.1038/bjc.2014.457.
- [355] E. Ulukaya, F.M. Frame, B. Cevatemre, D. Pellacani, H. Walker, V.M. Mann, M.S. Simms, M.J. Stower, V.T. Yilmaz, N.J. Maitland, Differential Cytotoxic Activity of a Novel Palladium-Based Compound on Prostate Cell Lines, Primary Prostate Epithelial Cells and Prostate Stem Cells, *PLoS One*. 8 (2013). doi:10.1371/journal.pone.0064278.
- [356] R. Akhtar, S. Chandel, P. Sarotra, B. Medhi, Current status of pharmacological treatment of colorectal cancer, *World J. Gastrointest. Oncol*. 6 (2014) 177. doi:10.4251/wjgo.v6.i6.177.
- [357] H.R. Hagland, K. Søreide, Cellular metabolism in colorectal carcinogenesis: Influence of lifestyle, gut microbiome and metabolic pathways, *Cancer Lett*. 356 (2015) 273–280. doi:10.1016/j.canlet.2014.02.026.
- [358] G. Martini, T. Troiani, C. Cardone, P. Vitiello, V. Sforza, D. Ciardiello, S. Napolitano, C.M. Della Corte, F. Morgillo, A. Raucci, A. Cuomo, F. Selvaggi, F. Ciardiello, E. Martinelli, Present and future of metastatic colorectal cancer treatment: A review of new candidate targets, *World J. Gastroenterol*. 23 (2017) 4675–4688.
- [359] G.J. Patti, O. Yanes, G. Siuzdak, Innovation: Metabolomics: the apogee of the omics trilogy., *Nat. Rev. Mol. Cell Biol*. 13 (2012) 263–9. doi:10.1038/nrm3314.
- [360] C. Balcells, C. Foguet, J. Tarragó-Celada, P. de Atauri, S. Marin, M. Cascante, Tracing metabolic fluxes using mass spectrometry: stable isotope-resolved metabolomics (SIRM) in health and disease, *Trends Anal. Chem.* (2019). doi:10.1016/J.TRAC.2018.12.025.
- [361] C. Balcells, C. Foguet, J. Tarragó-Celada, P. de Atauri, S. Marin, M. Cascante, Tracing metabolic fluxes using mass spectrometry: stable isotope-resolved metabolomics (SIRM) in health and disease, *Trends Anal. Chem.* (2019). doi:10.1016/J.TRAC.2018.12.025.
- [362] I. Marín de Mas, E. Aguilar, A. Jayaraman, I.H. Polat, A. Martín-Bernabé, R. Bharat, C. Foguet, E. Milà, B. Papp, J.J. Centelles, M. Cascante, Cancer cell metabolism as new targets for novel designed therapies, *Future Med. Chem.* 6 (2014) 1971–1810. <http://www.ncbi.nlm.nih.gov/pubmed/11221831>.
- [363] C. Matito, F. Mastorakou, J.J. Centelles, J.L. Torres, M. Cascante, Antiproliferative effect of antioxidant polyphenols from grape in murine Hepa-1c1c7, *Eur J Nutr*. 49 (2003) 43–49. doi:10.1007/s00394-003-0398-2.
- [364] C.M. Henry, E. Hollville, S.J. Martin, Measuring apoptosis by microscopy and flow cytometry, *Methods*. 61 (2013) 90–97. doi:10.1002/0471142735.im1438s112.
- [365] I. Vermes, H. Clemens, H. Steffens-Nakken, C. Reutelingsperger, A novel assay for apoptosis Flow cytometric detection of phosphatidylserine early apoptotic cells using fluorescein labelled expression on Annexin V, *J. Immunol. Methods*. 184 (1995) 39–51.

- [366] Y. Wu, L. Li, Sample normalization methods in quantitative metabolomics, *J. Chromatogr. A*. 1430 (2016) 80–95. doi:10.1016/j.chroma.2015.12.007.
- [367] H. Beltran, D.S. Rickman, K. Park, S.S. Chae, A. Sboner, T.Y. MacDonald, Y. Wang, K.L. Sheikh, S. Terry, S.T. Tagawa, R. Dhir, J.B. Nelson, A. de la Taille, Y. Allory, M.B. Gerstein, S. Perner, K.J. Pienta, A.M. Chinnaiyan, C.C. Collins, M.E. Gleave, F. Demichelis, D.M. Nanus, M.A. Rubin, Molecular Characterization of Neuroendocrine Prostate Cancer and Identification of New Drug Targets, *Cancer Discov.* 1 (2011) 487–495. doi:10.1158/2159-8290.CD-11-0130.
- [368] M. Cerasuolo, D. Paris, F.A. Iannotti, D. Melck, R. Verde, E. Mazzarella, A. Motta, A. Ligresti, Neuroendocrine transdifferentiation in human prostate cancer cells: An integrated approach, *Cancer Res.* 75 (2015) 2975–2986. doi:10.1158/0008-5472.CAN-14-3830.
- [369] S. Shaheen, M. Ahmed, F. Lorenzi, A.S. Nateri, Spheroid-Formation (Colonsphere) Assay for in Vitro Assessment and Expansion of Stem Cells in Colon Cancer, *Stem Cell Rev. Reports.* 12 (2016) 492–499. doi:10.1007/s12015-016-9664-6.
- [370] X.Y. Han, B. Wei, J.F. Fang, S. Zhang, F.C. Zhang, H.B. Zhang, T.Y. Lan, H.Q. Lu, H.B. Wei, Epithelial-Mesenchymal Transition Associates with Maintenance of Stemness in Spheroid-Derived Stem-Like Colon Cancer Cells, *PLoS One.* 8 (2013). doi:10.1371/journal.pone.0073341.
- [371] M. Stadler, M. Scherzer, S. Walter, S. Holzner, K. Pudelko, A. Riedl, C. Unger, N. Kramer, B. Weil, J. Neesen, M. Hengstschläger, H. Dolznig, Exclusion from spheroid formation identifies loss of essential cell-cell adhesion molecules in colon cancer cells, *Sci. Rep.* 8 (2018) 1–16. doi:10.1038/s41598-018-19384-0.
- [372] V. Härmä, J. Virtanen, R. Mäkelä, A. Happonen, J.P. Mpindi, M. Knuuttila, P. Kohonen, J. Lötjönen, O. Kallioniemi, M. Nees, A comprehensive panel of three-dimensional models for studies of prostate cancer growth, invasion and drug responses, *PLoS One.* 5 (2010). doi:10.1371/journal.pone.0010431.
- [373] E. Proctor, M. Waghray, C.J. Lee, D.G. Heidt, M. Yalamanchili, C. Li, F. Bednar, D.M. Simeone, Bmi1 Enhances Tumorigenicity and Cancer Stem Cell Function in Pancreatic Adenocarcinoma, 8 (2013). doi:10.1371/journal.pone.0055820.
- [374] K. Zhang, D.J. Waxman, PC3 prostate tumor-initiating cells with molecular profile FAM65B^{high}/MFI2^{low}/LEF1^{low} increase tumor angiogenesis, *Mol. Cancer.* 9 (2010) 319. doi:10.1186/1476-4598-9-319.
- [375] L. Patrawala, T. Calhoun-Davis, R. Schneider-Broussard, D.G. Tang, Hierarchical organization of prostate cancer cells in xenograft tumors: The CD44+ α 2 β 1+ cell population is enriched in tumor-initiating cells, *Cancer Res.* 67 (2007) 6796–6805. doi:10.1158/0008-5472.CAN-07-0490.
- [376] J.R. Hernandez, J.J. Kim, J.E. Verdone, X. Liu, G. Torga, K.J. Pienta, S.M. Mooney, C.D.Á. Ovol, Á.Z.E.B.Á.E. Cdh, Alternative CD44 splicing identifies epithelial prostate cancer cells from the mesenchymal counterparts, *Med. Oncol.* 32 (2015) 1–9. doi:10.1007/s12032-015-0593-z.

- [377] N. Kirschner, M. Haftek, C.M. Niessen, M.J. Behne, M. Furuse, I. Moll, J.M. Brandner, CD44 regulates tight-junction assembly and barrier function, *J. Invest. Dermatol.* 131 (2011) 932–943. doi:10.1038/jid.2010.390.
- [378] J. Chen, Q. Xia, B. Jiang, W. Chang, W. Yuan, Z. Ma, Z. Liu, X. Shu, Prognostic value of cancer stem cell marker ALDH1 expression in colorectal cancer: A systematic review and meta-analysis, *PLoS One.* 10 (2015) 1–15. doi:10.1371/journal.pone.0145164.
- [379] S.L. Xu, D.Z. Zeng, W.G. Dong, Y.Q. Ding, J. Rao, J.J. Duan, Q. Liu, J. Yang, N. Zhan, Y. Liu, Q.P. Hu, X. Zhang, Y.H. Cui, H.F. Kung, S.C. Yu, X.W. Bian, Distinct patterns of ALDH1A1 expression predict metastasis and poor outcome of colorectal carcinoma, *Int J Clin Exp Pathol.* 7 (2014) 2976–2986.
- [380] Y. Ye, S. Zhang, Y. Chen, X. Wang, P. Wang, High ALDH1A1 expression indicates a poor prognosis in gastric neuroendocrine carcinoma, *Pathol. Res. Pract.* 214 (2018) 268–272. doi:10.1016/j.prp.2017.10.015.
- [381] Y. Liu, D. Lv, J. Duan, S. Xu, J. Zhang, X. Yang, X. Zhang, Y. Cui, X. Bian, S. Yu, ALDH1A1 expression correlates with clinicopathologic features and poor prognosis of breast cancer patients: a systematic review and meta-analysis, *BMC Cancer.* 14 (2014) 444. doi:10.1186/1471-2407-14-444.
- [382] M. Sun, H. Zhao, Q. Xiao, Z. Yu, Z. Song, W. Yao, H. Tang, S. Guan, F. Jin, M. Wei, Combined expression of aldehyde dehydrogenase 1A1 and beta-catenin is associated with lymph node metastasis and poor survival in breast cancer patients following cyclophosphamide treatment, *Oncol Rep.* 34 (2015) 3163–3173. doi:10.3892/or.2015.4273.
- [383] X. Li, L. Wan, J. Geng, C.L. Wu, X. Bai, Aldehyde Dehydrogenase 1A1 Possesses Stem-Like Properties and Predicts Lung Cancer Patient Outcome, *J. Thorac. Oncol.* 7 (2012) 1235–1245. doi:10.1097/JTO.0b013e318257cc6d.
- [384] R.A. Simon, P.A. di Sant’Agnese, L.S. Huang, H. Xu, J.L. Yao, Q. Yang, S. Liang, J. Liu, R. Yu, L. Cheng, W.K. Oh, G.S. Palapattu, J. Wei, J. Huang, CD44 expression is a feature of prostatic small cell Carcinoma and Distinguishes it from its Mimickers, *Hum. Pathol.* 40 (2009) 252–258. doi:10.1016/j.humpath.2008.07.014.
- [385] E. Aguilar Fadó, Metabolic reprogramming and vulnerabilities of prostate cancer stem cells independent of epithelial- mesenchymal transition, (2014).
- [386] C. Bastide, C. Bagnis, P. Mannoni, J. Hassoun, F. Bladou, A Nod Scid mouse model to study human prostate cancer, *Prostate Cancer Prostatic Dis.* 5 (2002) 311–315. doi:10.1038/sj.pcan.4500606.
- [387] D.D. Mickey, R. Stone, H. Wunderli, H. Mickey, R.T. Vollmer, F. David, D. Urology, D. Surgery, D. Universitymedicalcenter, N.C.D.D. M, Heterotransplantation of a Human Prostatic Adenocarcinoma Cell Line in Nude Mice, *Cancer Res.* 37 (1977) 4049–4058.
- [388] S.C. Dolfi, L.L.-Y. Chan, J. Qiu, P.M. Tedeschi, J.R. Bertino, K.M. Hirshfield, Z.N. Oltvai, A. Vazquez, The metabolic demands of cancer cells are coupled to their

- size and protein synthesis rates, *Cancer Metab.* 1 (2013) 20. doi:10.1186/2049-3002-1-20.
- [389] S.Y.C. Choi, S.L. Ettinger, D. Lin, H. Xue, X. Ci, N. Nabavi, R.H. Bell, F. Mo, P.W. Gout, N.E. Fleshner, M.E. Gleave, C.C. Collins, Y. Wang, Targeting MCT4 to reduce lactic acid secretion and glycolysis for treatment of neuroendocrine prostate cancer, *Cancer Med.* 7 (2018) 3385–3392. doi:10.1002/cam4.1587.
- [390] V. Rajendran, M.V. Jain, In Vitro Tumorigenic Assay: Colony Forming Assay for Cancer Stem Cells., *Methods Mol. Biol.* 1692 (2018) 89–95. doi:10.1007/978-1-4939-7401-6_8.
- [391] M.V. Jain, J.R. Jangamreddy, J. Grabarek, F. Schweizer, T. Klonisch, A. Cieślarpobuda, M.J. Łos, Nuclear localized Akt enhances breast cancer stem-like cells through counter-regulation of p21 Waf1/Cip1 and p27 kip1, *Cell Cycle.* 14 (2015) 2109–2120. doi:10.1080/15384101.2015.1041692.
- [392] M. Luo, M. Brooks, M.S. Wicha, Asparagine and Glutamine : Co-conspirators Fueling Metastasis, *Cell Metab.* 27 (2018) 947–949. doi:10.1016/j.cmet.2018.04.012.
- [393] J. Liao, P. Liu, G. Hou, J. Shao, J. Yang, K. Liu, W. Lu, S. Wen, Regulation of stem-like cancer cells by glutamine through β -catenin pathway mediated by redox signaling, *Mol. Cancer.* 16 (2017) 1–13. doi:10.1186/s12943-017-0623-x.
- [394] I. Elia, D. Broekaert, S. Christen, R. Boon, E. Radaelli, M.F. Orth, C. Verfaillie, T.G.P. Grünewald, S.M. Fendt, Proline metabolism supports metastasis formation and could be inhibited to selectively target metastasizing cancer cells, *Nat. Commun.* 8 (2017) 1–11. doi:10.1038/ncomms15267.
- [395] A. Bansal, M.C. Simon, Glutathione metabolism in cancer progression and treatment resistance, *J. Cell Biol.* 217 (2018) 2291–2298.
- [396] R. El-Ansari, M.L. Craze, L. Alfarsi, D. Soria, M. Diez-Rodriguez, C.C. Nolan, I.O. Ellis, E.A. Rakha, A.R. Green, The combined expression of solute carriers is associated with a poor prognosis in highly proliferative ER+ breast cancer, *Breast Cancer Res. Treat.* 175 (2019) 27–38. doi:10.1007/s10549-018-05111-w.
- [397] L.C. Costello, R.B. Franklin, The Intermediary Metabolism of the Prostate : A Key to Understanding ..., *Oncology.* 21201 (2000) 269–282.
- [398] S. Schaffer, H.W. Kim, Effects and Mechanisms of Taurine as a Therapeutic Agent, *Biomol Ther.* 26 (2018) 225–241.
- [399] Y. Tang, Y. Kim, E. Choi, Y.J. Hwang, Taurine Attenuates Epithelial-Mesenchymal Transition-Related Genes in Human Prostate Cancer Cells, *Adv. Exp. Med. Biol.* 975 (2017) 1203–1212. doi:10.1007/978-94-024-1079-2.
- [400] G.L.S. Sholler, W. Ferguson, G. Bergendahl, J.P. Bond, K. Neville, D. Eslin, V. Brown, W. Roberts, R.K. Wada, J. Oesterheld, D. Mitchell, J. Foley, N.S. Parikh, F. Eshun, P. Zage, J. Rawwas, S. Sencer, D. Pankiewicz, M. Quinn, M. Rich, J. Junewick, J.M. Kravka, Maintenance DFMO Increases Survival in High Risk Neuroblastoma, *Sci. Rep.* 8 (2018) 1–9. doi:10.1038/s41598-018-32659-w.

- [401] M. Prunotto, A. Compagnone, M. Bruschi, G. Candiano, S. Colombatto, A. Bandino, A. Petretto, S. Moll, M.L. Bochaton-Piallat, G. Gabbiani, V. Dimuccio, M. Parola, L. Citti, G. Ghiggeri, Endocellular polyamine availability modulates epithelial-to-mesenchymal transition and unfolded protein response in MDCK cells, *Lab. Invest.* 90 (2010) 929–939. doi:10.1038/labinvest.2010.65.
- [402] T. Abaffy, J.R. Bain, M.J. Muehlbauer, I. Spasojevic, S. Lodha, E. Bruguera, S.K. O'Neal, S.Y. Kim, H. Matsunami, A Testosterone Metabolite 19-Hydroxyandrostenedione Induces Neuroendocrine Trans-Differentiation of Prostate Cancer Cells via an Ectopic Olfactory Receptor, *Front. Oncol.* 8 (2018). doi:10.3389/fonc.2018.00162.
- [403] M. Reina-campos, J.F. Linares, A. Duran, C.M. Metallo, J. Moscat, M.T. Diaz-meco, M. Reina-campos, J.F. Linares, A. Duran, T. Cordes, A.L. Hermitte, M.G. Badur, Increased Serine and One-Carbon Pathway Metabolism by PKC δ / ϵ Deficiency Promotes Neuroendocrine Prostate Cancer Article Increased Serine and One-Carbon Pathway Metabolism by PKC δ / ϵ Deficiency Promotes Neuroendocrine Prostate Cancer, *Cancer Cell.* 35 (2019) 385-400.e9. doi:10.1016/j.ccell.2019.01.018.
- [404] S. Nakanishi, J.L. Cleveland, Targeting the polyamine-hypusine circuit for the prevention and treatment of cancer, *Amino Acids.* 48 (2016) 2353–2362. doi:10.1007/s00726-016-2275-3.
- [405] E. Albers, Critical Review Metabolic Characteristics and Importance of the Universal Methionine Salvage Pathway Recycling Methionine from 5' - Methylthioadenosine, *IUBMB Life.* 61 (2009) 1132–1142. doi:10.1002/iub.278.
- [406] D. Sahu, S. Gupta, A.M. Hau, K. Nakashima, M.Z. Leivo, S.C. Searles, P. Elson, J.S. Bomalaski, D.E. Casteel, G.R. Boss, D.E. Hansel, Argininosuccinate Synthetase 1 Loss in Invasive Bladder Cancer Regulates Survival through General Control Nonderepressible 2 Kinase ϵ Mediated Eukaryotic Initiation Factor 2 α Activity and Is Targetable by Pegylated Arginine Deiminase, *Am. J. Pathol.* 187 (2017) 200–213. doi:10.1016/j.ajpath.2016.09.004.
- [407] C. Tsai, H. Chi, L. Chi, H. Yang, M. Tsai, K.-F. Lee, H.-W. Huang, L.-F. Chou, A.-J. Cheng, C.-W. Yang, C.-S. Wang, K.-H. Lin, Argininosuccinate synthetase 1 contributes to gastric cancer invasion and progression by modulating autophagy, *FASEB J.* 32 (2018) 2601–2614. doi:10.1096/fj.201700094R.
- [408] S. Rabinovich, L. Adler, K. Yizhak, A. Sarver, A. Silberman, S. Agron, N. Stettner, Q. Sun, A. Brandis, D. Helbling, S. Korman, S. Itzkovitz, D. Dimmock, I. Ulitsky, S.C.S. Nagamani, E. Ruppin, A. Erez, Diversion of aspartate in ASS1-deficient tumours fosters de novo pyrimidine synthesis, *Nature.* 527 (2015) 379–383. doi:10.1038/nature15529.
- [409] R. Keshet, A. Erez, Arginine and the metabolic regulation of nitric oxide synthesis in cancer, *Dis. Model. Mech.* 11 (2018) dmm033332. doi:10.1242/dmm.033332.
- [410] C. Foguet, C. Balcells, T.M. Thomson, J.B. Cazier, P. de Atauri, M. Cascante, Identification of the molecular drivers of prostate cancer stem cells, (2019) in

preparation.

- [411] R.S. Blanc, S. Richard, Arginine Methylation: The Coming of Age, *Mol. Cell.* 65 (2017) 8–24. doi:10.1016/j.molcel.2016.11.003.
- [412] J. Strobel, F. Müller, O. Zolk, B. Endreß, J. König, M.F. Fromm, R. Maas, Transport of asymmetric dimethylarginine (ADMA) by cationic amino acid transporter 2 (CAT2), organic cation transporter 2 (OCT2) and multidrug and toxin extrusion protein 1 (MATE1), *Amino Acids.* 45 (2013) 989–1002. doi:10.1007/s00726-013-1556-3.
- [413] N.N. Pavlova, S. Hui, J.M. Ghergurovich, J. Fan, A.M. Intlekofer, R.M. White, J.D. Rabinowitz, C.B. Thompson, J. Zhang, As Extracellular Glutamine Levels Decline, Asparagine Becomes an Essential Amino Acid, *Cell Metab.* 27 (2018) 428-438.e5. doi:10.1016/j.cmet.2017.12.006.
- [414] S. Avasarala, M. Van Scoyk, M. Kumar, K. Rathinam, S. Zerayesus, X. Zhao, W. Zhang, M.R. Pergande, J.A. Borgia, J. Degregori, J.D. Port, R.A. Winn, R.K. Bikkavilli, PRMT1 Is a Novel Regulator of Epithelial-Mesenchymal- Transition in Non-small Cell Lung Cancer, *J. Biol. Chem.* 290 (2015) 13479–13489. doi:10.1074/jbc.M114.636050.
- [415] K.R.K. Reddy, C. Dasari, D. Duscharla, B. Supriya, N.S. Ram, M. V. Surekha, J.M. Kumar, R. Ummanni, Dimethylarginine dimethylaminohydrolase-1 (DDAH1) is frequently upregulated in prostate cancer, and its overexpression conveys tumor growth and angiogenesis by metabolizing asymmetric dimethylarginine (ADMA), *Angiogenesis.* 21 (2018) 79–94. doi:10.1007/s10456-017-9587-0.
- [416] L. Kaminski, S. Torrino, M. Dufies, Z. Djabari, R. Haider, F.-R. Roustan, E. Jaune, K. Laurent, N. Nottet, J.-F. Michiels, M. Gesson, S. Rocchi, N.M. Mazure, M. Durand, J.F. Tanti, D. Ambrosetti, S. Clavel, I. Ben-Sahra, F. Bost, PGC-1 α inhibits polyamine synthesis to suppress prostate cancer aggressiveness, *Cancer Res.* 79 (2019) canres.2043.2018. doi:10.1158/0008-5472.can-18-2043.
- [417] L. Huang, J. Liu, X.O. Zhang, K. Sibley, S.M. Najjar, M.M. Lee, Q. Wu, Inhibition of protein arginine methyltransferase 5 enhances hepatic mitochondrial biogenesis, *J. Biol. Chem.* 293 (2018) 10884–10894. doi:10.1074/jbc.RA118.002377.
- [418] W.P. Katt, R.A. Cerione, Glutaminase regulation in cancer cells: A druggable chain of events, *Drug Discov. Today.* 19 (2014) 450–457. doi:10.1016/j.drudis.2013.10.008.
- [419] B.R.B. Pires, A.L. Mencialha, G.M. Ferreira, W.F. De Souza, NF-kappaB Is Involved in the Regulation of EMT Genes in Breast Cancer Cells, (2017) 1–20. doi:10.1371/journal.pone.0169622.
- [420] P.E. Porporato, V.L. Payen, B. Baselet, P. Sonveaux, Metabolic changes associated with tumor metastasis, part 2: Mitochondria, lipid and amino acid metabolism, *Cell. Mol. Life Sci.* 73 (2016) 1349–1363. doi:10.1007/s00018-015-2100-2.
- [421] E. Chan-Penebre, K.G. Kuplast, C.R. Majer, P.A. Boriack-Sjodin, T.J. Wigle, L.D. Johnston, N. Rioux, M.J. Munchhof, L. Jin, S.L. Jacques, K.A. West, T. Lingaraj, K.

- Stickland, S.A. Ribich, A. Raimondi, M.P. Scott, N.J. Waters, R.M. Pollock, J.J. Smith, O. Barbash, M. Pappalardi, T.F. Ho, K. Nurse, K.P. Oza, K.T. Gallagher, R. Kruger, M.P. Moyer, R.A. Copeland, R. Chesworth, K.W. Duncan, A selective inhibitor of PRMT5 with in vivo and in vitro potency in MCL models, *Nat. Chem. Biol.* 11 (2015) 432–437. doi:10.1038/nchembio.1810.
- [422] N. Srour, S.Y. Mersaoui, S. Richard, M-TAP Dance: Targeting PRMT1 and PRMT5 Family Members to Push Cancer Cells Over the Edge, *Cancer Cell.* 36 (2019) 3–5. doi:10.1016/j.ccell.2019.06.004.
- [423] S. Hager, C.J. Ackermann, M. Joerger, S. Gillessen, A. Omlin, Anti-tumour activity of platinum compounds in advanced prostate cancer—a systematic literature review, *Ann. Oncol.* 27 (2016) 975–984. doi:10.1093/annonc/mdw156.
- [424] L.B. Saltz, S. Clarke, E. Díaz-Rubio, W. Scheithauer, A. Figer, R. Wong, S. Koski, M. Lichinitser, T.S. Yang, F. Rivera, F. Couture, F. Sirzén, J. Cassidy, Bevacizumab in combination with oxaliplatin-based chemotherapy as first-line therapy in metastatic colorectal cancer: A randomized phase III study, *J. Clin. Oncol.* 26 (2008) 2013–2019. doi:10.1200/JCO.2007.14.9930.
- [425] M.P. Barr, S.G. Gray, A.C. Hoffmann, R.A. Hilger, J. Thomale, J.D.O. Flaherty, D.A. Fennell, D. Richard, J.J.O. Leary, K.J.O. Byrne, Generation and Characterisation of Cisplatin-Resistant Non-Small Cell Lung Cancer Cell Lines Displaying a Stem- Like Signature, *PLoS One.* 8 (2013) 1–19. doi:10.1371/journal.pone.0054193.
- [426] A.M. Buckley, B.A.S. Bibby, M.R. Dunne, S.A. Kennedy, M.B. Davern, N. Kennedy, S.G. Maher, J.O. Sullivan, Characterisation of an Isogenic Model of Cisplatin Resistance in Oesophageal Adenocarcinoma Cells, *Pharmaceuticals.* 12 (2019) 1–20. doi:10.3390/ph12010033.
- [427] O. Piskareva, H. Harvey, J. Nolan, R. Conlon, L. Alcock, P. Buckley, P. Dowling, M. Henry, F.O. Sullivan, I. Bray, R.L. Stallings, The development of cisplatin resistance in neuroblastoma is accompanied by epithelial to mesenchymal transition in vitro, *Cancer Lett.* 364 (2015) 142–155. doi:10.1016/j.canlet.2015.05.004.
- [428] P.W. Stacpoole, Therapeutic Targeting of the Pyruvate Dehydrogenase Complex/Pyruvate Dehydrogenase Kinase (PDC/PDK) Axis in Cancer, *J. Natl. Cancer Inst.* 109 (2017) 1–14. doi:10.1093/jnci/djx071.
- [429] W. Yu, Y. Chen, J. Dubrulle, F. Stossi, V. Putluri, A. Sreekumar, N. Putluri, D. Baluya, S.Y. Lai, V.C. Sandulache, Cisplatin generates oxidative stress which is accompanied by rapid shifts in central carbon metabolism, *Sci. Rep.* 8 (2018) 1–12. doi:10.1038/s41598-018-22640-y.
- [430] E. Panieri, M.M. Santoro, ROS homeostasis and metabolism: a dangerous liason in cancer cells, *Cell Death Dis.* 7 (2016) e2253. doi:10.1038/cddis.2016.105.
- [431] Y. Choi, H. Kim, W. Shim, M.A. Anwar, J.-W. Kwon, H.-K. Kwon, H.J. Kim, H. Jeong, H.M. Kim, D. Hwang, H.S. Kim, S. Choi, Mechanism of Cisplatin-Induced Cytotoxicity Is Correlated to Impaired Metabolism Due to Mitochondrial ROS Generation, *PLoS One.* 10(8) (2015) 1–21. doi:10.1371/journal.pone.0135083.

- [432] T.M. Stewart, T.T. Dunston, P.M. Woster, R.A. Casero, Polyamine catabolism and oxidative damage, *J. Biol. Chem.* 293 (2018) 18736–18745. doi:10.1074/jbc.TM118.003337.
- [433] R. Tummala, P. Diegelman, S.M. Fiuza, L.A.E. Batista de Carvalho, M.P.M. Marques, D.L. Kramer, K. Clark, S. Vujcic, C.W. Porter, L. Pendyala, Characterization of Pt-, Pd-spermine complexes for their effect on polyamine pathway and cisplatin resistance in A2780 ovarian carcinoma cells., *Oncol. Rep.* 24 (2010) 15–24. doi:10.3892/or.
- [434] K. Takubo, G. Nagamatsu, C.I. Kobayashi, A. Nakamura-ishizu, H. Kobayashi, E. Ikeda, N. Goda, Y. Rahimi, R.S. Johnson, T. Soga, A. Hirao, M. Suematsu, Regulation of Glycolysis by Pdk Functions as a Metabolic Checkpoint for Cell Cycle Quiescence in Hematopoietic Stem Cells, *Cell Stem Cell.* 12 (2013) 49–61. doi:10.1016/j.stem.2012.10.011.
- [435] S.Y. Lee, H.M. Jeon, M.K. Ju, C.H. Kim, G. Yoon, S.I. Han, Wnt / Snail Signaling Regulates Cytochrome c Oxidase and Glucose Metabolism, *Cancer Res.* 72 (2012) 3607–3618. doi:10.1158/0008-5472.CAN-12-0006.
- [436] E. Bauer, X. Domingo, C. Balcells, I.H. Polat, M. Crespo, J. Quirante, J. Badía, L. Baldomà, M. Font-Bardia, M. Cascante, Synthesis, characterization and biological activity of new cyclometallated platinum(IV) iodido complexes, *Dalt. Trans.* 46 (2017) 14973–14987. doi:10.1039/C7DT03448B.
- [437] N. Tamura, K. Hirano, K. Kishino, K. Hashimoto, O. Amano, J. Shimada, H. Sakagami, Analysis of Type of Cell Death Induced by Topoisomerase Inhibitor SN-38 in Human Oral Squamous Cell Carcinoma Cell Lines, *Anticancer Res.* 32 (2012) 4823–4832.
- [438] S. Wu, S. Pan, Z. Xiao, J. Hsu, M. Chen, K. Lee, C. Teng, NPRL-Z-1 , as a New Topoisomerase II Poison , Induces Cell Apoptosis and ROS Generation in Human Renal Carcinoma Cells, *PLoS One.* 9 (2014). doi:10.1371/journal.pone.0112220.
- [439] X. Zhong, M. Xiong, X. Meng, R. Gong, Comparison of the multi-drug resistant human hepatocellular carcinoma cell line Bel-7402 / ADM model established by three methods, *J. Exp. Clin. Cancer Res.* 29 (2010) 1–8.
- [440] L. Li, X. Huang, R. Huang, S. Gou, Z. Wang, H. Wang, Pt (IV) prodrugs containing microtubule inhibitors displayed potent antitumor activity and ability to overcome cisplatin resistance, *Eur. J. Med. Chem.* 156 (2018) 666–679. doi:10.1016/j.ejmech.2018.07.016.
- [441] X. Qin, L. Fang, F. Chen, S. Gou, Conjugation of platinum (IV) complexes with chlorambucil to overcome cisplatin resistance via a “ joint action ” mode toward DNA, *Eur. J. Med. Chem.* 137 (2017) 167–175. doi:10.1016/j.ejmech.2017.05.056.
- [442] G.A. Masters, H.F. Graham, S. Temin, S.B. Jr, D. Trent, C.G. Azzoli, G. Hospital, G. Giaccone, L. Cancer, J.R. Brahmer, J. Thomas, S.K. Comprehensive, J. Hopkins, P.M. Ellis, J. Cancer, N. Rackear, U. Against, F. Lauderdale, H. Joan, D.H. Johnson, Systemic Therapy for Stage IV Non – Small-Cell Lung Cancer : American Society of Clinical Oncology Clinical Practice Guideline Update, *J. Clin. Oncol.* 33 (2018).

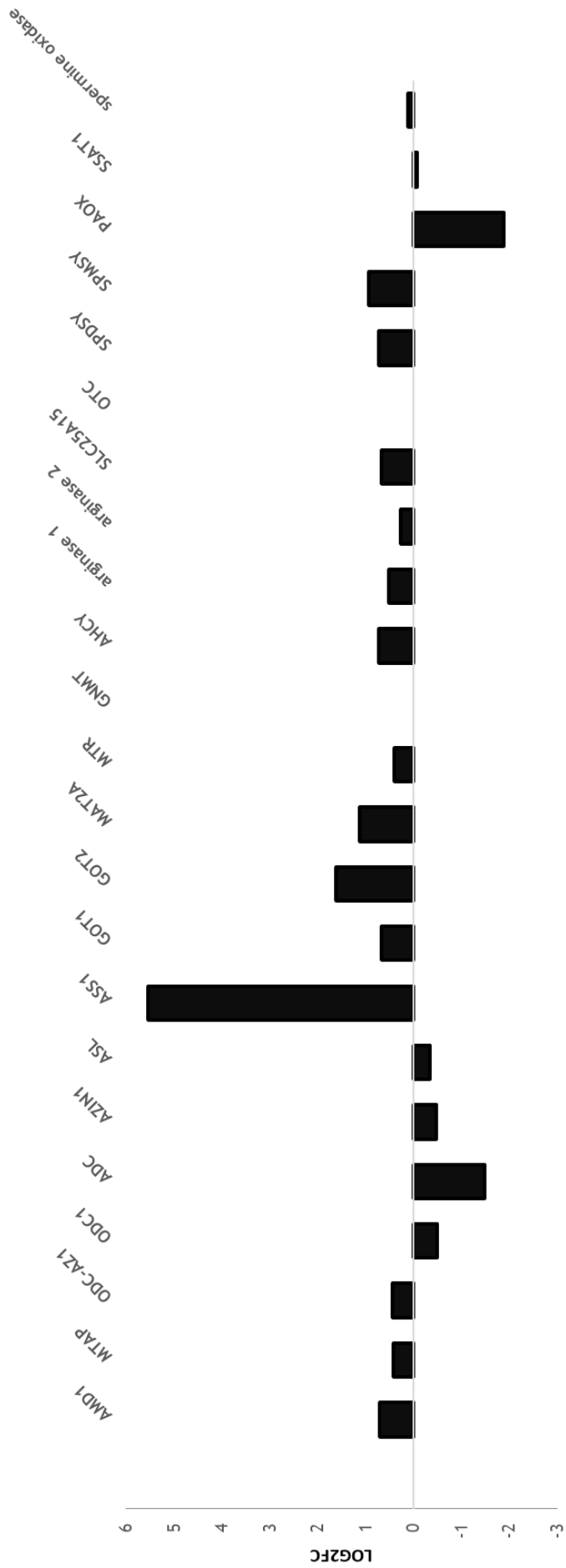
- doi:10.1200/JCO.2015.62.1342.
- [443] M. Solé, C. Balcells, M. Crespo, J. Quirante, J. Badía, L. Baldomà, M. Font-Bardia, M. Cascante, Synthesis, characterization and biological activity of new cyclometallated platinum (IV) complexes containing a para-tolyl ligand, *Dalt. Trans.* 47 (2018) 8956–8971. doi:10.1039/C7DT03448B.
- [444] S. Göschl, H.P. Varbanov, S. Theiner, M.A. Jakupec, M. Galanski, B.K. Keppler, The role of the equatorial ligands for the redox behavior, mode of cellular accumulation and cytotoxicity of platinum(IV) prodrugs, *J. Inorg. Biochem.* 160 (2016) 264–274. doi:10.1016/j.jinorgbio.2016.03.005.
- [445] J. Zhao, W. Hua, G. Xu, S. Gou, Biotinylated platinum(IV) complexes designed to target cancer cells, *J. Inorg. Biochem.* 176 (2017) 175–180. doi:10.1016/j.jinorgbio.2017.08.017.
- [446] E. Petruzzella, J.P. Braude, J.R. Aldrich-Wright, V. Gandin, D. Gibson, A Quadruple-Action Platinum(IV) Prodrug with Anticancer Activity Against KRAS Mutated Cancer Cell Lines, *Angew. Chemie - Int. Ed.* 56 (2017) 11539–11544. doi:10.1002/anie.201706739.
- [447] N. Muramatsu, A.P. Minton, Tracer diffusion of globular proteins in concentrated protein solutions, *PNAS.* 85 (1988) 2984–2988.
- [448] M. Arrio-dupont, G. Foucault, M. Vacher, P.F. Devaux, S. Cribier, Translational Diffusion of Globular Proteins in the Cytoplasm of Cultured Muscle Cells, *Biophys. J.* 78 (2000) 901–907. doi:10.1016/S0006-3495(00)76647-1.
- [449] J. a Dix, a S. Verkman, Crowding effects on diffusion in solutions and cells., *Annu. Rev. Biophys.* 37 (2008) 247–263. doi:10.1146/annurev.biophys.37.032807.125824.
- [450] G. Rivas, J.A. Fernandez, A.P. Minton, Direct Observation of the Self-Association of Dilute Proteins in the Presence of Inert Macromolecules at High Concentration via Tracer Sedimentation Equilibrium: Theory, Experiment, and Biological Significance, *Biochemistry.* 38 (1999) 9379–9388. doi:10.1021/bi990355z.
- [451] S. Mittal, L.R. Singh, Macromolecular crowding decelerates aggregation of a b-rich protein, bovine carbonic anhydrase: a case study, *J. Biochem.* 156 (2014) 273–282. doi:10.1093/jb/mvu039.
- [452] G.A. Siddiqui, A. Naeem, Aggregation of globular protein as a consequences of macromolecular crowding : A time and concentration dependent study, *Int. J. Biol. Macromol.* 108 (2018) 360–366. doi:10.1016/j.ijbiomac.2017.12.001.
- [453] N. Asaad, J.B.F.N. Engberts, Cytosol-Mimetic Chemistry : Kinetics of the Trypsin-Catalyzed Hydrolysis of p-Nitrophenyl Acetate upon Addition of Polyethylene Glycol and N-tert-Butyl Acetoacetamide, *J. Am. Chem. Soc.* 125 (2003) 6874–6875. doi:10.1021/ja034298f.
- [454] C.G. Poggi, K.M. Slade, Macromolecular Crowding and the Steady-State Kinetics of Malate Dehydrogenase, *Biochemistry.* 54 (2015) 260–267.

- [455] S.N. Olsen, Applications of isothermal titration calorimetry to measure enzyme kinetics and activity in complex solutions, *Thermochim. Acta.* 448 (2006) 12–18. doi:10.1016/j.tca.2006.06.019.
- [456] H.-X. Zhou, G. Rivas, A.P. Minton, Macromolecular Crowding and Confinement : Biochemical , Biophysical , and Potential Physiological, *Annu. Rev. Biophys.* 37 (2008) 375–397. doi:10.1146/annurev.biophys.37.032807.125817.
- [457] J.R. Wenner, V. a Bloomfield, Crowding effects on EcoRV kinetics and binding., *Biophys. J.* 77 (1999) 3234–3241. doi:10.1016/S0006-3495(99)77154-7.
- [458] B.K. Derham, J.J. Harding, The effect of the presence of globular proteins and elongated polymers on enzyme activity, *Biochim. Biophys. Acta.* 1764 (2006) 1000–1006. doi:10.1016/j.bbapap.2006.01.005.
- [459] R. Homchaudhuri, L.; Sarma, Navanita; Swaminathan, Effect of Crowding by Dextrans and Ficolls on the Rate of Alkaline Phosphatase-Catalyzed Hydrolysis: A Size-Dependent Investigation, *Biopolymers.* 83 (2006) 477–486. doi:10.1002/bip.
- [460] M.T. Morán-Zorzano, A.M. Viale, F.J. Muñoz, N. Alonso-Casajús, G.G. Eydallín, B. Zugasti, E. Baroja-Fernández, J. Pozueta-Romero, Escherichia coli AspP activity is enhanced by macromolecular crowding and by both glucose-1,6-bisphosphate and nucleotide-sugars, *FEBS Lett.* 581 (2007) 1035–1040. doi:10.1016/j.febslet.2007.02.004.
- [461] L. Pitulice, I. Pastor, E. Vilaseca, S. Madurga, A. Isvoran, M. Cascante, F. Mas, Influence of Macromolecular Crowding on the Oxidation of ABTS by Hydrogen Peroxide Catalyzed by HRP, *J. Biocatal. Biotransformation.* 2 (2013) 1–7.
- [462] U. Deichmann, S. Schuster, J.P. Mazat, A. Cornish-Bowden, Commemorating the 1913 Michaelis-Menten paper Die Kinetik der Invertinwirkung: Three perspectives, *FEBS J.* 281 (2014) 435–463. doi:10.1111/febs.12598.
- [463] L. Michaelis, M.L. Menten, Die Kinetik der Invertinwirkung, *Biochem. Z.* 49 (1913) 333–369.
- [464] D.D.L. Minh, C. Chang, J. Trylska, V. Tozzini, J.A. Mccammon, The Influence of Macromolecular Crowding on HIV-1 Protease Internal Dynamics, (2006) 6006–6007. doi:10.1021/ja060483s.
- [465] H. Berry, Monte Carlo Simulations of Enzyme Reactions in Two Dimensions : Fractal Kinetics and Spatial Segregation, *Biophys. J.* 83 (2002) 1891–1901. doi:10.1016/S0006-3495(02)73953-2.
- [466] S. Schnell, T.E. Turner, Reaction kinetics in intracellular environments with macromolecular crowding: Simulations and rate laws, *Prog. Biophys. Mol. Biol.* 85 (2004) 235–260. doi:10.1016/j.pbiomolbio.2004.01.012.
- [467] G. Schreiber, G. Haran, H.-X. Zhou, Fundamental aspects of protein-protein association kinetics., *Chem. Rev.* 109 (2009) 839–60. doi:10.1021/cr800373w.
- [468] V. Zewe, H.J. Fromm, Kinetic Studies of Rabbit Muscle Lactate Dehydrogenase, *J. Biol. Chem.* 237 (1962) 1668–1675.

- [469] V. Zewe, H.J. Fromm, Kinetic Studies of Rabbit Muscle Lactate Dehydrogenase . II . Mechanism of the Reaction *, *Biochemistry*. 4 (1965) 782–792. doi:10.1021/bi00880a024.
- [470] E. Vilaseca, A. Isvoran, S. Madurga, I. Pastor, J.L. Garcés, F. Mas, New insights into diffusion in 3D crowded media by Monte Carlo simulations: effect of size, mobility and spatial distribution of obstacles., *Phys. Chem. Chem. Phys.* 13 (2011) 7396–407. doi:10.1039/c0cp01218a.
- [471] T.J. Smith, C.A. Stanley, Untangling the glutamate dehydrogenase allosteric nightmare, *Trends Biochem. Sci.* 33 (2008) 557–564. doi:10.1016/j.tibs.2008.07.007.
- [472] A.P. Minton, How can biochemical reactions within cells differ from those in test tubes?, *J. Cell Sci.* 119 (2006) 2863–2869. doi:10.1242/jcs.03063.
- [473] S.A. Wacker, M.J. Bradley, J. Marion, E. Bell, Ligand-induced changes in the conformational stability and flexibility of glutamate dehydrogenase and their role in catalysis and regulation, *Protein Sci.* 19 (2010) 1820–1829. doi:10.1002/pro.459.
- [474] M. Li, C. Li, A. Allen, C.A. Stanley, T.J. Smith, The structure and allosteric regulation of mammalian glutamate dehydrogenase, *Arch. Biochem. Biophys.* 519 (2012) 69–80. doi:10.1016/j.abb.2011.10.015.
- [475] D.E. Koshland Jr, The structural basis of negative cooperativity : receptors and enzymes, *Curr. Opin. Struct. Biol.* 6 (1996) 757–761.
- [476] B.Y.P.C. Engel, K. Dalziel, Kinetic Studies of Glutamate Dehydrogenase with Glutamate and Norvaline as Substrates, *Biochem. J.* 116 (1969) 621–631.
- [477] P. Engel, K. Dalziel, Kinetic Studies of Glutamate Dehydrogenase, *Biochem. J.* 118 (1970) 409–419.
- [478] P.C. Engel, A marriage full of surprises ; forty-five years living with glutamate dehydrogenase, *Neurochem. Int.* 59 (2011) 489–494. doi:10.1016/j.neuint.2011.03.014.
- [479] B.I. Kurganov, Analysis of negative cooperativity for glutamate dehydrogenase, *Biophys. Chem.* 87 (2000) 185–199.
- [480] S. Aghajanian, P.C. Engel, Use of protein engineering to explore subunit interactions in an allosteric enzyme : construction of inter-subunit hybrids in *Clostridium symbiosum* glutamate dehydrogenase, *Protein Eng.* 11 (1998) 569–575.
- [481] M.A. Hamza, P.C. Engel, Homotropic allosteric control in clostridial glutamate dehydrogenase : Different mechanisms for glutamate and NAD+?, *FEBS Lett.* 582 (2008) 1816–1820. doi:10.1016/j.febslet.2008.04.049.
- [482] A. Cornish-Bowden, The physiological significance of negative cooperativity revisited, *J. Theor. Biol.* 319 (2013) 144–147. doi:10.1016/j.jtbi.2012.12.010.
- [483] G. Adair, The Hemoglobin system. VI The oxygen dissociation curve of hemoglobin,

-
- J. Biol. Chem. (1925) 529–545.
- [484] E. di Cera, *Thermodynamic Theory of Site-specific Binding Processes in Biological Macromolecule*, Cambridge University Press, Cambridge, 1995. doi:10.1017/CBO9780511524837.
- [485] J.L. Garcés, F. Mas, J. Puy, J. Galceran, J. Salvador, Use of activity coefficients for bound and free sites to describe metal–macromolecule complexation, *J. Chem. Soc., Faraday Trans. 94* (1998) 2783–2794.
- [486] J.L. Garcés, L. Acerenza, E. Mizraji, F. Mas, A Hierarchical Approach to Cooperativity in Macromolecular and Self-Assembling Binding Systems, *J. Biol. Phys.* 34 (2008) 213–235. doi:10.1007/s10867-008-9116-x.
- [487] C. Balcells, I. Pastor, L. Pitulice, M. Via, S. Madurga, E. Vilaseca, A. Isvoran, M. Cascante, F. Mas, Macromolecular Crowding upon in-vivo-like enzyme kinetics: effect of enzyme-obstacle size ratio, *New Front. Chem.* 24 (2015) 3–16.
- [488] P.S. Steeg, Targeting metastasis, *Nat. Rev. Cancer.* 16 (2016) 201–218. doi:10.1038/nrc.2016.25.
- [489] I.A. Cree, P. Charlton, Molecular chess? Hallmarks of anti-cancer drug resistance, *BMC Cancer.* 17 (2017) 1–8. doi:10.1186/s12885-016-2999-1.
- [490] A.R. Lima, M. de L. Bastos, M. Carvalho, P. Guedes de Pinho, Biomarker discovery in human prostate cancer: An update in metabolomics studies, *Transl. Oncol.* 9 (2016) 357–370. doi:10.1016/j.tranon.2016.05.004.
- [491] M. Jahani, F. Noroznezhad, K. Mansouri, Arginine: Challenges and opportunities of this two-faced molecule in cancer therapy, *Biomed. Pharmacother.* 102 (2018) 594–601. doi:10.1016/j.biopha.2018.02.109.
- [492] J. Zhao, W. Hua, G. Xu, S. Gou, Biotinylated platinum(IV) complexes designed to target cancer cells, *J. Inorg. Biochem.* 176 (2017) 175–180. doi:10.1016/j.jinorgbio.2017.08.017.
- [493] A.A. Tulub, V.E. Stefanov, Cisplatin stops tubulin assembly into microtubules . A new insight into the mechanism of antitumor activity of platinum complexes, 28 (2001) 191–198.
- [494] S. Fang, L. Yu, H. Mei, J. Yang, T. Gao, A. Cheng, W. Guo, K. Xia, G. Liu, Cisplatin promotes mesenchymal-like characteristics in osteosarcoma through Snail, (2016) 5007–5014. doi:10.3892/ol.2016.5342.
- [495] I. Pozdnyakova, P. Wittung-Stafshede, Non-linear effects of macromolecular crowding on enzymatic activity of multi-copper oxidase, *Biochim. Biophys. Acta - Proteins Proteomics.* 1804 (2010) 740–744. doi:10.1016/j.bbapap.2009.11.013.

Appendix 1



Transcript levels (LOG2FC) of the urea cycle reactions and polyamine metabolism in PC-3M and PC-3S analyzed by RNASeq. Abbreviations: adenosylhomocysteinase (AHCY), adenosylmethionine decarboxylase 1 (AMD1), glutaminase (GLS), S-methyl-5'-thioadenosine phosphorylase (MTAP), 5-methyltetrahydrofolate-homocysteine methyltransferase (MTR), ornithine aminotransferase (OAT), proline dehydrogenase (PRODH), pyrroline-5-carboxylate (P5C), pyrroline-5-carboxylate reductase (PYCR), S-adenosylmethionine (SAM), S-adenosyl homocysteine (SAH).

Appendix 2

Antiproliferative screening of cyclometallated Pd (II) compounds containing nitro ligands and ester/methyl-ester ligands

Cyclometallated compounds containing nitro ligands

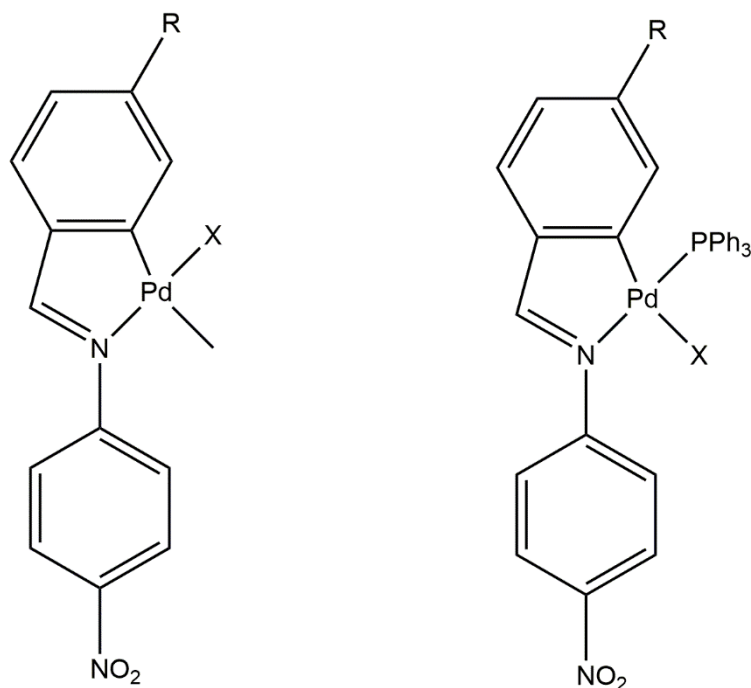


Figure S5.1. Structures of screened palladium cyclometallated nitro compounds. Left structure: **1a** (X = OAc, R = H), **1b** (X = OAc, R = Me), **2a** (X = Cl, R = H), **2b** (X = Cl, R = Me). Right structure: **3a** (X = OAc, R = H), **3b** (X = OAc, R = Me), **4a** (X = Cl, R = H), **4b** (X = Cl, R = Me).

Compound	IC ₅₀ (μM) ^a			
	A549	MDA-MB-231	MCF-7	HCT-116
1a	>100	65 ± 12	>100	35 ± 3
1b	>100	63 ± 3	>100	27 ± 1
2a	>100	> 100	>100	44 ± 4
2b	>100	29 ± 5	58 ± 6	19 ± 6

3a	>100	58 ± 3	>100	>100
3b	>100	>100	>100	>100
4a	>100	>100	>100	34 ± 1
4b	>100	52 ± 11	>100	31 ± 6
cisplatin^b	5.19 ± 0.09	12.31 ± 0.40	24.84 ± 0.40	6.47 ± 0.42

Table S5.2. Antiproliferative activity on A549 lung, MDA-MB-231 and MCF-7 breast, and HCT-116 colorectal cancer cell lines for the novel palladium (II) compounds and cisplatin as reference compound. IC₅₀ values (μM) of compounds **1a-4b** and cisplatin (cis-[PtCl₂(NH₃)₂]), assessed by MTT cell viability assay. Data shown represents mean ± SD of n=3 of at least two independent experiments. Cisplatin is taken as the reference compound.

Cyclometallated compounds containing ester and methyl-ester ligands

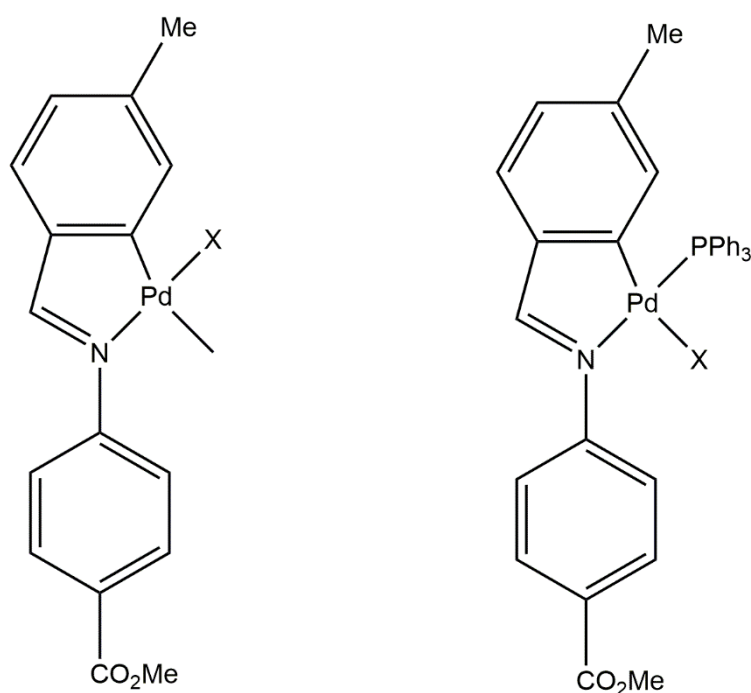


Figure S5.3. Structures of screened palladium cyclometallated methyl-ester compounds. Left structure: **1-methylester** (X = OAc), **2-methylester** (X = Cl). Right structure: **3-methylester** (X = OAc), **4-methylester** (X = Cl).

IC₅₀ (μM)^a

Compound	A549	MDA-MB-231	MCF-7	HCT-116
1-ester	>100	>100	>100	48 ± 2
1-methylester	>100	40 ± 1	>100	>100
2-ester	>100	> 100	>100	26.9 ± 0.9
2-methylester	>100	13.6 ± 0.2	>100	25.4 ± 2
3-ester	59 ± 2	24 ± 1	>100	49 ± 2
3-methylester	>100	45 ± 1	51 ± 1	> 100
4-ester	27 ± 1	>100	>100	72 ± 4
4-methylester	>100	51 ± 1	>100	33 ± 2
cisplatin^b	5.19 ± 0.09	12.31 ± 0.40	24.84	21.1 ± 0.3

Table S5.4. Antiproliferative activity on A549 lung, MDA-MB-231 and MCF-7 breast, and HCT-116 colorectal cancer cell lines for the novel palladium (II) compounds and cisplatin as reference compound. IC₅₀ values (μM) of compounds **1-ester** to **4-methylester** and cisplatin (cis-[PtCl₂(NH₃)₂]), assessed by MTT cell viability assay. Data shown represents mean ± SD of n=3 of at least two independent experiments. Cisplatin is taken as the reference compound.

Appendix 3

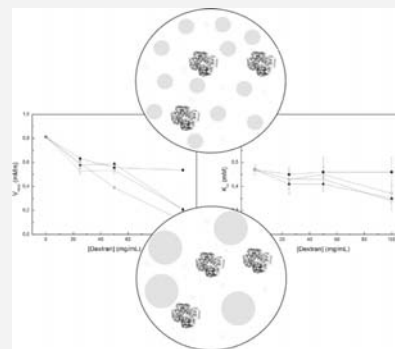
Macromolecular Crowding Effect upon *in Vitro* Enzyme Kinetics: Mixed Activation–Diffusion Control of the Oxidation of NADH by Pyruvate Catalyzed by Lactate Dehydrogenase

Cristina Balcells,[†] Isabel Pastor,^{*,†} Eudald Vilaseca,[†] Sergio Madurga,[†] Marta Cascante,[‡] and Francesc Mas[†]

[†]Department of Physical Chemistry and Research Institute of Theoretical and Computational Chemistry (IQTCUB), University of Barcelona (UB), 08028 Barcelona, Spain

[‡]Department of Biochemistry and Molecular Biology and Institute of Biomedicine (IBUB), University of Barcelona (UB) and IDIBAPS, 08028 Barcelona, Spain

ABSTRACT: Enzyme kinetics studies have been usually designed as dilute solution experiments, which differ substantially from *in vivo* conditions. However, cell cytosol is crowded with a high concentration of molecules having different shapes and sizes. The consequences of such crowding in enzymatic reactions remain unclear. The aim of the present study is to understand the effect of macromolecular crowding produced by dextran of different sizes and at diverse concentrations in the well-known reaction of oxidation of NADH by pyruvate catalyzed by L-lactate dehydrogenase (LDH). Our results indicate that the reaction rate is determined by both the occupied volume and the relative size of dextran obstacles with respect to the enzyme present in the reaction. Moreover, we analyzed the influence of macromolecular crowding on the Michaelis–Menten constants, v_{\max} and K_m . The obtained results show that only high concentrations and large sizes of dextran reduce both constants suggesting a mixed activation–diffusion control of this enzymatic reaction due to the dextran crowding action. From our knowledge, this is the first experimental study that depicts mixed activation–diffusion control in an enzymatic reaction due to the effect of crowding.



INTRODUCTION

It is well-known that up to 40% of the volume of cytosol is occupied by a wide variety of macromolecules and solutes.¹ For this reason, any solute moving through the intracellular environment will see its diffusion rate affected with respect to diffusion in aqueous solution,^{2–8} either being reduced or presenting anomalous diffusion at short times.

Macromolecular crowding inside the cell does affect not only diffusion processes but also biochemical reaction processes by inducing the enzyme to undergo protein folding, self-association, or protein-binding processes,^{9–22} which in turn alter enzymatic activity. Thus, in order to obtain more accurate rates for enzymatic reactions, it is important to perform studies of biochemical processes in nature-like microenvironments that try to mimic this effect. Indeed, there are an important number of works which have studied how enzyme kinetics is affected by crowded environments, even *in vitro*.^{23–41}

The best approach for these sorts of studies would certainly be using cell extracts. However, the experimental data collection and their interpretation would be challenging because cell extracts are complex media that present a high heterogeneity in their geometrical and physical properties. Therefore, the major experimental studies on crowding effect have used purified macromolecules as crowding agents. Dextran is one of them, and its use is widely spread due to its lack of

reactivity and high solubility in water. Moreover, its flexibility and random coil shape in solution are suitable for modeling many macromolecules present in the natural state of the cell. It is also readily available in various sizes and large quantities.

In recent years, the effects of crowding on enzyme catalysis have been explored by different works, excellently depicted by Zhou et al.⁸ and Norris and Malys.³⁴ Most of them indicate that, under Michaelis–Menten conditions in crowded media, excluded volume is the major player in modulating enzymatic behavior. Moreover, gathering all of the contributions published so far, some general trends are encountered. For instance, a slight reduction in the apparent substrate-binding affinity constant, K_m is usually reported, despite the characteristics of the crowding agent.^{9,24,26–32} In contrast, in crowded media experiments, k_{cat} can increase in some cases^{24,25,30–33} or it can also decrease.^{9,25,27,28}

Previously, we reported how the kinetic behavior of two enzymatic reactions is influenced by crowding. Our first study, the hydrolysis of *N*-succinyl-L-phenyl-Ala-*p*-nitroanilide catalyzed by α -chymotrypsin,³⁷ showed that the total volume excluded by dextrans, but not its size, is the property that makes

Received: December 4, 2013

Revised: March 11, 2014

Published: March 24, 2014



Chymotrypsin under Crowded Environment. *Biochimie* **2011**, *93*, 1424–1433.

(36) Hou, S.; Ziebaczyk, N.; Kalwarczyk, T.; Kaminski, T. S.; Wieczorek, S. A.; Holyst, R. Influence of Nano-Viscosity and Depletion Interactions on Cleavage of DNA by Enzymes in Glycerol and Poly(Ethylene Glycol) Solutions: Qualitative Analysis. *Soft Matter* **2011**, *7*, 3092–3099.

(37) Pastor, I.; Vilaseca, E.; Madurga, S.; Garcés, J. L.; Cascante, M.; Mas, F. Effect of Crowding by Dextran on the Hydrolysis of *N*-Succinyl-L-phenyl-Ala-*p*-nitroanilide Catalyzed by α -Chymotrypsin. *J. Phys. Chem. B* **2011**, *115*, 1115–1121.

(38) Akabayov, S. R.; Akabayov, B.; Richardson, C. C.; Wagner, G. Molecular Crowding Enhanced ATPase Activity of the RNA Helicase eIF4A Correlates with Compaction of Its Quaternary Structure and Association with eIF4G. *J. Am. Chem. Soc.* **2013**, *135*, 10040–10047.

(39) Akabayov, B.; Akabayov, S. R.; Lee, S. J.; Wagner, G.; Richardson, C. C. Impact of Macromolecular Crowding on DNA Replication. *Nat. Commun.* **2013**, *4*, No. 1615.

(40) Liu, J.; Peng, J.; Shen, S.; Jin, Q.; Li, C.; Yang, Q. Enzyme Entrapped in Polymer-Modified Nanopores: The Effects of Macromolecular Crowding and Surface Hydrophobicity. *Chem.—Eur. J.* **2013**, *19*, 2711–2719.

(41) Pitulice, L.; Pastor, I.; Vilaseca, E.; Madurga, S.; Isvoran, A.; Cascante, M.; Mas, F. Influence of Macromolecular Crowding on the Oxidation of ABTS by Hydrogen Peroxide Catalyzed by HRP. *J. Biocatal. Biotransformation* **2013**, *2*, 1, doi: 10.4172/2324-9099.1000107.

(42) Cornish-Bowden, A. *Fundamentals of Enzyme Kinetics*, 3rd ed.; Portland Press: London, U.K., 2004.

(43) Lonhienne, T. G. A.; Winzor, D. A Potential Role for Isothermal Calorimetry in Studies of the Effects of Thermodynamic Non-Ideality in Enzyme-Catalyzed Reactions. *J. Mol. Recognit.* **2004**, *17*, 351–361.

(44) Minh, D. D.; Chang, C.; Trylska, J.; Tozzini, V.; McCammon, J. A. The Influence of Macromolecular Crowding on HIV-1 Protease Molecular Dynamics. *J. Am. Chem. Soc.* **2006**, *128*, 6006–6007.

(45) Berry, H. Monte-Carlo Simulations of Enzyme Kinetics in Two Dimensions: Fractal Kinetics and Spatial Segregation. *Biophys. J.* **2002**, *83*, 1891–1901.

(46) Schnell, S.; Turner, T. E. Reaction Kinetics in Intracellular Environments with Macromolecular Crowding: Simulations and Rate Laws. *Prog. Biophys. Mol. Biol.* **2004**, *85*, 235–260.

(47) Pitulice, L. *Aspecte fractale ale structurii și dinamicii biomoleculilor*. Ph.D. thesis, Vest Timișoara University, Timișoara, Romania, 2009. Pitulice, L.; Vilaseca, E.; Pastor, I.; Madurga, S.; Garcés, J. L.; Isvoran, A.; Mas, F. Monte Carlo Simulations of Enzymatic Reactions in Crowded Media. Effect of the Enzyme-Obstacle Relative Size. *Math. Biosci.* **2014**, DOI: 10.1016/j.mbs.2014.03.012.

(48) Zewe, V.; Fromm, H. J. Kinetics Studies of Rabbit Muscle Lactate Dehydrogenase. *J. Biol. Chem.* **1962**, *237*, 1668–1675.

(49) Zewe, V.; Fromm, H. J. Kinetics Studies of Rabbit Muscle Lactate Dehydrogenase II. Mechanism of Reaction. *Biochemistry* **1965**, *4*, 782–792.

(50) Stambaugh, R.; Post, D. Substrate and Product Inhibition of Rabbit Muscle Lactic Dehydrogenase Heart (H_4) and Muscle (M_4) Isozyme. *J. Biol. Chem.* **1966**, *241*, 1462–1467.

(51) Griffin, J. H.; Criddle, R. S. Substrate-Inhibited Lactate Dehydrogenase. Reaction Mechanism and Essential Role of Dissociated Subunits. *Biochemistry* **1970**, *9*, 1195–1205.

(52) Saxton, M. J. Anomalous Diffusion Due to Obstacles: A Monte Carlo Study. *Biophys. J.* **1994**, *66*, 394–401.

(53) Pastor, I.; Vilaseca, E.; Madurga, S.; Garcés, J. L.; Cascante, M.; Mas, F. Diffusion of α -Chymotrypsin in Solution-Crowded Media. A Fluorescence Recovery after Photobleaching Study. *J. Phys. Chem. B* **2010**, *114*, 4028–4034; *J. Phys. Chem. B* **2010**, *114*, 12182 (erratum).

(54) Vilaseca, E.; Isvoran, A.; Madurga, S.; Garcés, J. L.; Pastor, I.; Mas, F. New Insights into Diffusion in 3D Crowded Media by Monte Carlo Simulations: Effect of Size, Mobility and Spatial Distribution of Obstacles. *Phys. Chem. Chem. Phys.* **2011**, *13*, 7396–7407.

(55) Vilaseca, E.; Pastor, I.; Isvoran, A.; Madurga, S.; Garcés, J. L.; Mas, F. Diffusion in Macromolecular Crowded Media. Monte Carlo Simulation of Obstructed Diffusion vs. FRAP Experiments. *Theor. Chem. Acc.* **2011**, *128*, 795–805.

Review

MACROMOLECULAR CROWDING UPON IN-VIVO-LIKE ENZYME-KINETICS: EFFECT OF ENZYME-OBSTACLE SIZE RATIO

*Cristina Balcells*¹, *Isabel Pastor*^{1,2}, *Laura Pitulice*³,
*Claudia Hernández*¹, *Mireia Via*¹, *Josep Lluís Garcés*⁴,
*Sergio Madurga*¹, *Eudald Vilaseca*¹, *Adriana Isvoran*³,
*Marta Cascante*⁵, and *Francesc Mas*^{1,*}

¹ Department of Physical Chemistry and Research Institute of Theoretical and Computational Chemistry (IQTUB) of Barcelona University, C/ Martí I Franquès, 1, 08028-Barcelona (Spain)

² Small Biosystems Lab, Department of Fundamental Physics, University of Barcelona, Barcelona and CIBER-BBN, Carlos III Health Institute, Madrid (Spain)

³ Department of Biology-Chemistry, West University of Timisoara, Timisoara (Romania)

⁴ Department of Chemistry, University of Lleida, Lleida (Spain)

⁵ Department of Biochemistry and Molecular Biology and Institute of Biomedicine (IBUB) of Barcelona University, Barcelona (Spain)

ABSTRACT

In the present work, the volume exclusion phenomenon, also known as macromolecular crowding, has been applied to the field of enzyme kinetics. It has been approached by adding polymeric obstacles in the media of different enzymatic reactions. The concentration and size of these obstacles have been changed systematically in order to obtain kinetic information about each reaction. Results indicate that the performance of a certain enzyme always depends on the amount of excluded volume. However, only large, oligomeric proteins display an obstacle size-dependent behavior. Besides, crowding can hinder diffusion to the extent of being capable of shifting reaction control from activation to diffusion.

Keywords: Enzyme kinetics, crowding, Dextran, excluded volume effects, enzymatic reaction control

* corresponding author: fmas@ub.edu

16. Pozdnyakova, I.; Wittung-Stafshede, P. Non-linear effects of macromolecular crowding on enzymatic activity of multi-copper oxidase. *Biochimica et Biophysica Acta - Proteins and Proteomics* **2010**, *1804*(4), 740–744.
17. Pastor, I.; Vilaseca, E.; Madurga, S.; Garcés, J.L.; Cascante, M.; Mas, F.. Effect of crowding by dextrans on the hydrolysis of N-Succinyl-L-phenyl-Ala-p-nitroanilide catalyzed by α -chymotrypsin. *The Journal of Physical Chemistry. B* **2011**, *115*(5), 1115–21.
18. Pitulice, L.; Pastor, I.; Vilaseca, E.; Madurga, S.; Isvoran, A.; Cascante, M.; Mas, F. Influence of Macromolecular Crowding on the Oxidation of ABTS by Hydrogen Peroxide Catalyzed by HRP. *Journal of Biocatalysis & Biotransformation* **2013**, *2*, 1-5.
19. Balcells, C.; Pastor, I.; Vilaseca, E.; Madurga, S.; Cascante, M.; Mas, F. Macromolecular crowding effect upon in vitro enzyme kinetics: mixed activation-diffusion control of the oxidation of NADH by pyruvate catalyzed by lactate dehydrogenase . *The Journal of Physical Chemistry. B* **2014**, *118*, 4062–8.
20. Pastor, I.; Pitulice, L.; Balcells, C.; Vilaseca, E.; Madurga, S.; Isvoran, A.; Cascante, M.; Mas, F. Effect of crowding by Dextrans in enzymatic reactions. *Biophysical Chemistry* **2014**, *185*, 8-13.
21. Poggi, C. G.; Slade, K. M. Macromolecular Crowding and the Steady-State Kinetics of Malate Dehydrogenase. *Biochemistry* **2015**, *54*, 260–267.
22. Bismuto, E.; Irace, G. The effect of molecular confinement on the conformational dynamics of the native and partly folded state of apomyoglobin. *FEBS Letters* **2001**, *509*, 476–480.
23. Cornish-Bowden, A. *Fundamentals of Enzyme Kinetics*, 4th Ed. Wiley-VCH, Weinheim, Germany, **2012**.
24. Schnell, S. Validity of the Michaelis-Menten equation – steady-state or reactant stationary assumption: that is the question. *FEBS Journal* **2014**, *281*, 464-472.

Cite this: *Dalton Trans.*, 2017, **46**,
14973

Synthesis, characterization and biological activity of new cyclometallated platinum(IV) iodido complexes†

Emma Bauer,^a Xavier Domingo,^a Cristina Balcells,^{b,c} Ibrahim H. Polat,^{b,c}
Margarita Crespo,^{b,*a,c} Josefina Quirante,^{b,*c,d} Josefa Badía,^{b,c,e}
Laura Baldomà,^{b,c,e} Mercè Font-Bardia^{b,f} and Marta Cascante^{b,c}

The synthesis of six novel cyclometallated platinum(IV) iodido complexes is accomplished by intermolecular oxidative addition of methyl iodide (compounds **2a–2c**) or iodine (compounds **3a–3c**) upon cyclometallated platinum(II) compounds [PtX((CH₃)₂N(CH₂)₃NCH(4-ClC₆H₃))] (**1a–1c**: X = Cl, CH₃ or I). The X-ray molecular structures of platinum(II) compound **1c** and platinum(IV) compounds **3b** and **3a'** (an isomer of **3a**) are reported. The cytotoxic activity against a panel of human adenocarcinoma cell lines (A-549 lung, MDA-MB-231 and MCF-7 breast, and HCT-116 colon), DNA interaction, topoisomerase I, II α , and cathepsin B inhibition, and cell cycle arrest, apoptosis and ROS generation of the investigated complexes are presented. Remarkable antiproliferative activity was observed for most of the synthesized cycloplatinated compounds (series **1–3**) in all the selected carcinoma cell lines. The best inhibition was provided for the octahedral platinum(IV) compounds **2a–2c** exhibiting a methyl and an iodido axial ligand. Preliminary biological results point to a different mechanism of action for the investigated compounds. Cyclometallated platinum(II) compounds **1a–1c** modify the DNA migration as cisplatin. In contrast, cyclometallated platinum(IV) compounds **2a–2c** and **3a–3c** did not modify the DNA tertiary structure neither in the absence nor in the presence of ascorbic acid, which made them incapable of reducing platinum(IV) compounds **2b** and **2c** in a buffered aqueous medium (pH 7.40) according to ¹H NMR experiments. Remarkable topoisomerase II α inhibitory activity is reported for platinum(IV) complexes **2b** and **3a** and in addition, for the last one, a moderate cathepsin B inhibition is reported. Cell cycle arrest (decrease in G₀/G₁ and G₂ phases and arrest in the S phase), induction of apoptosis and ROS generation are related to the antiproliferative activity of some representative octahedral cyclometallated platinum(IV) compounds (**2b** and **2c**).

Received 14th September 2017,
Accepted 29th September 2017

DOI: 10.1039/c7dt03448b

rsc.li/dalton

^aDepartament de Química Inorgànica i Orgànica, Secció de Química Inorgànica, Facultat de Química, Universitat de Barcelona, Diagonal 645, 08028-Barcelona, Spain. E-mail: margarita.crespo@qi.ub.es

^bDepartment of Biochemistry and Molecular Biomedicine, Faculty of Biology, Universitat de Barcelona, Av. Diagonal 643, 08028-Barcelona, Spain

^cInstitut de Biomedicina de la Universitat de Barcelona (IBUB), Av. Diagonal 643, 08028-Barcelona, Spain

^dLaboratori de Química Orgànica, Facultat de Farmàcia, Universitat de Barcelona, Av. Joan XXIII, 27-31, 08028-Barcelona, Spain. E-mail: quirantese@ub.edu

^eDepartament de Bioquímica i Fisiologia, Secció de Bioquímica i Biologia Molecular, Facultat de Farmàcia, Av. Joan XXIII, 27-31, 08028-Barcelona, Spain

^fUnitat de Difracció de RX, Centres Científics i Tecnològics de la Universitat de Barcelona (CCiTUB), Universitat de Barcelona, Solé i Sabarís 1-3, 08028-Barcelona, Spain

† Electronic supplementary information (ESI) available: Fig. S1–S4 showing the NMR spectra of **2b** and **2c** in D₂O-d⁶-DMSO in the absence and in the presence of ascorbic acid at different storage periods. The crystallographic data of compounds **1c**, **3b** and **3a'**. CCDC 1565438–1565440. For ESI and crystallographic data in CIF or other electronic format see DOI: 10.1039/c7dt03448b

Introduction

Following the well-established square-planar platinum(II) anti-cancer drugs, octahedral platinum(IV) complexes currently attract a great deal of attention as they display a number of advantages related to their inertness and to the possibility of tuning their properties through the additional axial ligands.^{1–4} Although several platinum(IV) complexes have undergone clinical trials, none has been approved to date, and the rational design of new platinum(IV) potential antitumor agents still remains a challenge.

On the other hand, in the last few years, the antitumor properties of cyclometallated platinum(II) compounds have been studied by several groups^{5–12} including ours.^{13–16} These compounds present several advantages such as high stability and increased lability of the leaving groups due to the strong *trans*-effect of C-donor ligands. Surprisingly, very little attention has

- 70 G. M. Sheldrick, *Acta Crystallogr., Sect. C: Cryst. Struct. Commun.*, 2015, **71**, 3–8.
- 71 T. Mosmann, *J. Immunol. Methods*, 1983, **65**, 55–63.
- 72 C. Matito, F. Mastorakou, J. J. Centelles, J. L. Torres Simón and M. C. Serratos, *Eur. J. Nutr.*, 2003, **42**, 43–49.
- 73 A. Abdullah, F. Huq, A. Chowdhury, H. Tayyem, P. Beale and K. Fisher, *BMC Chem. Biol.*, 2006, **6**, 3.
- 74 A. Casini, C. Gabbiani, F. Sorrentino, M. P. Rigobello, A. Bindoli, T. J. Geldbach, A. Marrone, N. Re, C. G. Hartinger, P. J. Dyson and L. Messori, *J. Med. Chem.*, 2008, **51**, 6773–6781.
- 75 M. Tarrado-Castellarnau, R. Cortés, M. Zanuy, J. Tarragó-Celada, I. H. Polat, R. Hill, T. W. M. Fan, W. Link and M. Cascante, *Pharmacol. Res.*, 2015, **102**, 218–234.



The importance of post-translational modifications in systems biology approaches to identify therapeutic targets in cancer metabolism

Alfonso Martín-Bernabé^{1,2,3,4,5}, Cristina Balcells^{1,5},
Josep Tarragó-Celada^{1,5}, Carles Foguet^{1,5},
Sandrine Bourgoïn-Voillard^{2,3,4}, Michel Seve^{2,3,4} and
Marta Cascante¹

Abstract

Cancer metabolism is reprogrammed to fulfill the needs of proliferation and migration, which is accomplished through different levels of regulation. In recent years, new advances in protein post-translational modifications (PTMs) research have revealed a complex layer of regulatory mechanisms through which PTMs control cell signaling and metabolic pathways, contributing to the diverse metabolic phenotypes found in cancer. Despite the efficacy of current modeling approaches to study cancer metabolism they still lack the capacity to integrate PTMs in their predictions. Here we will review the importance of PTMs in cancer metabolic reprogramming and suggest ways in which computational predictions could be enhanced through the integration of PTMs.

Addresses

¹ Department of Biochemistry and Molecular Biomedicine, Universitat de Barcelona and Institute of Biomedicine of Universitat de Barcelona (IBUB), Barcelona, Spain

² Univ. Grenoble Alpes, LBFA et BEeSy, PROMETHEE Proteomic Platform, Grenoble, France

³ Inserm, U1055, PROMETHEE Proteomic Platform, Grenoble, France

⁴ CHU de Grenoble, Institut de Biologie et de Pathologie, PROMETHEE Proteomic Platform, Grenoble, France

Corresponding author: Cascante, Marta (martacascante@ub.edu)

Email addresses: alf.martin@gmail.com (A. Martín-Bernabé),

crisgatsu@gmail.com (C. Balcells), jtarragocelada@ub.edu

(J. Tarragó-Celada), cfoguet@ub.edu (C. Foguet),

sandrine.bourgoïn@univ-grenoble-alpes.fr (S. Bourgoïn-Voillard),

michel.seve@univ-grenoble-alpes.fr (M. Seve)

⁵ These authors contributed equally to this work.

Introduction

Cancer is a complex and heterogeneous disease, which involves alteration of multiple biological processes. Some of these alterations are geared towards metabolic reprogramming, which provides advantages to cancer cells in terms of energy production and synthesis of biomolecules and is essential for tumor progression. Understanding metabolic reprogramming in heterogeneous tumor cell populations is key to identify metabolic vulnerabilities in cancer that can be exploited in therapy [1].

Metabolism is a complex network of biochemical reactions that requires a systemic view. Computational models have emerged as platforms to integrate multi-omics data (genomics, transcriptomics, proteomics, metabolomics, etc.), and therefore to understand the underlying metabolic phenotype. However current modeling approaches have a limited capacity to integrate modifications that occur at a post-translational level hence limiting their usefulness at analyzing cancer metabolic reprogramming.

Here, we review recent studies regarding the role of post-translational modifications (PTMs) in cancer metabolic reprogramming, mainly focusing on central carbon metabolism. In this context, we assess how computational predictions through genome-scale metabolic models (GSMs) and kinetic models could be enhanced through the integration of PTMs.

Metabolic reprogramming in cancer

The most common metabolic adaptation in cancer is the Warburg effect, consisting of high glucose uptake, glycolytic activity, and lactate production even under aerobic conditions [2]. However, metabolic reprogramming is not limited to the Warburg effect and usually involves the enhancement of other essential metabolic pathways including pentose phosphate pathway (PPP), glutaminolysis, and amino acid and lipid metabolisms [3].

Tumor cells display metabolic flexibility, which allows them to undergo metabolic switches and use different energy and carbon sources depending on their

Current Opinion in Systems Biology 2017, 3:161–169

This review comes from a themed issue on **Clinical and translational systems biology (2017)**

Edited by **Jesper Tegnér** and **David Gomez-Cabrero**

For a complete overview see the **Issue** and the **Editorial**

Available online 19 May 2017

<http://dx.doi.org/10.1016/j.coisb.2017.05.011>

2452-3100/© 2017 Elsevier Ltd. All rights reserved.

42. Nguyen TL, Durán RV: **Prolyl hydroxylase domain enzymes and their role in cell signaling and cancer metabolism.** *Int J Biochem Cell Biol* 2016, **80**:71–80.
43. Luo W, Hu H, Chang R, Zhong J, Knabel M, O'Meally R, Cole RN, Pandey A, Semenza GL: **Pyruvate kinase M2 is a PHD3-stimulated coactivator for hypoxia-inducible factor 1.** *Cell* 2011, **145**:732–744.
44. Kikuchi D, Minamishima YA, Nakayama K: **Prolyl-hydroxylase PHD3 interacts with pyruvate dehydrogenase (PDH)-E1 β and regulates the cellular PDH activity.** *Biochem Biophys Res Commun* 2014, **451**:288–294.
45. German NJ, Yoon H, Yusuf RZ, Scadden DT, Kaelin WG, Haigis MC: **PHD3 loss in cancer enables metabolic reliance on fatty acid oxidation via deactivation of ACC2.** *Mol Cell* 2016, **63**:1006–1020.
46. Theurillat JP, Udeshi ND, Errington WJ, Svinkina T, Baca SC, Pop M, Wild PJ, Blattner M, Groner AC, Rubin MA, Moch H, Privé GG, Carr SA, Garraway LA: **Prostate cancer. Ubiquitylome analysis identifies dysregulation of effector substrates in SPOP-mutant prostate cancer.** *Science* 2014 Oct 3, **346**:85–89.
47. Xu YM, Wang HJ, Chen F, Guo WH, Wang YY, Li HY, Tang JH, Ding Y, Shen YC, Li M, *et al.*: **HRD1 suppresses the growth and metastasis of breast cancer cells by promoting IGF-1R degradation.** *Oncotarget* 2015, **6**:42854–42867.
48. Han C, Yang L, Choi HH, Baddour J, Achreja A, Liu Y, Li Y, Li J, Wan G, Huang C, *et al.*: **Amplification of USP13 drives ovarian cancer metabolism.** *Nat Commun* 2016, **7**:13525.
49. Liu K, Li F, Han H, Chen Y, Mao Z, Luo J, Zhao Y, Zheng B, Gu W, Zhao W: **Parkin regulates the activity of pyruvate kinase M2.** *J Biol Chem* 2016, **291**:10307–10317.
 This work elucidated the role of Parkin in tumor cell metabolism by ubiquitination of PKM2.
50. Bian X, Chen H, Yang P, Li Y, Zhang F, Zhang J, Wang W, Zhao W, Zhang S, Chen Q, *et al.*: **Nur77 suppresses hepatocellular carcinoma via switching glucose metabolism toward gluconeogenesis through attenuating phosphoenolpyruvate carboxykinase sumoylation.** *Nat Commun* 2017, **8**:1–14.
51. Tan M, Peng C, Anderson KA, Chhoy P, Xie Z, Dai L, Park J, Chen Y, Huang H, Zhang Y, *et al.*: **Lysine glutarylation is a protein posttranslational modification regulated by SIRT5.** *Cell Metab* 2014, **19**:605–617.
52. Hirschev MD, Zhao Y: **Metabolic regulation by lysine malonylation, succinylation, and glutarylation.** *Mol Cell Proteomics* 2015, **14**:2308–2315.
53. Du Y, Cai T, Li T, Xue P, Zhou B, He X, Wei P, Liu P, Yang F, Wei T: **Lysine malonylation is elevated in type 2 diabetic mouse models and enriched in metabolic associated proteins.** *Mol Cell Proteomics* 2015, **14**:227–236.
54. Xu H, Chen X, Xu X, Shi R, Suo S, Cheng K, Zheng Z, Wang M, Wang L, Zhao Y, *et al.*: **Lysine acetylation and succinylation in HeLa cells and their essential roles in response to UV-induced stress.** *Sci Rep* 2016, **6**:30212.
55. Zhou L, Wang F, Sun R, Chen X, Zhang M, Xu Q, Wang Y, Wang S, Xiong Y, Guan K: **SIRT5 promotes IDH2 desuccinylation and G6PD deglutarylation to enhance cellular antioxidant defense.** *EMBO Rep* 2016, **36**:1–12.
56. Marín de Mas I, Aguilar E, Jayaraman A, Polat IH, Martín-Bernabé A, Bharat R, Foguet C, Milà E, Papp B, Centelles JC, *et al.*: **Cancer cell metabolism as new targets for novel designed therapies.** *Future Med Chem* 2014, **6**:1791–1810.
57. Megchelenbrink W, Katzir R, Lu X, Ruppín E, Notebaart R a: **Synthetic dosage lethality in the human metabolic network is highly predictive of tumor growth and cancer patient survival.** *Proc Natl Acad Sci U S A* 2015, **112**:12217–12222.
 This study presents a method that can systematically identify metabolic vulnerabilities specific for cancer cells overexpressing a given metabolic gene.
58. Yizhak K, Chaneton B, Gottlieb E, Ruppín E: **Modeling cancer metabolism on a genome scale.** *Mol Syst Biol* 2015, **11**:817–817.
59. König M, Bulik S, Holzhütter H-G: **Quantifying the contribution of the liver to glucose homeostasis: a detailed kinetic model of human hepatic glucose metabolism.** *PLoS Comput Biol* 2012, **8**:e1002577.
60. Stanford NJ, Lubitz T, Smallbone K, Klipp E, Mendes P, Liebermeister W: **Systematic construction of kinetic models from genome-scale metabolic networks.** *PLoS One* 2013, **8**.
61. Khodayari A, Maranas CD: **A genome-scale Escherichia coli kinetic metabolic model satisfying flux data for multiple mutant strains.** *Nat Commun* 2016, **7**:1–12.

Cite this: *Dalton Trans.*, 2018, **47**,
8956

Synthesis, characterization and biological activity of new cyclometallated platinum(IV) complexes containing a *para*-tolyl ligand†

Mònica Solé,^{‡a} Cristina Balcells,^{‡b,c} Margarita Crespo,^{‡*a,c}
Josefina Quirante,^{‡*c,d} Josefa Badia,^{‡c,e} Laura Baldomà,^{‡c,e}
Mercè Font-Bardia,^{‡f} and Marta Cascante,^{‡b,c,g}

The synthesis of three new cyclometallated platinum(II) compounds containing a *para*-tolyl ligand and a tridentate [C,N,N'] (**cm1**) or a bidentate [C,N] ligand and an additional ligand such as SEt₂ (**cm2**) or PPh₃ (**cm3**) is reported. The X-ray molecular structure of platinum(II) compound **cm3** is also presented. Intermolecular oxidative addition of methyl iodide or iodine upon **cm1**, **cm2** and **cm3** produced six novel cyclometallated platinum(IV) compounds. The cytotoxic activity against a panel of human adenocarcinoma cell lines (A-549 lung, MDA-MB-231 and MCF-7 breast, and HCT-116 colon), DNA interaction, topoisomerase I, II α , and cathepsin B inhibition, and cell cycle arrest, apoptosis and ROS generation of the investigated complexes are presented. The best results for antiproliferative activity were obtained for platinum(IV) compounds **cm1MeI** and **cm1I₂** arising from oxidative addition of methyl iodide and iodine, respectively, to **cm1**. Cyclometallated platinum(IV) compounds **cm1MeI** and **cm3MeI** induce significant changes in the mobility of DNA and, in addition, **cm1MeI**, **cm3MeI** and **cm1I₂**, showed considerable topoisomerase II α inhibitory activity. Moreover, the compounds exhibiting the higher antiproliferative activity (**cm1MeI** and **cm1I₂**) were found to generate ROS and to suppress HCT-116 colon cancer cell growth by a mixture of cell cycle arrest and apoptosis induction. ¹H NMR experiments carried out in a buffered aqueous medium (pH 7.40) indicate that compound **cm1MeI** is not reduced by common biologically relevant reducing agents such as ascorbic acid, glutathione or cysteine.

Received 23rd March 2018,

Accepted 14th June 2018

DOI: 10.1039/c8dt01124a

rsc.li/dalton

^aDepartament de Química Inorgànica i Orgànica, Secció de Química Inorgànica, Facultat de Química, Universitat de Barcelona, Diagonal 645, 08028-Barcelona, Spain. E-mail: margarita.crespo@qi.ub.es

^bDepartment of Biochemistry and Molecular Biomedicine, Faculty of Biology, Universitat de Barcelona, Av. Diagonal 643, 08028-Barcelona, Spain

^cInstitut de Biomedicina de la Universitat de Barcelona (IBUB), Av. Diagonal 643, 08028-Barcelona, Spain

^dLaboratori de Química Orgànica, Facultat de Farmàcia, Universitat de Barcelona, Av. Joan XXIII, 27-31, 08028-Barcelona, Spain. E-mail: quirantese@ub.edu

^eDepartament de Bioquímica i Fisiologia, Secció de Bioquímica i Biologia Molecular, Facultat de Farmàcia, Av. Joan XXIII, 27-31, 08028-Barcelona, Spain

^fUnitat de Difracció de RX, Centres Científics i Tecnològics de la Universitat de Barcelona (CCiTUB), Universitat de Barcelona, Solé i Sabarís 1-3, 08028-Barcelona, Spain

^gCentro de Investigación Biomédica en Red de Enfermedades Hepáticas y digestivas (CIBEREHD), Instituto de Salud Carlos III (ISCIII), Madrid, Spain

† Electronic supplementary information (ESI) available: Fig. S1–S4 showing the NMR spectra of **cm1MeI** in D₂O–d⁶-DMSO in the absence of reduction agents and in the presence of ascorbic acid, glutathione or cysteine at different storage periods. CCDC 1830967 for **cm3**. For ESI and crystallographic data in CIF or other electronic format see DOI: 10.1039/c8dt01124a

‡ These authors contributed equally to this work.

Introduction

Metal containing anticancer drugs started to be relevant more than 40 years ago with the discovery of the therapeutic potential of cisplatin. More recently, platinum(IV) compounds have attracted great interest due to their advantages over platinum(II) analogues.^{1–6} Platinum(IV) compounds exhibit an octahedral coordination that permits the modification of some important physicochemical properties such as lipophilicity, stability and the reduction potential through the two extra coordination positions. Moreover, they are kinetically inert compared to platinum(II) analogues, which allows the possibility of oral administration.

On the other hand, platinum(II) cyclometallated compounds, especially those with nitrogen donor atoms, attract great interest due to their antitumour properties.⁷ They benefit from a strong σ (M–C) bond that improves their stability in front of biological reduction and labilises the *trans* ligands allowing the exchange in cellular uptake.

Surprisingly, very little attention has been devoted to cyclometallated platinum(IV) compounds although these species

- 37 N. D'Arcy and B. Gabrielli, *Curr. Med. Chem.*, 2017, **24**, 1504–1519.
- 38 S. P. Fricker, *Metallomics*, 2010, **2**, 366–377.
- 39 S. Diaz-Moralli, M. Tarrado-Castellarnau, A. Miranda and M. Cascante, *Pharmacol. Ther.*, 2013, **138**, 255–271.
- 40 M. Zanuy, A. Ramos-Montoya, O. Villacañas, N. Canela, A. Miranda, E. Aguilar, N. Agell, O. Bachs, J. Rubio-Martinez, M. D. Pujol, W. N. P. Lee, S. Marin and M. Cascante, *Metabolomics*, 2012, **8**, 454–464.
- 41 N. P. Fusté, R. Fernández-Hernández, T. Cemeli, C. Mirantes, N. Pedraza, M. Rafel, J. Torres-Rosell, N. Colomina, F. Ferrezuelo, X. Dolcet and E. Garí, *Nat. Commun.*, 2016, 1–14.
- 42 G. Wu, L. Xu, N. Lin and B. Liu, *BMC Cancer*, 2013, **13**, 1–9.
- 43 G. R. Bean, Y. T. Ganesan, Y. Dong, S. Takeda, H. Liu, P. M. Chan, Y. Huang, L. A. Chodosh, G. P. Zambetti, J. J. D. Hsieh and E. H. Y. Cheng, *Sci. Signaling*, 2013, **6**, 1–14.
- 44 I. Vermes, H. Clemens, H. Steffens-Nakken and C. J. Reutelingsperger, *Immunol. Methods*, 1995, **184**, 39–51.
- 45 C. M. Henry, E. Hollville and S. J. Martin, *Methods*, 2013, **61**, 90–97.
- 46 M. W. Lee, S. C. Park, Y. G. Yang, S. O. Yim, H. S. Chae, J. H. Bach, H. Lee, K. Y. Kim, W. B. Lee and S. S. Kim, *FEBS Lett.*, 2002, **512**, 313–318.
- 47 E. Giannoni, F. Buricchi, G. Raugei, G. Ramponi and P. Chiarugi, *Mol. Cell. Biol.*, 2005, **25**, 6391–64033.
- 48 P. Gao, H. Zhang, R. Dinavahi, F. Li, Y. Xiang, V. Raman, Z. M. Bhujwalla, D. W. Felsher, L. Cheng, J. Pevsner, L. A. Lee, G. L. Semenza and C. V. Dang, *Cancer Cell*, 2007, **12**, 230–238.
- 49 A. L. Fitzgerald, A. A. Osman, T. X. Xie, A. Patel, H. Skinner, V. Sandulache and J. N. Myers, *Cell Death Dis.*, 2015, **6**, 1678–1610.
- 50 C. Garrido, L. Galluzzi, M. Brunet, P. E. Puig, C. Didelot and G. Kroemer, *Cell Death Differ.*, 2006, **13**, 1423–1433.
- 51 A. Tubbs and A. Nussenzweig, *Cell*, 2017, **168**, 644–656.
- 52 A. Miyajima, J. Nakashima, K. Yoshioka, M. Tachibana, H. Tazaki and M. Murai, *Br. J. Cancer*, 1997, **76**, 206–210.
- 53 S. Dasari and P. B. Tchounwou, *Eur. J. Pharmacol.*, 2014, **740**, 364–378.
- 54 V. Pichler, S. Göschl, E. Schreiber-Brynzak, M. A. Jakupec, M. Galanski and B. K. Keppler, *Metallomics*, 2015, **7**, 1078–1090.
- 55 S. Göschl, H. P. Varbanov, S. Theiner, M. A. Jakupec, M. Galanski and B. K. Keppler, *J. Inorg. Biochem.*, 2016, **160**, 264–274.
- 56 M. A. Casado-Lacabra, A. J. Canty, M. Lutz, J. Patel, A. L. Spek, H. Sun and G. van Koten, *Inorg. Chim. Acta*, 2002, **327**, 15–19.
- 57 G. M. Sheldrick, *Acta Crystallogr., Sect. C: Struct. Chem.*, 2015, **71**, 3–8.
- 58 T. Mosmann, *J. Immunol. Methods*, 1983, **65**, 55–63.
- 59 C. Matito, F. Mastorakou, J. J. Centelles, J. L. Torres Simón and M. C. Serratos, *Eur. J. Nutr.*, 2003, **42**, 43–49.
- 60 A. Casini, C. Gabbiani, F. Sorrentino, M. P. Rigobello, A. Bindoli, T. J. Geldbach, A. Marrone, N. Re, C. G. Hartinger, P. J. Dyson and L. Messori, *J. Med. Chem.*, 2008, **51**, 6773–6781.
- 61 M. Tarrado-Castellarnau, R. Cortés, M. Zanuy, J. Tarragó-Celada, I. H. Polat, R. Hill, T. W. M. Fan, W. Link and M. Cascante, *Pharmacol. Res.*, 2015, **102**, 218–234.

RESEARCH ARTICLE

Model-driven discovery of long-chain fatty acid metabolic reprogramming in heterogeneous prostate cancer cells

Igor Marín de Mas^{1,2,3}, Esther Aguilar^{1,2}, Erika Zodda^{1,2,4}, Cristina Balcells^{1,2}, Silvia Marin^{1,2}, Guido Dallmann⁵, Timothy M. Thomson⁴, Balázs Papp^{3*}, Marta Cascante^{1,2*}

1 Department of Biochemistry and Molecular Biomedicine, Faculty of Biology, Universitat de Barcelona, Barcelona, Spain, **2** Institute of Biomedicine of University of Barcelona (IBUB) and Associated Unit with CSIC, Barcelona, Spain, **3** Synthetic and Systems Biology Unit, Institute of Biochemistry, Biological Research Center of the Hungarian Academy of Sciences, Szeged, Hungary, **4** Department of Cell Biology, Barcelona Institute for Molecular Biology (IBMB), National Research Council (CSIC), Barcelona, Spain, **5** Biocrates Life Sciences AG, Innsbruck, Austria

* pappb@brc.hu (BP); martacascante@ub.edu (MC)



OPEN ACCESS

Citation: Marín de Mas I, Aguilar E, Zodda E, Balcells C, Marin S, Dallmann G, et al. (2018) Model-driven discovery of long-chain fatty acid metabolic reprogramming in heterogeneous prostate cancer cells. *PLoS Comput Biol* 14(1): e1005914. <https://doi.org/10.1371/journal.pcbi.1005914>

Editor: Nathan E Lewis, University of California San Diego, UNITED STATES

Received: July 7, 2017

Accepted: December 1, 2017

Published: January 2, 2018

Copyright: © 2018 Marín de Mas et al. This is an open access article distributed under the terms of the [Creative Commons Attribution License](https://creativecommons.org/licenses/by/4.0/), which permits unrestricted use, distribution, and reproduction in any medium, provided the original author and source are credited.

Data Availability Statement: All relevant data are within the paper and its Supporting Information files.

Funding: This work was supported by the European Commission Seventh Framework Programme FP7 (METAFLUX-Marie Curie FP7-PEOPLE-2010 ITN-264780); the Spanish Government and the European Union FEDER funds (SAF2014-56059-R, SAF2015-70270-REDT and SAF2015-66984-C2-1-R); Generalitat de Catalunya-

Abstract

Epithelial-mesenchymal-transition promotes intra-tumoral heterogeneity, by enhancing tumor cell invasiveness and promoting drug resistance. We integrated transcriptomic data for two clonal subpopulations from a prostate cancer cell line (PC-3) into a genome-scale metabolic network model to explore their metabolic differences and potential vulnerabilities. In this dual cell model, PC-3/S cells express Epithelial-mesenchymal-transition markers and display high invasiveness and low metastatic potential, while PC-3/M cells present the opposite phenotype and higher proliferative rate. Model-driven analysis and experimental validations unveiled a marked metabolic reprogramming in long-chain fatty acids metabolism. While PC-3/M cells showed an enhanced entry of long-chain fatty acids into the mitochondria, PC-3/S cells used long-chain fatty acids as precursors of eicosanoid metabolism. We suggest that this metabolic reprogramming endows PC-3/M cells with augmented energy metabolism for fast proliferation and PC-3/S cells with increased eicosanoid production impacting angiogenesis, cell adhesion and invasion. PC-3/S metabolism also promotes the accumulation of docosahexaenoic acid, a long-chain fatty acid with antiproliferative effects. The potential therapeutic significance of our model was supported by a differential sensitivity of PC-3/M cells to etomoxir, an inhibitor of long-chain fatty acid transport to the mitochondria.

Author summary

The coexistence within the same tumor of a variety of subpopulations, featuring different phenotypes (intra-tumoral heterogeneity) represents a challenge for diagnosis, prognosis and targeted therapies. In this work, we have explored the metabolic differences underlying tumor heterogeneity by building cell-type-specific genome-scale metabolic models

47. Pidgeon GP, Kandouz M, Meram A, Honn KV. Mechanisms controlling cell cycle arrest and induction of apoptosis after 12-lipoxygenase inhibition in prostate cancer cells. *Cancer Res.* 2002; 62(9):2721–7. PMID: [11980674](#).
48. Galluzzi L, Kepp O, Vander Heiden MG, Kroemer G. Metabolic targets for cancer therapy. *Nat Rev Drug Discov.* 2013; 12(11):829–46. <https://doi.org/10.1038/nrd4145> PMID: [24113830](#).
49. Irizarry RA, Hobbs B, Collin F, Beazer-Barclay YD, Antonellis KJ, Scherf U, Speed TP. Exploration, normalization, and summaries of high density oligonucleotide array probe level data. *Biostatistics.* 2003; 4(2):249–64. <https://doi.org/10.1093/biostatistics/4.2.249> PMID: [12925520](#).
50. Hamilton JJ and Reed JL. Identification of Functional Differences in Metabolic Networks Using Comparative Genomics and Constraint-Based Models. *PLoS ONE.* 2012; 7(4): e34670. <https://doi.org/10.1371/journal.pone.0034670> PMID: [22666308](#).
51. Llaneras F and Pico J. A procedure for the estimation over time of metabolic fluxes in scenarios where measurements are uncertain and/or insufficient. *BMC Bioinformatics.* 2007; 8:421. <https://doi.org/10.1186/1471-2105-8-421> PMID: [17971203](#).
52. Reed JL and Palsson B. Genome-scale in silico models of e. coli have multiple equivalent phenotypic states: assessment of correlated reaction subsets that comprise network states. *Genome Res.* 2004; 14(9):1797–1805. <https://doi.org/10.1101/gr.2546004> PMID: [15342562](#).
53. Mahadevan R and Schilling C H. The effects of alternate optimal solutions in constraint-based genome-scale metabolic models. *Metabolic Engineering.* 2003; 5:264–276. PMID: [14642354](#).
54. Hoppe A, Hoffmann S, Gerasch A, Gille C, Holzhütter H. FASIMU: flexible software for flux-balance computation series in large metabolic networks. *BMC Bioinformatics.* 2011; 12:28. <https://doi.org/10.1186/1471-2105-12-28> PMID: [21255455](#).



Contents lists available at ScienceDirect

Lung Cancer

journal homepage: www.elsevier.com/locate/lungcan

Tumor-associated metabolic and inflammatory responses in early stage non-small cell lung cancer: Local patterns and prognostic significance

Laura Millares^{a,b,c}, Esther Barreiro^{b,d}, Roldan Cortes^{e,f,g}, Anabel Martinez-Romero^d, Cristina Balcells^{e,f}, Marta Cascante^{e,f,g}, Ana Belen Enguita^{b,h}, Carlos Alvarez^{b,i}, Ramón Rami-Porta^{b,j}, Julio Sánchez de Cos^k, Luis Seijo^{b,l}, Eduard Monsó^{b,m,n,*}, Grupo Colaborativo en Cáncer de Pulmón CIBERES- CIBERONC- SEPAR - Plataforma Biobanco Pulmonar¹

^a Fundació Parc Taulí- Institut d' Investigació i Innovació Parc Taulí (I3PT), Barcelona, Spain

^b Centro de Investigación Biomédica en Red de Enfermedades Respiratorias (CIBERES), Instituto de Salud Carlos III (ISCIII), Madrid, Spain

^c Universitat Autònoma de Barcelona, Esfera UAB, Barcelona, Spain

^d Pulmonology Department-Muscle Wasting and Cachexia in Chronic Respiratory Diseases and Lung Cancer Research Group, IMIM-Hospital del Mar, Parc de Salut Mar, Health and Experimental Sciences Department (CEXS), Universitat Pompeu Fabra (UPF), Barcelona Biomedical Research Park (PRBB), Barcelona, Spain

^e Institut de Biomedicina (IBUB), Universitat de Barcelona, Spain

^f Department of Biochemistry and Molecular Biology, Faculty of Biology, and IDIBAPS, Unit Associated with CSIC, Barcelona, Spain

^g Centro de Investigación Biomédica en Red de Enfermedades Hepáticas y Digestivas (CIBEREHD), Instituto de Salud Carlos III (ISCIII), Madrid, Spain

^h Department of Pathology, Hospital 12 Octubre, Madrid, Spain

ⁱ Department of Respiratory Medicine, Hospital 12 Octubre, Madrid, Spain

^j Department of Thoracic Surgery, Hospital Universitario Mutua de Terrassa, Barcelona, Spain

^k Department of Respiratory Medicine, Hospital San Pedro de Alcántara, Cáceres, Spain

^l Department of Respiratory Medicine, Universidad de Navarra, Madrid, Spain

^m Department of Respiratory Medicine, Hospital Universitario Parc Taulí, Barcelona, Spain

ⁿ Department of Medicine, Universitat Autònoma de Barcelona (UAB), Barcelona, Spain

ARTICLE INFO

Keywords:

IL1 β
 Pentose phosphate pathway
 PDL1
 Early-stage
 NSCLC
 Prognosis
 Inflammation

ABSTRACT

Introduction: Non-small cell lung cancer (NSCLC) patients diagnosed in early stage and surgically-treated have five-year mortality rate > 20%. The identification of biomarkers able to predict progression and death may help to identify patients needing closer follow-up.

Methods: A retrospective cohort of early-stage surgically-treated NSCLC patients enrolled in the International Association for the Study of Lung Cancer (IASLC) Staging Project was created, and tissue Microarrays (TMAs) were constructed with tumor and non-tumor lung tissue. Pentose phosphate pathway (PPP) proteins (transketolase [TKT] and transketolase-like 1 [TKTL1]), inflammatory markers (cyclooxygenase-2 [COX-2], tumor necrosis factor alpha [TNF- α], interleukin 1 beta [IL1 β], nuclear factor kappa-light-chain-enhancer of activated B cells [NF κ B]-p65 and antigen Ki-67), and programmed death-ligand 1 (PDL1) were measured by immunohistochemistry.

Results: NSCLC patients with adenocarcinoma (ADC) or squamous cell carcinoma (SCC) were included in the study (n = 199). TKT and TKTL1 were significantly higher in ADC than in non-tumor tissue (p < 0.001). Higher values were also observed in NSCLC for all the inflammatory markers, with figures > 30% above those of non-tumor tissue (p < 0.001). PDL1 analysis showed a higher percentage of positivity in ADC than in non-tumor tissue (p < 0.001). Multivariate Cox proportional hazards modeling confirmed that high IL1 β level in tumor tissue was independently associated with 3-year mortality in NSCLC [HR = 2.05, 95% CI (1.1–3.7), p = 0.019], a relationship driven by ADC subtype.

Conclusion: This study confirms an increase in metabolic activity and an inflammatory response in tumor tissue

* Corresponding author at: Hospital Parc Taulí, Parc Taulí 1, 08208, Sabadell, Barcelona, Spain.

E-mail addresses: lmillares@tauli.cat (L. Millares), ebarreiro@imim.es (E. Barreiro), roldancg@gmail.com (R. Cortes), anabelmr.94@hotmail.es (A. Martinez-Romero), crisgatsu@gmail.com (C. Balcells), martacascante@ub.edu (M. Cascante), abenguita@hotmail.com (A.B. Enguita), carlosjose.alvarez@salud.madrid.org (C. Alvarez), rramip@yahoo.es (R. Rami-Porta), juli1949@separ.es (J. Sánchez de Cos), lseijo@unav.es (L. Seijo), emonso@tauli.cat (E. Monsó).

¹ See Appendix A.

- 801–808, <http://dx.doi.org/10.3892/ol.2015.3976>.
- [7] D. Hanahan, R.A. Weinberg, The hallmarks of cancer, *Cell* 100 (2000) 57–70.
- [8] D. Hanahan, R.A. Weinberg, Hallmarks of cancer: the next generation, *Cell* 144 (2011) 646–674, <http://dx.doi.org/10.1016/j.cell.2011.02.013>.
- [9] R.S. Herbst, J.V. Heymach, S.M. Lippman, Lung cancer, *N. Engl. J. Med.* 359 (2008) 1367–1380, <http://dx.doi.org/10.1056/NEJMra0802714>.
- [10] S. Diaz-Moralli, M. Tarrado-Castellarnau, C. Alenda, A. Castells, M. Cascante, Transketolase-like 1 expression is modulated during colorectal cancer progression and metastasis formation, *PLoS One* 6 (2011) e25323, <http://dx.doi.org/10.1371/journal.pone.0025323>.
- [11] M. Tarrado-Castellarnau, P. de Atauri, M. Cascante, Oncogenic regulation of tumor metabolic reprogramming, *Oncotarget* 7 (2016) 62726–62753, <http://dx.doi.org/10.18632/oncotarget.10911>.
- [12] K.C. Patra, N. Hay, The pentose phosphate pathway and cancer, *Trends Biochem. Sci.* 39 (2014) 347–354, <http://dx.doi.org/10.1016/j.tibs.2014.06.005>.
- [13] L.-H. Hu, J.-H. Yang, D.-T. Zhang, S. Zhang, L. Wang, P.-C. Cai, J.-F. Zheng, J.-S. Huang, The TKTL1 gene influences total transketolase activity and cell proliferation in human colon cancer LoVo cells, *Anticancer Drugs* 18 (2007) 427–433, <http://dx.doi.org/10.1097/CAD.0b013e328013d99e>.
- [14] G. Kayser, W. Sienele, B. Kubitz, D. Mattern, E. Stickeler, B. Passlick, M. Werner, A. Zur Hausen, Poor outcome in primary non-small cell lung cancers is predicted by transketolase TKTL1 expression, *Pathology (Phila.)* 43 (2011) 719–724, <http://dx.doi.org/10.1097/PAT.0b013e32832834c352b>.
- [15] S. Langbein, M. Zerilli, A. Zur Hausen, W. Staiger, K. Rensch-Boschert, N. Lukan, J. Popa, M.P. Ternullo, A. Steidler, C. Weiss, R. Grobholz, F. Willeke, P. Alken, G. Stassi, P. Schubert, J.F. Coy, Expression of transketolase TKTL1 predicts colon and urothelial cancer patient survival: Warburg effect reinterpreted, *Br. J. Cancer* 94 (2006) 578–585, <http://dx.doi.org/10.1038/sj.bjc.6602962>.
- [16] D.F. Quail, J.A. Joyce, Microenvironmental regulation of tumor progression and metastasis, *Nat. Med.* 19 (2013) 1423–1437, <http://dx.doi.org/10.1038/nm.3394>.
- [17] R.M. Bremnes, T. Dønnem, S. Al-Saad, K. Al-Shibli, S. Andersen, R. Sirera, C. Camps, I. Marinze, L.-T. Busund, The role of tumor stroma in cancer progression and prognosis: emphasis on carcinoma-associated fibroblasts and non-small cell lung cancer, *J. Thorac. Oncol.* 6 (2011) 209–217, <http://dx.doi.org/10.1097/JTO.0b013e3181f8a1bd>.
- [18] T.F. Gajewski, H. Schreiber, Y.-X. Fu, Innate and adaptive immune cells in the tumor microenvironment, *Nat. Immunol.* 14 (2013) 1014–1022, <http://dx.doi.org/10.1038/ni.2703>.
- [19] N.A. Bhowmick, E.G. Neilson, H.L. Moses, Stromal fibroblasts in cancer initiation and progression, *Nature* 432 (2004) 332–337, <http://dx.doi.org/10.1038/nature03096>.
- [20] E.M. Conway, L.A. Pikor, S.H.Y. Kung, M.J. Hamilton, S. Lam, W.L. Lam, K.L. Bennewith, Macrophages, inflammation, and lung cancer, *Am. J. Respir. Crit. Care Med.* 193 (2016) 116–130, <http://dx.doi.org/10.1164/rccm.201508-1545CI>.
- [21] M.B. Amin, S. Edge, E. Greene, et al., *AJCC Cancer Staging Manual*, 8th edition, Springer, 2016.
- [22] J.B. Brierley, M.K. Gospodarowicz, Ch Wittekind, *UICC TNM Classification of Malignant Tumours*, 8th edition, Wiley Blackwell, Oxford, 2016.
- [23] P. Goldstraw, K. Chansky, J. Crowley, R. Rami-Porta, H. Asamura, W.E.E. Eberhardt, A.G. Nicholson, P. Groome, A. Mitchell, V. Bolejack, International association for the study of lung cancer staging and prognostic factors committee, advisory boards, and participating institutions, international association for the study of lung cancer staging and prognostic factors committee advisory boards and participating institutions, the IASLC lung cancer staging project: proposals for revision of the TNM stage groupings in the forthcoming (eighth) edition of the TNM classification for lung cancer, *J. Thorac. Oncol.* 11 (2016) 39–51, <http://dx.doi.org/10.1016/j.jtho.2015.09.009>.
- [24] R. Rami-Porta (Ed.), *IASLC Staging Manual in Thoracic Oncology*, Editorial Rx Press, Fort Myers, FL, 2016.
- [25] R. Rami-Porta, V. Bolejack, D.J. Giroux, K. Chansky, J. Crowley, H. Asamura, P. Goldstraw, The IASLC lung cancer staging project: the new database to inform the eighth edition of the TNM classification of lung cancer, *J. Thorac. Oncol.* 9 (2014) 1618–1624, <http://dx.doi.org/10.1097/JTO.0000000000000334>.
- [26] J. Sánchez de Cos Escuin, M. Serra Mitjans, J. Hernández Hernández, H. Hernández Rodríguez, Registro del Grupo Cooperativo de Cáncer de Pulmón-II de la Sociedad Española de Neumología y Cirugía Torácica. Estudio descriptivo, *Arch. Bronconeumol.* 49 (2013) 462–467, <http://dx.doi.org/10.1016/j.arbres.2013.05.002>.
- [27] E. Monsó, L.M. Montuenga, J. Sánchez de Cos, C. Villena, por el Grupo Colaborativo en Cáncer de Pulmón CIBERES-RTICC-SEPAR-Plataforma Biobanco Pulmonar, Biological Marker Analysis as Part of the CIBERES-RTIC Cancer-SEPAR strategic project on lung cancer, *Arch. Bronconeumol.* (2015), <http://dx.doi.org/10.1016/j.arbres.2014.11.010>.
- [28] D.J. Giroux, R. Rami-Porta, K. Chansky, J.J. Crowley, P.A. Groome, P.E. Postmus, V. Rusch, J.-P. Sculier, F.A. Shepherd, L. Sobin, P. Goldstraw, International association for the study of lung cancer International staging committee, the IASLC lung cancer staging project: data elements for the prospective project, *J. Thorac. Oncol.* 4 (2009) 679–683, <http://dx.doi.org/10.1097/JTO.0b013e3181a52370>.
- [29] Plataforma Biobanco Pulmonar - Bienvenidos a la PBP, (n.d.). <http://biobancopulmonar.ciberes.org/> (Accessed August 28, 2014).
- [30] L. Jiang, X. Su, T. Zhang, X. Yin, M. Zhang, H. Fu, H. Han, Y. Sun, L. Dong, J. Qian, Y. Xu, X. Fu, P.R. Gavine, Y. Zhou, K. Tian, J. Huang, D. Shen, H. Jiang, Y. Yao, B. Han, Y. Gu, PD-L1 expression and its relationship with oncogenic drivers in non-small cell lung cancer (NSCLC), *Oncotarget* 8 (2017) 26845–26857, <http://dx.doi.org/10.18632/oncotarget.15839>.
- [31] P.S. Ward, C.B. Thompson, Metabolic reprogramming: a cancer hallmark even Warburg did not anticipate, *Cancer Cell* 21 (2012) 297–308, <http://dx.doi.org/10.1016/j.ccr.2012.02.014>.
- [32] C. Ricciardelli, N.A. Lokman, S. Cheruvu, I.A. Tan, M.P. Ween, C.E. Pyragius, A. Ruszkiewicz, P. Hoffmann, M.K. Oehler, Transketolase is upregulated in metastatic peritoneal implants and promotes ovarian cancer cell proliferation, *Clin. Exp. Metastasis* 32 (2015) 441–455, <http://dx.doi.org/10.1007/s10085-015-9718-1>.
- [33] M. Krockenberger, A. Honig, L. Rieger, J.F. Coy, M. Sutterlin, M. Kapp, E. Horn, J. Diel, U. Kammerer, Transketolase-like 1 expression correlates with subtypes of ovarian cancer and the presence of distant metastases, *Int. J. Gynecol. Cancer* 17 (2007) 101–106, <http://dx.doi.org/10.1111/j.1525-1438.2007.00799.x>.
- [34] H. Schultz, D. Kähler, D. Branscheid, E. Vollmer, P. Zabel, T. Goldmann, TKTL1 is overexpressed in a large portion of non-small cell lung cancer specimens, *Diagn. Pathol.* 3 (2008) 35, <http://dx.doi.org/10.1186/1746-1596-3-35>.
- [35] M. Grimm, S. Hoefert, O. Luz, S. Reinert, J. Polligkeit, Transketolase-like protein 1 expression in recurrent oral squamous cell carcinoma after curative resection: a case report, *Oral Surg. Oral Med. Oral Pathol. Oral Radiol.* 116 (2013) e173–178, <http://dx.doi.org/10.1016/j.oooo.2011.12.022>.
- [36] X. Xu, A. Zur Hausen, J.F. Coy, M. Löchelt, Transketolase-like protein 1 (TKTL1) is required for rapid cell growth and full viability of human tumor cells, *Int. J. Cancer* 124 (2009) 1330–1337, <http://dx.doi.org/10.1002/ijc.24078>.
- [37] S. Zhang, J.-H. Yang, C.-K. Guo, P.-C. Cai, Gene silencing of TKTL1 by RNAi inhibits cell proliferation in human hepatoma cells, *Cancer Lett.* 253 (2007) 108–114, <http://dx.doi.org/10.1016/j.canlet.2007.01.010>.
- [38] Y. Dong, M. Wang, Knockdown of TKTL1 additionally complements cisplatin-induced cytotoxicity in nasopharyngeal carcinoma cells by regulating the levels of NADPH and ribose-5-phosphate, *Biomed. Pharmacother. Biomed. Pharmacother.* 85 (2017) 672–678, <http://dx.doi.org/10.1016/j.biopha.2016.11.078>.
- [39] S. Diaz-Moralli, E. Aguilar, S. Marin, J.F. Coy, M. Dewerchin, M.R. Antoniewicz, O. Meca-Cortés, L. Notebaert, B. Ghesquière, G. Eelen, T.M. Thomson, P. Carmeliet, M. Cascante, A key role for transketolase-like 1 in tumor metabolic reprogramming, *Oncotarget* 7 (2016) 51875–51897, <http://dx.doi.org/10.18632/oncotarget.10429>.
- [40] A. Jayachandran, P.-H. Lo, A.C. Chueh, P. Prithviraj, R. Molania, M. Davalos-Salas, M. Anaka, M. Walkiewicz, J. Cebon, A. Behren, Transketolase-like 1 ectopic expression is associated with DNA hypomethylation and induces the Warburg effect in melanoma cells, *BMC Cancer* 16 (2016) 134, <http://dx.doi.org/10.1186/s12885-016-2185-5>.
- [41] A.M. Lewis, S. Varghese, H. Xu, H.R. Alexander, Interleukin-1 and cancer progression: the emerging role of interleukin-1 receptor antagonist as a novel therapeutic agent in cancer treatment, *J. Transl. Med.* 4 (2006) 48, <http://dx.doi.org/10.1186/1479-5876-4-48>.
- [42] I.A. Bhat, N.A. Naykoo, I. Qasim, F.A. Ganie, Q. Yousuf, B.A. Bhat, R. Rasool, S.A. Aziz, Z.A. Shah, Association of interleukin 1 beta (IL-1 β) polymorphism with mRNA expression and risk of non small cell lung cancer, *Meta Gene* 2 (2014) 123–133, <http://dx.doi.org/10.1016/j.mgene.2013.12.002>.
- [43] Y. Carmi, S. Dotan, P. Rider, I. Kaplanov, M.R. White, R. Baron, S. Abutbul, M. Huszar, C.A. Dinarello, R.N. Apte, E. Voronov, The role of IL-1 β in the early tumor cell-induced angiogenic response, *J. Immunol. Baltim. Md* 1950 190 (2013) 3500–3509, <http://dx.doi.org/10.4049/jimmunol.1202769>.
- [44] S. Nakao, T. Kuwano, C. Tsutsumi-Miyahara, S. Ueda, Y.N. Kimura, S. Hamano, K. Sonoda, Y. Saijo, T. Nukiwa, R.M. Strieter, T. Ishibashi, M. Kuwano, M. Ono, Infiltration of COX-2-expressing macrophages is a prerequisite for IL-1 β -induced neovascularization and tumor growth, *J. Clin. Invest.* 115 (2005) 2979–2991, <http://dx.doi.org/10.1172/JCI23298>.
- [45] F.R. Balkwill, A. Mantovani, Cancer-related inflammation: common themes and therapeutic opportunities, *Semin. Cancer Biol.* 22 (2012) 33–40, <http://dx.doi.org/10.1016/j.semcancer.2011.12.005>.
- [46] M. Seike, N. Yanaihara, E.D. Bowman, K.A. Zanetti, A. Budhu, K. Kumamoto, L.E. Mechanic, S. Matsumoto, J. Yokota, T. Shibata, H. Sugimura, A. Gemma, S. Kudoh, X.W. Wang, C.C. Harris, Use of a cytokine gene expression signature in lung adenocarcinoma and the surrounding tissue as a prognostic classifier, *J. Natl. Cancer Inst.* 99 (2007) 1257–1269, <http://dx.doi.org/10.1093/jnci/djm083>.
- [47] F. Passiglia, G. Bronte, M. Castiglia, A. Listi, V. Calò, F. Toia, G. Cicero, D. Fanale, S. Rizzo, V. Bazan, A. Russo, Prognostic and predictive biomarkers for targeted therapy in NSCLC: for whom the bell tolls? *Expert Opin. Biol. Ther.* 15 (2015) 1553–1566, <http://dx.doi.org/10.1517/14712598.2015.1071348>.
- [48] M. Ilie, V. Hofman, M. Dietel, J.-C. Soria, P. Hofman, Assessment of the PD-L1 status by immunohistochemistry: challenges and perspectives for therapeutic strategies in lung cancer patients, *Virchows Arch.* 468 (2016) 511–525, <http://dx.doi.org/10.1007/s00428-016-1910-4>.
- [49] C.T. Hiley, J. Le Quesne, G. Santis, R. Sharpe, D.G. de Castro, G. Middleton, C. Swanton, Challenges in non-molecular testing in de novo small-cell lung cancer patients with advanced disease, *Lancet Lond. Engl.* 388 (2016) 1002–1011, [http://dx.doi.org/10.1016/S0140-6736\(16\)31340-X](http://dx.doi.org/10.1016/S0140-6736(16)31340-X).
- [50] D.M. Pardoll, The blockade of immune checkpoints in cancer immunotherapy, *Nat. Rev. Cancer* 12 (2012) 252–264, <http://dx.doi.org/10.1038/nrc3239>.



Contents lists available at ScienceDirect

Trends in Analytical Chemistry

journal homepage: www.elsevier.com/locate/trac

Tracing metabolic fluxes using mass spectrometry: Stable isotope-resolved metabolomics in health and disease

Cristina Balcells^{a, b, 1}, Carles Foguet^{a, b, c, 1}, Josep Tarragó-Celada^{a, b, 1}, Pedro de Atauri^{a, b, c}, Silvia Marin^{a, b, c, **}, Marta Cascante^{a, b, c, *}

^a Department of Biochemistry and Molecular Biomedicine, Faculty of Biology, Universitat de Barcelona, Diagonal, 643, 08028 Barcelona, Spain

^b Institute of Biomedicine of Universitat de Barcelona (IBUB), Barcelona, Spain

^c Centro de Investigación Biomédica en Red de Enfermedades Hepáticas y Digestivas (CIBEREHD), Instituto de Salud Carlos III (ISCIII), Madrid, Spain

ARTICLE INFO

Article history:
Available online xxx

Keywords:
SIRM
MFA
MS
Metabolic fluxes
Metabolic regulation
Cancer metabolism
Metabolic diseases

ABSTRACT

Tracing metabolic fluxes, defined as the reaction and transport rates in living cells, is essential to characterize metabolic phenotypes. One of the most informative methods to predict fluxes is stable isotope-resolved metabolomics (SIRM). In SIRM, a biological system is fed with substrates labeled with stable heavy isotopes. This isotopic label propagates along metabolic pathways and is incorporated into metabolites. After incubation, metabolites are extracted, and the incorporation of the isotopic label is quantified with isotope-sensitive analytical techniques, either mass spectrometry (MS) or nuclear magnetic resonance (NMR). Here we review the most suitable and widely-used MS platforms and methodologies for SIRM. We also provide an overview of state of the art in the analysis of SIRM data to trace metabolic fluxes, covering both local flux predictions and network-wide flux analysis. Finally, we highlight the role of SIRM in shaping our current understanding of metabolism in both health and pathological conditions.

© 2019 Elsevier B.V. All rights reserved.

1. Introduction

Metabolic fluxes, defined as the reaction and transport rates in living cells, are a close reflection of the metabolic phenotype [1]. Hence, tracing metabolic fluxes is key to understanding the mechanisms of metabolic regulation in both health and disease. Extracellular fluxes (rates of uptake and secretion of metabolites) can be quantified by measuring changes in metabolite concentrations in the extracellular media [2]. However, intracellular fluxes cannot be directly estimated from measurements of intracellular metabolite concentrations as they are not informative of the fluxes leading to and originating from any given metabolite [3–5]. This

limitation has led to the development of stable isotope-resolved metabolomics (SIRM).

In SIRM, a biological system is fed with one or more metabolic substrates labeled with stable heavy isotopes (¹³C, ¹⁵N, ²H, ¹⁸O, etc.). These labeled molecules, usually referred to as tracers, are metabolized by the system of interest through different metabolic pathways. An isotopic label propagates in a time, flux and pathway-dependent manner, generating characteristic labeling patterns in metabolites, which can provide information about the fluxes through pathways leading to such metabolites [1,2].

The propagation of a label from tracers to metabolites is quantified by isotope-sensitive analytical techniques, namely nuclear magnetic resonance (NMR) and mass spectrometry (MS). NMR measures the resonance of nuclei with a net spin under a magnetic field. NMR, which is commonly used as a structural determination technique, can be used to quantify the abundance of positional isotopomers (isomers with heavy isotopes substitutions in specific positions) with isotopes that possess a net nuclear spin (e.g., ¹³C and ¹⁵N) [6,7]. By contrast, MS separates and quantifies ionized molecules based on their mass-to-charge ratio (*m/z*). Therefore, as the mass of an ionized molecule will increase upon heavy isotope incorporation, MS can be used to quantify the relative abundance of

* Corresponding author. Department of Biochemistry and Molecular Biomedicine, Faculty of Biology, Universitat de Barcelona, Av. Diagonal, 643, 08028 Barcelona, Spain.

** Corresponding author. Department of Biochemistry and Molecular Biomedicine, Faculty of Biology, Universitat de Barcelona, Av. Diagonal, 643, 08028 Barcelona, Spain.

E-mail addresses: silviamarin@ub.edu (S. Marin), martacascante@ub.edu (M. Cascante).

¹ These authors contributed equally to this work, and they are listed in alphabetic order.

- line, *J. Biol. Chem.* 283 (2008) 20621–20627. <https://doi.org/10.1074/jbc.M706494200>.
- [98] C.L. Perez, M.R. Van Gilst, A ¹³C isotope labeling strategy reveals the influence of insulin signaling on lipogenesis in *C. elegans*, *Cell Metab.* 8 (2008) 266–274. <https://doi.org/10.1016/j.cmet.2008.08.007>.
- [99] S.B. Crown, N. Marze, M.R. Antoniewicz, Catabolism of branched chain amino acids contributes significantly to synthesis of odd-chain and even-chain fatty acids in 3T3-L1 adipocytes, *PLoS One* 10 (2015) e0145850. <https://doi.org/10.1371/journal.pone.0145850>.
- [100] J.S. Kirkwood, C.L. Miranda, G. Bobe, C.S. Maier, J.F. Stevens, 18O-Tracer metabolomics reveals protein turnover and CDP-choline cycle activity in differentiating 3T3-L1 pre-adipocytes, *PLoS One* 11 (2016) 1–18. <https://doi.org/10.1371/journal.pone.0157118>.
- [101] G. Aubert, O.J. Martin, J.L. Horton, L. Lai, R.B. Vega, T.C. Leone, T. Koves, S.J. Gardell, M. Krüger, C.L. Hoppel, E.D. Lewandowski, P.A. Crawford, D.M. Muoio, D.P. Kelly, The failing heart relies on ketone bodies as a fuel, *Circulation* 133 (2016) 698–705. <https://doi.org/10.1161/CIRCULATIONAHA.115.017355>.
- [102] P. Mirtschink, J. Krishnan, F. Grimm, A. Sarre, M. Hörl, M. Kayikci, N. Fankhauser, Y. Christinat, C. Cortijo, O. Feehan, A. Vukolic, S. Sossalla, S.N. Stehr, J. Ule, N. Zamboni, T. Pedrazzini, W. Krek, HIF-driven SF3B1 induces KHK-C to enforce fructolysis and heart disease, *Nature* 522 (2015) 444–449. <https://doi.org/10.1038/nature14508>.
- [103] L. Gu, G.-F. Zhang, R.S. Kombu, F. Allen, G. Kutz, W.-U. Brewer, C.R. Roe, H. Brunengraber, Parenteral and enteral metabolism of anaplerotic triheptanoin in normal rats. II. Effects on lipolysis, glucose production, and liver acyl-CoA profile, *Am. J. Physiol. Endocrinol. Metab.* 298 (2010) E362–E371. <https://doi.org/10.1152/ajpendo.00384.2009>.
- [104] N. Carinhas, A. Koshkin, D.A.M. Pais, P.M. Alves, A.P. Teixeira, 13 C-metabolic flux analysis of human adenovirus infection: implications for viral vector production, *Biotechnol. Bioeng.* 114 (2017) 195–207. <https://doi.org/10.1002/bit.26063>.
- [105] S. Watanabe, M. Zimmermann, M.B. Goodwin, U. Sauer, C.E. Barry, H.I. Boshoff, Fumarate reductase activity maintains an energized membrane in anaerobic *Mycobacterium tuberculosis*, *PLoS Pathog.* 7 (2011) e1002287. <https://doi.org/10.1371/journal.ppat.1002287>.
- [106] E.H. Ma, G. Bantug, T. Griss, S. Condotta, R.M. Johnson, B. Samborska, N. Mainolfi, V. Suri, H. Guak, M.L. Balmer, M.J. Verway, T.C. Raissi, H. Tsui, G. Boukhaled, S. Henriques da Costa, C. Frezza, C.M. Krawczyk, A. Friedman, M. Manfredi, M.J. Richer, C. Hess, R.G. Jones, Serine is an essential metabolite for effector T cell expansion, *Cell Metab.* 25 (2017) 345–357. <https://doi.org/10.1016/j.cmet.2016.12.011>.
- [107] P. Sadiku, J.A. Willson, R.S. Dickinson, F. Murphy, A.J. Harris, A. Lewis, D. Sammut, A.S. Mirchandani, E. Ryan, E.R. Watts, A.A.R. Thompson, H.M. Marriott, D.H. Dockrell, C.T. Taylor, M. Schneider, P.H. Maxwell, E.R. Chilvers, M. Mazzone, V. Moral, C.W. Pugh, P.J. Ratcliffe, C.J. Schofield, B. Ghesquiere, P. Carmeliet, M.K.B. Whyte, S.R. Walmsley, Prolyl hydroxylase 2 inactivation enhances glycogen storage and promotes excessive neutrophilic responses, *J. Clin. Invest.* 127 (2017) 3407–3420. <https://doi.org/10.1172/JCI90848>.
- [108] D. Drago, V. Basso, E. Gaude, G. Volpe, L. Peruzzotti-Jametti, A. Bachi, G. Musco, A. Andolfo, C. Frezza, A. Mondino, S. Pluchino, Metabolic determinants of the immune modulatory function of neural stem cells, *J. Neuroinflammation* 13 (2016) 1–18. <https://doi.org/10.1186/s12974-016-0667-7>.
- [109] N.J. Matheson, J. Sumner, K. Wals, R. Rapiteanu, M.P. Weekes, R. Vigan, J. Weinelt, M. Schindler, R. Antrobus, A.S.H. Costa, C. Frezza, C.B. Clish, S.J.D. Neil, P.J. Lehner, Cell surface proteomic map of HIV infection reveals antagonism of amino acid metabolism by Vpu and Nef, *Cell Host Microbe* 18 (2015) 409–423. <https://doi.org/10.1016/j.chom.2015.09.003>.
- [110] C. Des Rosiers, C.A. Fernandez, F. David, H. Brunengraber, Reversibility of the mitochondrial isocitrate dehydrogenase reaction in the perfused rat liver. Evidence from isotopomer analysis of citric acid cycle intermediates, *J. Biol. Chem.* 269 (1994) 27179–27182. <http://www.ncbi.nlm.nih.gov/pubmed/7961626>.
- [111] G.-F. Zhang, S. Sadhukhan, R.A. Ibarra, S.M. Lauden, C.-Y. Chuang, S. Sushailo, P. Chatterjee, V.E. Anderson, G.P. Tochtrop, H. Brunengraber, Metabolism of γ -hydroxybutyrate in perfused rat livers, *Biochem. J.* 444 (2012) 333–341. <https://doi.org/10.1042/BJ20112046>.
- [112] S.Y. Lunt, V. Muralidhar, A.M. Hosios, W.J. Israelsen, D.Y. Gui, L. Newhouse, M. Ogrodzinski, V. Hecht, K. Xu, P.N.M. Acevedo, D.P. Hollern, G. Bellinger, T.L. Dayton, S. Christen, I. Elia, A.T. Dinh, G. Stephanopoulos, S.R. Manalis, M.B. Yaffe, E.R. Andrechek, S.M. Fendt, M.G. Vander Heiden, Pyruvate kinase isoform expression alters nucleotide synthesis to impact cell proliferation, *Mol. Cell.* 57 (2015) 95–107. <https://doi.org/10.1016/j.molcel.2014.10.027>.
- [113] A.R. Grassian, S.J. Parker, S.M. Davidson, A.S. Divakaruni, C.R. Green, X. Zhang, K.L. Slocum, M. Pu, F. Lin, C. Vickers, C. Joud-Caldwell, F. Chung, H. Yin, E.D. Handly, C. Straub, J.D. Growney, M.G. Vander Heiden, A.N. Murphy, R. Pagliarini, C.M. Metallo, IDH1 mutations alter citric acid cycle metabolism and increase dependence on oxidative mitochondrial metabolism, *Cancer Res.* 74 (2014) 3317–3331. <https://doi.org/10.1158/0008-5472.CAN-14-0772-T>.
- [114] S. Christen, D. Lorendeau, R. Schmieder, D. Broekaert, K. Metzger, K. Veys, I. Elia, J.M. Buescher, M.F. Orth, S.M. Davidson, T.G.P. Grünwald, K. De Bock, S.-M. Fendt, Breast cancer-derived lung metastases show increased pyruvate carboxylase-dependent anaplerosis, *Cell Rep.* 17 (2016) 837–848. <https://doi.org/10.1016/j.celrep.2016.09.042>.
- [115] I. Marín de Mas, E. Aguilar, E. Zozda, C. Balcells, S. Marin, G. Dallmann, T.M. Thomson, B. Papp, M. Cascante, Model-driven discovery of long-chain fatty acid metabolic reprogramming in heterogeneous prostate cancer cells, *PLoS Comput. Biol.* 14 (2018) e1005914. <https://doi.org/10.1371/journal.pcbi.1005914>.
- [116] M. Tarrado-Castellarnau, P. de Atauri, J. Tarragó-Celada, J. Perarnau, M. Yuneva, T.M. Thomson, M. Cascante, De novo MYC addiction as an adaptive response of cancer cells to CDK4/6 inhibition, *Mol. Syst. Biol.* 13 (2017) 940. <https://doi.org/10.15252/msb.20167321>.
- [117] J.R. Krycer, K. Yugi, A. Hirayama, D.J. Fazakerley, L.E. Quek, R. Scalzo, S. Ohno, M.P. Hodson, S. Ikeda, F. Shoji, K. Suzuki, W. Domanova, B.L. Parker, M.E. Nelson, S.J. Humphrey, N. Turner, K.L. Hoehn, G.J. Cooney, T. Soga, S. Kuroda, D.E. James, Dynamic metabolomics reveals that insulin primes the adipocyte for glucose metabolism, *Cell Rep.* 21 (2017) 3536–3547. <https://doi.org/10.1016/j.celrep.2017.11.085>.
- [118] E. Brunk, S. Sahoo, D.C. Zielinski, A. Altunkaya, A. Dräger, N. Mih, F. Gatto, A. Nilsson, G.A. Preciat Gonzalez, M.K. Aurich, A. Prlic, A. Sastry, A.D. Danielsdottir, A. Heinken, A. Noronha, P.W. Rose, S.K. Burley, R.M.T. Fleming, J. Nielsen, I. Thiele, B.O. Palsson, Recon3D enables a three-dimensional view of gene variation in human metabolism, *Nat. Biotechnol.* 36 (2018) 272–281. <https://doi.org/10.1038/nbt.4072>.



Review

Metabolic Plasticity and Epithelial-Mesenchymal Transition

Timothy M. Thomson ^{1,2,*}, Cristina Balcells ^{3,4}  and Marta Cascante ^{3,5}

¹ Department of Cell Biology, Molecular Biology Institute of Barcelona, Science Research Council, 08028 Barcelona, Spain

² Networked Center for Research in Liver and Digestive Diseases (CIBEREHD), Instituto de Salud Carlos III (ISCIII), 28029 Madrid, Spain

³ Department of Biochemistry and Molecular Biomedicine-Institute of Biomedicine (IBUB), University of Barcelona, 08028 Barcelona, Spain

⁴ Department of Materials Science and Physical Chemistry, University of Barcelona, 08028 Barcelona, Spain

⁵ Networked Center for Research in Liver and Digestive Diseases (CIBEREHD) and metabolomics node at INB-Bioinformatics Platform, Instituto de Salud Carlos III (ISCIII), 28029 Madrid, Spain

* Correspondence: titbmc@ibmb.csic.es

Received: 30 April 2019; Accepted: 28 June 2019; Published: 3 July 2019



Abstract: A major transcriptional and phenotypic reprogramming event during development is the establishment of the mesodermal layer from the ectoderm through epithelial-mesenchymal transition (EMT). EMT is employed in subsequent developmental events, and also in many physiological and pathological processes, such as the dissemination of cancer cells through metastasis, as a reversible transition between epithelial and mesenchymal states. The remarkable phenotypic remodeling accompanying these transitions is driven by characteristic transcription factors whose activities and/or activation depend upon signaling cues and co-factors, including intermediary metabolites. In this review, we summarize salient metabolic features that enable or instigate these transitions, as well as adaptations undergone by cells to meet the metabolic requirements of their new states, with an emphasis on the roles played by the metabolic regulation of epigenetic modifications, notably methylation and acetylation.

Keywords: epithelial-mesenchymal transition; metabolism; plasticity; epigenetics; drug resistance

1. Introduction

Cells undergoing switches from epithelial to mesenchymal states experience radical changes in motility, proliferation, morphology and interactions with their environment. Epithelial cells that undergo EMT lose cell-cell contacts, undergo extensive cytoskeletal remodeling and exponentially increase their motility and their ability to invade, through extracellular structures as individual cells [1]. At the same time, they adjust their rate of proliferation to the degree of motility, such that highly motile cells with strong acquired mesenchymal phenotypes may exhibit a diminished proliferative potential [2], while cells at “intermediate” states of EMT may retain or increase their proliferation rates relative to their initial epithelial states [3]. This suggests a balance between motility and proliferation [4,5], that may depend on the relative availability of common resources that can be spent on either motility or on proliferation. Indeed, cells can undergo EMT (or also mesenchymal–epithelial transition (MET)) to different extents [6], adopting a range of phenotypes. While “extreme” EMT can lead to stable mesenchymal phenotypes prone to enter pre-senescent states [5], “intermediate” forms of EMT endow cells with features shared with stem cells, including self-renewal or survival under stress and in non-adherent growth conditions [7,8].

178. Civenni, G.; Bosotti, R.; Timpanaro, A.; Vázquez, R.; Merulla, J.; Pandit, S.; Rossi, S.; Albino, D.; Allegrini, S.; Mitra, A.; et al. Epigenetic control of mitochondrial fission enables self-renewal of stem-like tumor cells in human prostate cancer. *Cell Metab.* **2019**. [CrossRef]
179. Gao, X.; Sanderson, S.M.; Dai, S.; Reid, M.A.; Cooper, D.E.; Lu, M.; Richie, J.P., Jr.; Ciccarella, A.; Calcagnotto, A.; Mikhael, P.G.; et al. Dietary methionine restriction targets one carbon metabolism in humans and produces broad therapeutic responses in cancer. *bioRxiv* **2019**. [CrossRef]



© 2019 by the authors. Licensee MDPI, Basel, Switzerland. This article is an open access article distributed under the terms and conditions of the Creative Commons Attribution (CC BY) license (<http://creativecommons.org/licenses/by/4.0/>).